DUKE POWER COMPANY
OCONEE NUCLEAR STATION

RELOAD DESIGN METHODOLOGY

NFS-1001A

APRIL 1984

DUKE POWER COMPANY

OCONEE NUCLEAR STATION

RELOAD DESIGN METHODOLOGY

Technical Report

NFS-1001

April 23, 1979

Revision 4 June 1981

July 29, 1981

Dockets Nos. 50-269, 50-270
and 50-287

Mr. William O. Parker, Jr.
Vice President - Steam Production
Duke Power Company
P. O. Box 33189
422 South Church Street
Charlotte, North Carolina 28242

Dear Mr. Parker:

The staff has completed the review of Technical Report NFS-1001, "Oconee Nuclear Station Reload Design Methodology" which was submitted by letter dated April 23, 1979 and revised by letters dated May 20, 1980, January 28, April 22 and June 16, 1981. The results of our review are contained in the enclosed Safety Evaluation.

We have found the revised report to be an acceptable method of performing reload design calculations for future Oconee Nuclear Station, Units 1, 2 and 3 reloads.

If you have any questions on this subject, please contact me.

Sincerely,

Philip C. Wagner

Philip C. Wagner, Project Manager
Operating Reactors Branch #4
Division of Licensing

Enclosure:
Safety Evaluation

cc w/enclosure:
See next page

ABSTRACT

This Technical Report describes Duke Power Company's Reload Design Methodology for the Oconee Nuclear Station. Included in this report are descriptions of Fuel Design, Fuel Cycle Design, Fuel Mechanical Performance, Maneuvering Analysis, Thermal Hydraulic Design, Technical Specifications Review and Development, Accident Analysis Review, and the Development of Core Physics Parameters.

TABLE OF CONTENTS

2

LIST OF TABLES

LIST OF FIGURES

1. INTRODUCTION

The design of a commercial light water reactor is such that the reactor core is loaded with a specified number of fuel assemblies which are generally identical in design but different in the amount of fissile material content. In the initial core the fuel assemblies differ in the initial enrichment of the fuel, and in subsequent fuel cycles they differ in the amount of the burnup of the fuel as well. The reactor is refueled at intervals varying from 6 to 18 months. The refueling of a reactor consists of removing part of the core (a certain number of irradiated fuel assemblies, the number and identity of which are determined by a fuel management scheme) and loading an equal number of fresh and possibly previously burned fuel assemblies called the "reload batch." In general, after refueling, the neutronic, thermal-hydraulic, safety, and operating parameters of the core would be different from the previous fuel cycle. The design analyses required to determine the mechanical design, enrichment and number of assemblies of the reload batch as well as the core loading pattern, the nuclear and thermal-hydraulic characteristics of the reloaded core, and the safety analyses demonstrating the safety of operation of the reloaded reactor is called reload design.

This report describes the various aspects of the reload design. In the following paragraphs, a brief overview of the major elements of the reload design process and the reload design criteria are provided. Subsequent sections provide detailed discussion including descriptions of design methods, analytical formulation, and calculational procedures of the major reload design tasks used for Oconee reload design.

The reload design is essentially a series of analytical exercises with the objective to design the reload core in such a manner that the reactor can be operated up to a specified power level for a specified number of days with acceptable safety criteria. It consists of the development of the basic specifications of the reload batch (mechanical characteristics of the fuel assembly, fuel rod and associated structures, fuel enrichment, pellet dimensions; shape and enrichment, fuel stack length, fill gas pressure, number of assemblies, uranium loading, etc.); it sets forth the number and identity of each residual fuel assembly, selects the location of each fuel assembly and control rod in

the core for the new fuel cycle, establishes the core characteristics and operating limits and protection system setpoints and demonstrates that the operation of the reactor during the new fuel cycle will be within safety considerations already evaluated and approved or provides new safety analyses to demonstrate conformance to applicable safety criteria.

In arriving at the final reload design, the designer tries to meet the requirements imposed by the operational considerations, fuel economics considerations and safety considerations. These requirements are called reload design criteria and are as follows:

1. Initial core excess reactivity will be sufficient to enable full power operation for the desired length of the cycle.

2. Technical Specification limits of specified core parameters (quadrant power tilt, power imbalance, control rod positions, xenon conditions, coolant flow) and on core protection system trip setpoints after allowance for appropriate measurement tolerances should have adequate margin from nominal values of these parameters during operational conditions throughout the cycle so that sufficient operating flexibility is retained for the fuel cycle.

3. The fuel assemblies to be discharged at the end of the fuel cycle will attain maximum permissible burnup so that maximum energy extraction consistent with the fuel mechanical integrity criteria is achieved.

4. Values of important core parameters (moderator temperature coefficient, Doppler coefficient, ejected rod worth, boron worth, total control rod group worth, maximum linear heat rate of the fuel pin at various elevations in the core, and shutdown margin) predicted for the cycle are conservative with respect to their values assumed in the safety analysis of various postulated accidents, and if they are not conservative, acceptable reanalysis of applicable accidents is performed.

5. The power distributions within the reactor core for all possible (or permissible) core conditions that could exist during the operation of the

cycle will not lead to exceeding the thermal design criteria of the fuel and exceeding the LOCA-limited peak linear heat rates.

6. Fuel management will produce fuel rod power and burnup consistent with the mechanical integrity analysis of the fuel rod--that is, the clad tensile strain is less than 1%, the effective clad stress is less that the yield strength, and clad collapse will not occur during the life of the fuel.

7. The mechanical design of the reload fuel, including its vibration, flow, structural characteristics, and seismic and LOCA response, is compatible with the residual fuel.

The reload design process is comprised of the coordinated effort of designers and analysts from many areas, each of which generates specified information in a sequential and sometimes iterative manner to develop the final reload design, meeting the design criteria. The major elements of the reload design process are (1) fuel design, (2) fuel cycle design , (3) fuel mechanical performance analysis, (4) maneuvering analysis, (5) thermal-hydraulic analysis, (6) safety analysis and Technical Specification development, and (7) reload report, and (8) development of core physics parameters.

The fuel design consists of the fuel assembly design (material selection, fuel rod lattice and fuel rod number specification, spacer grid design--number of spacer grids, material selection, mixing vanes, etc.--, and fuel assembly end fittings design) and fuel rod design (rod dimensions, cladding type and dimensions, pellet density and dimensions, design of fuel stack spacers, fuel stack length, fuel rod fill gas pressure and composition, and specified tolerances on fuel rod design parameters). The physical properties of the fuel assembly, fuel pin, and non-fuel regions established by the fuel design process are necessary input into other phases of reload design.

The fuel cycle design establishes the number and enrichment of the reload batch fuel assemblies, specifies the number and identity of residual fuel assemblies, and determines the arrangement (location and orientation) of the fuel assemblies and the locations of control rods and their grouping in such a manner that the

specified criterion on energy production and certain specified criteria on fuel burnup, power distribution and control rod worth requirements are satisfied.

The fuel mechanical performance analysis consists of the evaluations to confirm that the fuel assembly mechanical performance with regard to vibrations, hydraulic loading (fuel assembly lift-off), and seismic and LOCA reponse are acceptable. It also includes the evaluation of the extent of fuel densification and its effect; the evaluation of the fuel rod mechanical performance with regard to clad stress, strain, and clad collapse; and the evaluation of the extent of fuel rod bowing and its effects. In the absence of any changes in the mechanical design of the fuel assembly, no reevaluation of the mechanical performance of the fuel assembly is needed. The extent of fuel densification and its effects depends on the fuel fabrication process, the initial density of the fabricated fuel pellet, and the analytical model utilized for the evaluation; if any of these factors changes for a particular reload, a reanalysis of fuel densification and its effect is required. The fuel rod mechanical performance is influenced by the fuel density, operating RCS pressure, initial fill gas pressure, fuel rod design dimensions, fuel pellet density, and the predicted power history of the fuel rod; and if any of these factors changes for a particular reload, a reevaluation of the fuel mechanical performance is required. Fuel rod bowing is recognized to increase with fuel burnup. Since fuel rod bowing is considered to have the potential to decrease the thermal-hydraulic performance in certain flow channels in the core, an evaluation of the magnitude of rod bowing and its effect on DNBR is required for each reload considering the maximum expected fuel assembly burnup during that cycle. The thermal analysis establishes the maximum permissible power density of a fuel rod to preclude center fuel melting during steady-state and anticipated transient conditions. The thermal analysis needs to be repeated for a particular reload only if there is a change in the fuel design or there is a change in the regulatory requirements.

The maneuvering analysis involves detailed power distribution evaluation in three dimensions by simulating various anticipated and postulated design conditions and is performed to confirm that the fuel cycle design is acceptable from the point of view of safety requirements. The data generated in the maneuvering analysis are used to define the core safety limits pertaining to

the thermal design limits of the fuel and the limiting conditions on control rod position, axial imbalance, and xenon distribution.

The thermal-hydraulic analyses establish the maximum permissible power distribution for various flow conditions, the permissible combination of core pressure and core coolant temperature and the minimum permissible core pressure to ensure that a minimum DNBR of 1.3 or greater can be maintained during anticipated transients. The need to perform the thermal-hydraulic analysis in conjunction with a reload arises when there is a change in the fuel design, a change in the input assumptions of the original analysis, or a change in the regulatory criteria.

The results of the maneuvering analysis in conjunction with the results of thermal and thermal-hydraulic analyses, as appropriate, are used either to confirm that the existing Technical Specifications continue to be valid for the reload cycle or to generate new Technical Specifications limits. The accident analyses are reviewed to ensure that important core safety parameters predicted for the reload cycle are conservative compared to their values used in the existing accident analysis, and where necessary, appropriate accidents are reanalyzed.

A number of physics parameters pertinent to the reload cycle should be calculated to confirm that important core parameters for the reload cycle are conservative compared to their values used in the accident analyses. Other physics parameters are calculated to enable an orderly and safe startup of the cycle, to perform startup testing, and to perform core follow calculations. These parameters include the critical boron concentration as a function of core burnup and for various conditions, ejected and stuck rod worths, control rod group and total group worths, reactivity worths of xenon and samarium, core excess reactivity, moderator and Doppler reactivity coefficients, reactivity worth of boron, effective delayed neutron fractions and decay constants.

The final phase of the reload design is the integration and documentation of the results of all other phases into a report called the reload report. This report includes a description of the reload core, the fuel design, results of nuclear, thermal, thermal-hydraulic, and fuel mechanical analysis, accident analysis review, and proposed Technical Specifications, if any.

Considerable design and engineering effort is needed to incorporate a new fuel design into a reload design; and unless there is sufficient economic or engineering incentive or regulatory requirements, a new fuel design is not usually attempted for a reload cycle. Therefore, a typical reload design involves only a change in the fuel cycle design and as such is an extrapolation from the original core design, with many of the design variables being constrained by the original core design. In the following sections each of the major phases of the reload design process is discussed in more detail, and Figure 1-1 shows a flow chart of the various phases.

Figure 1-i

ELEMENTS OF RELOAD DESIGN

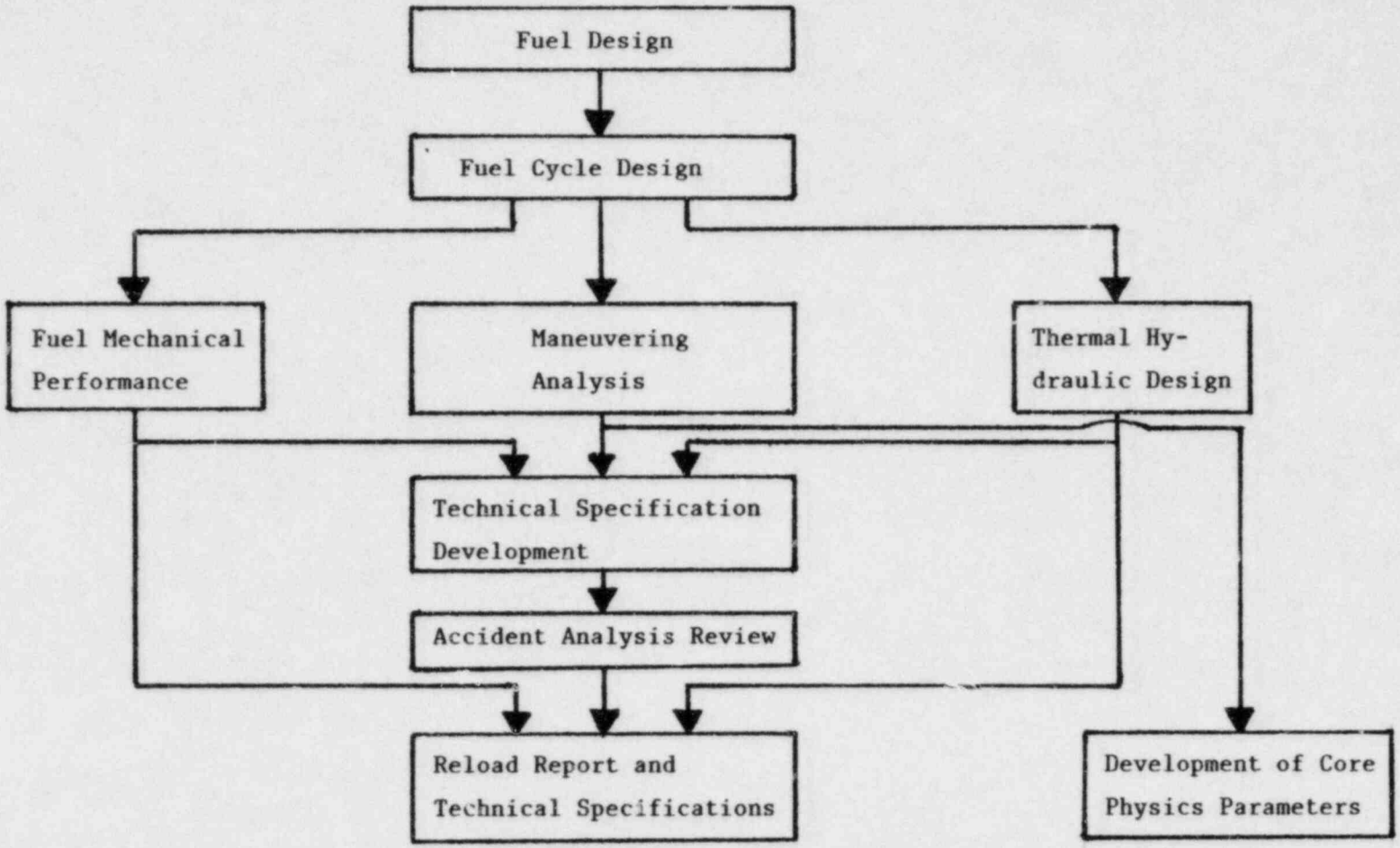

2. FUEL DESIGN

The fuel design consists of the fuel assembly design (material selection, fuel rod lattice and fuel rod number specification, spacer grid design--number of spacer grids, material selection, and fuel assembly end fittings design) and fuel rod design (rod dimensions, cladding type and dimensions, pellet density and dimensions, design of fuel stack spacers, fuel stack length, fuel rod fill gas pressure and composition, and specified tolerances on fuel rod design paramenters).

2.1 Fuel Pellet

The fuel is in the form of UO_2 cylindrical pellets which are sintered, ground, and dried to obtain the desired density, dimensions, and moisture content. The ends of the pellets are chamfered to minimize the effects of differential thermal expansion. The pellet radius is constrained to be less than the clad inner radius and is set to accommodate radial growth resulting from a peak pellet burnup of 55,000 MWD/MTU without the plastic clad strain exceeding 1%. The pellet radius is also determined from economic and nuclear calculations performed to minimize fuel cycle costs.

2.2 Fuel Rod

The fuel rod is composed of a cylindrical metal cladding, top and bottom fuel spacers, and a column of fuel pellets. Zircaloy -4 has proven to be an acceptable clad material because of its nuclear and material properties. The thickness of the clad is determined from heat transfer and clad strain and stress requirements. Fuel spacers hold the column of fuel pellets in position within the fuel rod and are designed to permit axial growth and thermal expansion of the fuel column. The void spaces at the top and bottom of the fuel rod are of sufficient volume to accommodate the fission gas release during the fuel burnup.

The volume is designed to maintain the internal pin pressure less than the primary system pressure at coolant temperatures greater than 425°F for Condition I and II occurences. All fuel rods are pre-pressurized with helium gas to

aid heat transfer, to prevent cladding collapse due to fuel densification effects, and to avoid hydrogen contamination. The fuel rods when loaded are sealed by Zr-4 endcaps welded at each end.

2.3 Fuel Assembly Design

Fuel assembly design consists of specifying the number, location, material and fabrication techniques for fuel rods and non-fuel components such as guide tubes, instrument tubes, spacer grids, end fittings, and spacer sleeves.

Generally the number of fuel rods per assembly and the number of assemblies per plant is determined by trying to limit the linear heat rate of the fuel. The fuel pellet radius and rod pitch are determined by both neutronics and economic calculations aimed at minimizing the fuel cycle costs through optimizing the fuel-to-moderator ratio. The overall assembly pitch is constrained by the size and number of assemblies in the core.

Instrument tubes are typically located in the center of the fuel assembly and guide tubes are symetrically dispersed throughout the assembly, and provide continuous guidance for the control rod assembly. Both the control rod guide tubes and the instrument tubes are made from Zr-4.

The lower end fitting positions the assembly in the lower core plate. The lower ends of the fuel rod rest on the grid of the lower end fitting. The guide tubes penetrate the end fitting and are attached to it.

The upper end fitting positions the upper end of the fuel assembly in the upper core grid plate and provides means for handling and identification of the assembly. An internal hollow post in the center of the end fitting provides a means for supporting control rod assemblies and for retention of either an orifice rod assembly or a burnable poison assembly. Attached to the upper end fitting is a holdown spring. This spring provides a holdown force to oppose hydraulic forces resulting from the primary coolant flow. These end fittings are cast stainless steel.

Spacer grids are constructed from strips of metal which are slotted and fitted together in an "egg crate" fashion. These spacer grids provide support for the fuel rods in the X-Y direction (keeps them at a fixed distance apart) and are located axially along the fuel rods to decrease the amount of fuel assembly and fuel rod bow. Oconee uses spacer grids constructed from Inconel-718 arranged in a 15 x 15 lattice. Each assembly contains eight of these grids. The spacer grids are held in position axially by the frictional grip force exerted on the fuel rods and guide tubes by the spacer grids.

Because of the considerable design, engineering and testing needed to incorporate a new fuel design into a reload core, it is usually not attempted unless there is sufficient economic, engineering, or regulatory justification. If however sufficient justification exists, the new fuel design is typically documented in a generic topical report and the reload report would reference this topical report.

2.4 Core Component Data

The basic physical dimensions and materials of the fuel pellet, fuel rod, fuel assembly, control rods, and orifice rods are used in the fuel cycle design, thermal-hydraulic design, and fuel mechanical performance. Table 2-1 contains a summary of this data for the B&W Mark-B2 assembly and is intended as an example.

TABLE 2-1

OCONEE

SYSTEM AND COMPONENT DATA

MARK B2 CORE COMPONENT DESIGN DATA

Fuel Assembly Designation	Mark B2
Calculated Fuel Assembly Total Weight, lbs.	1550
Material Between Active Core Limits per Assembly, lbs.	
Zircaloy	274
Inconel	9.2
UO_2	1172
Fuel Assembly Cell Flow Areas, in.	39.76
Assembly Pitch, in.	8.587
Spacer Grid Assemblies	
Spacer Grid Material	Inconel 718
Spacer Grid Material Density, lbs/in^3	0.296
Number of Spacer Grids per Assembly	
Total	8
Between Active Core Limits	6
Spacer Grid Weight, lbs.	
Intermediate, each	1.5
End, each	1.6
Total per Fuel Assembly	12.4

Fuel Rods	
Fuel Rod Pitch, in.	0.568
Fuel Rod Array	15 x 15
Number of Fuel Rods per Assembly	208
Fuel Rod Weight, lbs.	
Per Fuel Rod	7.0
Clad	1.15
Fuel Rod Clad OD, in.	0.430
Fuel Rod Clad ID, in.	0.377
Fuel Rod Clad Wall Thickness, in. minimum	0.024
Fuel Rod Length, in.	153.6875
Fuel Rod Clad Material	Zircaloy-4
Fuel Rod Clad Material Density, lbs/in.^{3}	0.237

Fuel Column Starts, From Bottom of Fuel Rods, in.	4-1/8
Fuel Pellet Diameter, in.	0.370
Fuel Pellet Length, in.	0.700
Pellet Density, g/cc (93.5% of Theoretical)	10.248
Pellet Dish Depth, in.	0.018
Pellet Dish Factor	0.983014
Diametrical Gap, in.	0.007
Fuel Column Length, in.	144
Unit Fuel Cell Flow Area, in.	0.1774
Material	UO_2
U per Fuel Rod, kg	2.2530
U per Assembly, kg	468.6240
UO_2 per Fuel Rod, kg	2.5559
UO_2 per Fuel Assembly, kg	531.6272
U/UO_2 Ratio Used for Calculation	0.8815
Metal/Water Ratio	0.828227

Control Rod Guide Tubes

Control Rod Guide Tubes Attachment to Spacer Grids	None
No. of Control Rod Guide Tubes per Assembly	16
Guide Tube Material	Zircaloy-4
Guide Tube Material Density, lbs/in.^{3}	0.237
Weight of control rod guide tubes, lbs.	
Per Control Rod Guide Tube	1.06
Total per Assembly	16.9
Between Active Core Limits	14.1
Guide Tube OD, in.	0.530
Guide Tube ID, in.	0.498
Guide Tube Wall Thickness, in.	0.016
Guide Tube Length, in.	155.625

Instrumentation Tube

Number of Instrumentation Tubes per Assembly	1
Instrumentation Tube Attachment to Spacer Grids	None
Instrumentation Tube Material	Zircaloy-4
Instrumentation Tube Material Density, lbs/ft.^{3}	0.237
Instrumentation Tube Weight, lbs.	
Per Tube	1.40
Between Active Core Limits	1.30
Instrumentation Tube OD, in.	0.493
Instrumentation Tube ID, in.	0.441
Instrumentation Tube Wall Thickness, in.	0.026
Instrumentation Tube Cell Flow Area, in.^{2}	0.0867
Length of Instrumentation Tube, in.	154.9375

Spacer Sleeves

Spacer Sleeve, OD, in.	0.550
Spacer Sleeve, ID, in.	0.498
Spacer Sleeve Material	Zircaloy-4
Spacer Sleeve Weight, lbs.	
Per Assembly	1.39

Spacer Sleeve Length, in.	
6 Sleeves at	19.593
1 Sleeve at	18.781
Length of 7 Spacer Sleeves, in.	136.339
Control Rod	
Cladding OD, in.	0.440
Cladding ID, in.	0.398
Cladding Wall Thickness	0.021
Cladding Length, in.	149.500
Cladding Material	SS304
Absorber OD, in.	0.392
Absorber Length, in.	134.0
Absorber Material	Ag-In-Cd
Axial Power Shaping Rod	
Cladding OD, in.	0.440
Cladding ID, in.	0.398
Cladding Wall Thickness, in.	0.021
Cladding Length, in.	38.500
Cladding Material	SS304
Absorber OD, in.	0.375
Absorber Length, in.	36
Absorber Material	Ag-In-Cd
Follower Tube OD, in.	0.440
Follower Tube ID, in.	0.376
Follower Tube Wall Thickness, in.	0.032
Follower Tube Length, in.	113.750
Follower Tube Material	Zircaloy-4

Burnable Poison Rod	
Cladding OD, in.	0.430
Cladding ID, in.	0.360
Cladding Wall Thickness, in.	0.035
Cladding Length, in.	157.250
Cladding Material	Zircaloy-4
Burnable Poison Material OD, in.	0.340
Burnable Poison Lengh, in.	126.000
Burnable Poison Material	Al_2O_3-B4C
Orifice Rod	
Orifice Rod OD, in.	0.480
Orifice Rod Length, in.	10.000
Orifice Rod Length, in. (0.489 dia. section)	7.000
Orifice Rod Material	SS304
Orifice Rod Spring OD, in.	0.381
Orifice Rod Spring Wire Dia., in.	0.063
Orifice Rod Spring Material	Inconel X-750

3. FUEL CYCLE DESIGN

3.1 Preliminary Fuel Cycle Design

The purpose of the preliminary fuel cycle design (PFCD) is to determine the number and enrichment of the fresh and possibly burned assemblies to be inserted during the next refueling. A preliminary fuel shuffling scheme is developed and check calculations on certain key parameters are performed.

The input required for the PFCD consists of general ground rules and design bases developed from cycle energy, contract, and operating requirements. The output of the PFCD is the number and enrichment of the feed assemblies.

The majority of this section will discuss the calculations necessary to determine the above information.

3.1.1 Overview of Nuclear Calculational System

The nuclear calculational system enables the nuclear designer to numerically model and simulate the nuclear reactor core. The current system in use at Duke Power is outlined in Figure 3-1. A brief description of each code is included as Apperdix A to this report.

3.1.1.1 Cross Section Generation

In order to model the neutronics of a reload core, it is necessary to generate nuclear cross sections for subsequent use in a diffusion theory code. The cross section generator sometimes referred to as a lattice code is EPRI-CELL. Basic input consists of the geometry and materials constituting the fuel assembly, specific power, soluble boron concentration, temperature for the pellet, clad, and moderator, effective resonance temperature, fuel enrichment, number of depletion steps and the length of each step, etc.

The output of the EPRI-CELL run is a set of nuclear cross sections which characterize that particular assembly. These are then formatted into table set structure through the use of an auxiliary code called NUPUNCHER for input to PDQØ7.

This procedure is repeated for the different fuel assemblies comprising the reactor core as well as for a spread of enrichments covering the typical range of reload enrichments.

Non-fuel cross sections with the exception of burnable poison assemblies and control rods are also generated using EPRI-CELL. Cross sections for burnable poison assemblies and control rods for use in diffusion theory calculations are generated by matching reaction rates between the diffusion theory code PDQØ7 and CPM (a collision probability code).

3.1.1.2 Diffusion Theory Calculations

Once the cross sections have been generated they are input to PDQØ7 which solves the diffusion depletion equations in one, two, or three dimensions. Two types of PDQØ7 calculations are routinely run; the color set calculation and the quarter core calculation. The color set calculation is a single assembly or four quarter assemblies pin mesh x-y geometry PDQØ7. This is used to calculate assembly parameters necessary for input to EPRI-NODE. The quarter core PDQØ7 is a pin mesh x-y geometry calculation which yields radial power distributions, local pin peaking, reactivity versus burnup, and other nuclear parameters of interest.

3.1.1.3 Nodal Calculations

The output from the color set PDQØ7 calculations discussed in Section 3.1.1.2 is processed by the auxiliary codes EPRI-FIT, and SUPERLINK and input to the nodal code EPRI-NODE. EPRI-NODE is a three dimensional nodal code that is currently in use to provide three dimensional information such as three dimensional power distributions and integral and differential rod worth, etc.

3.1.2 Calculations and Results of PFCD

Once the calculational models are prepared for the cycle of interest (steps discussed in 3.1.1 are complete), the nuclear designer chooses a feed enrichment, number of assemblies, and preliminary loading pattern for the reload core. Calculations using either or both EPRI-NODE and PDQØ7 are performed to verify cycle lifetime and power peaking. The process is iterated until the number and enrichment of feed assemblies as well as a preliminary shuffle scheme has been determined which yield the desired cycle lifetime and a reasonable power distribution.

The preliminary number and enrichment of the feed assemblies must typically be determined eighteen months prior to reactor shutdown for refueling to assure that an adequate quantity of separative work is available. Changes to these preliminary estimates are normally possible up to twelve months prior to reactor shutdown. Therefore, it is necessary that the results of the PFCD be complete at that time.

3.2 Final Fuel Cycle Design

Having determined the number and enrichment of the fuel assemblies during the PFCD, the final fuel cycle design (FFCD) concentrates on optimizing the placement of fresh and burned assemblies, control rod groupings, and burnable poison assemblies (if any) to result in an acceptable fuel cycle design. It must meet the following design criteria with appropriate reductions to account for calculational uncertainties:

1. Radial Pin Peak < 1.714 (inner flow zone)
   < 1.629 (outer flow zone)

2. Moderator Temperature Coefficient ≤ 0.0 at >95% hot full power.

3. Maximum pellet burnup $\leq$ 55,000 MWD/MTU.

4. Shutdown Margin at HZP ≥ 1.0 % $\Delta\rho$.

5. Ejected rod worth at HZP $\leq$ 1.0% $\Delta\rho$.

6. Ejected rod worth at HFP $\leq$ 0.65% $\Delta\rho$.

During the FFCD, nuclear calculations are performed to generate these parameters for input to fuel mechanical performance, thermal and thermal-hydraulic performance, maneuvering analysis, and accidents and transients analyzed during the safety analysis.

3.2.1 Fuel Shuffle Optimization and Cycle Depletion

Beginning of cycle (BOC) power distribution calculations are performed using combinations of EPRI-SHUFFLE and PDQØ7. Initial runs start with the fuel shuffle scheme developed in the PFCD and modify the shuffle scheme in an attempt to minimize the power peaking. This is accomplished by a trial and error type search until an acceptable BOC power distribution results. The cycle is then depleted using point depletion in steps corresponding to 0, 4, 12, 25, 50, 100, 150...EFPD to verify that power peaking versus burnup remains acceptable. The shuffling variations include re-arranging the location of the burned or fresh fuel assemblies, location of control rods (groups 5, 6, 7) and rotation of the spent fuel assemblies. These calculations are typically performed assuming quarter core symmetry. 1

The shuffle pattern determined by optimizing power distribution may later need to be modified based upon results obtained in the remaining nuclear calculations.

3.2.2 Rod Worth Calculations

Control rods serve several functions in the Oconee reactor. The primary function is to provide adequate shutdown capability during normal and accident conditions. They are also used in the "rods in" mode to maintain criticality during power maneuvers and to compensate for reactivity loss due to fuel

depletion. Since the presence of control rods influences both power distributions and criticality, it is necessary in many calculations to evaluate not only the reactivity effect but also the perturbation that a given rod configuration has on the power distribution.

Oconee may be designed and operated in either a "rods out" (feed and bleed) or a "rods in" mode. A typical "rods in" design allows for the first regulating bank (7) to be almost fully inserted into the reactor core during HFP operation. This regulating bank is typically withdrawn two months prior to the end of the fuel cycle to provide the additional reactivity to operate to EOC. Shutdown margin for a "rods in" design is typically less before the regulating bank is removed than at EOC and is normally calculated for that point in the cycle instead of EOC.

Most calculations of control rod worth are used in the safety analysis of the reload core. The calculations discussed in subsequent sections include the following:

1. Choice of Control Rod Groupings and Worths
2. Shutdown Margin
3. Ejected Rod Worth
4. Dropped Rod Worth

3.2.2.1 Control Rod Groupings and Worths

Control rod locations in Oconee are fixed, however, the rods in a particular group may vary from cycle to cycle. The control and rod groupings are determined by nuclear calculations to evaluate the effects that a particular rod grouping has on power distribution, group worth, and ejected rod worth. The worth of each regulating bank (5, 6, 7) is calculated in quarter core geometry using either PDQØ7 or EPRI-NODE at BOC, EOC, and before and after control rod interchange at HFP and HZP. The total rod worth (all rods in) is calculated at BOC, EOC, and any limiting burnup at HZP only for use in the shutdown margin calculation.

The locations chosen during the FFCD are confirmed during the maneuvering analysis.

3.2.2.2 Shutdown Margin

Searches for the highest worth stuck rod are performed at BOC, EOC, or any limiting burnup for HZP conditions using full core EPRI-NODE and/or PDQØ7 calculations. Table 3-1 summarizes the results of a shutdown margin calculation. The total rod worth described in section 3.2.2.1 is shown as Item 1. This value is reduced by an estimate of the worth lost by the control rod poison due to burnup (Item 2). Item 3 is the worth of the highest stuck rod. The total worth reduced by the control rod burnup penalty and the stuck rod worth is shown as the net worth (Item 4). A calculational uncertainty of 10% is subtracted off in step 5 and step 6 shows the available rod worth.

The required rod worth is calculated next in steps 7-10. The power deficit obtained by running an EPRI-NODE or PDQØ7 case at HFP and a second case at HZP and subtracting the reactivities is shown as item 7. The maximum allowable inserted rod worth, item 8, is obtained from the allowable rod insertion and the integral rod worth curve for that insertion (generated by EPRI-NODE). This accounts for any rod insertion allowed at HFP. An axial flux redistribution occurs when the power level is reduced from HFP to HZP. This redistribution causes an increase in reactivity.

If Item 7 is calculated using a 3-D code such as EPRI-NODE no additional penalty is required here. However, if Item 7 was calculated using 2-D PDQØ7 an additional reactivity penalty is assessed as Item 9. The sum of these required worths (Item 10) is the total required worth.

The shutdown margin is shown as Item 11 and is defined as the total available worth minus the total required worth. For Oconee this is required to be $\geq$ 1.0% $\Delta\rho$.

3.2.2.3 Ejected Rod Worth

The maximum allowable ejected rod worth is limited by the Technical Specifications. For Oconee these limits are shown in Table 3-2. A calculated limit for setting rod withdrawal positions has been established by applying a 15% uncertainty to the Technical Specification limits.

To verify that the ejected rod worths are within this calculational limit, ejected rod worth calculations are performed at BOC and EOC at both HFP and HZP.

The calculation of ejected rod worths is accomplished using full core two dimensional pin mesh PDQØ7 or EPRI-NODE calculations. The HZP ejected rod worth calculations are performed with control groups 5 through 7 fully inserted in the core and with group 8 centered.

Single rods in groups 5, 6, and 7 are removed in subsequent cases and the worth of the ejected rod is calculated by subtracting the reactivities of the cases before and after the rod was removed. The fuel and moderator temperature is held constant and equal to the HZP moderator temperature for these calculations. The highest worth calculated by the above procedure is the worst ejected rod at HZP. If the ejected rod worth exceeds the calculational limit, rod position limits are imposed or a new control rod grouping is developed.

The HFP ejected rod worths are performed in a similar manner to the HZP calculations with the exceptions that for a "rods out" design only groups 7 and 8 are inserted into the core and that the fuel temperature and moderator temperatures correspond to those of HFP conditions. The HFP ejected rod worths are performed without thermal feedback to be conservative. If the ejected rod worth exceeds the calculational limit, rod position limits are imposed or a new control rod grouping is developed. 1

3.2.2.4 Dropped Rod

The analysis of the rod drop worth is required to determine the reactivity insertion resulting from the rod drop. Full core calculations using EPRI-NODE are performed with thermal-hydraulic feedback.

Search cases are run dropping full length control rods until the highest worth rod has been identified. This value of dropped rod worth is used as input to the accident analysis evaluation.

3.2.3 Power Distribution Calculations

For Oconee emphasis in the FFCD is on radial power distributions both on an assembly and local rod basis. Thermal and thermal-hydraulic analyses have been performed on the Oconee reactors which indicate that radial pin peaks shown in Table 3-3 will result in acceptable DNB and Center Fuel Melt (CFM) margins. These margins are calculated and confirmed during the maneuvering analyses.

Power distributions are calculated both with the 2-D PDQØ7 model and the 3-D EPRI-NODE model. The local radial peaking factor, maximum pin to assembly power ratio, calculated by PDQØ7 is multiplied by the three dimensional peak calculated by EPRI-NODE to produce maximum three dimensional power peaks in a fuel rod.

3.2.4 Fuel Burnup Calculations

One of the current design criterion is that maximum pellet burnup is $\leq$ 55,000 MWD/MTU. This criterion is confirmed during the final fuel cycle design. Depletion calculations from 2-D quarter core pin mesh PDQØ7 models yield core and assembly average burnup as well as single fuel rod burnups. From these values a maximum ratio of single rod to assembly average burnup can be calculated for each assembly. This data is then used in conjunction with 3-D EPRI-NODE depletion calculations (where the axial burnup distribution is calculated) to arrive at a local burnup limit which can be compared to the design limit of 55,000 MWD/MTU.

Generally, the assembly average burnups are in the 30,000 to 33,000 MWD/MTU range and sufficient margin to the 55,000 MWD/MTU limit exists to make the detailed calculation described above unnecessary.

3.2.5 Reactivity Coefficients and Deficits

Reactivity coefficients define the reactivity insertion for small changes in reactor parameters such as moderator temperature, fuel temperature, and power level. These parameters are input to safety analysis and used in modeling the reactor response during accidents and transients. Whereas reactivity coefficients represent reactivity effects over small changes in reactor parameters, reactivity deficits usually apply to reactivity inserted from larger changes typical of HFP to HZP. An example of a reactivity deficit is the power deficit from HFP to HZP used in the shutdown margin calculation. A different way of looking at the terms is that the coefficient when integrated over a given range yields the deficit, or the coefficient is the partial derivative of reactivity with respect to one specific parameter.

Coefficients of reactivity are calculated using PDQØ7 or EPRI-NODE. First a nominal case is established at some reference conditions. Then one parameter of interest is varied up and/or down by a fixed amount in another calculation and the resulting change in core reactivity divided by the parameter change is the reactivity coefficient.

3.2.5.1 Doppler Coefficient

The Doppler Coefficient or Fuel Temperature Coefficient (FTC) is the change in core reactivity produced by a small change in fuel temperature. The major component of the Doppler coefficient arises from the behavior of the Uranium-238 and Plutonium-240 resonance absorption cross sections. As the fuel temperature increases, the resonances broaden increasing the chance that a neutron will be absorbed and thus decreasing the core reactivity.

If Case 1 represents the reference case with an effective fuel temperature T_1 (and K^1 effective) and Case 2 represents a second case where the fuel temperature has been increased or decreased by approximately 50°F and is T_2, (and K^2 effective) the Doppler coefficient is mathematically calculated from the following equation:

$$FTC = \frac{\dfrac{K^1_{eff} - K^2_{eff}}{K^1_{eff} \times K^2_{eff}}}{T_1 - T_2} = \Delta\rho/^{\circ}F$$

In the final fuel cycle design both HFP and HZP Doppler coefficients are calculated.

3.2.5.2 Moderator Temperature Coefficient

The Moderator Temperature Coefficient (MTC) is the change in reactivity produced by a small change in moderator temperature. In Oconee the average core moderator temperature is increased as power is escalated from 0 to 15% HFP. At and above 15% HFP the average moderator temperature is held constant at 580°F. However, for accident and transient analyses it is necessary to know the moderator temperature coefficient at HFP and also at HZP.

These analyses can be performed with either EPRI-NODE and/or PDQØ7 by effecting a change in the core average moderator temperature. Two cases are run with the moderator temperature at +5°F and -5°F around the HZP (±2.5°F at HFP) average temperature. If these cases and the resulting K effectives are identified as Case 1 ($TMOD_1$, K^1_{eff}) and Case 2 ($TMOD_2$, K^2_{eff}), the moderator temperature coefficient is calculated from the following equation: | 1

$$MTC = \frac{\dfrac{K^1_{eff} - K^2_{eff}}{K^1_{eff} \times K^2_{eff}}}{(TMOD_1 - TMOD_2)} = \Delta\rho/°F$$

3.2.5.3 Temperature Coefficient

The fractional change in reactivity due to a small change in core temperatures is defined as the core temperature coefficient of reactivity. This is equal to the sum of the moderator and Doppler temperature coefficients and may be explicitly calculated at HZP for isothermal conditions (TFUEL=TMOD) by varying both the fuel and moderator temperatures approximately ±5°F about the average moderator temperature at HZP. Similarly the temperature coefficient at HFP may be explicitly calculated by varying the moderator and fuel temperatures by ±2.5°F. This calculation may be performed with PDQØ7 and/or EPRI-NODE. | 1

3.2.5.4 Power Coefficient and Power Deficit

The power coefficient of reactivity is the core reactivity change resulting from an incremental change in core power level. The power deficit is usually the total reactivity change associated with a power level change from HZP to HFP.

The power coefficient is defined by the following equation:

$$\alpha p = \frac{\frac{K^1_{eff} - K^2_{eff}}{K^1_{eff} \times K^2_{eff}}}{P_1 - P_2}$$

where: K^1_{eff} is K effective for the core at power P_1 (%)
K^2_{eff} is K effective for the core at power P_2 (%).

Neglecting second order effects this equation is equivalent to the following:

$$\alpha p = MTC \frac{\Delta TMOD}{\Delta P} + FTC \frac{\Delta TFUEL}{\Delta P}$$

where: MTC is the moderator temperature coefficient and FTC is the fuel temperature coefficient (Doppler coefficient).

In Oconee the core average moderator temperature is constant at approximately 580°F above 15% HFP. Therefore, for power levels above 15% HFP the power coefficient can be reduced to just the fuel temperature contribution or

$$\alpha p = FTC \frac{\Delta TFUEL}{\Delta P}$$

Since the power coefficient should include flux redistribution effects resulting from axial variations in burnup and isotopics as well as non-uniform fuel temperature distributions it should be performed using a 3-D simulator with thermal hydraulic feedback. If the calculation is performed using a 2-D model then it should be corrected for the 3-D effects.

A typical power coefficient calculation for HFP would proceed in the following manner. The HFP case is run using EPRI-NODE and the core Keffective is calculated ($K^1_{effective}$). Then a second EPRI-NODE case is run with the core power level reduced 5% while holding everything else constant. The Keffective from this case, $K^2_{effective}$, is used along with the results from the reference case to calculate the power coefficient:

$$\alpha p = \frac{\dfrac{K^1_{eff} - K^2_{eff}}{K^1_{eff} \times K^2_{eff}}}{P_1 - P_2} = \frac{\Delta\rho}{\%\ \text{POWER}}$$

The power deficit is calculated for use in the shutdown margin calculation (see Section 3.2.2.2) and is the reactivity change from HZP to HFP. This calculation should be performed in three dimensions to satisfactorily model the axial flux redistribution, however, a two dimensional calculation may be performed and corrected for this flux redistribution phenomenon. Two EPRI-NODE or PDQ07 runs are made to calculate the power deficit. The first is made at 100% HFP and the second at HZP. These calculations are usually performed at least two times during the cycle burnup.

The HFP and the HZP case should have the equilibrium xenon concentration corresponding to HFP. The power deficit is calculated from the following equation:

$$\text{Power Deficit}_{\text{HZP - HFP}} = \frac{K^1_{eff} - K^2_{eff}}{K^1_{eff} \times K^2_{eff}} \times 100 = \%\Delta\rho$$

where: $K^1_{effective}$ is core Keffective at HZP and $K^2_{effective}$ is core Keffective at HFP.

3.2.5.5 Miscellaneous Coefficients

For reload design, certain coefficients of reactivity are not routinely calculated. These include moderator density coefficient, moderator pressure coefficient, and moderator void coefficient.

3.2.6 Boron Related Parameters

Critical boron concentrations at BOC and EOC for HFP and HZP and various rod positions are calculated using PDQØ7 and/or EPRI-NODE. Table 3-4 lists conditions that critical boron concentrations and boron worths are calculated. In addition to these, an all rods out (ARO) critical boron letdown curve, and a critical boron letdown curve at nominal rod index are generated for HFP equilibrium conditions.

3.2.7 Xenon Worth

The HFP equilibrium xenon worth is calculated at BOC (4 EFPD) and at EOC. These values are compared to previous cycle values in the reload report.

Calculations using either PDQØ7 or EPRI-NODE are performed for HFP equilibrium xenon conditions. If PDQØ7 is being used, a second no xenon case is run by either zeroing out the number density for xenon or zeroing out the xenon cross section. If EPRI-NODE is being used the power level on the xenon card can be set to zero and the time in hours set to 40.0 to obtain a no xenon concentration.

The difference in reactivities between the equilibrium and no xenon cases is the xenon worth.

3.2.8 Kinetics Parameters

The kinetics behavior of the nuclear reactor is often described in terms of solutions to the Inhour equation for six effective groups of delayed neutrons. Transient and accident analyses often involve kinetic modeling of the reactor core. The rate of change in power from a given reactivity insertion can be calculated by solving the kinetics equations if the six group effective delayed neutron fractions, the six group precursor decay constants, and the prompt neutron lifetime are known.

The computer codes used to calculate these parameters are PDQØ7 and DELAY. PDQØ7 is used to obtain spatially averaged isotope fission fractions as a function of burnup, and DELAY calculates kinetics parameters and then uses these parameters to solve the Inhour equation and thereby relate the stable reactor period to the

reactivity insertion. This information is also needed for startup physics testing. The sum of the six group β^i effective, β effective, for the new reload cycle is compared to that of the previous cycle in the reload report.

Table 3-1

Shutdown Margin Calculation

	BOC, % Δρ	EOC, % Δρ
Available Rod Worth		
1. Total rod worth, HZP	8.91	8.79
2. Worth reduction due to burnup of poison material	-.36	- .42
3. Maximum stuck rod, HZP	-2.17	-2.01
4. Net Worth	6.38	6.36
5. Less 10% uncertainty	-0.64	-0.64
6. Total available worth	5.74	5.72
Required Rod Worth		
7. Power deficit, HFP to HZP	1.31	2.12
8. Max allowable inserted rod worth	0.40	0.60
9. Flux redistribution	0.59	1.20
10. Total required worth	2.30	3.92
11. Shutdown Margin (total avail. worth minus total required worth)	3.44	1.80

Note: Required shutdown margin is 1.00% Δρ.

Table 3-2

Ejected Rod Worths

Condition	Technical Specification Limit	Calculational Limit
HZP (Banks 5-8 in.)	1.00% $\Delta\rho$	0.85% $\Delta\rho$
HFP (Banks 7-8 in.)	0.65% $\Delta\rho$	0.55% $\Delta\rho$

Table 3-3

Radial Pin Peak

FLOW ZONE	Maximum Allowable Radial Pin Peak	Calculational Limit*
Inner	1.714	1.587
Outer	1.629	1.508

*An 8% reduction has been applied to the radial peaks to account for calculational uncertainty and to provide a margin for the 3-D calculations performed during the maneuvering analysis.

Table 3-4

Boron Parameters

Critical Boron - BOC, ppm (no Xenon)

HZP, group 8 inserted

HZP, group 7 and 8 inserted

HFP, group 7 and 8 inserted

Critical Boron - EOC, ppm (equilibrium Xenon)

HZP, group 8 37.5% WD

HFP, group 8 37.5% WD

Boron Worth - HFP, ppm/%$\Delta\rho$

BOC (xx ppm)

EOC (17 ppm)

Figure 3-1

NUCLEAR FLOW CHART
FOR EPRI-aRMP

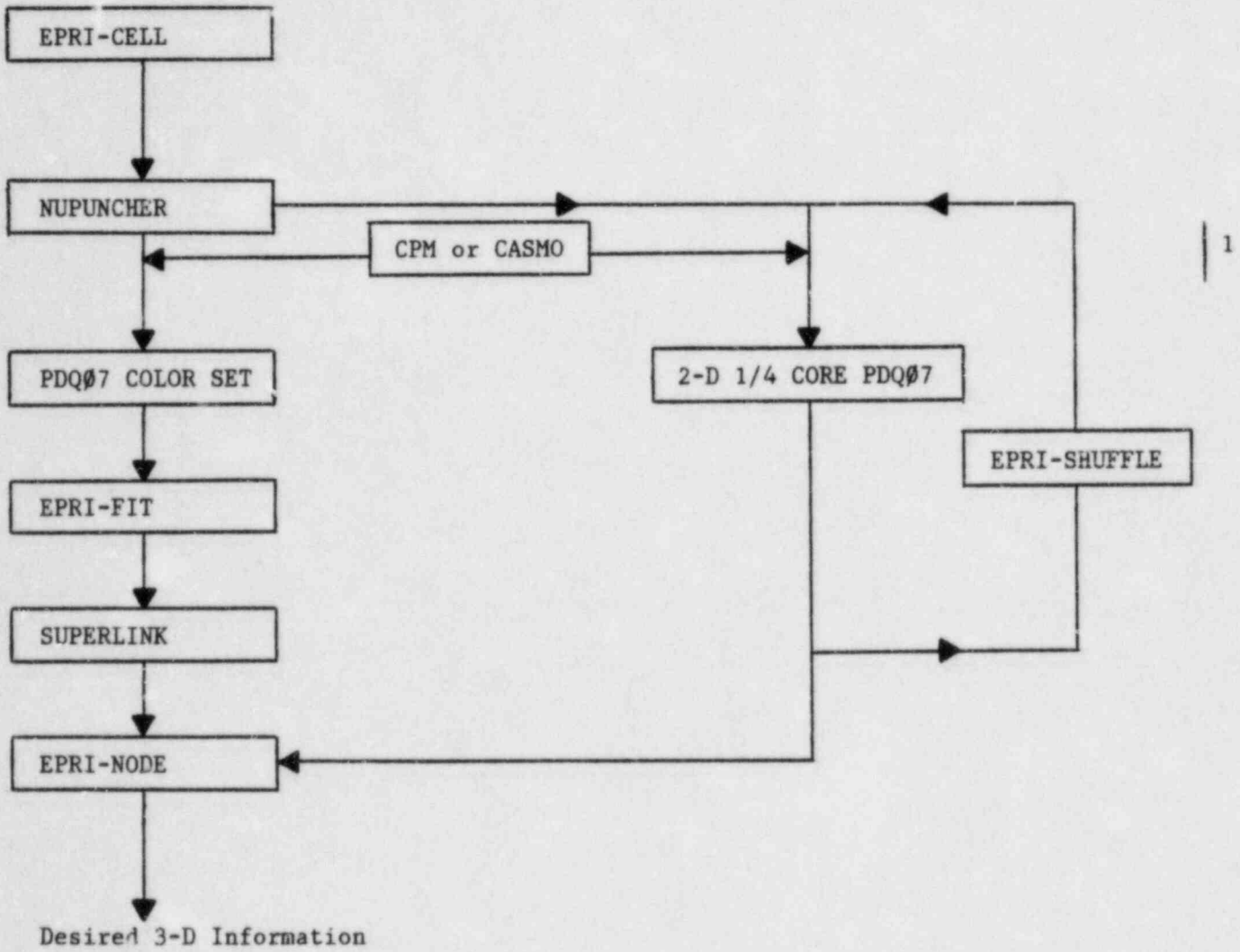

4. FUEL MECHANICAL AND THERMAL PERFORMANCE

4.1 Introduction

Each fuel cycle design requires that thorough fuel mechanical and thermal assessments be performed. A reload design utilizes fuel designs that are bound by previous fuel assembly design analyses. Occasionally, however, minor differences in the design will occur (such as a change from 94% TD fuel to 95% TD fuel). These changes must then be assessed in regard to the following:

- Cladding creep collapse,
- Cladding strain,
- Cladding stress,
- Fuel pin temperature, and
- Fuel pin pressure

Design analyses that envelope the operation of all current fuel designs have been completed by the fuel vendor, and reanalysis is normally not required for a new fuel cycle design. Rather, a specific fuel cycle design is compared against the enveloping design analyses. The assessment must compare cladding and pellet designs against the pellet and cladding geometries and densities, etc., that have been considered in the enveloping design analyses. Further, the individual radial power histories during the fuel cycle (current and previous batches) must be compared against the generic radial power envelopes that have been used in the design analyses. In most cases, the design analyses will envelope the fuel cycle design being considered and no reanalysis is required. However, in some cases, either the radial power history or fuel geometry may lie outside of the enveloping design analyses, thus requiring partial or full reanalysis. The following subsections describe the types of comparisons that must be made to justify a fuel cycle design without reanalysis and provides some detail concerning the types of analyses that must be performed if required by either the fuel cycle design or by changes in the fuel design itself.

Table 4-1 presents a summary of all types of fuel thermal and mechanical performance assessment criteria that are used to determine whether a fuel cycle design, the cladding, and the pellets are enveloped by existing analyses. As shown in Table 4-1, several of these analyses require either a comparison against a fuel pin power versus burnup envelope or a comparison against an assembly radial power versus burnup envelope. Examples of these power history envelopes are presented in Figures 4-1 and 4-2. These envelopes change, as reanalysis is occasionally required, resulting in an expanded power history envelope. Figure 4-3 presents a flow chart for the fuel pin pressure and linear heat rate to melt analyses. Figure 4-4 is a mechanical analysis flow diagram.

4.2 Cladding Collapse

Cladding creepdown under the influence of external (system) pressure is a phenomenon that must be evaluated during each reload fuel cycle design to ensure that the most limiting fuel rod does not exceed the cladding collapse exposure limit. Cladding creep is a function of neutron flux, cladding temperature, applied stress, cladding thickness, and initial ovality. Acceptability of a fuel cycle design is demonstrated by comparing the power histories of all the fuel assemblies against the generic assembly power history used in existing design analyses, similar to Figure 4-2. The generic power history must be completely enveloping to avoid reanalysis. Duke Power Company uses its own PDQ edit code to automatically perform this comparison for all fuel assemblies at each depletion step. Changes in pellet or cladding design are also assessed in a similar manner: direct comparison with the fuel rod geometries of Table 4-1 and reanalysis, if necessary. Four separate fuel designs have been analyzed to form the generic cladding creep collapse analysis.

The CROV[1] computer code calculates ovality changes in the fuel rod cladding due to thermal and irradiation creep and is used to perform the fuel rod creep collapse analysis when required. CROV predicts

the conditions necessary for collapse and the resultant time to collapse. Conservative inputs to the CROV cladding collapse analysis include the use of minimum cladding wall thickness and maximum initial ovality (conservatively assumed to be uniformly oval), all as allowed by manufacturing specifications. Other conservatisms included are minimum prepressurization pressure and zero fission gas release. Internal pin pressure and cladding temperatures, input to CROV, are calculated by TACO[16] (or TACO2[6] when approved) using a radial power history similar to that of Figure 4-2, a generic pin to assembly local peak, and a standard axial flux shape. | Rev. 4

The conservative fuel rod geometry and conservative power history are used to predict the number of EFPH required for complete cladding collapse. To demonstrate acceptability, the maximum expected residence time of the cycle is compared against the EFPH required for complete collapse.

4.3 Cladding Strain Analysis

The limit on cladding strain is that uniform strain of the cladding should not exceed 1.0%.

A generic strain analysis has been completed by the fuel vendor using TACO (or TACO2 when approved) to ensure that the strain criterion above is not exceeded. To determine whether the fuel and fuel cycle designs are enveloped by existing analyses, the criteria of Table 4-1 are reviewed. | Rev. 4

Should reanalysis be required, TACO (or TACO2 when approved) will be used to determine the fuel rod dimensional changes that occur between the two power levels considered by the conservative design power ramp used in the strain analysis. Then, the maximum tensile (elastic and plastic) strain, which occurs at the cladding I.D., is determined from the following equation: | Rev. 4

$$\text{Strain} = \frac{(\text{Pellet O.D.})_{\text{peak}} - (\text{Pellet O.D.})_o \times 100}{(\text{Pellet O.D.})_o} \leq 1\%$$

where (Pellet O.D.) peak = the maximum pellet O.D. at the local power peak, and

$(\text{Pellet O.D.})_o$ = pellet O.D. prior to and after a local power ramp.

Pellet O.D. dimensions are used to calculate cladding strain because the strain itself is caused by pellet thermal expansion.

The strain analysis is completed in two parts:

- Part 1 employs TACO (or TACO2 when approved) to determine when pellet contact occurs. A conservative fuel rod geometry is used in conjunction with a ≤ 1.5 axial flux shape, and the core average linear heat rate at 100% power to characterize gap closure. If contact occurs prior to 30,000 MWD/MTU, then Part 2 will use a ramp from 2 KW/FT to a final linear heat rate that is consistent with centerline fuel melt. Whereas, if contact occurs after 30,000 MWD/MTU, then the ramp's peak linear power is reduced to a lower value that is consistent with maximum local powers that could occur at burnups greater than 30,000 MWD/MTU. | Rev.

- Part 2 of the strain analysis is the power ramp calculation, also performed on TACO (or TACO2 when approved), which calculates the change in fuel pellet O.D. that occurs from the change in power level induced by the power ramp. The change in pellet O.D. is then used to perform the hand calculation of cladding strain using the equation above. The cladding and pellet are assumed to be in hard contact at the initiation of this ramp. | Rev.

Thus, there are two major conditions in this scenario that make it conservative. The first is the extreme power change that is used to simulate the worst case peaking. The second is that the pellet is assumed to be in hard contact at inititation of the ramp. This is a conservative assumption since the power ramp is

initiated from 2 KW/FT, and pellet/cladding contact is not expected to occur at this low linear heat rate.

4.4 Cladding Stress Analysis

The cladding stress analysis for a new fuel cycle design is similarly bounded by a conservative design analysis that uses Section III of the ASME Boiler and Pressure Vessel Code as a guide in classifying the stresses into various categories, assigning appropriate limits to these categories, and combining these stresses to determine stress intensity. Each new fuel cycle design is assessed against the criteria stated in Table 4-1 to determine if reanalysis is required. The stress analysis is very conservative, and reanalysis should not be required for standard Mark B reloads. However, an assessment is made for each reload design using the criteria of Table 4-1.

The fuel rod stress analysis considers those stresses that are not relaxed by small material deformation, and this anaysis complies with the following design critera:

- All fuel cladding stresses (primary and secondary) shall not exceed minimum unirradiated yield strength for condition I and II occurrences.

- The stress intensity value of the primary membrane stresses in the fuel rod cladding, which are not relieved by small material deformation of the cladding, shall not exceed 2/3 of the minimum unirradiated yield strength.

The above criteria keep the primary loads well below material allowable.

In performing the stress analysis, all the loads were selected to represent the worst case loads and were then combined. This repre-

sents a conservative approach since they cannot occur simultaneously. This insures that the worst case conditions for condition I and II events are satisfied. In addition, these input parameters were chosen so that they conservatively envelope all Mk-B design conditions.

The primary membrane stresses result from the compressive pressure loading. Stresses resulting from creep ovalization are addressed in the creep collapse analysis.

Since the internal fuel rod pressure cannot exceed system pressure for condition I and II occurrences (at coolant temperatures greater than 425°F), the need to address tensile stresses at hot zero power (HZP) conditions and higher is eliminated. The tensile stresses were addressed at cold conditions. The minimum internal fuel rod pressure at HZP conditions is combined with the maximum design system pressure during a transient to simulate the maximum pressure differential across the cladding. The tensile stress analyzed occurs at cold (room temperature) conditions at BOL. This is the worst case since the grid loads will be maximum at that point.

The worst case compressive pressure loads were combined with the other worst case loads. These are described below:

- The maximum grid loads will occur at BOL. During operation, the contact force will relax with time due to fuel rod creepdown and ovalization as well as grid spring relaxation.

- The maximum radial thermal stress will occur at the maximum rated power (power level corresponding to centerline fuel melt). This stress cannot physically occur at the same time the maximum pressure loading occurs, but is assumed to do so for conservatism. (Maximum cladding temperature gradient is combined with minimum pin pressure.)

- The ovality bending stresses are calculated at BOL conditions. A linear stress distribution is assumed. The creep collapse analysis calculates the stress increase with time and ovalization.

- Flow induced vibration and differential fuel rod growth stresses are also addressed.

4.5 Fuel Pin Pressure Analysis

The pin pressure analysis is assessed against the design basis analysis criteria and envelopes as indicated in Table 4-1. If any of the parameters of this table are violated, then a reanalysis is performed.

Pin pressure analysis is performed using TACO (or TACO2 when approved). The rod is assumed to have a 1.5 symmetric axial flux shape, with a pin power history similar to that presented in Figure 4-1. Incore fuel densification is minimized in this analysis to yield a smaller plenum volume and a maximum pin pressure. | Rev. 4

Figure 4-5 presents the result of an analysis of pin pressure versus burnup, performed by Duke Power Company, using TACO (or TACO2 when approved). This analysis was performed for an extended burnup fuel cycle design, using the pin power history indicated in Figure 4-1, but with lower, more realistic axial flux shapes than the 1.5 cosine shape that is used for Reload Design purposes. (Refer to Table 4-2 for the axial flux shapes used in this extended burnup analysis.) To satisfy mechanical design criteria, pin pressure must be less than system pressure (2200 psia). | Rev. 4

4.6 Linear Heat Rate Capability

Linear heat rate capability of all fuel rods in a reload batch is assessed by comparison against the criteria and envelopes of Table

4-1. Any rod whose geometry or power history falls outside of those criteria must be reanalyzed.

The Linear Heat Rate to Melt (LHRTM) analysis is performed using TACO (or TACO2 when approved), assuming maximum incore pellet densification. This analysis assumes a conservative pin power history, similar to that of Figure 4-1, and a 1.5 cosine axial flux shape. In this analysis, very small axial segments of the fuel rod are spiked to high linear heat rates at each burnup step until centerline fuel melt occurs. The resulting heat rate required to reach centerline fuel melt at each burnup is then plotted versus burnup. | Rev. 4

Figure 4-6 is a plot of fuel LHRTM versus burnup for an extended burnup fuel cycle design. This TACO (or TACO2 when approved) analysis, performed by Duke Power Company, represents the pin power history of Figure 4-1, but with more realistic axial flux shapes than the 1.5 cosine that is used for reload fuel cycles. (Refer to Table 4-2 for the axial flux shapes used in this analysis.) The minimum LHRTM occurs early in life due to fuel densification, but quickly increases due to the offsetting effects of cladding creepdown, pellet swelling, and fuel relocation. (No credit is taken for fuel relocation in LHRTM analyses). | Rev. 4

TABLE 4-1
FUEL MECHANICAL PERFORMANCE ASSESSMENT CRITERIA

Item No.	Parameter Reviewed[1]	Analysis Category: Cladding Collapse[2]	Cladding Strain	Cladding Stress	Pin Pressure	Linear Heat Rate Capability
1	Pin Power History vs Burnup	NA	NA	NA	Figure 4-1	Figure 4-1
2	Radial Assembly Power History vs Burnup	Figure 4-2	NA	NA	NA	NA
3	Clad O.D.	Yes	Yes	Yes	Yes	Yes
4	Clad I.D.	Yes	Yes	Yes	Yes	Yes
5	Clad Thickness	Yes	Yes	Yes	Yes	Yes
6	Clad Initial Ovality	Yes	NA	NA	NA	NA
7	Pellet Diameter	Yes	Yes	Yes	Yes	Yes
8	Pellet Density	Yes	Yes	Yes	Yes	Yes
9	Initial Prepressure	Yes	Yes	Yes	Yes	Yes

NOTES:
1. These criteria are the more significant items reviewed for a reload fuel cycle design, and do not include minor assumptions that are part of the bases.
2. The cladding collapse review actually is performed separately for each type of Mark B fuel design (four sets of parameters exist, corresponding to four separate fuel designs).

TABLE 4-2

Axial Flux Shapes Used for Thermal Analysis
(Reference, Figures 4-5, 4-6)

Burnup Range	Peak of Axial Cosine Shapes
0 - 15,100	1.28
15,100 - 35,000	1.22
> 35,000	1.16

NOTE: Standard reload design analyses always employ a 1.5 P/P axial flux shape for pin pressure and LHRTM analysis.

FIGURE 4-1 PIN POWER VERSUS BURNUP ENVELOPE FOR THERMAL ANALYSIS ASSESSMENTS (EXAMPLE ONLY)

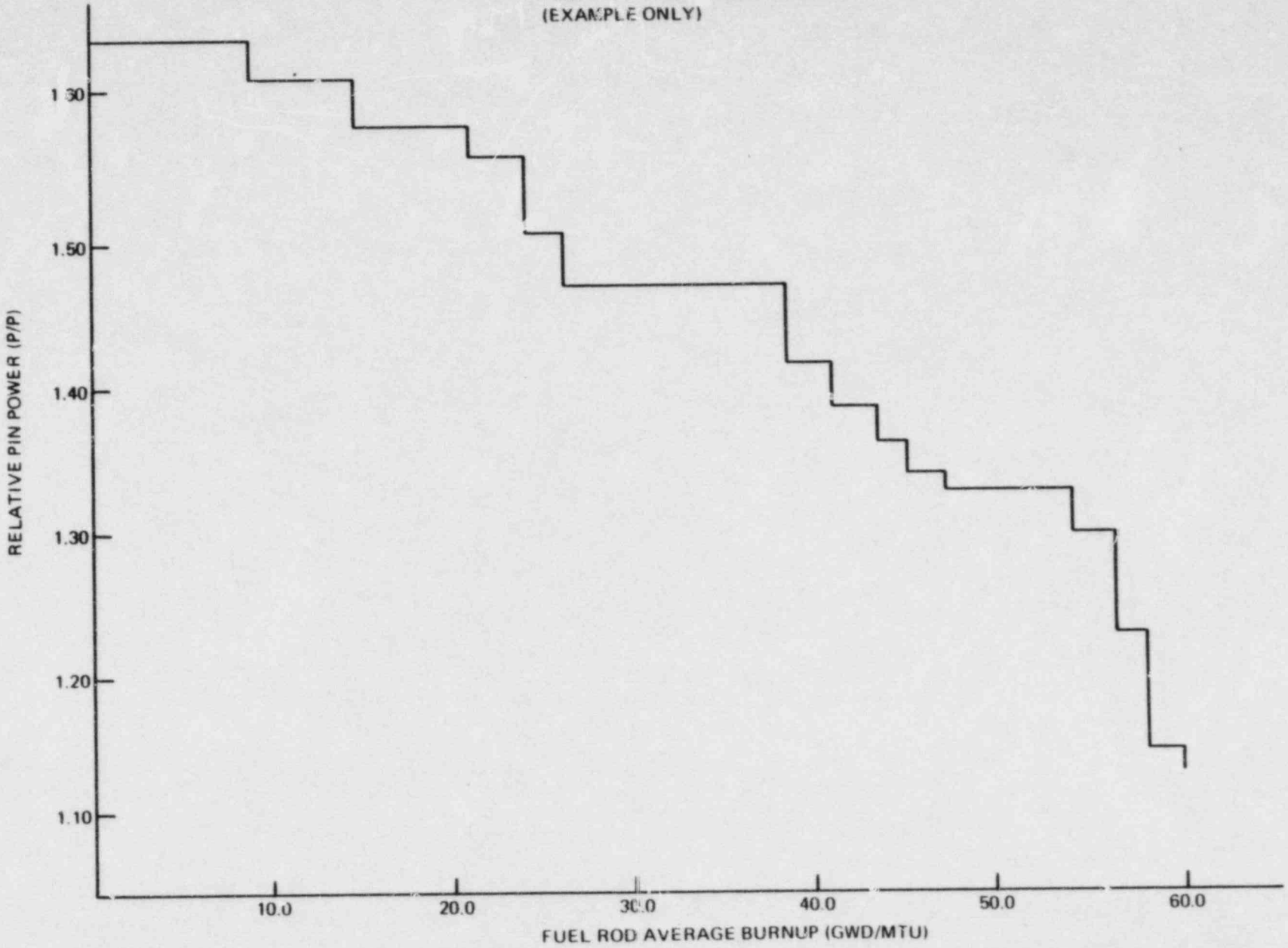

FIGURE 4-2 RADIAL ASSEMBLY POWER VERSUS BURNUP
FOR CREEP COLLAPSE ANALYSIS ASSESSMENTS
(EXAMPLE ONLY)

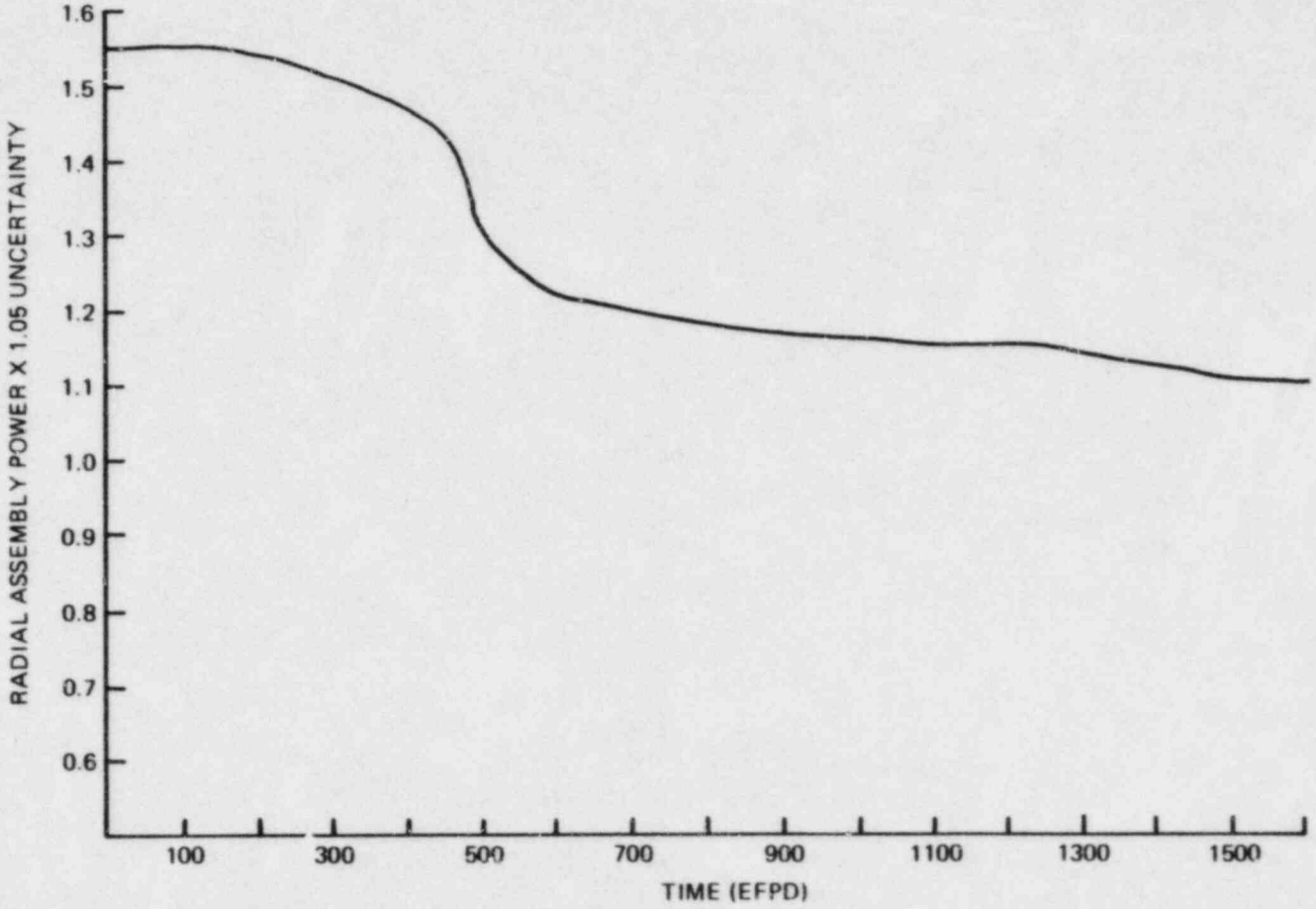

FIGURE 4-3 THERMAL ANALYSIS FLOW DIAGRAM

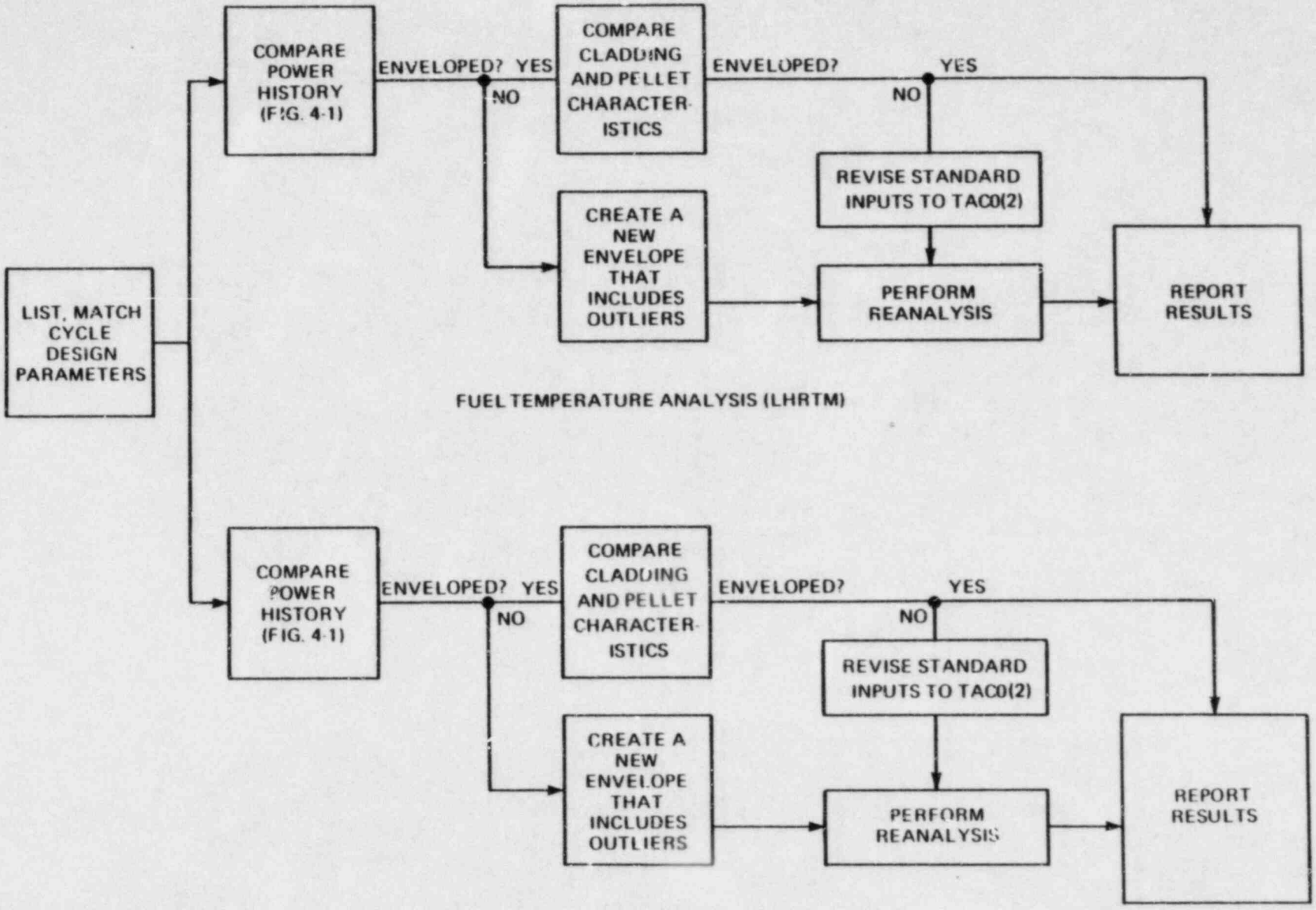

FIGURE 4-4 MECHANICAL ANALYSES FLOW DIAGRAM

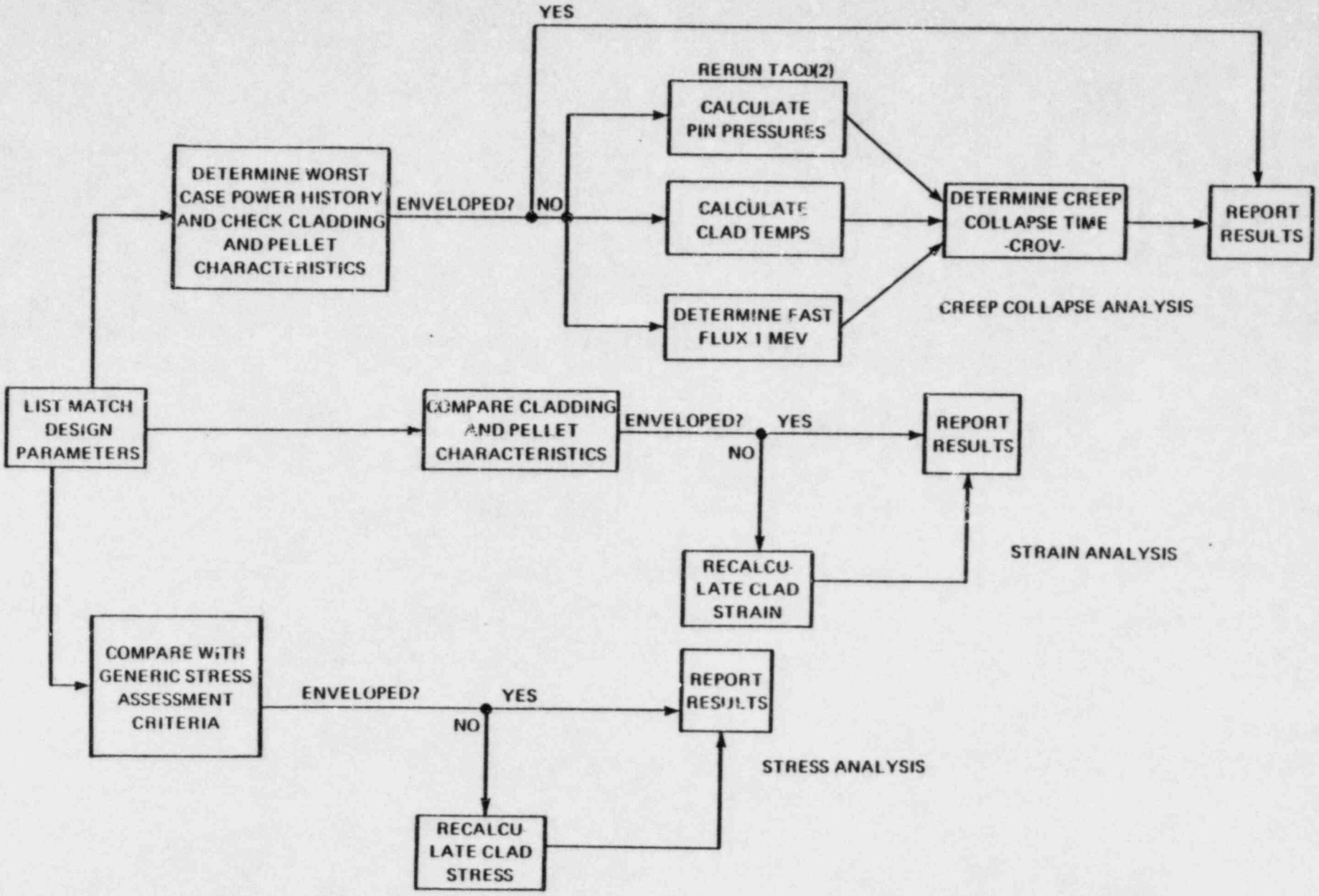

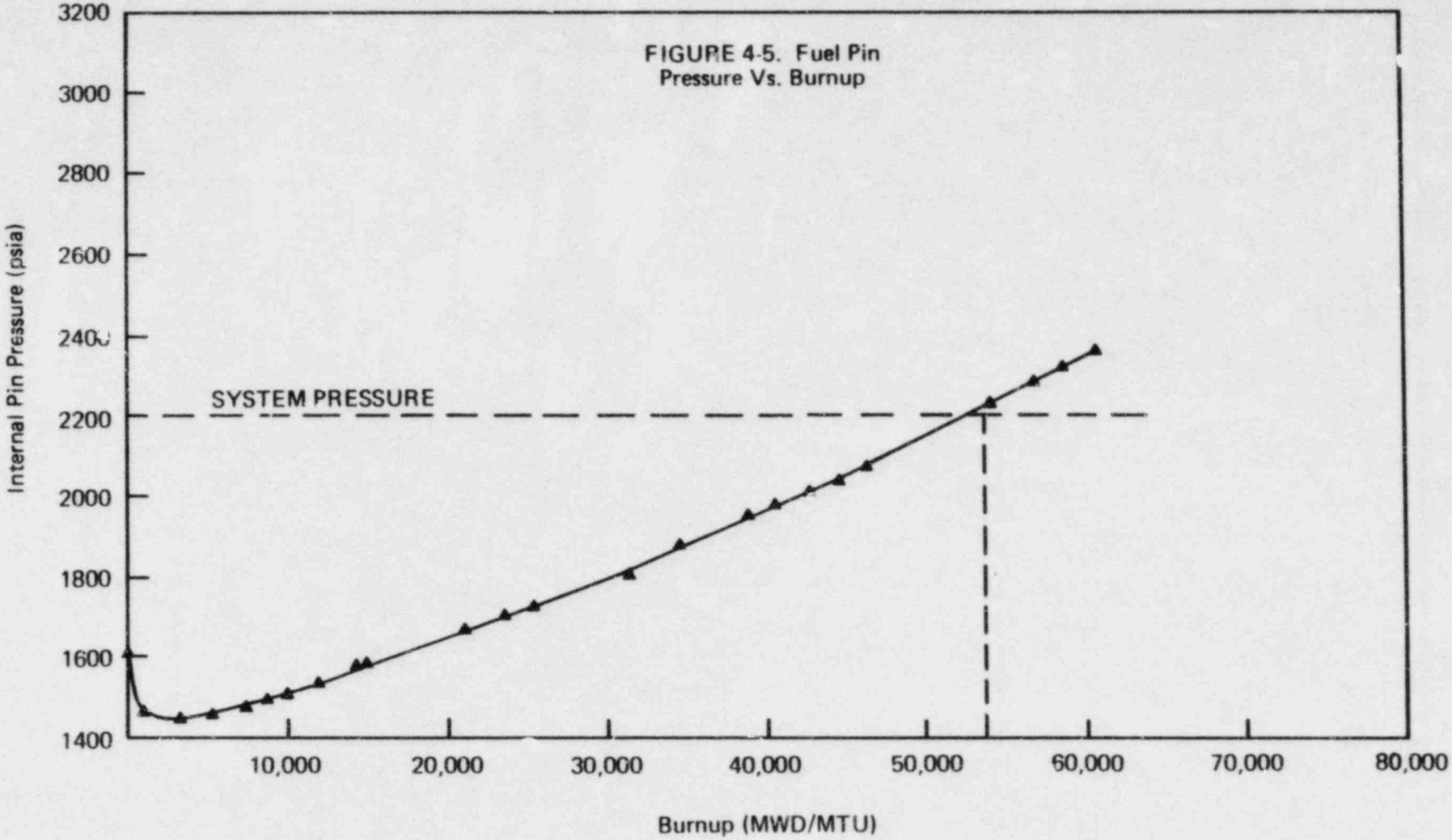
FIGURE 4-5. Fuel Pin
Pressure Vs. Burnup
Internal Pin Pressure (psia)
3200
3000
2800
2600
2400
2200
2000
1800
1600
1400
SYSTEM PRESSURE
10,000
20,000
30,000
40,000
50,000
60,000
70,000
80,000
Burnup (MWD/MTU)

Figure 4-6
Fuel Linear Heat Rate to Melt Vs Burnup

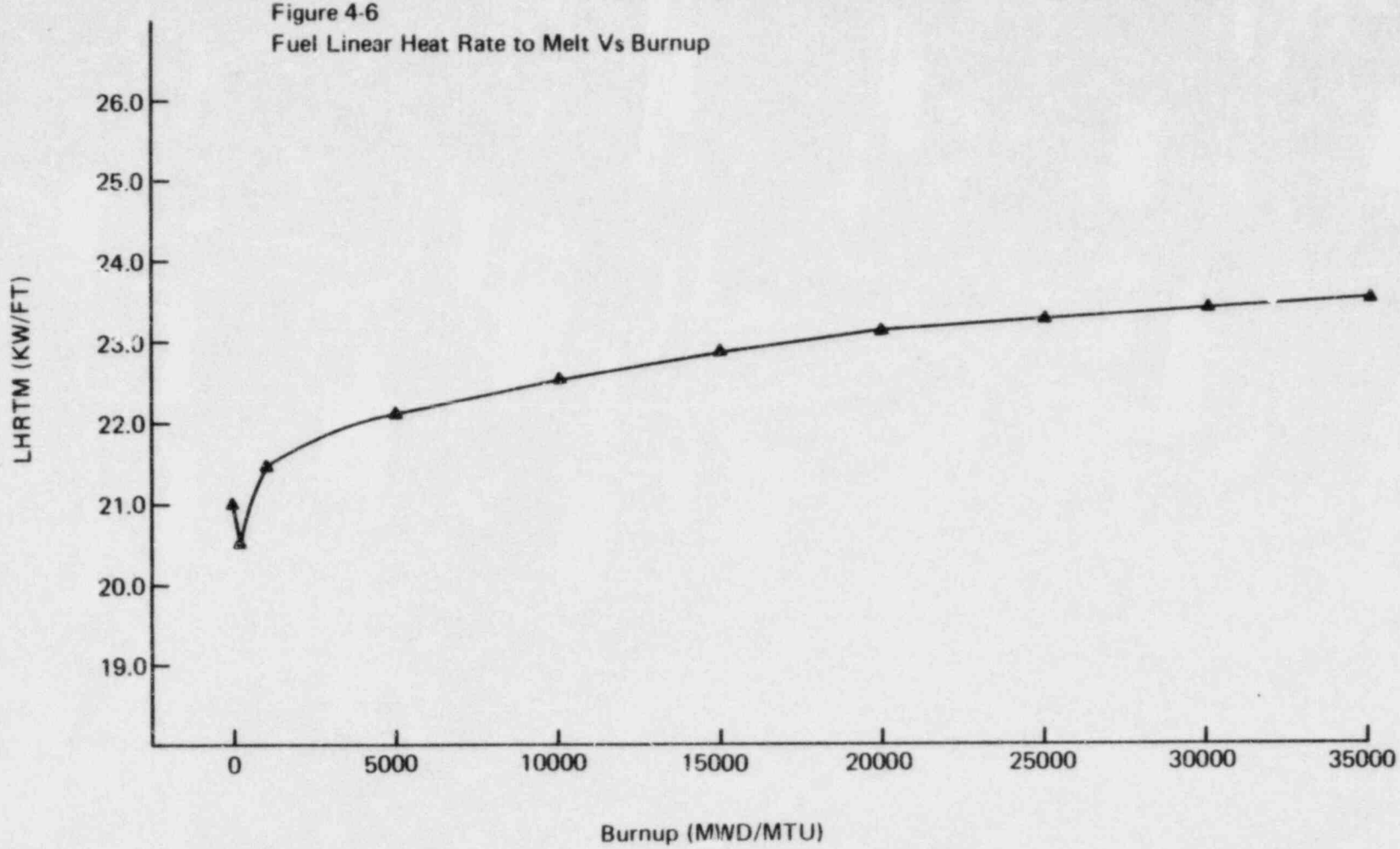

5. MANEUVERING ANALYSIS

The purpose of a maneuvering analysis is to generate three dimensional power distributions and imbalances for a variety of rod positions, xenon distributions, and power levels.

The maneuvering analysis can be divided into five discrete phases. The first is the fuel cycle depletion performed to establish a nominal rod index and fuel depletion history. The second is the generation of integral rod worth curves at several burnup steps. The third step is the power maneuver performed in the nominal manner at BOC (4EFPD) and usually after a rod pull or at EOC. The fourth phase is to perform control rod and APSR scans at the most severe times of the power transient. The fifth step is to perform selected control rod and APSR scans at the various depletion steps. Each of these phases involves the running of multiple EPRI-NODE cases and generation of three dimensional power distributions, rod positions, and imbalance for each case. | 1

This data is processed by the Node Utility Code (NUC) to calculate CFM, DNBR, and LOCA margins and to produce "fly speck" graphs to be used to set Technical Specification (see Section 7.1) limits on rod position, offset versus power level, and reactor protective system setpoints. | 1

5.1 Fuel Cycle Depletion

If the three dimensional EPRI-NODE model has not been previously depleted during the FFCD with rod positions which limit imbalance to within $\pm$ 5%, then the fuel cycle depletion is performed as the first step of the maneuvering analysis. The depletion is typically performed in steps of 0, 4, 12, 25, 50, 100, 150 ... EFPD adjusting rod positions and soluble boron where necessary to hold imbalance within $\pm$ 5% and the reactor near critical. The xenon, power, and exposure files for these cases are saved for use in later analyses.

5.2 Integral Rod Worth

EPRI-NODE cases are run at BOC (4EFPD) and after a rod pull or at EOC stepping the control rods into the core to calculate an integral rod worth curve for groups 7, 6, and 5 with a 25% overlap. These cases input the exposure history calculated from the nominal depletion discussed in Section 5.1. The resulting integral rod worth curve is used in determining rod positions for maintaining criticality during the power maneuver and to define rod insertion limits based on shutdown margin and ejected rod worth. 1

5.3 Power Maneuver

5.3.1 "Rods In" Design 1

The burnup and xenon distribution from the BOC (4EFPD) depletion case at 100% HFP forms the input starting point for the 100-30-100 power maneuver. First an EPRI-NODE case is run reducing power to 30% HFP and holding everything else constant. The difference in reactivity between the 100% and 30% cases represents the power deficit. Using the integral rod worth curve generated in Section 5.2, the change in rod position necessary to compensate this power deficit is calculated.

The next step is to run a third case reducing the power level to 30% with the above estimated control rod positions. Subsequent cases may be necessary to correct the rod positions to maintain the problem near critical. APSR positions are also varied to maintain imbalance within $\pm$5% where possible.

The transient is performed using one hour time steps for updating the xenon concentrations, rod positions, and power levels (soluble boron concentration is held constant). The power is held at 30% until peak xenon occurs. When peak xenon has occurred (approximately six hours) the power is raised back to 100% and the control rods are withdrawn enough to compensate for the power deficit and the increased xenon worth. The transient is followed using one hour steps inserting the control rods as xenon burns out and maintaining imbalance by varying APSR position until xenon concentration approaches its new equilibrium concentration.

The power and xenon distributions, rod positions, and imbalance from this nominal 100-30-100 power maneuver are saved and used in the next phase of the analysis.

5.3.2 "Rods Out" Design

For a "Rods Out" fuel cycle design, the power maneuver is simulated by inserting group 7 to 50% and allowing EPRI-NODE to calculate the reduced power level which results in criticality. This reduced power level is used in place of the 30% power level of the "Rods In" Design. The remainder of the calculations proceed similarly to those previously discussed for the "Rods In" Design. 1

5.4 Control Rod Scans Off the Power Maneuver

Control rod scans are performed at the most severe times during the power maneuver intentionally trying to produce large offsets and high power peaking to evaluate the effect of mispositioned control rods on power peaking. During these scans control groups 6 and 7 with appropriate overlap are inserted and/or removed to produce large offsets and high power peaks. APSR scans are also performed to determine the offset and power peaking that results as these rods are moved. 1

The resulting power distributions and offset from these rod scans are used to evaluate CFM and DNBR margins which lead to the core safety limits on power and imbalance (see Section 7.2).

5.5 Control Rod Scans Off Fuel Cycle Depletion

Control rod scans on groups 6 and 7 with overlap are also performed from the fuel cycle depletion cases usually at 4 EFPD, 100 EFPD, after any rod pull, and at EOC. APSR scans are also performed at these times during the fuel cycle.

The resulting power distributions, rod positions, and offset from these rod scans are also evaluated for CFM, DNBR, and LOCA margins and used in setting Technical Specification limits.

6. THERMAL HYDRAULIC DESIGN

6.1 Introduction

The thermal-hydraulic analyses establish the maximum permissible core power and power distribution for various operating conditions and the permissible combination of core outlet pressure and reactor outlet temperature to ensure that a minimum DNBR of 1.3 or greater can be maintained during the steady state overpower condition or during anticipated transients. The need to perform the thermal-hydraulic analyses in conjunction with a reload arises when there is a change in the fuel design, a change in the input assumptions of the original analysis, or a change in the regulatory criteria.

6.2 Thermal-Hydraulic Design Criterion

The general criterion for thermal-hydraulic performance is that no core damage due to critical heat flux take place during steady state operations or during anticipated transients.

The critical heat flux criterion is expressed as a departure from nucleate boiling ratio, or DNBR. Nucleate boiling refers to the heat transfer regime where small steam bubbles are forming on the clad surface and efficiently transferring heat (small temperature difference between clad and water). As fuel rod power is increased, the bubble generation increases to a point where the bubbles form an insulating blanket over the heating surface, causing a large rise in clad temperature. This point is the critical heat flux, or departure from nucleate boiling. The DNB ratio is the ratio of this critical heat flux at a given point on a fuel rod to the actual heat flux at that same point, or location.

DNBR is calculated using the Babcock & Wilcox BAW-2 correlation. This correlation, approved by NRC, has replaced the older and more conservative Westinghouse W-3 correlation used initially for the Oconee cores. The BAW-2 correlation, like the W-3, is an empirical correlation of hundreds of experimental data points covering the range of temperatures, pressures, mass velocities, and coolant

qualities typical of PWRs. Validity limits on the BAW-2 which are observed during all thermal-hydraulic analyses follow:

- Coolant Quality: -3% to +26% (analysis conservatively limited to +22%)
- Mass Velocity : 0.95×10^6 to 4.0×10^6 Lbm/hr-ft^2
- Pressure : 1750 to 2457 psia

The minimum DNBR, during normal operation and anticipated transients is limited to 1.30. A DNBR of 1.30 corresponds to a 95 percent probability at a 95 percent confidence level that DNB will not occur. Existing analyses conservatively use a DNBR criterion of 1.4326 to accommodate rod bow (Refer to Section 6.10).

6.3 Analysis Methodology

In order to show that the design criterion of 1.4326 minimum DNBR is met, analysis of core conditions with respect to coolant flow, core pressure, core inlet temperature, power level, and power distribution must be performed. The objective of the analysis is to define permissible values of these parameters such that the criterion is met. Assuring that the many possible variations of power distribution in three dimensions meet the DNBR criterion, for example, requires a systematic analysis of possible power distributions and comparison with predicted conditions meeting the DNBR criterion. A flow chart of this analysis methodology is provided in Figure 6.1.

The steady state thermal-hydraulic analysis covers the overpower (112% full power) condition as a reference point, then determines the allowable pressure-temperature operating limits, and finally determines power distribution limits called generic DNBR curves that conservatively envelope the allowable core operating conditions. Subsequently, the transient thermal-hydraulic analysis of the two pump coastdown is completed, and results of this analysis are used to determine a flux/flow reactor trip setpoint. This setpoint ensures that the DNBR criterion is met upon loss of one or more primary coolant pumps.

6.4 Core Inlet Conditions

The first block of the Figure 6.1, Core Inlet Conditions, represents the hand calculations required to determine the core mass flow rate and the core inlet temperature (enthalpy) for each plant operating condition to be analyzed.

The reactor coolant pumps are constant volumetric flow pumps; thus the RCS mass flow rate varies with cold leg temperature. Further, the integrated control system maintains a constant average temperature over the power range of 15-100 percent, which requires that cold leg temperature decrease with increasing core power. These two factors when combined require that an iterative calculation be used to determine core inlet temperature and mass flow rate over the power range analyzed. Additional density changes (flow corrections) are made to account for parametric variations in the core inlet temperature and outlet pressure as well as for the temperature and pressure errors which are applied during the analysis.

6.5 Reference Design DNBR Analysis

This section represents block number 2 of Figure 6.1 and discusses the method used to determine the reference design DNBR, which is reported in Table 6-1, Thermal-Hydraulic Design Conditions, of each Reload Report.

A two stage analysis is used to determine this reference DNBR: 1) a core-wide analysis and 2) a hot assembly/hot channel analysis. These two stages are described in subsections 6.5.1 and 6.5.2, which follow.

6.5.1 Core-Wide Analysis

The CHATA[10] (Core Hydraulic And Thermal Analysis) program is used to determine the core-wide flow distribution. CHATA is a closed channel model (no energy or mass interchange among assemblies) that varies flow to each assembly until each one has the same pressure drop and the sum of the assembly flows is equal to the input core flow. 3

Total core flow effective for heat transfer is input into CHATA, which models single fuel assemblies on an eighth-core symmetric basis to determine the core flow distribution. The calculated result of particular importance that is derived from this CHATA core flow distribution is the hot assembly flow, which is subsequently input into the hot assembly analysis described in Subsection 6.5.2.

Primary inputs to this core-wide analysis are core flow effective for heat transfer, individual fuel assembly geometries, form loss coefficients, the generic radial peaking distribution, the 1.5 design cosine axial flux shape, and core operating conditions.

Core flow rate is one of the most important inputs to the thermal-hydraulic analyses, and the possibility exists that this input flow can change depending on measured flow. Reloads are now being designed based on 106.5% of the original design reactor coolant system flow rate of 88,000 gpm per pump. The 106.5% figure was selected based on the lowest measured flow rate less measurement uncertainties.

Core flow is equal to total loop flow less the bypass flow, which is defined as that part of the flow that does not contact the active heat transfer surface area. These bypass flow paths are 1) core shroud, 2) core barrel annulus, 3) control rod guide tubes and instrument tubes, and 4) all interfaces separating the inlet and outlet regions. A typical value of the design bypass flow is 8.10%; however, this flow rate is dependent on the number of orifice rod and burnable poison rod assemblies. Removal of orifice rod assemblies and/or changes in the number of burnable poison rod assemblies and retainers cause both changes in the core bypass flow rate and in the core flow distribution. Such changes will either be reflected appropriately in the core-wide flow distribution or will be conservatively enveloped.

The basic assumption for the core inlet flow distribution. which is based on vessel model flow tests and Oconee 1 core pressure drop measurements, is that the isothermal flow distribution is relatively flat with a maximum deviation of

less than 5% for 4-pump flow conditions. Therefore, the hot assembly is assumed to receive only 95% of the nominal assembly flow for this isothermal, four pump condition.

These isothermal flow maldistribution factors are considered during the core-wide CHATA analysis by the use of an additional form loss coefficient located at the entrance of the "hot" assembly. However, it is important to note that the numerical value of this form loss coefficient is determined in an isothermal flow distribution analysis to be consistent with the fact that the vessel model flow test is an isothermal model. Subsequently, when the CHATA core-wide model is run at power conditions, a significantly larger hot assembly flow maldistribution results due to the radial peaking factor of the hot assembly. Further conservatisms imposed on the hot assembly during the core-wide analysis are minimum spacing effects on the flow area and on the form loss coefficients.

6.5.2 Hot Assembly/Hot Channel Analysis

The second step toward determining the reference design DNBR is the hot assembly/hot channel analysis, which is also represented by block number 2 of Figure 6.1. The term "hot" assembly refers to that fuel assembly with the highest radial peaking factor(actually the intersection of four 1/4 assemblies). The term hot channel refers to the subchannel with the highest single pin peaking factor. This subchannel occurs within the hot assembly and is generally formed by the intersection of four fuel pins, although the hot channel could occur in a pin-control rod subchannel. (Hot channel factors are always included in all subchannel types within the hot bundle to permit this possibility.)

The conservative hot assembly flow rate from Section 6.5.1 is input into the TEMP[14] (Thermal Energy Mixing Program) code for detailed analysis of the single "hot" assembly. The Oconee hot assembly pin by pin peaking distribution conservatively models the intersection of the pin arrays of four 1/4 assemblies, with a relatively flat local peaking gradient, to conservatively minimize beneficial energy mixing effects. This generic pin-by-pin power distribution includes the design radial peaking factor of 1.714 at the hot channel. All hot

3

channel factors are applied, so that the resulting DNBR calculated represents the worst case (lowest) DNBR for the reactor core for the specified input conditions. The assembly-wide modeling utilizes an open channel calculation; that is, it calculates energy interchange between channels at each calculational increment up the channel. This energy interchange reduces the enthalpy rise in the hot channel, thereby raising the minimum DNBR and permitting a higher allowable peaking factor for the reactor core for conditions when DNBR is limiting. However, the model does not include mass interchange between subchannels.

The outputs of primary importance from the hot assembly/hot channel analysis are the hot channel minimum DNBR and the hot channel flow rate. The hot channel minimum DNBR from the 112% overpower analysis is the reference design DNBR. In general, these outputs of minimum DNBR and hot channel flow are used to establish the equivalent hot channel model of Section 6.6, which itself is used for parametric studies.

6.5.3 Hot Channel Factors

The following hot channel factors are utilized in the thermal-hydraulic analyses of Sections 6.5, 6.6, 6.7, and 6.9. Additional hot channel factors are included in the analyses of Section 6.8 and are described therein.

The flow area reduction factor, is 0.98 on the hot unit and the hot pin-rod cells, and is 0.97 on the instrument guide tube, wall and corner cells. This factor, a statistical computation from measured as-built rod gaps, is applied to the channel flow area at each increment.

The hot channel factor on average pin power, is 1.0107.
This factor accounts for variations in average pin power caused by differences in the absolute number of grams of U-235 per rod. The loading tolerance on U-235 per fuel stack and variation on the powder lot mean enrichment are considered in determining the factor.

The hot channel factor due to manufacturing tolerances, is 1.014.
Variations in pellet density, pellet cross-sectional area, weight per unit length, local enrichment, and local outer clad diameter are all accounted for in this factor.

6.6 Equivalent Two Channel Model

Results of the hot channel analysis performed using the TEMP code, described in Subsection 6.5.2, are used to build a closed, dual channel model that is used for all subsequent parametric analyses. This two channel model contains an average channel and a hot channel and is modeled using the CHATA code.

The hot channel model in CHATA contains all of the conservatisms used in TEMP and is forced to duplicate the hot channel minimum DNBR calculated by TEMP. This matching of the CHATA hot channel with that of TEMP is accomplished by use of an engineering hot channel factor on enthalpy rise, $F_{L\Delta h}$, that is applied during the CHATA analysis. This factor is varied until the CHATA hot channel minimum DNBR equals that in TEMP.

In parametric analyses, the average channel represents a pseudo-core average channel and acts as the "driver" of the hot channel. Thus, an accurate, yet efficient representation of the TEMP hot channel is created for use in parametric analyses, such as the pressure-temperature core protection safety limits and the generic DNBR curves, described in Subsections 6.7 and 6.8.

6.7 Determination of Pressure-Temperature Core Protection Safety Limits

The curves shown in Figure 6.2, Core Protection Safety Limits, represent values of reactor outlet temperature and core outlet pressure for which a minimum DNBR of 1.4326 (or 22% quality) is obtained for various pump combinations. The thermal-hydraulic analysis considers all conservatisms discussed in Section 6.5. To determine the allowable range of pressure-temperature combinations for each pump combination, a series of DNBR calculations is done using the equivalent two channel model for a range of core outlet pressures and reactor outlet temperatures. The results of these calculations are used to generate the locus of pressure-temperature points corresponding to the minimum DNBR of 1.4326. For the 3-pump and 2-pump cases, the minimum core flows as a fraction of 4-pump flow are standard, previously verified numbers; their corresponding power levels are calculated using the flux-flow ratio determined for each reload.

Section 7.3.1 discusses calculation of Pressure-Temperature Trip Setpoints.

6.8 Determination of Power Distribution Limits

6.8.1 Summary

Calculation of power-power imbalance limits based on the DNBR criterion involves a synthesis of thermal-hydraulic analysis and the results of the maneuvering analysis. Margin to DNBR is calculated in the maneuvering analysis for design power transients at various burnups. The method used to generate these DNBR margins efficiently is to precalculate a set of generic curves plotting the total peaking factor producing the minimum allowable DNBR (1.4326) for the overpower condition associated with each pump combination. These curves of allowable total peaking are plotted versus distance up the channel for a range of axial peaking factors as shown in Figure 6-3. The fact that the curves are generic means that they can be generated once and used for all maneuvering analyses until fuel design or core flow rate changes impacting the thermal-hydraulic analyses are made. The following two sections describe the thermal-hydraulic analyses involved in obtaining the generic DNBR curves. Since the curves are plotted in terms of maximum allowable total peaking factors that envelope all core operating power distributions, their comparison to actual peaking during the maneuvering analysis becomes a relatively simple numeric exercise rather than a thermal-hydraulic analysis. Conversion of these calculated DNBR margins into Power-Power Imbalance limits is described in Section 7.2.2.2.

6.8.2 Generic DNBR Curves

Sections 6.3, 6.4, 6.5, and 6.6 have described the methods used to arrive at a dual channel model which can be used for performing parametric studies. This subsection will summarize how this dual channel model is used in determining the generic DNBR curves.

These parametric variations on the reference hot channel analysis are based on the concept that for specified reactor core operating conditions - power level, flow rate, temperature and pressure - all channels in the core have the same

pressure drop regardless of variations in local peaking and axial power shape. In other words, hot channel flow rate will be adjusted by the code to satisfy core-wide pressure drop as local conditions are varied. The axial power shapes input to these parametric hot channel runs are smooth cosine curves whose peak can be specified at various distances up the channel for each series of axial peaking factors. To obtain the maximum allowable peaking factor for each data point, power input to the channel is increased until the limiting DNBR of 1.4326 is reached. This process determines a maximum allowable total peak for a specified axial peak and its location.

After completion of these parametric analyses, two sets of generic DNBR curves or Maximum Allowable Peaking (MAP) curves are determined. One set is used for DNB operational offset limits, and the second set is used for RPS DNB offset limits. The generic DNBR curves used as operational limits are a conservative overlay of 1) the generic DNBR curves used for RPS offset limits, and 2) another set of MAP curves which have the reference design DNBR as their basis. Both sets of limits consider the extremities of the P-T core protection envelope (619°F and 1800 psig) as potential core operating conditions. Thus both the operational DNB offset limits and the RPS DNB offset limits have considered the worst case temperature and pressure envelope permitted by the RPS.
The last step in the thermal-hydraulic analysis is to take actual power shapes that gave the lowest DNBRs during the maneuvering analysis and input these irregularly shaped axial curves into the hot channel code to verify conservatism of the corresponding cosine curves used to develop the generic DNBR curves. A typical set of generic DNB curves is provided in Figure 6.3.

6.8.3 Hot Channel Factors

The following additional hot channel factors on local heat flux are utilized in the thermal-hydraulic analyses for developing the generic DNBR curves:

1.026 = penalty incurred to increase calculated axial powers since flux depressions at the spacer grids are ignored.

1.024 = the ratio of the total nuclear uncertainty of 1.075 to the radial nuclear uncertainty of 1.05.

Thus, in determining the generic DNB curves, the normal value of Fq" is increased from 1.014 to 1.065.

6.9 Transient Analysis - Determination of the Flux - Flow Ratio

During a loss of one or more reactor coolant pumps, the core is prevented from violating the 1.4326 minumum DNBR criterion by a reactor trip that is initiated by exceeding the allowable reactor power to reactor coolant flow ratio setpoint. Loss of one or more reactor coolant (RC) pumps is also detected by the RC pump monitors. That is, independently of the power to flow trip, loss of one RC pump will result in an automatic reactor runback. Similarly, loss of two or more RC pumps from above 55% full power will cause a reactor trip.

The thermal-hydraulic analysis that is used to set the power to flow trip setpoint for coastdown protection conservatively assumes the loss of two RC pumps. The transient is analyzed using the RADAR[15] code to assure that the 1.4326 minimum DNBR criterion is not violated at anytime during the loss of one or more RC pumps. 3

The steady state thermal-hydraulic analysis provides the starting point for the transient analysis. The power to flow setpoint itself is derived from this analysis by varying the time of reactor trip following the loss of two RC pumps (that is by considering various trip setpoints) until the minimum ratio required to maintain the minimum DNBR of 1.4326 has been determined. Calculation of the actual (error corrected) power to flow setpoint used at the nuclear station is described in Section 7.3.2.

6.10 Application of the Rod Bow Penalty

In existing thermal-hydraulic analyses, a very conservative DNBR penalty is included to account for rod bowing effects. This penalty (11.2%), however, has been reduced by 1% because of the flow area (rod pitch) reduction factor already included in the thermal hydraulic analysis.

2

For some reloads, additional credit can be applied based on the fact that primary coolant flow can be proven to be higher than the 106.5% design flow.

The resulting net penalty is applied directly to the final DNBR margins or by increasing the 1.3 DNBR criteria by the percent penalty, resulting in a DNBR criterion of 1.4326.

In future fuel cycle designs, this penalty will be revised to reflect the true effect of measured rod bowing on minimum DNBR (if any additional penalty is required). References 12 and 13 document the methods to be used for determining the true rod bow penalty. Then, a determination will be made to either maintain the current margin which exists or to eliminate part or all of this margin. 2

FIGURE 6.1
THERMAL HYDRAULIC ANALYSIS METHODOLOGY

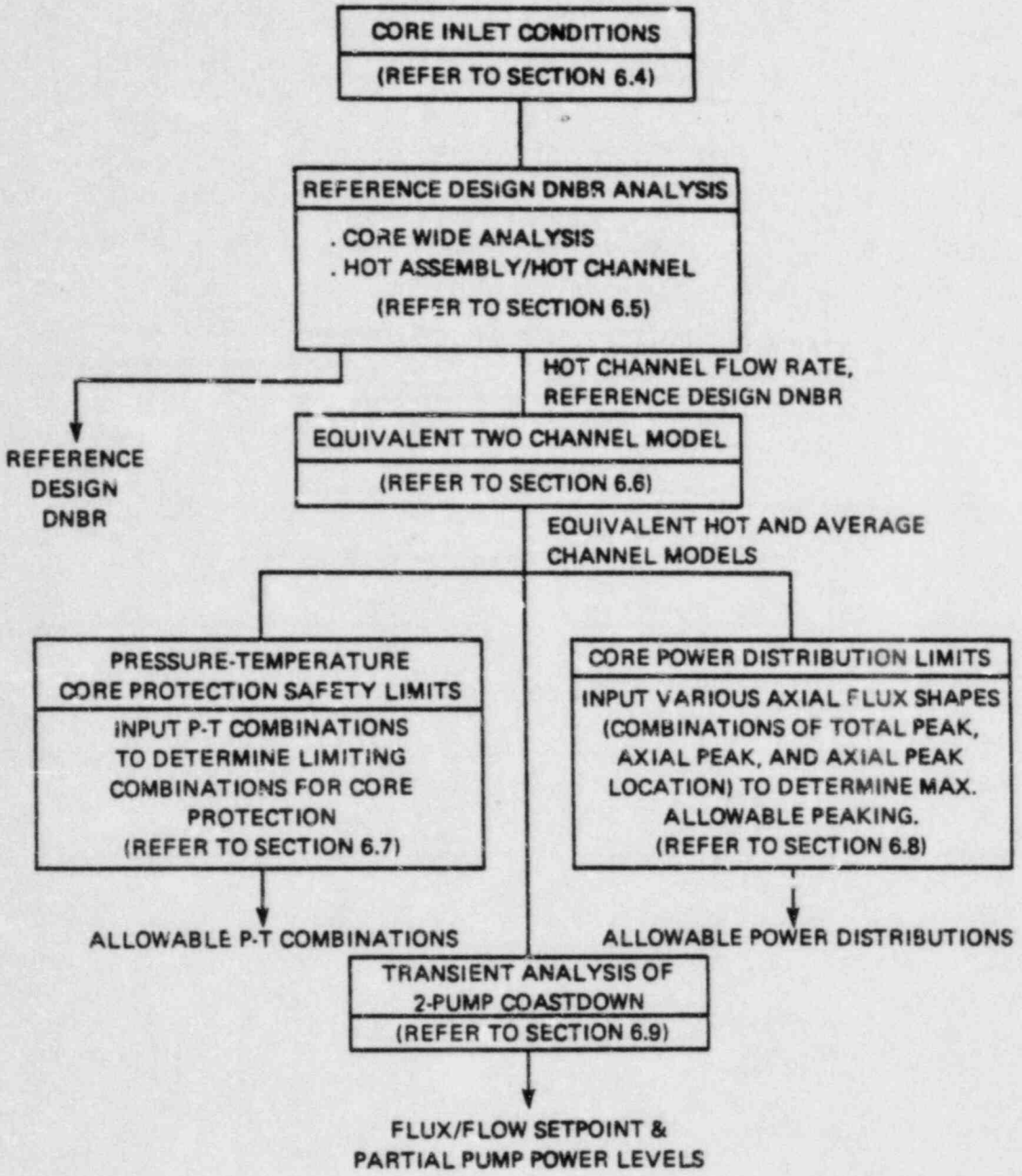

FIGURE 6.2
STEADY STATE PRESSURE-TEMPERATURE
CORE PROTECTIVE SAFETY LIMIT

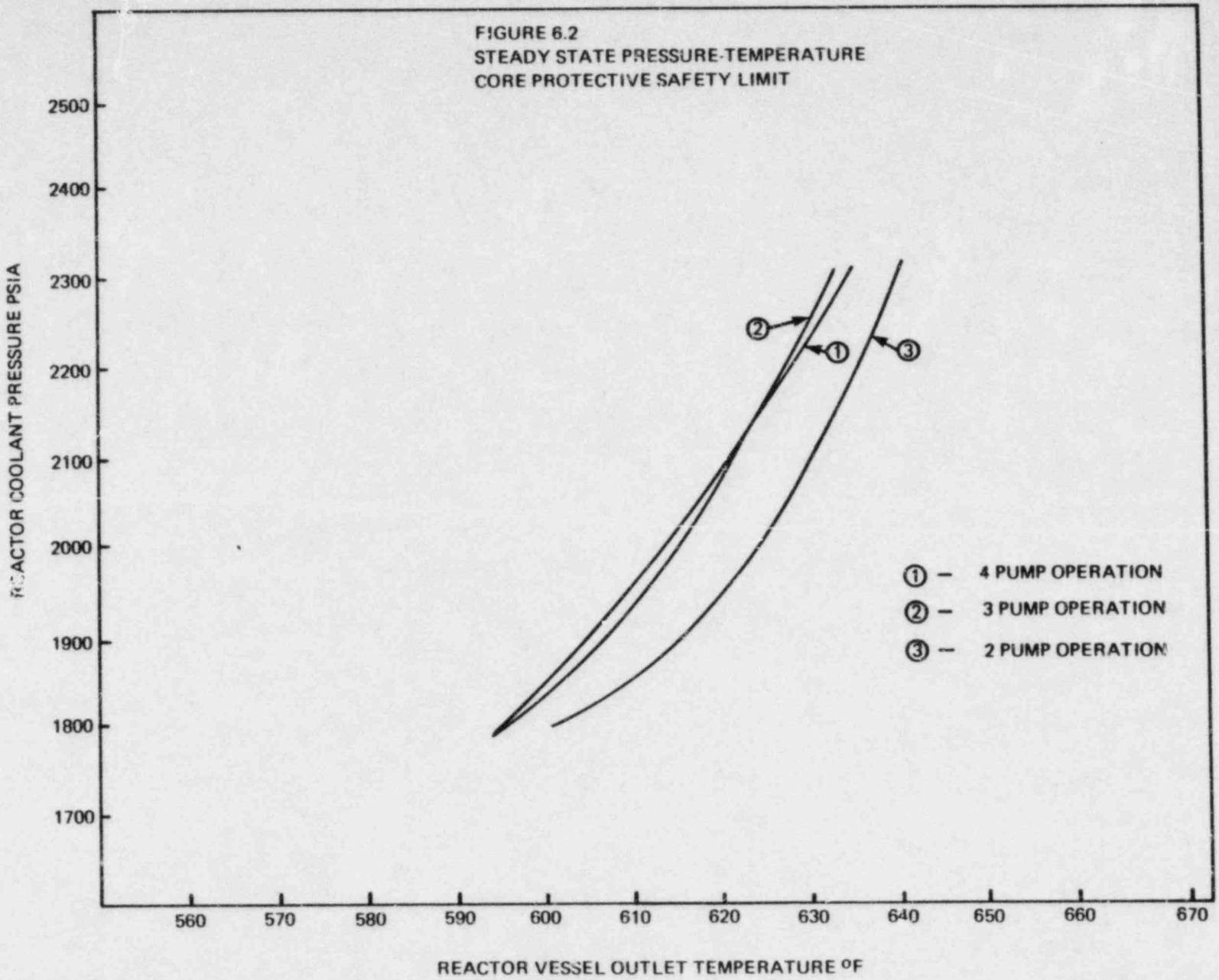

FIGURE 6.3
MAXIMUM ALLOWABLE PEAKING

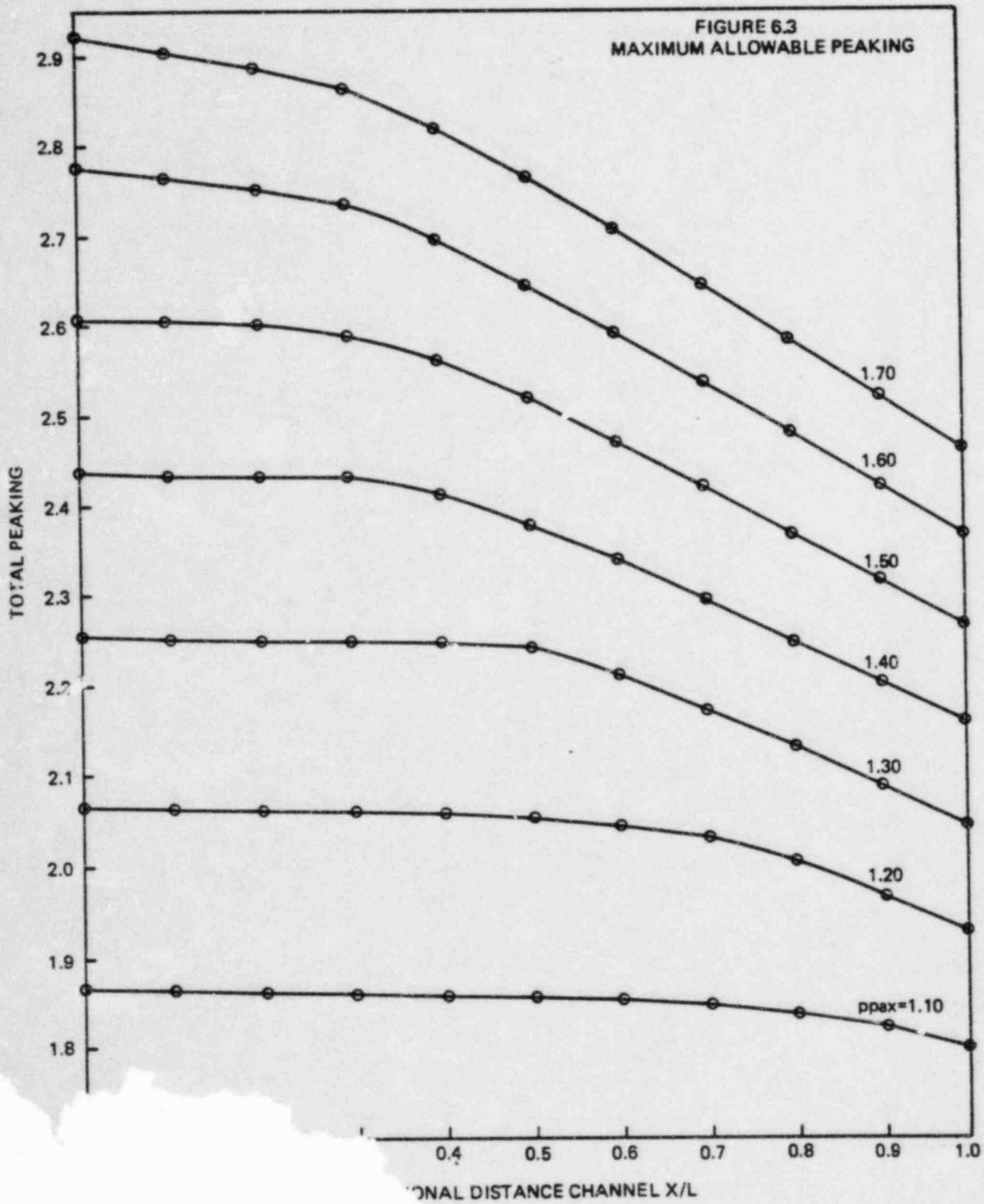

7. TECHNICAL SPECIFICATIONS REVIEW AND DEVELOPMENT

7.1 Technical Specifications Review

One of the license conditions applicable to the operation of a power reactor is that the reactor facility should be operated in accordance with the "Technical Specifications". Technical Specifications are criteria for safe operation of the reactor and are established from applicable design evaluations, safety analyses, and other considerations. Included in the Technical Specifications are safety limits, limiting system settings, limiting conditions for operation, surveillance requirements, identification of design features, and identification of administrative controls.

The Technical Specifications on core safety limits, certain limiting safety system settings, and certain limiting conditions for operation are established on the basis of, among other things, the nuclear and thermal-hydraulic characteristics of the core and applicable accident analyses. Since the nuclear and thermal-hydraulic behavior of the core and accident analyses may be affected by the reload design, the Technical Specifications (and their bases), particularly the sections pertaining to core safety limits, limiting safety system settings, limiting conditions for operation, surveillance requirements, and reactor design features are reviewed to confirm their continued validity for the reload cycle, and modifications are made as necessary to ensure safety of operation and/or to improve flexibility in operation. Technical Specifications ally affected by a typical reload design are (i) core safety limits, limiting safety system settings based on core safety limits and fuel gn limits, and (iii) limiting conditions for operation based on LOCA-power tribution limits and shutdown margin and ejected rod worth limits. The following subsections describe the manner in which these Technical Specification limits are developed.

7.2 Development of Core Safety Limits

The core safety limits define limits on the values of pertinent core parameters such that if core operation is within these limits, the integrity of the fuel cladding is maintained. Fuel cladding integrity can be assured (within per-

missible tolerances) by maintaining the minimum DNBR in the core at or above the design minimum value of 1.3 and by limiting the maximum linear heat rate in the core to less than or equal to the center fuel melt LHR limit. In order to achieve this condition, values of pertinent core parameters which correspond to a minimum DNBR of 1.3 and/or the center fuel melt LHR limit are calculated, and these values form the core safety limits. Core safety limits are specified on core pressure-core outlet temperature combinations (P-T limits) and on reactor power-power imbalance combinations. In calculating these limits it is assumed that all other pertinent variables are at their design limits (maximum or minimum, as appropriate).

7.2.1 Determination of Core Safety P-T Limits

The P-T limits are based entirely on the DNBR criterion, and they represent the values of core outlet pressure--vessel outlet temperature combinations for which a minimum DNBR of 1.3 is predicted when other pertinent parameters are at their respective design limits. The thermal-hydraulic analysis of Section 6.7 defines the values of core outlet pressure as a function of vessel outlet temperature for which a minimum DNBR of 1.3 is predicted for the maximum design conditions during 4-pump, 3-pump, and 2-pump modes of operation. (The design conditions during 4-pump operation consist of a reactor power of 112% power, a combination of radial peak of 1.71 with an axial peak of 1.5, and a minimum reactor coolant flow of 374,880 gpm). The core safety limit is obtained by superimposing the P-T curves corresponding to 4-pump, 3-pump, and 2-pump modes of operation and by drawing the enveloping curve as shown in Figure 7-1.

7.2.2 Determination of Core Safety Power-Power Imbalance Limits

The core safety power-power imbalance limits define the values of reactor power as a function of axial imbalance such that for these values a minimum DNBR of 1.3 and/or a linear heat rate equal to the center fuel melt limit is predicted when other pertinent parameters (RCS flow, pressure and temperature, and hot channel factors) are at their design limits. These limits indirectly represent the limits on the DNBR criterion-limited power peaks and the center fuel melt criterion-limited power peaks. Since power peaking is not directly measurable

by the RPS, the DNBR criterion-limited power peaks and the center fuel melt criterion-limited power peaks are separately correlated to RPS measurable reactor power and power imbalance, and limits are then established on reactor power-power imbalance combinations to satisfy the DNBR and center fuel melt criteria. The power-power imbalance limits separately established for the DNBR and center fuel melt criteria are then superimposed, and the resulting most limiting power-power imbalance envelope forms the core safety limit.

7.2.2.1 Calculation of Power-Power Imbalance Limits for Center Fuel Melt Criterion

The power-power imbalance limits based on the center fuel melt criterion are determined by a synthesis of the results of the fuel thermal analysis and the results of the maneuvering analysis.

The fuel thermal analysis (Section 4.6) establishes the maximum permissible linear heat rate in the core to prevent center fuel melting (center fuel melt linear heat rate limit). Using the center fuel melt linear heat rate limit (CFMLHR), the allowable total peaking factor is established by the relation:

$$MAPF = \frac{CFMLHR}{LHR \times FOP}$$

where LHR is the average linear heat rate in the core (including densification effects) and FOP is the power level expressed as a fraction of rated power.

The maneuvering analysis (Section 5) establishes the maximum calculated total peaking factors for various core conditions (power levels, xenon conditions, control rod positions and burnups). These calculated maximum total peaking factors are increased by several conservative factors to obtain the worst case expected total peaking factor corresponding to each condition. The individual conservative factors and their values are as follows:

1. Nuclear uncertainty factor = 1.075

2. Spacer grid effect factor = 1.026

3. Radial-local factor = varies with location of the assembly in the core (typical value is 1.10)

4. Engineering hot channel factor = 1.014

5. Densification power spike factor: varies with axial location of the peak in the core.

The nuclear uncertainty factor accounts for the uncertainty in the calculated peak due to the limitations of the analytical models; the spacer grid effect factor accounts for the flux distortion caused by the spacer grids; and the radial-local factor is applied to account for the fact that the calculations are performed using an assembly-by-assembly model rather than by using a pin-by-pin model. The engineering hot channel factor accounts for the manufacturing tolerances of critical fuel rod design parameters (pellet enrichment, pellet density, pellet diameter, etc.). The densification power spike factor accounts for the local flux enhancement resulting from gaps in the fuel column induced by fuel densification. Although fuel rod bowing is considered to have the potential for enhancing the power peaks, no explicit allowance is provided for the rod bow power spike factor on the basis that the other conservatism factors (nuclear uncertainty factor and engineering hot channel factor) are adequate to offset the effect of the rod bow power spike factor without an additional allowance.

The worst case expected maximum total peaking factors calculated in this manner for different power levels are compared to the respective allowable total peaking factors, and the central fuel melt margin for each condition can be determined. The central fuel melt margin at a particular power level is given by:

CFM Margin (%) =

$$\frac{\text{allowable total peak - worst case expected maximum total peak}}{\text{allowable total peak}} \times 100$$

Core conditions which correspond to non-negative margins are acceptable conditions, and core conditions which correspond to negative margins cannot be permitted. In order to preclude core conditions with negative margins, limits should be established on acceptable values of power peaking conditions for each power level, and corresponding reactor trip setpoints should be established so as to trip the reactor when conditions approach unacceptable values. Since power peaking cannot directly be measured by the RPS, power peaks are first correlated with the RPS-measurable axial offset for each power level. The outputs of the maneuvering calculations include the maximum total peaking factor in the core, its location and the corresponding core axial offset. In order to determine the axial offset limits that correspond to an acceptable center fuel melt margin for a particular power level, the center fuel melt margin for each calculated maximum total peak for that power level is plotted against the corresponding axial offset. These plots include the data for the entire cycle. For each plot two straight lines are drawn, one conservatively enveloping the data corresponding to positive offsets and the other conservatively enveloping the data corresponding to negative offsets. The maximum allowable positive and negative offsets are found by extrapolating these straight lines to zero margin. Figure 7-2 illustrates the analysis for the 100% FP case.

In practice, detailed calculations are performed only for the 100% FP case, and the limits for other power levels are determined by conservatively extrapolating the 100% FP limits to other power levels by using the power feedback effect on peaking factors and by validating these limits by comparison with results of a limited number of maneuvering calculations at these power levels. Offset limits are typically established for power levels of 112% FP, 100% FP, 80% FP, and 50% FP.

7.2.2.2 Calculation of Power-Power Imbalance Limits for DNBR Criterion

The power-power imbalance limits based on the DNBR criterion are determined by a synthesis of the results of the thermal-hydraulic analysis and the results of the maneuvering analysis.

The thermal-hydraulic analysis establishes the maximum allowable total peaking factors as a function of core elevation for various axial flux shapes to prevent

violation of the DNBR criterion (Section 6.8). The maneuvering analysis generates the power distribution in the core (including the maximum total peaking factor and the associated axial peaking factor for each fuel assembly in a ½-core representation and the core axial offset) for various design conditions and for various times in the cycle. For each power distribution, the calculated maximum total peaking factors of each of the assemblies is increased by a radial uncertainty factor of 1.05, a radial-local factor, and the resulting adjusted peak is compared to the allowable peaking factor for that axial peaking factor and axial peak location. The DNBR margin is then obtained as: | 1 | 1

$$\text{DNBR margin (\%)} = \frac{\text{(allowable total peak - adjusted maximum total peak)}}{\text{allowable total peak}} \times 100$$

For each calculated power distribution, the DNBR margin is calculated for each assembly in the ½-core, and then the minimum DNBR margin in the core for each power distribution is determined.

In order to determine the axial offset limits that correspond to the acceptable DNBR margin, the minimum DNBR margins are plotted for each calculated power distribution against the corresponding axial offset, and the maximum allowable positive and negative offset limits are determined in a manner similar to that used to establish the center fuel melt limited offset limits. In this case also, offset limits are established typically for power levels of 112% FP, 100% FP, 80% FP and 50% FP at full flow conditions.

7.2.2.3 Calculation of the Core Safety Limits on Power-Power Imbalance

The core safety limits on power-power imbalance are the most limiting values of the center fuel melt power imbalance limits and the DNBR power imbalance limits for each power level. To determine the core safety limits, first the limiting offsets at 112% FP, 100% FP, 80% FP, and 50% FP are determined by superimposing the DNBR and center fuel melt offset limits at each power level. The following example illustrates the procedure:

Power Level (% FP)	(CFM Offset Limits (%)		DNBR Offset Limits (%)		Limiting Offset (%)		
	-ve	+ve	-ve	+ve	-ve	+ve	
112	31	29	35	33	31	29	1
100	49	47	55	50	49	47	

The limiting offsets at each power level are converted to imbalance limits using the relation:

Power imbalance = axial offset x fraction of full power.

The resulting imbalance limits are plotted on a power-power imbalance graph, as shown in Figure 7-3. The following additional steps are required to complete the procedure of determining the core safety limits on power-power imbalance:

1. Draw a horizontal straight line corresponding to 112% FP.

2. From points where this line intersects the imbalance limit envelope, draw two straight lines, one on the positive imbalance and one on the negative imbalance side, that conservatively envelope the imbalance points.

These three straight lines define the power-power imbalance limits for 4-pump operation.

The power-power imbalance limits for 3-pump and 2-pump modes of operation can be determined by reducing the thermal power associated with each break point of the 4-pump curve to the values of the maximum allowable core thermal power for 3-pump and 2-pump modes and by drawing straight lines parallel to the 4-pump envelope through the points defined by the 3-pump and 2-pump thermal power and the 4-pump imbalance limits. The maximum thermal power for the 3-

pump mode is obtained by multiplying the 3-pump flow (74.7% of the full flow) by the flux-flow trip setpoint and adding the allowance for calibration and instrumentation error for power measurement (6.5%) to the product. The maximum allowable core thermal power for the 2-pump case (one-pump for each loop) is determined by a similar manner.

7.3 Development of Limiting Safety Settings

The reactor protection system contains several trip functions designed to prevent the process variables from exceeding the safety limits, to ensure that the fuel design limits (minimum DNBR and center fuel melt LHR limit) are not exceeded during conditions of normal operation and anticipated transients, and to enable reactor shutdown during accident conditions. These trip functions, their intended purpose, and their setpoints are shown in Table 7-1. The trip setpoints are established by reducing the safety limits or other design analysis limits by appropriate error adjustment factors, which account for any uncertainty in the measurement of that variable and the calibration and instrumentation errors.

In general, the trip setpoints requiring modification for a reload cycle are the P-T trip setpoints and the power-flow-imbalance trip setpoints as a result of a change in the core safety limits and/or a change in the flux/flow trip setpoints. | 1

7.3.1 Determination of RPS P-T Trip Setpoints

The P-T trip function defines values of RCS pressure as a function of RC outlet temperature at which the RPS should trip and provides protection of the P-T core safety limits.

The P-T trip setpoints are derived by error-adjusting the P-T core safety limits and by considering the high RCS pressure, low RCS pressure, and high RC outlet temperature trip setpoints. Error adjustment is performed on the RCS pressure (to account for the difference in pressure between the core outlet and the point of measurement and to account for the error in the measurement of pressure by the RPS) and the RC outlet temperature (to account for the error in temperature measurement by the RPS). The P-T trip setpoints are to be modi-

fied whenever the P-T core safety limits are changed, P-T error adjustment factors are changed, or the high RC outlet temperature trip setpoints are changed, or the low RCS pressure trip setpoint is changed.

In order to determine the P-T trip setpoints, first the locus of pressure-temperature points constrained by the high RCS pressure trip setpoint (2300 psig), the high RCS temperature trip setpoint (619°F), and the low RCS pressure trip setpoint (1800 psig) are identified on the Core Safety P-T Limit curve, as shown in Figure 7-4. Referring to Figure 7-4, the straight lines AB, BC, and DE respectively represent the locus of P-T points constrained by the high RCS pressure trip, the high RCS temperature trip, and the low RCS pressure trip setpoints. Next, the pressure-temperature points C and D are adjusted for the difference between the core pressure and the RCS pressure at the measurement location and for the errors in the temperature and pressure measurements by the RPS. Referring to Figure 7-4, C' and D' are the error adjusted points, and the straight line C'D' joining these points defines the locus of RPS P-T trip setpoints. 4

7.3.2 Determination of RPS Power-Flow-Imbalance Trip Setpoints

The power-flow-imbalance trip setpoints define the values of reactor power at which RPS trip should occur whenever the combinations of power, flow, and their uncertainties produce limiting values of power and flow which result in the design minimum DNBR during a flow transient and whenever the combination of power, imbalance, and their uncertainties correspond to the core safety limits on power-imbalance. This trip function is established by considering maximum allowable power-to-flow ratio and by considering the maximum allowable values of power as a function of imbalance. The maximum allowable power-to-flow ratio is constrained by the requirement that the minimum DNBR, in the event of a limiting flow transient, is equal to or greater than the design limit of 1.3. Thus the power-flow-imbalance trip setpoints ensure core protection during transients involving a flow reduction (by the power-to-flow trip portion of the trip function) and during conditions involving adverse power distributions (by the power-imbalance trip portions of the trip function).

In order to determine the power-flow-imbalance trip setpoints, first the maximum allowable power-to-flow ratio is to be obtained. The maximum allowable power-to-flow ratio (also called the flux/flow trip setpoint) is obtained by reducing the calculated flux/flow ratio (Section 6.9) by an error adjustment factor, which takes into account the noise in the RPS flow signal and other electronic errors in the RPS flow instrumentation. Next, the core safety power-imbalance limits are error-adjusted both on the power level limit and the imbalance limit. The error adjustment factor for power level is 6.5% FP, which includes 4% FP allowance for the neutron flux error (uncertainty in correlating the RPS measured neutron flux to reactor power), 2% FP allowance for the calorimetric error, and ½% FP allowance for any setpoint error. The error adjustment factor for imbalance accounts for the uncertainty in the measurement of axial imbalance by the out-of-core detector system, and it is a function of the imbalance limit and the power level. To establish the RPS power-flow-imbalance trip setpoints, the error adjusted power and imbalance are plotted on a figure with imbalance as the horizontal axis and power as the vertical axis. The envelope obtained by the straight lines passing through pairs of these points and the horizontal straight line drawn passing through the point representing 112% power for the 4-pump case or the maximum power allowed by the flux/flow trip setpoint, as illustrated in Figure 7-5. | 4 | 1

7.4 Development of Limiting Conditions for Operation

The limiting conditions of operation generally requiring modification in conjunction with a reload cycle are the LOCA-limited power distribution limits, shutdown margin-limited control rod insertion limits, and the ejected rod worth-limited control rod insertion limits.

The LOCA-limited power distribution limits are limits on pertinent core parameters (such as control rod positions, axial imbalance, quadrant power tilt, and xenon conditions which influence the power distribution in the core) such that the power distributions in the core during normal operation are within the values assumed in the safety analysis of the loss of coolant accident.

The shutdown margin-limited control rod insertion limits are limits on the maximum allowable control rod insertions satisfying the shutdown margin

criterion, and the ejected rod worth-limited control rod insertion limits are limits on the maximum allowable control rod insertions satisfying the ejected rod worth criterion.

7.4.1 Determination of LOCA-Limited Power Distribution Limits

The ECCS analysis establishes acceptable values of the linear heat rate in the core such that the performance of the Emergency Core Cooling System conforms to the requirements of the Final Acceptance Criteria. The values of the allowable linear heat rates established by the currently applicable ECCS analysis for Oconee class reactors are 15.5 kw/ft. at the 2 ft. core elevation, 16.6 kw/ft. at the 4 ft. elevation, 18 kw/ft. at the 6 ft. elevation, 17 kw/ft. at the 8 ft. elevation, and 16 kw/ft. at the 10 ft. elevation. The maximum operating linear heat rates at the designated core elevations should be maintained at or below the allowable values. The maximum operating linear heat rate is a function of the power level and the maximum operating peaking factor. Thus, for a given power level the maximum operating linear heat rate varies with the maximum operating peaking factor. Therefore, for a given power level the maximum operating linear heat rates can be maintained within the allowable linear heat rates by maintaining the maximum operating power peaks at the designated axial locations within the allowable peaking factor. The allowable peaking factor at axial location z for the power level FOP is given by:

$$APF\ (FOP,z) = \frac{ALHR\ (z)}{LHR \times FOP,}$$

where APF (FOP,z) is the allowable peaking factor at elevation z for power levels equal to or less than FOP, ALHR (z) is the allowable linear heat rate at axial location z, and LHR is the densified average linear heat rate at 100% FP.

The power peaking factor in the core changes with fuel burnup, axial imbalance, full length control rod position, and part length control rod position. In addition, the peaking factor is influenced by the existence of any quadrant power tilt and non-equilibrium xenon conditions. Therefore, allowable ranges of these core operation parameters would have to be established in order that the maximum operating peaking factors at the designated axial locations be within

the allowable values. Although the fuel densification phenomenon has the potential for enhancing power peaks, no explicit allowance is provided for power spikes associated with this phenomenon in the LOCA power distribution limits on the basis that the densification power spikes do not enhance the local heat flux.

The effect of a positive quadrant power tilt on the maximum peaking factor has been conservatively established to be an increase of 1.5% in peaking factor per percent positive quadrant tilt. The current Technical Specifications permit reactor operation with a positive quadrant tilt of 5.00%, which amounts to a possible 7.5% increase in peaking factor. Therefore, the allowable peaking factor would have to be reduced by 7.5% to account for the permitted quadrant tilt condition.

The effect of non-equilibrium xenon conditions on peaking factors is quantified by the analysis of the power peaking factors occurring during various power maneuvers. Based on the results of this analysis, it has been determined that for "rods in" operation the effect of non-equilibrium xenon on power peaking can be accounted for by reducing the maximum allowable peaking factor by 8% for power levels equal or greater than 90% full power. For "rods out" operation the non-equilibrium xenon peaking factor is 5%.

The allowable peaking factor for "rods out" operation after accounting for quadrant tilt and xenon becomes:

$$APF\ (FOP,z) = \frac{ALHR\ (Z)}{LHRx\ FOP \times 1.075 \times 1.05}$$

1

The remaining core parameters which influence the maximum operating power peaks are the full length control rod position, part length control rod position, axial imbalance, and core burnup. The permissible values of these quantities are to be determined such that resulting power peaks, after accounting for any uncertainties, would be within the maximum allowable power peaks.

The maneuvering analysis establishes the relationship of operating peaking factors at various axial locations with the core imbalance and control rod positions. The maneuvering analysis calculations include part length cont l rod scans inducing a range of values of core axial offset for different full

length control rod positions. The calculations are performed for various power levels and for the full range of core burnups. The calculations yield the values of the maximum peaking factor at the different axial planes corresponding to various full-length control rod positions, various axial offsets, and for different part length rod positions, and these calculations also yield the variations of the maximum peaking factor with axial offset. The calculated maximum peaks at each axial plane are increased by the nuclear uncertainty factor (1.075), the spacer grid effect factor (1.026), the radial-local factor (its value varies with the radial location of the assembly containing the maximum peak), the power level uncertainty factor (1.02) and the engineering hot channel factor (1.014) to obtain the worst case operating peaking factors.

To determine the allowable values of full-length and part-length control rod positions and the axial offsets, first an operating range for the full-length control rod position is chosen and then the ranges of axial offsets and part-length control rod positions for which the worst case operating peaking factors at the designated axial planes are less than or equal to their respective allowable values are determined. If the resulting ranges of axial offset and part-length control rod position are acceptable from the standpoint of operational flexibility, the assumed full-length control rod position ranges and the calculated range of axial offset and part-length control rod position are taken as the operating limit for the full-length control rod positions, axial offsets and part-length control rod positions. If, however, the resulting ranges of axial offsets and part-length control positions are unacceptable from the standpoint of operational flexibility, a more restrictive full-length control rod position bank is selected and the corresponding axial offset and part-length control rod position limits established.

Since the core peaking factors do not remain constant throughout the entire fuel cycle, the operating limits on control rod positions and axial offsets should be based on the composite results of calculations for representative times in the cycle. In order to provide maximum operating flexibility, the operating limits on control rod positions and axial offsets are established for different cycle burnup intervals (e.g., BOC - 100EFPD, 100 EFPD - 250 EFPD and 250 EFPD-EOC). The operating limits applicable to each burnup interval are generated on the

basis of the results of maneuvering calculations corresponding to the beginning and end of each burnup interval. (For each burnup interval, the control rod grouping and the nominal position of the regulating control rod groups are the same).

Calculations of axial offset limits, part length control rod position limits, and full length control rod position limits are performed for various power levels (typically for 102% FP, 92% FP, 80% FP, and 50% FP). The offset limits at each power level are converted to imbalance limits by multiplying the offset limits by the applicable power fraction. Typical operating limits established in this manner are shown in Figures 7-6 - 7-8. | 1

7.4.2 Determination of Control Rod position Limits Based on Shutdown Margin Criterion

The criterion on shutdown margin is that a minimum of 1% Δk/k shutdown margin should be available at all times. The shutdown margin decreases with increasing power and also with increasing inserted rod worth. Therefore, associated with each power level, there is a maximum allowable full length control rod insertion limit which corresponds to a minimum shutdown margin of 1% Δk/k. Shutdown margin limited rod insertion limits are determined by evaluating the shutdown margins at different power levels (typically at 100% FP, 50% FP, and 15% FP) and by using the integral group worth results. Since shutdown margins change with cycle burnup, shutdown margin limited rod insertion limits are calculated for different burnup intervals of the fuel cycle. The shutdown margin limited rod insertion limits are identified in Figure 7-6.

7.4.3 Determination of Control Rod Position Limits Based on Ejected Rod Worth Criterion

The criterion on the ejected rod worth is that its value shall not exceed 1% Δk/k at hot zero power (HZP) conditions and 0.65% Δk/k at hot full power (HFP) conditions. The limits at intermediate power levels are assumed to vary linearly with power--that is, the ejected rod worth at 80% FP is 0.72, the limit at 20% FP is 0.93, etc. The ejected rod worth is a function of, among other things, the inserted control rod group worth and the cycle burnup

(through changes in power distribution). For a fixed burnup the ejected rod worth changes with control rod insertions; therefore limits on the allowable control rod insertion should be placed at various power levels so that the ejected rod worth criterion is satisfied. In order to determine the ejected rod worth limited control rod position limits, the ejected rod worths are calculated corresponding to the most limiting of the shutdown margin and LOCA-limited full length rod insertion limits for different power levels. The calculated ejected rod worths are increased by 15% and compared to the allowable values. If the adjusted calculated ejected rod worths are within the allowable values, no further calculations are needed; otherwise, the control rod insertion limit is changed to the value that corresponds to acceptable ejected rod worths. When the ECCS-limited and ejected rod worth limited rod insertion limits are more limiting than the shutdown margin limited insertion limits, the ECCS and ejected rod worth limited rod insertion limits are combined by superposition into a single rod insertion limit. 1

Table 7-1

Reactor Protection System Trip Functions

Reactor Trip	Monitored Parameter	Trip Setpoint During 4-Pump Operation	Purpose of Trip	
1. Overpower trip	Neutron flux	105.5% FP	To provide core protection during transients involving uncontrolled power increase.	
2. Power-flow-imbalance trip	Neutron flux, RC flow and power imbalance	Flux/Flow = 1.08	To provide core protection during transients involving a flow reduction and during core conditions involving excessive power peaking	1
3. RCS pressure-temperature trip	RCS pressure and RC outlet temperature	Function of RC outlet temperature	To provide core protection during transients involving a reduction in pressure or a reduction in core heat removal and to ensure reactor shut down during a LOCA.	
4. Low RCS pressure trip	RCS pressure	1800 psig	To provide core protection during transients involving a pressure reduction	
5. RC Pump Monitor trip	Neutron flux and pump contact monitor voltage	Loss of two pumps above 55% FP	To provide core protection during loss of RC pumps	
6. High RCS pressure trip	RCS pressure	2300 psig	To provide protection of RCS pressure boundary from excessive pressures	4
7. High RCS temperature trip	RC outlet temp.	619°F	To prevent excessive temperature in the RCS	
8. High RC pressure trip	RB pressure	4 psig	To ensure reactor shutdown during a LOCA and SLB inside containment.	

FIGURE 7-1
STEADY STATE PRESSURE-TEMPERATURE
CORE PROTECTIVE SAFETY LIMIT

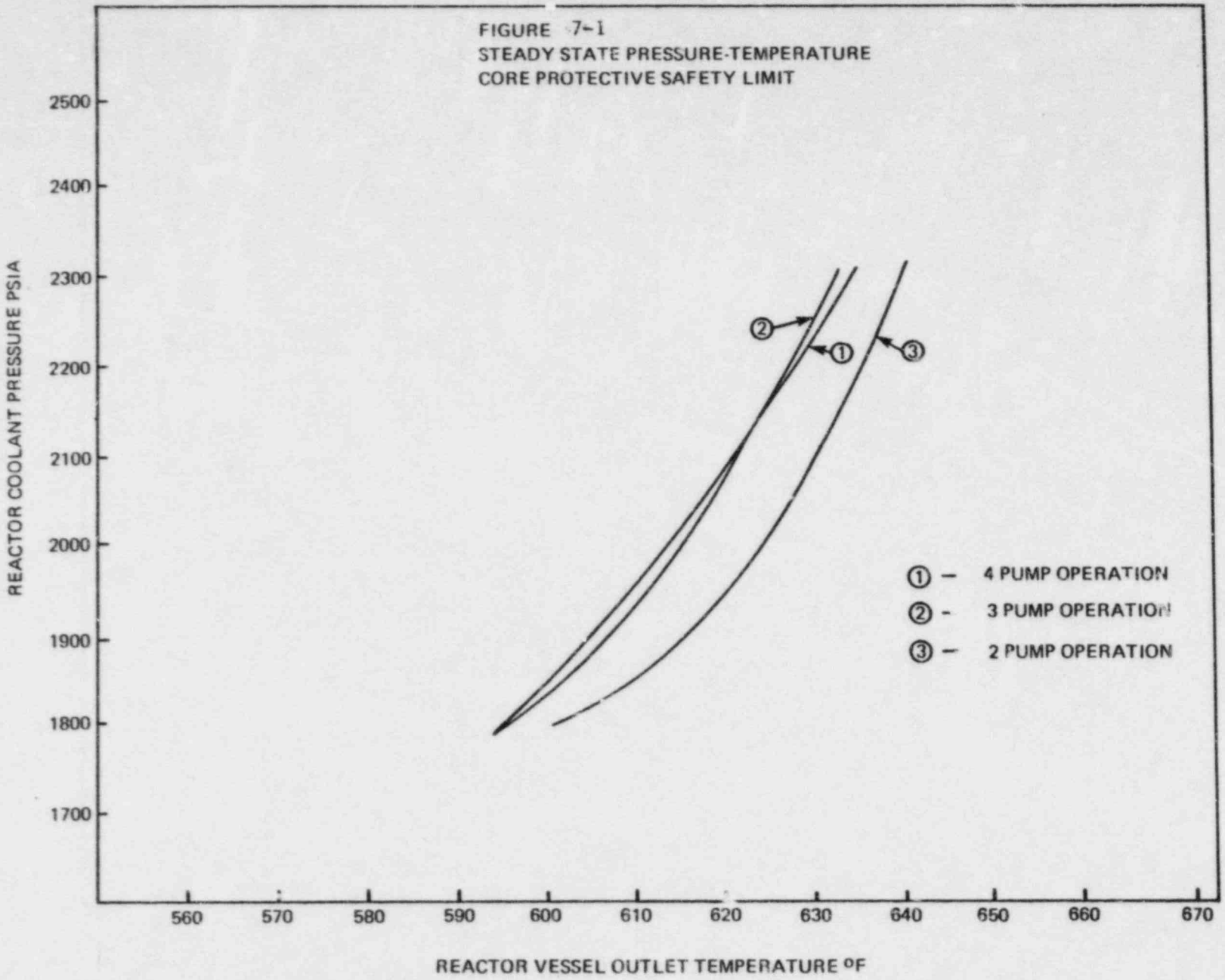

Figure 7-2

Margin To Center Fuel Melt LHR Versus Core Offset

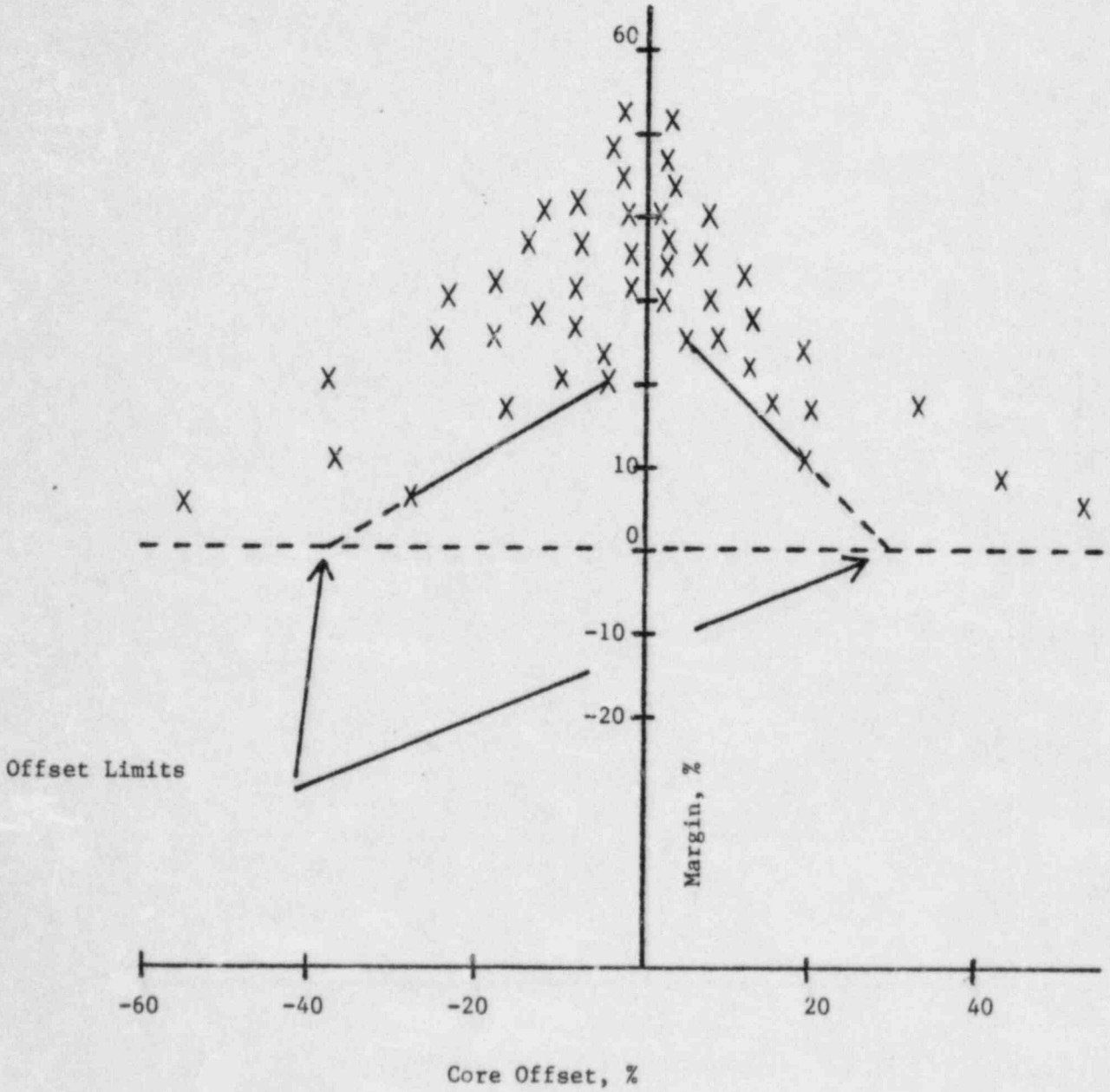

Figure 7-3 Core Protection Safety Limits

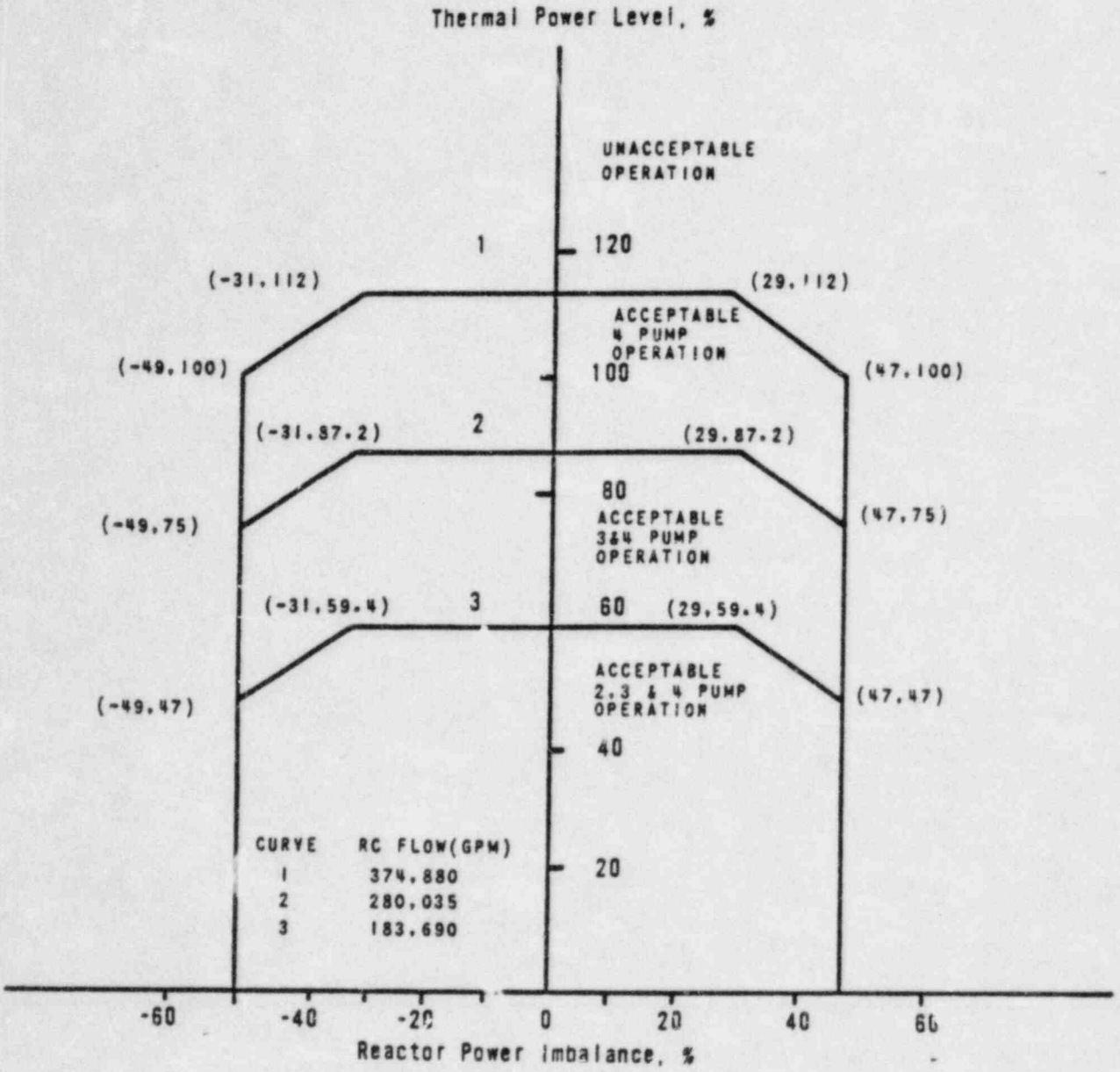

Figure 7-4

Determination of RPS P-T Trip Setpoints

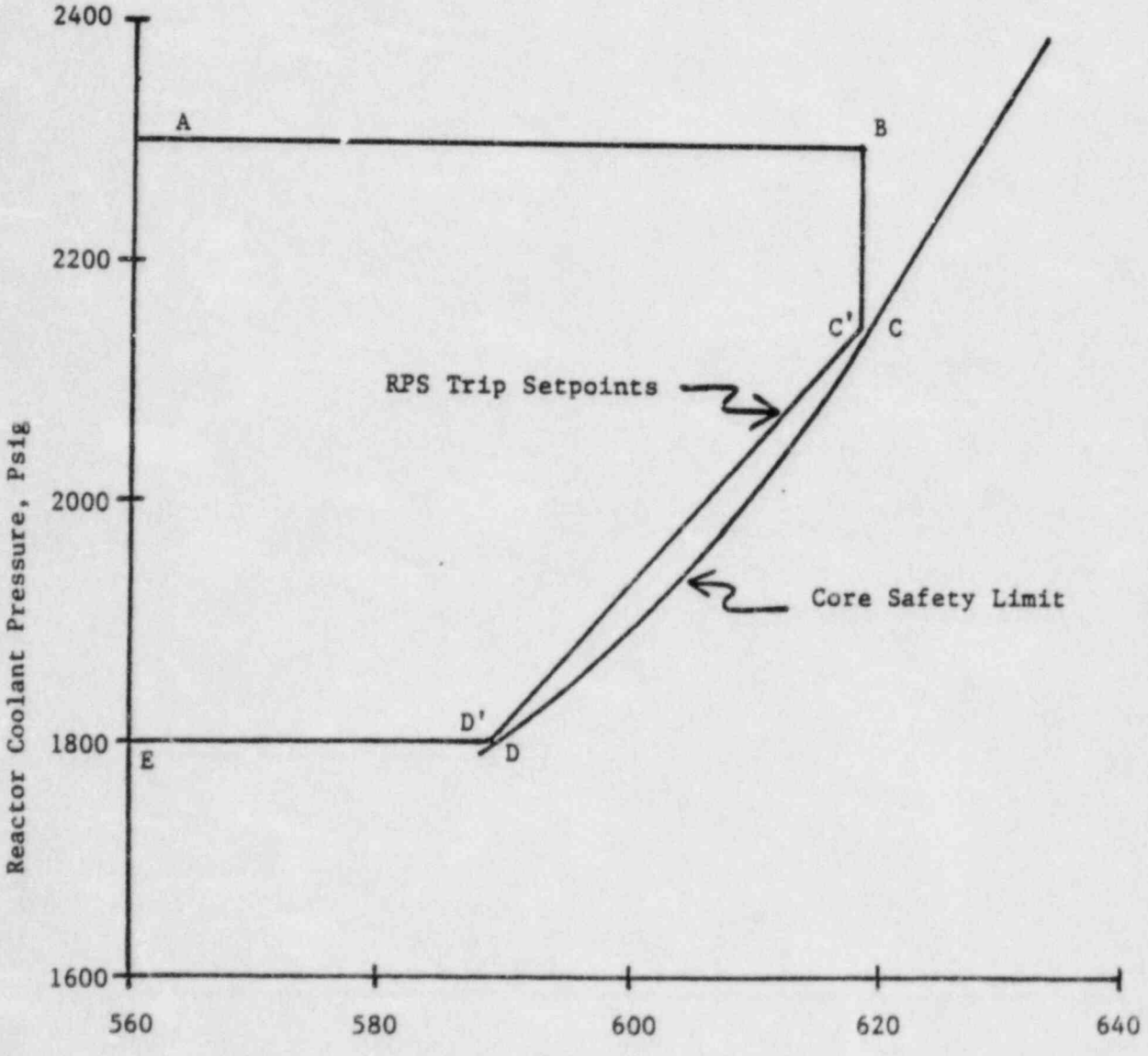

Figure 7-5 Protective System Maximum Allowable Setpoints

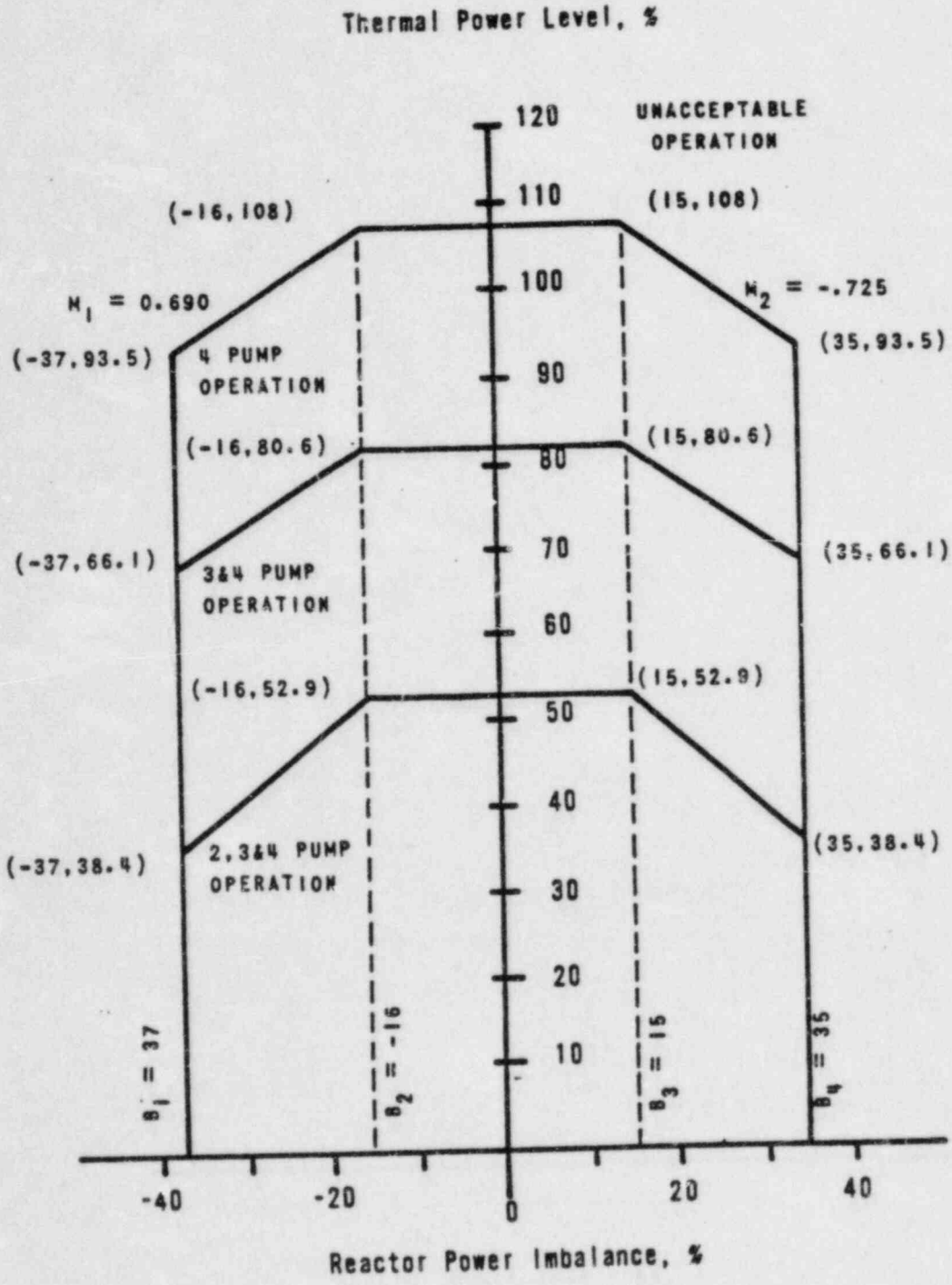

Figure 7-6 Rod Position Limits for Four-Pump Operation, (0 to 200 ± 10 EFPD)

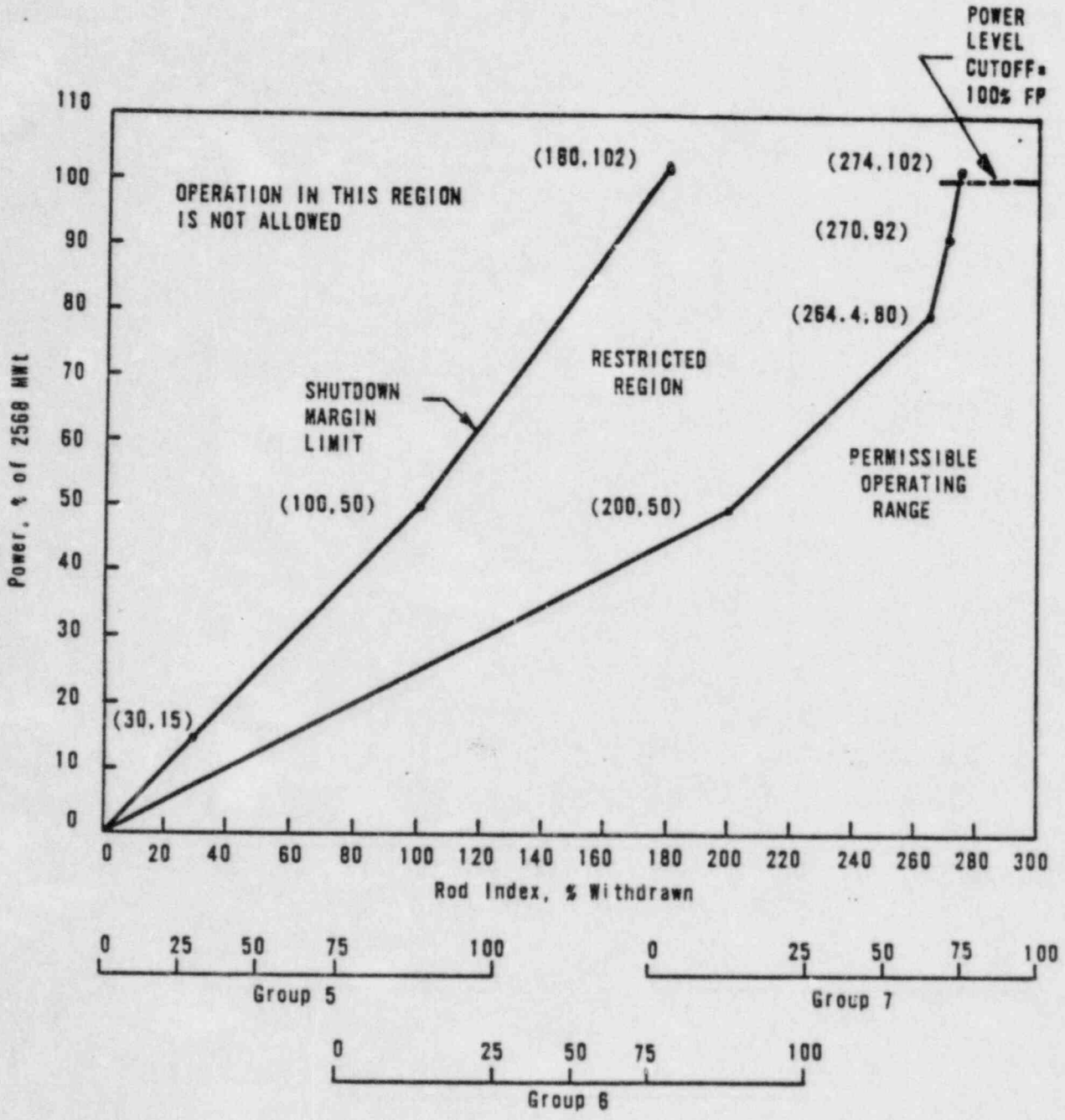

Figure 7-7 Power Imbalance Limits,
(0 to 200 ± 10 EFPD)

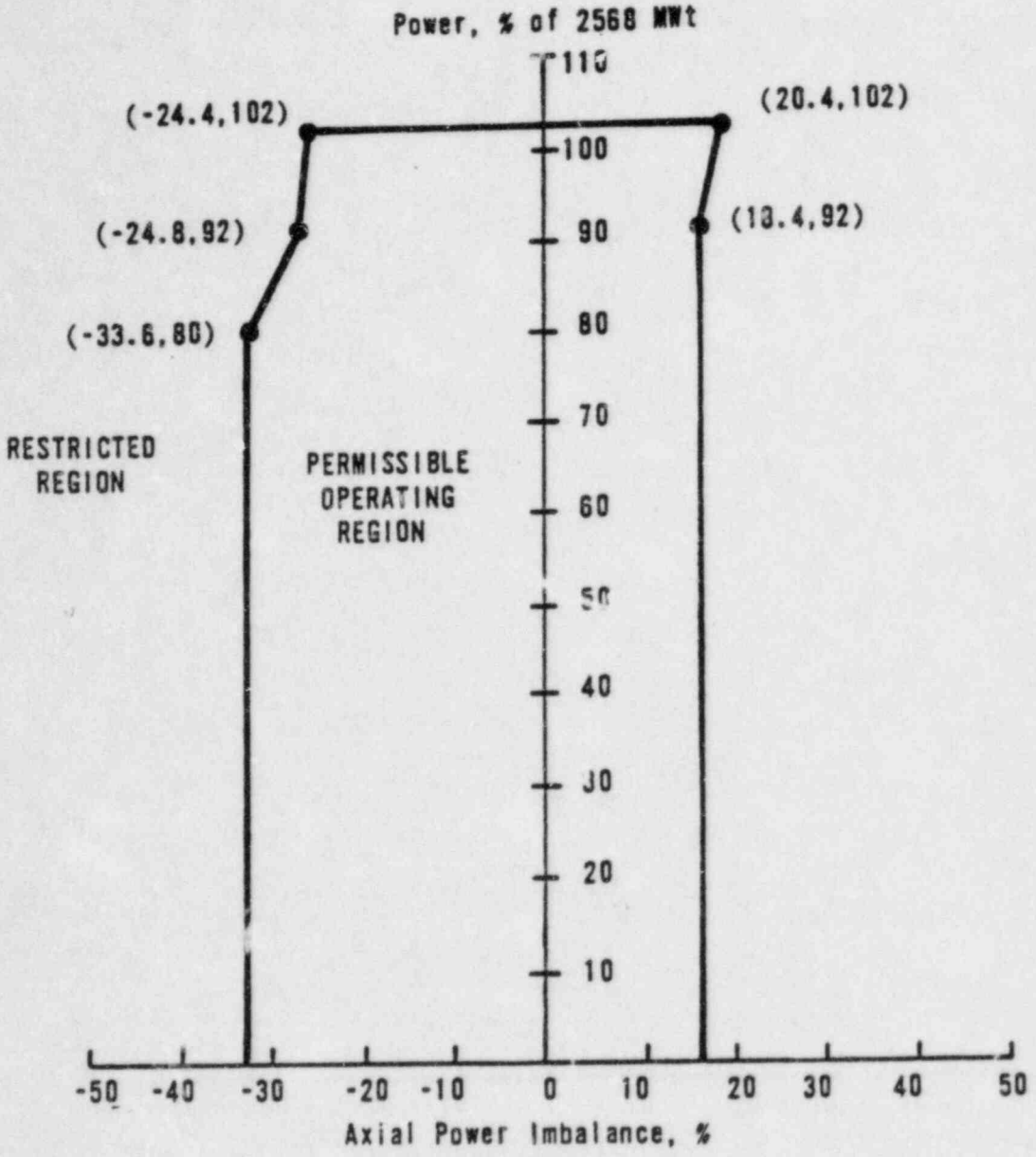

Figure 7-8 APSR Position Limits,
(From 0 to 200 ± 10 EFPD)

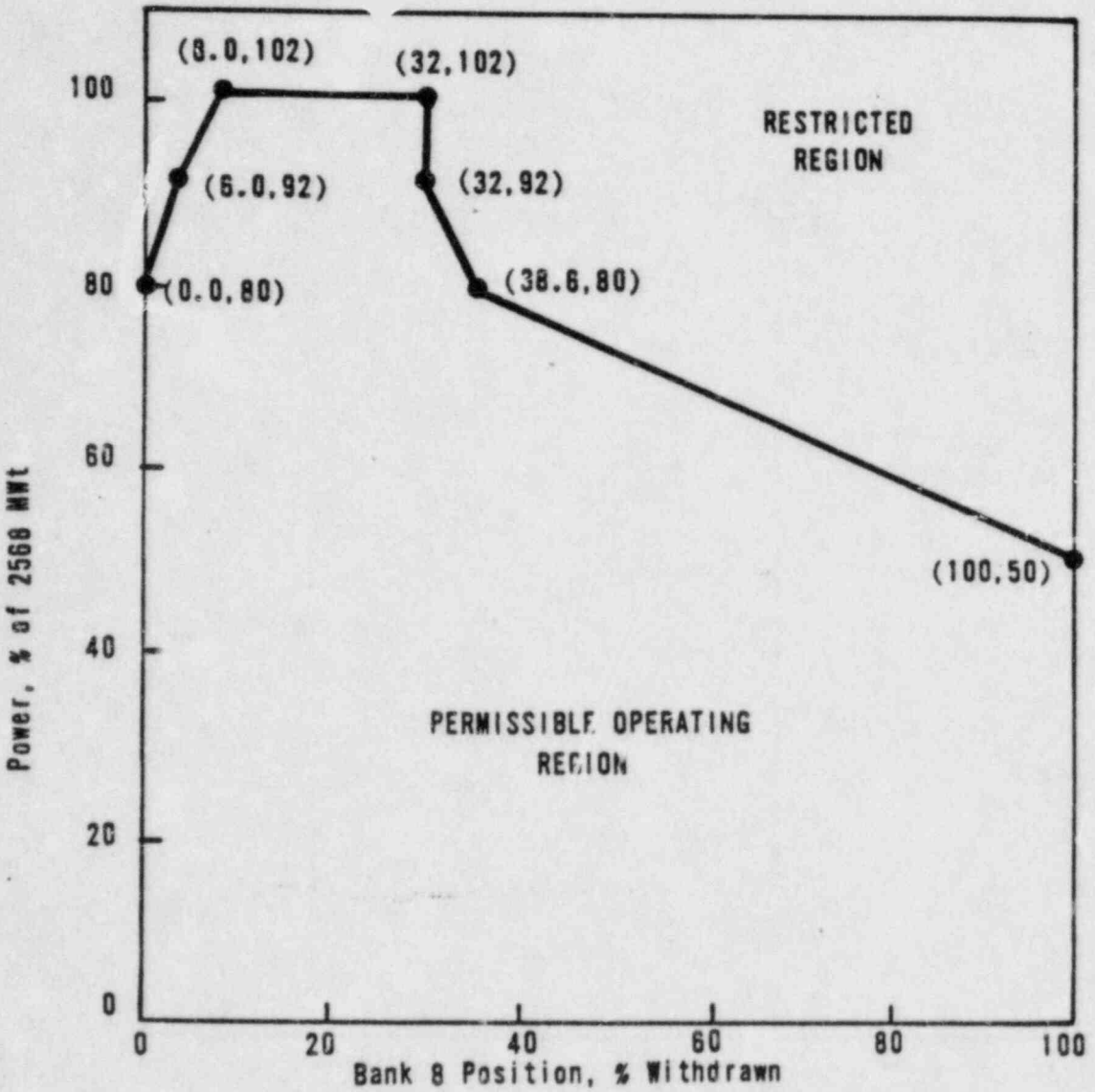

8. ACCIDENT ANALYSIS REVIEW

8.1 Introduction

A major aspect of the safety consideration of a reactor is the safety analysis of postulated accidents. These safety analyses enable one to confirm that the reactor system is designed to mitigate such events and that the resulting consequences of such events are acceptable. The most important considerations affecting the calculated consequences of the various postulated accidents are (a) the values of plant parameters assumed in the analysis, (b) the performance characteristics of the mitigating systems assumed in the analysis, and (c) the analytical models used. In general, the accident analyses documented in the FSAR[8] and Fuel Densification Reports[2 3 4 & 5] are based on values of plant parameters that correspond to the most adverse conditions expected to exist throughout the life of the plant, are based on conservative performance characteristics of the mitigating systems, and were performed utilizing generally accepted analytical methodology. Therefore, the reference safety analyses (FSAR and Fuel Densification Analysis Reports) are intended to be valid for the entire life of the plant.

The primary goal of safety analysis during the reload design process is to ensure the continued safe operation of the facility with the refueled core. The reference safety analyses and facility Technical Specifications establish the bases and conditions for safe operation of the initial core. An equivalent level of safety for the refueled core is established when it is determined that the reload design satisfies the original bases and conditions. In particular, the accident analyses contained in the licensing basis safety analyses remain valid if a reload design predicts steady-state and transient parameters that lie within the ranges of the values assumed in the original analyses. Thus, reload safety analysis may consist of verifying that the core physics, fuel performance, thermal-hydraulic, and mechanical design parameters for the reload design are bounded by the licensing basis analysis values.

8.2 Overview of Accident Analysis Review

The role of accident analysis review in typical Oconee reload design consists of a systematic review of the reference analysis of all postulated accidents. In this review each accident is examined by comparing the values of important plant parameters and RPS trip functions and trip setpoints assumed in the reference accident analysis to the corresponding values predicted for the fuel cycle under consideration. The safety parameters of interest for the reload cycle are obtained from appropriate nuclear design, thermal-hydraulic design, and fuel performance analyses. If the safety analysis review confirms that all pertinent plant parameters and RPS trip functions and trip setpoints for the reload cycle are conservative with respect to their values assumed in the accident analyses, it is concluded that the reference accident analyses continue to be valid for the fuel cycle, and therefore in these situations no reanalyses of accidents are performed. If, however, one or more plant parameters or RPS trip functions or trip setpoints assumed in the reference accident analyses are found to be non-conservative for the fuel cycle, a reanalysis of affected accidents is performed. This process is shown schematically in Figure 8-1.

The safety parameters of interest for the reload cycle are obtained from appropriate nuclear design, thermal-hydraulic design, and fuel performance analyses. Table 8-1 presents a list of the key safety parameters that are reviewed for each reload design. The table indicates the conservative direction that each parameter value should take relative to the reference analysis value.

In addition to the safety parameters addressed above, the reference analyses also incorporate the RPS trip functions and setpoints. (The role of the functions and the determination of the setpoint values is discussed in Chapter 7 of this report.) If a particular reload design results in revised setpoint values, a review of the reference accident analyses is performed and the effect of the revision on the analyses is evaluated.

In some cases, the reference analysis calculations explicitly include the various conservative engineering factors, densification and rod bow factors, and fuel pin design parameters. If a reload design results in changes in these values, their impact on the reference analyses is evaluated.

8.3 Discussion of Individual Accidents

A discussion of each of the accidents addressed in the reference analyses follows. For each event, a brief description of the accident is followed by a listing and discussion of the key safety parameters associated with the accident.

8.3.1 Uncompensated Operating Reactivity Changes

8.3.1.1 Accident Description

During the normal operation of the reactor, the overall reactivity of the core changes because of fuel depletion and variations in fission product poison concentrations. These reactivity changes, if not compensated for, could produce an increase or decrease in reactor power (depending on the direction of the reactivity change) and consequently change the fuel and moderator temperatures. Ultimately, core operating limits could be exceeded.

Normal functioning of the Integrated Control System would compensate for the reactivity changes. In the absence of automatic or manual compensatory responses, the reactor coolant system average temperature will change to compensate for the reactivity disturbances.

The reference analyses demonstrate that the reactor protective system prevents safety limits from being exceeded.

8.3.1.2 Key Safety Parameters

The reference analyses are based on the following parameter values:

Doppler Coefficient, $\Delta k/k/°F$	-1.17×10^{-5}
Moderator Temperature Coefficient, $\Delta k/k/°F$	$+0.5 \times 10^{-4}$

These values are representative of beginning of core life for the first cycle and provide least negative bounds for the expected range of values. That is, more negative (less positive) values would lessen the severity of the accident by amplifying the compensating moderator and Doppler feedback effects.

8.3.2 Start-Up Accident

8.3.2.1 Accident Description

During reactor startup, an uncontrolled positive reactivity insertion by maloperation of control rods could result in a nuclear excursion. In addition to the Reactor Protection System trip functions, several design features have been utilized to minimize the possibility of inadvertent rod withdrawal. In the absence of all other protection actions, the excursion is terminated by the negative Doppler coefficient.

The core protection criteria for this accident specify that the reactor thermal power shall not exceed 112% FP and that the RCS pressure not exceed code allowable limits.

The reference analyses demonstrate that the reactor is completely protected against any startup accident involving the withdrawal of any or all control rods, since in no case does the thermal power exceed 112% and peak pressure never exceeds code allowable limits.

8.3.2.2 Key Safety Parameters

The reference analyses are based on the following parameter values:

Doppler Coefficient, $\Delta k/k/°F$	-1.17×10^{-5}
Moderator Temperature Coefficient, $\Delta k/k/°F$	$+0.5 \times 10^{-4}$
Total Rod Worth, $\Delta k/k$	10.0

The reactivity coefficient values are representative of beginning of core life for the first core and provide a least negative bound for the expected range of values. That is, more negative (less positive) values would lessen the severity of the accident by amplifying the compensating moderator and Doppler feedback effects. The total rod worth value is a maximum worth that provides for the largest positive reactivity insertion.

8.3.3 Rod Withdrawal Accident at Rated Power Operation

8.3.3.1 Accident Description

A rod withdrawal accident presupposes an operator error or equipment failure which results in accidental withdrawal of a control rod group while the reactor is at rated power. As a result, the power level increases, the coolant and fuel rod temperatures increase, and core damage would eventually occur if the withdrawal were not terminated by operator or protection system action.

The reference analysis of this accident utilizes Reactor Protection System action to mitigate the effects of the rod withdrawal and demonstrates that thermal power and system pressure remain below acceptable limits. These results satisfy the core protection criteria for this accident.

8.3.3.2 Key Safety Parameters

The reference analyses are based on the following parameter values:

Doppler Coefficient, $\Delta k/k/°F$	-1.17×10^{-5}
Moderator Temperature Coefficient, $\Delta k/k/°F$	$+0.5 \times 10^{-4}$
Total Rod Worth, % $\Delta k/k$	10.0

The reactivity coefficient values are representative of beginning of core life for the first cycle and provide least negative bounds for the expected range of values. That is, more negative (less positive) values would lessen the severity of the accident by amplifying the compensating moderator and Doppler feedback effects. The total rod worth value is a maximum worth that provides for the largest positive reactivity insertion.

8.3.4 Moderator Dilution Accident

8.3.4.1 Accident Description

Moderator dilution, a periodic operational procedure, occurs when the soluble boron concentration of the coolant make-up flow is less than the average concentration of the coolant in the primary system. An uncontrolled moderator dilution accident occurs when the process continues for long periods of time at excessive make-up flow rates. The postive reactivity insertion caused by the decreasing soluble boron concentration would cause an increase in reactor power and hence increased coolant and fuel rod temperatures.

The automatic dilution process incorporates several design interlocks and alarms to prevent improper operation. However, if a dilution accident were to occur, the Reactor Protection System would function to safely mitigate the event.

The criteria for reactor protection for this accident are:

1. Reactor thermal power shall be less than 112% FP.

2. RCS pressure shall be less than the code allowable limits.

3. The reactor minimum shutdown margin of 1% $\Delta k/k$ subcritical shall be maintained.

The reference analyses evaluate plant responses to dilution rates ranging from 70 gpm to 500 gpm of unborated make-up water. In all cases, thermal power and system pressure remain below the specified limits and the shutdown margin is maintained. Additional analyses demonstrate complete protection during refueling operations.

8.3.4.2 Key Safety Parameters

Doppler Coefficient, $\Delta k/k/°F$	-1.17×10^{-5}
Moderator Temperature Coefficient, $\Delta k/k/°F$	$+0.94 \times 10^{-4}$
Boron Worth, ppm/% $\Delta k/k$	75

The reactivity coefficient values are representative of beginning of core life conditions and provide least negative bounds on the range of expected values. More negative (less positive) values would lessen the severity of the accident by amplifying the compensating moderator and Doppler feedback effects. The boron worth value is a conservatively low value (high reactivity worth per ppm) that produces a high positive reactivity insertion rate.

8.3.5 Cold Water Accident

8.3.5.1 Accident Description

A cold water accident involves the introduction of a slug of coolant water into the reactor core with a temperature lower than that of the coolant in the core. Or, a cold water accident may involve a sudden increase in reactor coolant flow rate (idle pump startup) which would reduce the average coolant temperature in the core. In the presence of negative reactivity coefficients, a reduction in coolant and fuel temperatures would yield a positive reactivity insertion and thus increase the power level.

The power increase response to this type of accident is inherently self-limiting due to the compensating reactivity feedback effects. Furthermore, the Reactor Protection System provides a high neutron flux trip function. The protection criteria for this accident are that the minimum DNBR be greater than 1.3 and that system pressure limits not be exceeded.

The reference analysis for this event demonstrates that thermal power and system pressure remain below the specified limits and DNBR remains above 1.3.

8.3.5.2 Key Safety Parameters

The reference analysis is based on the following parameter values:

Doppler Coefficient, $\Delta k/k/°F$	-1.3×10^{-5}
Moderator Temperature Coefficient, $\Delta k/k/°F$	-3.0×10^{-4}

The MTC value is representative of end of core life conditions and provides a most negative bound on the range of expected values. A less negative value would lessen the severity of the accident by decreasing the positive reactivity insertion. The Doppler value assumed is a conservative, least negative bound. Values in the conservative direction (more negative) would also lessen the severity of the accident through enhanced feedback effects during a power increase.

8.3.6 Loss of Coolant Flow

8.3.6.1 Accident Description

A reduction in reactor coolant flow rate occurs if one or more of the reactor coolant pumps should fail. A pumping failure can occur from mechanical failures or from a loss of electrical power. The effects of loss or reduction in coolant flow are an increase in coolant temperature and system pressure which could result in exceeding the core thermal limits if the reactor is not tripped promptly. The core protection criteria of concern in this event is the minimum DNBR, which must be greater than 1.3 for electrical malfunction events and greater than 1.0 for mechanical malfunction events. Reactor protection is provided by three RPS trip functions: power - number of RC pumps, power - flow - imbalance, and RC pressure - temperature.

The reference analyses demonstrate that the reactor can sustain a loss-of-coolant-flow accident without damage to the fuel. The minimum DNBR reached for the loss of flow due to electrical failure analyses was greater than 1.3. The analysis for the loss of flow due to mechanical failure (locked rotor) demonstrated a minimum DNBR greater than 1.0.

8.3.6.2 Key Safety Parameters

The reference analyses were based on the following parameter values:

Doppler Coefficient, $\Delta k/k/°F$	-1.2×10^{-5}
Moderator Temperature Coefficient, $\Delta k/k/°F$	$+0.5 \times 10^{-4}$

Reactor Coolant Flow, gpm	352,000
Core Power Peaking Factors	
radial-local	1.783
axial (cosine)	1.5

These reactivity coefficient values provide least negative bounds for the expected range of values. More negative values would amplify the compensating feedback effects due to increasing temperatures. The assumed reactor coolant flow is extremely conservative compared to the available flow (greater than 108.5%). The core power peaking factors considered in this analysis are those corresponding to the maximum design condition. The combination of 1.783 (radial-local) x 1.5 (axial cosine) is more conservative with respect to DNBR criteria than any other power shape that exists in typical reload cores.

In addition, the effects of a loss of coolant flow accident are strongly influenced by the flow coastdown characteristics, fuel densification and rod bow effects, and hot channel power peak augmentation factors. These parameters are not expected to change during the normal reload design process. If changes do occur, their impact on the reference analyses will be evaluated.

8.3.7 Stuck-Out, Stuck-In, or Dropped-In Control Rod Accident

8.3.7.1 Accident Description

In the event that a control rod becomes significantly misaligned from the other control rods in its group, the effect of such a condition on localized power peaking (flux distortion) and on available shutdown margin must be considered. A stuck-out control rod reduces the available shutdown worth and hence reduces the shutdown margin. The effects of this accident are mitigated by requiring a shutdown margin of 1% $\Delta k/k$, with the control rod of greatest worth fully withdrawn from the core. A stuck-in or dropped-in control rod causes neutron flux distortions that could result in localized power densities and heat fluxes in excess of the design limits if the reactor is allowed to return to full power. The effects of this type of accident are mitigated by

providing sufficient margin between the expected, distorted power peaks and the design limits to prevent the limits from being exceeded. The core protection criteria of concern for these events are that the minimum DNBR shall be greater than 1.3 and that the system pressure shall not exceed code allowable limits.

The reference analyses demonstrate that, even in the absence of ICS action (to accomplish a power runback to 60% FP) or a reactor trip, thermal power does not exceed the original values nor does system pressure exceed allowable limits.

8.3.7.2 Key Safety Parameters

The reference analyses are based upon the following parameter values:

Doppler Coefficient, $\Delta k/k/°F$	-1.3×10^{-5}
Moderator Temperature Coefficient, $\Delta k/k/°F$	-3.0×10^{-4}
Maximum Dropped Control Rod Worth, % $\Delta k/k$	
HFP, No Xe	0.46
HFP, W/Xe	0.36

The MTC value is representative of end of core life conditions and maximizes the positive reactivity insertion during the initial temperature decrease. The Doppler value is a conservative, least negative value that minimizes the compensating feedback effects during a return to power.

8.3.8 Loss of Electric Power

8.3.8.1 Loss of Load Transient

8.3.8.1.1 Accident Description

The effect of of a loss-of-load condition on a unit would be that the unit generator breakers would open and thus disconnect the unit from the transmission system. When this occurs, a runback signal causes an automatic power reduction to 15 percent power. Depending on the initial power level at the time of the loss of load, the Reactor Protection System may initiate a reactor trip on high reactor coolant temperature or pressure.

The loss-of-load accident does not result in any fuel damage or excessive pressures on the reactor coolant system. There is no resultant radiological hazard to station operating personnel or to the public as only secondary system steam is discharged to the atmosphere. Unit operation with 1 percent defective fuel and 1 gpm steam generator tube leakage is demonstrated to be safe by the reference analyses. For these conditions, the steam relief accompanying a loss-of-load accident would not change the whole body dose because the primary contributors are normally released through the condenser air ejector.

8.3.8.1.2 Key Safety Parameters

The course and consequences of this accident are independent of the parameters affected in the reload design.

8.3.8.2 Complete Loss of All Station Power

8.3.8.2.1 Accident Description

The hypothetical initiator of this accident is the complete loss of all station power except the station batteries. The loss of power results in gravity insertion of the control rods and trip of the turbine stop valves. The main steam safety valves prevent excessive temperatures and pressures in the reactor coolant system. The reactor coolant system flow decays without fuel damage occurring, and decay heat removal is provided by natural circulation. The turbine-driven emergency feedwater pump, taking its suction from the condenser hotwell and upper surgetank, provides feedwater to the steam generators. Condenser cooling is maintained through a gravity feed line from Lake Keowee. The station batteries provide power for the necessary control and auxiliary systems.

The reference analyses demonstrate that neither fuel damage nor excessive pressures occur.

8.3.8.2.2 Key Safety Parameters

The course and consequences of this accident are independent of the parameters affected in the reload design.

8.3.9 Steam Line Failure

8.3.9.1 Accident Description

The steam line failure accident assumes a break in the secondary system pressure boundary that results in inadequate secondary pressure control. The worst case steam line failure involves the maximum break size (34 inch diameter) at rated power and end of core life. Under these conditions, the rapidly decreasing secondary pressure results in an excessive primary system cooldown which, under the influence of a negative moderator temperature coefficient, produces a positive reactivity insertion. If feedwater flow continues to the affected steam generator the excessive heat removal and concurrent primary cooldown will continue and the reactor may experience a return to low power levels if the positive reactivity inserted exceeds the shutdown margin. The reactor coolant contraction accompanying the primary cooldown may result in ECCS actuation.

The criteria for unit protection and the release of fission products to the environment are:

1. That the core will remain intact for effective core cooling, assuming minimum tripped rod worth with a stuck rod.

2. That no steam generator tube loss of primary boundary integrity will occur due to the loss of secondary pressure and resultant temperature gradients.

3. That doses will be within 10CFR100 limits.

The reference analyses consider three major accident scenarioes: (1) the base case that assumes proper ICS and operator actions; (2) a case that assumes ICS action but no operator action; and (3) a case that assumes neither ICS nor

operator action. The reference analyses demonstrate that the protection criteria are satisfied.

8.3.9.2 Key Safety Parameters

The reference analyses were based upon the following parameter values:

Doppler Coefficient, $\Delta k/k/°F$	-1.2×10^{-5}
Moderator Temperature Coefficient, $\Delta k/k/°F$	-3.0×10^{-4}
Available Scram Worth, % $\Delta k/k$	3.46

The MTC value used in the analyses provides a most negative bound for the expected range of values. Less negative values would decrease the positive reactivity insertion and thus lessen the severity of the accident. The Doppler Coefficient is a least negative value that minimizes the compensating feedback effects during a return to power. A minimum rod worth value yields the most adverse effects.

8.3.10 Steam Generator Tube Failures

8.3.10.1 Accident Description

The occurrence of a double-ended rupture of one steam generator tube would result in the release of the activity contained in the reactor coolant to the secondary system. The initial leak rate is in excess of the normal makeup flow and hence would result in a low reactor coolant system pressure or pressure-temperature trip. Continued primary to secondary flow would result in the automatic initiation of the high pressure injection system which would provide sufficient makeup to compensate for the tube leakage and thus terminate the depressurization.

The volume of primary coolant released to the atmosphere through steam relief would produce acceptable consequences.

8.3.10.2 Key Safety Parameters

The course and consequences of this accident are independent of the parameters affected in the reload design.

8.3.11 Fuel Handling Accidents

The reference analyses for the fuel handling accident are not affected by the reload design process.

8.3.12 Rod Ejection Accident

8.3.12.1 Accident Description

For reactivity to be added to the core at a rapid rate, physical failure of a pressure barrier component in the control rod drive assembly must occur. Such a failure could cause a pressure differential to act on a control rod assembly and rapidly eject the assembly from the core region. The power excursion due to the rapid increase in reactivity is limited by the Doppler effect and terminated by the Reactor Protection System.

The criterion for reactor protection in this accident is that the reactor will be operated in such a manner that a control rod ejection accident will not further damage the reactor coolant system.

The consequences of the rod ejection accident are largely dependent upon the rate at which thermal energy is released to the coolant. In turn, the amount of thermal energy is a function of the worth of the ejected rod and the initial power level. The reference analyses include calculations for a range of ejected rod worths at rated power and hot zero power and at beginning and end of core life. The effects of varying the Doppler and moderator coefficients and rod worths are also calculated. The analyses demonstrate that the reactivity transient resulting from this accident will be limited by the Doppler effect and terminated by the RPS with no serious core damage or additional loss of the coolant system integrity.

8 3.12.2 Key Safety Parameters

The reference analyses are based upon the following parameter values:

	BOL	EOL
Doppler Coefficient, Δk/k/°F	-1.17×10^{-5}	-1.33×10^{-5}
Moderator Temperature Coefficient, Δk/k/°F	$+0.5 \times 10^{-4}$	-3.0×10^{-4}
Delayed Neutron Fraction	0.0071	0.0053
Neutron Lifetime, μ_s	24.8	23.0
Ejected Rod Worth, % Δk/k		
HZP	1.0	1.0
HFP	0.65	0.65

The analyses calculate the effects of an ejected rod using a spectrum of reactivity coefficients between the values shown. The MTC bounds define the range of allowable values based upon Technical Specification limits. The results of the Doppler sensitivity study show the highest neutron power for the least negative coefficients. Thus, more negative values would lessen the severity of the accident. The kinetics parameters are nominal values that are representative of the range of values expected in the reload design work. The rod worth values provide upper limits for the calculations. Lower rod worths would lessen the severity of the accident.

8.3.13 loss of Coolant Accident

8.3.13.1 Accident Description

A loss of coolant accident (LOCA) occurs when a break in the reactor coolant pressure boundary results in coolant expulsion in excess of the normal make-up flow rate. The blowdown rate, the time period before reactor trip and ECCS actuation and the amount of stored energy initially removed from the core are all dependent upon the break size. In order to evaluate this accident, a range of rupture sizes from small leaks up to the complete severance of a 36 inch ID primary coolant pipe have been evaluated.

Should a break occur, depressurization of the RCS causes coolant to flow out of the pressurizer into the primary loop resulting in a pressure and level decrease in the pressurizer. A reactor trip occurs when the low pressure or pressure-temperature trip setpoints are reached. The Engineered Safeguards system is actuated when the appropriate setpoints are reached. The consequences of the accident are limited in two ways:

1. The reactor trip and borated water injection complement void formation in causing a rapid decrease in nuclear power to a residual level corresponding to the delayed fission and fission product decay.

2. Injection of borated water ensures sufficient flooding of the core to prevent excessive clad temperatures.

The core protection criteria for a LOCA are specified in the regulatory requirements of 10CFR50.46. Briefly, the five criteria are:

1. The peak cladding temperature shall not exceed 2200°F.

2. The percentage of local cladding oxidation shall not exceed 17%.

3. The percentage of hydrogen generation resulting from whole-core cladding oxidation shall not exceed 1%.

4. Calculated changes in the core geometry shall be such that the core remains amenable to cooling.

5. The mode of long term cooling shall be established.

The reference analyses[11] demonstrate that these criteria are satisfied at all times.

8.3.13.2 Key Safety Parameters

The reference analyses are based upon two major input parameters that are affected by the reload design process. They are:

Average Fuel Temperature, °F (@ 18 kw/ft)		3120
Peak Linear Heat Rate, kw/ft		
Core Elevation, ft	2	15.5
	4	16.6
	6	18.0
	8	17.0
	10	16.0

These parameter values are the limiting values applicable to the generic ECCS analysis.

Table 8-1

ACCIDENT ANALYSIS REVIEW

KEY SAFETY PARAMETER CHECKLIST

Parameter (Units)	Reference Analysis Value(s)	Conservative Direction	Reload Cycle Value(s)
Doppler Coefficient, $\Delta k/k/°F$	-1.17×10^{-5}	more negative	
Moderator Temperature Coefficient, $\Delta k/k/°F$	BOL $+0.5 \times 10^{-4}$ EOL -3.0×10^{-4}	less positive less negative	
Delayed Neutron Fraction, (nominal)	BOL 0.0071 EOL 0.0053		
Neutron Lifetime (nominal), micro-seconds	BOL 24.8 EOL 23.0		
Total Rod Worth, % $\Delta k/k$	10.0	smaller	
Maximum Ejected Rod Worth, % $\Delta k/k$	HFP 0.65 HZP 1.0	smaller smaller	
Maximum Dropped Rod Worth, % $\Delta k/k$	HFP, no Xe 0.46 HFP, w/Xe 0.36	smaller smaller	
Minimum Tripped Rod Worth (for SLB), % $\Delta k/k$	3.46	larger	
Minimum Shutdown Margin, % $\Delta k/k$	1.0	larger	

Table 8-1 (cont'd)

ACCIDENT ANALYSIS REVIEW

KEY SAFETY PARAMETER CHECKLIST

Parameter (Units)	Reference Analysis Value(s)	Conservative Direction	Reload Cycle Value(s)
Boron Worth, PPM/ % Δk/k	75	larger	
Average Fuel Temperature at 18 kW/ ft, °F	3120	smaller	
Peak Linear Heat Rate, kΔ/ft			
Core Elevation, ft 2	15.5	smaller	
4	16.6	smaller	
6	18.0	smaller	
8	17.0	smaller	
10	16.0	smaller	
Reactor Coolant Flow, gpm	352,000	larger	
Core Power Peaking Factors			
radial-local	1.783	smaller	
axial (cosine)	1.5	smaller	

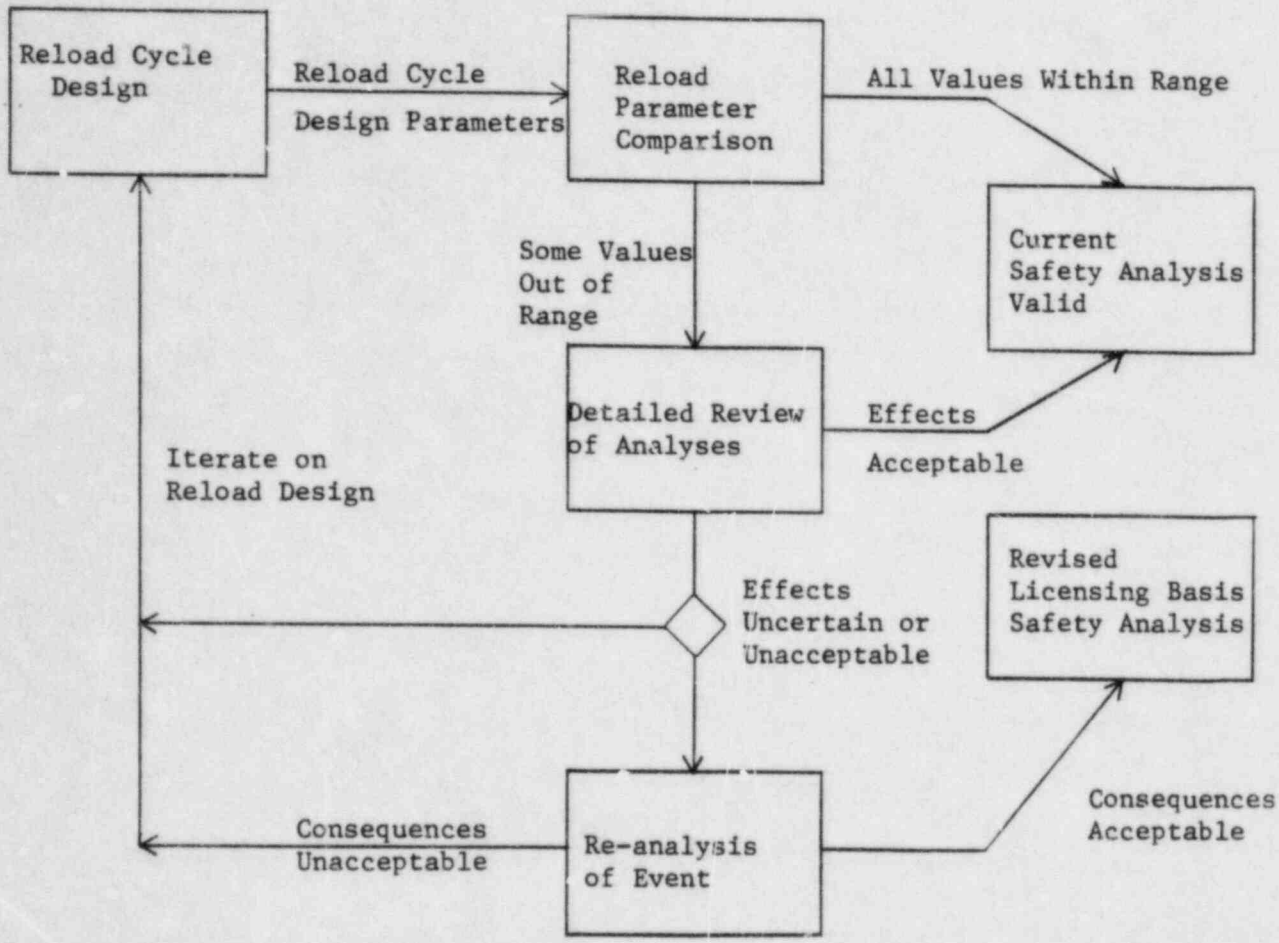

Figure 8-1

Accident Analysis Review Process

9. DEVELOPMENT OF CORE PHYSICS PARAMETERS

Upon completion of the Final Fuel Cycle Design and the Maneuvering Analysis both PDQØ7 and EPRI-NODE depletions, rod scans, boron concentrations and worths, power distributions, etc. have been generated primarily for HFP and some HZP conditions. The purpose of this stage of developing core physics parameters is to provide additional calculations to supplement those already performed. The results of these calculations are used for startup test predictions and core physics parameters throughout the cycle.

9.1 Startup Test Predictions

After each refueling, the reactor undergoes a startup test program aimed at verifying that the reactor core is correctly loaded, control rods are in the correct locations and are functioning properly, and to verify reactor behavior is as predicted by the nuclear simulators which were used in generating the data used in the plant's safety analysis.

9.1.1 Critical Boron Concentrations and Boron Worths

EPRI-NODE and/or PDQØ7 may be used to calculate critical boron concentrations and boron worths at a variety of rod configurations, at HZP and HFP, as a function boron concentration, at different xenon concentrations, and at different times in the fuel cycle. EPRI-NODE and PDQØ7 both are capable of critical boron searches and when critical boron concentrations are desired are usually run in this mode. An acceptable alternative, however, is to not search on critical boron but to correct the input boron concentration to the critical boron concentration using a calculated boron worth and the calculated reactivity.

Table 9-1 shows some of the critical boron calculations normally performed for startup physics tests. Table 9-2 shows the soluble boron worths usually performed for startup physics tests. The boron worths are usually calculated by running two identical cases except that the soluble boron concentration is different. The differential boron worth is calculated by subtracting the reactivities and dividing by the boron difference. Differential boron worths are usually quoted in %ρ/100 PPM or in PPM/%ρ (the latter is sometimes referred to as the inverse boron worth).

Critical boron concentration at 68°F, 532°F, and HFP with all rods out except APSR's is calculated as a function of cycle burnup. Figure 9-1 illustrates the form in which these results are displayed.

Differential boron worth is calculated as a function of boron concentration and also as a function of cycle burnup. Figures 9-2 and 9-3 show the results of these types of calculations. Integral boron worth calculation is performed at BOC (4EFPD) as a function of boron concentration. The results of this are displayed in the format illustrated by Figure 9-4.

9.1.2 Xenon Worths

Xenon worth is calculated as a function of cycle burnup using either PDQØ7 or EPRI-NODE. The nominal HFP depletion cases with equilibrium xenon are used as input to a second set of cases where the xenon concentration is set to zero (or the xenon cross sections are set to zero). The difference in reactivities between the equilibrium xenon and no xenon cases equals the equilibrium xenon worth at HFP. The results are displayed in a format similar to Figure 9-5.

9.1.3 Rod Worths

9.1.3.1 Group Worths

The worth of groups 1 to 8 and the integral rod worth curves for groups 5-7 are calculated at BOC HZP for use in the zero power physics testing. The rod groups are sequentially inserted or withdrawn from the EPRI-NODE calculation assuming no control rod overlap. The group worth is the difference in reactivity between the fully inserted case and the fully withdrawn case.

At HFP equilibrium xenon BOC (4EFPD), the above rod worths are calculated in a similar manner except that when calculating the intergral rod worth curves a control rod overlap of 25% is used.

At HFP and HZP group 8 rod scans are performed where group 8 is stepped in small increments into or out of the core. The HZP results are used to provide tables of rod worth versus position and plots of relative rod worth versus position. The HFP results are used to provide the same information plus a table of imbalance as a function of rod index. Rod scans on group 7 are performed at BOC HFP to provide a table of imbalance versus rod position.

9.1.3.2 Stuck Rod Worth

The maximum worth of a single control rod stuck out of the reactor core at HZP is calculated during the final fuel cycle design. The worth of the stuck rod is used by the site engineers in the reactivity balance procedures to guarantee shutdown margin. If the stuck rod worth is to be measured during the startup test program, then a recalculation of the worth is performed simulating the test conditions. This worth would then be provided as a startup test prediction.

9.1.3.3 Dropped Rod Worth

The maximum worth of a single control rod dropped into the reactor core is calculated during the final fuel cycle design. If this parameter is to be measured during the startup test program, then a recalculation of the worth is performed simulating the test conditions. This worth would then be provided as a startup test prediction.

9.1.3.4 Ejected Rod Worth

During startup physics testing the maximum ejected control rod worth at HZP is measured and compared to the predicted worth. The maximum ejected rod worth is calculated during the final fuel cycle design (Section 3.2.2.3) and a recalculation of this parameter is not usually necessary since the calculation is performed at conditions similar to those used in the testing.

9.1.4 Reactivity Coefficients

9.1.4.1 HZP Coefficients

At HZP the isothermal temperature coefficient is measured by reducing the average moderator temperature 5°F to 527°F taking data once equilibrium is reached then increasing the temperature 10°F to 537°F taking data and establishing equilibrium. The temperature is then reduced 5°F back to the original 532°F value. The calculations used for predicting the isothermal temperature coefficient should be run at 527°F and 537°F using either EPRI-NODE or PDQØ7. The resulting reactivity change is then divided by the 10°F temperature change to yield the HZP isothermal temperature coefficient.

The Doppler or fuel temperature coefficient at HZP can be calculated by varying the fuel temperature while maintaining the moderator temperature constant at 532°F. The resulting reactivity change divided by the change in fuel temperature is the Doppler coefficient at HZP.

The predicted moderator coefficient is calculated by subtracting the Doppler coefficient from the isothermal coefficient and is compared to the measured moderator coefficient obtained by subtracting the predicted Doppler coefficient from the measured isothermal coefficient. Alternately, the moderator temperature coefficient can also be explicitly calculated.

9.1.4.2 HFP Coefficients

Both a temperature coefficient of reactivity and a power doppler coefficient of

reactivity are measured at HFP. Changes in temperature or power are compensated for by control rod insertion or withdrawal. A calculated Doppler coefficient is subtracted from the temperature coefficient to obtain the moderator coefficient.

A moderator coefficient is calculated by running one equilibrium HFP case at BOC (4EFPD EPRI-NODE or PDQØ7) and a second case which has lowered the moderator temperature $5^{o}F$. The difference in reactivity divided by the temperature change is the moderator coefficient. | 1

A third case is run to determine the power doppler. In this case the power level is reduced to 95% HFP. The difference in reactivity between the HFP and the 95% HFP cases divided by 5% FP is the power doppler coefficient. | 1

9.1.5 Power Distributions

Power distributions, both assembly radial and total peaking factors, are measured at 40 and 100% HFP for Oconee reload startups. Calculations using EPRI-NODE are run at these power levels and nominal conditions to provide predicted power distributions to compare to measured. Typical power distributions generated are shown in Table 9-3. | 1

9.1.6 Kinetics Parameters

Kinetics parameters are calculated using the methodology and codes as discussed in section 3.2.8. These parameters include the six group β^{i} effective and λ^{i}, total β effective and λ, and reactivity versus positive and negative doubling times. These kinetics parameters are generated for two sets of HZP conditions. The first is with group 8 inserted and the second is with groups 5 through 8 inserted. In addition to the BOC HZP parameters, one set of BOC HFP parameters are generated with groups 5-7 at 100% WD and group 8 at 37.5% WD. | 1

9.2 Core Physics Report

The purpose of the core physics report is to document the predicted behavior of the reactor core as a function of burnup and power level. It is intended to be used for operator guidance and the site engineer. Portions of the information included will reiterate data found in the final fuel cycle design report and the startup test prediction report, however, much data not needed for these reports is useful to the operator and site engineers.

This report will include sufficient information to calculate reactivity balance throughout the cycle. Table 9-4 lists items typical of what will be calculated for this report. Any additional calculations will be performed using either EPRI-NODE or PDQ07.

Table 9-1

CRITICAL BORON CONCENTRATIONS (PPM)

HZP, NOXE, ØEFPD

ARO

CRGP 1-7 out	CRGP8=37.5%WD
CRGP 7 in	CRGP8=37.5%WD
CRGP 6,7 in	CRGP8=37.5%WD
CRGP 5-7 in	CRGP8=37.5%WD
CRGP 4-7 in	CRGP8=37.5%WD
CRGP 3-7 in	CRGP8=37.5%WD
CRGP 2-7 in	CRGP8=37.5%WD
CRGP 1-7 in	CRGP8=37.5%WD

HFP, NOXE, ØEFPD

CRGP 1-6 out, CRGP 7 in,

CRGP 8=37.5%WD

HFP, EQXE, 4EFPD

ARO

CRGP 1-7 out	CRGP8=37.5%WD
CRGP 7 in	CRGP8=37.5%WD
CRGP 6,7 in	CRGP8=37.5%WD
CRGP 5-7 in	CRGP8=37.5%WD

HFP,EQXE,EOC

CRGP 1-7 out	CRGP8=37.5%WD

Table 9-2

BORON WORTH (PPMB/%Δρ)

HZP, NOXE, CRGP 7 and 8 in

Ø EFPD, XX PPMB

Ø EFPD, XXXX PPMB

Rod Patch, XXX PPMB

EOC, XXX PPMB

HFP, EQXE, CRGP 7 and 8 in

4 EFPD, XXXX PPMB

Rod Patch, 17 PPMB

EOC, 17 PPMB

Table 9-3

RADIAL AND TOTAL PEAKING POWER MAPS

CONDITIONS

POWER LEVEL % HFP	BURNUP EFPD
40	2
100	4
100	12
100	25

1

Table 9-4

Core Physics Data

A. Critical Boron Concentrations
   1. ARO HFP Versus Burnup
   2. ARO HZP Versus Burnup
   3. ARO 68°F Versus Burnup

B. Critical Boron Concentrations required for 1% shutdown with highest worth rod stuck out (NoXe)
   1. HZP Versus Burnup
   2. 68°F Versus Burnup

C. Differential Boron Worth HFP, HZP versus burnup.

D. Power Distributions from the Cycle Depletion

E. Rod Worths BOC, EOC, HFP and HZP

F. Imbalance versus APSR position BOC, EOC at HFP

G. Imbalance versus Group 7 position BOC, EOC at HFP

H. Xenon worth versus Power Level

I. Xenon Worth versus Burnup

FIGURE 9-1

BORON LETDOWN CURVES

CRGP 1-7=100%WD

CRGR 8-37.5%WD

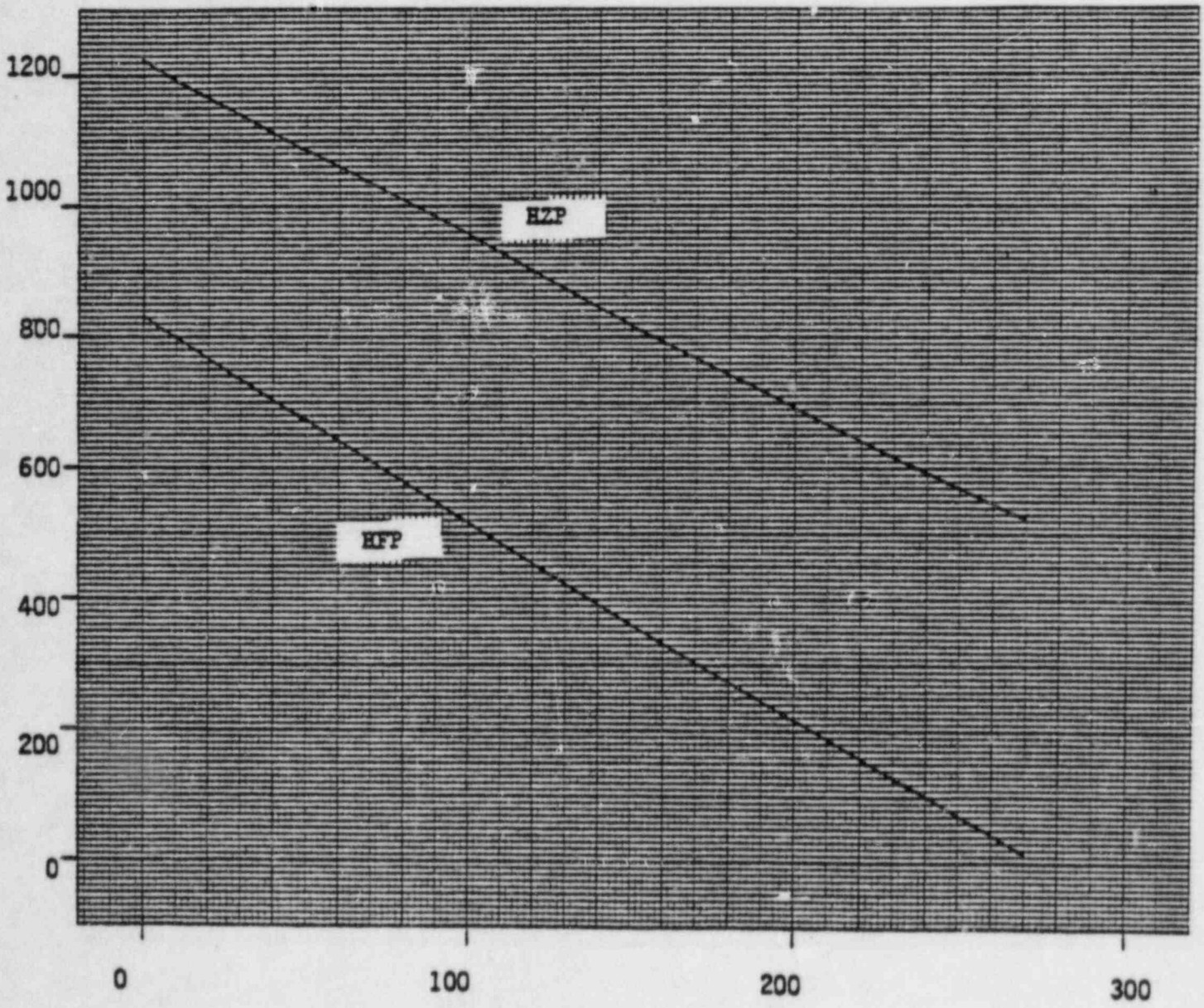

FIGURE 9-2

DIFFERENTIAL BORON WORTH

VERSUS BURNUP

HFP, EQXE

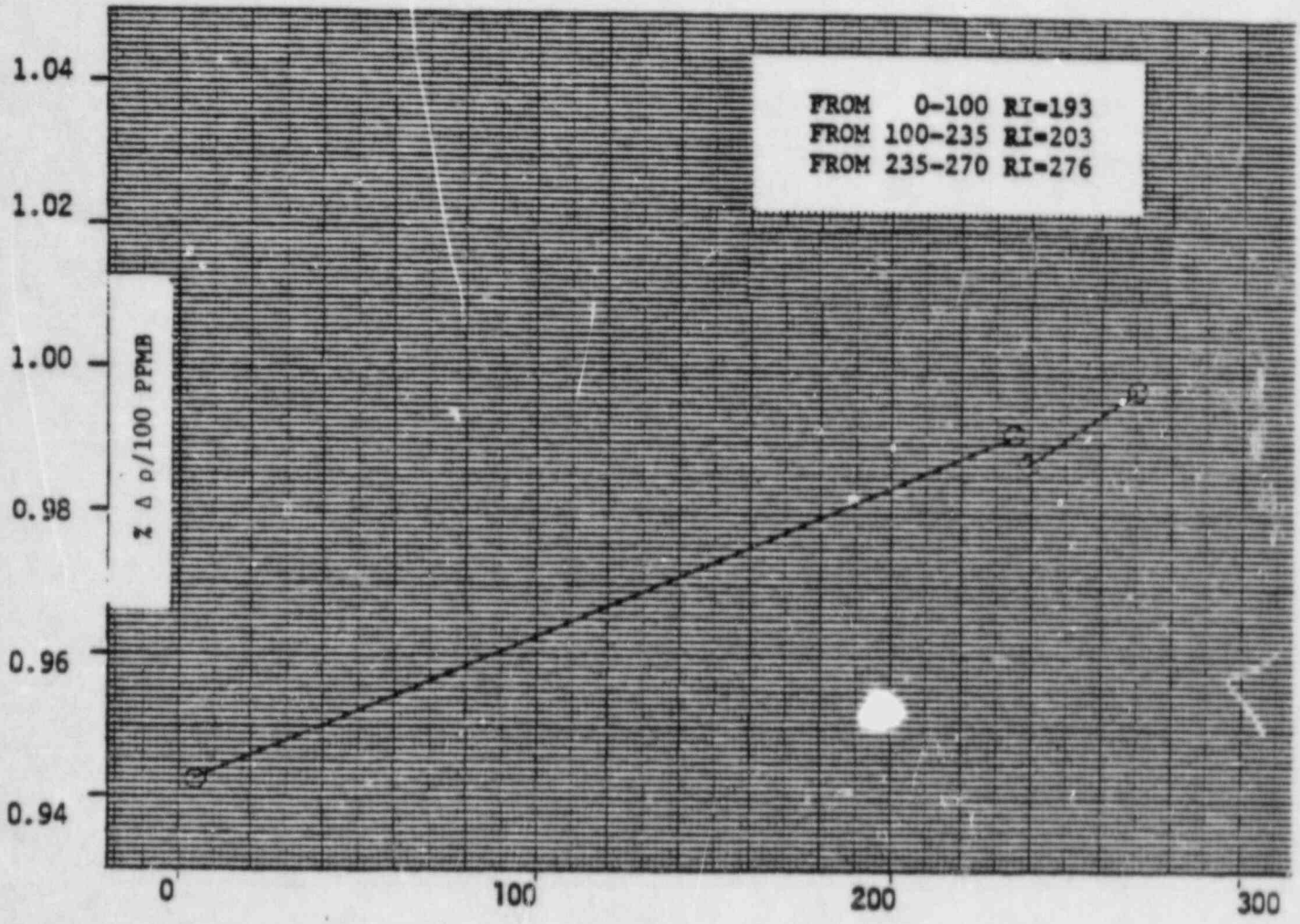

FIGURE 9-3

DIFFERENTIAL BORON WORTH

HFP, 4 EFPD, EQXE, RI=XXX

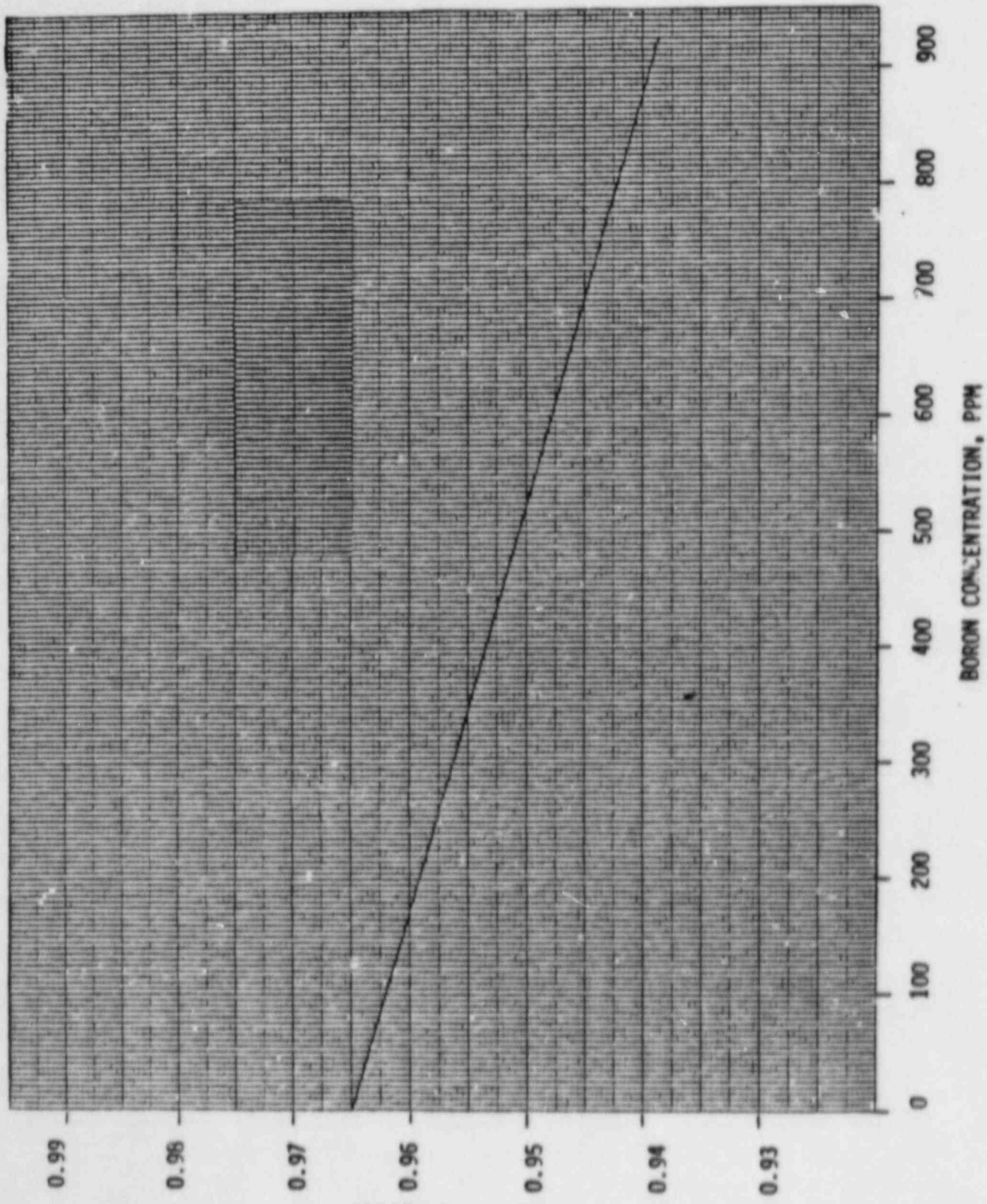

FIGURE 9-4

INTEGRAL BORON WORTH

HFP, 4 EFPD, EQXE, RI=XXX

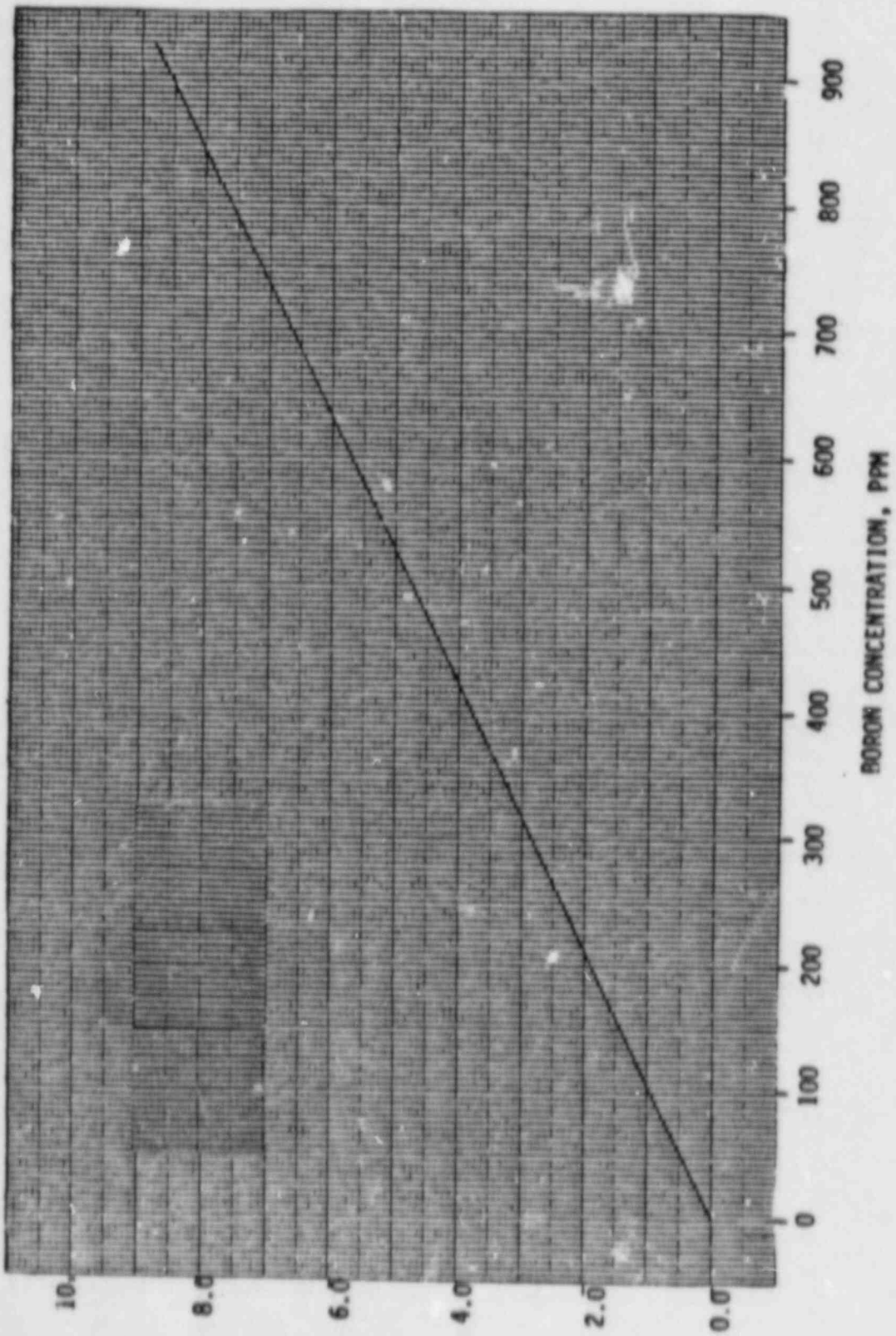

FIGURE 9-5

EQUILIBRIUM XENON WORTH
VERSUS BURNUP AT HFP

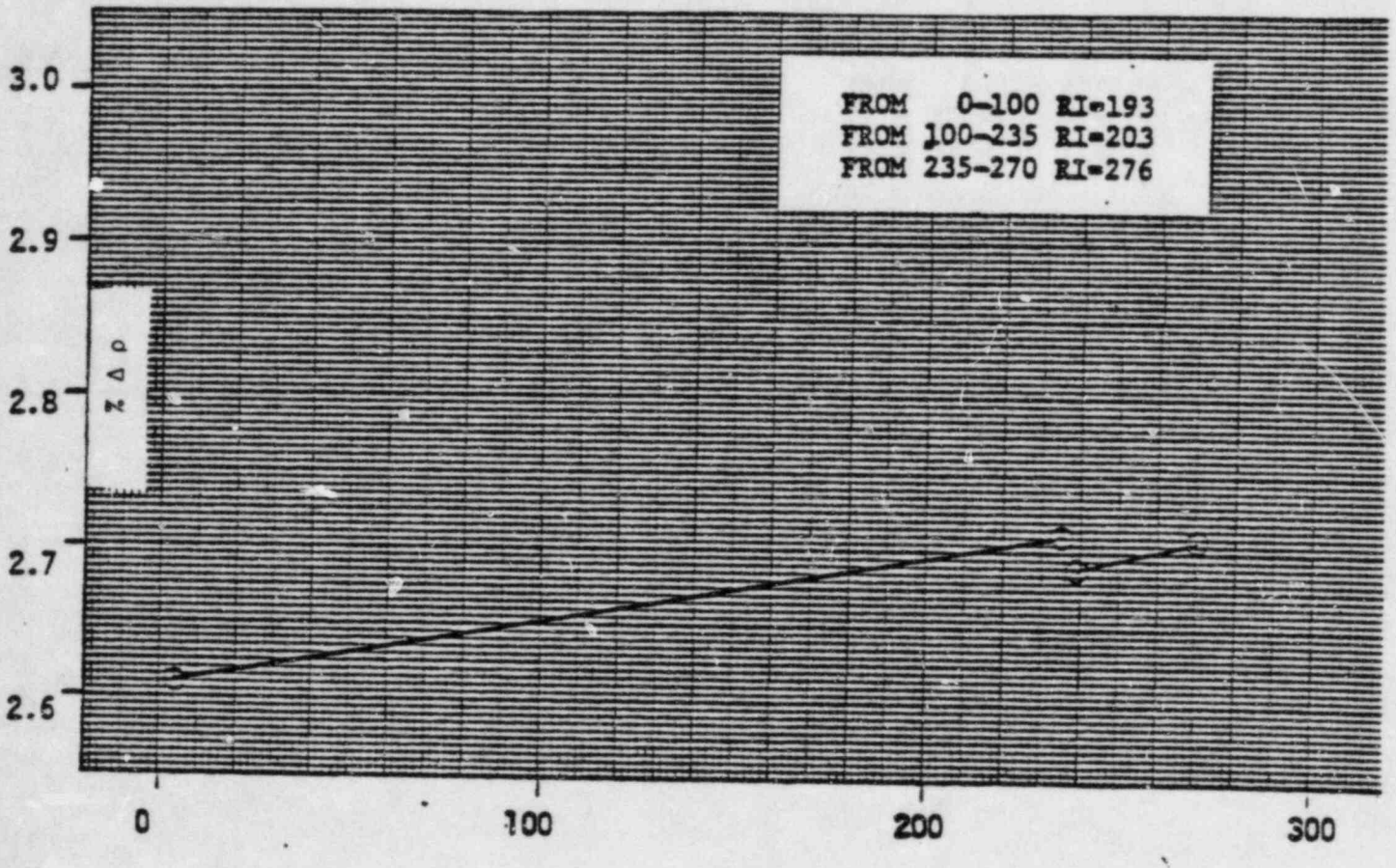

10. REFERENCES

1. Program to Determine In-Reactor Performance of B&W Fuels - Cladding Creep Collapse, BAW-10084, Rev. 2, Babcock & Wilcox, Lynchburg, Virginia, October, 1978. | 2

2. R. A. Turner, Fuel Densification Report, BAW-10054, Rev. 2, Babcock & Wilcox, Lynchburg, Virginia, May 1973.

3. Oconee 1 Fuel Densification Report, Revision 1, BAW-1387, Rev. 1, Babcock & Wilcox, Lynchburg, Virginia, April 1973.

4. A. J. Eckert, H. W. Wilson, and K. E. Yoon, Oconee 2 Fuel Densification Report, BAW-1395, Babcock & Wilcox, Lynchburg, Virginia, June 1973. | 3

5. Oconee 3 Fuel Densification Report, BAW-1399, Babcock & Wilcox, Lynchburg, Virginia, November 1973.

6. TACO2 - Fuel Pin Performance Analysis, BAW-10141, Babcock & Wilcox, Lynchburg, Virginia, August 1979. | 2

7. Correlation of Critical Heat Flux in a Bundle Cooled by Pressurized Water, BAW-10000A, Babcock & Wilcox, Lynchburg, Virginia, June 1976.

8. Oconee Nuclear Station, Units 1, 2, and 3, Final Safety Analysis Report, Docket Nos. 50-269, -270, and -287.

9. Electric Power Research Institute (EPRI), Advanced Recycle Methodology Program (ARMP) System Documentation, September 1977.

10. J. M. Alcorn and R. H. Wilson, CHATA - Core Hydraulics and Thermal Analysis, BAW-10110, Rev. 1, Babcock & Wilcox, Lynchburg, Virginia, May 1977. | 3

11. R. C. Jones, J. R. Biller, and B. M. Dunn, ECCS Analysis of B&W's 177-FA Lowered Loop NSS, BAW-10103A, Rev. 3, Babcock & Wilcox, Lynchburg, Virginia, July 1977. | 1

12. J. H. Taylor (B&W) to D. B. Vassallo (NRC), Letter, "Determination of the Fuel Rod Bow DNB Penalty," December 13, 1978. | 2

13. D. B. Vassallo (USNRC) to J. H. Taylor (B&W), Letter "Calculation of the Effect of Fuel Rod Bowing on the Critical Heat Flux for Pressurized Water Reactors," June 12, 1978. | 2

14. J. M. Alcorn, H. C. Cheatwood, C. D. Morgan, and R. H. Wilson, TEMP - Thermal Energy Mixing Program, BAW-10021, Babcock & Wilcox, Lynchburg, Virginia, April 1970. | 3

15. J. R. Gloudemans and H. C. Cheatwood, RADAR - Reactor Thermal and Hydraulic Analysis During Reactor Flow Coastdown, BAW-10069A, Rev. 1, Babcock & Wilcox, Lynchburg, Virginia, October 1974. | 3

16. TACO - Fuel Performance Analysis, BAW - 10087A, Rev. 1, Babcock & Wilcox, Lynchburg, Virginia, August 1977. | 4

APPENDIX A - CODE SUMMARY

Appendix A

Code Summary

CASMO

CASMO is a multigroup two-dimensional transport theory code for burnup calculations on BWR and PWR assemblies. This code has been developed by Studsvick Energiteknik AB and supported by EPRI. 1

CHATA

CHATA is a steady state closed channel thermal-hydraulic code which can be used in a multichannel or single channel configuration. It calculates flow, pressure drop, coolant properties, and DNBR. It has several different options that give it the capability to iterate on an input parameter, such as finding the maximum power for a specified DNBR and pressure drop. It can be used to calculate assembly-by-assembly core flow distribution and a hot channel analysis, and is suitable for parametric studies because of its short running time.

COMETHE-III-J

The COMETHE code calculates fuel pin thermal and mechanical behavior as a function of burnup. This code was developed by Belgo Nucleaire and licensed in this country by the S. M. Stoller Corp. EPRI is sponsoring the distribution and further development of this code for the utilities. The code does all the calculations described for TAFY and includes a relocation and cracking model to determine fuel-clad interaction forces.

CROV

The Creep Ovalization Analysis Program for Fuel Cladding (CROV) calculates ovality changes in fuel rod cladding due to thermal and irradiation induced creep. CROV conservatively predicts the ovality time history and time to collapse under a prescribed pressure, inside and outside temperature, and flux level time history loading.

The creep rate calculation utilizes a modified von Mises flow rule and includes a strain-hardening model. Empirical constants used in the creep rate equation are conservatively representative of B&W zircaloy-4 cladding at a temperature range between 600^{o}F and 750^{o}F.

DELAY

DELAY calculates core averaged delayed neutron fractions for six energy groups, core averaged decay constants for six energy groups, core averaged delayed neutron fraction with and without importance factor, estimated prompt neutron lifetime, and reactivity versus period. Input consists primarily of isotopic fission fractions versus burnup and enrichment from PDQØ7 calculations.

EPRI-CELL

EPRI-CELL computes the space, energy and burnup dependence of the neutron spectrum within cylindrical cells of Light Water Reactor fuel rods. Its primary output consists of broad group, microscopic, exposure dependent cross-sections for subsequent use in multidimensional diffusion theory depletion analysis. EPRI-CELL utilizes three industry accepted subcodes; GAM-1, THERMOS, and CINDER.

EPRI-CPM

EPRI-CPM is a multigroup two-dimensional collision probability code for burnup calculations on BWR and PWR assemblies. The code handles a geometry consisting of cylindrical fuel rods of varying composition in a square pitch array with allowance for fuel rods loaded with gadolinium, burnable absorber rods, cluster control rods, in-core instrument channels, water gaps, boron steel curtains and cruciform control rods in the regions separating fuel assemblies.

EPRI-FIT

EPRI-FIT is a program which processes the PDQØ7 integral file and calculates and edits values needed by the EPRI-NODE code. EPRI-FIT greatly reduces the hand calculation time needed to extract these values from the PDQØ7 printout and improves the quality assurance. A data file under the local name of COLOR is written which contains the EPRI-FIT edited data and is used as input to the SUPERLINK program.

EPRI-NODE

EPRI-NODE is a multidimensional model code similar in theory to FLARE. The EPRI-NODE program computes the core effective multiplication factor, the three-dimensional core power distribution, core coolant flow and temperature distribution, and fuel exposure distribution. The program includes the effects of partially inserted full-length control rods, part-length rods, and up to 13 different fuel assembly types with different enrichments and burnable absorber shim loadings. EPRI-NODE has a capacity to represent the core with 32 axial nodes for each fuel assembly and 30x30 nodes in the XY plane.

The program iterates to account for the interaction between power distribution and core nuclear properties which depend on coolant flow and coolant temperature distributions, fuel temperature distribution and xenon distribution. The program computes the time dependence of xenon following changes in power level and/or changes in power distribution. The program permits fuel shuffling from one location to another and fresh fuel insertion for burnup cycle calculations. Individual steps can by stacked for either xenon transient or fuel cycle burnup calculations.

EPRI-NUPUNCHER

NUPUNCHER prepares cross section tables in HARMONY format from cross section data produced by EPRI-CELL and placed on the ECDATA file. NUPUNCHER reduces significantly the tedious task of hand transferring values from the EPRI-CELL printout to macroscopic and microscopic tables in card image HARMONY format. Two, three and four group cross section data may be obtained with one dimensional HARMONY interpolating tables.

EPRI-PDQØ7 MODIFICATIONS

PDQØ7 is the industry accepted multigroup one, two, or three dimensional diffusion depletion code. EPRI-ARMP uses PDQØ7/Version II with minor modifications to allow options for mixed number density, improved removal treatment, peak power editing, and re-editing.

EPRI-SHUFFLE

The EPRI-SHUFFLE program will read a PDQØ7 concentration file, make certain modifications to this file, and write a new updated concentration file. This procedure is accomplished by defining "assembly regions" in the program input. Assembly regions are square arrays of mesh points containing depletable nuclide concentrations and superimposed on the original PDQØ7 geometry. These assembly regions are then used to describe the movement of existing nuclide concentrations by translation, reflection and/or rotation. In addition, new fuel concentrations can replace spent fuel concentrations in selected assembly regions described in the program's input.

EPRI-SUPERLINK

SUPERLINK accesses data on the files produced by EPRI-FIT and together with relevant input information for file management and for data processing control produces polynomial coefficients for use in EPRI-NODE.

PDQØ7

See EPRI-PDQØ7 Modifications.

NODE UTILITY CODE (NUC)

The NUC program is a package of subroutines that performs any necessary utility function to EPRI-NODE files. The major subroutines are:

I. FILE - this mode lists, merges, purges, adds, rearranges, edits, etc. the NODE cases on one or more history files.

II. FLEX - this mode takes an existing file, expands or collapses it to a new problem size, and then stores it on a new disk.

III. COPY - this mode copies a given history file from disk storage (working file) to magnetic tape storage (permanent backup file) and vice versa.

IV. MARGINS - this mode performs those operations which are necessary to calculate CFM, DNB, and LOCA margins from an input history file(s). It also plots the results in the form of a "fly speck" graph.

TACO2

TACO2 conservatively predicts fuel pin temperature and fuel pin pressure. It includes models for fuel densification, fuel swelling, fuel restructuring, gas release, cladding creep, and gap closure. 3

TEMP

TEMP is a steady state open channel thermal hydraulic code that considers energy mixing between channels and is used to calculate flow distribution among individual channels in an assembly or a cluster of fuel pins. It calculates flow, pressure drop, coolant parameters up the channel, and DNBR.

RADAR

RADAR performs a thermal analysis of a slow reactor transient such as the loss of a primary pump, computing as a function of time fuel pin and clad surface temperatures, DNBR, and coolant thermodynamic conditions when given pin power and either channel flow or pressure drop as a function of time.

TACO

TACO conservatively predicts fuel pin temperature and fuel pin pressure. It includes models for fuel densification, fuel swelling, fuel restructuring, gas release, cladding creep, and gap closure. 4

QUESTIONS AND ANSWERS

ATTACHMENT

DUKE POWER COMPANY
OCONEE NUCLEAR STATION

OCONEE RELOAD DESIGN METHODOLOGY TECHNICAL REPORT

RESPONSES TO NRC QUESTIONS OF OCTOBER 16, 1980

Q. 1. Paragraph 3.2.5. Reactivity Coefficients and Deficits.

The described procedure for the calculation of the reactivity deficits involves PDQ07 or EPRI-NODE. However, it is not clear whether for widely different states the reactivity difference due to the spectral component is also included. The same comment applies to the differential boron worth calculation.

A. 1. The lattice code EPRI-CELL does change cross section libraries as a function of moderator temperature. These cross sections are then used in PDQ07 Version 2 for both color set calculations, which lead to input for EPRI-NODE, and for quarter core calculations. Therefore, the spectral component is included in the calculations of reactivity coefficients and reactivity deficits.

The effects of soluble boron on the flux spectrum is accounted for in two ways. First the soluble boron concentration input to the EPRI-CELL fuel depletion is varied from 1200 ppm at BOL to 400 ppm at 6000 MWD/MTU and is held constant at this concentration for the rest of the depletion. Second, the non-fuel cross sections (eg. control rod guide tubes, reflector, etc.) are generated as a function of soluble boron concentration.

Q. 2. Table 3-1, Shutdown Margin Calculation.

Give a description of the manner in which the "Worth reduction due to burnup of poison material" has been calculated.

A. 2. CPM has been used to generate a curve of control rod reactivity reduction (% $\Delta\rho$) as a function of fuel burnup at HFP Nominal conditions. This is changed to a % reduction in control rod worth versus burnup. For rodded fuel cycles the control rod bank that is inserted is conservatively assumed to have been inserted for the whole cycle. For unrodded (feed & bleed) cycles the lead regulating bank is conservatively assumed to have been inserted 20% for the whole cycle. Knowing the worth of the rod groups, the integral rod worth curve, and the accumulated burnup that each has seen, the burnup penalty can be calculated.

Q. 3. Paragraph 3.2.8, Kinetics Parameters.

Present a more detailed description of the DELAY code. Provide the source of the code, e.g., Duke Power Company.

A. 3. The DELAY code has been written by Duke Power Company. The following four pages have been extracted from the DELAY code manual and describe the theory, equations, and data sources for the code.

1.0 INTRODUCTION

DELAY is a utility type code which calculates the six group delayed neutron β's, λ's and also reduces them by a group independent effectiveness value. In addition to this, DELAY calculates the prompt neutron lifetime and then solves the In-hour equation to correlate reactivity insertion and doubling time.

Input for DELAY is available from two dimensional quarter core PDQ calculations and EPRI-CELL fuel depletion calculations.

2.0 THEORY

2.1.1 β_i, λ_i and β_i^{eff} Calculation

β_i is defined as the fraction of fission neutrons produced that appear as delayed neutrons of delayed group i. λ_i is defined as the effective decay constant for the precursors that produce delayed neutrons in delayed group i. These quantities are defined by the following equations:

$$(1) \qquad \beta_i \sum_{jg} \nu_{jg} \Sigma^F_{jg} \phi_{jg} = \sum_{jg} \beta_{ijg} \nu_{jg} \Sigma^F_{jg} \phi_{jg}$$

and

$$(2) \qquad \lambda_i \sum_{jg} C_{ijg} = \sum_{jg} \lambda_{ijg} C_{ijg}$$

where

$(\nu \Sigma^F \phi)$ is the neutron production rate, C denotes the concentration of delayed neutron precursors, and the subscripts i, j, g refer to the delayed neutron group, fissioning isotope, and incident neutron energy group respectively.

The concentration of delayed neutron precursors is related to the fission rate by

$$(3) \qquad \lambda_{ijg} C_{ijg} = k \beta_{ijg} \nu_{ijg} \Sigma^F_{ijg} \phi_{ijg}$$

Using equation 3, the solution to equations (1) and (2) becomes:

$$(4a) \qquad \beta_i = \sum_{jg} \beta_{ijg} \rho_{jg}$$

$$(4b) \qquad \beta_i^{effective} = \beta_i \cdot \text{EFFECTIVENESS FACTOR}$$

$$(5) \qquad \lambda_i = \frac{\beta_i}{\sum_{jg} (\beta_{ijg} \rho_{jg} / \lambda_{ijg})}$$

where

(6) $$P_{jg} = \frac{\nu_{jg}\Sigma^{F}_{jg}\phi_{jg}}{\sum_{g}\nu_{jg}\Sigma^{F}_{jg}\phi_{jg}}$$

is the fraction of the total neutron production rate arising from fissions of isotope j by incident neutrons of group g. Equation (5) is solved using integrated fission rate data from PDQ calculations. Suggested effectiveness factors are 0.961 for Oconee and 0.97 for McGuire.

2.1.2 Delayed Neutron Data

Tomlinson's values of delayed neutron parameters have been chosen for DELAY. The values have been reproduced here as Table I for documentation purposes and have been used in DELAY.

2.2 Prompt Neutron Lifetime

The prompt neutron lifetime, ℓ^* is defined

(7) $$\ell^* = \frac{1}{V_1\Sigma_{T1}} + \frac{k_2}{V_2\Sigma_{T2}}$$

where

(8) $$\Sigma_{T1} = \frac{\nu\Sigma_{F1}}{k_1}$$

(9) $$\Sigma_{T2} = \frac{\Sigma_{R1}}{\Sigma_{T1}} \quad \frac{\nu\Sigma_{F2}}{k_2}$$

(10) $$V_i = \frac{\sigma_a^{B-10} \text{ at } 2200 \text{ m/sec}}{\sigma_{ai}^{B-10}} \times 220000 \frac{\text{cm}}{\text{sec}} / \frac{\text{m}}{\text{sec}}$$

The parameters and their units are defined in Table 2.

2.3 Reactivity Calculation

The In-hour equation has been simplified to include only the asymptotic reactor period. The form programmed into DELAY is the following:

$$\rho = \frac{\ell^*}{T} + \sum_{i=1}^{6} \frac{\beta_i^{\text{effective}}}{1+\lambda_i T}$$

where T = asymptotic reactor period
ρ = reactivity

TABLE 1

Delayed Neutron Data
From Tomlinson AERE-R-6993

Fast Fission

Isotope	Group	λ (sec^{-1})	± S.D.	Relative Abundance	± S.D.	Absol. Gp. Yield (n/100F)	± S.D.
U235	1	.0127	.0003	.038	.004	.063	.007
	2	.0317	.0012	.213	.007	.351	.016
	3	.115	.004	.188	.024	.310	.042
	4	.311	.012	.407	.010	.672	.034
	5	1.40	.012	.128	.012	.211	.022
	6	3.87	.548	.026	.004	.043	.007
U238	1	.0132	.0004	.013	.001	.058	.007
	2	.0321	.0009	.137	.003	.602	.037
	3	.139	.007	.162	.030	.712	.129
	4	.358	.021	.388	.018	1.708	.120
	5	1.41	.099	.225	.019	.989	.089
	6	4.02	.317	.075	.007	.330	.036
Pu239	1	.0129	.0003	.038	.004	.024	.003
	2	.0311	.0007	.280	.006	.179	.013
	3	.134	.004	.216	.027	.138	.019
	4	.331	.018	.328	.015	.210	.018
	5	1.26	.171	.103	.013	.066	.010
	6	3.21	.378	.035	.007	.022	.004
Pu240	1	.0129	.0006	.028	.004	.022	.004
	2	.0313	.0007	.273	.006	.238	.024
	3	.135	.016	.192	.079	.162	.065
	4	.333	.046	.350	.030	.315	.040
	5	1.36	.304	.128	.027	.119	.027
	6	4.04	1.16	.029	.009	.024	.007
Pu242*	1	.0129		.004		.006	
	2	.0295		.195		.31	
	3	.131		.162		.26	
	4	.338		.411		.66	
	5	1.39		.213		.35	
	6	3.65		.010		.016	

TABLE 2

Parameters for Prompt Neutron Lifetime Calculation

Parameter	Description	Units	Source
k_1	$k_{effective}$, fast group	none	PDQ
k_2	$k_{effective}$, thermal group	none	PDQ
Σ_R	Removal cross section to thermal group	cm^{-1}	PDQ flux weighted edit fuel only
$\nu\Sigma_{F1}$	Neutron production cross section in fast group	cm^{-1}	PDQ flux weighted edit fuel only
$\nu\Sigma_{F2}$	Neutron production cross section in thermal group	cm^{-1}	PDQ flux weighted edit fuel only
Σ_{T1}	Total cross section fast group	cm^{-1}	equation 8
Σ_{T2}	Total cross section in thermal group	cm^{-1}	equation 9
V_1	Neutron velocity, fast group	cm/sec	equation 10
V_2	Neutron velocity, thermal group	cm/sec	equation 10
$\sigma_{B_{10}}(2200m)$	Thermal cross section at 2200 m/sec for B10 (3.84E+3)	barns	Chart of the Nuclides
σ_{ai}	Average boron cross section for group i	barns	PDQ
ℓ^*	Prompt neutron lifetime	sec	equation 7

Q. 4. Paragraph 8.3.2 Start-up Accident

Give the variation of the total (and its components) reactivity for the start-up accident for the first 10 seconds after the accident initiation, (these would complement Fig. 14-1 and 14-2 of the Oconee FSAR Rev. 16).

A. 4. The approach taken in the review of FSAR transient analyses as an integral part of the reload design methodology is discussed in Section 8 of NFS-1001. For each FSAR analysis the main parameters of interest have been identified and documented in the FSAR. In order to assure that a reload core is in conformance with the assumptions in the analysis, it is necessary to determine that the parameters associated with the reload core are bounded by the parameters assumed in the FSAR. If this criterion is met, it can be concluded that the existing FSAR analysis remains valid for the reload core.

Question 4 requests additional information for the start-up accident concerning the variation of the components of the reactivity response. These parameters are an intermediate output of the analysis whose response is indicated by other documented parameters such as power level, but are not normally included in the analysis documentation. However, the components of the reactivity response are determined by the parameters which are reviewed and shown to be within the bounds of the FSAR analysis. The reactivity response determined by those parameters remains valid until the value of a parameter is no longer bounded for a reload core. The safety review methodology of Section 8 assures the identification of all pertinent reload core parameters affecting the reference safety analysis, confirmation of the validity of the reference safety analysis for the reload core, and the resolution of any non-conservative parameter.

In order to respond to the question, the variation of the total reactivity and its components were calculated from the results presented in FSAR Figures 14-1 and 14-2, utilizing the analysis assumptions specified in the FSAR. The variation of the total reactivity during a startup accident is the sum of three reactivity effects. The withdrawal of the control rod banks adds positive reactivity which causes the neutron power level to increase and raise the average core temperature. The increase in fuel temperature causes a negative reactivity feedback due to the negative Doppler coefficient. The increase in power level increases heat transfer from the fuel to the coolant, resulting in an increase in moderator temperature. This causes a positive reactivity feedback since a positive beginning of cycle moderator coefficient is assumed. The transient response is primarily determined by the rate of positive reactivity addition from the withdrawal of rods, and the Doppler feedback which slows or terminates the nuclear excursion. The moderator feedback has a smaller effect. Figures 4-1 and 4-2 show the variation of the reactivity consistent with FSAR Figures 14-1 and 14-2 respectively. It should be noted that these figures do not represent the first 10 seconds of the transients, considering that the initial conditions are 10E-9 rated power and 1% k/k subcritical. Figures 4-1 and 4-2 illustrate the time interval of greatest interest during the transient, Figure 4-1 is the same scale as Figure 14-1, and Figure 4-2 is the first one second of the response in Figure 14-2. For both transients the reactivity addition for the first 10 seconds following initiation of rod withdrawal would only cause a reduction in the subcriticality margin.

Revised 3/18/81

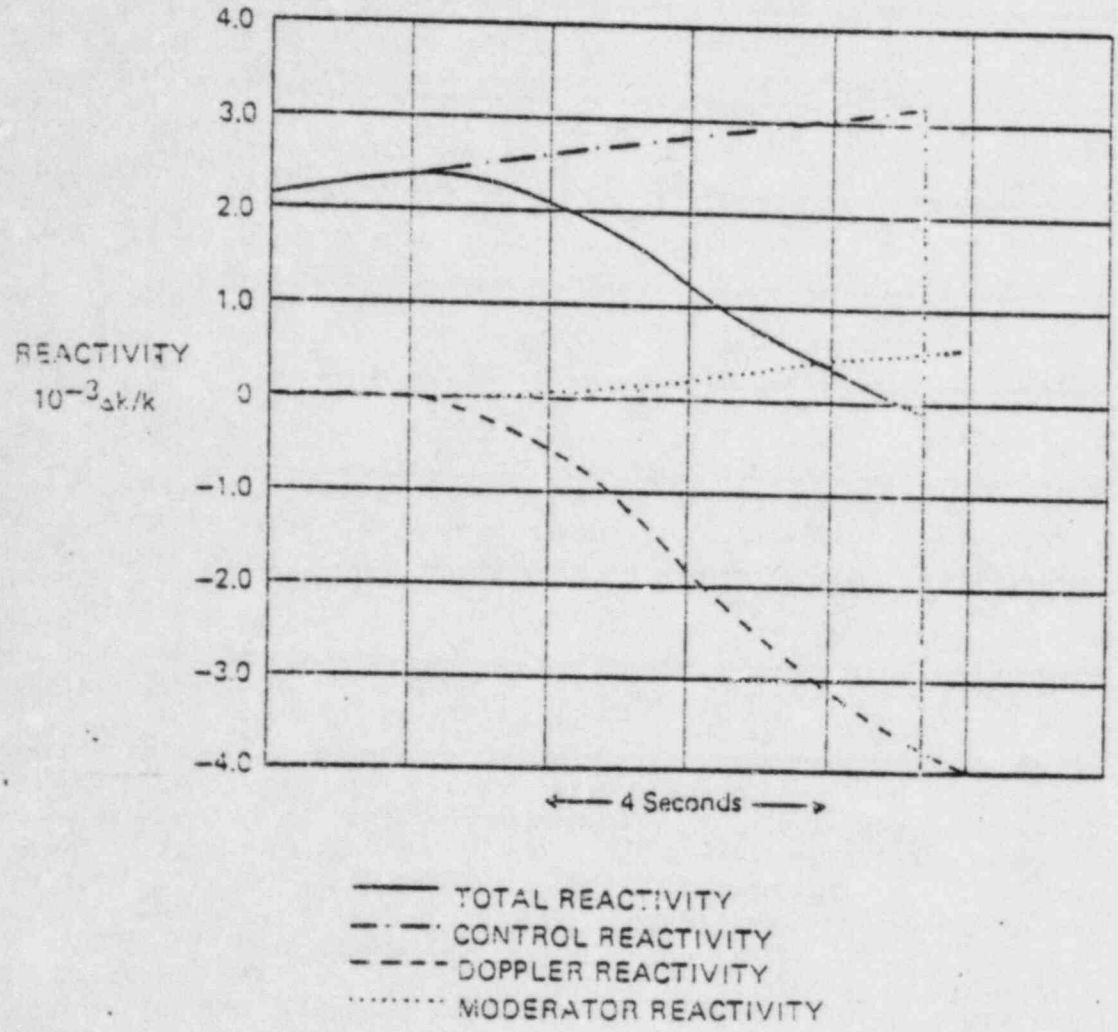

Figure 4-1. (FSAR Figure 14-1)

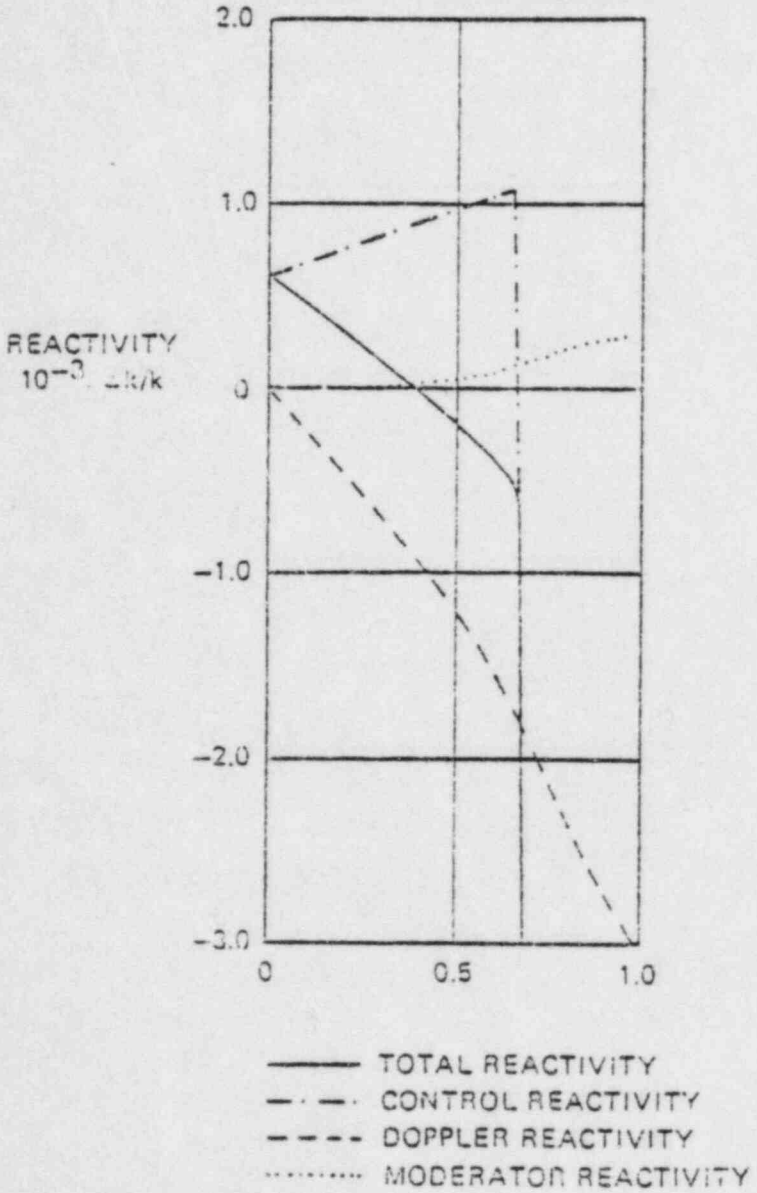

Figure 4-2. (FSAR Figure 14-2)

Q. 5. Paragraph 8.3.3. Rod Withdrawal Accident at Rated Power Operation

Give the variation of the reactivity as in 4. above.

A. 5. The reactivity response of the rod withdrawal accident at rated power simulation performed by B&W and used in the original FSAR analysis is not available. In order to respond to the question a similar analysis was performed by Duke Power Company using the RETRAN code and matching as accurately as possible the modeling assumptions of the original analysis. Figure 5-1, a revised FSAR Figure 14-9, shows the comparison between the original analysis (solid lines) and the new analysis (dashed lines). No attempt was made to match the results of the original analysis, the intent being to match the assumptions and initial conditions. The similarity between the results of the two analyses supports the conclusion that the reactivity response of the new analysis shown in Figure 5-2 is representative of the original analysis.

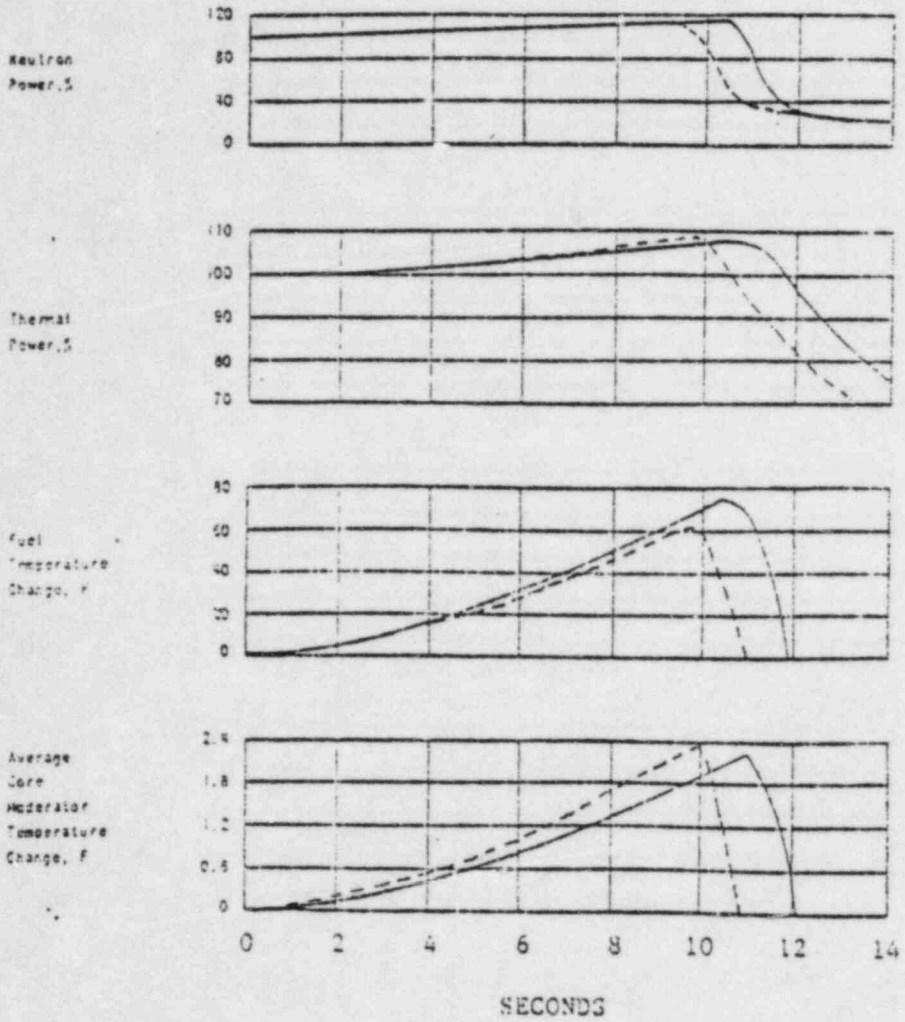

——— FSAR ORIGINAL ANALYSIS

----- DUKE RETRAN ANALYSIS

Figure 3-1 (FSAR Figure 14-9)

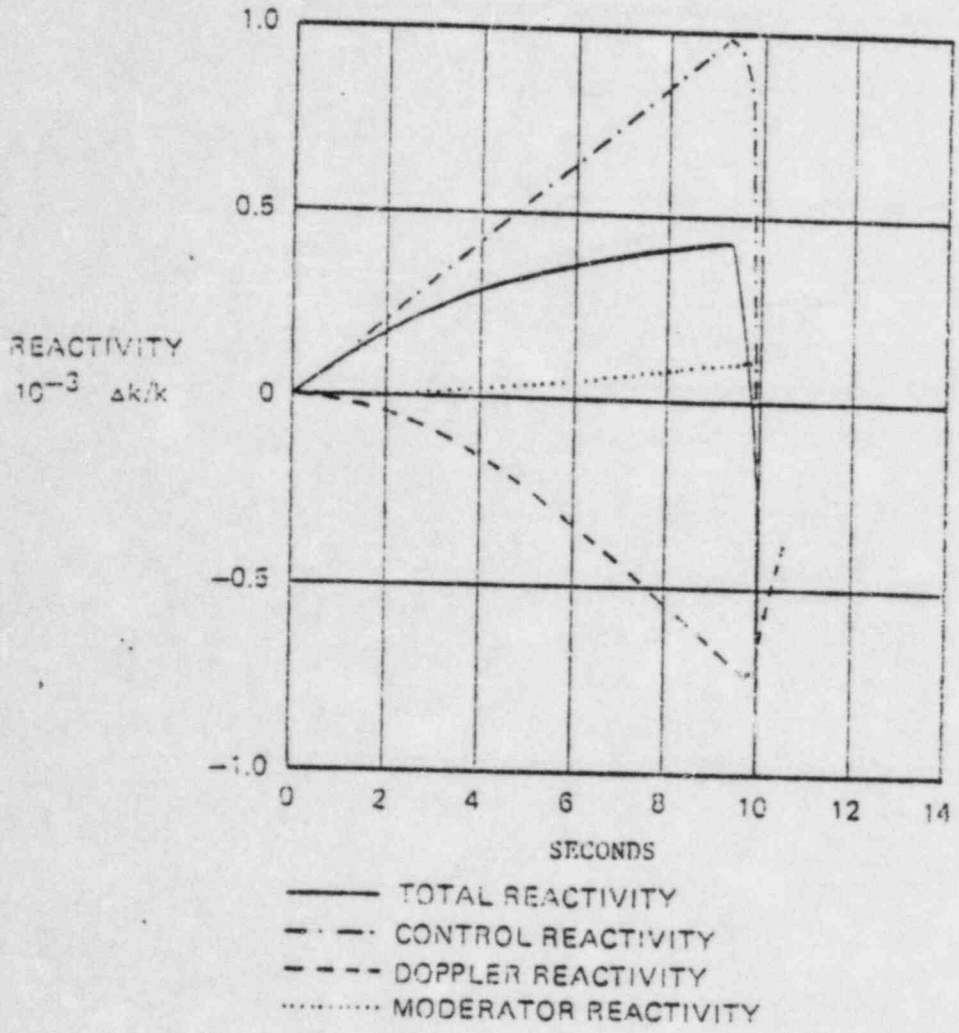

Figure 5-2 (FSAR Figure 14-9)

Q. 6. Paragraph 8.3, Discussion of Individual Accidents

Have the computer codes used in accident analysis (summarized in Appendix A) been updated and revised since the Oconee FSAR was issued? If so, would the general conclusions of the accident analysis change if the analysis was to be performed with the updated codes? Justify your conclusion.

A. 6. The computer codes summarized in Appendix A of NFS-1001 are primarily the nuclear, thermal, and thermal-hydraulic analysis codes intended for the reload core design. All the codes necessary for accident analyses are not included in that appendix.

The analysis of the loss of coolant accident was revised since the issuance of the Oconee FSAR using updated codes. BAW-10103 represents this revised analysis. Although many of the other accidents have not been reanalyzed utilizing updated codes, it is believed that the general conclusions of the existing analyses would not change if the analysis was repeated utilizing state-of-the-art computer codes. This conclusion is based on the premise that the earlier computer codes employed generally conservative modeling compared to the more accurate modeling utilized in current computer codes. Furthermore, the input parameters and assumptions employed in establishing the plant models have the dominant influence on accident consequences.

As discussed in the report, the safety analysis review performed during reload design involves a thorough review of the input data and assumptions used in the accident analyses and a comparison to the values generated by the reload design. The goal of the review is to verify that the reload design values remain bounded by the accident values and thus confirm that the safety analyses remain valid.

Q. 7. Paragraph 8.3.4. Moderator Dilution Accident

"Additional Analysis" is claimed to demonstrate complete protection during refueling operations. Give more information of this analysis.

A. 7. The "Additional Analysis" referred to is summarized in FSAR Section 14.1.2.4.2, the last paragraph on page 14-9. This paragraph is reproduced below.

During refueling or maintenance operations when the reactor closure head has been removed, the sources of dilution water makeup to the letdown storage tank--and therefore to the reactor coolant system--are locked closed, and the high pressure injection pumps are not operating. At the beginning of core life when the boron concentration is highest, the reactor is about 9.5 per cent $\Delta k/k$ subcritical with the maximum worth rod stuck out. To demonstrate the ability of the reactor to accept moderator dilution during shutdown, the consequences of accidentally filling the letdown storage tank with dilution water and starting the high pressure injection pumps have been evaluated. The entire water volume from the letdown storage tank could be pumped into the reactor coolant system (assuming only the coolant in the reactor vessel is diluted), and the reactor would still be 4.9 per cent $\Delta k/k$ subcritical.

Q. 8. Paragraph 8.3.6. Loss of Coolant Flow

It is stated that the hot channel power peak augmentation factors, fuel densification, and rod bow effects are not expected to change for the reloads; however, it is not stated how this conclusion has been arrived at.

A. 8. Hot channel power peak augmentation factors are associated with the mechanical design of the fuel assembly. The mechanical design is not normally modified in the reload design process. The fuel assembly design for Oconee has a history of very few modifications, none significantly affecting mechanical or nuclear performance. For example, the hot channel factors which account for the effect of statistical uncertainty in parameters such as enrichment, fuel rod loading, and geometry on the fuel rod heat flux and heat generation rate, remain valid for all fuel manufactured within the specified tolerances in these parameters.

The presently accepted treatment of the fuel densification effect on minimum DNBR analysis is the use of densified fuel stack length for calculating the heat flux. The original analysis was based on an initial fuel density of 92.5%, which produced the maximum stack length reduction compared to the subsequent reload fuel batches consisting of higher density fuel. For each reload, values of the densified heat flux are evaluated in the thermal hydraulic design analysis section of the reload report.

The effect of fuel rod bowing, dependent on the fuel assembly mechanical design and burnup, is explicitly factored into the thermal-hydraulic design of the reload core. The reactor protection system setpoints necessary for DNBR protection are established to provide the necessary margin to account for the effect of fuel rod bowing, as discussed in Sections 4.8 and 6.10 of NFS-1001.

Q. 9. Paragraph 8.3.9, Steam Line Failure

It is stated in the accident description that continued feedwater flow in the affected steam generator, combined with excessive heat removal and primary cool down the reactor may experience "a return to low power levels." There is not quantification of this power level, its potential consequences, or measures and actions for the return of the reactor to subcritical. Under what conditions is there a minimum of rod worth which could have the most adverse effects?

A. 9. The answers to these questions may be found in the Oconee FSAR, Chapter 14 and Supplement 3. However, a brief response summarizing the FSAR material follows.

A number of cases involving a variety of secondary system behavior during a steam line break are evaluated in the FSAR. Cases involving failure to isolate the affected steam generator, excessive feedwater addition due to malfunction in the feedwater control function, or of the auxiliary feedwater in additon to the continuing feedwater to the affected steam generator predict a return to power (1% FP, 8% FP, 35% FP, respectively) for a brief period of time. In each case, the reactor is returned to a subcritical condition by the action of the ECCS (high pressure injection, core flood tank and low pressure injection) within 350 seconds. The return to power situations are calculated to occur with the conservative assumption of the minimum tripped rod work associated with the minimum shutdown margin specified in the Technical Specifications and considering the highest-worth rod to be stuck out.

Q. 10. Supplement 2, Figure 4-1 and Paragraph 3.1.1.1.

Figure 4-1, Supplement 2 appears to contradict the statement in paragraph 3.1.1.1 that reads:

"NON-fuel cross sections with the exception of burnable poison assemblies and control rods are also generated using EPRI-CELL. Cross sections for burnable poison assemblies and control rods for use in diffusion theory calculations are generated by matching reaction rates between the diffusion theory code PDQ07 and CPM (a collision probability code)."

Give a more detailed description of the procedure for control rod and burnable poison cross section generation and the use of burnable poison cross sections in PDQ07-HARMONY depletion calculations.

A. 10. While there appears to be a contradiction both statements have merit. The ARMP procedure for generation of burnable poison cross sections was developed from CPM and PDQ07 calculations. The procedure however needs only EPRI-CELL and PDQ07 calculations to use it. Detailed description of the procedure can be found in the "Advanced Recycle Methodology Program System Documentation, September 1977." Part I Chapter 6 Section 4.2 describes the development of the procedure using CPM and PDQ07 while Section 4.3 describes the procedure using EPRI-CELL and PDQ07.

The procedure for developing control rod cross sections is described in Part I Chapter 6 Section 3.4 of the "Advanced Recycle Methodology Program System Documentation, September 1977."

Q. 11. Supplement 2, Paragraph 3.2, Comparison of ARMP PDQ07 to Cold Criticals.

The two-dimensional simulation of the criticals has not been performed at Duke nor with PDQ07, yet it was concluded that the results would have been identical with the PDQ07 results. Justify the above conclusion.

A. 11. The cold criticals have been simulated with PDQ07. The results have been published in Part I Chapter 2, Rev. 1 of the ARMP System Documentation. This work was performed under EPRI Research Project 118-1.

These benchmark calculations use standard ARMP methodology, standard ARMP codes (EPRI-CELL, NUPUNCHER, PDQ07) and Duke Power also uses these codes and methodology. Duke Power Company has been actively involved in developing in-core fuel management capability since 1969. Currently in the Nuclear Fuel Services Section, there are a total of nine employees with a cumulative thirty-two (32) man-years of PDQ experience. The level of individual experience ranges from one to nine years, and includes experience with Combustion Engineering, Westinghouse, and Babcock & Wilcox core design calculations. Therefore, Duke Power considers that if it had performed these benchmark calculations, the results would have been identical.

Q. 12. Supplement 2, paragraph 3.4, Conclusions.

The conclusions for the calculated results of the peak power are not tenable. There is no reason why the diffusion theory estimation by PDQ07 of the local radial peaking should be more conservative than those calculated with transport theory codes, or the measured values. This result must be regarded as fortuitous. For example (Fig. 3-4), many fuel assembly maxima were underpredicted by PDQ07. Justify the conclusion that PDQ07 will always be conservative in peak power predictions and present physical arguments for this justification.

A. 12. In Section 3, PDQ07's ability to conservatively predict the assembly local radial is addressed. In Figures 3-2, 3-3, and 3-4, it was shown that the maximum local radial as calculated by PDQ07 was conservative with respect to the measured or transport theory calculated values for three completely different lattice conditions. Each of these figures show the pinwise power distributions within a single fuel assembly.

In Figures 3-2, 3, 4, the eight highest measured (or EPRI-CPM calculated) pin powers were selected. The means and standard deviations of the (calculated-measured) difference were tabulated for all three groups together, and by each group (by Figure) individually.

In these samples, the mean was taken as the sample mean with the true standard deviation unknown. Then 95% confidence limits of the true mean were determined by:

$$\bar{D}_{U,L} = \bar{D} \pm \frac{t(.025,\ n-1) * S(D)}{\sqrt{n}}$$

Table 1 displays the results of this analysis.

Table 1

95% Confidence Level Estimates of the C-M Radial Local Means

Figure	n	$\bar{D}$	S (D)	$\bar{D}_U$	$\bar{D}_L$
3-2	8	.0070	.01739	.0215	-.0075
3-3	8	.02225	.01268	.0329	.0116
3-4	8	.0105	.008767	.0178	.0032
3-2,3,4	24	.01325	.01445	.0194	.0071

A. 12. cont'd.

Since $\bar{D}>0.0$ for all four sample groups, it is concluded that PDQ07 would overpredict the mean radial local of the highest power pins within an assembly. Furthermore, using 95% confidence limits estimates, PDQ07 over-predicts the mean radial local in the lower 2.5% interval ($\bar{D}_L>0.0$) for three of the four cases considered.

Besides the observations in Chapter 3 of Supplement 2, the Oconee fuel assembly employs a uniform lattice with a small interassembly water gap. A water hole's area is only as large as that of a fuel rod so that thermal flux peaking is minimized. Likewise, even at cold conditions, the nominal water gap between assemblies is only 12% of a pin pitch.

Thermal physics constants are standardly calculated using the Mixed Number Density (MND) procedure. Thermal absorption and fission constants are products of their respective 2200 m/sec cross sections and the cell average velocity (relative to 2200 m/sec). Thermal diffusion constants are treated in a similar fashion.

Thermal reaction rates in PDQ07 are proportional to the magnitude of the thermal flux. When excess thermalization occurs, e.g., near a water hole, MND cross sections conservatively yield higher thermal reaction rates than conventional cross sections.

This conservatism of the MND method is shown in Figure 1. Here a comparison was made of MND and conventional PDQ07 pin powers relative to EPRI-CPM. The data source for the MND PDQ07 and EPRI-CPM assembly simulation was Figure 3-4 of Supplement 2. It was shown that for the eight maximum pin powers, MND cross sections yielded a mean percent difference of .99%; while the conventional cross section PDQ07 had a nonconservative mean of -.31%.

The statistics presented in Supplement 2 justify use of a radial ONRF of 1.03 for unrodded fuel cycles. We have suggested use of 1.05 which allows approximately two percent conservatism for any local pin peak uncertainties.

The above statistics, physical geometry, and modeling procedures support the conclusion that no additional uncertainty is needed on the radial local peak. However, a 2% conservatism is built into the 1.05 radial ONRF we propose using.

A.12

FIGURE 1

PERCENT DIFFERENCE COMPARISON OF PIN POWERS

REFERENCE CALCULATION: EPRI-CPM

CODE USED	PDQ07	PDQ07	EPRI-CPM
MODEL	1/4 ASS'Y	1/4 ASS'Y	1/4 ASS'Y
X-SECTIONS	MND	CONV	CPM
%FP	100	100	100
PPMB	0.0	0.0	0.0

IT							
-.79 -1.58	.29 -.59	MND PDQ07 CONV PDQ07					
-.30 -.10	0.0 ⑥ -.96						
-.40 .20	.98 .69	.85 ② -.38	2.45 ⑤ .94				
-.40 .40	.98 .79	1.04 ③ -.28	1.76 ① -.19				
-.30 .30	.10 ⑧ -.58		1.13 ④ -.56	.58 ⑦ -.48	.41 .41		
-.82 .21	.30 .40	-.29 -.78	.60 .50	-.21 .41	-.54 .21	-1.28 0.0	
-1.25 .10	-.94 .21	-.52	-.73 .31	-1.05	-1.38 0.0	-1.61 -.11	-1.52 -.11

*NOTE: PIN #1 IS THE PEAK LOCAL RADIAL, #2 - THE SECOND HIGHEST PIN, ETC.

Q. 13. Supplement 2, paragraph 4.2, Oconee Fuel Cycle Simulation.

It appears that the EPRI-NODE-P almost consistently under-predicts the assembly peak power for cycles 2 and 3. Justify the conclusion in paragraph 4.3 that the EPRI-NODE-P "yielded consistently good power distributions..."

A. 13. Conclusions about power distributions are reached in view of the global behavior of EPRI-NODE-P. The Cycle 3 data was shown in Section 4 of Supplement 2 only for illustrative purposes since the measured data was not considered benchmark quality as the other four cycles.

The derived total ONRF from chapter 5 was 1.10 for rodded cycles. Only 6% of the products of the ONRF and calculated peak exceeded the cycle 2 measured peaks. Therefore, based on a 95/95 criterion, the agreement was judged good.

Q. 14. Supplement 2, Figure 4-2 through 4-127.

The EPRI-NODE-P calculated power distributions for the first four cycles of operation of Oconee 1 consistently underpredicted the relative power in assembly H-8, often by more than 10%. Is the reason for this anomaly known?

A. 14. Yes. It is current Duke design practice to perform only <u>one</u> radial power normalization at approximately 25 EFPD. The normalization is referenced to a two-dimensional discrete pin model PDQ07 power distribution.

The normalization is performed such that there is good radial power agreement in both the central <u>nine</u> (H-8 included) and the peripheral assembly regions. Since only the internal leakage factor, g_h, was adjusted for the central nine, agreement of the central nine as a whole was addressed rather H-8 specifically. This method yielded radial differences of 5% or less early in each cycle for H-8 as shown by Figures 4-4, 4-41, and 4-87. Assembly K-9 in Cycle 3 had a 20% larger radial at BOC than H-8, therefore the central nine normalization gave a more accurate agreement with a more limiting assembly. Cycles 1, 2, and 3 were all rodded cycles, and therefore rod interchanges severely changed the radial power shape. A radial power renormalization to PDQ07 after the rod interchange would have significantly improved radial and peak agreement.

The reactors at Oconee will soon all be operated in the unrodded mode and so only the statistics for Cycles 4 and 5 are representative of future design calculations.

In Cycle 4, the largest radial power difference for H-8 was 3.3%. In Cycle 5, differences of up to 10% were seen. However, H-8 was a low power assembly, and K-9 was the assembly of concern. Good agreement was shown between assemblies K-9 and also H-9 throughout this cycle.

The only other method of assuring less than 5% power difference to H-8 would have been to apply a K_∞ multiplier. Such an ad hoc method of normalization is contrary to Duke design practice.

Q. 15. Supplement 2, paragraph 5.2, Normality Test Results.

All data sets have been used with the assumption of normal distribution, yet some have failed the normality test. Justify the use of the data sets as normal.

A. 15. The D' test for normality is a very rigorous test, and in Table 5-1 of Supplement 2 it was shown that nine of 16 individual and grouped data sets passed the normality criteria outright - with a 5% level of significance.

Table 1 below presents the percent differences by which the other seven data sets missed the D' percentage point cutoff values for normality. Of these seven, four data sets were combinations of individual nonnormal datasets which in turn, carried inherent near-normality into the larger sets.

Table I

Nearly Normal Data Sets

Cycle	Type	N	Percent Difference from Cutoff	Figure
1	Radial	308	-2.16%	5-11
1,2	Radial	455	-1.75%	5-21
1,2,4,5	Radial	730	-1.56%	5-23
1	Peak	377	- .26%	5-16
3	Peak	211	-3.67%	5-19
1,2	Peak	612	-1.38%	5-24
1,2,4,5	Peak	1027	-1.72%	5-26

The argument presented in paragraph 5.2 was that although certain distributions did not pass the normality test criteria, an ocular inspection of the histograms indicated that, for engineering purposes, normality would be a reasonable approximation of these distributions. This is further supported by Table I above.

It should also be noted that cycle 4, cycle 5, and cycle 4 & 5 radial and peak power data sets passed the normality test. These unrodded cycles are typical of future Oconee reload designs.

Re Q. 11 NRC reviewer would like a copy of the work performed under EPRI Research Project 118-1.

Re A. 11 Enclosed is a copy of the EPRI-CELL Criticals Benchmarking portion of Project 118-1. Figures 6-5 and 6-6 of 118-1 correspond to Figures 3-2 and 3-3 in Supplement 2 of NFS-1001.

Rev. 1
October, 1978

Part I
Chapter 2

Advanced Recycle Methodology Program

System Documentation

Research Project 118-1

EPRI-CELL Criticals Benchmarking

October 30, 1978

Prepared for:

Electric Power Research Institute
3412 Hillview Avenue
Palo Alto, CA 94304

Principal Investigators

W. J. Eich (NAI)*
M. L. Kennedy (NAI)
R. D. Mosteller (Science Applications, Inc.)

EPRI Project Manager

B. A. Zolotar

Prepared by:

Nuclear Associates International Corporation
6003 Executive Boulevard
Rockville, MD 20852

With revisions by:
Electric Power Research Institute

* Current affiliation: Electric Power Research Institute
Palo Alto, CA 94303

TABLE OF CONTENTS

effect, however, adds several tenths of a percent in reactivity to very watery lattices but such are so far from reactor conditions that their analysis lacks most practical relevance.) Finally, the two items of input required for the simulation of grain heterogeneities have been entered for the MO_2 cases.

Box 3 of Figure 2-1 signifies the non-depletion EPRI-CELL (GAM/THERMOS) run which produces printed output (Box 4) and, by option, the few PDQ-7 input cards containing the macroscopic few group EPRI-CELL output in Table Set Format (Box 5). These cards are part of the input to a "one-dimensional" radial plane PDQ-7 - Box 7 (one mesh in the Z-direction with zero current boundaries). Another item of input is the axial buckling, B_Z^2, (Box 6) which has generally been measured. If this buckling was not available in the literature, then it has been accurately estimated from measured critical water heights and reflector savings measured in similar lattices. Since the criticals analyzed in the course of this Program have been restricted to arrays having relatively high moderator heights, dependence of the final value of k_{eff} (Box 8) is quite minimal on axial buckling uncertainty. Another item of input to these PDQs is a set of (four fast group) reflector constants which were developed to match the results of multigroup transport (P3) calculations[4]. These critical analyses could as validly have been conducted with 3 fast groups mutatis mutandis[5] but the effort had been initiated before the installation of the collapsed broad group edits. The Mixed Number Density model is implicit in the core and reflector thermal group constants used in these PDQ calculations.

The approach used in analyzing large-scale mock-up experiments differs in some respects from the procedure discussed above. That approach is described in more detail in Section 6 of this Chapter.

SECTION 6

LARGE-SCALE MOCK-UP RESULTS

6.1 Introduction

Figure 6-1 schematically illustrates the calculational process followed in the analysis of five large-scale mock-ups. The procedure is basically similar to the approach described in Section 2 of this chapter for critical lattices. There are three principal differences between the two methodologies:

(1) the large-scale mock-ups were analyzed for the verification of existing ARMP libraries and procedures rather than to aid in the development of the system

(2) the mock-ups were sufficiently heterogeneous that two-dimensional rectangular diffusion theory calculations were required in place of one-dimensional radial calculations

(3) separate EPRI-CELL calculations were required for different parts of lattices--fuel pins, water holes, and burnable poison pins

These mock-ups are of special interest because they permit accurate determination of the worth of burnable poison rods (BPR's). Heretofore, BPR contributions to reactivity in PWR's have been subsumed into core analyses which integrate a number of additional effects, such as control rod worth, Xenon worth, Doppler defect, and soluble boron worth. These mock-ups, however, determine the BPR worth up to 9 percent $\Delta\rho$ by means of straightforward soluble boron substitution. Furthermore, these particular BPR's have a boron loading which is approximately 70 percent heavier than that for PWR assemblies of any current design. The agreement achieved with the experimental data therefore uniquely validates the ARMP representation of burnable poisons and, in addition, further substantiates the benchmarking of EPRI-CELL against critical experiments, which is described in the preceding sections of this chapter.

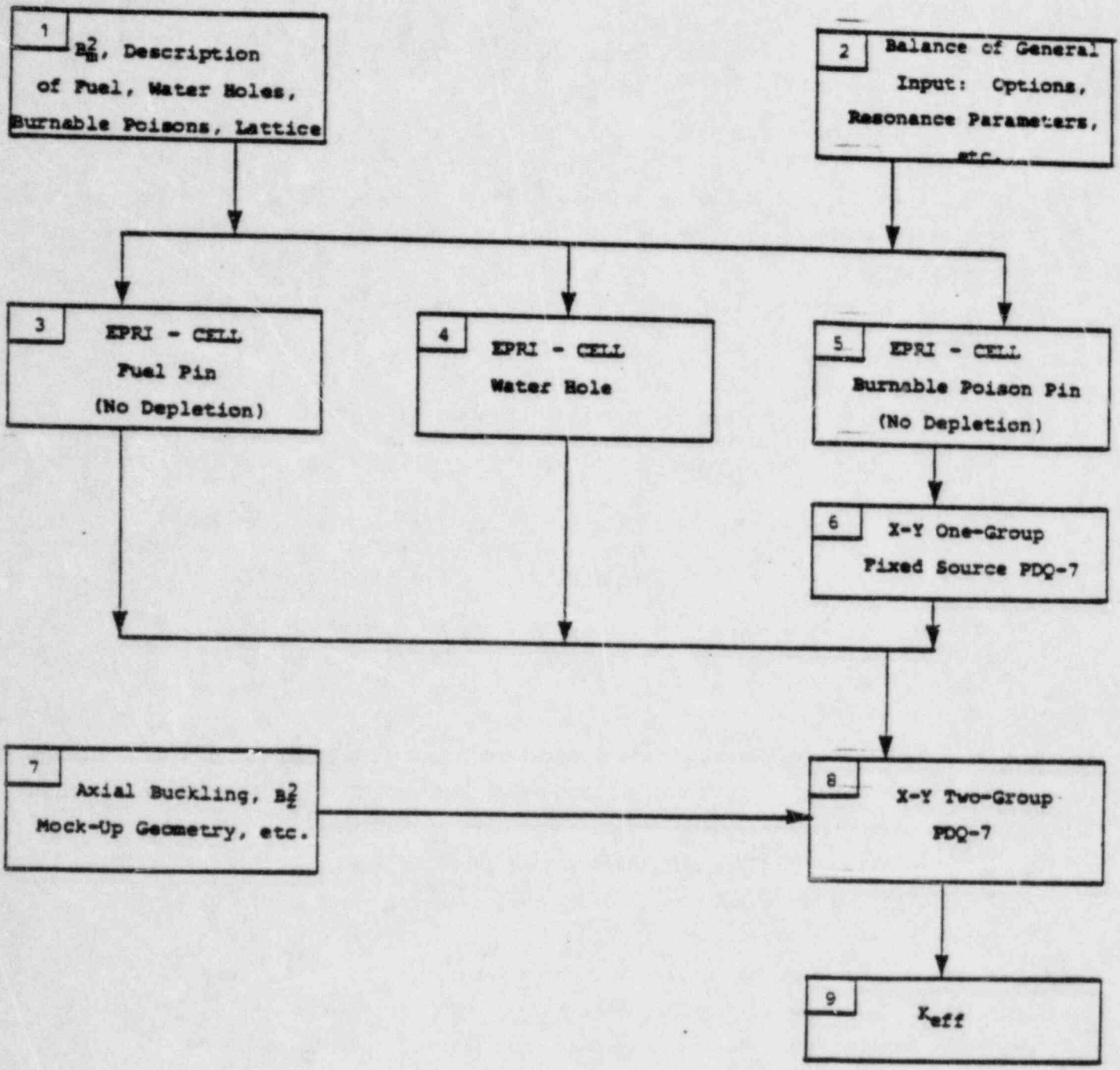

FIGURE 6-1 Flow Chart for Large-Scale Mock-Up Analysis

6.2 Description of Experiments[21]

The experimental configuration employed in these critical mock-ups is shown in Figure 6-2. The subassembly regions indicated there are fictitious in the sense that there is no structural material in the active region of the geometry and that there is no physical significance to the subassembly boundary. A subassembly region, however, does correspond to a 15 x 15 assembly in size and configuration. The outer buffer region was comprised only of fuel pins and borated moderator, but the contents of the subassembly regions were rearranged from case to case and the soluble boron concentration was adjusted until a multiplication factor of 1.0007 was achieved. The subassembly configurations for the different cases, or "loads," are summarized in Figure 6-3. All locations other than those indicated are fuel cells.

The fuel pins and burnable poison rods are described in Table 6-1. Unlike normal fuel pins, these pins are clad with aluminum. The BPR's are unclad cylinders of pyrex glass which have a much higher boron content than normal BPR's. Water holes contain nothing but borated water, and moderator characteristics are summarized in Table 6-1, as well. All measurements were performed at room temperature and pressure, with a moderator height of 145 cm.

For the loadings of interest in this study relative power densities were obtained for one octant of the central subassembly. These measurements were made at the midplane of the active height, using a sodium iodide (thallium activated) scintillation counter to count collimated fission-product gamma rays from activated fuel rods.

The five loadings considered here allow direct determination of BPR worth by the method of soluble boron substitution. In load 1 the subassemblies contain a uniform lattice of fuel pins, and the central region is identical to the buffer. In loads 2 and 3, 17

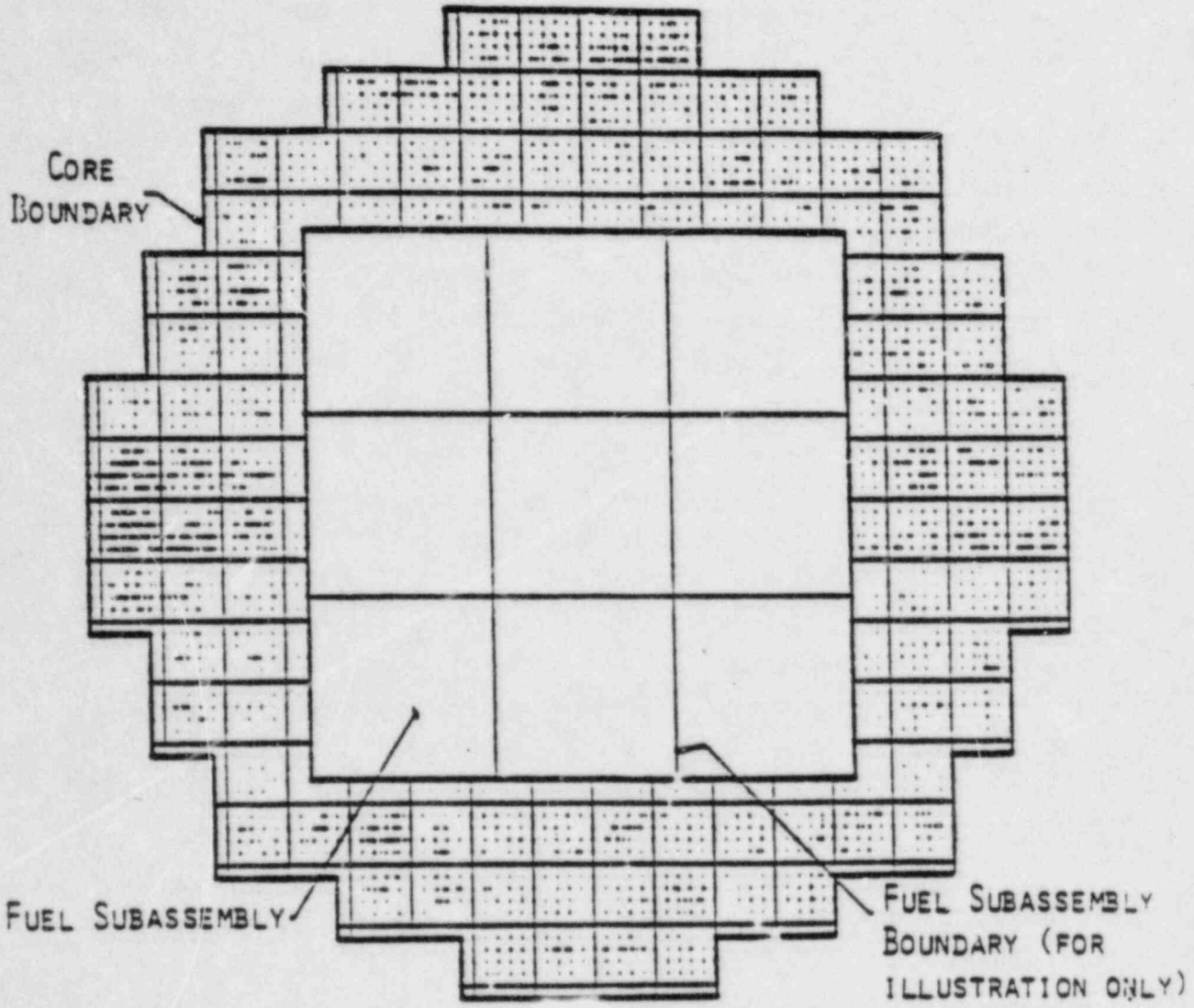

FIGURE 6.2 Geometry for Large-Scale Mock-Up Experiments

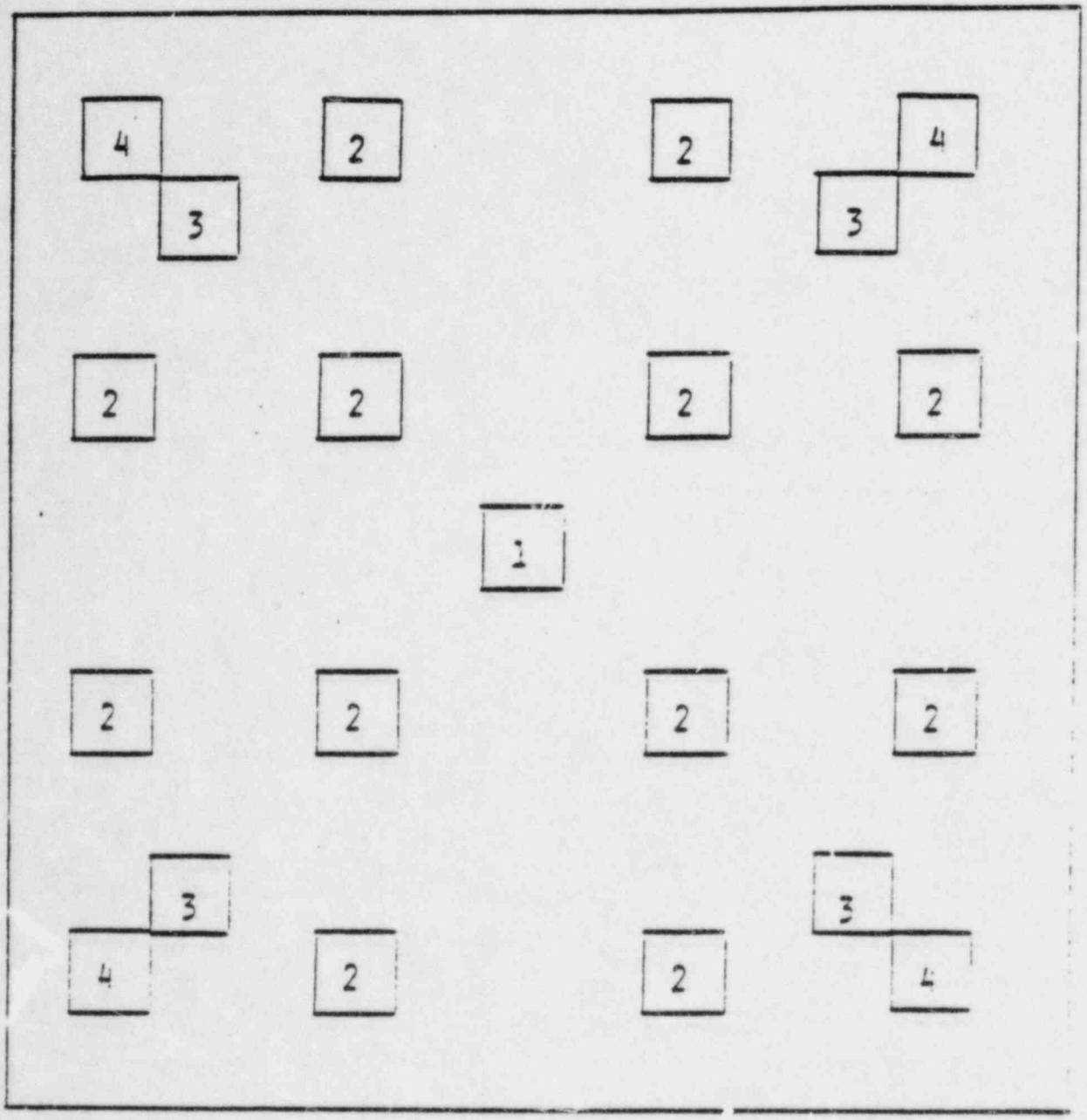

	Load 1	Load 2	Load 3	Load 8	Load 9
Location 1	Fuel	Water	Water	Water	Water
Locations 2	Fuel	Water	Water	Poison	Poison
Locations 3	Fuel	Water	Fuel	Poison	Fuel
Locations 4	Fuel	Fuel	Water	Fuel	Poison

FIGURE 6-3 Subassembly Configurations

TABLE 6-1

PHYSICAL CHARACTERISTICS OF PINS AND MODERATOR

Fuel Pin

Enrichment, w/o	2.459, ± .002
Pellet Material	UO_2
Pellet Density, g/cm^3	10.24 ± .04
Pellet Diameter, cm	1.0297 ± .0013
Active Fuel Length, cm	153.34 ± .89
Clad Material	6061 Aluminum
Clad Thickness, cm	.0813 ± .0025
Clad Outer Diameter, cm	1.2060 ± .0015
Fuel Pin Pitch, cm	1.636 ± .003

Burnable Poison Rod

Poison Material	Pyrex Glass
Poison Density, g/cm^3	2.244 ± .008
Poison Diameter, cm	1.170 ± .001
Boron Content, w/o	3.919 ± .002
Poison Length, cm	188.0 ± .1
Clad	None

Moderator

Water Density, g/cm^3	.9978
Water Temperature, °C	21 ± 1
Soluble Boron Content, ppm	
Load 1	1511 ± 3
Load 2	1335.5 ± 3
Load 3	1335.5 ± 3
Load 8	794 ± 3
Load 9	779 ± 3

fuel pins have been removed from each of the subassemblies, leaving borated water in their place. In both loads the subassemblies are octant symmetric, but the water hole locations are slightly different. In loads 8 and 9 the same fuel pins have been removed as in loads 2 and 3, respectively, but BPR's have been inserted in their place everywhere except in the central location of each subassembly. Comparison of results from loads 2 and 8 and from loads 3 and 9 therefore provides a value for the BPR worth in terms of the change in the soluble boron concentration.

6.3 Analytical Procedure

Loads 1, 2 and 8 first were simulated with the standard ARMP PWR procedures described in Part I, Chapter 6 of this documentation, following the process indicated in Figure 6-1. It is to be emphasized that only the standard procedures were used -- more detailed treatments normally employed during benchmarking against critical experiments, such as four energy groups and four mesh spaces per pin cell side in the two-dimensional PDQ calculation, were not needed because of the very low leakage of all these configurations.

This approach produces very good agreement with the experimental data for loads 1 and 8 but not as good for load 2. In the ARMP procedure, a four-group fine-mesh correction is applied to the multiplication factor when water holes are present (see Part I, Chapter 8, Section B), but the discrepancy in the result for load 2 is somewhat beyond the range of the recommended correction factor for operating PWR's. On the other hand, the water density in these mock-up experiments is about 50% greater than under normal operating conditions, and so the higher soluble boron density can produce a larger reactivity discrepancy.

Because the leakage from these mock-up experiments is quite low, a change in group structure would have very little effect and so only a fine-mesh correction is needed. A finer mesh spacing, two

mesh spaces per pin cell side rather than one, was selected and the two-dimensional calculations for loads 1, 2, and 8 were re-run.

As Figures 6-4, 6-5, and 6-6 illustrate, this change produced a significantly better value for the multiplication factor for load 2 and left the multiplication factors for loads 1 and 8, which were already in good agreement with the experimental data, essentially unchanged. (The convention adopted in these Figures is that water holes are represented by an "X" and that BPR's are represented by a "+".) In load 1, no non-fuel locations are present and so no correction is necessary. In load 8, the BPR parameterization itself, which preserves the reaction rate predicted by EPRI-CELL by adjusting the PDQ thermal KND absorption cross section for the BPR, produces a BPR worth which is mesh independent.

Calculations also have been performed for loads 3 and 9, and the results are presented in Figures 6-7 and 6-8, respectively.

Once this mesh change was made in PDQ-7, the ARMP system produced excellent agreement with the measured data from all [illegible] loads. No additional modification of any of the ARMP procedures was needed, and it should be emphasized that this one change was necessitated by the high density of the moderator, relative to normal operating conditions. EPRI-CELL therefore has been shown to describe accurately the neutronic behavior of BPR's, even when they are as heavily loaded as the ones in these experiments.

1.026 1.026	1.025 1.025	1.022 1.022	1.018 1.018	1.013 1.013	1.005 1.005	.997 .996	.986 .986
	1.024 1.024	1.021 1.021	1.017 1.017	1.012 1.012	1.004 1.004	.996 .996	.985 .985
		1.019 1.019	1.015 1.015	1.009 1.009	1.002 1.002	.993 .993	.983 .983
			1.011 1.011	1.005 1.005	.998 .998	.989 .989	.979 .979
				1.000 1.000	.992 .991	.984 .984	.973 .973
					.985 .985	.976 .976	.966 .966
						.968 .968	.958 .957
							.947 .947

Relative Pin Power in Central Subassembly

	K_{EFF}	K_∞	M^2
EXPERIMENT	1.0007	-	-
ARMP, STANDARD	.9999	1.0182	35.64
ARMP, FINER MESH	.9998	1.0179	35.64

ARMP, STANDARD
ARMP, FINER MESH

FIGURE 6-4 Comparison of Results for Load 1

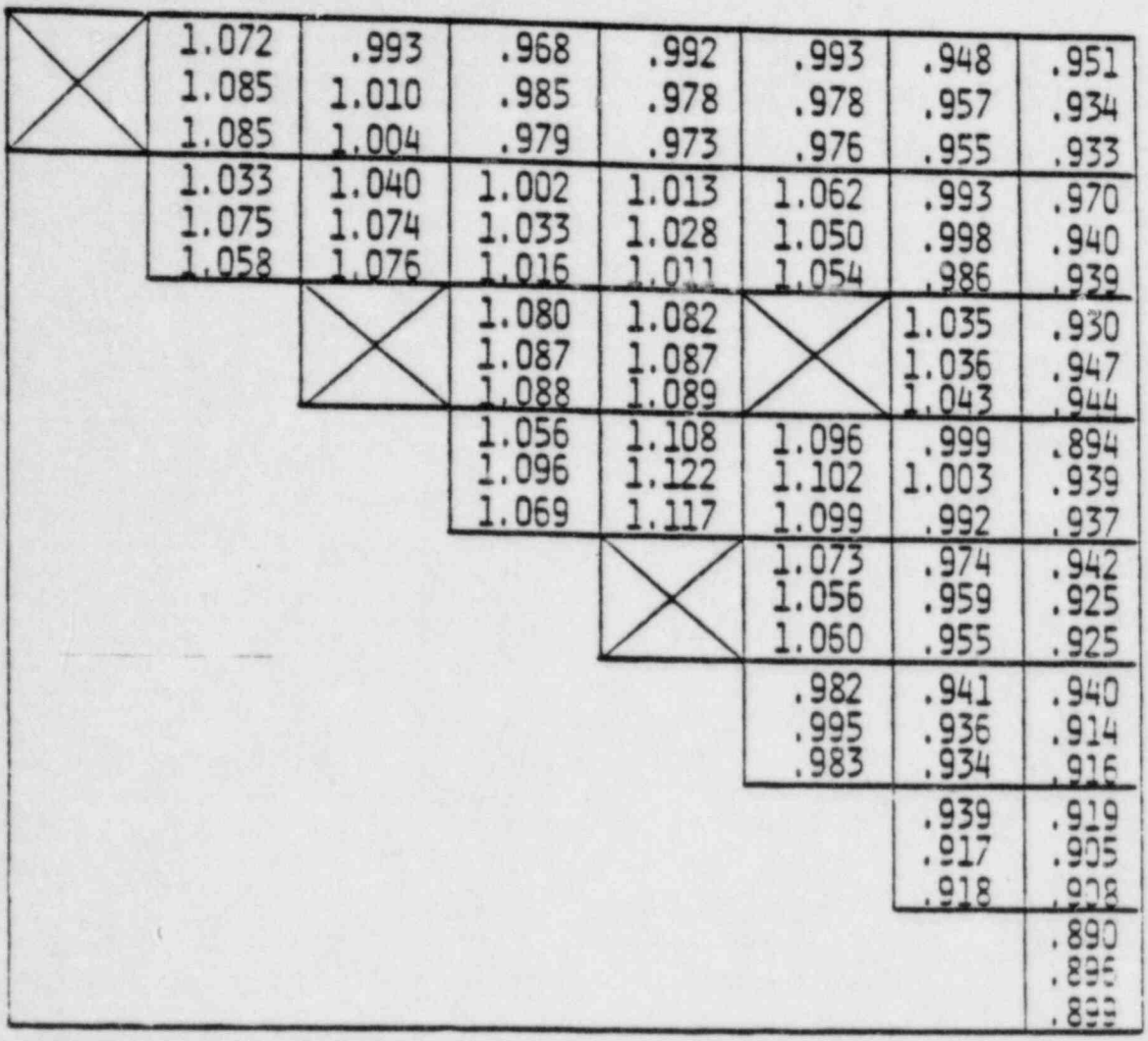

Relative Pin Power in Central Subassembly

	K_{EFF}	K_∞	M^2
EXPERIMENT	1.0007	-	-
ARMP, STANDARD	1.0052	1.0240	35.24
ARMP, FINER MESH	1.0018	1.0205	35.25

EXPERIMENT
ARMP, STANDARD
ARMP, FINER MESH

FIGURE 6-5 Comparison of Results for Load 2

	1.102 1.114 1.120	.986 .998 .996	1.003 .990 .991	1.015 .996 .998	1.005 1.005 1.004	1.045 1.046 1.046	1.079 1.087 1.085
	.995 .999 1.011	.907 .899 .890	.961 .924 .938	.943 .931 .945	.924 .914 .904	1.027 .993 1.003	1.061 1.077 1.078
			.864 .851 .844	.864 .855 .845		.961 .945 .932	1.044 1.070 1.072
			.878 .839 .860	.820 .816 .813	.896 .855 .851	1.007 .994 1.005	1.045 1.090 1.092
					.931 .926 .914	1.053 1.067 1.070	1.093 1.123 1.121
					1.028 1.021 1.030	1.095 1.115 1.116	1.147 1.153 1.150
						1.118 1.155 1.152	1.151 1.178 1.174
							1.158 1.196 1.191

Relative Pin Power in Central Subassembly

	K_{EFF}	K_∞	M^2
EXPERIMENT	1.0007	-	-
ARMP, STANDARD	.9993	1.0234	35.52
ARMP, FINER MESH	.9998	1.0234	35.54

EXPERIMENT
ARMP, STANDARD
ARMP, FINER MESH

FIGURE 6-6 Comparison of Results for Load 8

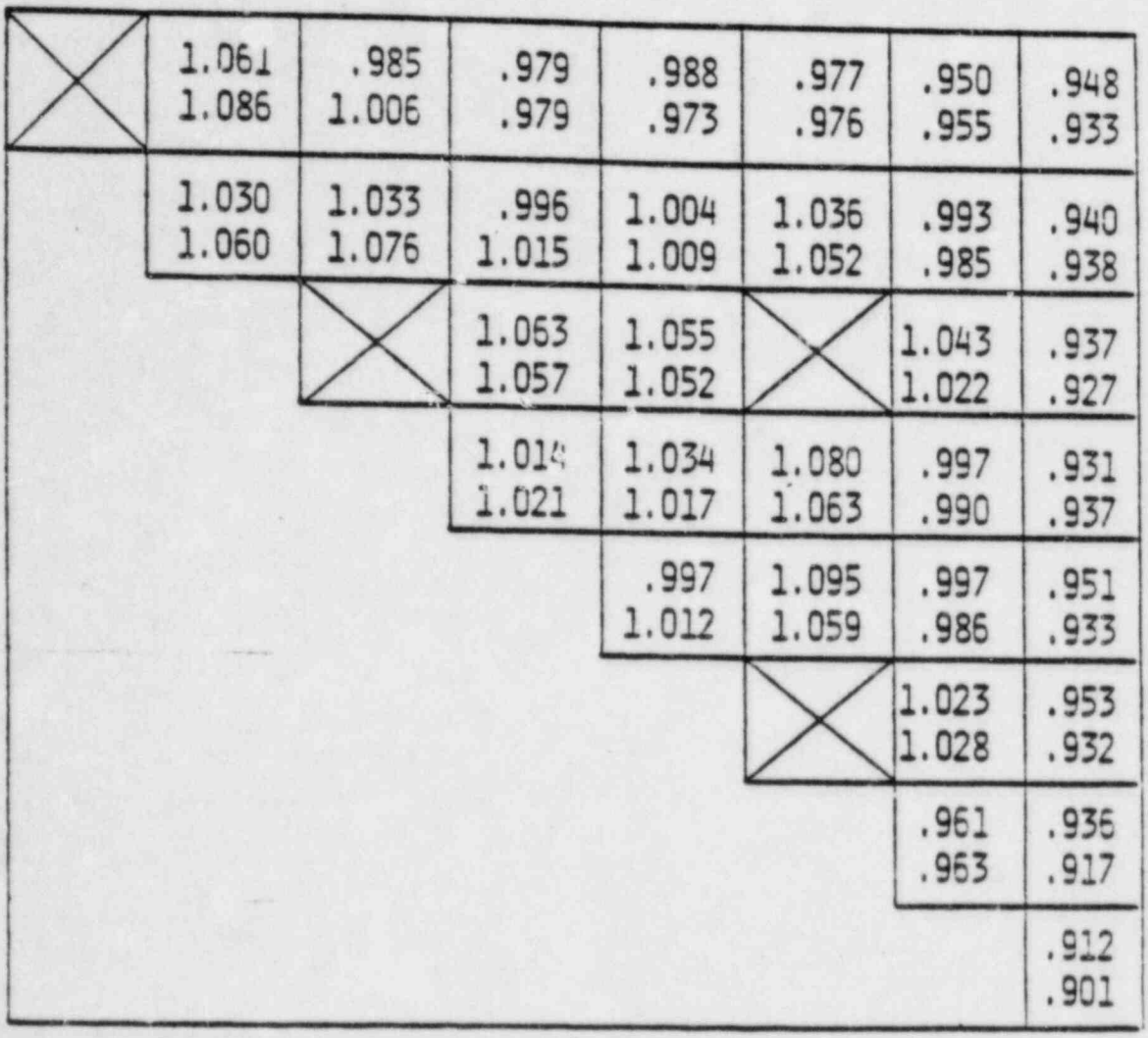

Relative Pin Power in Central Subassembly

	K_{EFF}	K_∞	M^2
EXPERIMENT	1.0007	-	-
ARMP, FINER MESH	1.0022	1.0209	35.25

EXPERIMENT
ARMP, FINER MESH

FIGURE 6-7 Comparison of Results for Load 3

	1.107 1.144	1.003 1.016	1.016 1.011	1.011 1.016	1.011 1.019	1.058 1.058	1.072 1.097
	1.013 1.032	.901 .908	.961 .959	.958 .965	.931 .919	1.036 1.014	1.070 1.088
			.882 .875	.900 .880		.954 .940	1.056 1.076
			.932 .941	.968 .949	.925 .897	.993 1.003	1.055 1.086
				.956 .956	.960 .903	1.018 1.010	1.082 1.094
						.996 .961	1.096 1.010
						1.045 1.055	1.094 1.127
							1.105 1.153

Relative Pin Power in Central Subassembly

	K_{EFF}	K_∞	M^2
EXPERIMENT	1.0007	-	-
ARMP, FINER MESH	.9997	1.0235	35.54

EXPERIMENT
ARMP, FINER MESH

FIGURE 6-8 Comparison of Results for Load 9

17. V.O. Uotinen, et al., "Lattices of Plutonium-Enriched Rods in Light Water--Part I: Experimental Results," Nucl. Tech., 15, 257 (1972).

18. H. Windsor and R. Goldstein, "Analysis of Lattices Containing Mixed-Oxide Fuel in Particulate Form," Trans. Am. Nucl. Soc., 15, 107 (1972).

19. Askew, et al., op cit.

20. Hellens, op cit.

21. M.N. Baldwin and M.E. Stern, "Physics Verification Program -- Part III, Task 4, Summary Report," BAW-3647-20 (1971).

Re Q. 12 Additional justification is required to support the conclusion that PDQ07 conservatively predicts maximum pin powers.

Re A. 12 Nuclear reactor cores are modeled in two dimensions at Duke Power Company using the PDQ07 code. A discrete pin geometry and two neutron energy group Mixed Number Density (MND) EPRI-CELL physics constants are used.

In the following figures, hot full power (HFP) PDQ07 and CASMO individual pin powers are presented from quarter-assembly calculations. These calculations were performed at beginning-of-life with no xenon; at this time pin power peaking is most severe. The enrichments used are typical of future reloads at Oconee. A variety of soluble boron concentrations and burnable poison (BP) weight percents (B_4C) were used. Also, water filled control rod guide tubes (CRGT) were used. All assemblies contained an instrument tube (IT). Table 1 identifies the five cases.

TABLE 1

Case	U-235 w/o	Absorber	PPM-Boron
1	3.08	1.0 w/o B_4C	500
2	3.08	1.0 w/o B_4C	1000
3	3.38	.2 w/o B_4C	1000
4	3.38	CRGT	1000
5	3.08	CRGT	0

In evaluating pin powers, the CASMO code solves the transport equation in two dimensions and seven neutron energy groups[1]. PDQ07 used only two energy groups in evaluating the diffusion equation. Therefore, the Duke PDQ07 model was tested not only by a higher order neutronics method, but also by more neutron energy groups.

In all five cases it is shown that PDQ07 predicts accurately and conservatively each assembly's maximum pin power. PDQ07 also predicted the same location of the maximum pin for each case as CASMO.

For pin powers equal to or greater than 1.000, pinwise powers usually agree within 1%. The CRGT cases, however, show PDQ07 to be up to 2% more conservative.

Therefore it is concluded from these comparisons, as well as those in NFS-1001 Supplement 2, that the two group MND PDQ07 accurately and conservatively predicts the maximum pin power within an assembly over a wide range of moderator and fuel temperatures, enrichments, soluble boron concentrations, and BP loadings.

1. These CASMO calculations were run using 69 energy groups in the microregion calculation.

FIGURE 1

QUARTER ASSEMBLY PINWISE POWERS - CASE 1

CODE	PDQ07	CASMO	
K-INF	1.1419	1.1421	
U-235 w/o	3.08	3.08	
PPMB	500	500	
B-4-C w/o	1.0	1.0	

IT							
1.044 1.050	1.009 1.012	CASMO PDQ07					
0.992 0.993	0.970 0.973	BP					
0.982 0.977	0.974 0.966	0.952 0.952	0.956 0.948				
0.981 0.975	0.973 0.965	0.952 0.952	0.946 0.947	BP			
0.986 0.980	0.967 0.968	BP	0.959 0.960	0.971 0.973	1.000 0.994		
1.003 1.000	0.997 0.992	0.981 0.986	0.997 0.994	1.010 1.007	1.024 1.022	1.041 1.043	
1.035 1.036	1.033 1.034	1.031 1.033	1.035 1.038	1.043 1.046	1.054 1.058	1.068 1.076	1.096 1.109

FIGURE 2

QUARTER ASSEMBLY PINWISE POWERS - CASE 2

CODE	PDQ07	CASMO	
K-INF	1.0938	1.0930	
U-235 w/o	3.08	3.08	
PPMB	1000	1000	
B-4-C w/o	1.0	1.0	

IT							
1.043 1.049	1.009 1.012	CASMO PDQ07					
0.992 0.993	0.971 0.974	BP					
0.983 0.978	0.975 0.967	0.953 0.954	0.958 0.950				
0.982 0.976	0.975 0.966	0.953 0.954	0.948 0.949	BP			
0.986 0.981	0.968 0.969	BP	0.960 0.961	0.972 0.974	1.000 0.994		
1.003 0.999	0.997 0.993	0.982 0.987	0.997 0.994	1.010 1.006	1.023 1.020	1.039 1.040	
1.034 1.035	1.032 1.033	1.030 1.032	1.034 1.036	1.042 1.045	1.052 1.056	1.065 1.073	1.092 1.105

FIGURE 3

QUARTER ASSEMBLY PINWISE POWERS - CASE 3

CODE	PDQØ7	CASMO	
K-INF	1.1891	1.1876	
U-235 w/o	3.38	3.38	
PPMB	1000	1000	
B-4-C w/o	0.2	0.2	

IT							
1.037 1.043	1.013 1.023	CASMO PDQØ7					
0.994 0.993	1.002 1.004	BP					
0.984 0.976	0.988 0.988	0.999 1.002	0.995 1.007				
0.982 0.972	0.986 0.986	0.999 1.003	1.003 1.014	BP			
0.984 0.975	0.995 0.994	BP	1.002 1.011	0.999 1.001	0.990 0.988		
0.988 0.980	0.992 0.991	1.001 1.002	0.994 0.996	0.991 0.986	0.990 0.983	0.995 0.989	
1.007 1.002	1.008 1.005	1.009 1.008	1.008 1.007	1.008 1.004	1.009 1.006	1.015 1.015	1.037 1.042

FIGURE 4

QUARTER ASSEMBLY PINWISE POWERS - CASE 4

CODE	PDQ07	CASMO	
K-INF	1.2210	1.2170	
U-235 w/o	3.38	3.38	
PPMB	1000	1000	
B-4-C w/o	CRGT	CRGT	

IT							
1.024 1.028	1.011 1.029	CASMO PDQ07					
0.990 0.989	1.028 1.031	CRGT					
0.980 0.971	0.996 1.006	1.041 1.050	1.030 1.063				
0.977 0.966	0.994 1.004	1.042 1.052	1.058 1.080	CRGT			
0.978 0.968	1.019 1.017	CRGT	1.046 1.062	1.028 1.030	0.983 0.985		
0.971 0.960	0.985 0.988	1.020 1.017	0.992 0.999	0.974 0.968	0.962 0.949	0.958 0.942	
0.980 0.967	0.983 0.975	0.988 0.983	0.984 0.977	0.977 0.966	0.972 0.959	0.974 0.961	0.993 0.984

FIGURE 5

QUARTER ASSEMBLY PINWISE POWERS - CASE 5

CODE	PDQ07	CASMO	
K-INF	1.3272	1.3267	
U-235 w/o	3.08	3.08	
PPMB	0	0	
B-4-C w/o	CRGT	CRGT	

IT							
1.026 1.030	1.013 1.031	CASMO PDQ07					
0.992 0.993	1.030 1.032	CRGT					
0.981 0.974	0.998 1.009	1.043 1.051	1.033 1.065				
0.978 0.969	0.996 1.006	1.044 1.053	1.060 1.080	CRGT			
0.979 0.970	1.019 1.016	CRGT	1.047 1.061	1.028 1.029	0.982 0.985		
0.971 0.960	0.985 0.988	1.020 1.016	0.992 0.995	0.974 0.968	0.960 0.948	0.956 0.941	
0.979 0.966	0.982 0.974	0.987 0.982	0.982 0.976	0.975 0.964	0.969 0.956	0.9[illegible] 0.[illegible]8	0.989 0.979

Section 5.0

DUKE POWER COMPANY
OCONEE NUCLEAR STATION

Attachment 1

Reload Design Methodology Technical Report
NFS - 1001

Revision 2

Pages

Title Page	4- 9 (New)
ii	4-10 (New)
iii	4-11 (New)
vi	4-12 (New)
vii	4-13 (New)
4-1	4-14 (New)
4-2	4-15 (New)
4-3	4-16 (New)
4-4	6- 9
4-5	6-10
4-6	6-11
4-7	10-1
4-8 (New)	10-2 (New)

DUKE POWER COMPANY
OCONEE NUCLEAR STATION
RELOAD DESIGN METHODOLOGY

Technical Report
NFS-1001

April 23, 1979
Revision 2 January 1981

4. FUEL MECHANICAL AND THERMAL PERFORMANCE

4.1 Introduction

Each fuel cycle design requires that thorough fuel mechanical and thermal assessments be performed. A reload design utilizes fuel designs that are bound by previous fuel assembly design analyses. Occasionally, however, minor differences in the design will occur (such as a change from 94% TD fuel to 95% TD fuel). These changes must then be assessed in regard to the following:

- Cladding creep collapse,
- Cladding strain,
- Cladding stress,
- Fuel pin temperature, and
- Fuel pin pressure

Design analyses that envelope the operation of all current fuel designs have been completed by the fuel vendor, and reanalysis is normally not required for a new fuel cycle design. Rather, a specific fuel cycle design is compared against the enveloping design analyses. The assessment must compare cladding and pellet designs against the pellet and cladding geometries and densities, etc., that have been considered in the enveloping design analyses. Further, the individual radial power histories during the fuel cycle (current and previous batches) must be compared against the generic radial power envelopes that have been used in the design analyses. In most cases, the design analyses will envelope the fuel cycle design being considered and no reanalysis is required. However, in some cases, either the radial power history or fuel geometry may lie outside of the enveloping design analyses, thus requiring partial or full reanalysis. The following subsections describe the types of comparisons that must be made to justify a fuel cycle design without reanalysis and provides some detail concerning the types of analyses that must be performed if required by either the fuel cycle design or by changes in the fuel design itself.

Table 4-1 presents a summary of all types of fuel thermal and mechanical performance assessment criteria that are used to determine whether a fuel cycle design, the cladding, and the pellets are enveloped by existing analyses. As shown in Table 4-1, several of these analyses require either a comparison against a fuel pin power versus burnup envelope or a comparison against an assembly radial power versus burnup envelope. Examples of these power history envelopes are presented in Figures 4-1 and 4-2. These envelopes change, as reanalysis is occasionally required, resulting in an expanded power history envelope. Figure 4-3 presents a flow chart for the fuel pin pressure and linear heat rate to melt analyses. Figure 4-4 is a mechanical analysis flow diagram.

4.2 Cladding Collapse

Cladding creepdown under the influence of external (system) pressure is a phenomenon that must be evaluated during each reload fuel cycle design to ensure that the most limiting fuel rod does not exceed the cladding collapse exposure limit. Cladding creep is a function of neutron flux, cladding temperature, applied stress, cladding thickness, and initial ovality. Acceptability of a fuel cycle design is demonstrated by comparing the power histories of all the fuel assemblies against the generic assembly power history used in existing design analyses, similar to Figure 4-2. The generic power history must be completely enveloping to avoid reanalysis. Duke Power Company uses its own PDQ edit code to automatically perform this comparison for all fuel assemblies at each depletion step. Changes in pellet or cladding design are also assessed in a similar manner: direct comparison with the fuel rod geometries of Table 4-1 and reanalysis, if necessary. Four separate fuel designs have been analyzed to form the generic cladding creep collapse analysis.

The CROV[1] computer code calculates ovality changes in the fuel rod cladding due to thermal and irradiation creep and is used to perform the fuel rod creep collapse analysis when required. CROV predicts

the conditions necessary for collapse and the resultant time to collapse. Conservative inputs to the CROV cladding collapse analysis include the use of minimum cladding wall thickness and maximum initial ovality (conservatively assumed to be uniformly oval), all as allowed by manufacturing specifications. Other conservatisms included are minimum prepressurization pressure and zero fission gas release. Internal pin pressure and cladding temperatures, input to CROV, are calculated by TACO2[6] using a radial power history similar to that of Figure 4-2, a generic pin to assembly local peak, and a standard axial flux shape.

The conservative fuel rod geometry and conservative power history are used to predict the number of EFPH required for complete cladding collapse. To demonstrate acceptability, the maximum expected residence time of the cycle is compared against the EFPH required for complete collapse.

4.3 Cladding Strain Analysis

The limit on cladding strain is that uniform strain of the cladding should not exceed 1.0%.

A generic strain analysis has been completed by the fuel vendor using TACO2 to ensure that the strain criterion above is not exceeded. To determine whether the fuel and fuel cycle designs are enveloped by existing analyses, the criteria of Table 4-1 are reviewed.

Should reanalysis be required, TACO2 will be used to determine the fuel rod dimensional changes that occur between the two power levels considered by the conservative design power ramp used in the strain analysis. Then, the maximum tensile (elastic and plastic) strain, which occurs at the cladding I.D., is determined from the following equation:

$$\text{Strain} = \frac{(\text{Pellet O.D.})_{\text{peak}} - (\text{Pellet O.D.})_o \times 100}{(\text{Pellet O.D.})_o} \leq 1\%$$

where $(\text{Pellet O.D.})_{\text{peak}}$ = the maximum pellet O.D. at the local power peak, and

$(\text{Pellet O.D.})_o$ = pellet O.D. prior to and after a local power ramp.

Pellet O.D. dimensions are used to calculate cladding strain because the strain itself is caused by pellet thermal expansion.

The strain analysis is completed in two parts:

- Part 1 employs TACO2 to determine when pellet contact occurs. A conservative fuel rod geometry is used in conjunction with a $\leq$ 1.5 axial flux shape, and the core average linear heat rate at 100% power to characterize gap closure. If contact occurs prior to 30,000 MWD/MTU, then Part 2 will use a ramp from 2 KW/FT to a final linear heat rate that is consistent with centerline fuel melt. Whereas, if contact occurs after 30,000 MWD/MTU, then the ramp's peak linear power is reduced to a lower value that is consistent with maximum local powers that could occur at burnups greater than 30,000 MWD/MTU.

- Part 2 of the strain analysis is the power ramp calculation, also performed on TACO2, which calculates the change in fuel pellet O.D. that occurs from the change in power level induced by the power ramp. The change in pellet O.D. is then used to perform the hand calculation of cladding strain using the equation above. The cladding and pellet are assumed to be in hard contact at the initiation of this ramp.

Thus, there are two major conditions in this scenario that make it conservative. The first is the extreme power change that is used to simulate the worst case peaking. The second is that the pellet is assumed to be in hard contact at initiation of the ramp. This is a conservative assumption since the power ramp is

initiated from 2 KW/FT, and pellet/cladding contact is not expected to occur at this low linear heat rate.

4.4 Cladding Stress Analysis

The cladding stress analysis for a new fuel cycle design is similarly bounded by a conservative design analysis that uses Section III of the ASME Boiler and Pressure Vessel Code as a guide in classifying the stresses into various categories, assigning appropriate limits to these categories, and combining these stresses to determine stress intensity. Each new fuel cycle design is assessed against the criteria stated in Table 4-1 to determine if reanalysis is required. The stress analysis is very conservative, and reanalysis should not be required for standard Mark B reloads. However, an assessment is made for each reload design using the criteria of Table 4-1.

The fuel rod stress analysis considers those stresses that are not relaxed by small material deformation, and this anaysis complies with the following design critera:

- All fuel cladding stresses (primary and secondary) shall not exceed minimum unirradiated yield strength for condition I and II occurrences.

- The stress intensity value of the primary membrane stresses in the fuel rod cladding, which are not relieved by small material deformation of the cladding, shall not exceed 2/3 of the minimum unirradiated yield strength.

The above criteria keep the primary loads well below material allowable.

In performing the stress analysis, all the loads were selected to represent the worst case loads and were then combined. This repre-

sents a conservative approach since they cannot occur simultaneously. This insures that the worst case conditions for condition I and II events are satisfied. In addition, these input parameters were chosen so that they conservatively envelope all Mk-B design conditions.

The primary membrane stresses result from the compressive pressure loading. Stresses resulting from creep ovalization are addressed in the creep collapse analysis.

Since the internal fuel rod pressure cannot exceed system pressure for condition I and II occurrences (at coolant temperatures greater than 425°F), the need to address tensile stresses at hot zero power (HZP) conditions and higher is eliminated. The tensile stresses were addressed at cold conditions. The minimum internal fuel rod pressure at HZP conditions is combined with the maximum design system pressure during a transient to simulate the maximum pressure differential across the cladding. The tensile stress analyzed occurs at cold (room temperature) conditions at BOL. This is the worst case since the grid loads will be maximum at that point.

The worst case compressive pressure loads were combined with the other worst case loads. These are described below:

- The maximum grid loads will occur at BOL. During operation, the contact force will relax with time due to fuel rod creepdown and ovalization as well as grid spring relaxation.

- The maximum radial thermal stress will occur at the maximum rated power (power level corresponding to centerline fuel melt). This stress cannot physically occur at the same time the maximum pressure loading occurs, but is assumed to do so for conservatism. (Maximum cladding temperature gradient is combined with minimum pin pressure.)

- The ovality bending stresses are calculated at BOL conditions. A linear stress distribution is assumed. The creep collapse analysis calculates the stress increase with time and ovalization.

- Flow induced vibration and differential fuel rod growth stresses are also addressed.

4.5 Fuel Pin Pressure Analysis

The pin pressure analysis is assessed against the design basis analysis criteria and envelopes as indicated in Table 4-1. If any of the parameters of this table are violated, then a reanalysis is performed.

Pin pressure analysis is performed using TACO2. The rod is assumed to have a 1.5 symmetric axial flux shape, with a pin power history similar to that presented in Figure 4-1. Incore fuel densification is minimized in this analysis to yield a smaller plenum volume and a maximum pin pressure.

Figure 4-5 presents the result of an analysis of pin pressure versus burnup, performed by Duke Power Company, using TACO2. This analysis was performed for an extended burnup fuel cycle design, using the pin power history indicated in Figure 4-1, but with lower, more realistic axial flux shapes than the 1.5 cosine shape that is used for Reload Design purposes. (Refer to Table 4-2 for the axial flux shapes used in this extended burnup analysis.) To satisfy mechanical design criteria, pin pressure must be less than system pressure (2200 psia).

4.6 Linear Heat Rate Capability

Linear heat rate capability of all fuel rods in a reload batch is assessed by comparison against the criteria and envelopes of Table

4-1. Any rod whose geometry or power history falls outside of those criteria must be reanalyzed.

The Linear Heat Rate to Melt (LHRTM) analysis is performed using TACO2, assuming maximum incore pellet densification. This analysis assumes a conservative pin power history, similar to that of Figure 4-1, and a 1.5 cosine axial flux shape. In this analysis, very small axial segments of the fuel rod are spiked to high linear heat rates at each burnup step until centerline fuel melt occurs. The resulting heat rate required to reach centerline fuel melt at each burnup is then plotted versus burnup.

Figure 4-6 is a plot of fuel LHRTM versus burnup for an extended burnup fuel cycle design. This TACO2 analysis, performed by Duke Power Company, represents the pin power history of Figure 4-1, but with more realistic axial flux shapes than the 1.5 cosine that is used for reload fuel cycles. (Refer to Table 4-2 for the axial flux shapes used in this analysis.) The minimum LHRTM occurs early in life due to fuel densification, but quickly increases due to the offsetting effects of cladding creepdown, pellet swelling, and fuel relocation. (No credit is taken for fuel relocation in LHRTM analyses).

TABLE 4-1
FUEL MECHANICAL PERFORMANCE ASSESSMENT CRITERIA

Item No.	Parameter Reviewed[1]	Analysis Category: Cladding Collapse[2]	Cladding Strain	Cladding Stress	Pin Pressure	Linear Heat Rate Capability
1	Pin rower History vs Burnup	NA	NA	NA	Figure 4-1	Figure 4-1
2	Radial Assembly Power History vs Burnup	Figure 4-2	NA	NA	NA	NA
3	Clad O.D.	Yes	Yes	Yes	Yes	Yes
4	Clad I.D.	Yes	Yes	Yes	Yes	Yes
5	Clad Thickness	Yes	Yes	Yes	Yes	Yes
6	Clad Initial Ovality	Yes	NA	NA	NA	NA
7	Pellet Diameter	Yes	Yes	Yes	Yes	Yes
8	Pellet Density	Yes	Yes	Yes	Yes	Yes
9	Initial Prepressure	Yes	Yes	Yes	Yes	Yes

NOTES:
1. These criteria are the more significant items reviewed for a reload fuel cycle design, and do not include minor assumptions that are part of the bases.
2. The cladding collapse review actually is performed separately for each type of Mark B fuel design (four sets of parameters exist, corresponding to four separate fuel designs).

TABLE 4-2

Axial Flux Shapes Used for Thermal Analysis
(Reference, Figures 4-5, 4-6)

Burnup Range	Peak of Axial Cosine Shapes
0 - 15,100	1.28
15,100 - 35,000	1.22
> 35,000	1.16

NOTE: Standard reload design analyses always employ a 1.5 P/P axial flux shape for pin pressure and LHRTM analysis.

FIGURE 4-1 PIN POWER VERSUS BURNUP ENVELOPE FOR THERMAL ANALYSIS ASSESSMENTS (EXAMPLE ONLY)

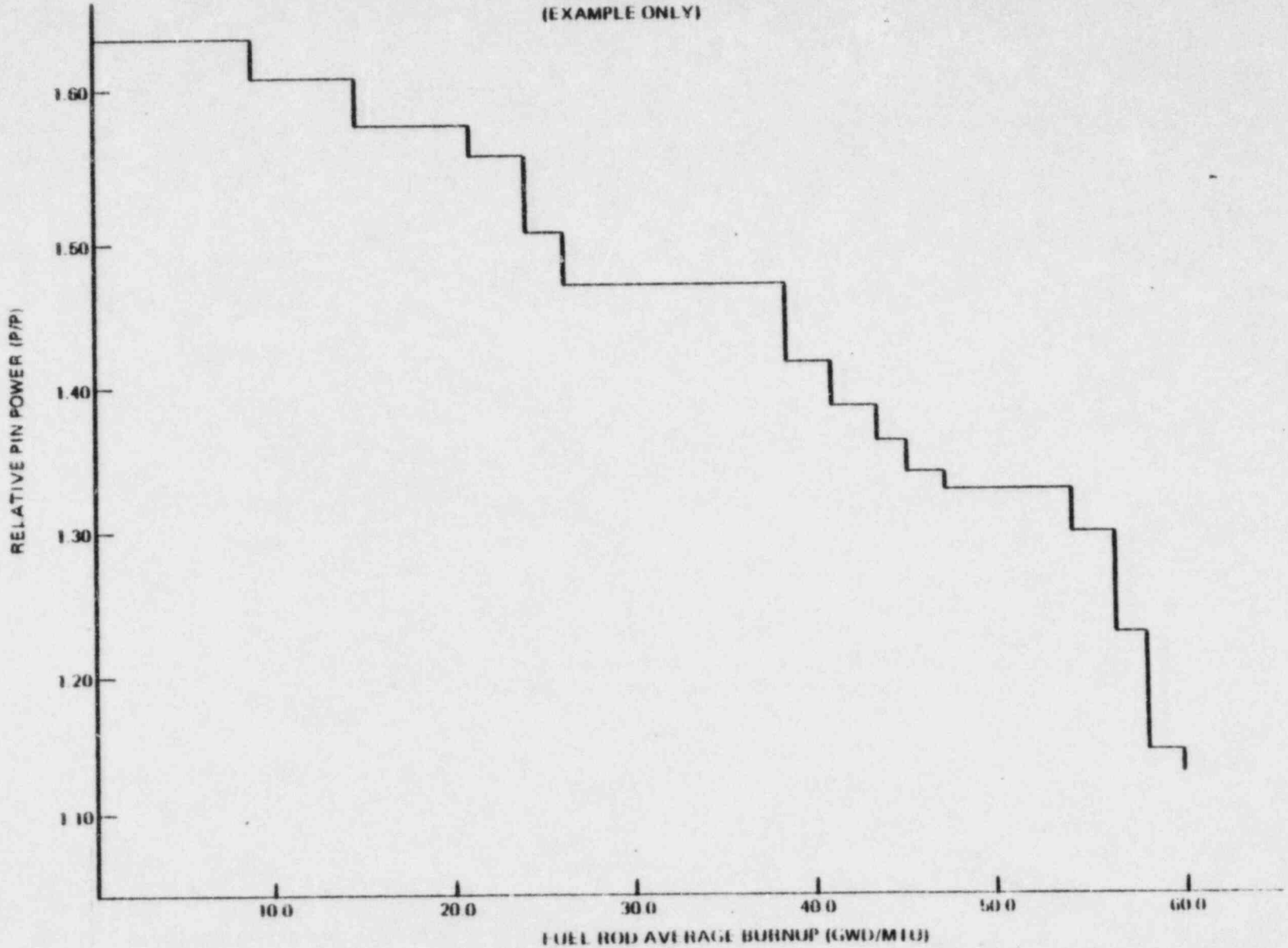

FIGURE 4 2 RADIAL ASSEMBLY POWER VERSUS BURNUP FOR CREEP COLLAPSE ANALYSIS ASSESSMENTS (EXAMPLE ONLY)

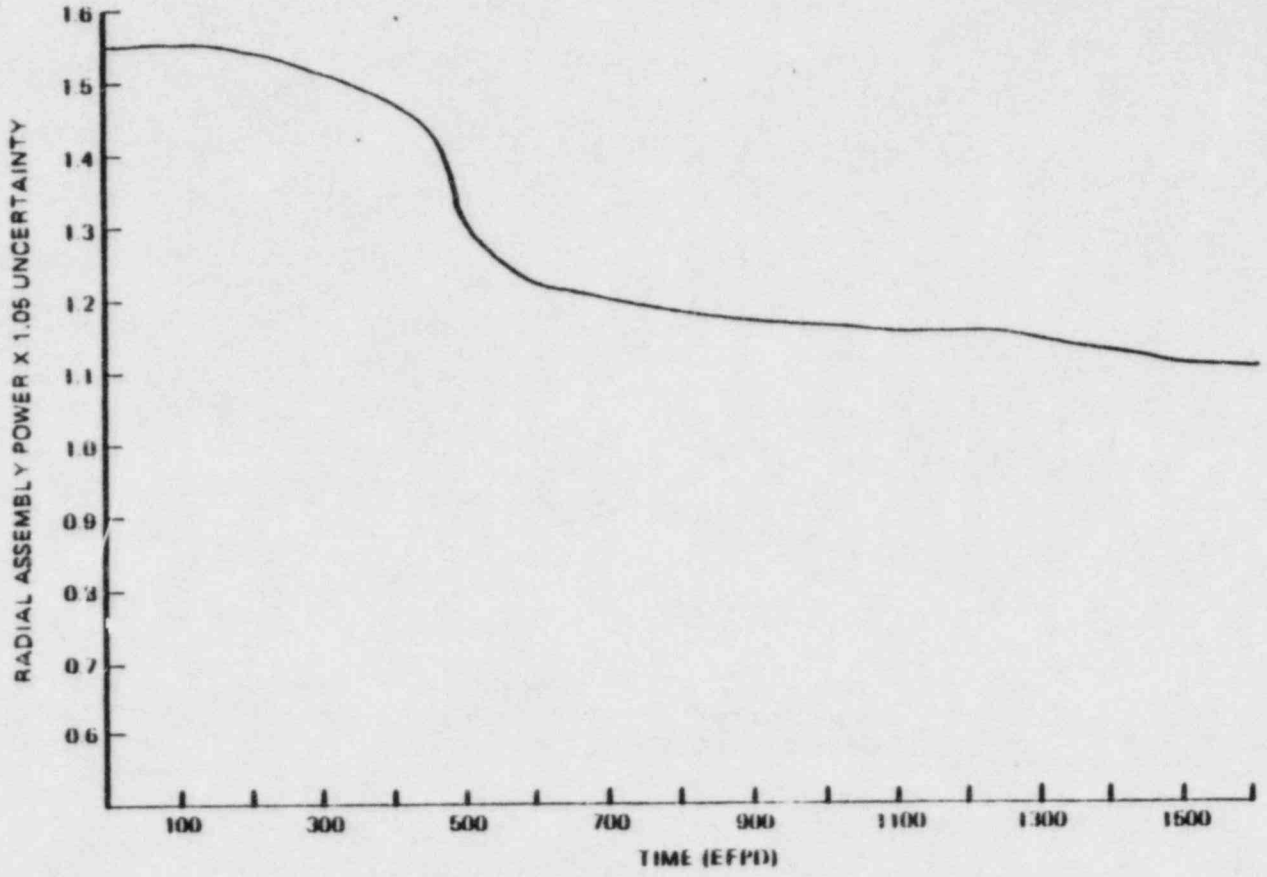

FIGURE 4-3 THERMAL ANALYSIS FLOW DIAGRAM

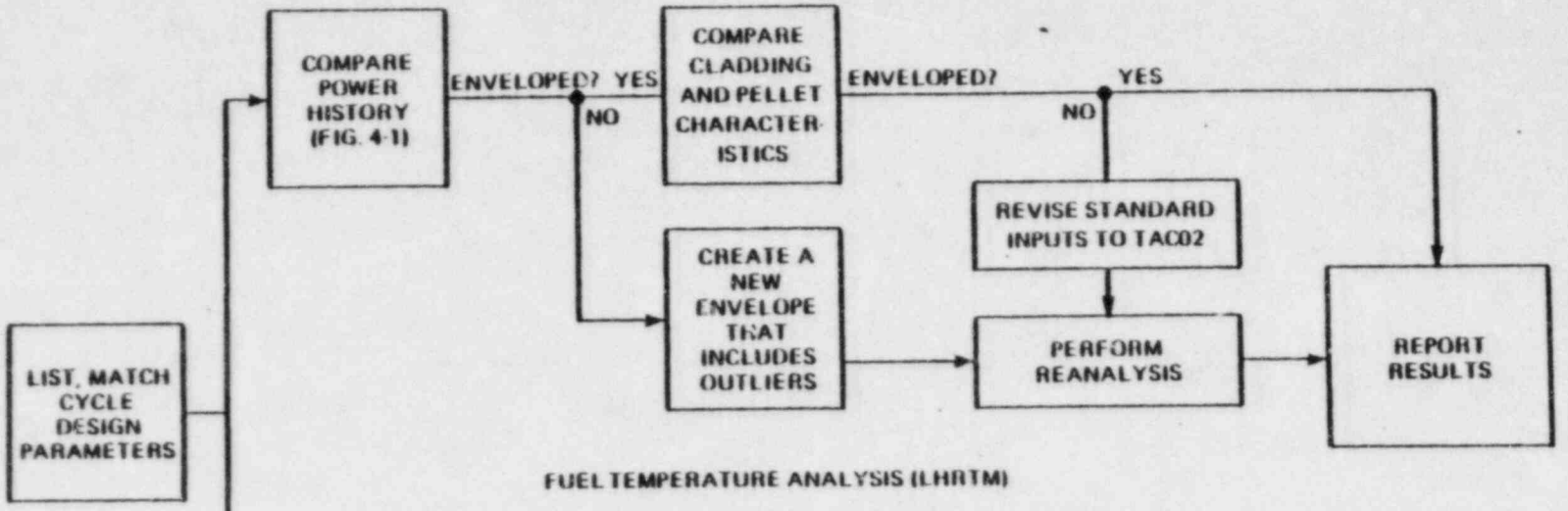

FUEL TEMPERATURE ANALYSIS (LHRTM)

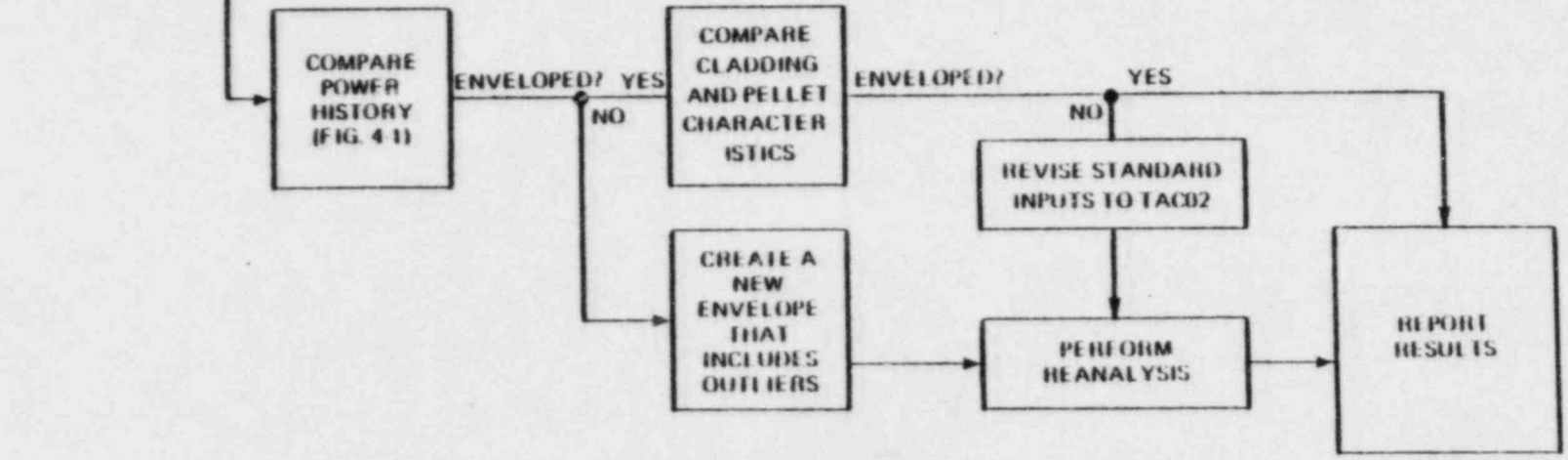

FUEL PIN PRESSURE ANALYSIS

FIGURE 4 4 MECHANICAL ANALYSES FLOW DIAGRAM

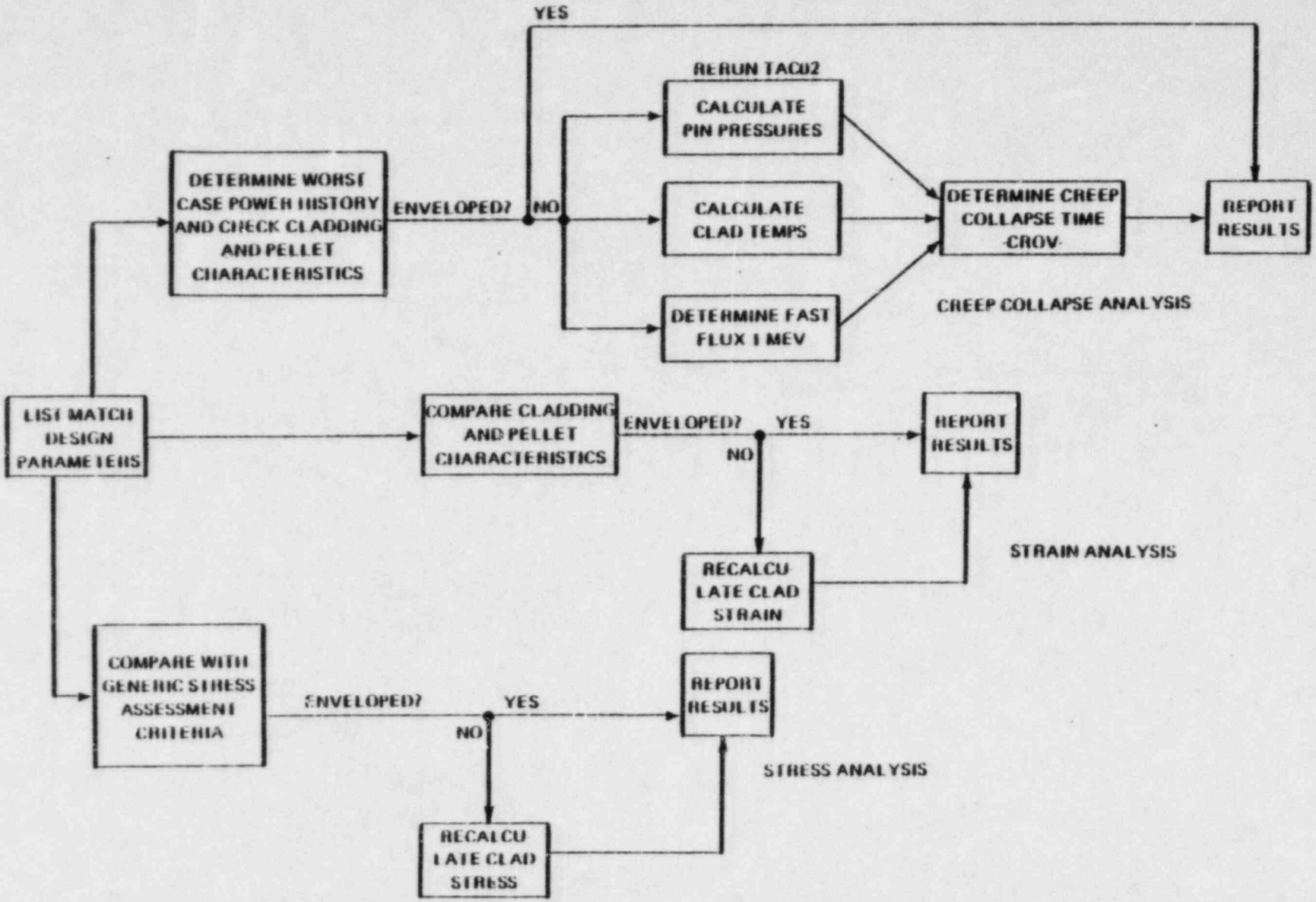

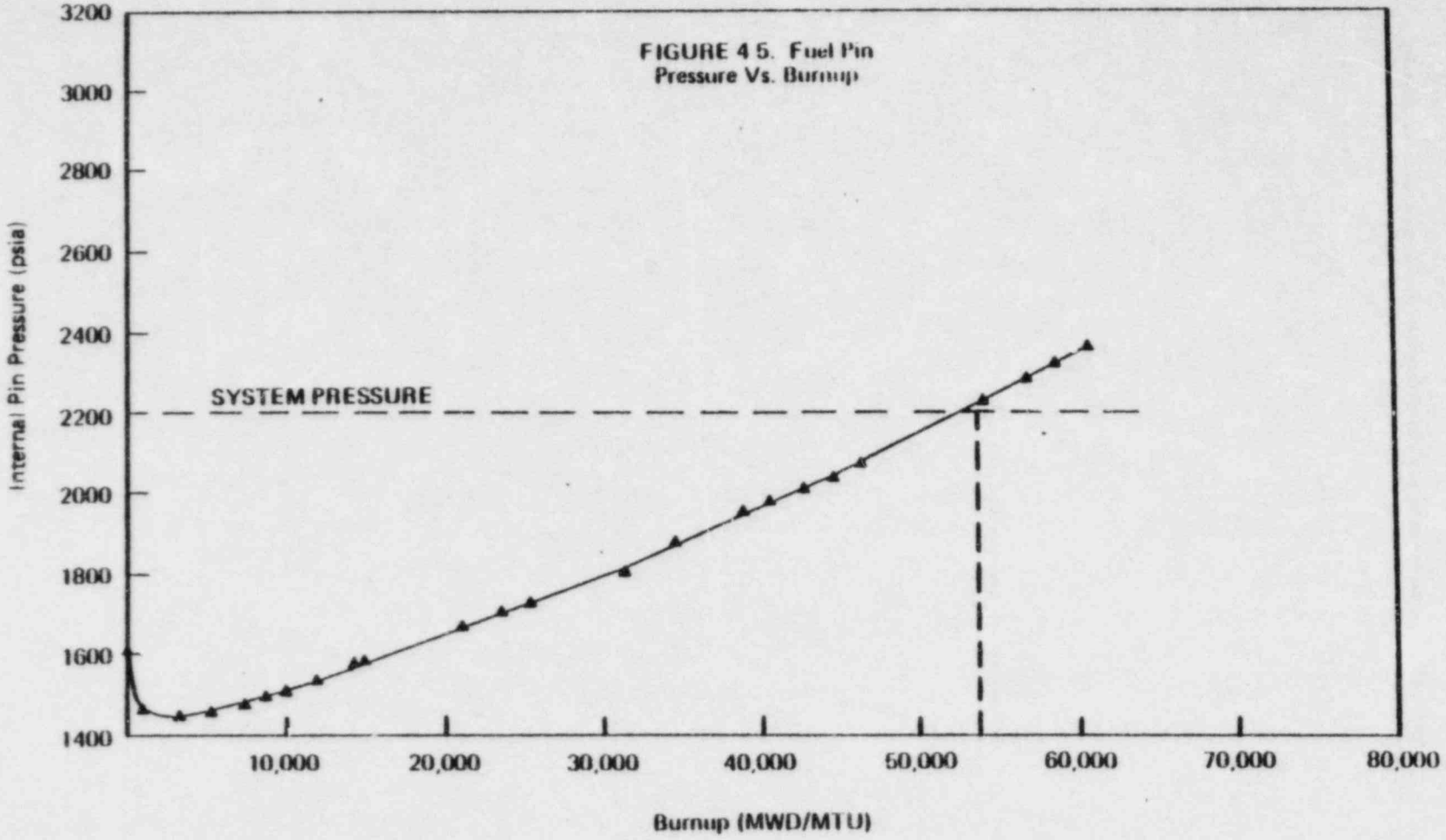

FIGURE 4.5. Fuel Pin Pressure Vs. Burnup

Figure 4.6
Fuel Linear Heat Rate to Melt Vs Burnup

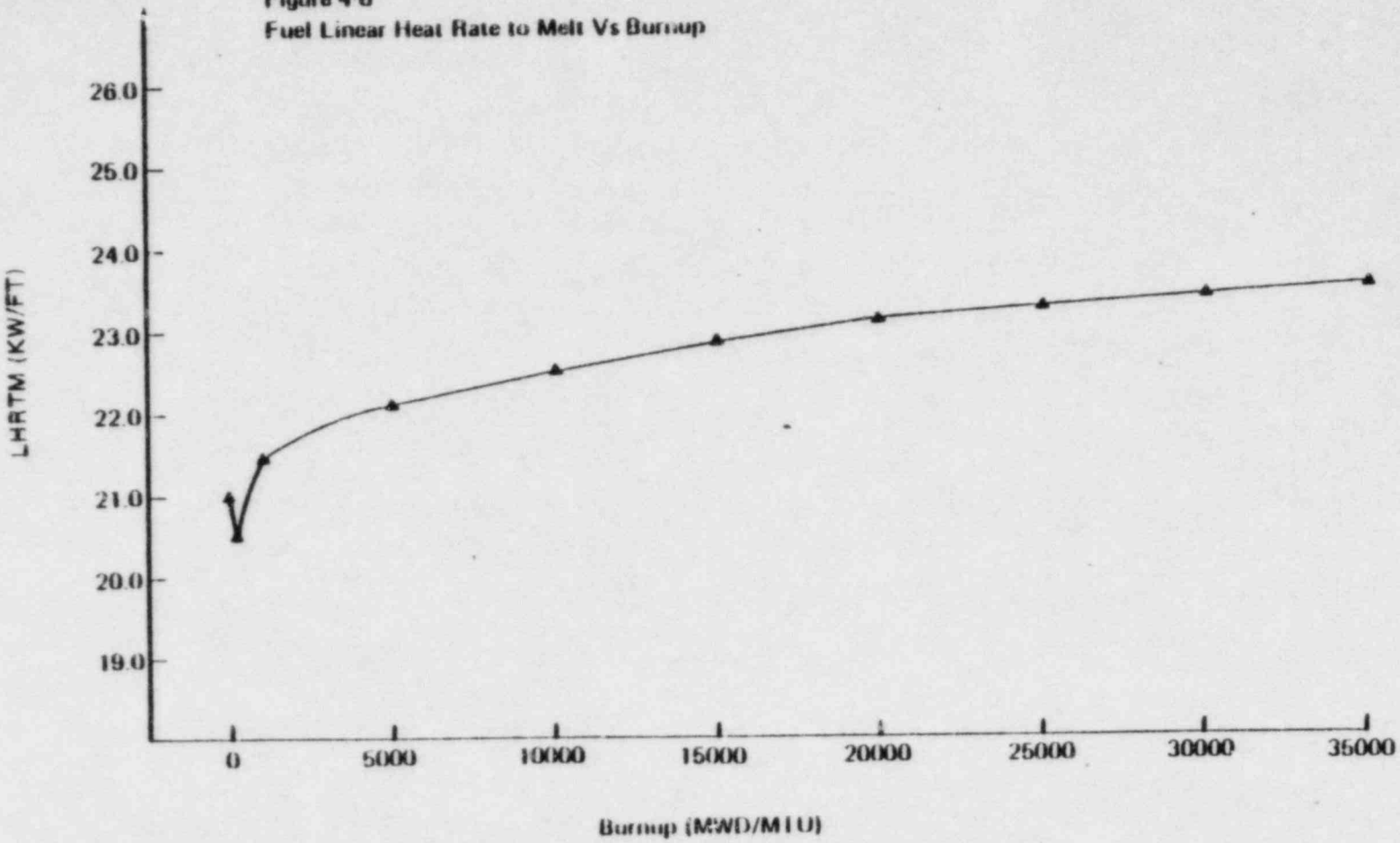

pressure drop regardless of variations in local peaking and axial power shape. In other words, hot channel flow rate will be adjusted by the code to satisfy core-wide pressure drop as local conditions are varied. The axial power shapes input to these parametric hot channel runs are smooth cosine curves whose peak can be specified at various distances up the channel for each series of axial peaking factors. To obtain the maximum allowable peaking factor for each data point, power input to the channel is increased until the limiting DNBR of 1.4326 is reached. This process determines a maximum allowable total peak for a specified axial peak and its location.

After completion of these parametric analyses, two sets of generic DNBR curves or Maximum Allowable Peaking (MAP) curves are determined. One set is used for DNB operational offset limits, and the second set is used for RPS DNB offset limits. The generic DNBR curves used as operational limits are a conservative overlay of 1) the generic DNBR curves used for RPS offset limits, and 2) another set of MAP curves which have the reference design DNBR as their basis. Both sets of limits consider the extremities of the P-T core protection envelope (619°F and 1800 psig) as potential core operating conditions. Thus both the operational DNB offset limits and the RPS DNB offset limits have considered the worst case temperature and pressure envelope permitted by the RPS.
The last step in the thermal-hydraulic analysis is to take actual power shapes that gave the lowest DNBRs during the maneuvering analysis and input these irregularly shaped axial curves into the hot channel code to verify conservatism of the corresponding cosine curves used to develop the generic DNBR curves. A typical set of generic DNB curves is provided in Figure 6.3.

6.8.3 Hot Channel Factors

The following additional hot channel factors on local heat flux are utilized in the thermal-hydraulic analyses for developing the generic DNBR curves:

1.026 = penalty incurred to increase calculated axial powers since flux depressions at the spacer grids are ignored.

1.024 = the ratio of the total nuclear uncertainty of 1.075 to the radial nuclear uncertainty of 1.05.

Thus, in determining the generic DNB curves, the normal value of Fq" is increased from 1.014 to 1.065.

6.9 Transient Analysis - Determination of the Flux - Flow Ratio

During a loss of one or more reactor coolant pumps, the core is prevented from violating the 1.4326 minimum DNBR criterion by a reactor trip that is initiated by exceeding the allowable reactor power to reactor coolant flow ratio setpoint. Loss of one or more reactor coolant (RC) pumps is also detected by the RC pump monitors. That is, independently of the power to flow trip, loss of one RC pump will result in an automatic reactor runback. Similarly, loss of two or more RC pumps from above 55% full power will cause a reactor trip.

The thermal-hydraulic analysis that is used to set the power to flow trip setpoint for coastdown protection conservatively assumes the loss of two RC pumps. The transient is analyzed using the RADAR code to assure that the 1.4326 minimum DNBR criterion is not violated at anytime during the loss of one or more RC pumps.

The steady state thermal-hydraulic analysis provides the starting point for the transient analysis. The power to flow setpoint itself is derived from this analysis by varying the time of reactor trip following the loss of two RC pumps (that is by considering various trip setpoints) until the minimum ratio required to maintain the minimum DNBR of 1.4326 has been determined. Calculation of the actual (error corrected) power to flow setpoint used at the nuclear station is described in Section 7.3.2.

6.10 Application of the Rod Bow Penalty

In existing thermal-hydraulic analyses, a very conservative DNBR penalty is included to account for rod bowing effects. This penalty (11.2%), however, has been reduced by 1% because of the flow area (rod pitch) reduction factor already included in the thermal-hydraulic analysis.

2

For some reloads, additional credit can be applied based on the fact that primary coolant flow can be proven to be higher than the 106.5% design flow.

The resulting net penalty is applied directly to the final DNBR margins or by increasing the 1.3 DNBR criteria by the percent penalty, resulting in a DNBR criterion of 1.4326. 2

In future fuel cycle designs, this penalty will be revised to reflect the true effect of measured rod bowing on minimum DNBR (if any additional penalty is required). References 12 and 13 document the methods to be used for determining the true rod bow penalty. Then, a determination will be made to either maintain the current margin which exists or to eliminate part or all of this margin.

10. REFERENCES

1. Program to Determine In-Reactor Performance of B&W Fuels - Cladding Creep Collapse, BAW-10084, Rev. 2, Babcock & Wilcox, Lynchburg, Virginia, October, 1978. | 2

2. R. A. Turner, Fuel Densification Report, BAW-10054, Rev. 02, Babcock & Wilcox, Lynchburg, Virginia, May 1973.

3. Oconee 1 Fuel Densification Report, Revision 1, BAW-1387, Rev. 1, Babcock & Wilcox, Lynchburg, Virginia, April 1973.

4. A. J. Eckert, H. W. Wilson, and Y. E. Yoon, Oconee 2 Fuel Densification Report, BAW-1395, Babcock & Wilcox, Lynchburg, Virginia, June 1973.

5. Oconee 3 Fuel Densification Report, BAW-1399, Babcock & Wilcox, Lynchburg, Virginia, November 1973.

6. TACO2 - Fuel Pin Performance Analysis, BAW-10141, Babcock & Wilcox, Lynchburg, Virginia, August 1979. | 2

7. Correlation of Critical Heat Flux in a Bundle Cooled by Pressurized Water, BAW-10000A, Babcock & Wilcox, Lynchburg, Virginia, June 1976.

8. Oconee Nuclear Station, Units 1, 2, and 3, Final Safety Analysis Report, Docket Nos. 50-269, -270, and -287.

9. Electric Power Research Institute (EPRI), Advanced Recycle Methodology Program (ARMP) System Documentation, September 1977.

10. J. M. Alcorn and R. H. Wilson, CHATA - Core Hydraulics and Thermal Analysis, BAW-10110, Babcock & Wilcox, Lynchburg, Virginia, January 1976.

11. R. C. Jones, J. R. Biller, and B. M. Dunn, ECCS Analysis of B&W's 177-FA Lowered Loop NSS, BAW-10103A, Rev. 3, Babcock & Wilcox, Lynchburg, Virginia, July 1977. | 1

12. J. H. Taylor (B&W) to D. B. Vassallo (NRC), Letter, "Determination of the Fuel Rod Bow DNB Penalty," December 13, 1978. 2

13. D. B. Vassallo (USNRC) to J. H. Taylor (B&W), Letter "Calculation of the Effect of Fuel Rod Bowing on the Critical Heat Flux for Pressurized Water Reactors," June 12, 1978. 2

DUKE POWER COMPANY
POWER BUILDING
422 SOUTH CHURCH STREET, CHARLOTTE, N. C. 28242

4144

WILLIAM O. PARKER, JR.
VICE PRESIDENT
STEAM PRODUCTION

June 16, 1981

TELEPHONE AREA 704
373-4083

Mr. Harold R. Denton, Director
Office of Nuclear Reactor Regulation
U. S. Nuclear Regulatory Commission
Washington, D. C. 20555

Attention: Mr. J. F. Stolz, Chief
Operating Reactors Branch No. 4

Re: Oconee Nuclear Station
Docket Nos. 50-269, -270, -287

Dear Sir:

In response to your letter dated June 2, 1981 requesting additional information regarding Technical Report NFS 1001, "Reload Design Methodology," please find the attached responses in Attachment 1 of this submittal. Attachment 2 transmits Revision 4 of Technical Report 1001, "Reload Design Methodology."

Very truly yours,

William O. Parker, Jr.

JLJ:scs

Attachments

bcc: w/o Attachment 2
K. S. Canady
N. A. Rutherford
R. L. Gill
R. C. Futrell
P. M. Abraham
R. H. Clark
R. M. Gribble
J. E. Smith
R. T. Bond
T. B. Owen
Section File OS-801.01

ATTACHMENT 1

DUKE POWER COMPANY
OCONEE NUCLEAR STATION

Response to NRC Letter of June 2, 1981

Question 492.1 (Section 6.7)

Provide a more detailed discussion on how the core outlet pressure - reactor outlet temperature curves are determined.

Response

The core outlet pressure - reactor outlet temperature curves (P-T Safety Limits, Figure 6.2) are determined by varying core outlet pressure and core inlet temperature using CHATA Command Routines 1 and 2 (CR 1/2). Using the equivalent two channel model, described in Section 6.6, core inlet temperature is varied at a constant pressure (one inlet temperature value per CHATA run) until the inlet temperature that yields a hot channel minimum DNBR of 1.4326 at that pressure has been determined. This single limiting combination of reactor coolant pressure and inlet temperature is then used to calculate the corresponding reactor vessel outlet temperature, using a simple reactor vessel heat balance.

This process is repeated over a range of pressures, typically 1800, 1900, 2000, 2100, 2200, and 2300 psia. For each of these pressures, a limiting inlet temperature is determined and a corresponding reactor outlet temperature is calculated. Finally, the resulting P-T Safety Limits are plotted for each allowable combination of operating reactor coolant pumps.

Question 492.2 (Section 6.8.2)

The method used to determine the Maximum Allowable Peaking (MAP) factor was to vary the hot channel power until the limiting DNBR was reached. Babcock and Wilcox varies the radial peaking factor rather than the power. Demonstrate that the Duke method is an acceptable and equivalent method when compared to the Babcock and Wilcox method.

Response

The Duke method is identical to the Babcock and Wilcox method; further, the operation of CHATA Command Routine 8 prohibits such a variation in this procedure. In addition to this response, it may also be helpful to review Reference 10 of NFS-1001, specifically page 10-3 and Appendix H, which describe the CHATA Command Routines.

The MAP curves are generated using CHATA Command Routines 1 and 8 (CR 1/8) and the equivalent two channel model described in Section 6.6. (This two channel model contains an average channel (Command Routine 1) that represents the overall core and a hot channel (Command Routine 8) that is "driven" by the average channel's pressure drop.

Command Routine 8 (CR8) accepts the average channel (CR1) pressure drop as a boundary condition, and varies hot channel flow and percent over power in the hot channel until the criteria of dP and minimum DNBR are satisfied in the hot channel.

The hot channel in CR8 is a single rod; therefore, for this single rod, overpower is functionally equivalent to pin peak. Usually the pin power input

data field in the CR8 hot channel model is set equal to the core overpower fraction (for example 1.12) such that CR8 will output the allowable pin peak directly.

Question 492.3 (Section 6.8.2)

More information is needed on the generic DNBR curves or MAP curves.

Item 1: Provide a detailed discussion of how the curves are developed.

Response

MAP curves are developed using the equivalent two channel model described in Section 6.6 and further described in Duke's response to question 492.2, above. CHATA Command Routines 1 and 8 are used for MAP analyses.

Maximum allowable total peaking (MAP) limits are determined both for RPS DNB offset limits and for "operational" DNB offset limits. These two types of MAP curves are described in the response to Item 2 of this question.

CHATA Command Routines 1 and 8 are used to vary (in a series of hundreds of separate computer analyses) the axial flux shape peak and axial peak location. One computer run is required for each combination of axial peak and axial peak location, for example, an axial peak of 1.7 at 80% of the active fuel length. CHATA CR 1/8 is run such that the average channel model (CR1) calculates and transmits the dP boundary condition to the hot channel (CR8). The hot channel model then determines the maximum rod power (peak) and the hot channel flow that satisfy the dP and DNBR boundary conditions.

The inputs to CR 1/8 for MAP analyses are core operating conditions (temperature, pressure, power, and average channel flow), average and hot channel geometries, hydraulic characteristics, average channel pin power (pin peak = 1.0), and a specific axial flux shape to be assessed. To develop a set of MAP curves, axial flux shape is varied from an axial peak of 1.1 to 2.0, with the location of the axial peak varying from the bottom to top of the active fuel length in increments of 10 percent of active fuel length. Output from the hot channel model (CR-8) is the allowable hot channel overpower fraction (functionally equivalent to pin peak for this single rod model). The output pin peak is then multiplied by the axial peak to yield the maximum allowable total peak for the flux shape being analyzed.

Item 2: State the differences between the RPS DNB offset curves and the DNB operational offset curves.

Response

Two types of MAP curves are developed. One type is used for the RPS DNB offset limits. Multiple subsets of RPS MAP limits are determined, one subset for each allowable combination of operating reactor coolant pumps. The second type of MAP curves is used for DNB operational offset limits.

RPS MAP curves are determined at two separate operating conditions (temperature and pressure) for each allowable combination of operating reactor coolant

pumps, as shown in Table 492.3-1. These two sets of RPS MAP curves (high temperature and low pressure) are overlayed at each allowable pump combination, and the conservative overlay is chosen for RPS DNB offset limits. The result of the RPS MAP analysis is three separate families of curves (similar to Figure 6.3), one for four RC pumps operating, one for three pumps, and one for two pumps.

Operational MAP curves are developed for operation with four reactor coolant pumps and are based on the most conservative overlay of the RPS MAP curves and a new set of MAP curves that are determined at the conditions stated in Table 492.3-2.

Item 3: State how the MAP curves which have the reference design DNBR as their basis are obtained.

Response

The MAP curves referred to in this item are the "operational" MAP curves, previously described. As stated in the Response to Item 2, above, the operational MAP curves are the conservative overlay of 1) the RPS MAP curves at four pump conditions and 2) MAP curves determined at 102% power and based on the reference DNBR at 102% power. The purpose of this additional overlay at 102% power is to insure that the operational offset limits preserve the initial DNB ratio assumed for DNB limited accidents.

Item 4: State how the extremities of the P-T core protection envelope are considered in developing the DNB offset limits.

Response

The low pressure and high temperature extremities of the variable P-T envelope are used as operating conditions for the RPS MAP analysis by performing the RPS MAP analyses at the operating conditions stated in Table 492.3-1. The extremities for the four pump RPS MAP analyses carry-through into the operational MAP limits because the operational MAP curves are an overlay of the RPS MAP curves and the 102% power reference DNB condition.

Table 492.3-1

MAP Analysis Input Operating Conditions

4 Pump Operation

High Temperature	Low Pressure
Core Power Level = 112% Rated T RV outlet = 619F	Core Power Level = 112% Rated * Tcore inlet = 544F (typical)
*Pcore = 2063 psia (typical)	Pcore = 1800 psia
MDNBR = 1.4326	MDNBR = 1.4326

3 Pump Operation

High Temperature	Low Pressure
Core Power Level = 87.2% Rated T RV outlet = 619F	Core Power Level = 87.2% Rated * Tcore inlet = 542 (typical)
*Pcore = 2065 PSIA	Pcore = 1800 psia
MDNBR = 1.4326	MDNBR = 1.4326

2 Pump Operation

High Temperature	Low Pressure
Core Power Level = 59.4% Rated T RV outlet = 619F	Core Power Level = 59.4% Rated * Tcore inlet = 552F (typcial)
* Pcore = 1870 psia	Pcore = 1800 psia
MDNBR = 1.4326	MDNBR = 1.4326
* Pcore is that pressure which results in a MDNBR = 1.4326 with a RV outlet temperature at the high temperature setpoint.	* Tcore inlet is that temperature that results in a MDNBR = 1.432o with a pressure at the low pressure setpoint.

Table 492.3-2

Operational MAP Input Operating Conditions

The following operating conditions describe the additional set of MAP curves that are developed at 4 pump conditions and are overlayed with the RPS MAP curves to form the operational MAP curves.

Core Power Level = 102% Rated*

Tcore inlet ≅ 557.2F (includes +2°F error)

Pcore = 2135.0 psia (includes -65 psi error)

MDNBR ≅ 2.38 (B&W-2)*

*NOTE: The maximum allowable total peak resulting from these constraints is the same as the maximum allowable peak that results from an analysis performed at 112% power and a DNBR of 2.05.

Question 492.4 (Section 7.3.1)

In determining the reactor protection system P-T set points, the applicant stated that the RCS high pressure trip set point was 2356 psig. In the Technical Specifications for Oconee Units 1, 2, and 3, the high pressure trip is at 2300 psig. Correct this discrepancy.

Response

The current value for the high pressure trip set point is indeed 2300 psig. This discrepancy will be corrected in the next revision of the report on the following pages:

1) Paragraph 2, page 7-0
2) Table 7-1, page 7-16
3) Figure 7-4, page 7-20

Question 492.5 (Section 7.3.1)

Provide the values that are used to error adjust the P-T set point curve. How are these numbers obtained?

Response

The error-adjustment of the P-T set point curve is the same as for previous Oconee reload designs. The error-adjustment for temperature is $+1^{\circ}F$. This conservatively accounts for the maximum temperature error in the instrumentation string. The pressure measurement error is $\pm$ 30 psi which is added to the minimum pressure difference between the core outlet and the pressure tap on the hot leg, $\Delta P = +30$ psi. The net error-adjustment for pressure is 0 psi.

Question 492.6 (Section 7.3.2)

On page 7-10 reference is made to the flux/flow ratio ratio calculated in Section 6.8. The flux/flow ratio is calculated in Section 6.9. Correct this discrepancy.

Response

This editorial correction will be in the next revision of the report.

Question 492.7 (Section 7.3.2)

Provide a reference for the 6.5 percent full power error-adjustment factor used in setting the RPS power-flow imbalance.

Response

The 6.5 percent full power error-adjustment is the same as for previous Oconee reload designs and is discussed in the B&W Topical Report, "RPS Limits and Setpoints", BAW-10121, on page 5-13. Although this report is based on the 205 class plant, this factor is the same for the Oconee Units (see Technical Specifications 2.3 and 4.1).

SUPPLEMENT 1

ABSTRACT

Measurement and calculational techniques and comparisons of calculated and measured results for core physics parameters are presented in this supplement. The measurements are from Oconee Unit 1, Cycles 1-5 and the calculations are performed with EPRI-NODE-P. Comparisons of calculated and measured parameters show good agreement and confirm the adequacy of present calculational procedures in predicting core physics parameters.

TABLE OF CONTENTS

LIST OF TABLES

LIST OF FIGURES

1. INTRODUCTION

This supplement presents measurement and calculational techniques and comparisons of calculated and measured results for some key core physics parameters. The physics parameters include hot zero power (HZP) and hot full power (HFP) critical boron concentrations, HZP control rod worths and ejected rod worths, and HZP isothermal temperature coefficients.

The measured data is from the Oconee Nuclear Station Unit 1, Cycles 1-5. The measurement techniques discussed are those currently used at the station. The HZP measurements were taken at beginning-of-cycle (BOC) during the Zero Power Physics Testing. The HFP boron concentration measurements were taken at various time steps throughout the cycles.

All calculations were performed with EPRI-NODE-P. In contrast to predictions, which are calculated before the measurements are taken, the calculations presented here were performed after the measurements were taken. Therefore, the plant conditions at the time of the measurements could be closely modeled with EPRI-NODE-P.

The comparisons of calculated and measured results present the means of the differences between the measured and calculated data and the corresponding standard deviations. The mean and standard deviation are defined as follows:

$$\text{Mean} = \bar{x} = \frac{\Sigma x_i}{n}$$

$$\text{Standard Deviation} = S = \sqrt{\frac{\Sigma (\bar{x} - x_i)^2}{n - 1}}$$

where: x_i = value for the $i^{\underline{th}}$ observation

n = number of observations.

2. CRITICAL BORON CONCENTRATIONS

2.1 Measurement Technique

Critical boron concentrations are measured at HZP and HFP by an acid-base titration of a reactor coolant system sample.

The measurement uncertainty for critical boron concentrations is due to (1) error in the titration method and (2) error due to differences between the sample concentration and the core average concentration. Based on conservative estimates of these errors, the total uncertainty associated with the critical boron concentration measurements is less than 20 ppmb.

2.2 Calculational Technique

Critical boron concentrations are calculated at HZP and HFP using EPRI-NODE-P in the boron search mode. Since the search does not yield an exactly critical value, fixed boron runs using EPRI-NODE-P are also made to calculate a boron worth, which is then used to correct the calculated boron concentration to exactly critical.

2.3 Comparison of Calculated and Measured Results

2.3.1 Hot Zero Power Comparison

The calculated and measured critical boron concentrations at HZP and BOC for Oconee Unit 1, Cycles 1-5 are compared in Table 2-1. Each entry corresponds to a different control rod position. The mean of the differences for these five cycles was found to be 32 ppmb with a standard deviation of 24 ppmb. Excluding cycle 3 data, which does not follow the biasing trend of the other cycles, the mean of the differences is 43 ppmb with a standard deviation of only 14 ppmb.

2.3.2 Hot Full Power Comparison

The calculated and measured critical boron concentrations at HFP for the reload cycles 2-5 of Oconee Unit 1, are compared in Table 2-2. The mean of

the differences for these cycles is 46 ppmb with a standard deviation of 19 ppmb.

The data displayed in Table 2-2 can be visualized better by examining plots of soluble boron concentration as a function of burnup. These boron letdown curves are shown in Figures 2-1 through 2-5.

2.4 Summary

The comparison between EPRI-NODE-P and measured critical boron concentrations at HZP and HFP indicate EPRI-NODE-P can adequately predict soluble boron concentrations over both "rods in and "unrodded" (feed-and-bleed) fuel cycles.

Table 2-1
OCONEE 1 CYCLES 1-5
CRITICAL BORON CONCENTRATIONS AT HOT ZERO POWER, BOC

Cycle	Critical Boron Conc., PPM		Difference, PPM
	Calculated	Measured	
1	1443	1476	33
	1441	1480	39
	1438	1467	29
	1403	1440	37
	1333	1364	31
	1336	1367	31
	1247	1262	15
	1246	1253	7
2	1257	1301	44
	1250	1296	46
	1221	1276	55
	1143	1194	51
	1059	1119	60
	1046	1099	53
	992	1043	51
	965	1013	48
3	1378	1373	- 5
	1357	1365	8
	1320	1331	11
	1376	1356	-20
	1356	1350	- 6
	1321	1324	3
	1241	1226	-15
	1019	1018	- 1
4	1290	1334	44
	1257	1310	53
	1003	1057	54
5	1376	1423	47
	1350	1405	55
	1349	1399	50
	1348	1412	64
	1045	1083	38
Mean	--	--	31.6
Standard Deviation	--	--	24.1
Mean (w/o Cycle 3 Data)	--	--	43.1
Standard Deviation	--	--	13.7

Difference = Measured - Calculated

TABLE 2-2
OCONEE 1, CYCLES 2-5
HOT FULL POWER CRITICAL BORON CONCENTRATIONS

Cycle	EFPD	Critical Boron Conc., PPM		Difference, PPM
		Calculated	Measured	
2	30.6	662	697	35
	52.2	592	645	53
	83.0	446	511	65
	103.5	383	428	45
	129.0	298	352	54
	156.0	217	265	48
	184.0	129	188	59
	203.8	66	127	61
	222.9	1	75	74
3	25.3	721	717	-4
	58.5	606	625	19
	91.2	499	504	5
	121.9	423	482	59
	143.9	361	403	42
	179.1	243	279	36
	203.3	173	212	39
	232.6	79	127	48
4	28.3	770	797	27
	56.6	672	702	30
	83.2	591	640	49
	103.4	524	583	59
	125.1	452	507	55
	150.6	373	430	57
	174.8	301	354	53
	194.5	234	316	82
	234.7	113	187	74
5	24.5	910	930	20
	44.4	848	877	29
	90.4	708	722	14
	118.1	604	670	66
	145.4	517	564	47
	175.3	417	461	44
	207.5	316	377	61
	239.7	217	266	49
Mean		--	--	45.7
Standard Deviation		--	--	19.7

Difference = Measured - Calculated

Figure 2-1

OCONEE 1, CYCLE 1

BORON LETDOWN CURVES

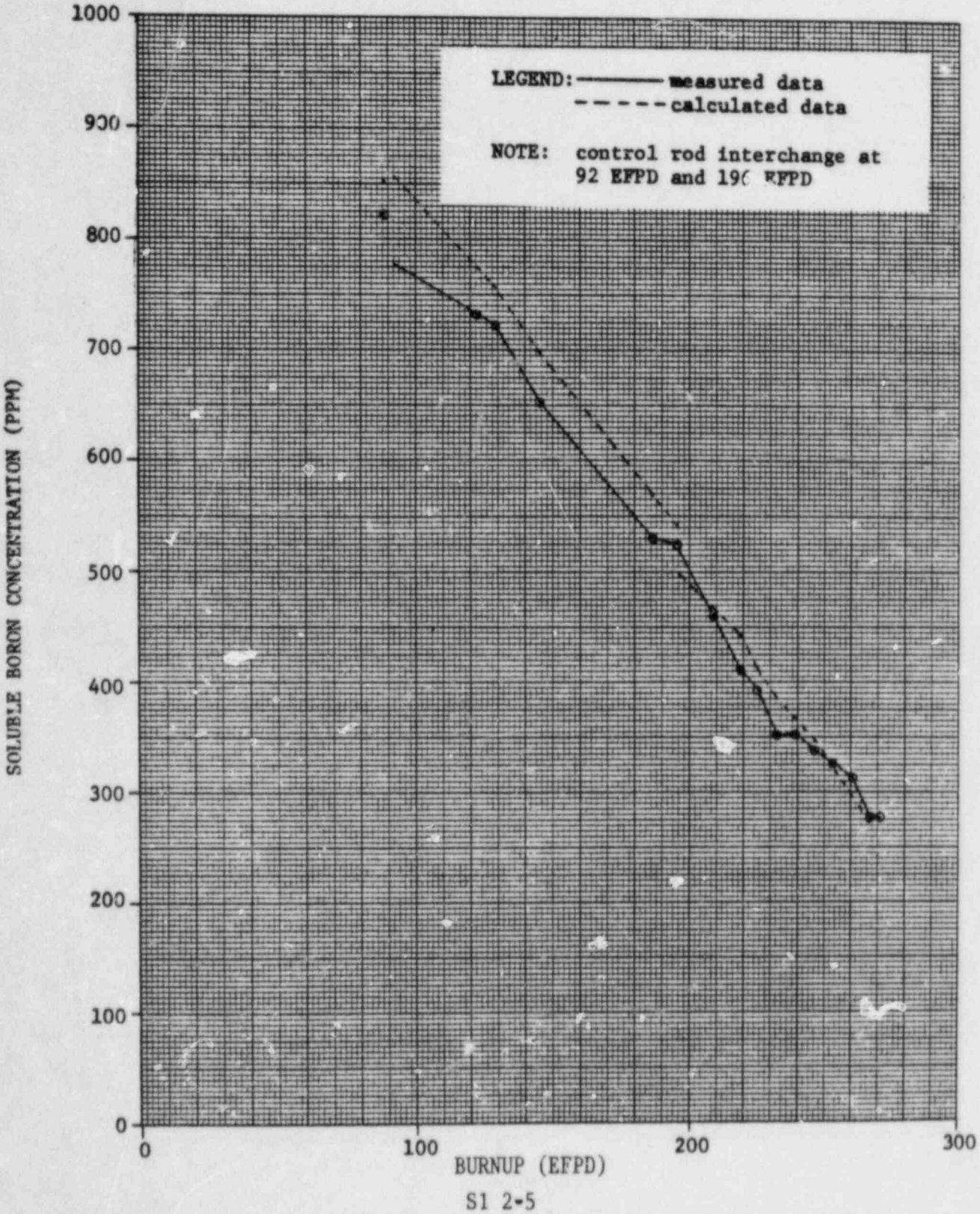

Figure 2-2

OCONEE 1, CYCLE 2

BORON LETDOWN CURVES

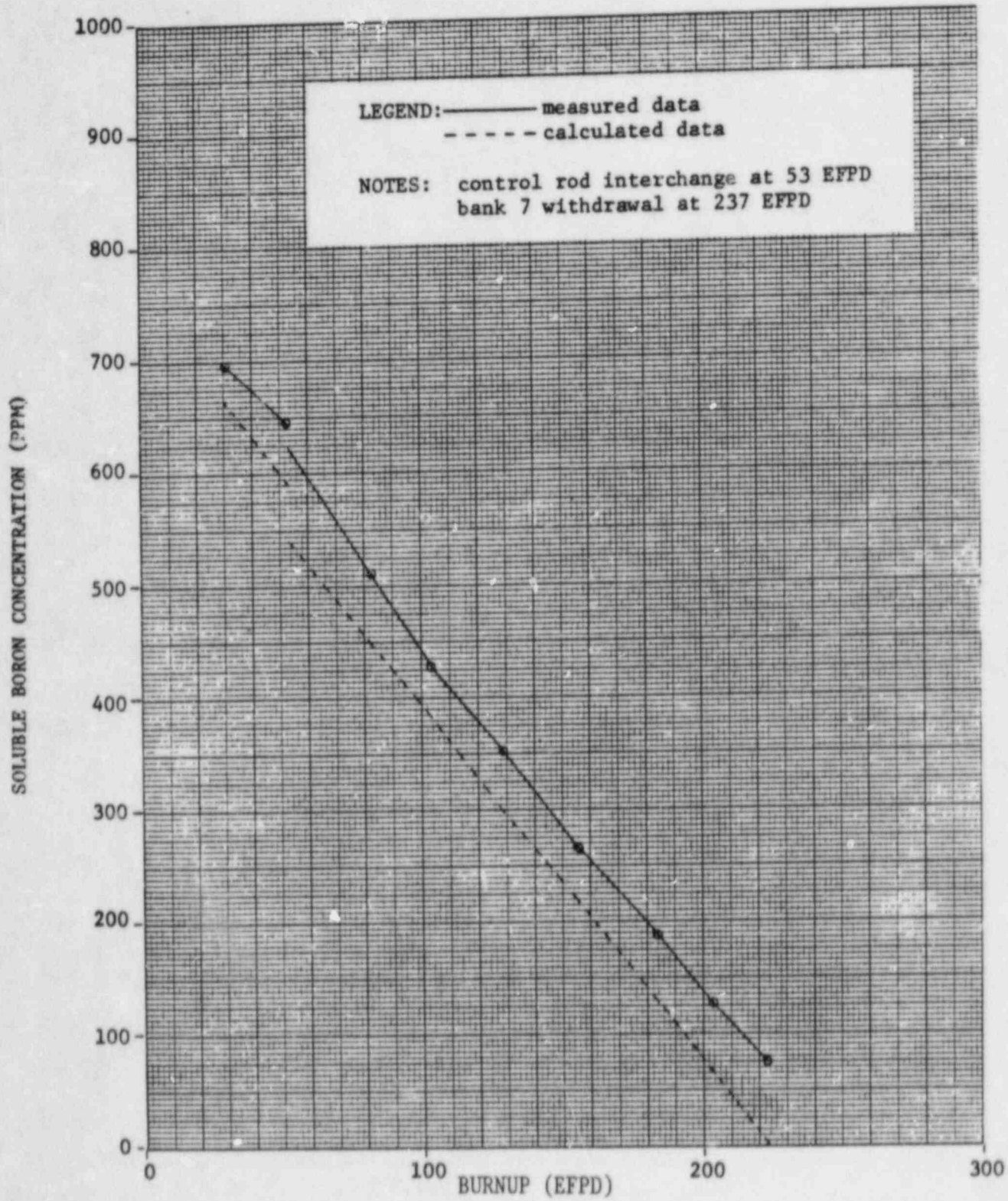

Figure 2-3

OCONEE 1, CYCLE 3

BORON LETDOWN CURVES

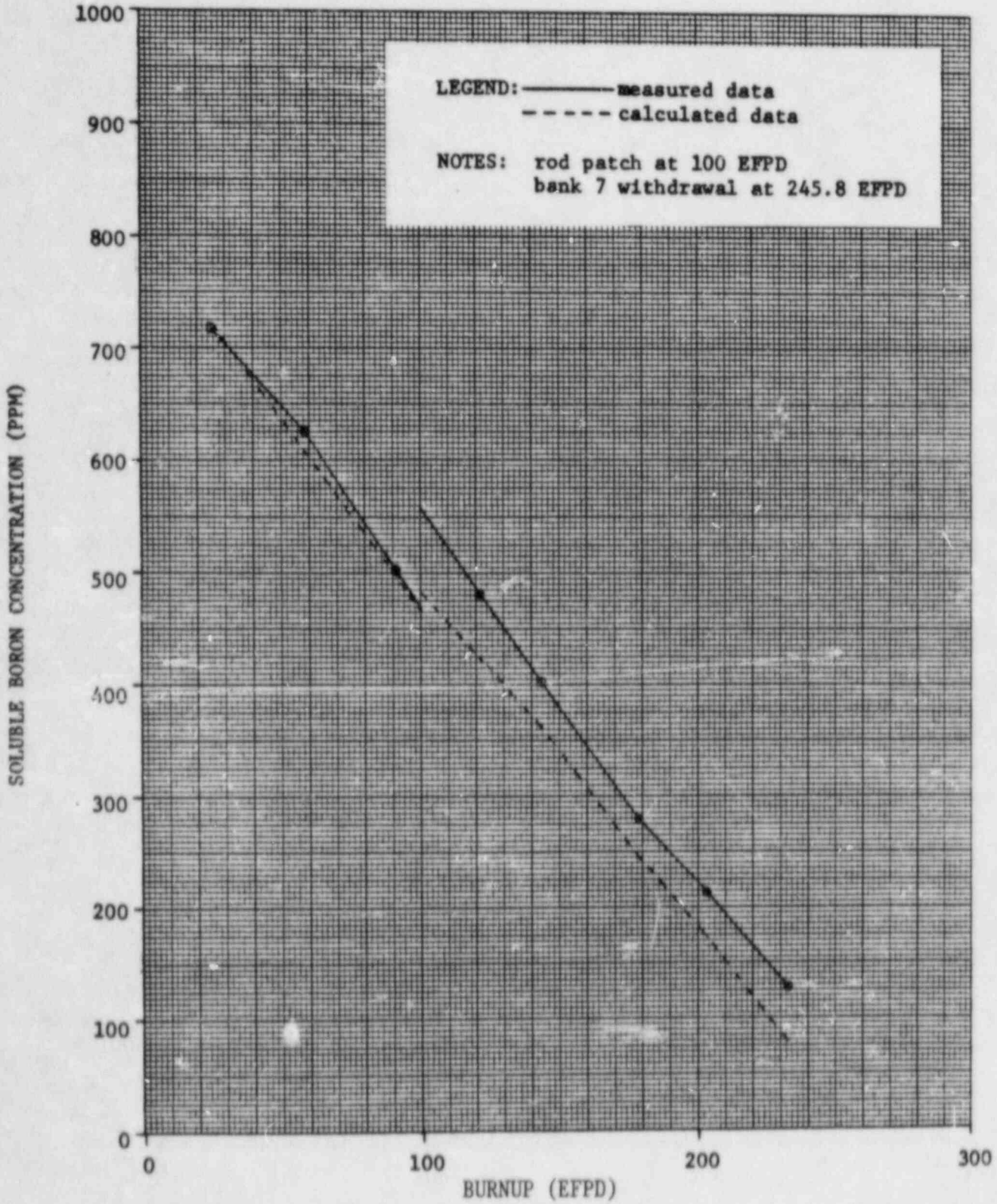

Figure 2-4

OCONEE 1, CYCLE 4

BORON LETDOWN CURVES

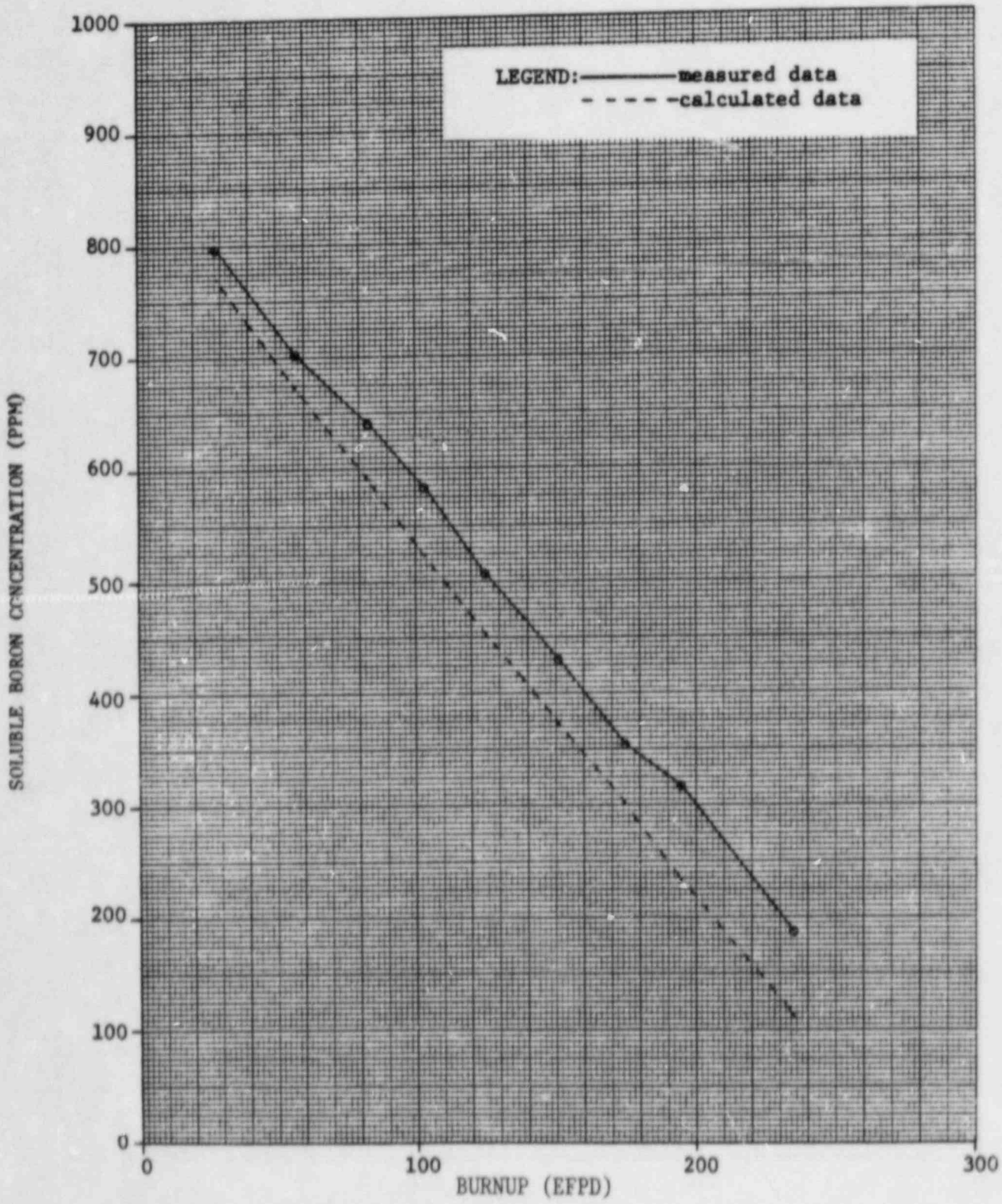

Figure 2-5

OCONEE 1, CYCLE 5

BORON LETDOWN CURVES

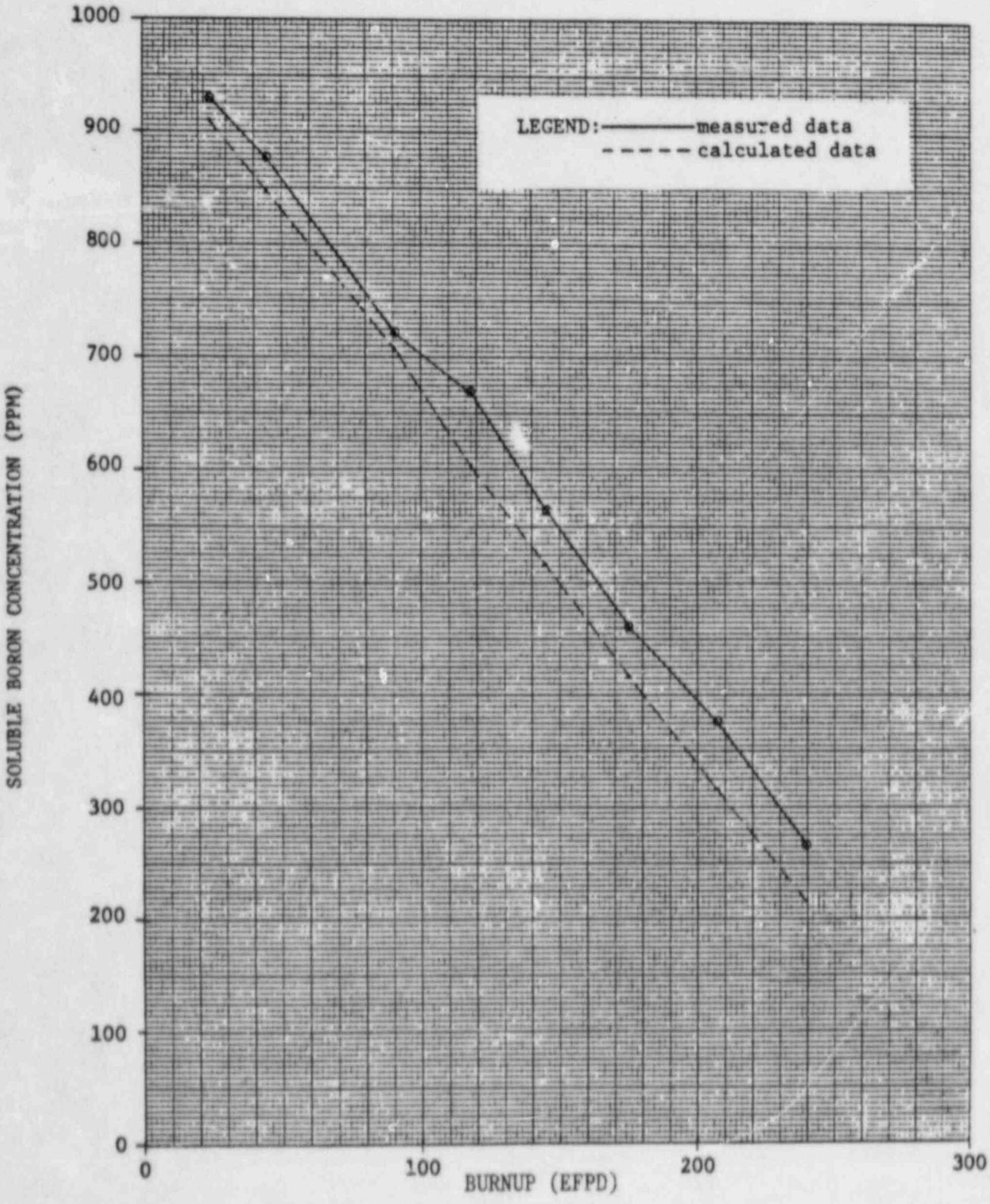

3. CONTROL ROD WORTHS

3.1 Measurement Techniques

Individual control rod group worths are measured by the boron swap technique. This technique involves a continuous decrease in boron concentration together with an insertion of the control rods in small, discrete steps. The change in reactivity due to each insertion is determined from reactimeter readings before and after the insertion. The worth of each rod group is the sum of all the reactivity changes for that group.

The worth of the total regulating banks 5-7 can be measured in two ways. The first is to add up the worths of the individual banks as determined from the reactimeter readings. The worth in this case is in terms of reactivity. This measurement technique is the approved test procedure method. The second way is to measure rod worth in terms of change in soluble boron concentration. This worth is defined as the difference between the equilibrium critical boron concentration when all the regulating rods are out and the concentration when all the regulating rods are in.

3.2 Calculational Techniques

Individual and total regulating rod group worths in terms of reactivity are calculated by making two EPRI-NODE-P runs. The first is a boron search run with the rod group(s) out. The boron concentration found in this run is then used in a fixed boron run with the rod group(s) in. The difference in reactivity between these two runs with constant boron concentration is the rod group(s) worth.

To calculate the total regulating rod groups worth in terms of soluble boron concentration, a boron search using EPRI-NODE-P is performed for both the rods-out case and the rods-in case. The resulting boron concentrations are then corrected to exact criticality and the group worths are determined as the difference between these critical boron concentrations.

3.3 Comparison of Calculated and Measured Results

3.3.1 Comparison in Terms of Reactivity

A comparison of calculated and measured control rod worths in terms of reactivity is shown in Table 3-1. This table compares the worths of the individual banks 5, 6 and 7 and the total regulating banks 5-7 at HZP and BOC for Oconee Unit 1, Cycles 1-5. The differences between measured and calculated worths for all the banks are small. For the total banks 5-7, the mean of the % difference was 7.98% with a standard deviation of 5.36%.

3.3.2 Comparison in Terms of Soluble Boron Concentration

The comparison of calculated and measured regulating bank worths in terms of soluble boron concentration for Oconee Unit 1, Cycles 2-5 at HZP and BOC is given in Table 3-2. The agreement between calculated and measured worths is very good. All the differences are less than the measurement uncertainty associated with the boron measurement. The mean of the differences between measured and calculated values for the total banks 5-7 was found to be -3.3 ppmb with a standard deviation of 13.5 ppmb. The mean of the % differences was -0.98% with a standard deviation of 4.26%.

3.4 Summary

The comparisons between the calculated and measured control rod worths at HZP indicate that EPRI-NODE-P can adequately predict control rod worths. This has been verified by comparing calculated worths to two independent measurement techniques for Oconee 1, Cycles 1-5.

Table 3-1
OCONEE 1 CYCLES 1-5
CONTROL ROD WORTHS AT HOT ZERO POWER, BOC

Cycle	Bank	Rod Worth, %Δρ Calculated	Rod Worth, %Δρ Measured	Difference %Δρ	% Difference
1[a]	7	0.973	1.11	0.14	12.6
	6	0.842	0.97	0.13	13.4
	5	0.642	0.68	0.04	5.9
	5-7	2.457	2.76	0.30	10.9
1	7	0.967	1.11	0.14	12.6
	6	1.007	1.10	0.09	8.2
	5	0.606	0.69	0.08	11.6
	5-7	2.580	2.90	0.32	11.0
2[b]	7	0.726	0.898	0.172	19.2
	6	0.893	0.912	0.019	2.1
	5	1.192	1.242	0.050	4.0
	5-7	2.811	3.052	0.241	7.9
3	7	1.235	1.228	-0.007	-0.6
	6	1.025	1.013	-0.012	-1.2
	5	1.332	1.376	0.044	3.2
	5-7	3.592	3.617	0.025	0.7
4	7	0.859	0.86	0.00	0.0
	6	0.891	0.89	0.00	0.0
	5	1.163	1.24	0.08	6.5
	5-7	2.913	2.99	0.08	2.7
5	7	1.155	1.36	0.20	14.7
	6	1.030	1.20	0.17	14.2
	5	1.012	1.19	0.18	15.1
	5-7	3.197	3.75	0.55	14.7
Mean	7	NA	NA	0.108	9.75
	6	NA	NA	0.066	6.12
	5	NA	NA	0.079	7.72
	5-7	NA	NA	0.253	7.98
Standard Deviation	7	NA	NA	0.089	8.15
	6	NA	NA	0.075	6.78
	5	NA	NA	0.053	4.66
	5-7	NA	NA	0.188	5.36

(a) Group 8 100% withdrawn; Group 8 inserted in all other cases.

(b) Group 7 not completely withdrawn; Group 5 not completely inserted.

$$\text{Difference} = \text{Measured} - \text{Calculated}$$

$$\%\ \text{Difference} = \frac{\text{Measured} - \text{Calculated}}{\text{Measured}} \times 100$$

Table 3-2

OCONEE 1 CYCLES 2-5

CONTROI ROD WORTHS - REGULATING BANKS, HZP, BOC

Cycle	Banks	Rod Worth, PPM		Difference, PPM	% Difference
		Calculated	Measured		
2	5 - 7	256	263	+ 7	+ 2.7
3	5 - 7	357	338	-19	- 5.6
4	5 - 7	287	277	-10	- 3.6
5	5 - 7	331	340	+ 9	+ 2.6
MEAN		-	-	-3.3	-0.98
STANDARD DEVIATION		-	-	13.5	4.26

Difference = Measured - Calculated

$$\% \text{ Difference} = \frac{\text{Measured - Calculated}}{\text{Measured}} \times 100$$

4. EJECTED ROD WORTHS

Ejected rod worth is defined here as the measured worth of the worst case ejected rod. No error adjustments have been included.

4.1 Measurement Technique

Ejected rod worths have previously been measured by three methods: boron swap, rod swap, and rod drop.

4.1.1 Boron Swap

The boron swap method is similar to the method used to measure control rod worth. It involves maintaining criticality by varying the boron concentration to compensate for the ejection of the worst case rod. The control rod positions are held constant. As was done for control rod worth, the ejected rod worth is determined from the reactimeter readings.

4.1.2 Rod Swap

For the rod swap method, criticality is maintained by varying the position of the controlling rod group (usually Group 5) to compensate for the ejection of the worst case rod. In this method, the boron concentration is held constant. The ejected rod worth is the reactivity due to the controlling rod group movement as determined from the differential rod worth measurement.

4.1.3 Rod Drop

The rod drop method starts with the ejected rod fully withdrawn. The rod is then tripped into the core and the reactivity is charted by the reactimeter. Rod position and boron concentration are held constant. The extrapolation to zero inverse time of a plot of reactivity vs. inverse time yields the ejected rod worth. The uncertainty associated with this method is much greater than that associated with either of the other two methods.

4.2 Calculational Techniques

Ejected rod worths are calculated using EPRI-NODE-P to simulate either boron swap, rod swap, or rod drop.

4.2.1 Boron Swap

For boron swap, a boron search run is first performed to determine the critical boron concentration at the rod group position. The boron concentration as calculated in the EPRI-NODE-P run should be corrected for exact criticality. Using this corrected boron concentration and a constant rod group position, the reactivity is determined with the worst case rod first in and then out. The ejected rod worth is the difference in reactivity between the worst case rod in and out.

4.2.2 Rod Swap

For rod swap, the reactivity is determined with the worst case rod first in and then out, keeping the boron concentration constant and the controlling rod group position constant at the least withdrawn position (least withdrawn corresponds to ejected rod out). The ejected rod worth is the difference in reactivity between the worst case rod in and out.

4.2.3 Rod Drop

To calculate ejected rod worths by rod drop, EPRI-NODE-P cases with the worst case rod first out and then in are run, with boron concentration and rod group position held constant. The ejected rod worth is the difference in reactivity between these two cases.

4.3 Comparison of Calculated and Measured Results

A comparison of calculated and measured ejected rod worths for Oconee Unit 1, Cycles 1-5 is given in Table 4-1. Overall, the agreement is good. The mean of all the differences between measured and calculated values is -0.0053%$\Delta\rho$ with a standard deviation of 0.0602%$\Delta\rho$.

4.4 Summary

The comparison between measured and calculated ejected rod worths indicate EPRI-NODE-P can adequately predict ejected rod worths.

TABLE 4-1

OCONEE 1, CYCLES 1-5

EJECTED ROD WORTHS

Cycle	Location	Measurement Technique	Worth %Δρ		Difference %Δρ
			Calculated	Measured	
1	H-2	Rod drop	0.287	0.33	0.04
	L-10	Rod drop	0.279	0.27	-0.01
	N-12	Rod drop	0.183	0.20	0.02
	K-9	Rod drop	0.122	0.15	0.03
2	L-14	Rod swap	0.580	0.46	-0.12
	L-14	Rod swap	0.232	0.20	-0.03
	L-14	Rod swap	0.239	0.15	-0.09
	H-8	Boron swap	0.554	0.639	0.085
3	K-13	Boron swap	0.537	0.57	0.03
4	D-12	Rod swap	0.385	0.39	0
	N-12	Rod swap	0.363	0.25	-0.11
	N-4	Rod swap	0.381	0.34	-0.04
	D-4	Rod swap	0.420	0.51	0.09
	F-8	Rod swap	0.109	0.12	0.01
	H-10	Rod swap	0.109	0.07	-0.04
	L-8	Rod swap	0.109	0.09	-0.02
	H-6	Rod swap	0.111	0.11	0
5	N-12	Boron swap	0.610	0.67	0.06
Mean	-	-	-	-	-0.0053
Standard Deviation	-	-	-	-	0.0602

Difference = Measured - Calculated

5. ISOTHERMAL TEMPERATURE COEFFICIENTS

The isothermal temperature coefficient is defined as the change in reactivity per unit change in moderator temperature at hot zero power, i.e.,

$$\alpha_T = \frac{\Delta\rho}{\Delta T}$$

5.1 Measurement Techniques

The isothermal temperature coefficient is measured by executing average moderator temperature changes of +5°F, -10°F and +5°F from initial equilibrium critical conditions. After each change, steady state conditions are established and pertinent data are recorded by the reactimeter or reactivity program at the resulting plateaus. The isothermal temperature coefficient is determined as the change in reactivity between plateaus divided by the change in temperature. Since three different temperature ramps are executed, three coefficients can be determined. The reported isothermal temperature coefficient is a temperature-weighted average of these three coefficients.

The uncertainty associated with the isothermal temperature coefficient measurement is dependent on the value of the coefficient. For acceptable coefficient values, the measurement uncertainty is less than $\pm 0.06 \times 10^{-4}$ $\Delta k/k/°F$.

5.2 Calculational Technique

The isothermal temperature coefficient at HZP is calculated using EPRI-NODE-P. Two cases with the same boron concentration and rod positions but different moderator temperatures are run. The isothermal temperature coefficient is the difference in reactivity between the two cases divided by the difference in the moderator temperatures.

5.3 Comparison of Calculated and Measured Results

A comparison of calculated and measured isothermal temperature coefficients at HZP and BOC for Oconee Unit 1, Cycles 1-5 is presented in Table 5-1. The

agreement between these calculated and measured coefficients is very good; all values agree within 0.2×10^{-4} $\Delta\rho/°F$. The mean of all the differences was found to be only $+0.027 \times 10^{-4}$ $\Delta\rho/°F$ with a standard deviation of 0.089×10^{-4} $\Delta\rho/°F$.

5.4 Summary

The comparison between calculated and measured isothermal temperature coefficients indicates that EPRI-NODE-P is an excellent predictor of isothermal temperature coefficients.

Table 5-1
OCONEE 1 CYCLES 1-5
ISOTHERMAL TEMPERATURE COEFFICIENTS AT HOT ZERO POWER, BOC

Cycle	Soluble Boron Conc., PPM	Temp. Coeff, 10^{-4} $\Delta\rho/^{o}F$ Calculated	Measured	Difference 10^{-4} $\Delta\rho/^{o}F$
1	1478	+1.09	+1.07	-0.02
	1428	+0.999	+1.052	+0.053
	1355	+0.736	+0.77	+0.03
	1263	+0.509	+0.51	0.00
	1253	+0.474	+0.5315	+0.058
	952	-0.301	-0.391	-0.09
2	1295	-0.035	+0.15	+0.19
	1194	-0.341	-0.17	+0.17
	1013	-0.120	-0.14	-0.02
3	1330	-0.0078	+0.046	+0.054
	1018	-0.708	-0.726	+0.018
4	1324	+0.121	+0.090	-0.031
	1057	-0.542	-0.701	-0.159
5	1405	+0.122	+0.20	+0.08
	1083	-0.719	-0.65	+0.07
Mean	--	--	--	+0.027
Standard Deviation	--	--	--	0.089

Difference = Measured - Calculated

6. REFERENCES

1. Comparison of Core Physics Calculations with Measurements, BAW-10120, Babcock & Wilcox, Lynchburg, Virginia, June 1978.

2. Duke Power Company, Oconee Nuclear Station Unit 1, Startup Physics Test Program, February 1980.

3. Duke Power Company, Oconee Nuclear Station Unit 1, Cycle 6, Zero Power Physics Test, TT/1/A/711/06.

SUPPLEMENT 2

ABSTRACT

Supplement 2 describes Duke Power Company's benchmarking of EPRI-NODE-P. Included in this supplement are measured Assembly Powers, Local Radial Comparisons, EPRI-NODE-P Calculations, Statistical Analyses, and Fitting Procedures.

TABLE OF CONTENTS

LIST OF TABLES

LIST OF FIGURES

LIST OF FIGURES

LIST OF FIGURES

1. INTRODUCTION AND SUMMARY

1.1 Introduction

The current nuclear code employed by Duke Power Company for three dimensional assembly power calculations is EPRI-NODE-P. This code has been benchmarked against two rodded cycles and two unrodded cycles of operation of the Oconee Unit 1 reactor.

This work encompassed: derivation of measured power distributions for cycles 1 through 5, simulations of these 5 cycles using EPRI-NODE-P, development of fitting procedures for the assembly axial power, and development of a statistical basis for estimating the calculational accuracy of EPRI-NODE-P.

1.2 Structure Of Supplement 2

This supplement is structured to provide smooth transitions between various major topics. Section 2 will describe the assembly measured power data base. Section 3 will compare calculated and measured local radial factors. Section 4 describes the EPRI-NODE-P Oconee simulations and presents comparisons of assembly radial and peak powers. Section 5 quantitatively compares calculated and measured powers from Section 4. EPRI-NODE-P reliability factors are calculated based on observed differences. Appendix A outlines the fitting procedure for the assembly axial power.

1.3 Summary

Local radial factors predicted by PDQ07 were examined and found consistently conservative relative to either measurements or more elegant neutronics codes. A large data base consisting of five cycles of Oconee-1 measured and EPRI-NODE-P calculated fuel assembly powers was assembled.

Calculated and measured powers were statistically combined to derive 95/95 Observed Nuclear Reliability Factors (ONRF) for EPRI-NODE-P. Using a variety of fuel cycle combinations, ONRF's were calculated for both assembly peak and radial powers.

ONRF's of 1.05 for the radial and 1.075 for the peak were found to be conservative for unrodded (feed and bleed) core operation.

2. MEASUREMENT DATA

2.1 Measured Assembly Power Data

The measured power data base used in this supplement comprises assembly power data from Oconee Unit 1 for cycles 1 to 5. All assembly power data are directly traceable to raw signals received from the incore detector system.

The measured assembly power data for Cycle 1 and at 30.6 EFPD in Cycle 2 were those used by Babcock & Wilcox in their calculational nuclear uncertainty analysis[5]. The remaining data was generated by B&W using similar methods to reprocess the raw detector signals[6,7].

2.2 Measurement System Description

The incore detectors at Oconee consist of pure Rhodium emitters which respond to the incident neutron flux. With each neutron absorption, a beta particle (β) is released according to the reaction:

$$^{103}_{45}Rh + ^{1}_{0}n \rightarrow ^{104}_{45}Rh + ^{0}_{-1}\beta + \text{energy} \qquad (2\text{-}1)$$

The current measured from the emitter to ground is proportional to the net emitter loss. After the emitter current has stabilized ($\sim 4\frac{1}{2}$ minutes), the current is then proportional to the local neutron flux (in the neighborhood of the eight pins surrounding the emitter). This emitter is called a Self Powered Neutron Detector (SPND). The SPND's are physically located inside the Fuel Assembly (FA) Instrument Tube (IT). The IT is situated in the center of the FA.

SPND signal magnitude is of the order of nanoamps. The reactor's on-line computer (OLC) performs a signal to power conversion approximately at ten minute intervals, logging signal data, core power, power distribution, and assorted other data pertinent to core operation.

SPND's are distributed in fixed positions to provide an adequate three dimensional assembly power measurement. In each instrumented FA, seven SPND's are located equidistantly along a "string". Each string also has a thermocouple and an insulated leadwire which is used to correct for gamma induced signals in the seven detector leads.

In Oconee, 52 of 177 FA contain detector strings. The locations of instrumented FA form a spiral as shown in Figure 2-1. Eight strings are located symmetrically in the interior; another 8 symmetrically farther out toward the periphery. The two sets of eight strings are used to supply corewise quadrant tilt information. An eighth core map of 29 FA three dimensional powers can be obtained; and using tilt data, full core maps of 177 radial FA powers and 1239 segment FA powers can be obtained.

The measured powers used in this supplement will be collapsed from 52x7 (full core) to 29x7 (eighth core) at each reactor state point. As shown on Figure 2-2, 11 of the 29 eighth core locations have symmetrically located detector strings. Relative powers (radial and seven-level) for each symmetric pair or symmetric octet were averaged to obtain the best estimate of the "true" measured power.

Power measurements were taken at approximately equilibrium Xenon conditions. Reactor power was also as close to 100% full power as practicable.

2.3 Measured Powers: Cycle 1 and Cycle 2 - 30.6 EFPD

This data base consisted of the same PDO data as Babcock and Wilcox used in its calculational nuclear reliability analysis. The raw emitter signals were reprocessed off-line at B&W using software which represented then current state-of-the-art experience obtained from the operation of Cycle 1 of Oconee 1.

The core state-points where these measurements were taken are shown in Tables 4-7 and 4-8. Seventeen state points were used in Cycle 1.

2.4 Measured Powers Beyond 30.6 EFPD - Cycle 2

In order to complete the measured assembly power data base using a consistent procedure, raw detector signal data were processed by B&W for the remainder of the cycles. As in Cycle 1, all data were taken at equilibrium Xenon conditions so as to mitigate any transient effects. Tables 4-8, 4-9, 4-10, and 4-11 show the selected reactor state-points.

No explicit estimate is made here of the measurement system accuracy during Cycles 1 to 5, since this component is conservatively treated in Section 5.

For failed detectors substitute signals are derived through a spline fitting procedure, provided that operating SPND's are adjacent on either side to the failed SPND. If two or more adjacent SPND's fail on a string, substitute signals are derived from either symmetric or adjacent locations. The same procedure is employed for entire string substitution. Since most of the failed strings in Cycle 3 had operable symmetric counterparts, it was judged that the radial power measurements were reasonable. However, the number of individual detector failures would disqualify the Cycle 3 power distributions from being used in a reliability factor program.

Cycle 3 radial powers and peak powers will be shown in this report for comparison only. No Cycle 3 data will be used in Section 5 where EPRI-NODE-P reliability factors will be derived.

Figure 2-1

Oconee
Instrument String Locations

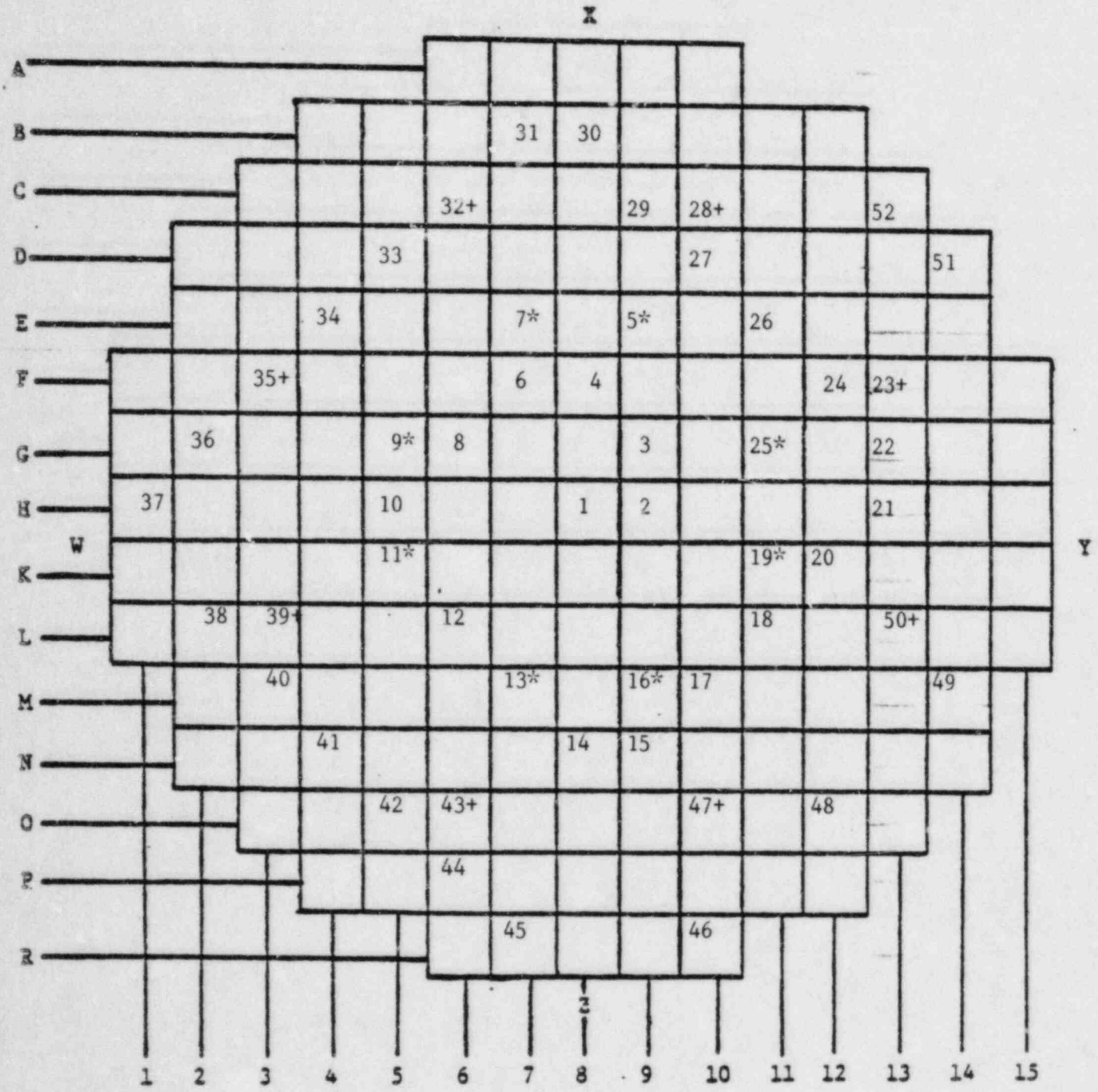

* - Inner Eight Symmetric Detector Strings

\+ - Outer Eight Symmetric Setector Strings

Figure 2-2

Oconee Fuel Assembly Map

Detector String Number Assignment
For Eighth-Core Averaging

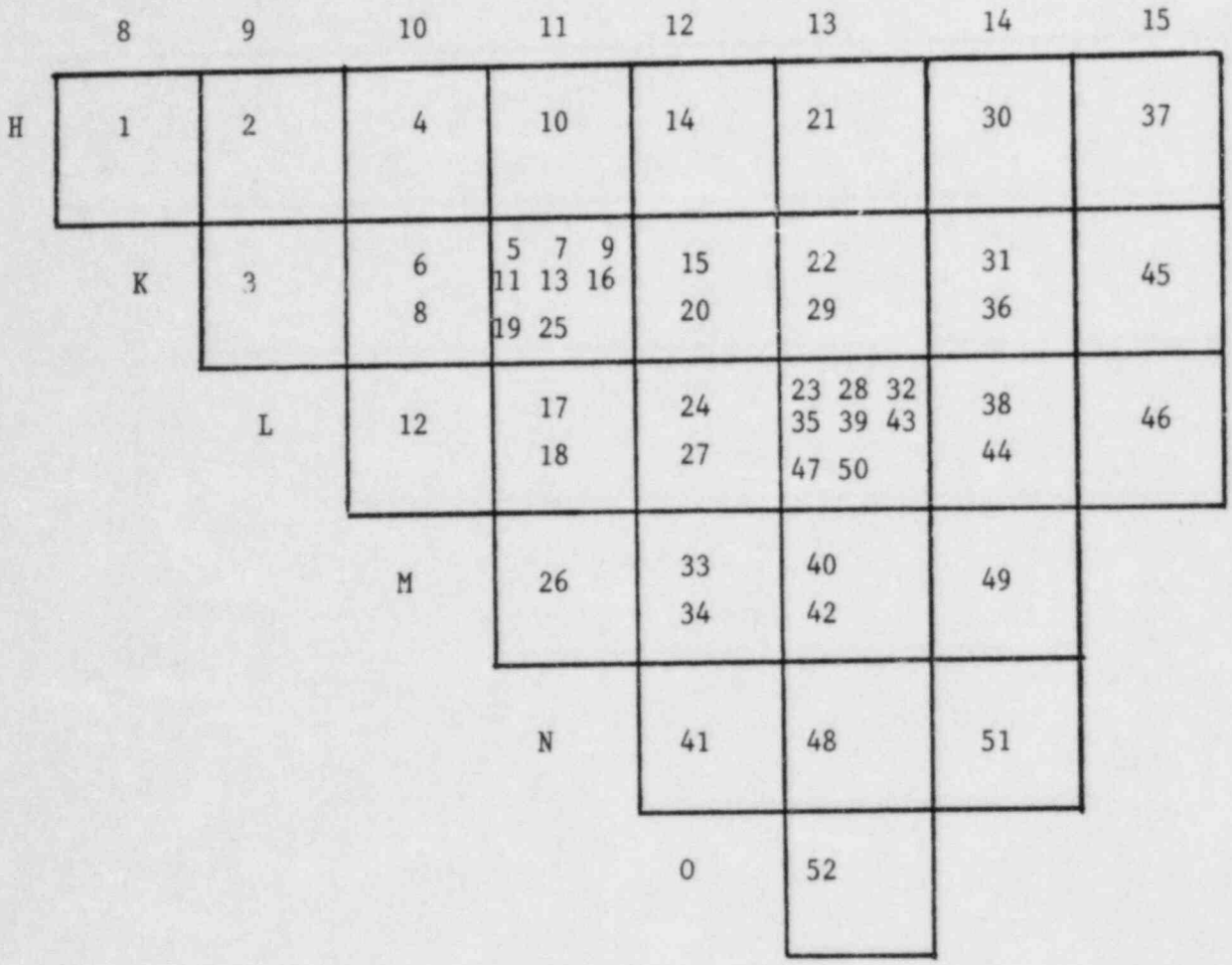

3. LOCAL RADIAL ANALYSIS

3.1 Local Radial Reliability Factor Analysis

In this document, the local radial is defined as the ratio of the maximum pin power to the assembly radial power (assembly average X-Y power). Commercial reactors, such as Oconee, are not instrumented to measure local radial factors. The only pinwise power data available to Duke Power are the room temperature B&W critical experiments[8] where pinwise powers were measured.

The calculational tools available for predicting the local radial factor are PDQ07, EPRI-CPM[9], and CASMO[10]. Both EPRI-CPM and CASMO are two dimensional transport theory codes. EPRI-CPM uses collision probabilities to solve the Boltzman transport equation, while CASMO employs transport probabilities. Both transport theory codes have been benchmarked against the KRITZ hot criticals.[11]

3.2 Comparisons of ARMP PDQ07 To Cold Criticals

In order to establish the local radial predictive accuracy of the ARMP PDQ07 code, a series of calculations[12] were performed and compared to measured pin powers in the B&W uranium criticals.

All criticals consisted of a central region of nine 15 x 15 lattices surrounded by a buffer region of fuel rods. This buffer region, in turn was reflected radially by borated water. Criticality was achieved by raising the moderator height.

The overall measurement error has been estimated to be 1.11% in the determination of relative pin powers. Additional descriptive information of the B&W uranium fuel criticals can be found in Reference 8.

In the two dimensional simulation of the criticals, the ARMP procedure was used in generating PDQ07 cross sections and usage of the PDQ07 code. Although the simulations of these criticals were not performed at Duke Power, the methods used would have been similar, resulting in identical PDQ07 results.

A typical B&W Mark B 15x15 fuel assembly (FA) was mocked by two such criticals described in Table 3-1. Load number 2 corresponds to an unrodded FA. While load number 8 corresponds to a FA with lumped burnable poison (LBP). Figure 3-1 depicts the two loading patterns. The results are shown in Figures 3-2 and 3-3.

In load 2, shown in Figure 3-2, the PDQ07 predicted local radial was 1.3% higher than the measured local radial. Likewise, the PDQ07 local radial in load 8 (Figure 3-3) was 3.3% higher.

To assess the overall local radial predictive behavior, the ten maximum pins were compared in each critical. In load number 2, the (C-M) mean was .0091 with a standard deviation of .01775. In load number 8, the mean was .0239 with a standard deviation of .01356. When the (C-M) differences from loads 2 and 8 are lumped together, the 20 data points give a mean of .0165 and a standard deviation of .01715.

The positive means of the C-M differences and small standard deviations shown above indicate that the ARMP PDQ07 discrete pin model yields radial local factors which are conservative.

3.3 ARMP PDQ07 Local Radials Compared to Simulated Hot Full Power Conditions

To assess the ARMP PDQ07 radial predictive capability at Hot Full Power (HFP) conditions, quarter assembly simulations were performed at Duke Power Company. The codes CASMO, EPRI-CPM, and PDQ07 were used to model a 2.75 w/o ^{235}U unrodded FA at beginning of life (BOL).

In an unrodded FA, usually the worst peaking occurs at BOL, since Xenon has not yet built up to equilibrium concentrations. And so this is a good time to test a two group diffusion theory model against multigroup transport theory codes: a) EPRI-CPM which provides a solution using collision probabilities, and b) CASMO which uses transmission probabilities.

The results of these calculations are shown in Figure 3-4. The ARMP PDQ07 conservatively overpredicted the maximum CASMO pin power by 2.5% and likewise overpredicted the CPM maximum pin by 1.8%. The mean difference of the 10

highest PDQ-CASMO pairs was .0143 RPD with a standard deviation of .01233. Comparisons of the 10 maximum pin powers for PDQ-CPM likewise gave a mean difference of .0084 RPD and a standard deviation of .00902.

3.4 Conclusions

In Section 3.1 it was demonstrated that the ARMP PDQ07 discrete pin model conservatively overpredicts measured peak powers from critical experiments. Also the ARMP PDQ07 discrete pin model conservatively overpredicts the hot full power pin powers when compared to two independent transport theory solutions.

Since this conservatism was demonstrated at hot and cold conditions, it is concluded that an uncertainty component applied to the assembly local radial is not necessary. This component would only be necessary if the ARMP-PDQ07 model were to underpredict the maximum pin power.

Table 3-1

B&W COLD CRITICALS USED FOR LOCAL

RADIAL UNCERTAINTY FACTOR ANALYSIS

Core Number	Core Load Number	Type of Fuel	Compositions of Central Fuel Assembly Control and Instrument Unit Cells
XI	2	UO_2	17 H_2O
XI	8	UO_2	1 H_2O, 16 Pyrex

FIGURE 3-1

B&W URANIUM CRITICAL EXPERIMENTS

GEOMETRY OF INTERIOR "ASSEMBLIES"

	LOAD 2	LOAD 8	
LOCATION 1	WATER	WATER	
LOCATION 2	WATER	POISON	
LOCATION 3	WATER	POISON	

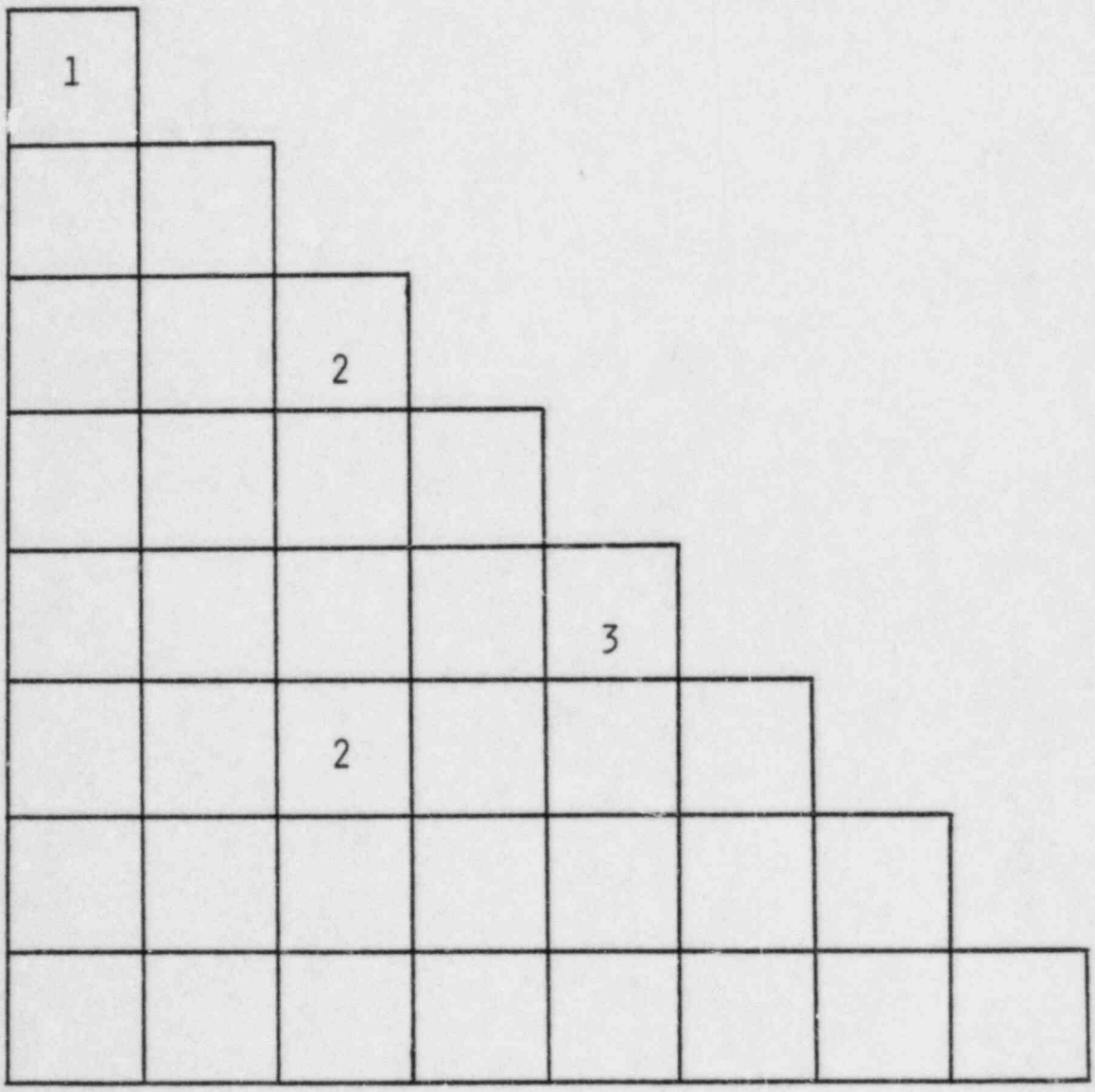

FIGURE 3-2

RELATIVE PIN POWERS IN CENTRAL ASSEMBLY OF B&W CRITICALS

UNRODDED LATTICE

LOAD 2 - 1335 PPM

	K_{EFF}
EXPERIMENT	1.0007
ARMP PDQ07, STANDARD	1.0052

*MAXIMUM PIN

EXPERIMENT 1.108

ARMP PDQ07, STANDARD 1.122

0. 0.							
1.072 1.085	1.033 1.075						
.993 1.010	1.040 1.074	0. 0.					
.968 .985	1.002 1.033	1.080 1.087	1.050 1.096				
.992 .978	1.013 1.028	1.082 1.087	1.108* 1.122	0. 0.			
.993 .978	1.062 1.050	0. 0.	1.096 1.102	1.073 1.056	.982 .995		
.948 .957	.993 .998	1.035 1.036	.999 1.003	.974 .959	.941 .936	.939 .917	
.951 .934	.970 .940	.930 .947	.894 .939	.942 .925	.940 .914	.919 .905	.890 .896

EXPERIMENT
ARMP PDQ07,
Standard

FIGURE 3-3

RELATIVE PIN POWERS IN CENTRAL ASSEMBLY OF B&W CRITICALS

BURNABLE POISON LATTICE

LOAD 8 794 PPM

	K_{EFF}
EXPERIMENT	1.0007
ARMP PDQ07, STANDARD	.9993

*MAXIMUM PIN

EXPERIMENT 1.158

ARMP PDQ07, STANDARD 1.196

0. 0.								
1.102 1.114	.995 .999							
.986 .998	.907 .899	0. 0.						
1.003 .990	.961 .924	.864 .851	.878 .839					
1.015 .996	.943 .931	.864 .855	.820 .816	0. 0.				
1.005 1.005	.924 .914	0. 0.	.896 .855	.931 .926	1.028 1.021			
1.043 1.046	1.027 .993	.961 .945	1.007 .994	1.053 1.067	1.095 1.115	1.118 1.155		
1.079 1.087	1.061 1.077	1.044 1.070	1.045 1.090	1.093 1.123	1.147 1.153	1.151 1.178	1.158* 1.196	EXPERIMENT ARMP PDQ07, Standard

FIGURE 3-4

OCONEE UNRODDED ASSEMBLY

PIN X PIN POWER DISTRIBUTION

HOT FULL POWER SIMULATION

CODE USED	CASMO	EPRI-CPM	ARMP PDQ07
K-INF	1.2973	1.2968	1.2962
K-EFF	1.2972	1.2967	1.2962
PPMB	0	0	0
EXPOSURE	0	0	0

*MAXIMUM PIN

CASMO	1.072
EPRI-CPM	1.080
ARMP PDQ07	1.099

0. 0. 0.								
1.009 1.015 1.007	1.012 1.022 1.025							
1.001 1.005 1.002	1.039 1.045 1.045	0. 0. 0.						
0.997 0.999 0.995	1.013 1.020 1.030	1.057 1.064 1.073	1.048 1.061 1.087					
0.995 0.995 0.991	1.011 1.017 1.027	1.057 1.063 1.074	1.072* 1.080 1.099	0. 0. 0.				
0.992 0.991 0.988	1.030 1.032 1.033	0. 0. 0.	1.056 1.063 1.075	1.036 1.036 1.042	0.989 0.988 0.992			
0.977 0.975 0.967	0.990 0.991 0.994	1.023 1.023 1.020	0.996 0.997 1.003	0.976 0.972 0.970	0.960 0.953 0.945	0.947 0.937 0.925		
0.963 0.959 0.947	0.967 0.963 0.954	0.972 0.967 0.962	0.967 0.962 0.955	0.958 0.950 0.940	0.948 0.939 0.926	0.940 0.930 0.915	0.936 0.924 0.910	CASMO CPM PDQ

4. EPRI-NODE-P POWER DISTRIBUTION COMPARISONS

4.1 EPRI-NODE-P Model

The primary three-dimensional nuclear code employed at Duke Power is EPRI-NODE-P. This code is used for all maneuvering analyses, core follow, and physics test data where three-dimensional core power distributions are required. In this section, comparisons of measured and EPRI-NODE-P calculated values will be shown for both radial and total peak powers. Comparisons were performed on a total of 55 reactor state points covering Cycles 1 through 5 of Oconee Unit I.

The Oconee core was modeled using quarter core symmetry. Each fuel assembly was modeled with one radial and 12 equidistant axial nodes.

The active stack height was set at 144 inches. Control rods could be positioned continuously in this model, with a maximum inserted length of 139 inches.

Methods described in the ARMP System Documentation[13] were used to generate fuel neutronics characteristics. Figure 4-1 shows a flow chart of the general methodology employed. In generating the input for EPRI-NODE, "as built" assembly uranium enrichments and loadings were used to model more closely actual core conditions.

EPRI-NODE-P employs fuel k_∞ fits versus moderator temperature for rodded, half-rodded, and nonrodded conditions. Assemblies having burnable poison rods are treated similarly. All k_∞ fits are referenced to either moderator temperature or fuel exposure. Also fuel temperature reactivity changes are included. Therefore, EPRI-NODE-P explicitly models the effects of thermal-hydraulic and Doppler (THD) feedbacks.

Since EPRI-NODE-P does not account explicitly for the core reflector and baffle, the following normalization procedure was employed. The assembly radial powers from EPRI-NODE-P were normalized <u>once</u> at BOC to discrete pin model PDQ07 radial powers when the core reached equilibrium Xenon and Samarium conditions (~25 EFPD). Since the two dimensional PDQ07 does not have thermal and hydraulic feedbacks, all EPRI-NODE-P normalization runs were performed likewise.

Plots comparing calculated and measured assembly axial powers are given in Appendix A.

4.2 Oconee Fuel Cycle Simulations

Using the EPRI-NODE-P model described in Section 4.1, Cycles 1 through 5 of Oconee 1 were depleted using THD feedbacks. The depletions were performed in a core follow mode, utilizing critical boron searches at each exposure step. Since all depletions were performed at greater than 90% full power, control banks 1 through 5 were not inserted into the core.

Table 4-1 shows by cycle: core operation mode, control bank interchange/withdrawal exposures, and core reload data. Assembly peaks were derived by the method described in Appendix A. The results of these depletions will be described below.

Cycle 1 operated in a rodded mode until end of cycle which occurred at 309.6 EFPD.[14] Control bank locations are shown in Figure 4-2 and the core loading pattern is shown on Figure 4-3.

Assembly radial powers in this cycle were normalized at 88.6 EFPD. There were two control rod bank interchanges during this cycle causing considerable global power shifts.

There were 25 depletion steps in this cycle; 17 of these time points are shown in Table 4-2. Assembly radial power comparisons are shown in Figures 4-4 to 4-20. Assembly peak powers are compared in Figures 4-21 to 4-37.

Cycle 2 operated in a rodded mode, having a transient bank interchange at 53 EFPD, and transient bank withdrawal at 237 EFPD. The reactor continued operation until 292 EFPD.[15] Figure 4-38 shows the control rod bank locations. Five 2.60 and 56 3.20 w/o ^{235}U enriched assemblies were loaded. Figure 4-39 shows the assembly enrichments, and Figure 4-40 shows the quarter core assembly shuffle used to rearrange fuel from EOC-1 to BOC-2.

The EPRI-NODE-P radial powers were normalized to a discrete pin quarter core POQ07 depletion at 22 EFPD. EPRI-NODE-P simulation of Cycle 2 employed 20 timesteps, 10 of these are shown in Table 4-3. These 10 state points are where comparisons to measured power data were made. Figures 4-41 to 4-50 show comparisons for assembly radial powers. Assembly peak powers are compared in Figures 4-51 to 4-60.

During Cycle 3, Unit 1 operated in the rodded mode. A transient bank interchange occurred at 100 EFPD, and transient bank withdrawal occurred at 245.8 EFPD. The reactor continued operation until 303.8 EFPD.[16] Figure 4-61 shows the locations of control banks 6, 7, and 8. Sixty 2.75 w/o ^{235}U enriched fuel assemblies were loaded as shown in Figure 4-62. The Cycle 2 to 3 assembly shuffle pattern is shown in Figure 4-63.

EPRI-NODE-P was normalized at 38.5 EFPD to a parallel quarter core discrete pin model PDQ07 depletion. Cycle 3 was simulated using 16 depletion time steps, 10 of which are shown on Table 4-4.

Figure 4-64 through 4-73 compare assembly radial powers, and Figures 4-74 through 4-83 compare total peak powers.

During startup testing at BOC-4, a quadrant tilt occurred that limited reactor operation to 75% full power for the first 10 EFPD. The reactor operational mode was changed to feed and bleed to provide additional safety margin. The reactor continued operation at full power until a control rod dropped about 2 EFPD before shutdown. The reactor power level was lowered to 50% full power, and operation continued until shutdown at 245.9 EFPD.[17]

During the refueling preceding Cycle 4, 34 of 52 detector strings were replaced. Therefore, the power measurement uncertainty was considerably improved. The measured power data from this cycle was included in the analysis of EPRI-NODE-P reliability factor.

The EPRI-NODE-P Cycle 4 model was normalized to the Duke Power discrete pin model PDQ07 depletion at 25 EFPD. The exposure steps used for power comparisons are shown on Table 4-5. The control bank patterns are shown on Figure 4-84. Core loading and quarter core assembly shuffle patterns are shown on Figures 4-85 and 4-86, respectively.

Calculated assembly radial and peak powers agreed very well with measured. Figures 4-87 to 4-95 compare the radials and Figures 4-96 to 4-104 compare the peaks.

During Cycle 5, the core also operated in a feed and bleed mode. Locations of control rod banks are given in Figure 4-105. Fifty six 3.02 w/o ^{235}U enriched assemblies were loaded as shown in Figure 4-106. Figure 4-107 shows the quarter core assembly shuffle pattern.

Ten equilibrium reactor state points were used for power comparisons as shown in Figure 4-6. As in Cycle 4, the EPRI-NODE-P radial assembly power distribution was normalized to the PDQ07 parallel depletion at 25 EFPD.

In Figures 4-108 to 4-117, the assembly EPRI-NODE-P and measured radial powers are compared. Figures 4-118 to 4-127 show the calculated and measured assembly peak powers.

4.3 Conclusions

EPRI-NODE-P yielded consistently good power distributions when compared to measured power distributions. This conclusion applies for both radial and peak power comparisons. Although the conclusions in this section are qualitative, quantitative statistical results of these comparisons will be shown in Section 5.

Table 4-1

OCONEE-1 CORE CONDITIONS

Cycle	Mode of Operation	Bank 7 Interchange (EFPD)	Bank 7 Withdrawal (EFPD)	Nominal Assembly Loading (w/o U-235/ # Assembly
1	Rodded	91.5 196.0	None	2.00/41, 2.10/56, 2.15/80
2	Rodded	53.0	237.0	2.60/5, 3.20/56
3	Rodded	100.0	245.8	2.75/60
4	Unrodded	-	-	2.79/56
5	Unrodded	-	-	3.02/56

Table 4-2

OCONEE UNIT 1 STATE POINTS

CYCLE 1

Point #	EFPD	Power (Percent)	Control Bank Position (% WD)			Axial Offset, % (Meas/Calc)
			Group 6	Group 7	Group 8	
1	88.6	96.4	94.9	22.6	2.0	-4.74/-3.10
2	122.2	98.1	96.7	24.3	0.5	-0.22/-1.98
3	129.0	97.4	98.6	27.2	1.6	-4.07/-2.34
4	145.6	100.7	98.4	24.5	0.7	-2.96/-2.62
5	169.7	100.1	92.9	20.4	4.1	-2.87/-2.47
6	186.4	100.5	98.6	26.0	0.6	-4.23/-4.33
7	195.8	99.5	99.6	27.8	1.3	-3.70/-4.28
8	208.9	99.8	96.4	20.2	3.9	-4.17/-4.51
9	225.5	98.8	93.3	18.1	0.7	-3.04/-4.91
10	232.4	99.0	90.1	16.3	3.4	-1.81/-4.85
11	239.6	100.8	96.7	18.8	4.3	-0.02/-4.28
12	246.4	100.8	96.0	20.8	4.3	-1.68/-5.97
13	253.4	100.4	94.3	20.3	2.7	-4.67/-6.24
14	260.4	100.2	91.8	17.0	4.9	-3.11/-4.50
15	267.4	100.1	92.1	16.1	4.9	-2.05/-4.05
16	270.7	99.2	96.3	21.3	6.9	-1.34/-6.27
17	281.6	90.5	92.1	17.2	12.0	-2.35/-6.37

Table 4-3

OCONEE UNIT 1 STATE POINTS

CYCLE 2

Point #	EFPD	Power (Percent)	Control Bank Position (% WD)			Axial Offset, % (Meas/Calc)
			Group 6	Group 7	Group 8	
1	30.6	98.9	84.7	10.2	6.2	-2.28/-3.30
2	52.5	97.9	85.5	9.5	4.7	-3.30/-3.24
3	83.0	98.7	84.9	6.4	3.4	-2.65/-5.35
4	103.5	98.8	85.8	7.6	3.5	-7.61/-5.58
5	129.0	97.2	83.2	3.4	4.0	-5.57/-3.20
6	156.0	98.7	85.2	6.3	3.3	-2.07/-4.51
7	184.0	99.9	85.3	6.6	2.9	-4.19/-4.63
8	203.8	99.6	84.6	5.6	5.7	-1.53/-3.78
9	222.9	99.7	81.5	2.9	6.1	-0.39/-4.05
10	259.9	99.9	100.0	83.7	15.6	-2.77/-3.90

Table 4-4

OCONEE UNIT 1 STATE POINTS

CYCLE 3

Point #	EFPD	Power (Percent)	Control Bank Position (% WD)			Axial Offset, % (Meas/Calc)
			Group 6	Group 7	Group 8	
1	25.3	99.8	94.1	20.3	18.2	-6.78/0.07
2	58.5	99.7	94.6	18.3	18.6	-4.88/-1.02
3	91.2	99.6	94.9	18.3	17.5	-4.72/-1.93
4	121.9	99.9	92.3	18.4	25.6	-5.97/-5.15
5	143.9	99.4	97.6	22.4	19.5	-2.38/-1.14
6	179.1	99.7	94.6	21.1	24.6	-4.54/-6.02
7	203.3	98.9	98.5	22.5	23.8	-4.88/-3.48
8	232.6	99.9	97.8	22.5	25.4	-5.92/-5.49
9	266.0	99.9	100.0	85.3	25.8	2.00/ 1.38
10	303.1	90.2	100.0	84.5	31.6	-2.55/-4.62

Table 4-5

OCONEE UNIT 1 STATE POINTS

CYCLE 4

Point #	EFPD	Power (Percent)	Control Bank Position (% WD)			Axial Offset, % (Meas/Calc)
			Group 6	Group 7	Group 8	
1	28.3	99.4	100.0	83.8	35.3	-2.16/2.44
2	56.6	99.7	100.0	80.7	32.5	-1.13/0.68
3	83.2	99.5	100.0	86.0	34.7	-2.00/-0.57
4	103.4	99.9	100.0	85.6	32.6	-2.15/-0.01
5	125.1	99.6	100.0	82.7	29.[illegible]	-1.61/-0.33
6	150.6	99.0	100.0	84.6	29.4	-2.90/-0.43
7	174.8	98.8	100.0	88.1	30.5	-3.15/-0.32
8	194.5	98.8	100.0	84.3	28.3	-2.04/-2.02
9	234.7	99.6	100.0	88.7	29.6	-2.42/-1.55

Table 4-6

OCONEE UNIT 1 STATE POINTS

CYCLE 5

Point #	EFPD	Power (Percent)	Control Bank Position (% WD)			Axial Offset, % (Meas/Calc)
			Group 6	Group 7	Group 8	
1	24.5	97.0*	100.0	89.6	26.1	-0.41/-0.78
2	44.4	97.0	100.0	90.0	28.6	-2.54/-3.62
3	90.4	99.5	100.0	88.7	25.6	-4.61/-3.17
4	118.1	99.0	100.0	90.1	26.1	-1.84/-2.86
5	145.4	99.5	100.0	87.8	22.3	-2.89/-2.70
6	175.3	98.8	100.0	87.8	22.3	-3.33/-3.22
7	207.5	99.1	100.0	90.1	25.9	-4.87/-4.29
8	239.7	98.2	100.0	88.4	19.8	-0.94/-1.81
9	263.6	98.5	100.0	89.8	20.3	-1.40/-1.59
10	288.1	93.8	100.0	91.2	20.4	-1.53/ 0.44

* Calculation performed at 97.5% Full Power

Figure 4-1 Outline of PWR Data Flow

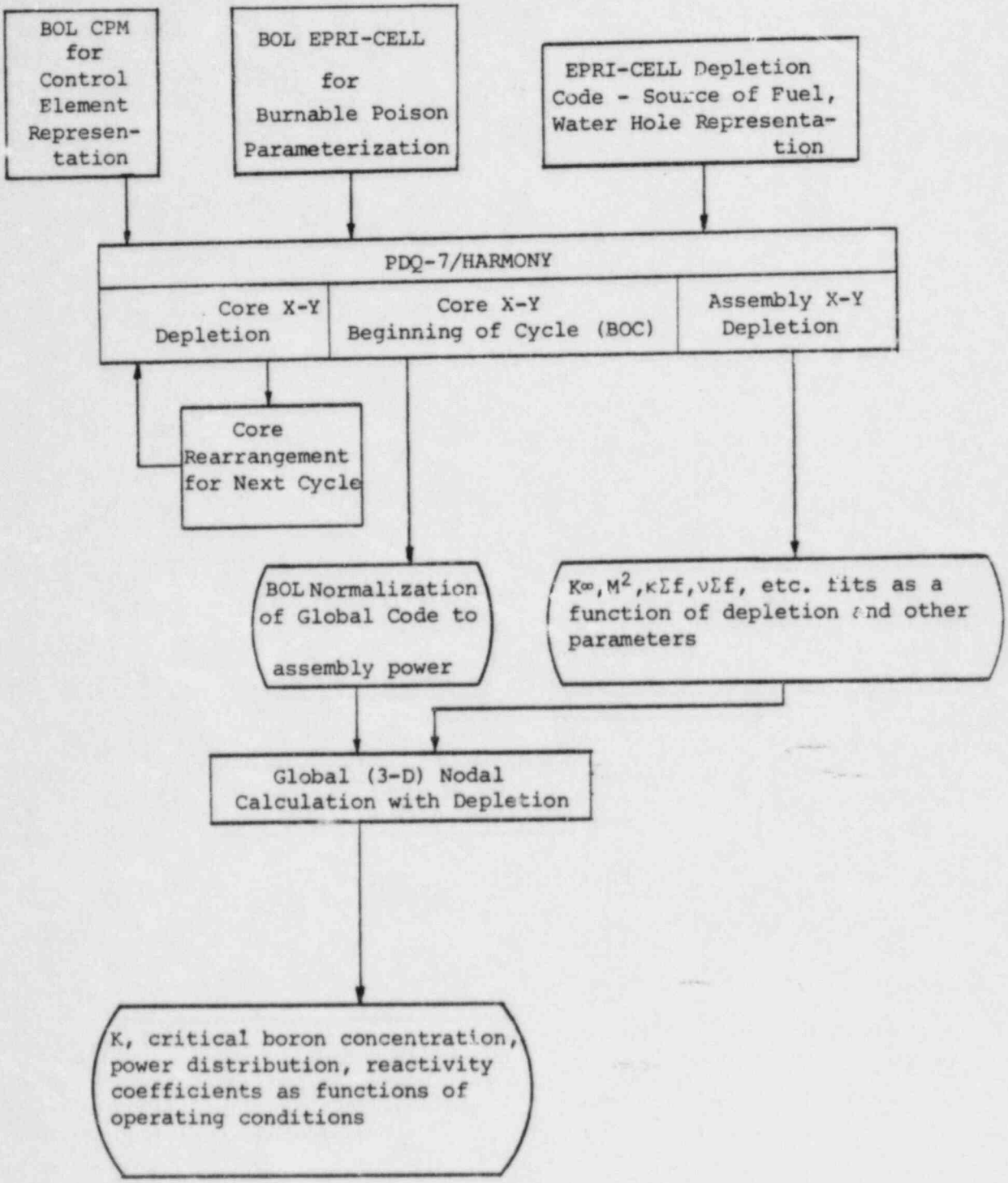

Figure 4-2
Oconee 1, Cycle 1
Control Rod Configuration

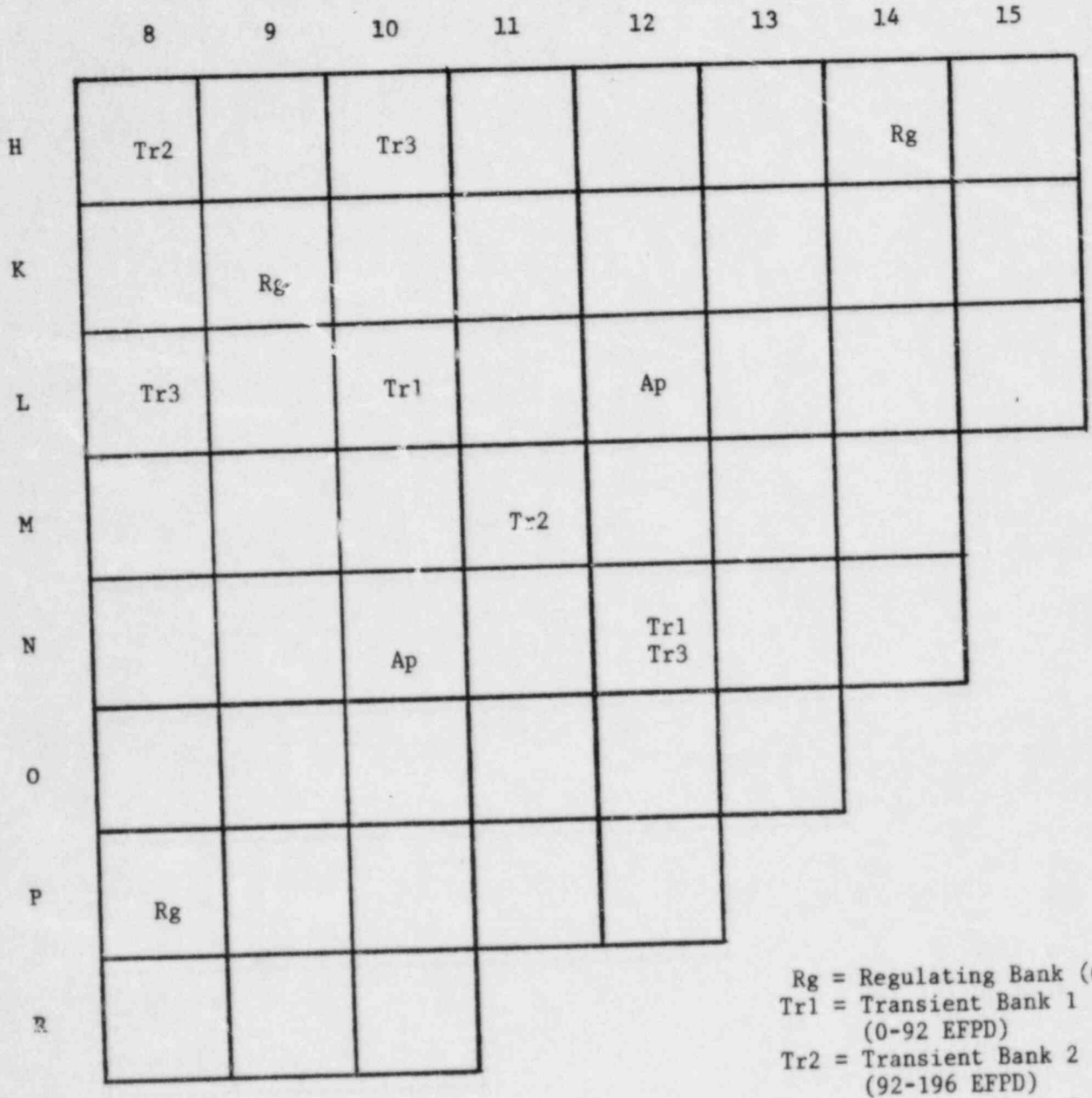

Rg = Regulating Bank (6)
Tr1 = Transient Bank 1 (7)
(0-92 EFPD)
Tr2 = Transient Bank 2 (7)
(92-196 EFPD)
Tr3 = Transient Bank 3 (7)
(196-310 EFPD)
Ap = APSR (8)

Figure 4-3
Oconee 1, Cycle 1
Quarter Core Loading Diagram

	8	9	10	11	12	13	14	15
H	2.00 1	2.00 1	2.00 1	2.00 1	2.00 1	2.10 2	2.15 3	2.15 3
K	2.00 1	2.00 1	2.00 1	2.00 1	2.10 2	2.10 2	2.15 3	2.15 3
L	2.00 1	2.00 1	2.00 1	2.10 2	2.10 2	2.10 2	2.15 3	2.15 3
M	2.00 1	2.00 1	2.10 2	2.10 2	2.10 2	2.15 3	2.15 3	
N	2.00 1	2.10 2	2.10 2	2.10 2	2.15 3	2.15 3	2.15 3	
O	2.10 2	2.10 2	2.10 2	2.15 3	2.15 3	2.15 3		
P	2.15 3	2.15 3	2.15 3	2.15 3	2.15 3			
R	2.15 3	2.15 3	2.15 3					

W/O U-235
Batch No.

Figure 4-4

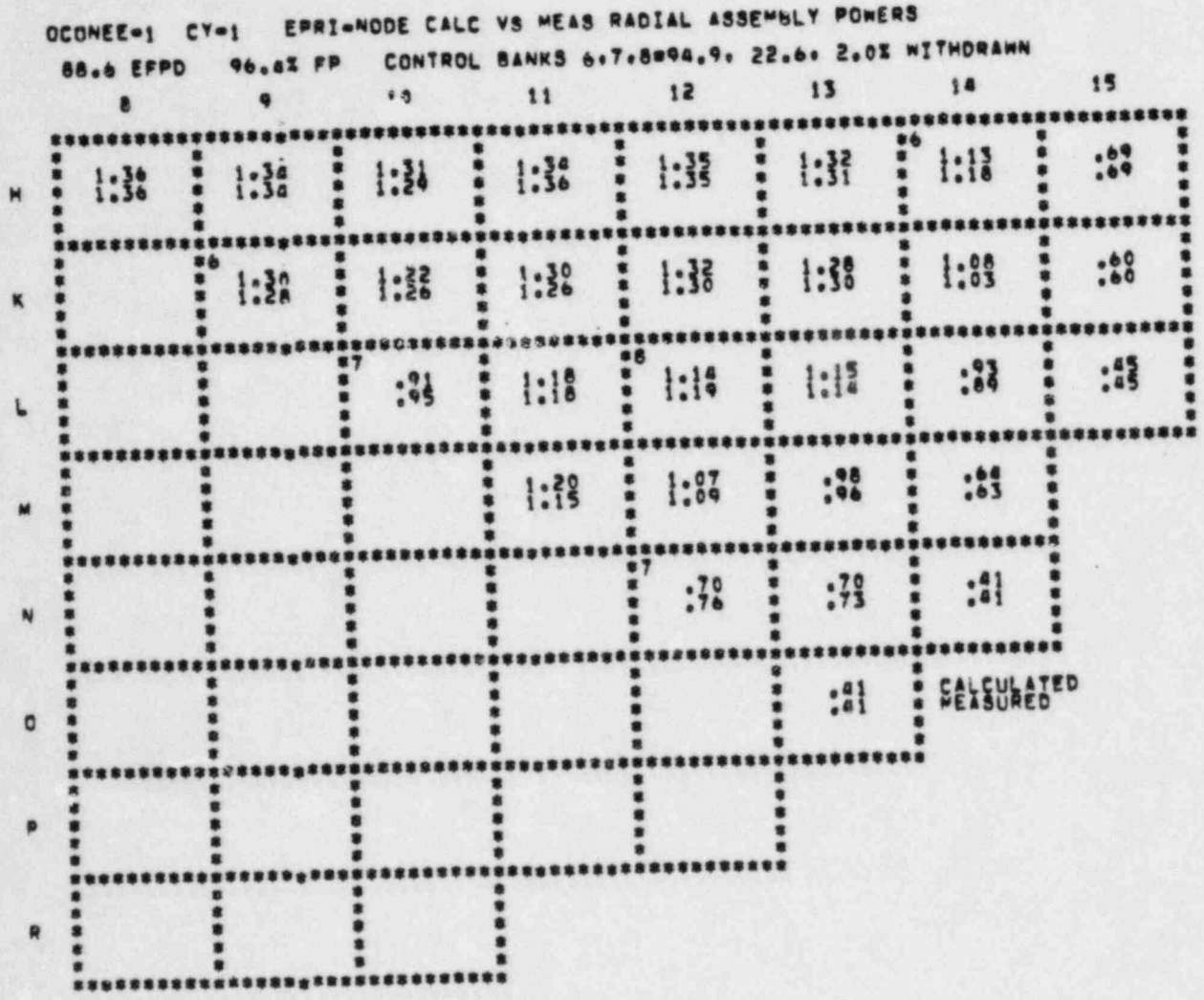
OCONEE-1 CY-1 EPRI-NODE CALC VS MEAS RADIAL ASSEMBLY POWERS
88.6 EFPD 96.8% FP CONTROL BANKS 6,7,8=94.9, 22.6, 2.0% WITHDRAWN
8 9 10 11 12 13 14 15
H K L M N O P R
1.36 1.36
1.34 1.34
1.31 1.24
1.34 1.36
1.35 1.35
1.32 1.31
1.13 1.18
.69 .69
6
1.30 1.28
1.32 1.26
1.30 1.26
1.32 1.30
1.28 1.30
1.08 1.03
.60 .60
7
.91 .95
1.18 1.18
8
1.14 1.19
1.15 1.14
.93 .89
.45 .45
1.20 1.15
1.07 1.09
.98 .96
.64 .63
7
.70 .76
.70 .73
.41 .41
.41 .41
CALCULATED
MEASURED

Figure 4-5

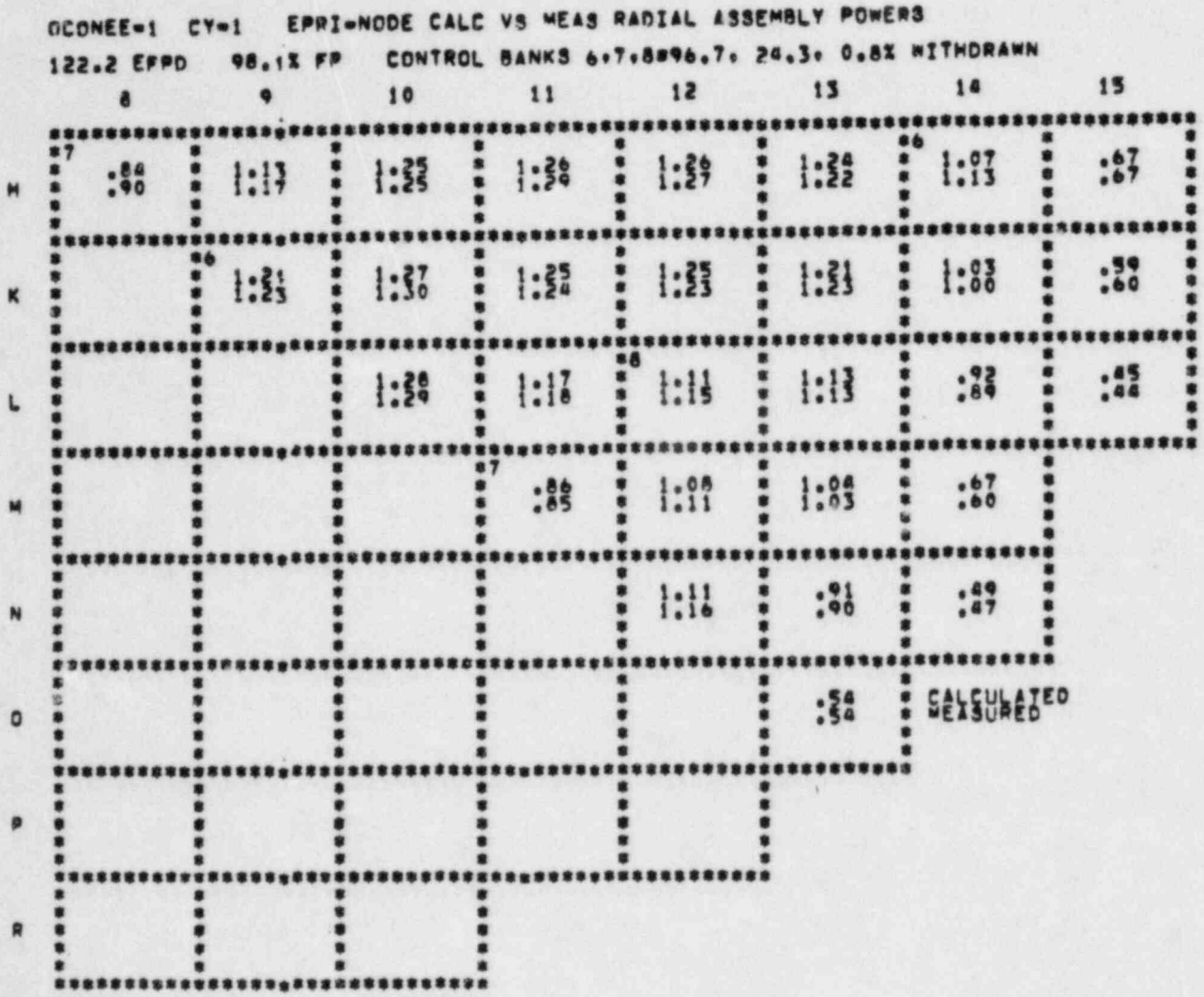
OCONEE-1 CY-1 EPRI-NODE CALC VS MEAS RADIAL ASSEMBLY POWERS
122.2 EFPD 98.1% FP CONTROL BANKS 6,7,8@96.7, 24.3, 0.8% WITHDRAWN
8 9 10 11 12 13 14 15
H
K
L
M
N
O
P
R
.84 .90
1.13 1.17
1.25 1.25
1.26 1.24
1.26 1.27
1.24 1.22
1.07 1.13
.67 .67
1.21 1.23
1.27 1.30
1.25 1.24
1.25 1.23
1.21 1.23
1.03 1.00
.59 .60
1.28 1.29
1.17 1.18
1.11 1.15
1.13 1.13
.92 .89
.85 .84
.86 .85
1.08 1.11
1.04 1.03
.67 .60
1.11 1.16
.91 .90
.49 .47
.54 .54
CALCULATED
MEASURED

Figure 4-6

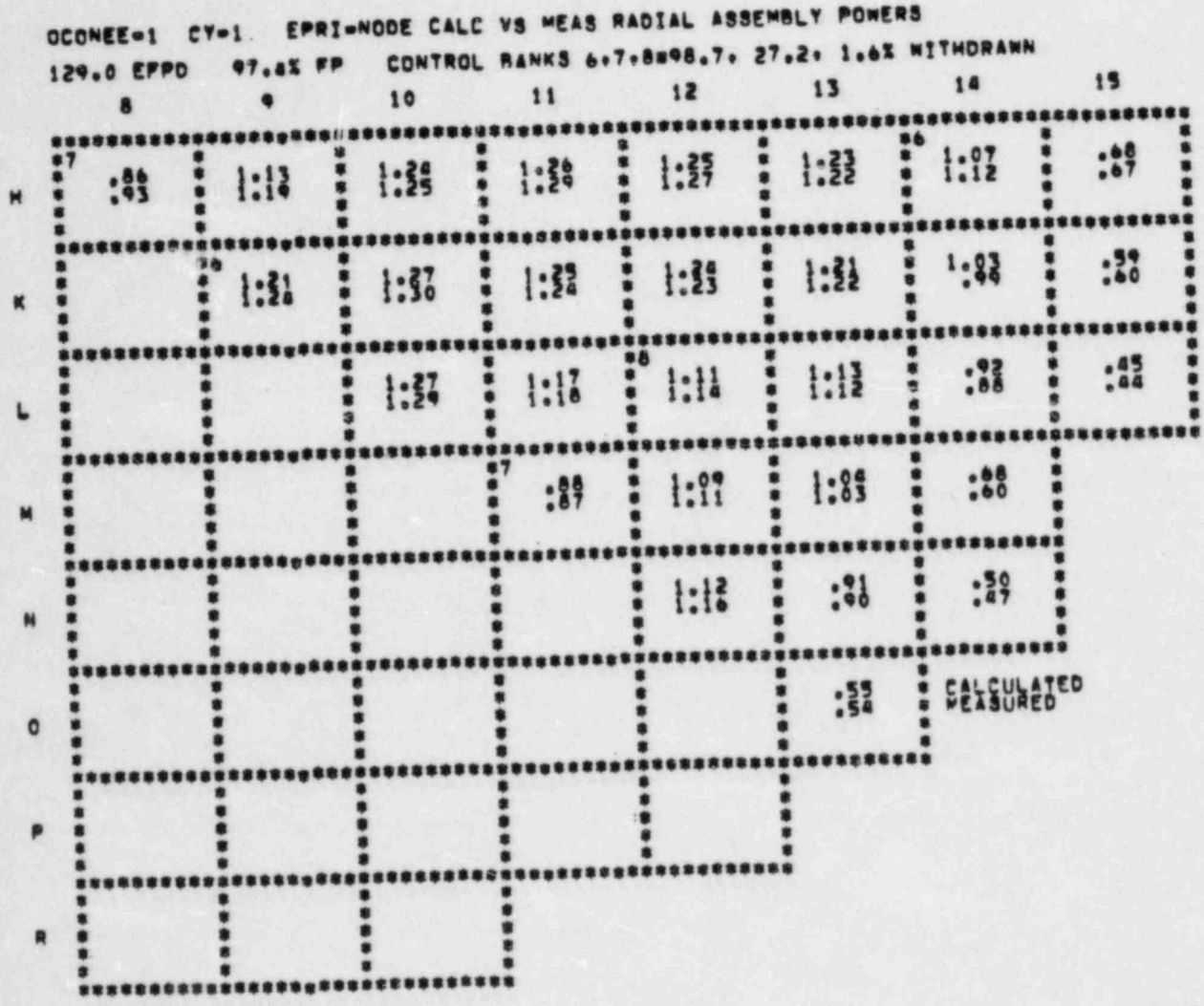
OCONEE-1 CY-1 EPRI-NODE CALC VS MEAS RADIAL ASSEMBLY POWERS
129.0 EFPD 97.6% FP CONTROL RANKS 6,7,8&8,7, 27,2, 1.6% WITHDRAWN
8 9 10 11 12 13 14 15
H
K
L
M
N
O
P
R
CALCULATED
MEASURED

Figure 4-7

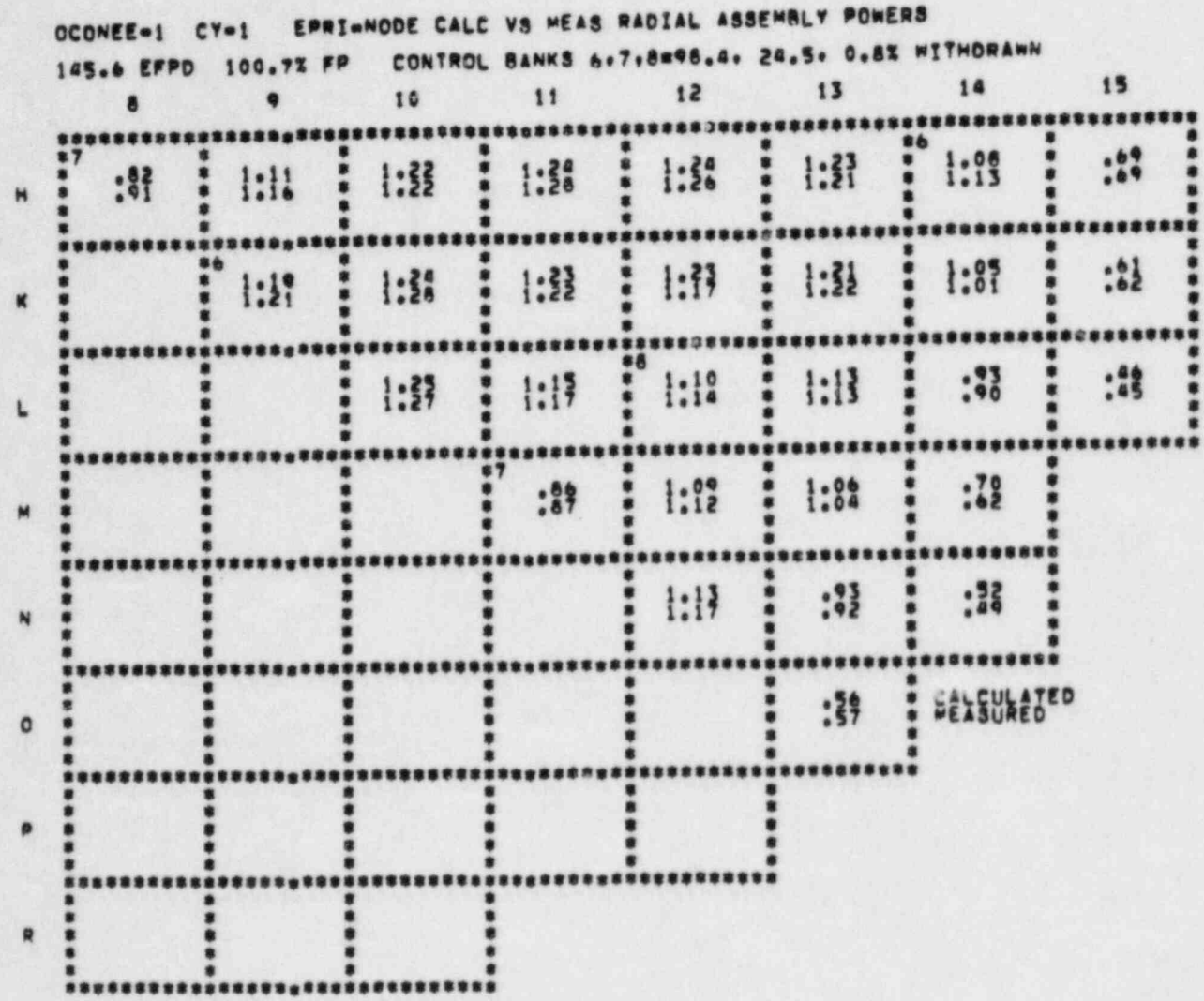
OCONEE-1 CY-1 EPRI-NODE CALC VS MEAS RADIAL ASSEMBLY POWERS
145.6 EFPD 100.7% FP CONTROL BANKS 6,7,8=98.4, 24.5, 0.8% WITHDRAWN
8 9 10 11 12 13 14 15
H K L M N O P R
.82 .91
1.11 1.16
1.22 1.22
1.24 1.28
1.24 1.26
1.23 1.21
1.08 1.13
.69 .69
1.10 1.21
1.24 1.26
1.23 1.22
1.23 1.17
1.21 1.22
1.05 1.01
.61 .62
1.25 1.27
1.15 1.17
1.10 1.14
1.13 1.15
.93 .90
.46 .45
.86 .87
1.09 1.12
1.06 1.04
.70 .62
1.13 1.17
.93 .92
.52 .44
.56 .57
CALCULATED
MEASURED

Figure 4-8

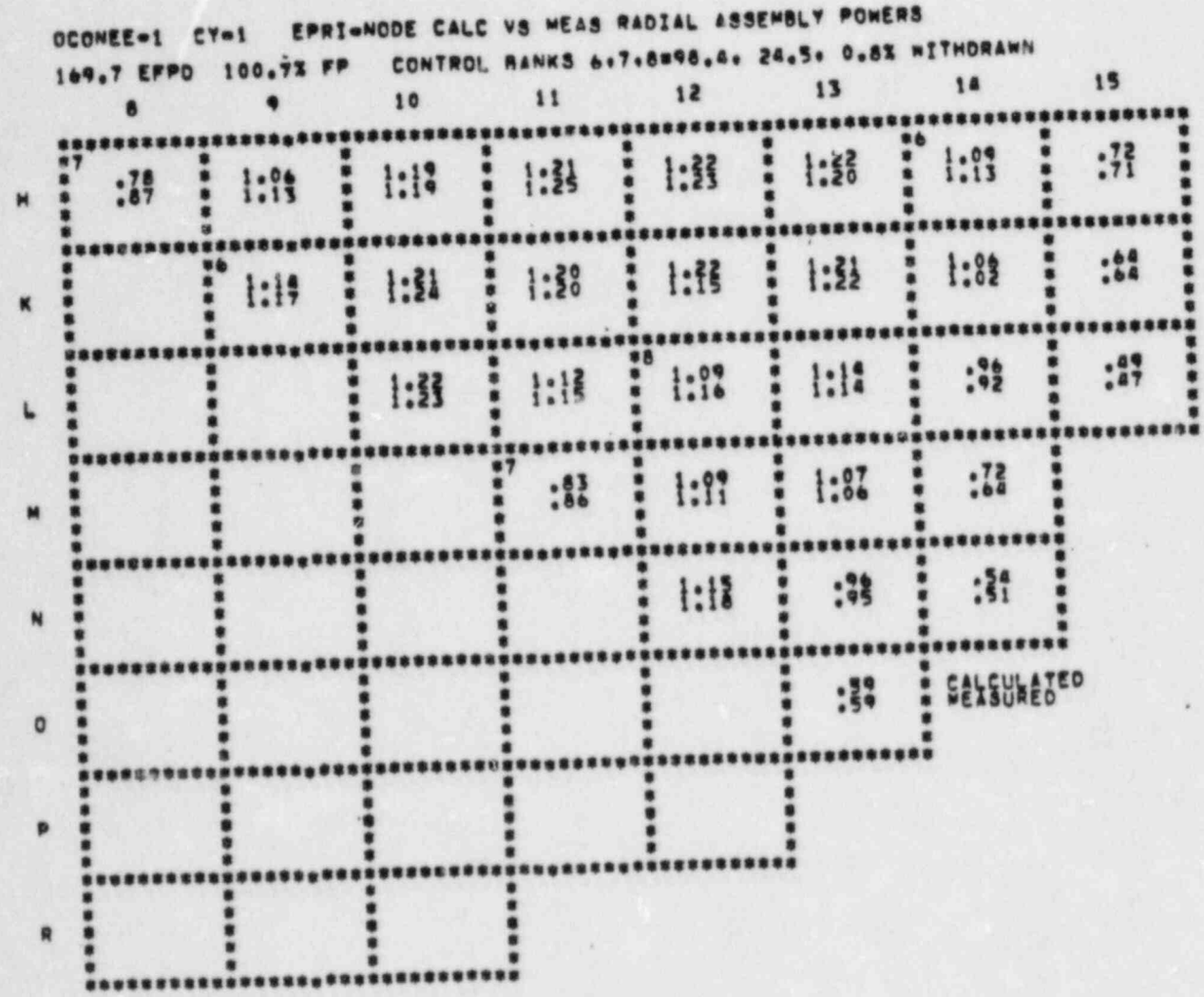
OCONEE-1 CY-1 EPRI-NODE CALC VS MEAS RADIAL ASSEMBLY POWERS
169.7 EFPD 100.7% FP CONTROL BANKS 6,7,8=98.4, 24.5, 0.8% WITHDRAWN
8 9 10 11 12 13 14 15
H
K
L
M
N
O
P
R
CALCULATED
MEASURED

Figure 4-9

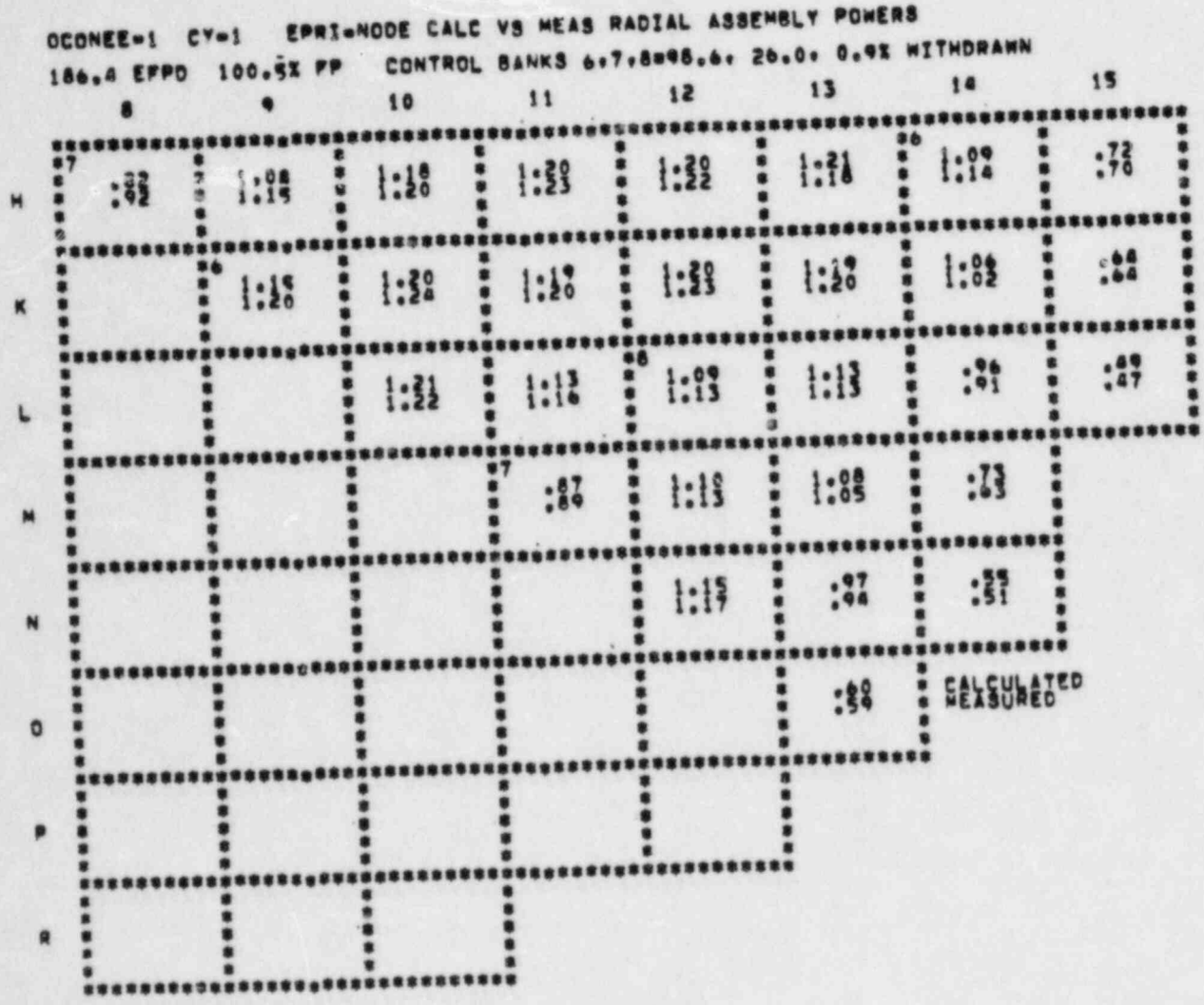
OCONEE-1 CY-1 EPRI-NODE CALC VS MEAS RADIAL ASSEMBLY POWERS
186.4 EFPD 100.5% FP CONTROL BANKS 6,7,8=98.6, 26.0, 0.9% WITHDRAWN
8 9 10 11 12 13 14 15
H
K
L
M
N
O
P
R
CALCULATED
MEASURED

Figure 4-10

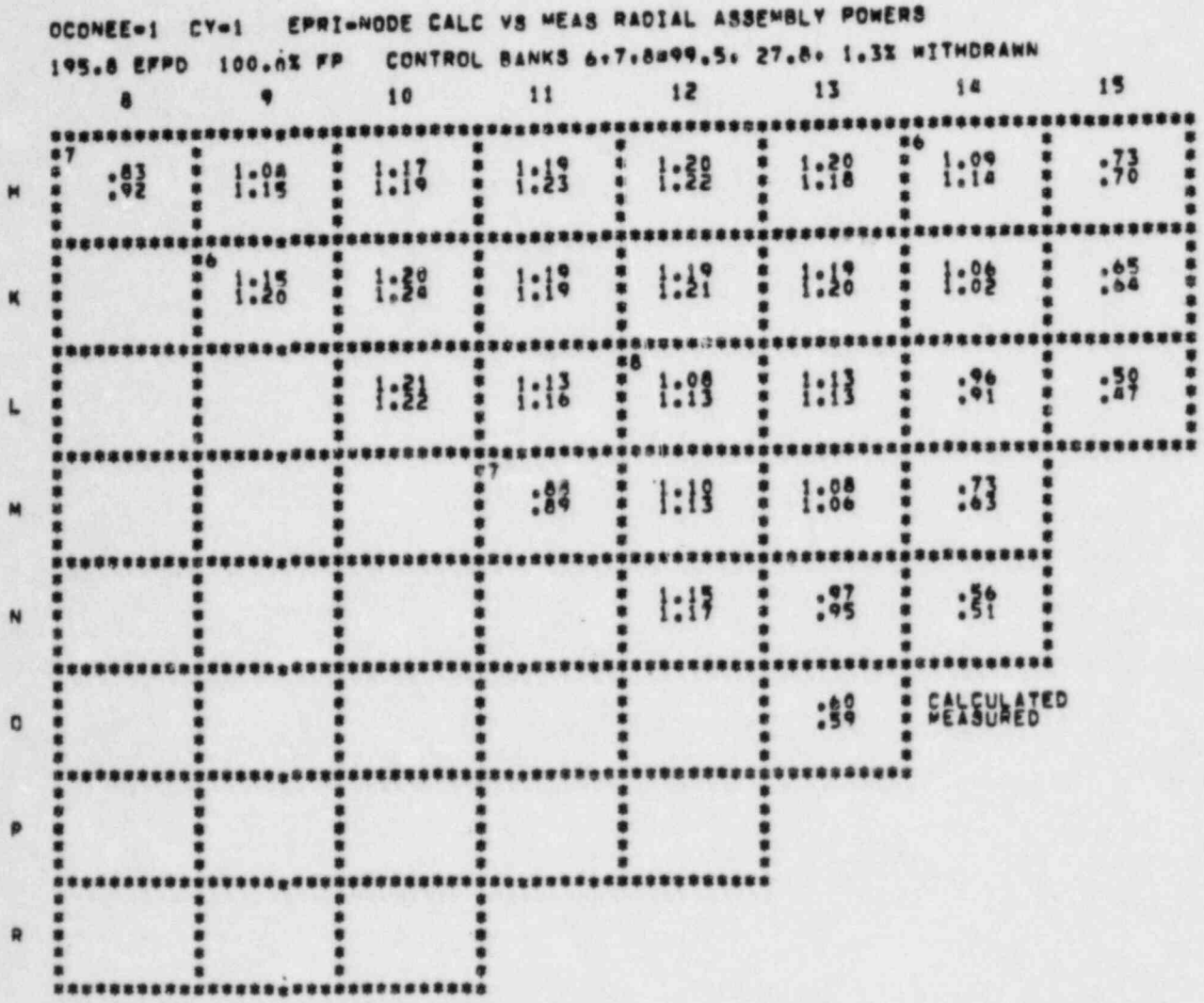
OCONEE-1 CY-1 EPRI-NODE CALC VS MEAS RADIAL ASSEMBLY POWERS
195.8 EFPD 100.0% FP CONTROL BANKS 6,7,8=99.5, 27.8, 1.3% WITHDRAWN
8 9 10 11 12 13 14 15
H
K
L
M
N
O
P
R
.83 .92
1.08 1.15
1.17 1.19
1.19 1.23
1.20 1.22
1.20 1.18
1.09 1.14
.73 .70
1.15 1.20
1.20 1.24
1.19 1.19
1.19 1.21
1.19 1.20
1.06 1.02
.65 .64
1.21 1.22
1.13 1.16
1.08 1.13
1.13 1.13
.96 .91
.50 .47
.84 .89
1.10 1.13
1.08 1.06
.73 .63
1.15 1.17
.97 .95
.56 .51
.60 .59
CALCULATED
MEASURED

Figure 4-11

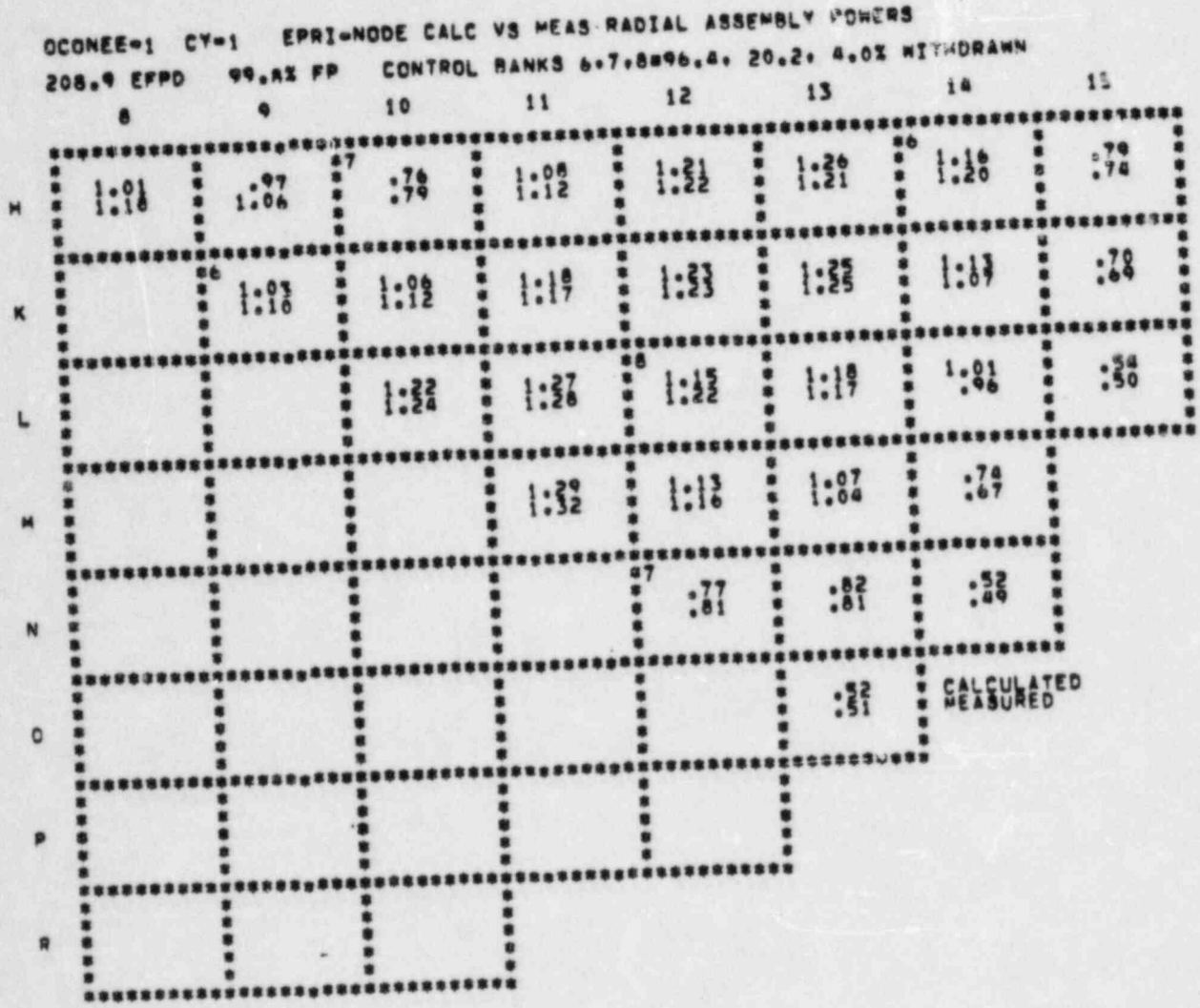
OCONEE-1 CY-1 EPRI-NODE CALC VS MEAS RADIAL ASSEMBLY POWERS
208.9 EFPD 99.8% FP CONTROL BANKS 6,7,8@96.4, 20.2, 4.0% WITHDRAWN
8 9 10 11 12 13 14 15
H K L M N O P R
1.01 1.10
.97 1.06
.76 .79
1.08 1.12
1.21 1.22
1.26 1.21
1.16 1.20
.79 .74
1.03 1.10
1.06 1.12
1.18 1.17
1.23 1.23
1.25 1.25
1.13 1.09
.70 .69
1.22 1.24
1.27 1.26
1.15 1.22
1.18 1.17
1.01 .96
.58 .50
1.29 1.32
1.13 1.16
1.07 1.04
.74 .67
.77 .81
.82 .81
.52 .49
.82 .81
CALCULATED
MEASURED

Figure 4-12

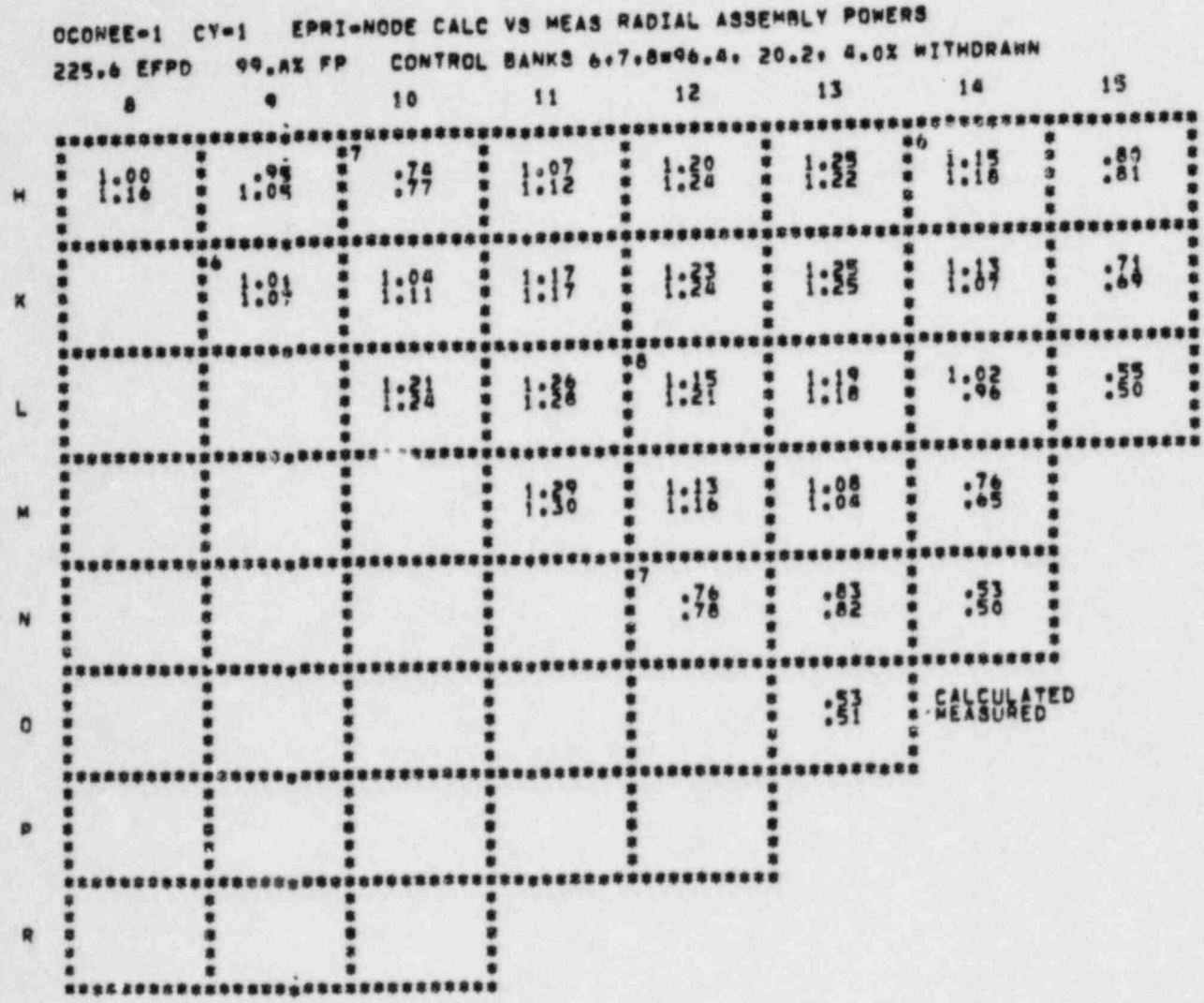
OCONEE-1 CY-1 EPRI-NODE CALC VS MEAS RADIAL ASSEMBLY POWERS
225.6 EFPD 99.8% FP CONTROL BANKS 6,7,8=96.4, 20.2, 4.0% WITHDRAWN
8 9 10 11 12 13 14 15
H K L M N O P R
1.00 1.16
.98 1.04
.74 .77
1.07 1.12
1.20 1.24
1.25 1.22
1.15 1.18
.80 .81
1.01 1.07
1.04 1.11
1.17 1.17
1.23 1.24
1.25 1.25
1.13 1.07
.71 .69
1.21 1.24
1.24 1.28
1.15 1.21
1.19 1.18
1.02 .96
.55 .50
1.29 1.30
1.13 1.16
1.08 1.04
.76 .65
.76 .78
.83 .82
.53 .50
.53 .51
CALCULATED
MEASURED

Figure 4-13

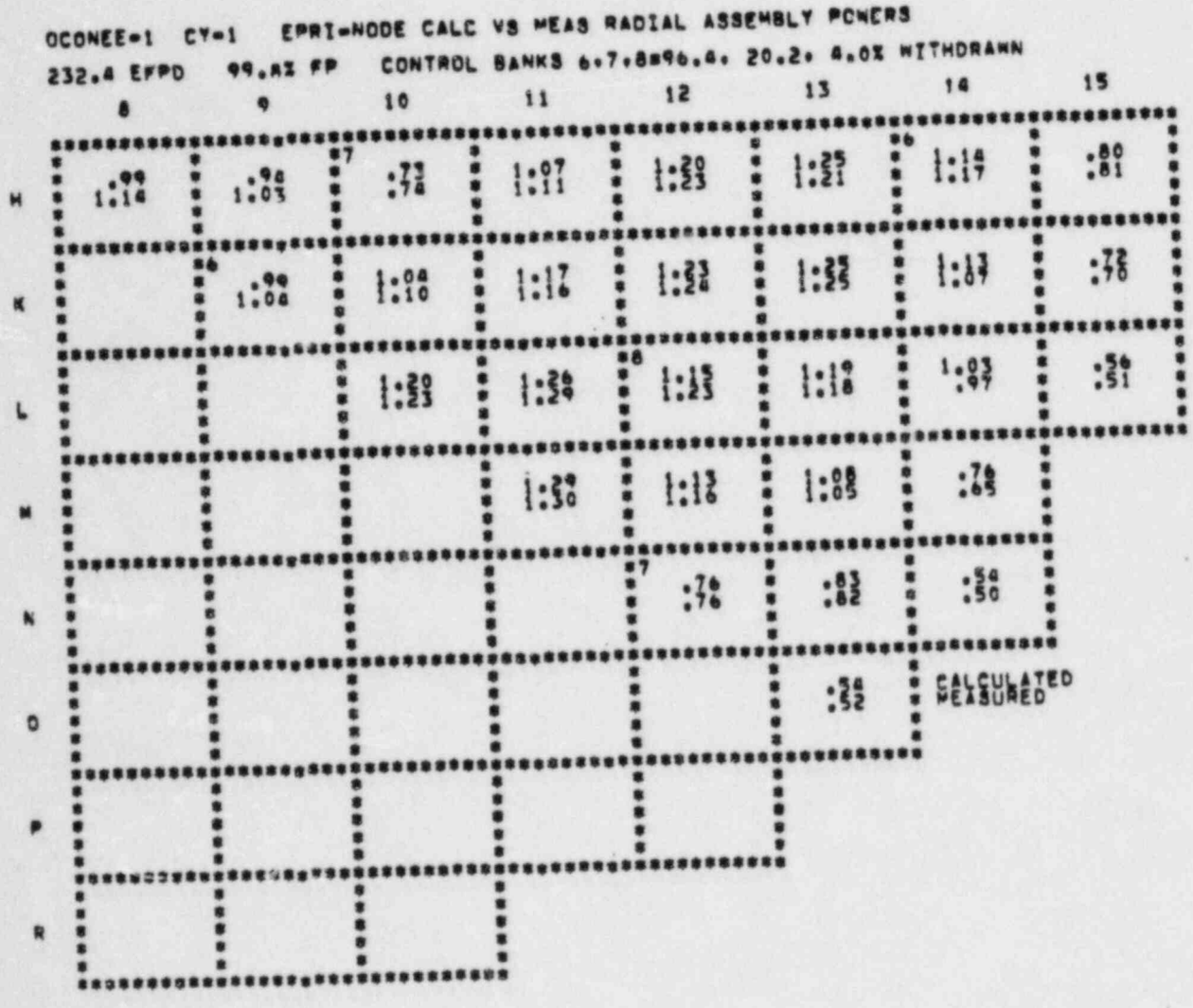
OCONEE-1 CY-1 EPRI-NODE CALC VS MEAS RADIAL ASSEMBLY POWERS
232.4 EFPD 99.8% FP CONTROL BANKS 6,7,8=96.4, 20.2, 4.0% WITHDRAWN
8 9 10 11 12 13 14 15
H K L M N O P R
.99 1.14
.96 1.03
.73 .74
1.07 1.11
1.20 1.23
1.25 1.21
1.14 1.17
.80 .81
.99 1.04
1.04 1.10
1.17 1.16
1.23 1.24
1.25 1.25
1.13 1.07
.72 .76
1.20 1.23
1.24 1.24
1.15 1.25
1.19 1.18
1.03 .97
.56 .51
1.29 1.30
1.13 1.16
1.08 1.05
.76 .65
.76 .76
.83 .82
.54 .50
.54 .52
CALCULATED
MEASURED

Figure 4-14

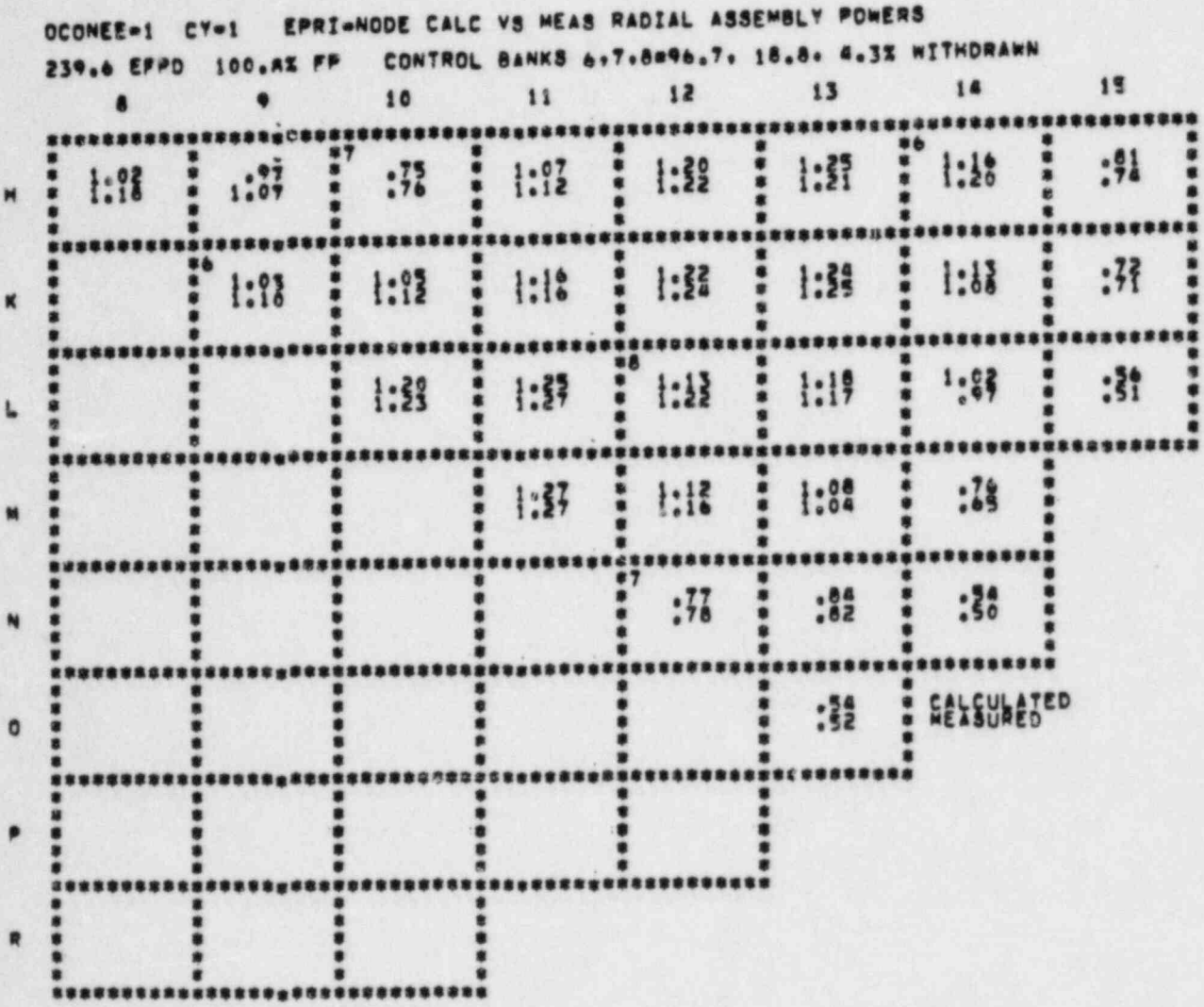
OCONEE-1 CY-1 EPRI-NODE CALC VS MEAS RADIAL ASSEMBLY POWERS
239.6 EFPD 100.A% FP CONTROL BANKS 6,7,8=96.7, 18.8, 4.3% WITHDRAWN
8
9
10
11
12
13
14
15
H
K
L
M
N
O
P
R
1.02 1.18
.97 1.09
.75 .76
1.07 1.12
1.20 1.22
1.25 1.21
1.16 1.20
.81 .74
1.03 1.10
1.05 1.12
1.16 1.16
1.22 1.24
1.24 1.25
1.13 1.08
.72 .71
1.20 1.23
1.25 1.27
1.13 1.22
1.18 1.17
1.02 .97
.86 .81
1.27 1.29
1.12 1.16
1.08 1.04
.76 .65
.77 .78
.84 .82
.54 .50
.54 .52
CALCULATED
MEASURED

Figure 4-15

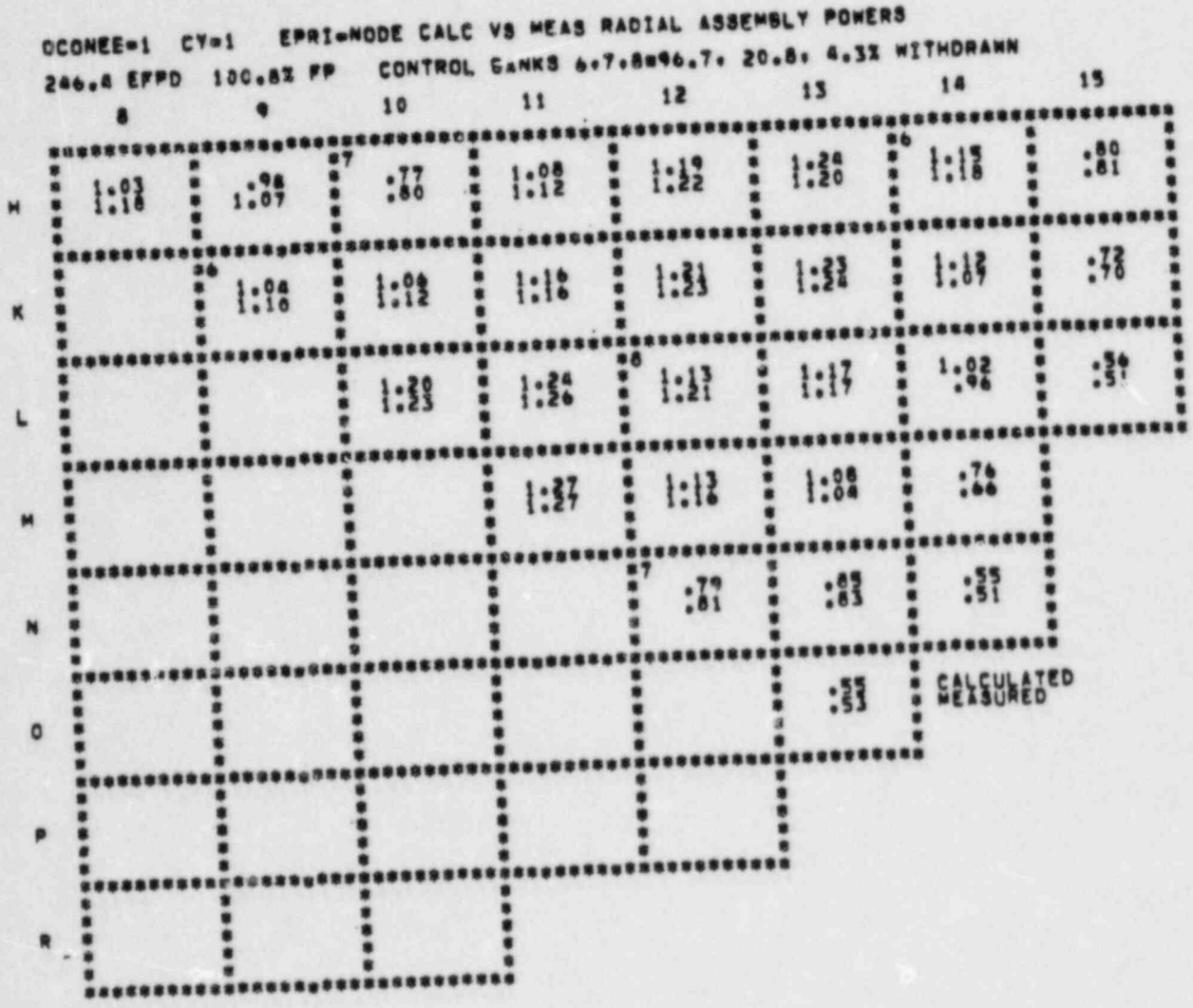
OCONEE-1 CY-1 EPRI-NODE CALC VS MEAS RADIAL ASSEMBLY POWERS
246.8 EFPD 100.8% FP CONTROL BANKS 6,7,8@96.7, 20.8, 4.3% WITHDRAWN
8 9 10 11 12 13 14 15
H
K
L
M
N
O
P
R
1.03 1.18
.98 1.07
.77 .80
1.08 1.12
1.19 1.22
1.24 1.20
1.15 1.18
.80 .81
1.04 1.10
1.08 1.12
1.16 1.16
1.21 1.23
1.23 1.24
1.12 1.09
.72 .70
1.20 1.23
1.24 1.26
1.13 1.21
1.17 1.17
1.02 .96
.54 .51
1.27 1.27
1.13 1.16
1.08 1.04
.74 .66
.79 .81
.68 .83
.55 .51
.55 .53
CALCULATED
MEASURED

Figure 4-16

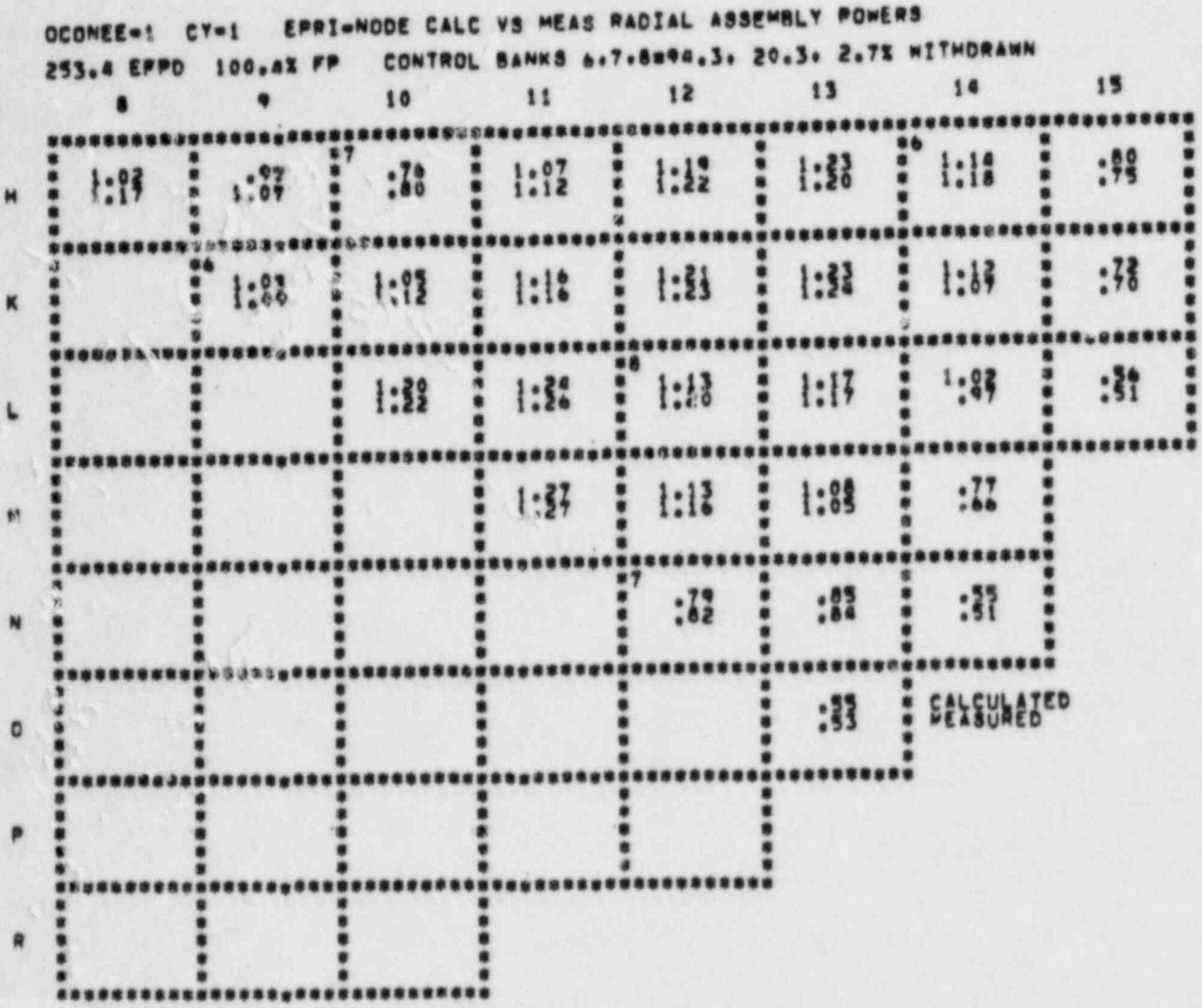
OCONEE-1 CY-1 EPRI-NODE CALC VS MEAS RADIAL ASSEMBLY POWERS
253.4 EFPD 100.0% FP CONTROL BANKS 6,7,8@94.3, 20.3, 2.7% WITHDRAWN
8 9 10 11 12 13 14 15
H K L M N O P R
1.02 1.17
1.07 1.09
.78 .80
1.07 1.12
1.19 1.22
1.23 1.20
1.14 1.18
.80 .75
1.01 1.00
1.05 1.12
1.16 1.16
1.21 1.23
1.23 1.24
1.12 1.09
.72 .76
1.20 1.22
1.24 1.26
1.13 1.18
1.17 1.17
1.02 1.09
.84 .81
1.27 1.24
1.13 1.16
1.08 1.05
.77 .66
.79 .82
.85 .84
.55 .51
.83 .83
CALCULATED
MEASURED

Figure 4-17

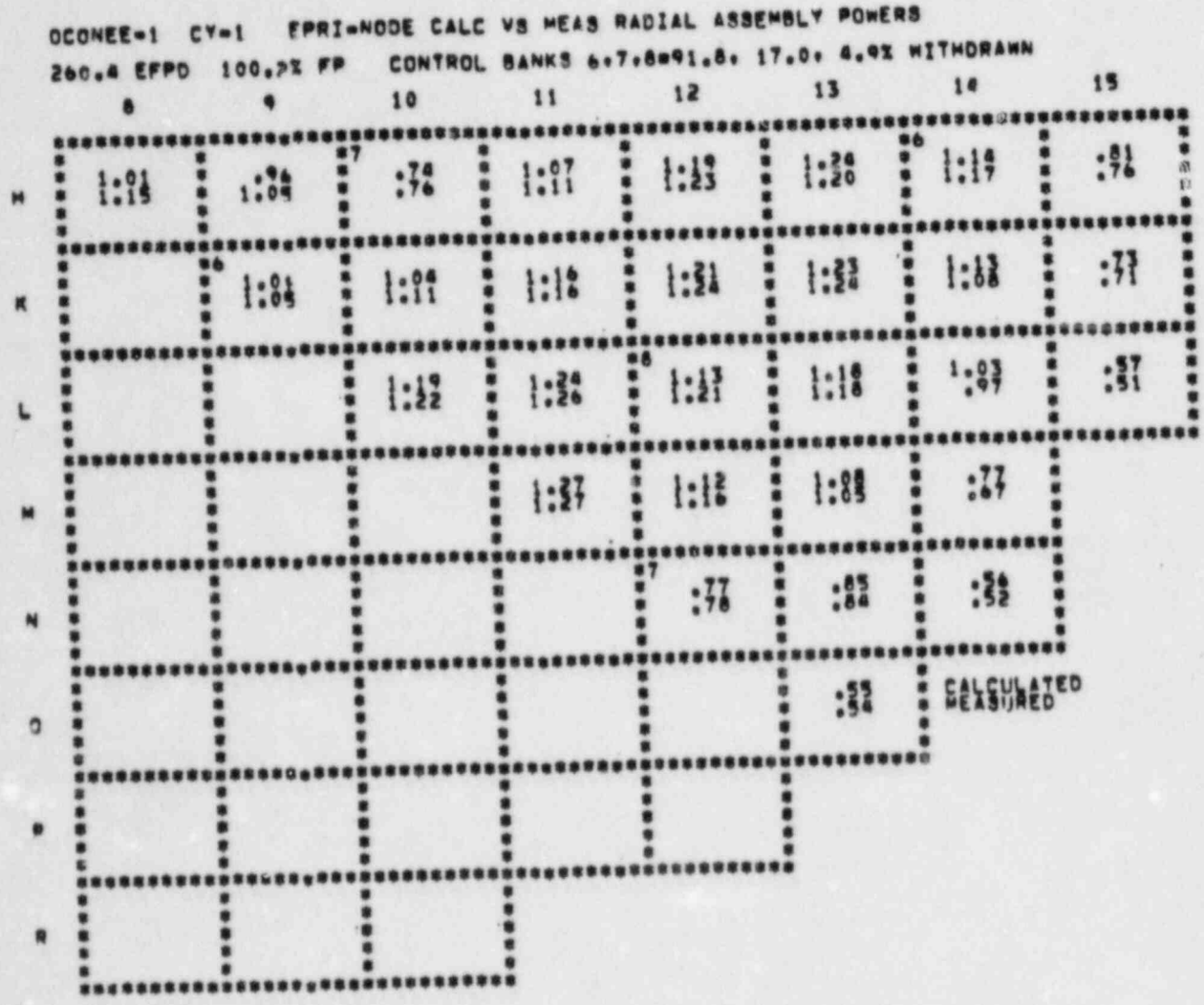
OCONEE-1 CY-1 EPRI-NODE CALC VS MEAS RADIAL ASSEMBLY POWERS
260.4 EFPD 100.2% FP CONTROL BANKS 6,7,8=91.8, 17.0, 4.9% WITHDRAWN
8 9 10 11 12 13 14 15
H K L M N O P R
1.01 1.15
.96 1.09
.74 .76
1.07 1.11
1.19 1.23
1.24 1.20
1.18 1.17
.81 .76
1.01 1.05
1.04 1.11
1.16 1.16
1.21 1.24
1.23 1.24
1.13 1.08
.73 .71
1.19 1.22
1.24 1.26
1.13 1.21
1.18 1.18
1.03 .97
.87 .81
1.27 1.27
1.12 1.16
1.08 1.05
.77 .69
.77 .78
.85 .84
.84 .82
.88 .84
CALCULATED
MEASURED

Figure 4-18

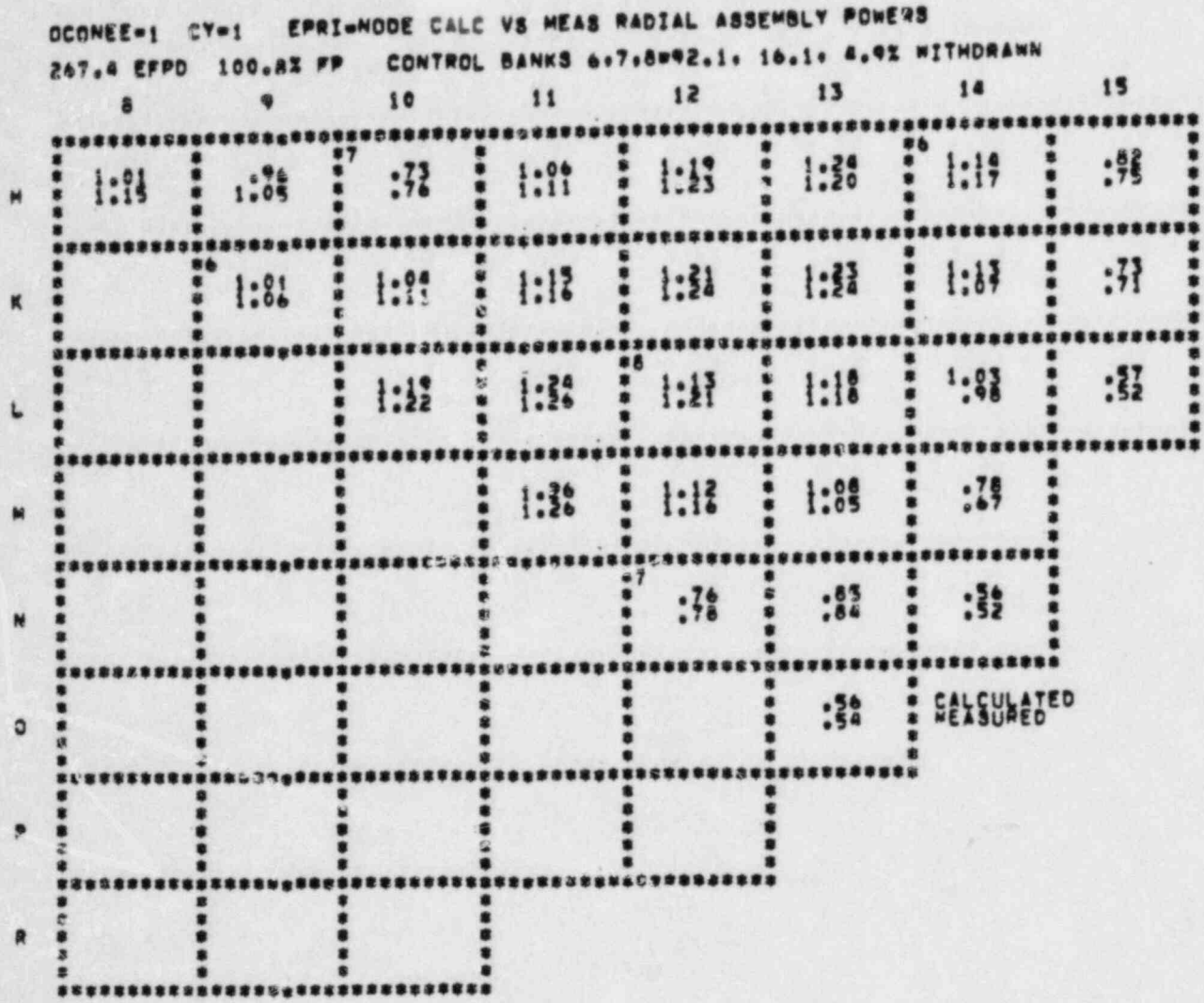
OCONEE-1 CY-1 EPRI-NODE CALC VS MEAS RADIAL ASSEMBLY POWERS
247.4 EFPD 100.8% FP CONTROL BANKS 6,7,8=92.1, 16.1, 4.9% WITHDRAWN
8 9 10 11 12 13 14 15
H
K
L
M
N
O
P
R
CALCULATED
MEASURED

Figure 4-19

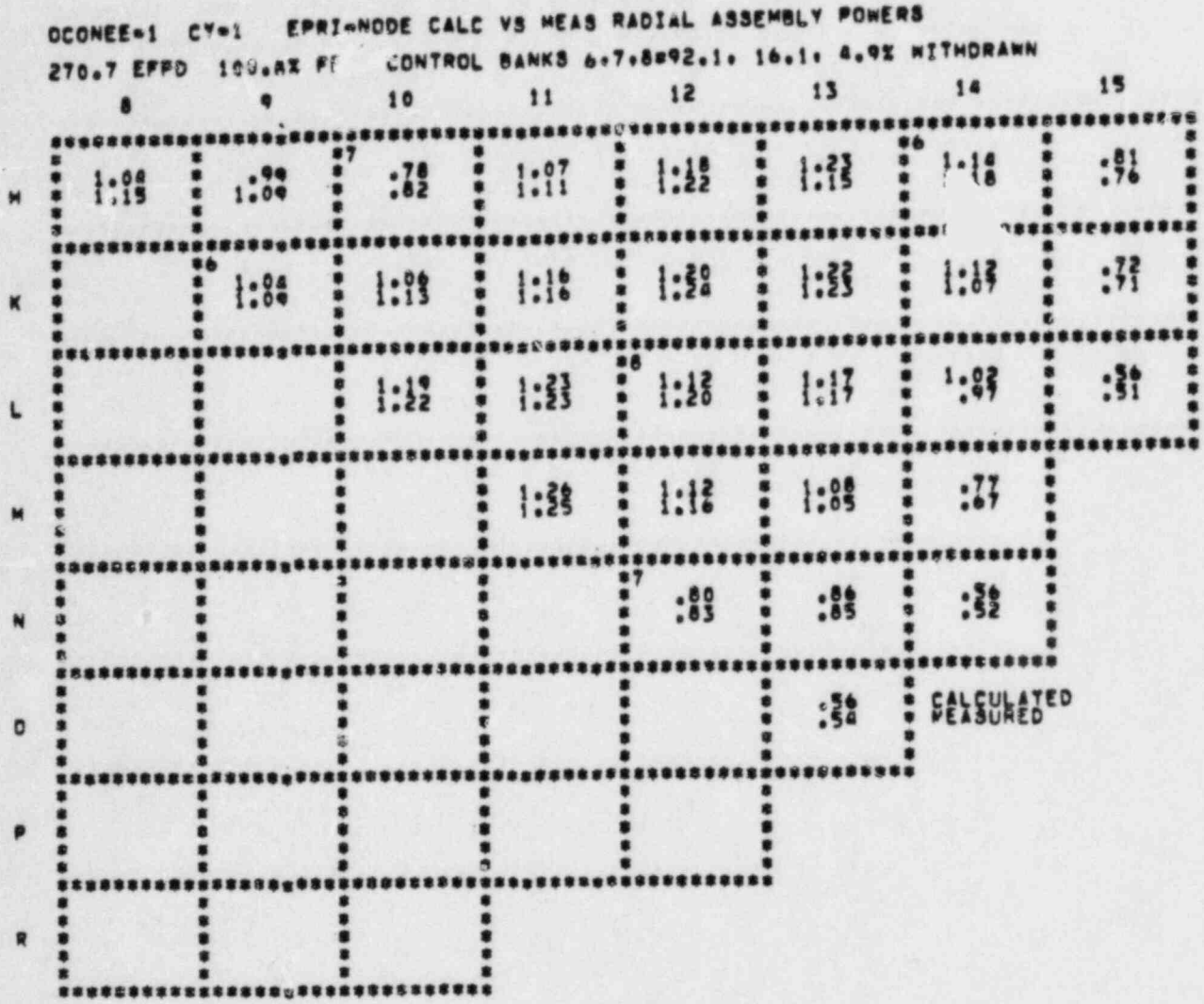
OCONEE-1 CY-1 EPRI-NODE CALC VS MEAS RADIAL ASSEMBLY POWERS
270.7 EFPD 100.0% FP CONTROL BANKS 6,7,8=92.1, 16.1, 4.9% WITHDRAWN
8 9 10 11 12 13 14 15
H
K
L
M
N
O
P
R
1.04 1.15
.99 1.09
.78 .82
1.07 1.11
1.18 1.22
1.23 1.15
1.14 1.8
.81 .76
1.04 1.09
1.06 1.13
1.16 1.16
1.20 1.24
1.22 1.23
1.12 1.07
.72 .71
1.19 1.22
1.23 1.23
1.12 1.20
1.17 1.17
1.02 .99
.56 .51
1.26 1.25
1.12 1.16
1.08 1.05
.77 .67
.80 .83
.86 .85
.56 .52
.56 .54
CALCULATED
MEASURED

Figure 4-20

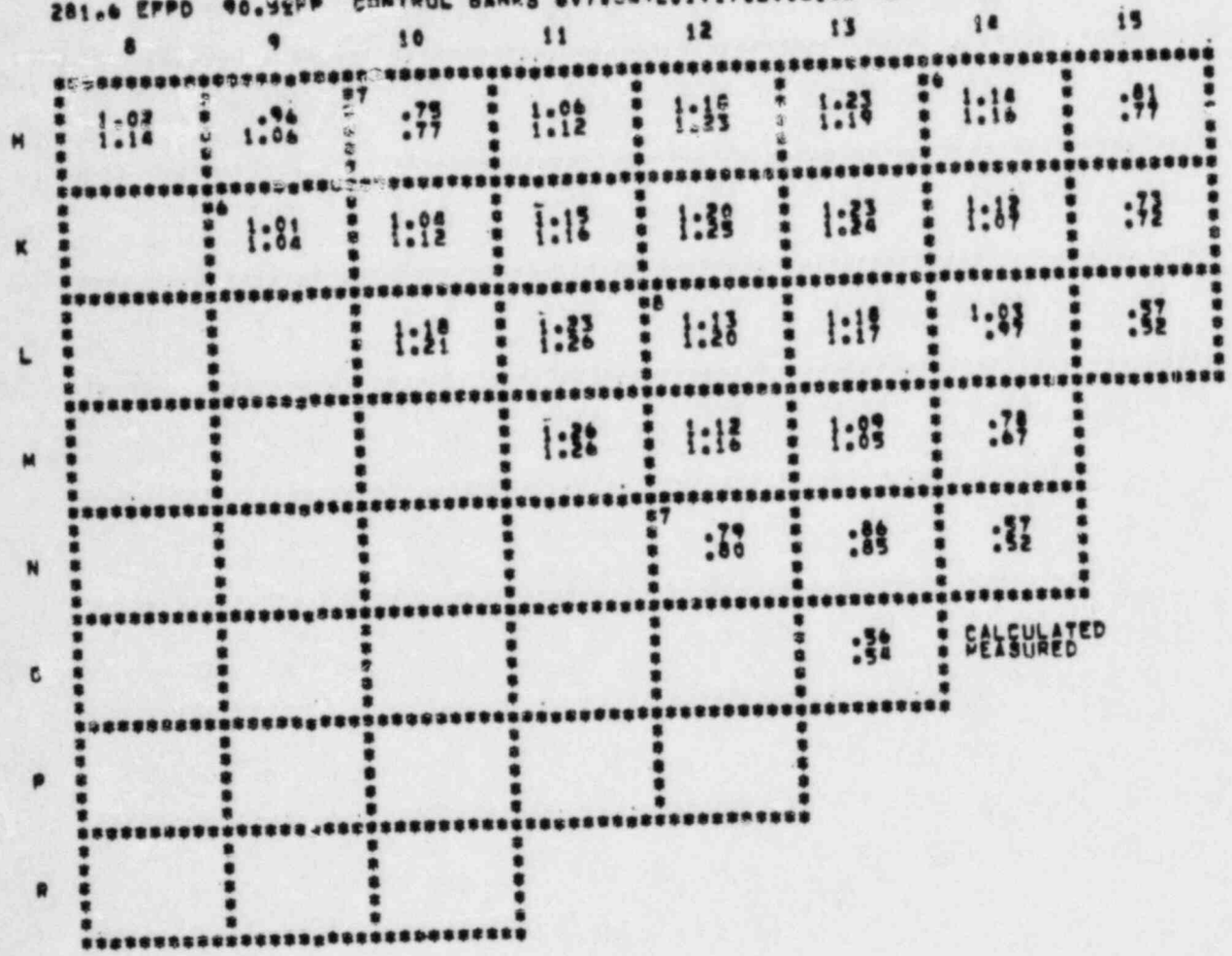
OCONEE CY=1 EPRI-NODE CALC VS MEAS RADIAL ASSEMBLY POWERS
281.4 EFPD 90.9%FP CONTROL BANKS 6,7,8@2.1,17.2,12.0% WITHDRAWN
8
9
10
11
12
13
14
15
H
K
L
M
N
C
P
R
1.02 1.14
.94 1.06
.75 .77
1.06 1.12
1.16 1.23
1.23 1.19
1.18 1.16
.81 .77
1.01 1.04
1.06 1.12
1.15 1.18
1.20 1.25
1.23 1.24
1.18 1.17
.73 .72
1.18 1.21
1.23 1.26
1.13 1.20
1.18 1.17
1.03 1.09
.87 .82
1.24 1.24
1.12 1.16
1.09 1.05
.78 .87
.79 .80
.86 .85
.87 .82
.56 .54
CALCULATED
MEASURED

Figure 4-21

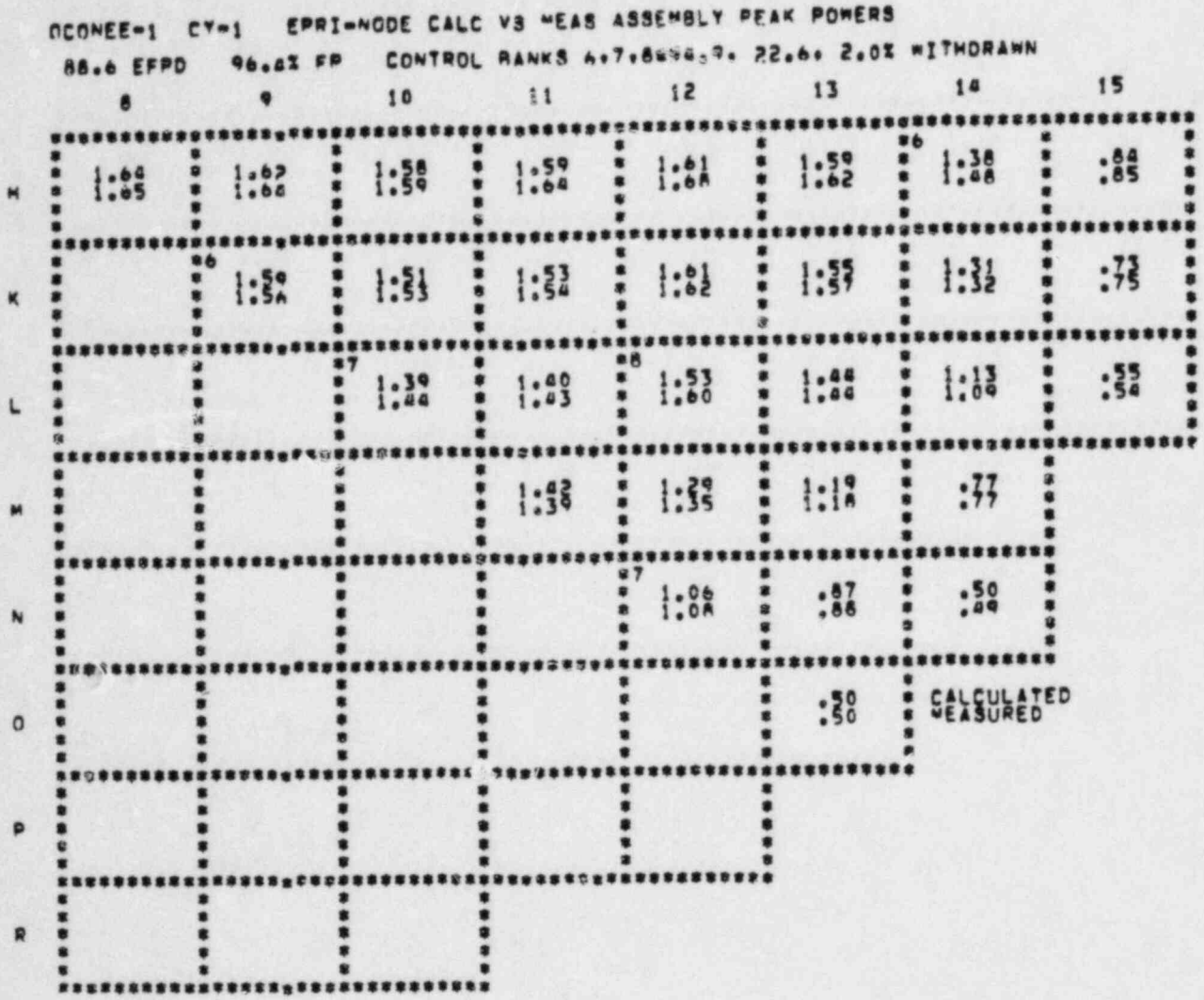
OCONEE-1 CY-1 EPRI-NODE CALC VS MEAS ASSEMBLY PEAK POWERS
88.6 EFPD 96.6% FP CONTROL RANKS 4,7,8,9, 22.6, 2.0% WITHDRAWN
8 9 10 11 12 13 14 15
H
K
L
M
N
O
P
R
1.64 1.65
1.62 1.66
1.58 1.59
1.59 1.64
1.61 1.68
1.59 1.62
#6 1.38 1.48
.84 .85
#6 1.59 1.58
1.51 1.53
1.53 1.54
1.61 1.62
1.55 1.57
1.31 1.32
.73 .75
#7 1.39 1.44
1.40 1.43
#8 1.53 1.60
1.48 1.46
1.13 1.09
.55 .54
1.42 1.38
1.29 1.35
1.19 1.18
.77 .77
#7 1.06 1.08
.87 .88
.50 .49
.50 .50
CALCULATED
MEASURED

Figure 4-22

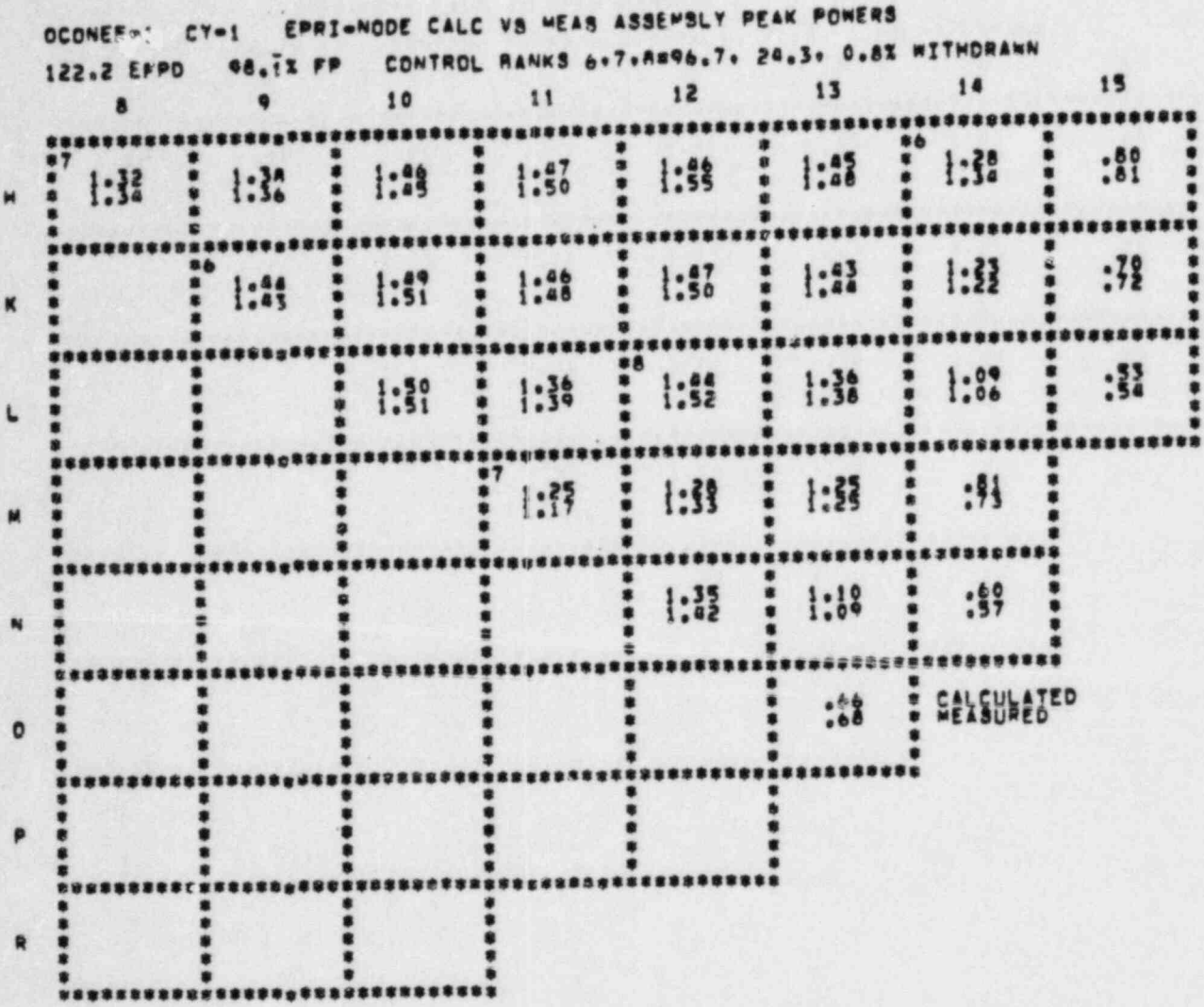
OCONEE 1 CY-1 EPRI-NODE CALC VS MEAS ASSEMBLY PEAK POWERS
122.2 EFPD 68.1% FP CONTROL BANKS 6,7,A=96.7, 24.3, 0.8% WITHDRAWN
8 9 10 11 12 13 14 15
H
K
L
M
N
O
P
R
CALCULATED
MEASURED

Figure 4-23

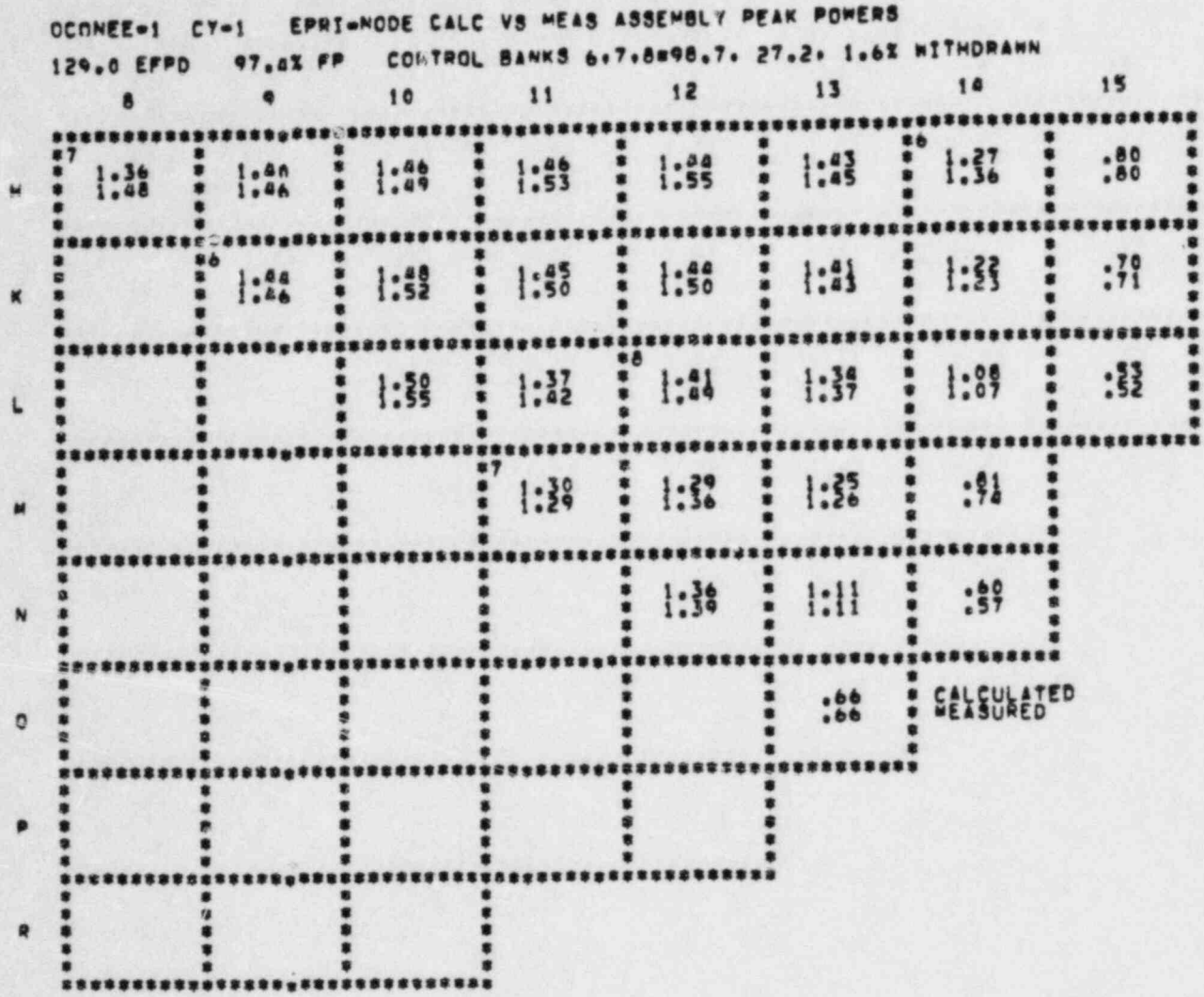
OCONEE-1 CY-1 EPRI-NODE CALC VS MEAS ASSEMBLY PEAK POWERS
129.0 EFPD 97.0% FP CONTROL BANKS 6,7,8=98.7, 27.2, 1.6% WITHDRAWN
8 9 10 11 12 13 14 15
H
K
L
M
N
O
P
R
1.36 1.48
1.40 1.46
1.46 1.49
1.46 1.53
1.44 1.55
1.43 1.45
1.27 1.36
.80 .80
1.44 1.46
1.48 1.52
1.45 1.50
1.44 1.50
1.41 1.43
1.22 1.23
.70 .71
1.50 1.55
1.37 1.42
1.41 1.44
1.34 1.37
1.08 1.07
.83 .52
1.30 1.29
1.29 1.36
1.25 1.26
.81 .74
1.36 1.39
1.11 1.11
.60 .57
.66 .66
CALCULATED
MEASURED

Figure 4-24

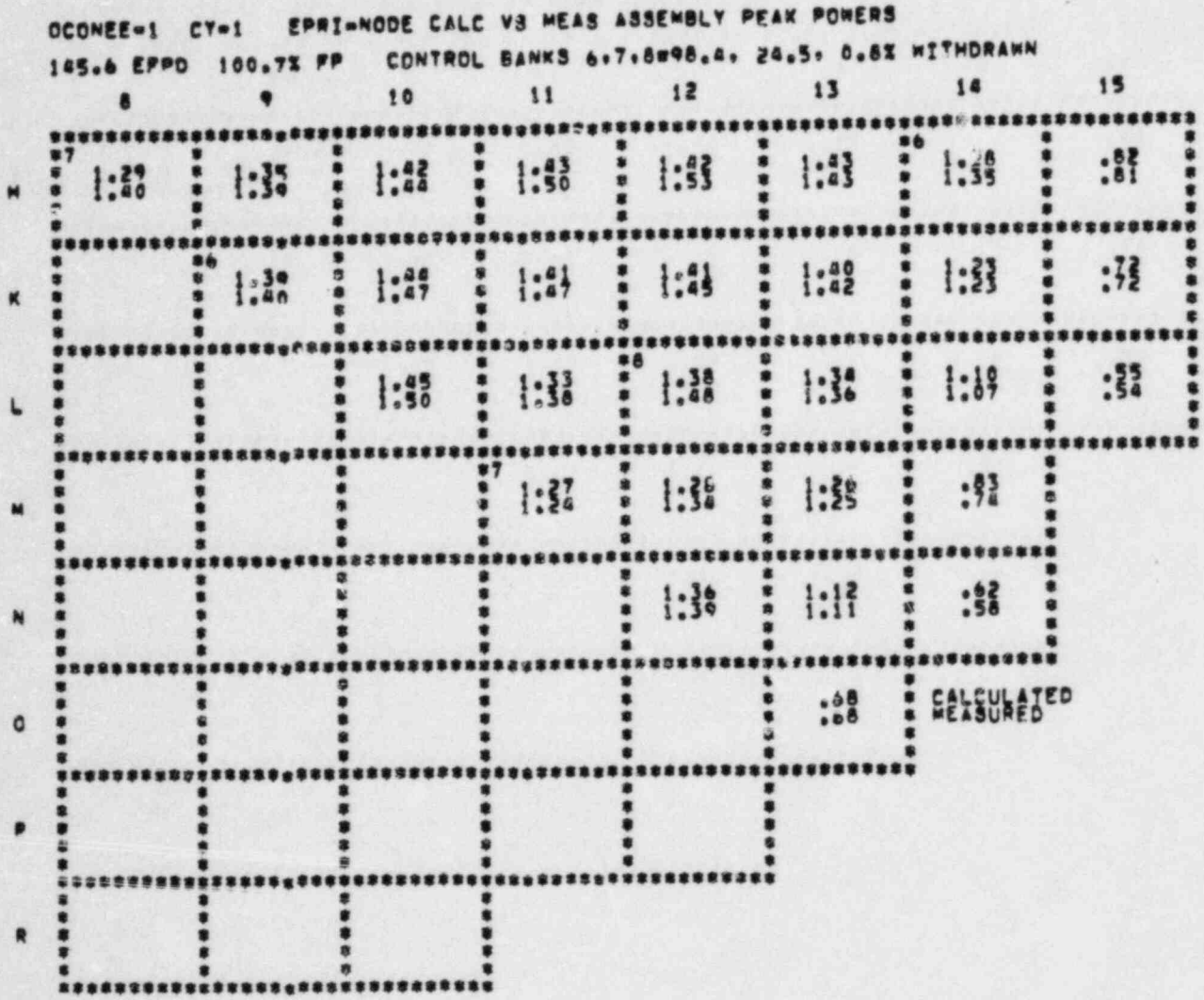
OCONEE-1 CY-1 EPRI-NODE CALC VS MEAS ASSEMBLY PEAK POWERS
145.6 EFPD 100.7% FP CONTROL BANKS 6,7,8=98.4, 24.5, 0.8% WITHDRAWN
8 9 10 11 12 13 14 15
H
K
L
M
N
O
P
R
1.29 1.40
1.35 1.39
1.42 1.44
1.43 1.50
1.42 1.53
1.43 1.43
1.28 1.35
.82 .81
1.38 1.40
1.46 1.47
1.41 1.47
1.41 1.45
1.40 1.42
1.23 1.23
.72 .72
1.45 1.50
1.33 1.38
1.38 1.48
1.34 1.36
1.10 1.09
.55 .54
1.27 1.24
1.26 1.38
1.30 1.25
.83 .74
1.36 1.39
1.12 1.11
.62 .58
.68 .68
CALCULATED
MEASURED

Figure 4-25

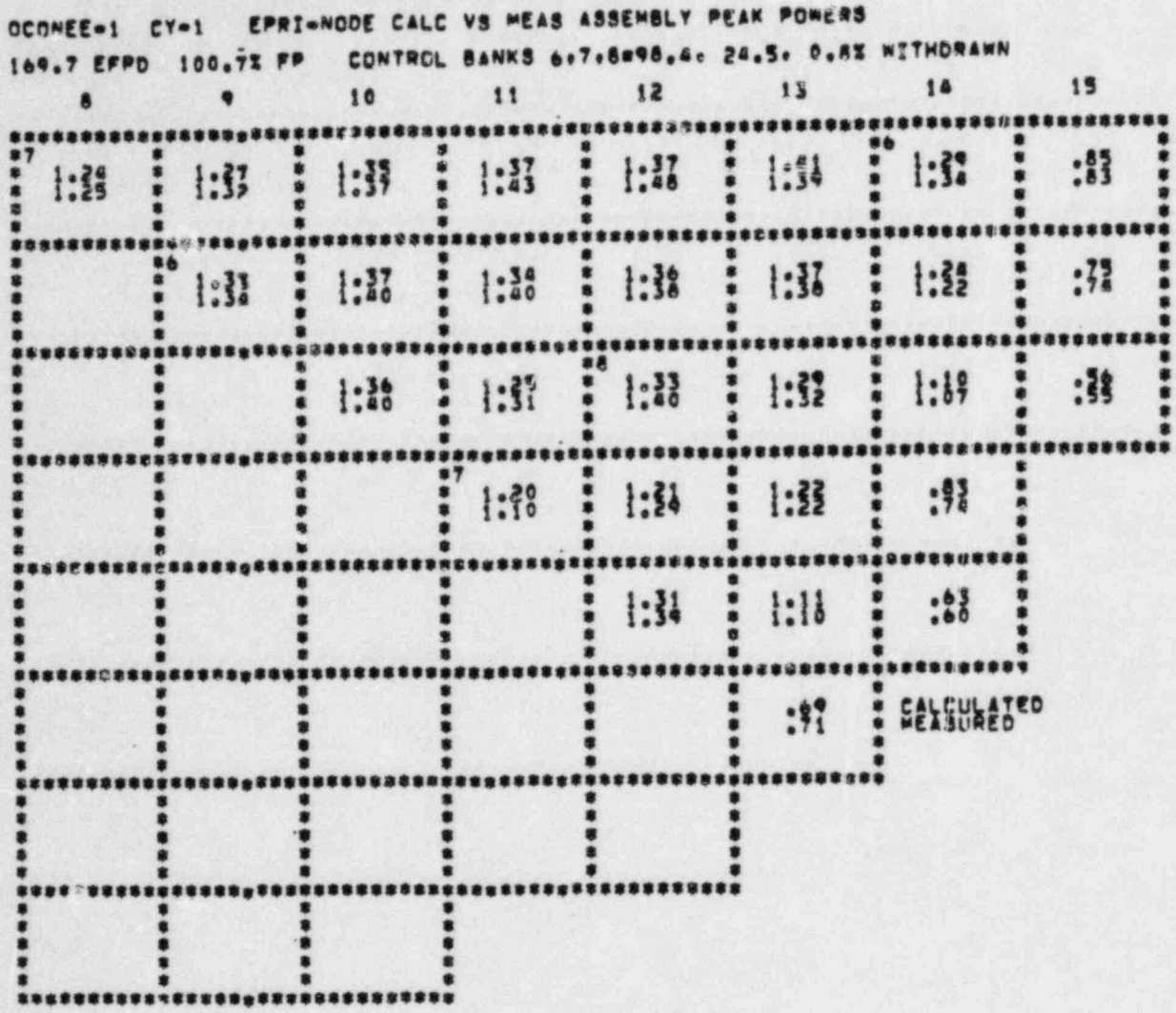
OCONEE-1 CY-1 EPRI-NODE CALC VS MEAS ASSEMBLY PEAK POWERS
169.7 EFPD 100.7% FP CONTROL BANKS 6,7,8=98.4, 24.5, 0.8% WITHDRAWN
8 9 10 11 12 13 14 15
H K L M N O P R
1.24 1.25
1.27 1.29
1.35 1.39
1.37 1.43
1.37 1.48
1.41 1.34
1.29 1.34
.85 .83
1.33 1.38
1.37 1.40
1.34 1.40
1.36 1.38
1.37 1.36
1.24 1.22
.75 .74
1.36 1.40
1.27 1.31
1.33 1.40
1.29 1.32
1.10 1.07
.96 .95
1.20 1.10
1.21 1.24
1.22 1.22
.83 .74
1.31 1.34
1.11 1.10
.63 .60
.89 .71
CALCULATED
MEASURED

Figure 4-26

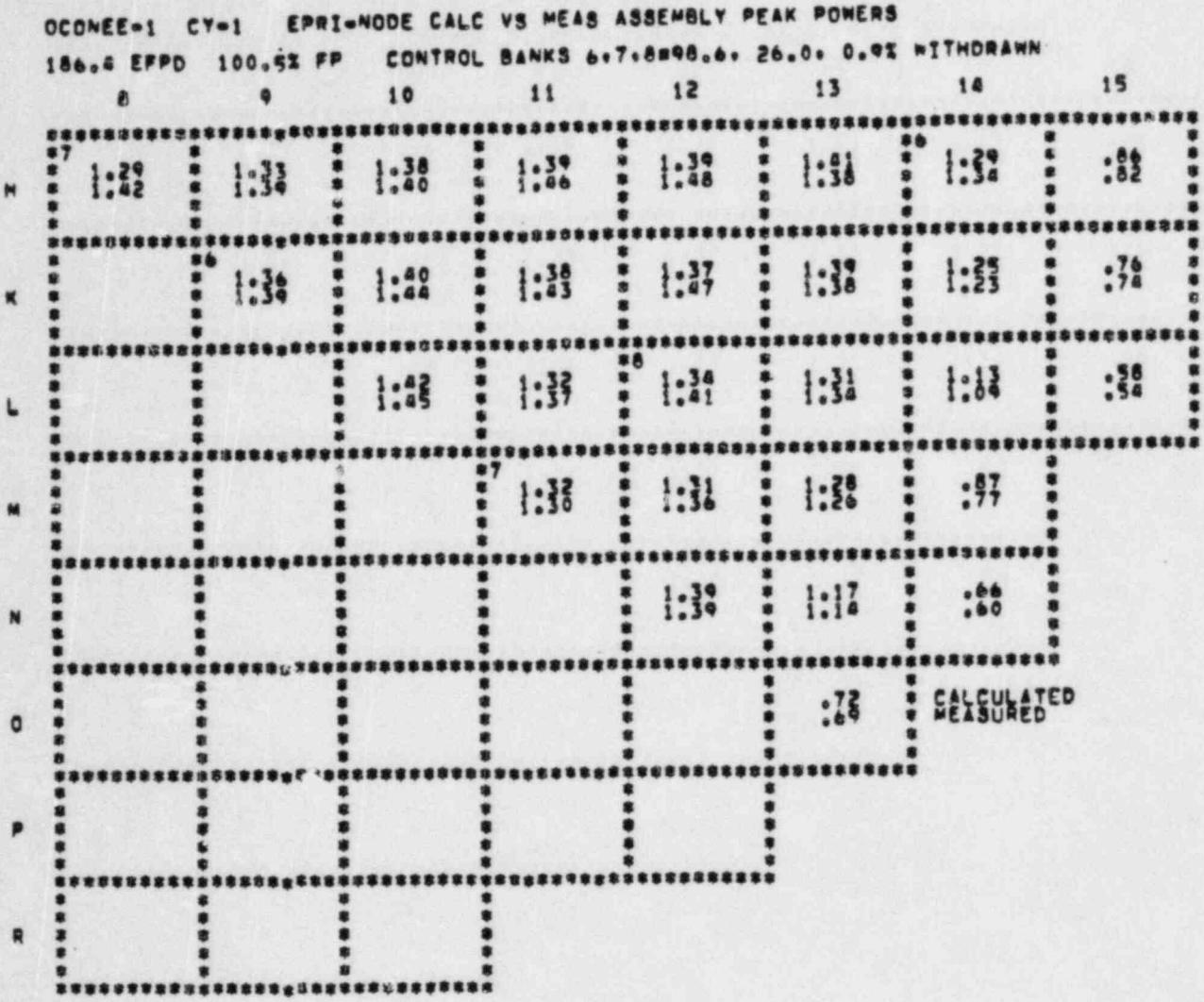
OCONEE-1 CY-1 EPRI-NODE CALC VS MEAS ASSEMBLY PEAK POWERS
186.4 EFPD 100.5% FP CONTROL BANKS 6,7,8=98.6, 26.0, 0.0% WITHDRAWN
8 9 10 11 12 13 14 15
H
K
L
M
N
O
P
R
CALCULATED
MEASURED

Figure 4-27

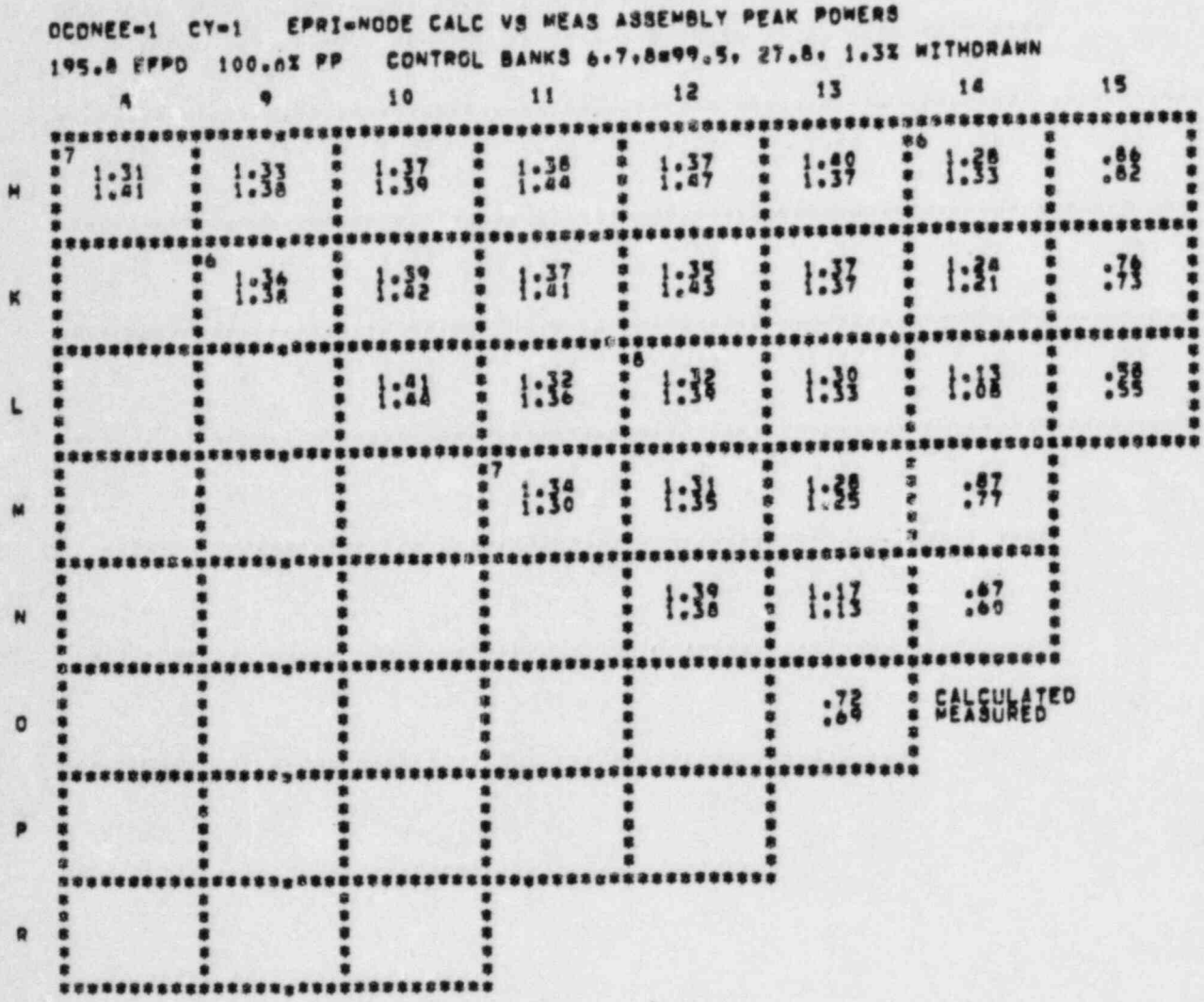
OCONEE-1 CY-1 EPRI-NODE CALC VS MEAS ASSEMBLY PEAK POWERS
195.8 EFPD 100.0% PP CONTROL BANKS 6,7,8=99.5, 27.8, 1.3% WITHDRAWN
8 9 10 11 12 13 14 15
H
K
L
M
N
O
P
R
CALCULATED
MEASURED

Figure 4-28

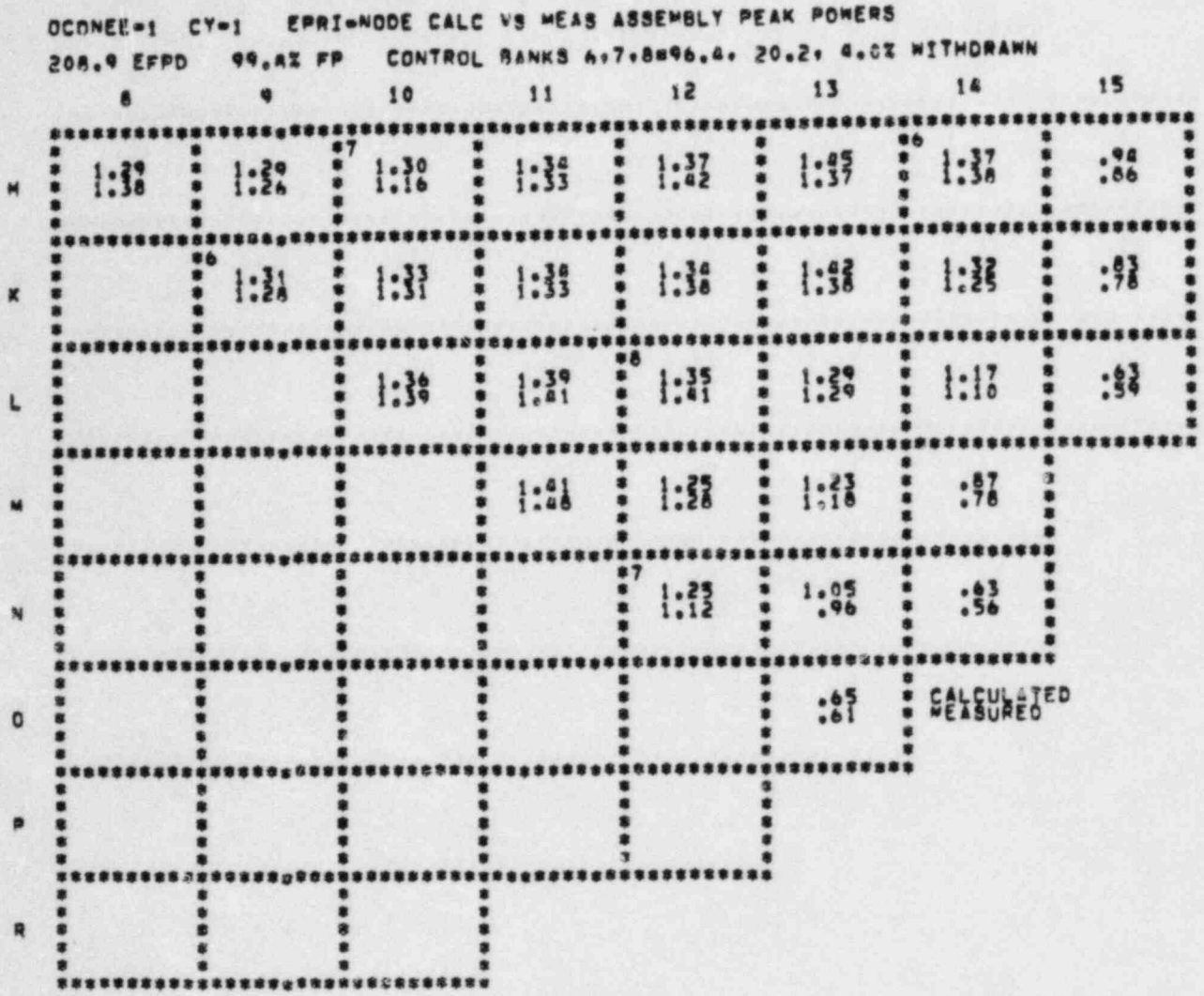
OCONEE-1 CY-1 EPRI-NODE CALC VS MEAS ASSEMBLY PEAK POWERS
208.9 EFPD 99.8% FP CONTROL BANKS 4,7,8=96.4, 20.2, 4.0% WITHDRAWN
8 9 10 11 12 13 14 15
H K L M N O P R
1.29 1.38
1.29 1.24
7
1.30 1.16
1.34 1.33
1.37 1.42
1.05 1.37
6
1.37 1.38
.94 .86
6
1.31 1.28
1.33 1.31
1.38 1.33
1.34 1.38
1.02 1.38
1.32 1.25
.83 .78
8
1.36 1.39
1.39 1.41
1.35 1.41
1.29 1.29
1.17 1.10
.63 .54
1.41 1.48
1.25 1.28
1.23 1.18
.87 .78
7
1.25 1.12
1.05 .96
.63 .56
.65 .61
CALCULATED
MEASURED

Figure 4-29

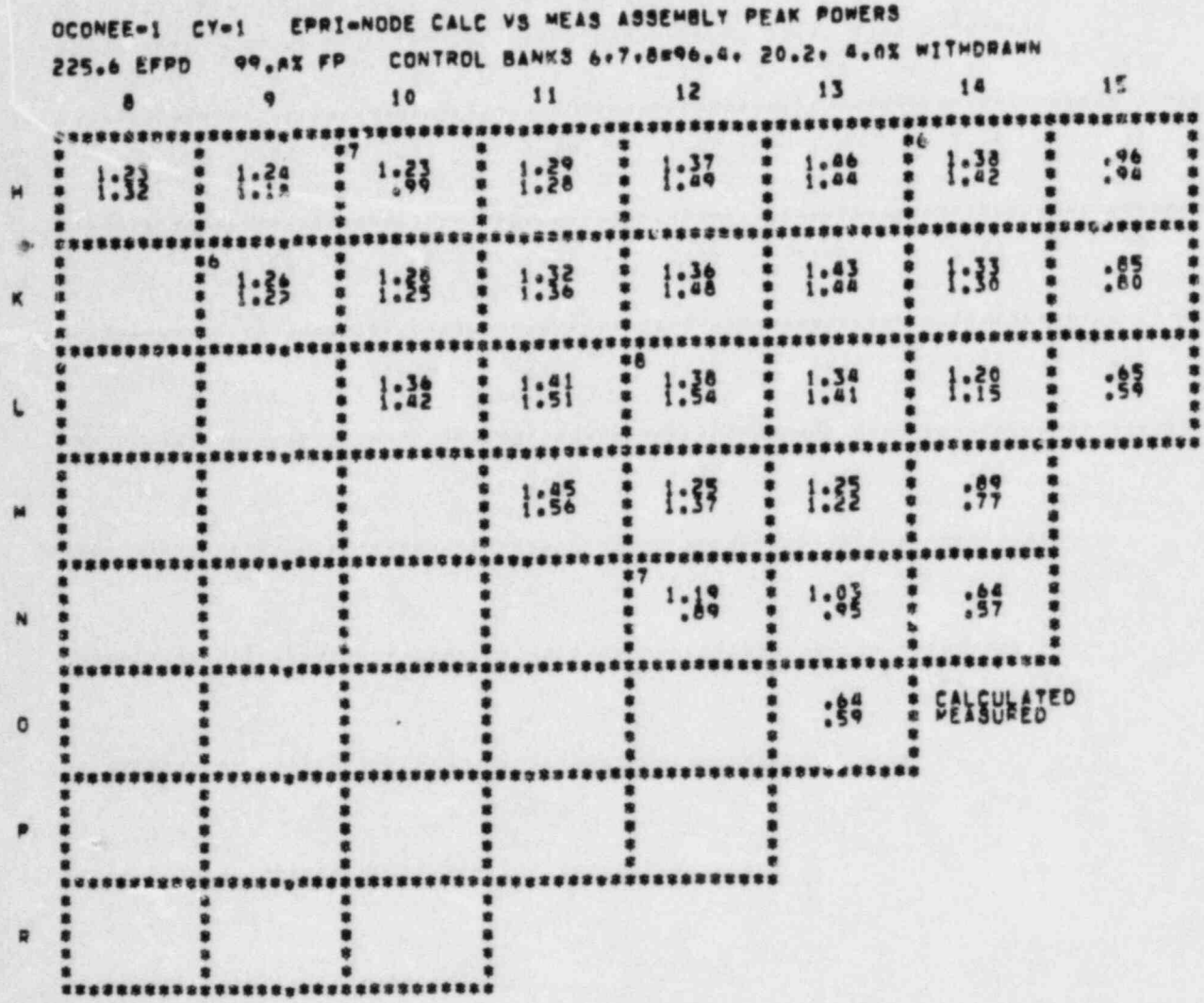
OCONEE-1 CY-1 EPRI-NODE CALC VS MEAS ASSEMBLY PEAK POWERS
225.6 EFPD 99.A% FP CONTROL BANKS 6,7,8=96.4, 20.2, 4.0% WITHDRAWN
8 9 10 11 12 13 14 15
H K L M N O P R
1.23 1.32
1.24 1.19
#7 1.23 .99
1.29 1.28
1.37 1.49
1.46 1.44
#6 1.38 1.42
.96 .94
#6 1.26 1.25
1.28 1.25
1.32 1.36
1.36 1.48
1.43 1.44
1.33 1.30
.85 .80
1.36 1.42
1.41 1.51
#8 1.38 1.54
1.34 1.41
1.20 1.15
.65 .54
1.45 1.56
1.25 1.37
1.25 1.22
.89 .77
#7 1.19 .89
1.03 .95
.64 .57
.64 .59
CALCULATED
MEASURED

Figure 4-30

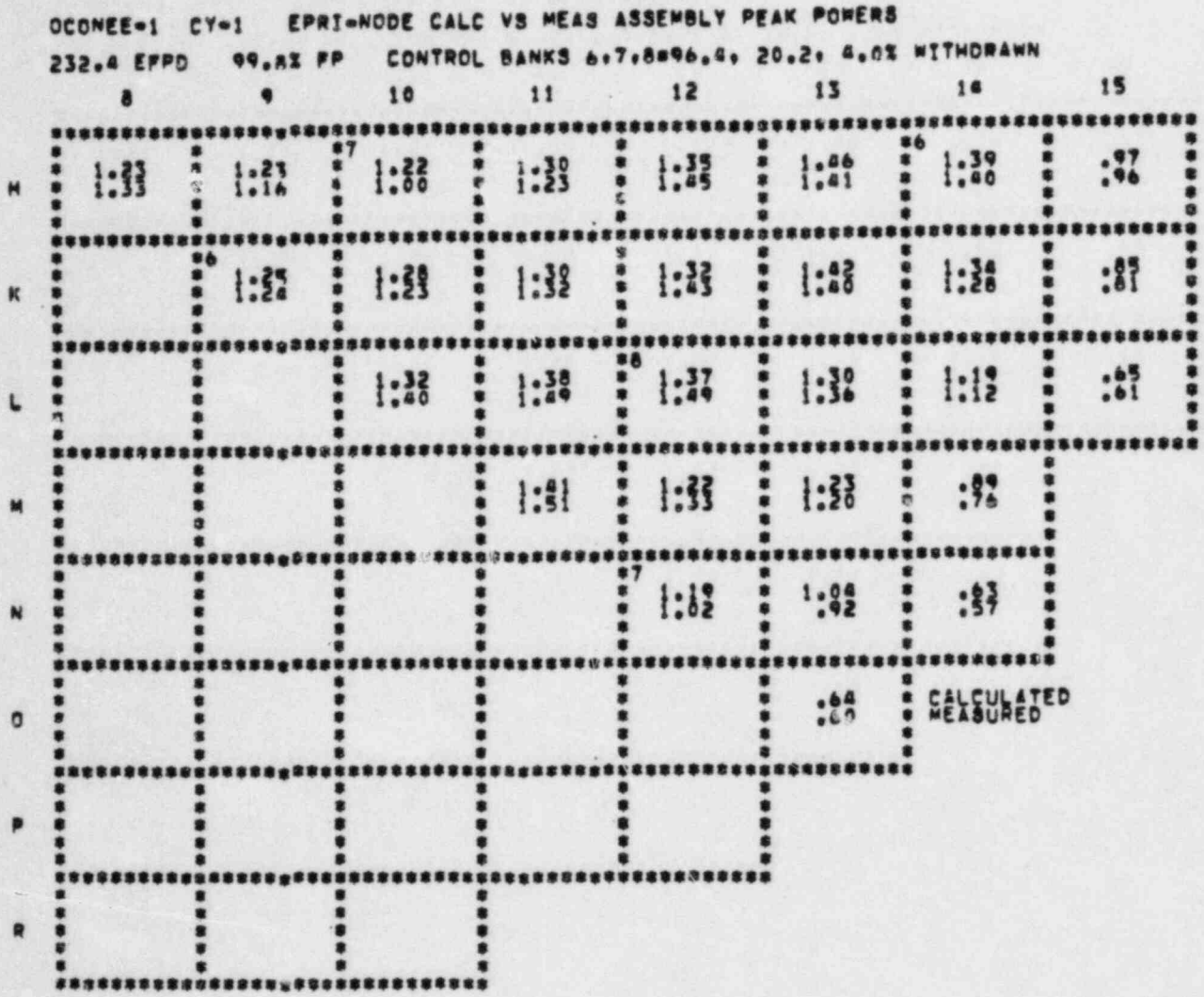
OCONEE-1 CY-1 EPRI-NODE CALC VS MEAS ASSEMBLY PEAK POWERS
232.4 EFPD 99.8% FP CONTROL BANKS 6,7,8=96.4, 20.2, 4.0% WITHDRAWN
8 9 10 11 12 13 14 15
H K L M N O P R
1.23 1.33
1.23 1.14
#7 1.22 1.00
1.30 1.23
1.35 1.45
1.06 1.41
#6 1.39 1.40
.97 .96
#6 1.25 1.24
1.28 1.23
1.30 1.32
1.32 1.45
1.42 1.40
1.34 1.28
.85 .81
1.32 1.40
1.38 1.49
#8 1.37 1.49
1.30 1.36
1.19 1.12
.65 .61
1.41 1.51
1.32 1.33
1.23 1.20
.89 .76
#7 1.19 1.02
1.04 .92
.63 .59
.64 .60
CALCULATED
MEASURED

Figure 4-31

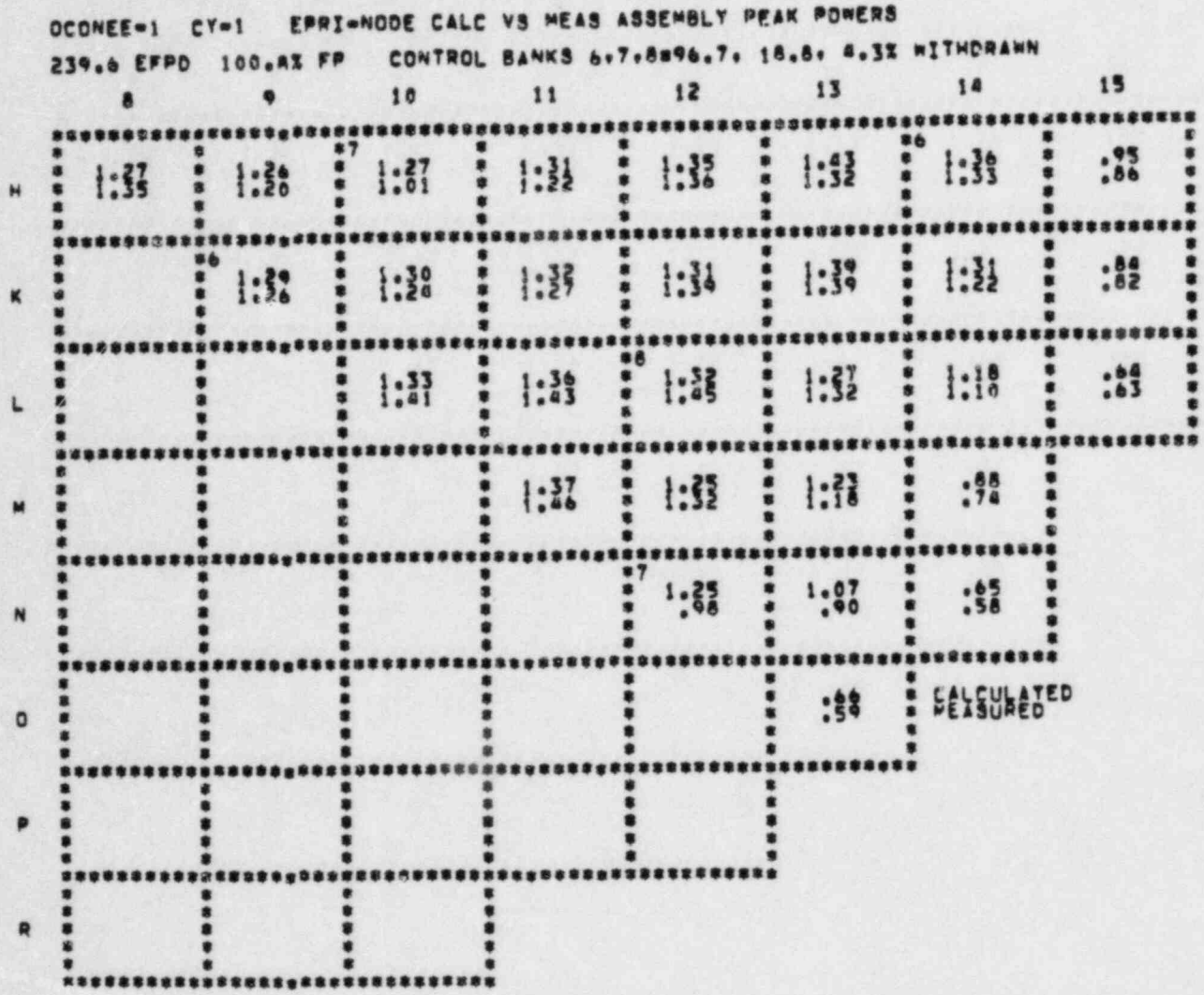
OCONEE-1 CY-1 EPRI-NODE CALC VS MEAS ASSEMBLY PEAK POWERS
239.6 EFPD 100.0% FP CONTROL BANKS 6,7,8=96.7, 18.8, 8.3% WITHDRAWN
8 9 10 11 12 13 14 15
H
K
L
M
N
O
P
R
1.27 1.35
1.26 1.20
#7 1.27 1.01
1.31 1.22
1.35 1.36
1.43 1.32
#6 1.36 1.33
.95 .86
#6 1.29 1.26
1.30 1.28
1.32 1.27
1.31 1.34
1.39 1.39
1.31 1.22
.84 .82
#8 1.33 1.41
1.36 1.43
1.32 1.45
1.27 1.32
1.18 1.10
.84 .83
1.37 1.46
1.25 1.32
1.23 1.18
.88 .74
#7 1.25 .98
1.07 .90
.65 .58
.84 .54
CALCULATED
MEASURED

Figure 4-32

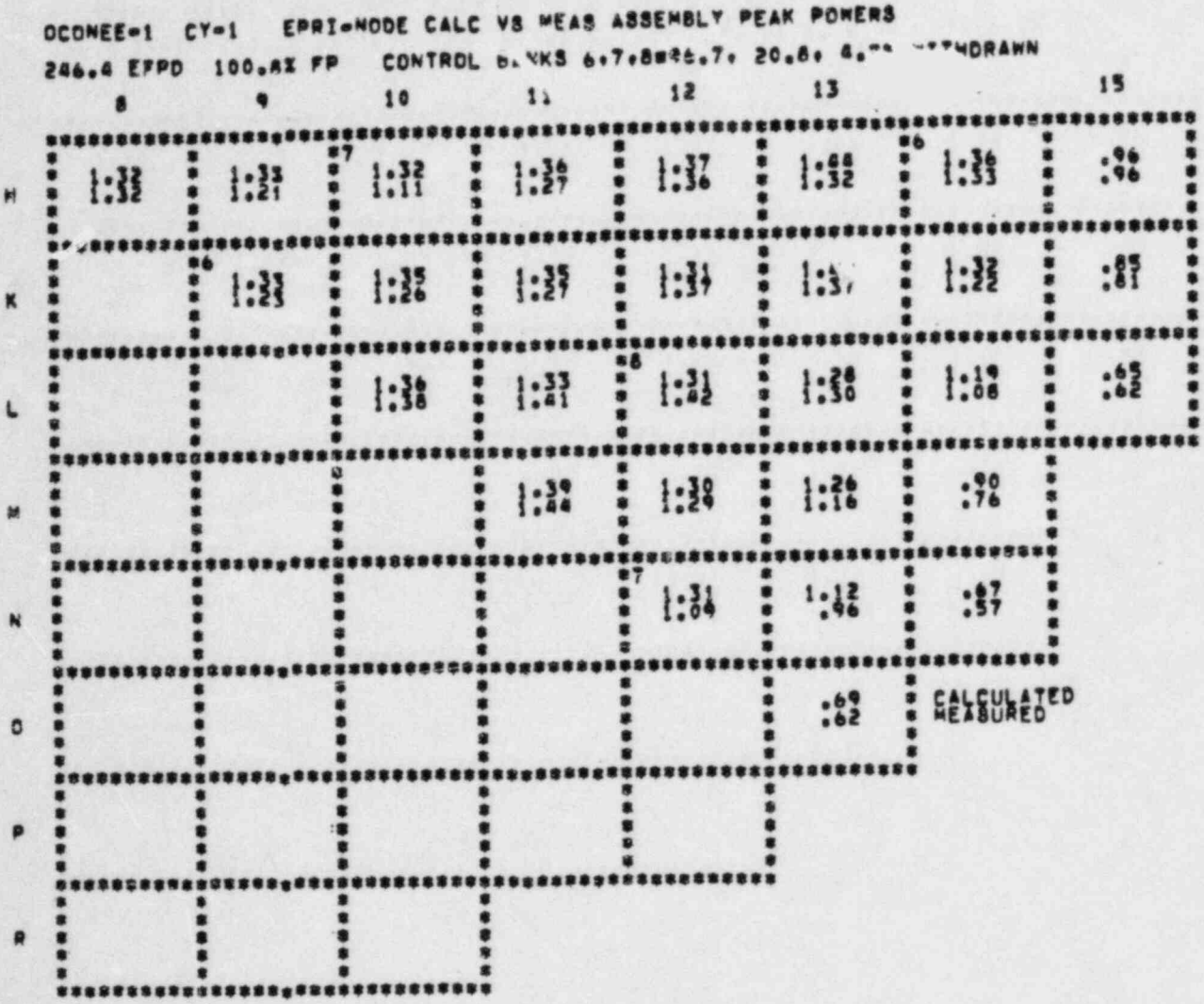
OCONEE-1 CY-1 EPRI-NODE CALC VS MEAS ASSEMBLY PEAK POWERS
246.4 EFPD 100.0% FP CONTROL BANKS 6,7,8##6,7, 20,6, 6,** **WDRAWN
8
9
10
11
12
13
15
H
K
L
M
N
O
P
R
1.32 1.32
1.33 1.21
7
1.32 1.11
1.36 1.27
1.37 1.36
1.68 1.32
6
1.36 1.33
.96 .96
6
1.33 1.23
1.35 1.26
1.35 1.27
1.31 1.39
1.32 1.22
.85 .81
1.36 1.38
1.33 1.41
8
1.31 1.42
1.28 1.30
1.19 1.08
.65 .62
1.39 1.44
1.30 1.24
1.26 1.16
.90 .76
7
1.31 1.04
1.12 .46
.87 .57
.69 .62
CALCULATED
MEASURED

Figure 4-33

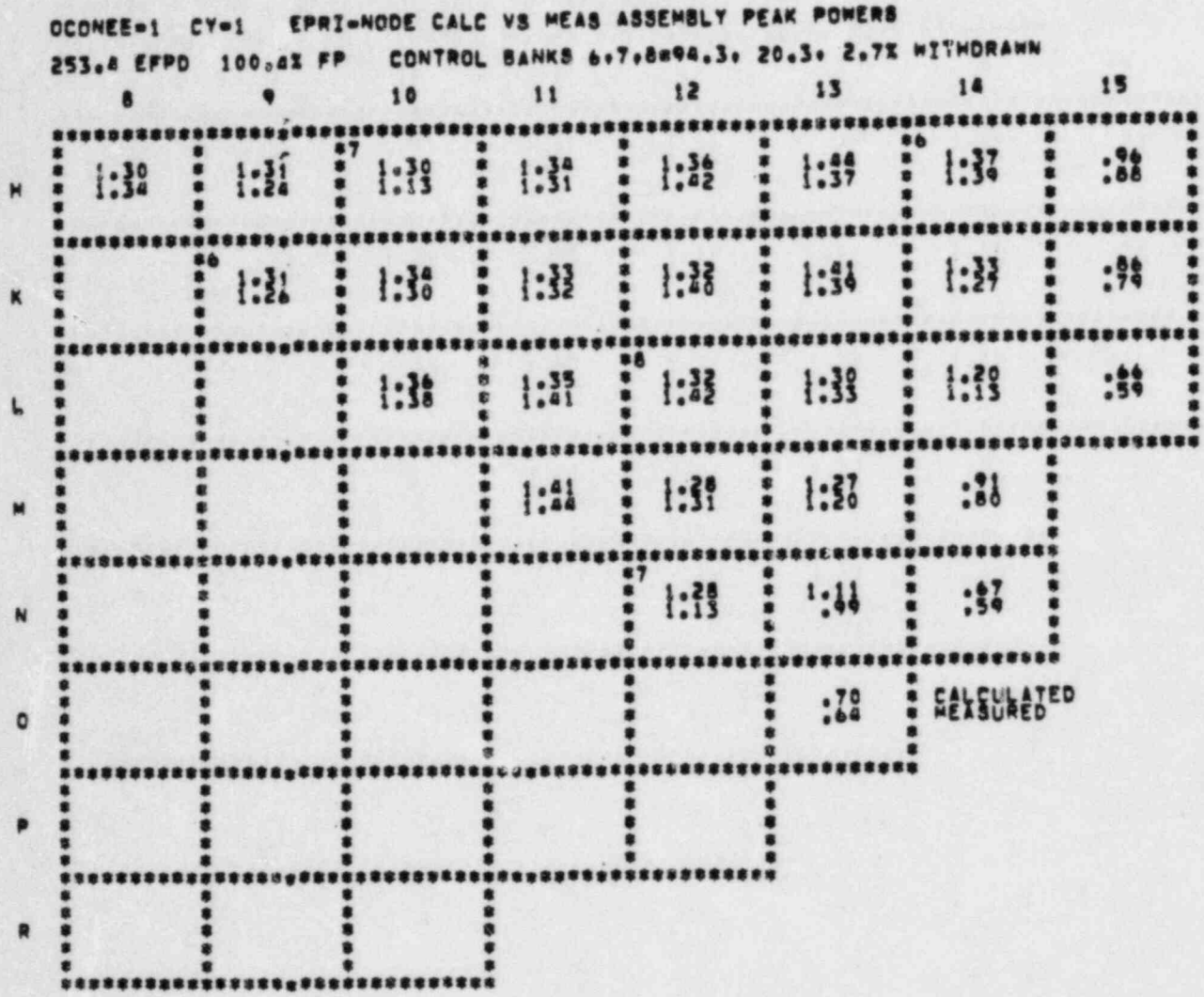
OCONEE=1 CY=1 EPRI-NODE CALC VS MEAS ASSEMBLY PEAK POWERS
253.8 EFPD 100.0% FP CONTROL BANKS 6,7,8=94.3, 20.3, 2.7% WITHDRAWN
8 9 10 11 12 13 14 15
H K L M N O P R
1.30 1.34
1.31 1.24
#7
1.30 1.13
1.34 1.31
1.36 1.42
1.44 1.37
#6
1.37 1.34
.96 .88
#6
1.31 1.26
1.34 1.30
1.33 1.32
1.32 1.40
1.41 1.34
1.33 1.27
.86 .79
1.36 1.38
1.35 1.41
#8
1.32 1.42
1.30 1.33
1.20 1.13
.66 .59
1.41 1.44
1.28 1.31
1.27 1.20
.91 .80
#7
1.28 1.13
1.11 .99
.87 .54
.70 .64
CALCULATED
MEASURED

Figure 4-34

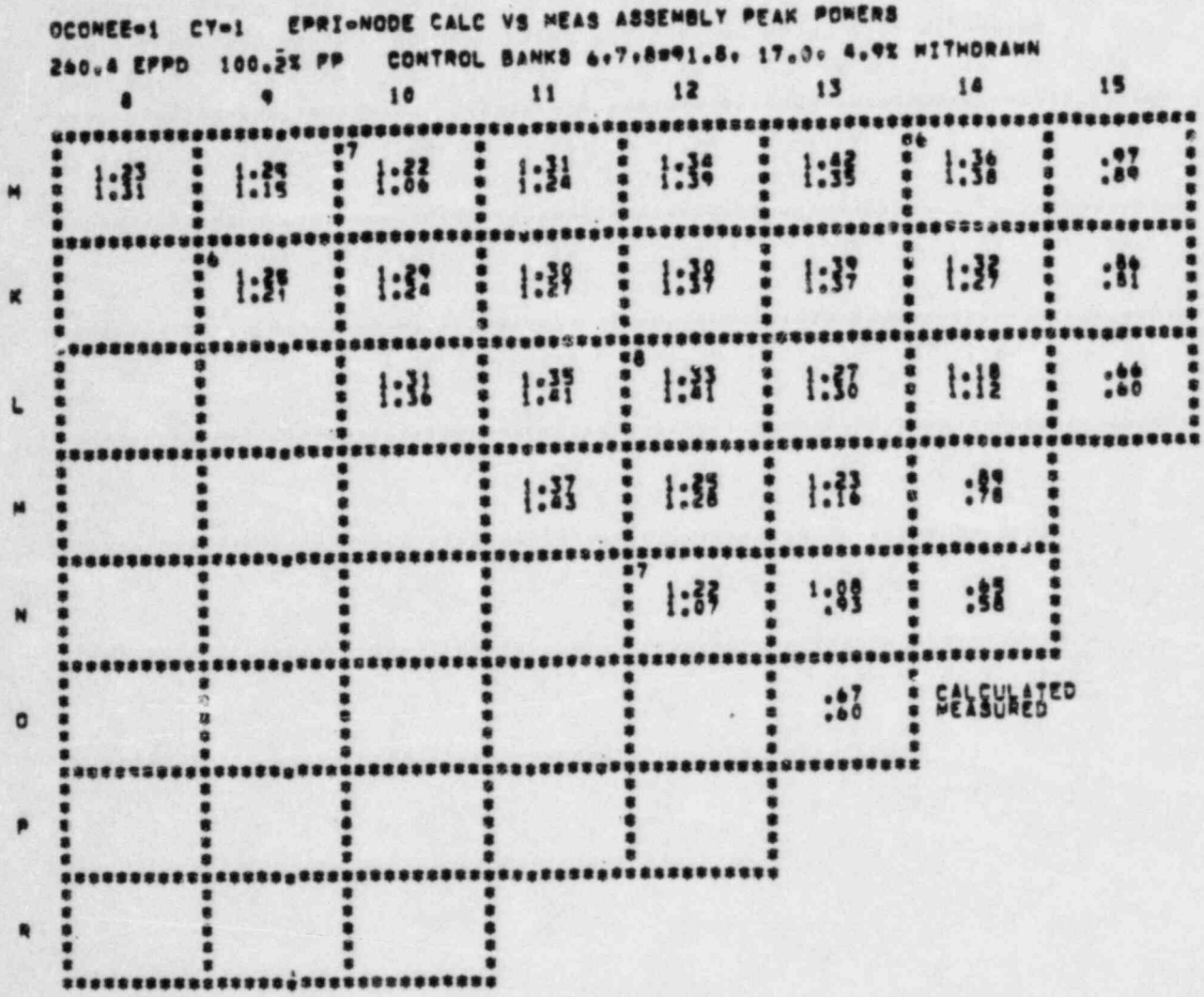
OCONEE-1 CY-1 EPRI-NODE CALC VS MEAS ASSEMBLY PEAK POWERS
240.4 EFPD 100.2% FP CONTROL BANKS 6,7,8=91.8, 17.0, 4.9% WITHDRAWN
8 9 10 11 12 13 14 15
H
K
L
M
N
O
P
R
1.23 1.31
1.25 1.15
7
1.22 1.06
1.31 1.24
1.34 1.34
1.42 1.35
6
1.36 1.38
.97 .89
6
1.25 1.21
1.29 1.24
1.30 1.29
1.39 1.39
1.39 1.37
1.32 1.29
.84 .81
8
1.31 1.36
1.35 1.41
1.33 1.41
1.27 1.36
1.18 1.12
.96 .80
1.37 1.43
1.25 1.28
1.23 1.16
.89 .78
7
1.22 1.09
1.08 1.03
.85 .58
.67 .60
CALCULATED
MEASURED

Figure 4-35

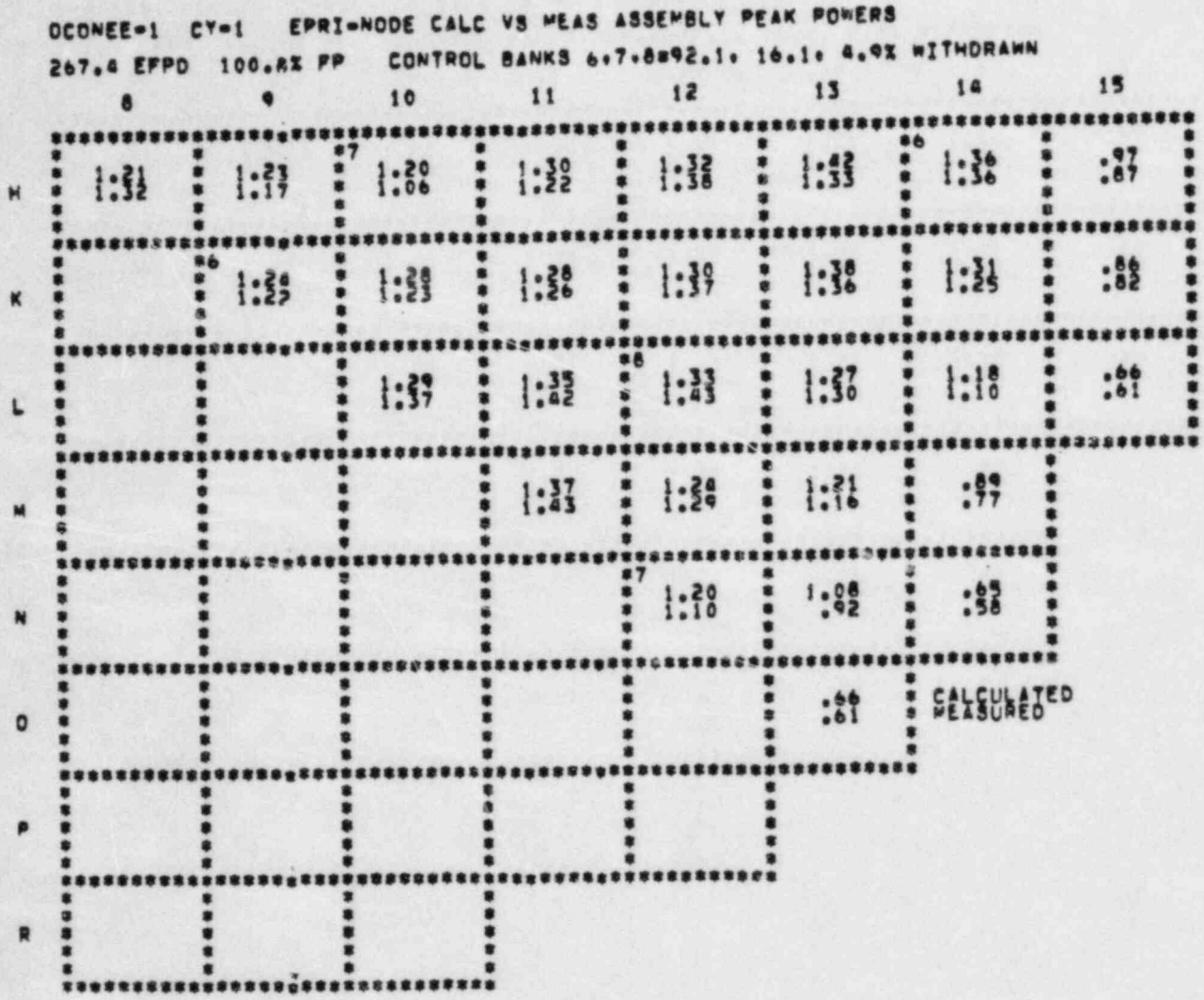
OCONEE-1 CY-1 EPRI-NODE CALC VS MEAS ASSEMBLY PEAK POWERS
267.4 EFPD 100.8% FP CONTROL BANKS 6,7,8=92.1, 16.1, 4.9% WITHDRAWN
8 9 10 11 12 13 14 15
H
K
L
M
N
O
P
R
1.21 1.32
1.23 1.17
#7 1.20 1.06
1.30 1.22
1.32 1.38
1.42 1.33
#6 1.36 1.36
.97 .87
#6 1.24 1.29
1.28 1.23
1.28 1.26
1.30 1.37
1.38 1.36
1.31 1.25
.86 .82
#8 1.29 1.37
1.35 1.42
1.33 1.43
1.27 1.30
1.18 1.10
.66 .61
1.37 1.43
1.28 1.29
1.21 1.16
.89 .77
#7 1.20 1.10
1.08 .92
.65 .58
.66 .61
CALCULATED
MEASURED

Figure 4-36

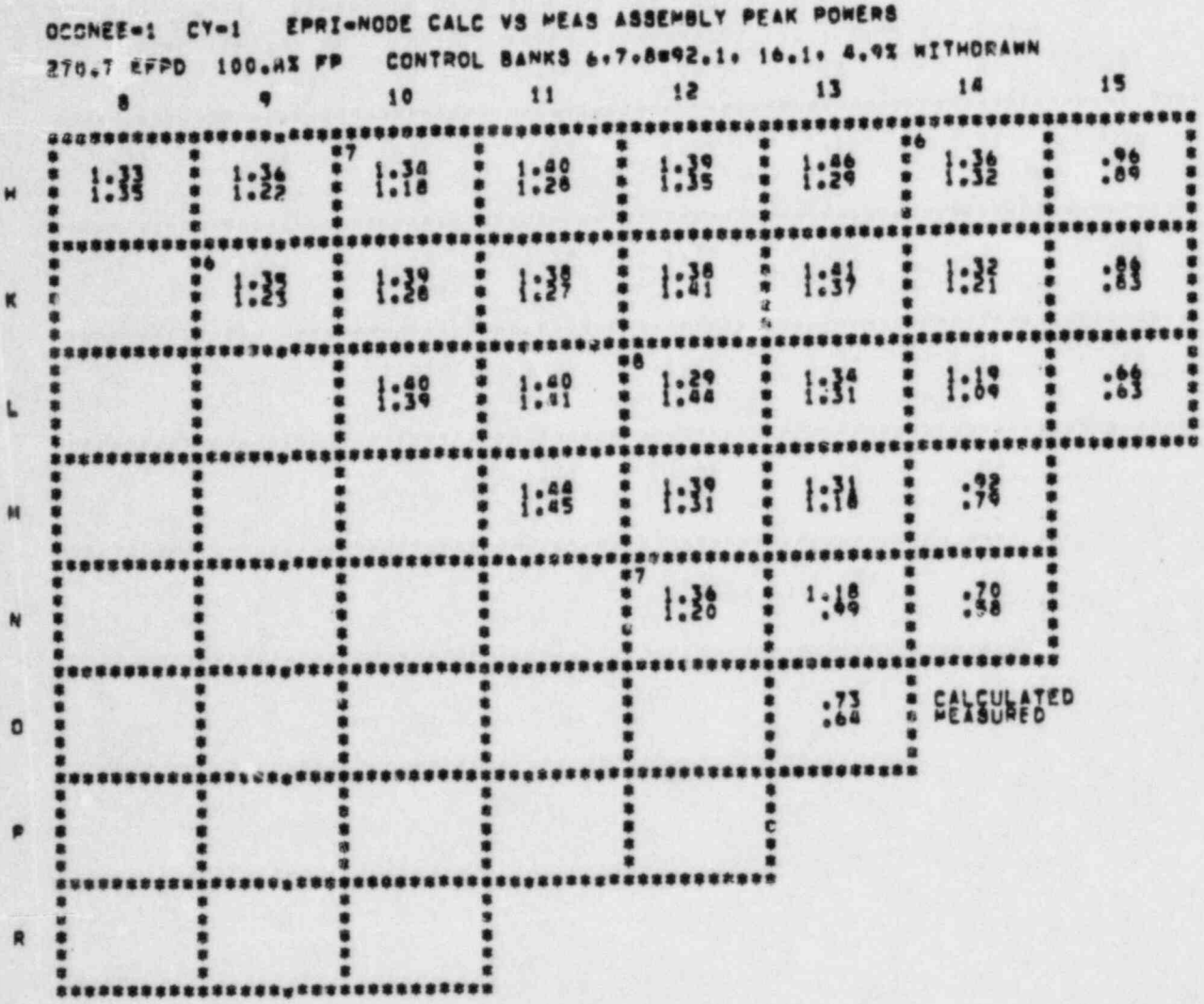
OCONEE-1 CY-1 EPRI-NODE CALC VS MEAS ASSEMBLY PEAK POWERS
270.7 EFPD 100.0% FP CONTROL BANKS 6,7,8@92.1, 16.1, 4.9% WITHDRAWN
8 9 10 11 12 13 14 15
H
K
L
M
N
O
P
R
1.33 1.35
1.36 1.22
1.34 1.18
1.40 1.28
1.39 1.35
1.46 1.29
1.36 1.32
.96 .89
1.35 1.23
1.39 1.28
1.38 1.27
1.38 1.41
1.41 1.37
1.32 1.21
.86 .83
1.40 1.39
1.40 1.41
1.29 1.44
1.34 1.31
1.19 1.09
.66 .63
1.44 1.45
1.39 1.31
1.31 1.18
.92 .76
1.36 1.20
1.18 .99
.70 .68
.73 .68
CALCULATED
MEASURED

Figure 4-37

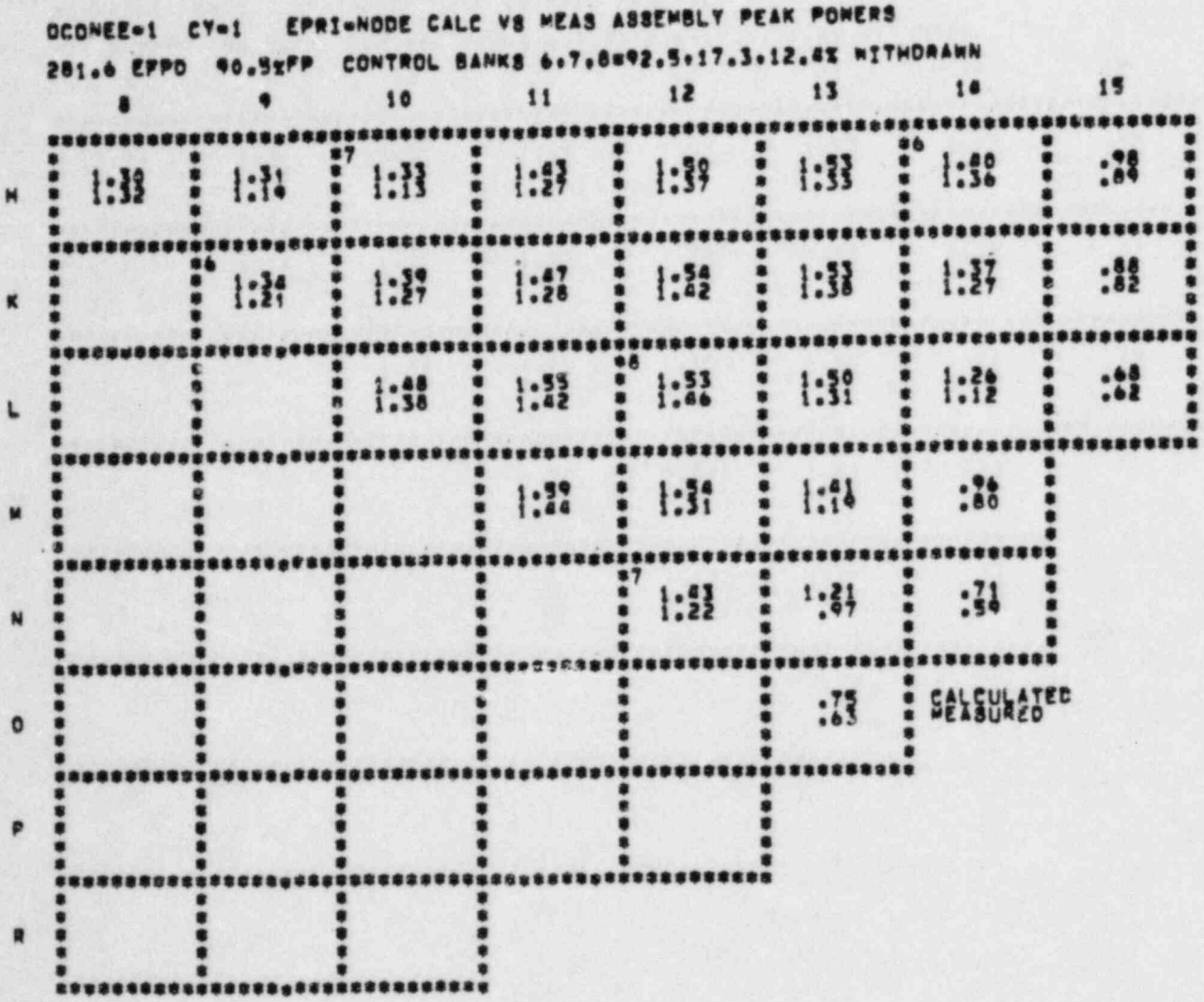
OCONEE-1 CY-1 EPRI-NODE CALC VS MEAS ASSEMBLY PEAK POWERS
281.6 EFPD 90.5%FP CONTROL BANKS 6,7,8=92.5,17.3,12.4% WITHDRAWN
8 9 10 11 12 13 14 15
H
K
L
M
N
O
P
R
1.30 1.32
1.31 1.14
7
1.33 1.13
1.43 1.27
1.50 1.37
1.53 1.33
6
1.40 1.36
.78 .84
6
1.34 1.21
1.39 1.27
1.47 1.28
1.54 1.42
1.53 1.38
1.37 1.27
.88 .82
8
1.48 1.38
1.55 1.42
1.53 1.46
1.50 1.31
1.26 1.12
.68 .62
1.59 1.44
1.54 1.31
1.41 1.14
.96 .80
7
1.43 1.22
1.21 .97
.71 .54
.75 .63
CALCULATED
MEASURED

Figure 4-38
Oconee 1, Cycle 2
Control Rod Configuration

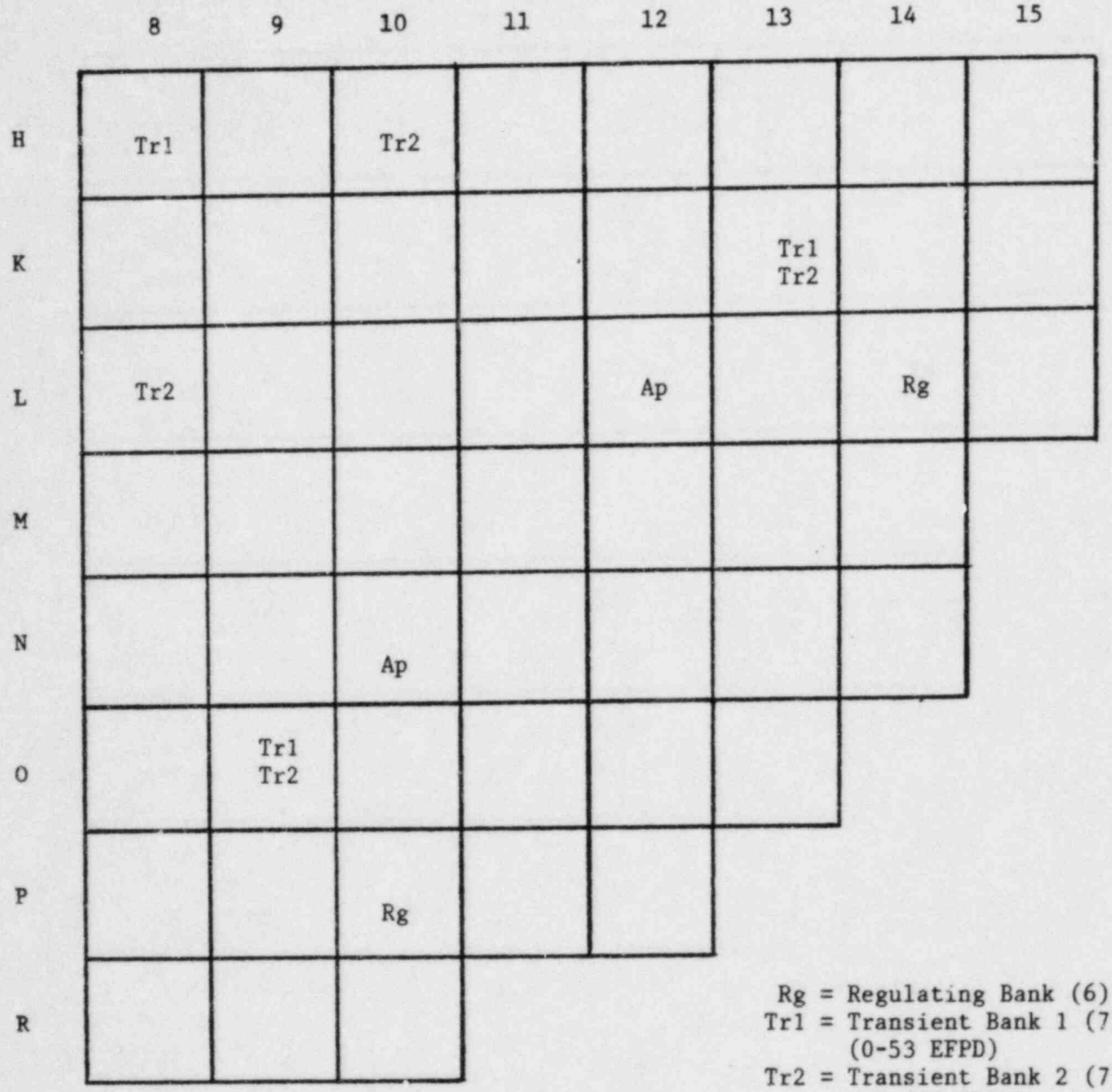

Rg = Regulating Bank (6)
Tr1 = Transient Bank 1 (7)
(0-53 EFPD)
Tr2 = Transient Bank 2 (7)
(53-292 EFPD)
Ap = APSR (8)

Figure 4-39
Oconee 1, Cycle 2
Quarter Core Loading Diagram

	8	9	10	11	12	13	14	15
H	2.60 4A	2.15 3	2.15 3	2.60 4A	2.15 3	3.20 4B	2.15 3	3.20 4B
K	2.15 3	2.10 2	2.15 3	2.15 3	2.10 2	2.10 2	2.15 3	3.20 4B
L	2.15 3	2.15 3	2.15 3	2.15 3	2.15 3	2.10 2	3.20 4B	3.20 4B
M	2.60 4A	2.15 3	2.15 3	3.20 4B	2.10 2	2.15 3	3.20 4B	
N	2.15 3	2.10 2	2.15 3	2.10 2	2.15 3	2.15 3	3.20 4B	
O	3.20 4B	2.10 2	2.10 2	2.15 3	2.15 3	3.20 4B		
P	2.15 3	2.15 3	3.20 4B	3.20 4B	3.20 4B			
R	3.20 4B	3.20 4B	3.20 4B					

W/O U-235
Batch No.

Figure 4-40
Oconee 1, Cycle 2
Quarter Core Shuffle Pattern

	8	9	10	11	12	13	14	15
H	F	0-13*	K-15	F	H-14	F	H-15	F
K	0-13*	M-11	M-14	K-14	L-13	L-11	M-13	F
L	R-9**	P-11	R-9**	L-14	L-15	K-13	F	F
M	F	P-9	P-10	F	M-12	N-13	F	
N	P-8	0-10	R-10	N-11	N-12	N-14	F	
O	F	M-10	0-9	0-12	P-12	F		
P	R-8	0-11	F	F	F			
R	F	F	F					

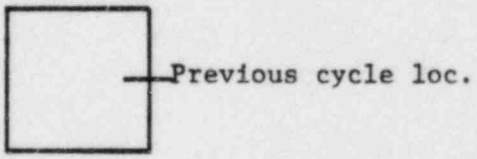

* Assembly location formerly on diagonal placed on the core flat.
** Moved from eighth core symmetric location to quarter core symmetric location.

Figure 4-41

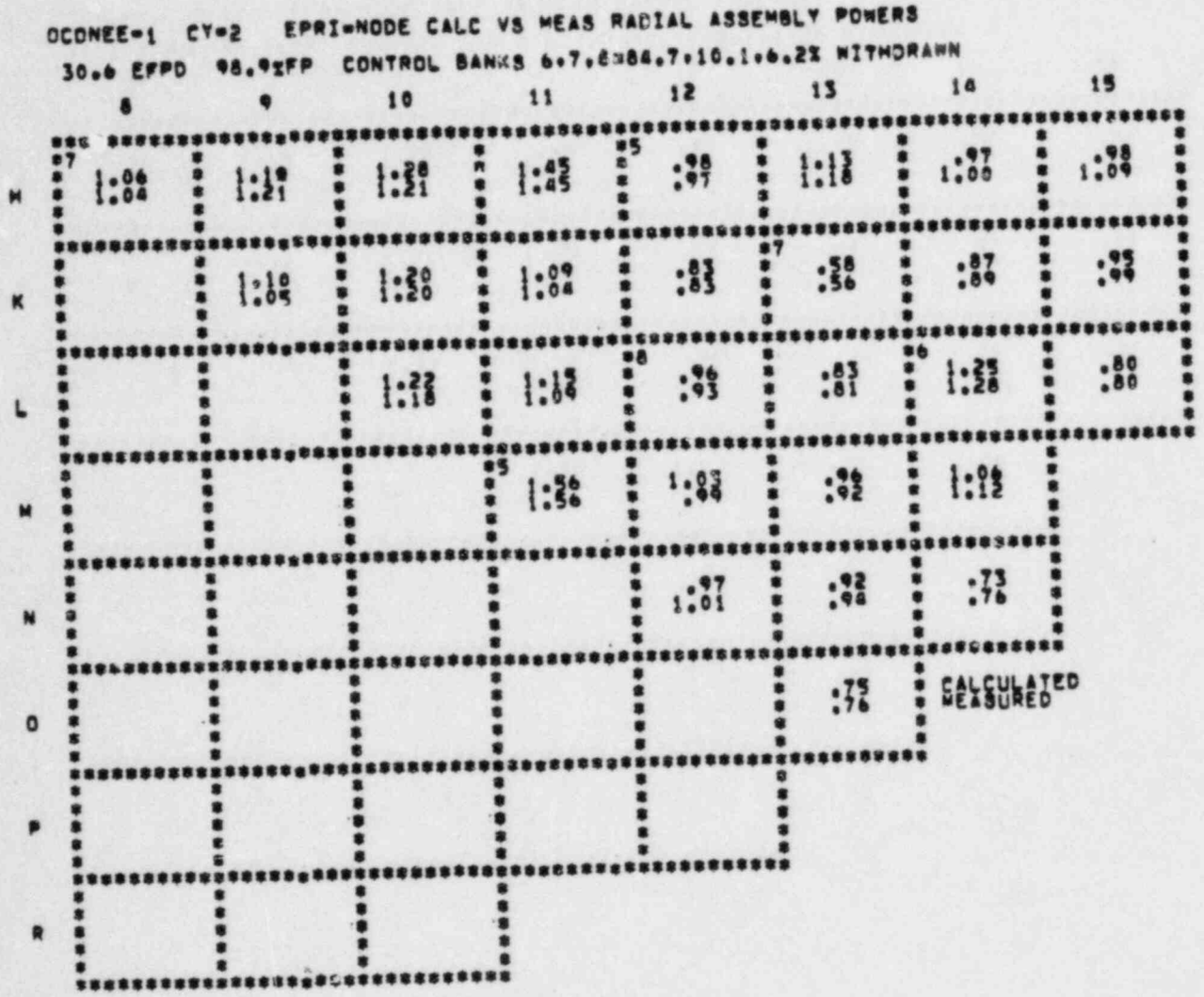
OCONEE-1 CY-2 EPRI-NODE CALC VS MEAS RADIAL ASSEMBLY POWERS
30.6 EFPD 98.9%FP CONTROL BANKS 6,7,8=84.7,10.1,6.2% WITHDRAWN
8
9
10
11
12
13
14
15
H
K
L
M
N
O
P
R
CALCULATED
MEASURED

Figure 4-42

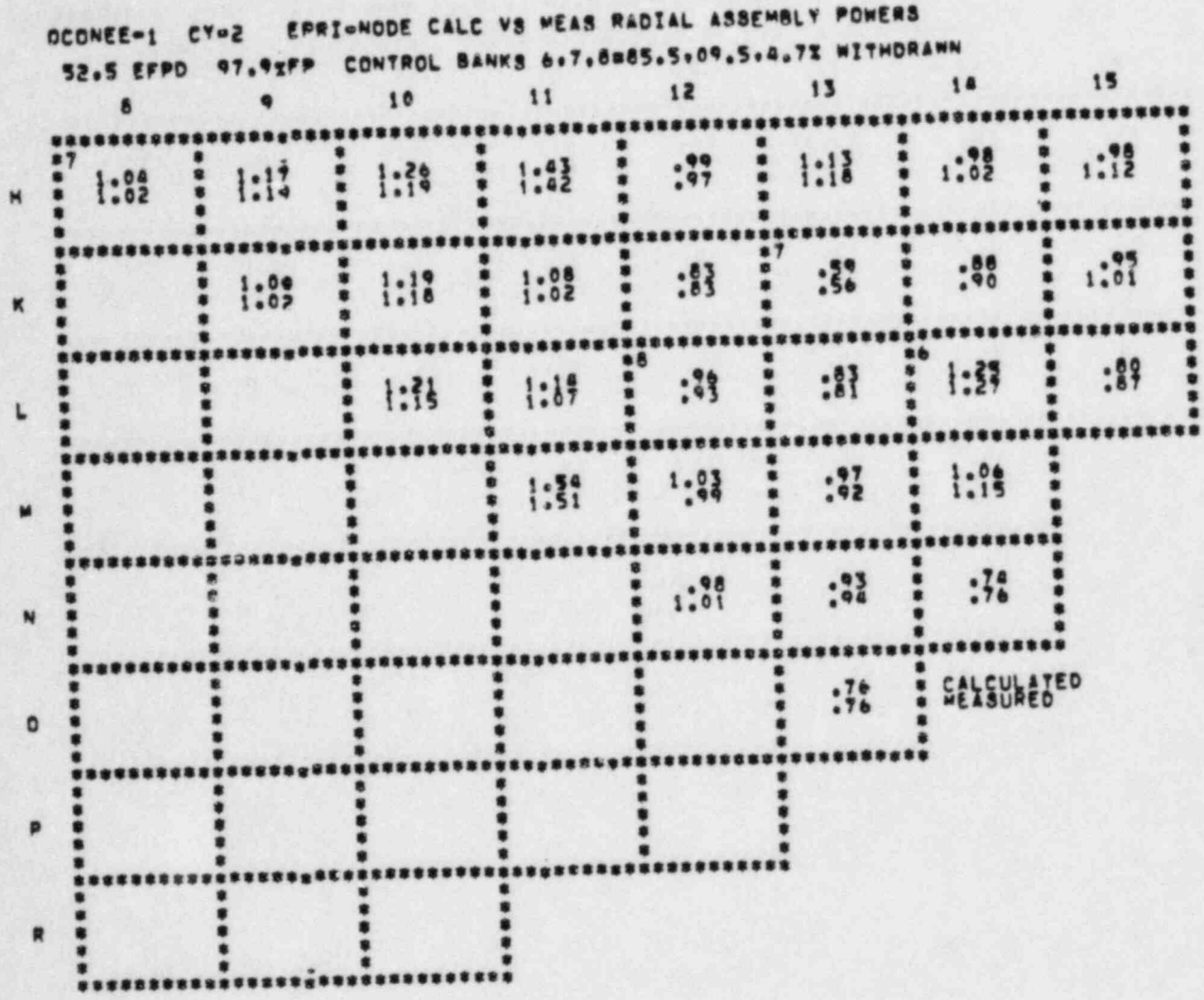
OCONEE-1 CY-2 EPRI-NODE CALC VS MEAS RADIAL ASSEMBLY POWERS
52.5 EFPD 97.9%FP CONTROL BANKS 6,7,8=85.5,09.5,4.7% WITHDRAWN
8 9 10 11 12 13 14 15
H
K
L
M
N
O
P
R
CALCULATED
MEASURED

Figure 4-43

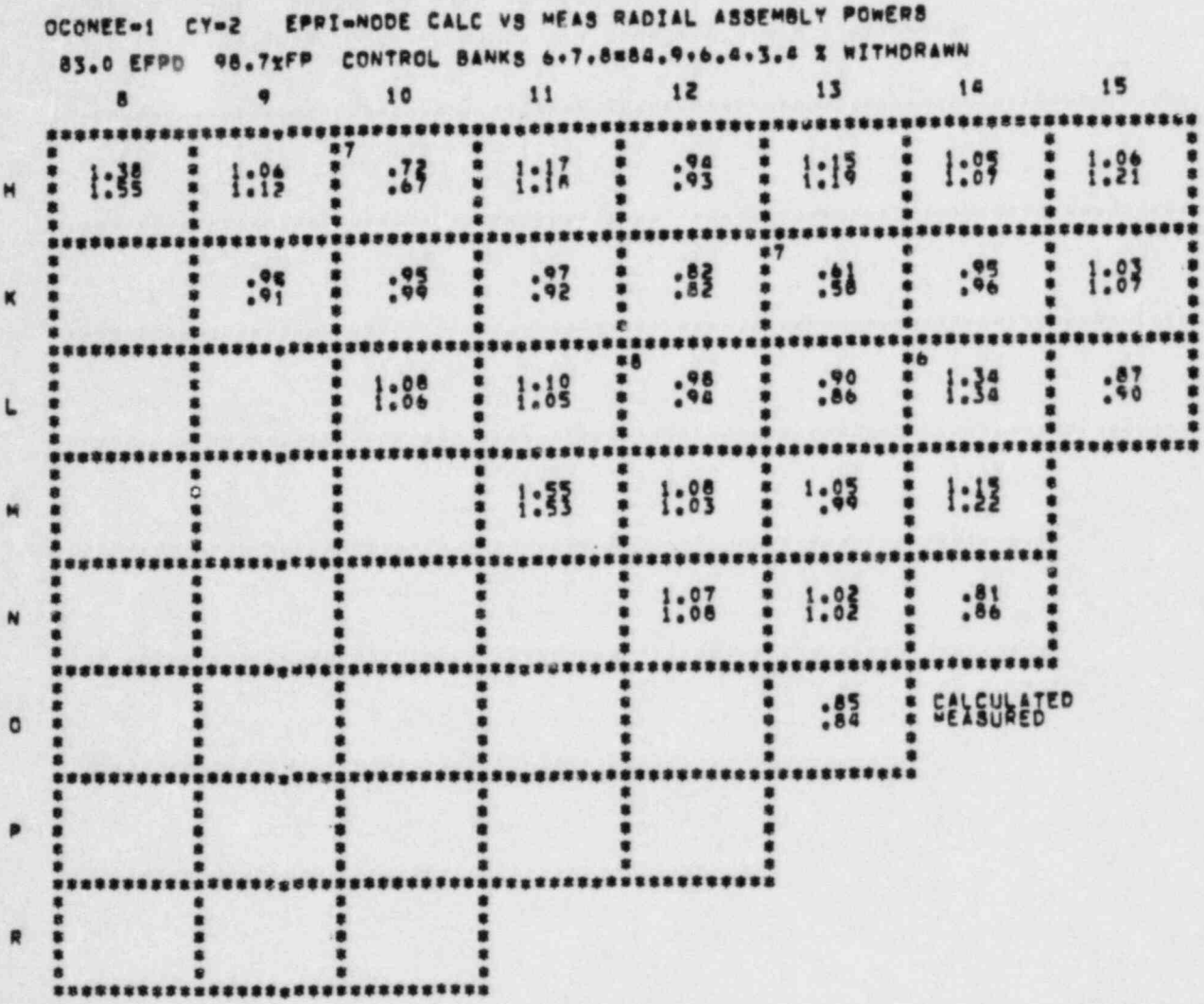
OCONEE-1 CY-2 EPRI-NODE CALC VS MEAS RADIAL ASSEMBLY POWERS
83.0 EFPD 98.7%FP CONTROL BANKS 6,7,8=84,9,6,4,3,4 % WITHDRAWN
8 9 10 11 12 13 14 15
H
K
L
M
N
O
P
R
1.38 1.55
1.04 1.12
#7 .72 .67
1.17 1.14
.98 .93
1.15 1.19
1.05 1.09
1.06 1.21
.96 .91
.95 .99
.97 .92
.82 .82
#7 .61 .58
.95 .96
1.03 1.09
1.08 1.06
1.10 1.05
#8 .98 .94
.90 .86
#6 1.34 1.34
.87 .90
1.55 1.53
1.08 1.03
1.05 .99
1.15 1.22
1.07 1.08
1.02 1.02
.81 .86
.85 .84
CALCULATED
MEASURED

Figure 4-44

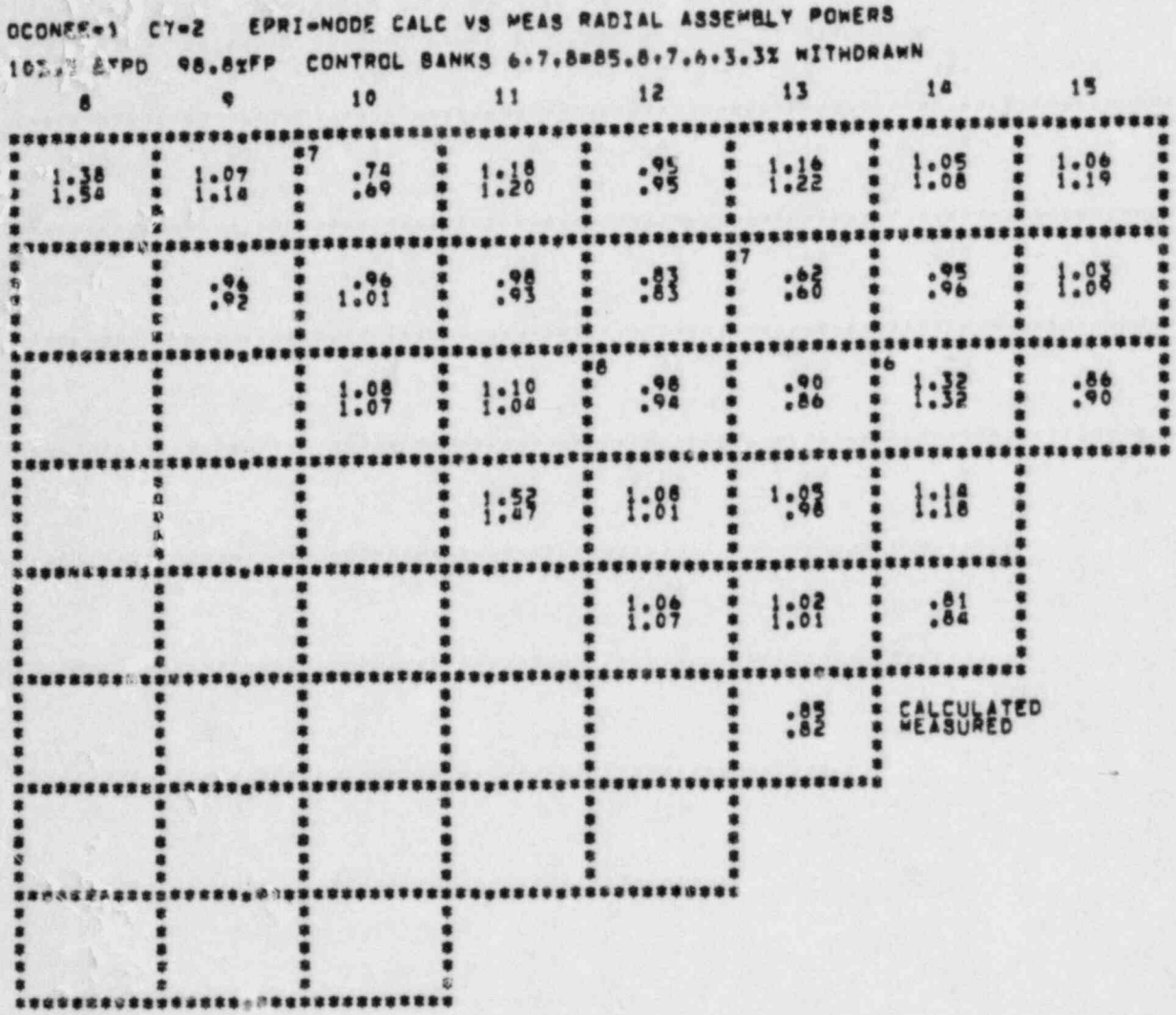
OCONEE-1 CY-2 EPRI-NODE CALC VS MEAS RADIAL ASSEMBLY POWERS
10[illegible] EFPD 98.8%FP CONTROL BANKS 6,7,8=85.8,7,6,3.3% WITHDRAWN
8 9 10 11 12 13 14 15
H K L M N P R
1.38 1.54
1.07 1.14
#7 .74 .69
1.18 1.20
.95 .95
1.16 1.22
1.05 1.08
1.06 1.19
.96 .92
.96 1.01
.98 .93
.83 .83
#7 .62 .60
.95 .96
1.03 1.09
#6 1.08 1.07
1.10 1.04
#6 .98 .94
.90 .86
#6 1.32 1.32
.86 .90
1.52 1.47
1.08 1.01
1.05 .98
1.14 1.18
1.06 1.07
1.02 1.01
.81 .84
.85 .82
CALCULATED
MEASURED

Figure 4-45

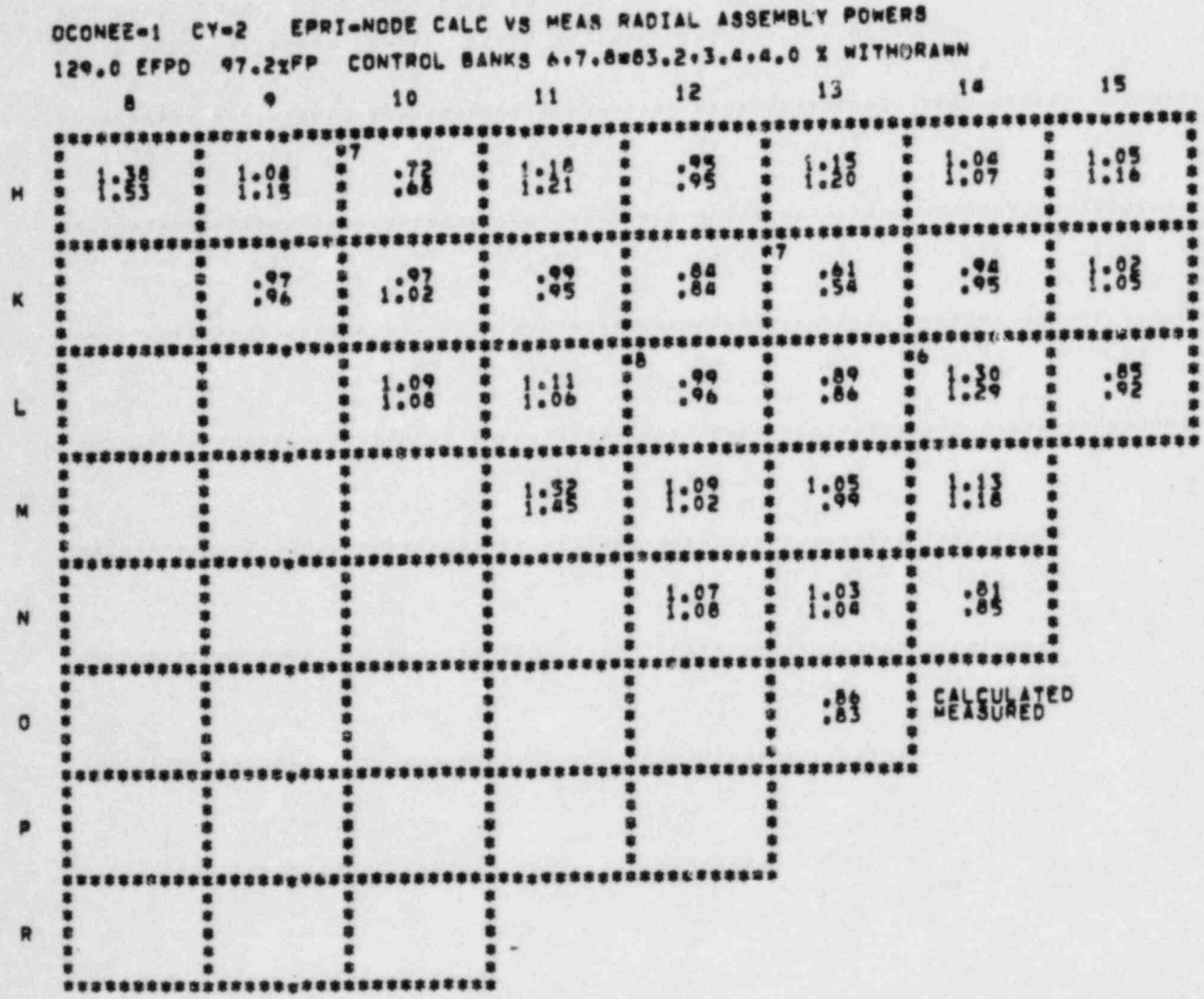
OCONEE-1 CY-2 EPRI-NODE CALC VS MEAS RADIAL ASSEMBLY POWERS
129.0 EFPD 97.2%FP CONTROL BANKS 6,7,8=83.2,3,4,4.0 % WITHDRAWN
8 9 10 11 12 13 14 15
H K L M N O P R
1.38 1.53
1.08 1.15
.7 .72 .68
1.18 1.21
.95 .95
1.15 1.20
1.04 1.07
1.05 1.16
.97 .96
.97 1.02
.99 .95
.84 .84
.7 .61 .54
.94 .95
1.02 1.05
.8 .99 .96
.89 .86
.6 1.30 1.29
.85 .92
1.09 1.08
1.11 1.06
1.32 1.45
1.09 1.02
1.05 .94
1.13 1.18
1.07 1.08
1.03 1.04
.81 .85
.86 .83
CALCULATED
MEASURED

Figure 4-46

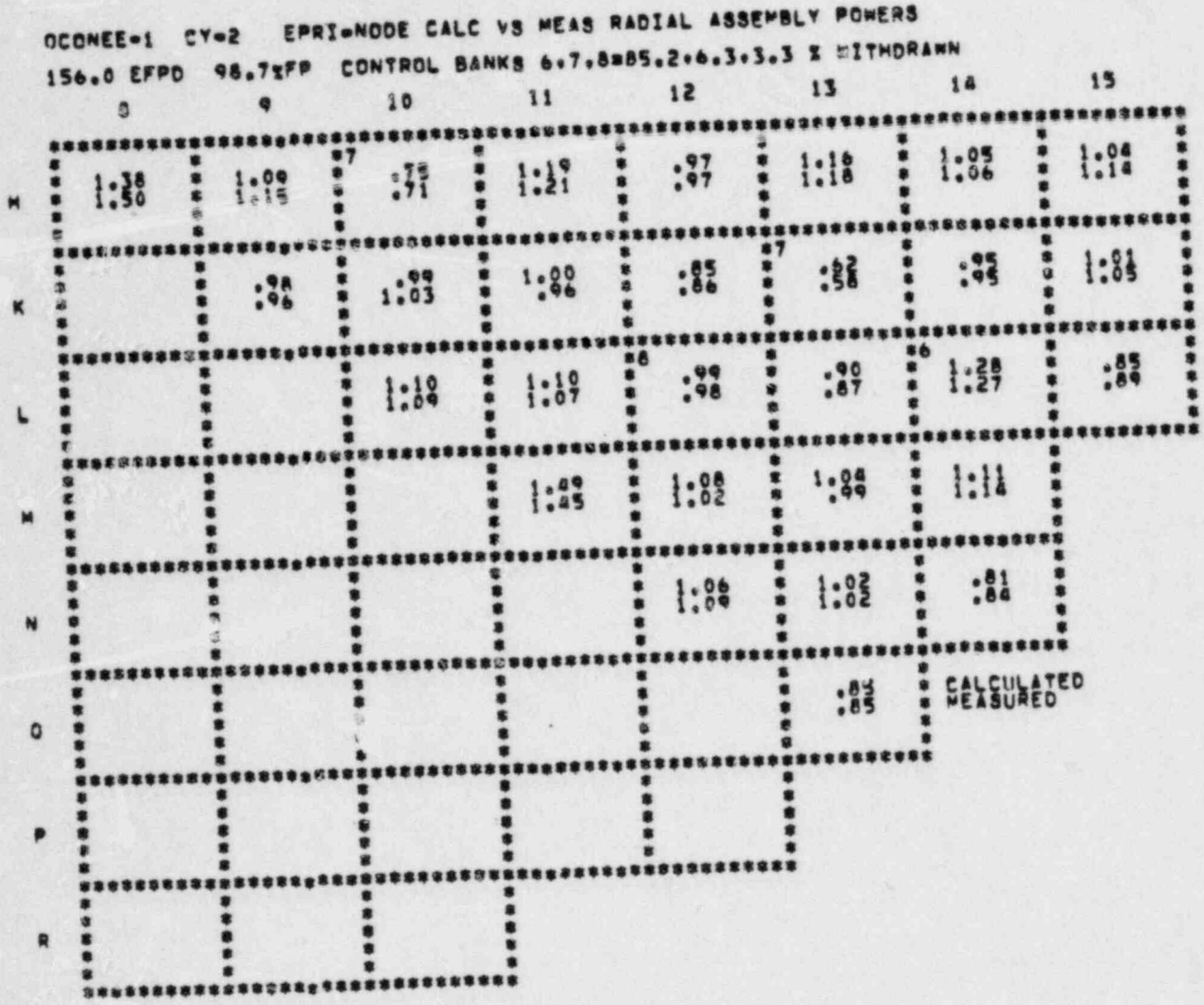
OCONEE-1 CY-2 EPRI-NODE CALC VS MEAS RADIAL ASSEMBLY POWERS
156.0 EFPD 98.7%FP CONTROL BANKS 6,7,8=85.2,6.3,3.3 % WITHDRAWN
8 9 10 11 12 13 14 15
H
K
L
M
N
O
P
R
1.38 1.50
1.09 1.15
.75 .71
1.19 1.21
.97 .97
1.16 1.18
1.05 1.06
1.04 1.14
.98 .96
1.00 1.03
1.00 .96
.85 .86
.62 .58
.95 .95
1.01 1.05
1.10 1.09
1.10 1.07
.99 .98
.90 .87
1.28 1.27
.85 .89
1.09 1.05
1.08 1.02
1.04 .99
1.11 1.14
1.06 1.09
1.02 1.02
.81 .84
.84 .85
CALCULATED
MEASURED

Figure 4-47

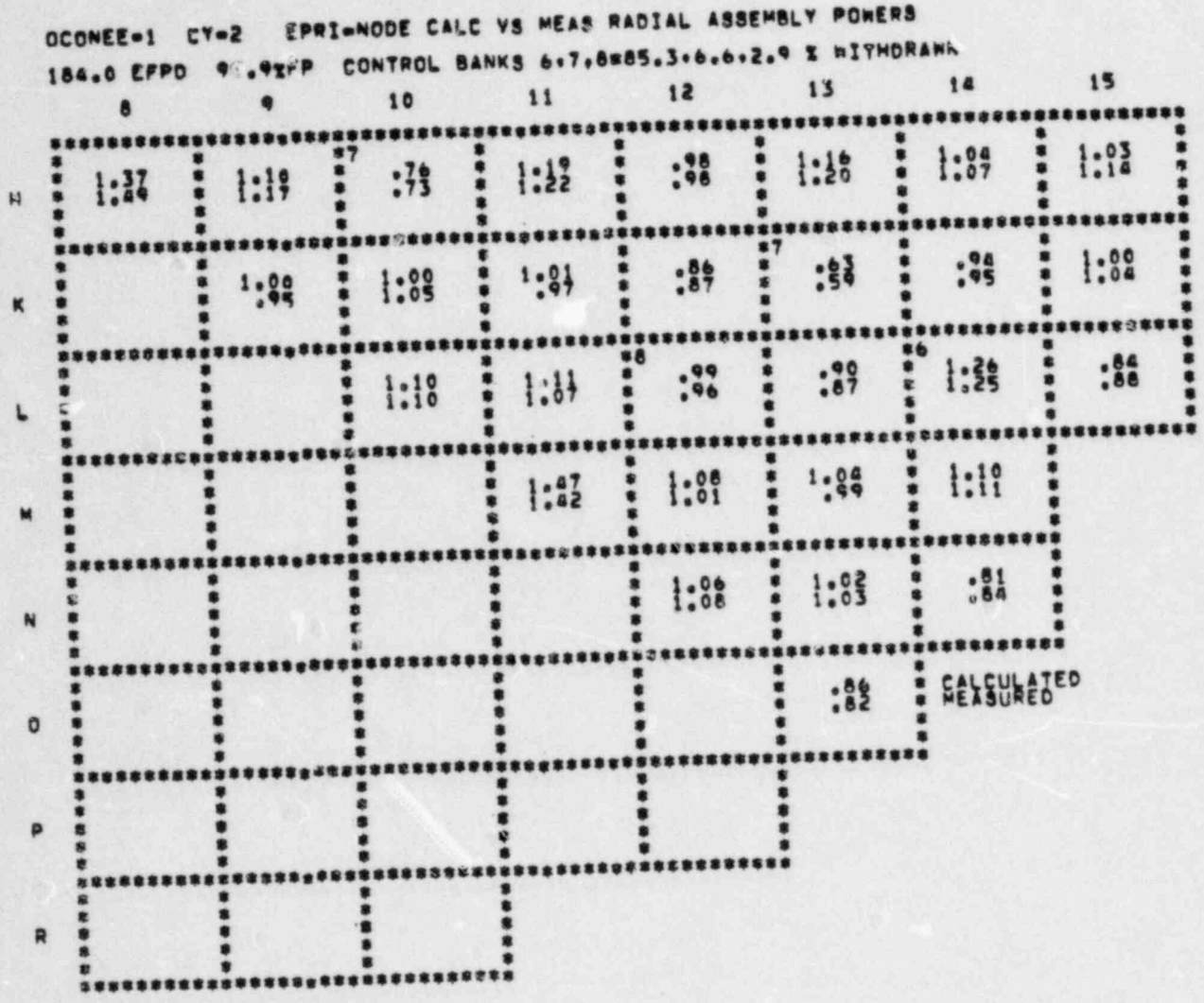
OCONEE-1 CY-2 EPRI-NODE CALC VS MEAS RADIAL ASSEMBLY POWERS
184.0 EFPD 9[illegible]FP CONTROL BANKS 6,7,8=85.3,6.6,2.9 % WITHDRAWN
8 9 10 11 12 13 14 15
H
K
L
M
N
O
P
R
1.37 1.44
1.18 1.17
.7 .76 .73
1.19 1.22
.98 .98
1.16 1.20
1.04 1.07
1.03 1.14
1.08 .94
1.00 1.05
1.01 .97
.86 .87
.7 .63 .54
.94 .95
1.00 1.04
1.10 1.10
1.11 1.07
.8 .99 .96
.90 .87
.6 1.26 1.25
.84 .88
1.07 1.02
1.08 1.01
1.04 .99
1.10 1.11
1.06 1.08
1.02 1.03
.81 .84
.86 .82
CALCULATED
MEASURED

Figure 4-48

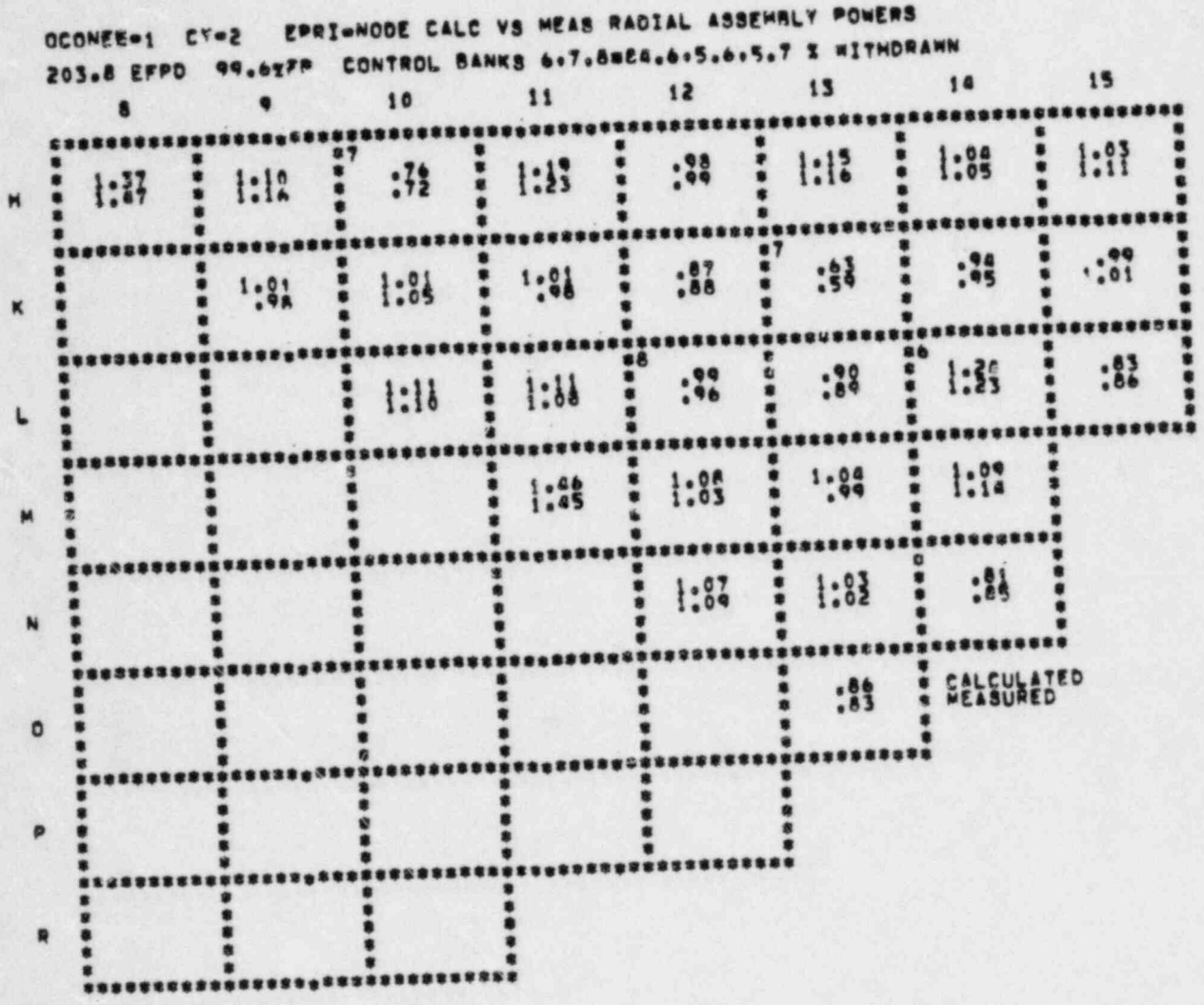
OCONEE-1 CY-2 EPRI-NODE CALC VS MEAS RADIAL ASSEMBLY POWERS
203.8 EFPD 99.6%FP CONTROL BANKS 6,7,8@24,6,5,6,5,7 % WITHDRAWN
8 9 10 11 12 13 14 15
H
K
L
M
N
O
P
R
CALCULATED
MEASURED

Figure 4-49

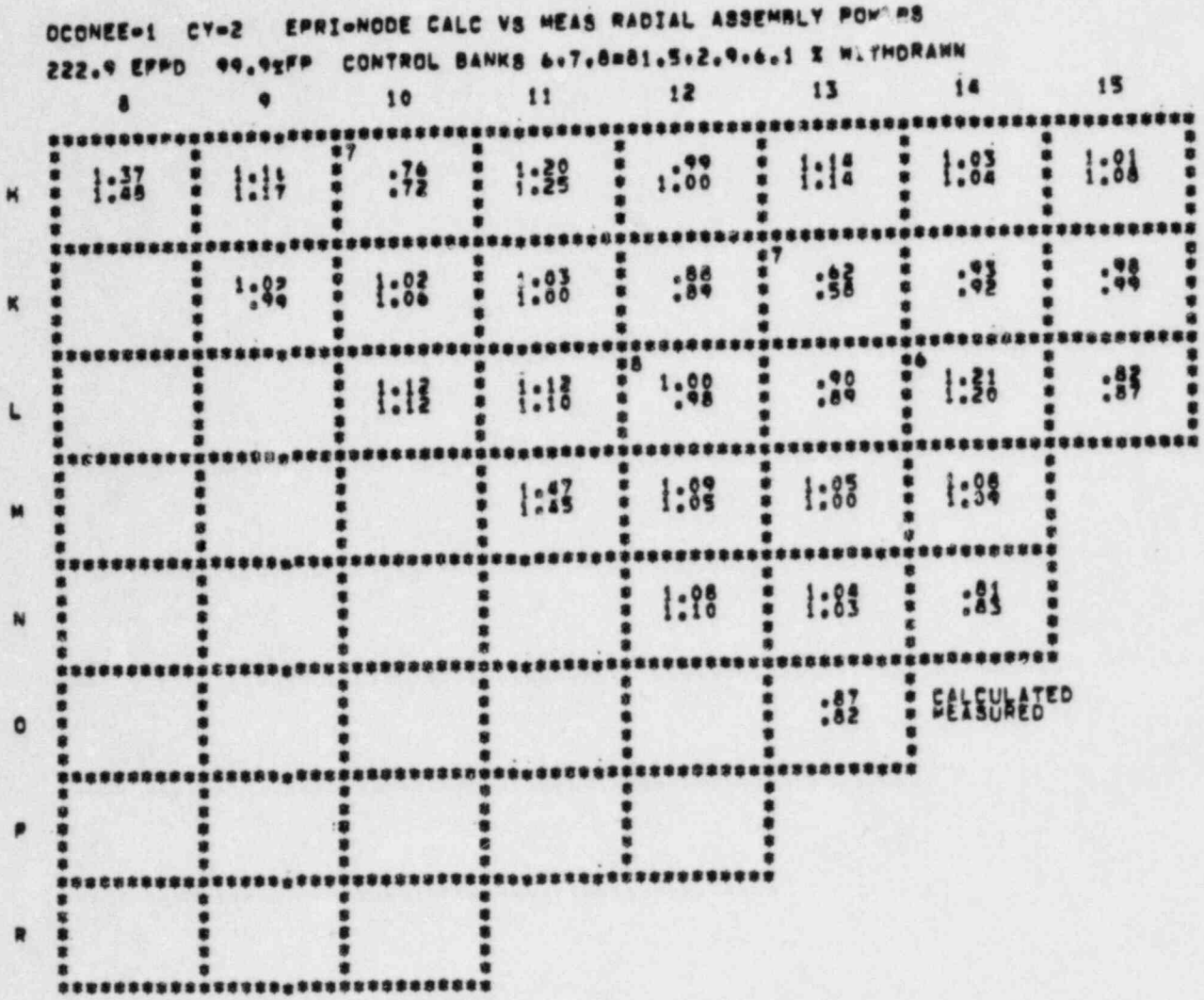
OCONEE-1 CY-2 EPRI-NODE CALC VS MEAS RADIAL ASSEMBLY POWERS
222.9 EFPD 99.9%FP CONTROL BANKS 6,7,8=81.5,2.9,6.1 % WITHDRAWN
8 9 10 11 12 13 14 15
H
K
L
M
N
O
P
R
1.37 1.48
1.11 1.17
.76 .72
1.20 1.25
.99 1.00
1.14 1.14
1.03 1.04
1.01 1.08
1.02 .99
1.02 1.06
1.03 1.00
.86 .89
.82 .58
.93 .92
.98 .99
1.12 1.12
1.12 1.10
1.00 .98
.90 .89
1.21 1.20
.82 .87
1.07 1.05
1.09 1.05
1.05 1.00
1.06 1.04
1.08 1.10
1.04 1.03
.81 .85
.87 .82
CALCULATED
MEASURED

Figure 4-50

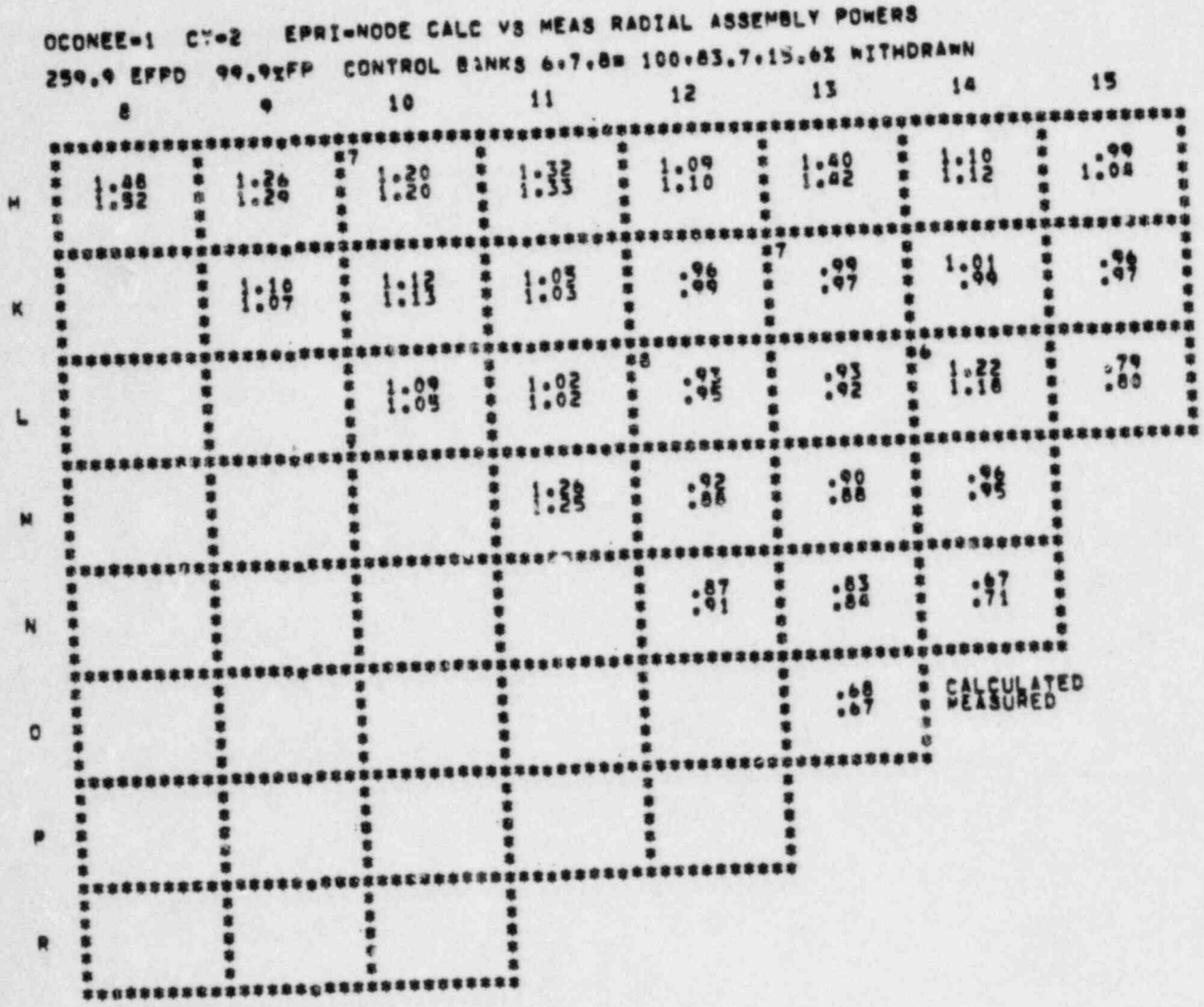
OCONEE-1 CY-2 EPRI-NODE CALC VS MEAS RADIAL ASSEMBLY POWERS
259.9 EFPD 99.9%FP CONTROL BANKS 6,7,8= 100,83.7,15.6% WITHDRAWN
8
9
10
11
12
13
14
15
H
K
L
N
N
O
P
R
1.48 1.52
1.26 1.24
1.20 1.20
1.32 1.33
1.09 1.10
1.40 1.42
1.10 1.12
.99 1.04
1.10 1.07
1.12 1.13
1.05 1.03
.96 .99
.99 .97
1.01 .94
.96 .97
1.09 1.05
1.02 1.02
.93 .95
.93 .92
1.22 1.18
.79 .80
1.20 1.25
.92 .88
.90 .88
.96 .95
.87 .91
.83 .84
.97 .71
.68 .67
CALCULATED
MEASURED

Figure 4-51

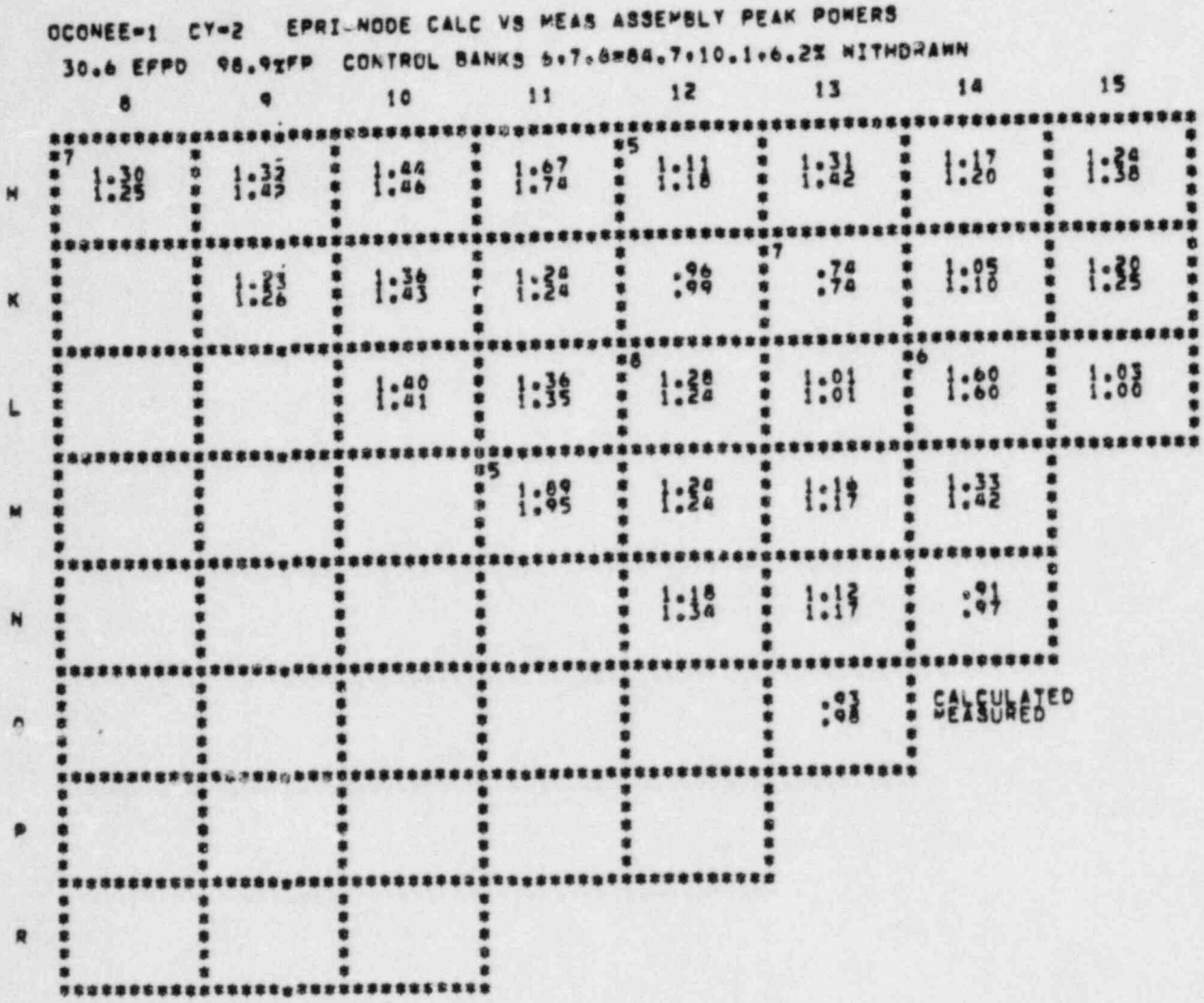
OCONEE-1 CY-2 EPRI-NODE CALC VS MEAS ASSEMBLY PEAK POWERS
30.6 EFPD 98.9%FP CONTROL BANKS 5,7,8=84.7,10.1,6.2% WITHDRAWN
8 9 10 11 12 13 14 15
H
K
L
M
N
P
R
#7 1.30 1.25
1.32 1.42
1.44 1.46
1.67 1.74
#5 1.11 1.18
1.31 1.42
1.17 1.20
1.24 1.38
1.23 1.26
1.36 1.43
1.24 1.24
.96 .99
#7 .74 .74
1.05 1.10
1.20 1.25
1.40 1.41
1.36 1.35
#8 1.28 1.24
1.01 1.01
#6 1.60 1.60
1.03 1.00
#5 1.09 1.05
1.24 1.24
1.19 1.17
1.33 1.42
1.18 1.34
1.13 1.17
.91 .97
.93 .98
CALCULATED
MEASURED

Figure 4-52

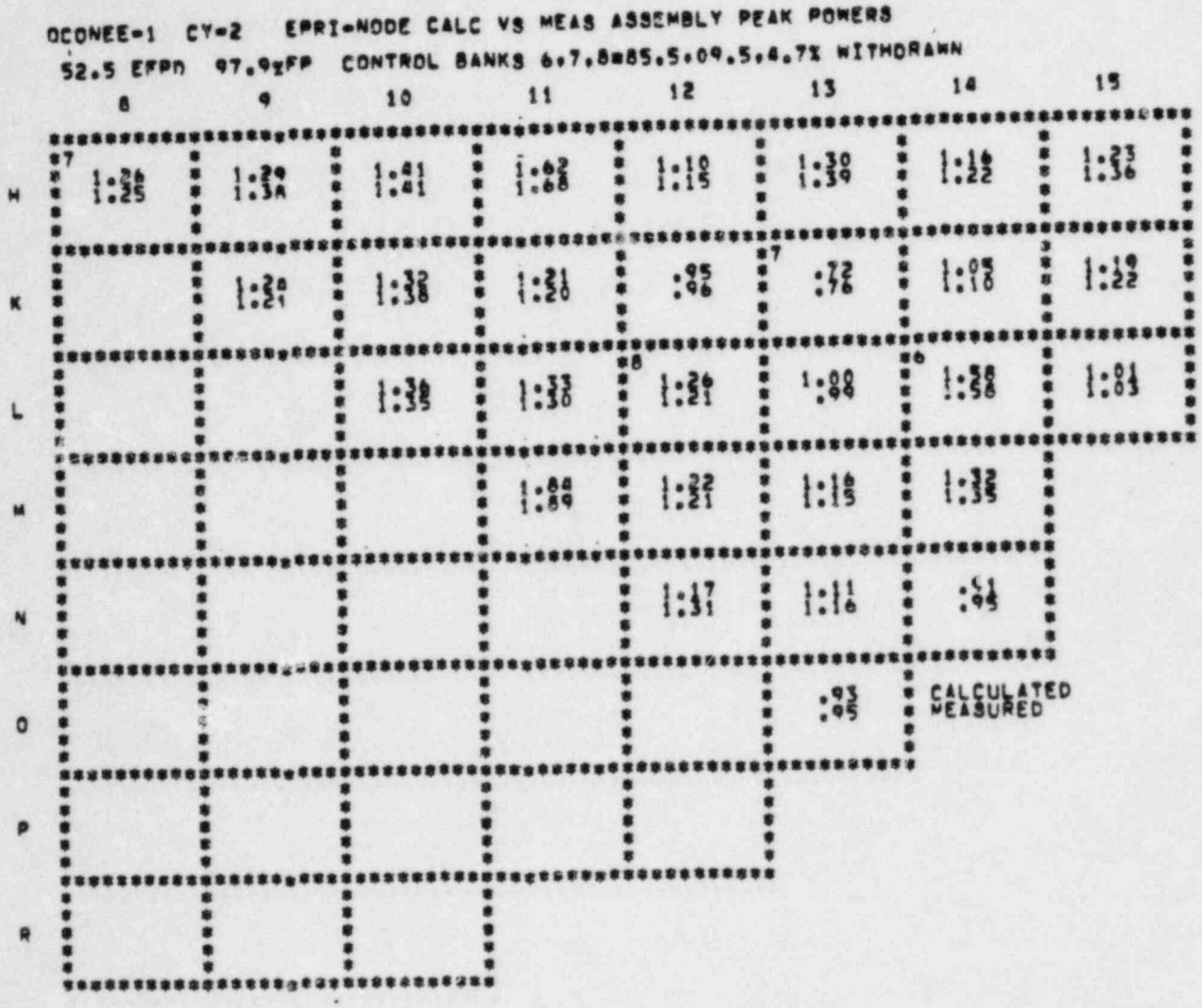
OCONEE-1 CY-2 EPRI-NODE CALC VS MEAS ASSEMBLY PEAK POWERS
52.5 EFPD 97.9%FP CONTROL BANKS 6,7,8@85.5,09.5,4.7% WITHDRAWN
8 9 10 11 12 13 14 15
H
K
L
M
N
O
P
R
CALCULATED
MEASURED

Figure 4-53

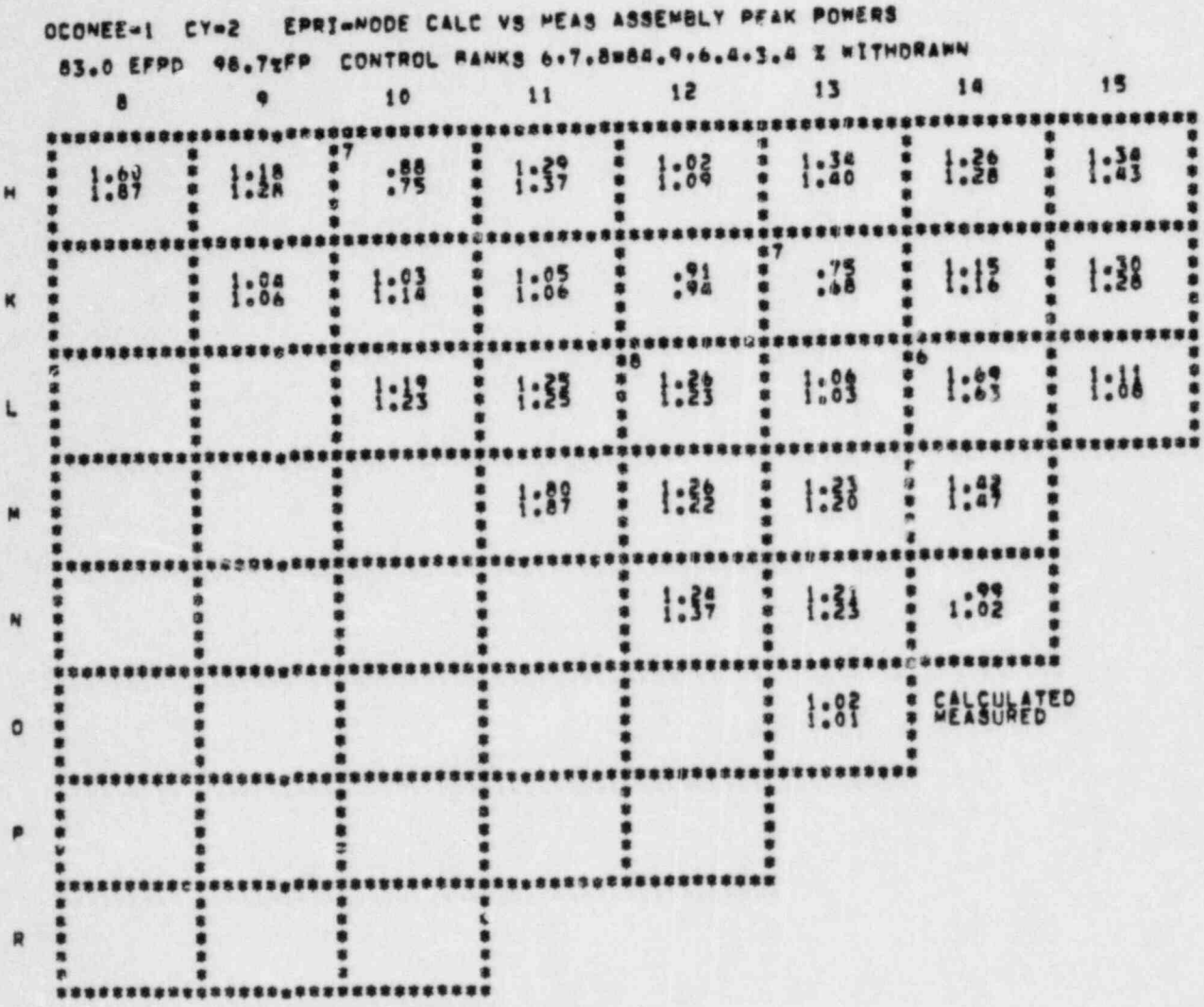
OCONEE-1 CY-2 EPRI-NODE CALC VS MEAS ASSEMBLY PEAK POWERS
83.0 EFPD 98.7%FP CONTROL BANKS 6,7,8,84,9,6,4,3,4 % WITHDRAWN
8
9
10
11
12
13
14
15
H
K
L
M
N
O
P
R
1:60 1.87
1:18 1.28
7
:88 .75
1:29 1.37
1:02 1.09
1:34 1.40
1:26 1.28
1:36 1.43
1:04 1.06
1:03 1.14
1:05 1.06
:91 .94
7
:75 .68
1:15 1.16
1:30 1.28
8
6
1:19 1.23
1:25 1.25
1:26 1.23
1:06 1.03
1:09 1.05
1:11 1.08
1:30 1.37
1:26 1.22
1:23 1.20
1:42 1.49
1:24 1.37
1:21 1.24
1:99 1.02
1:02 1.01
CALCULATED
MEASURED

Figure 4-54

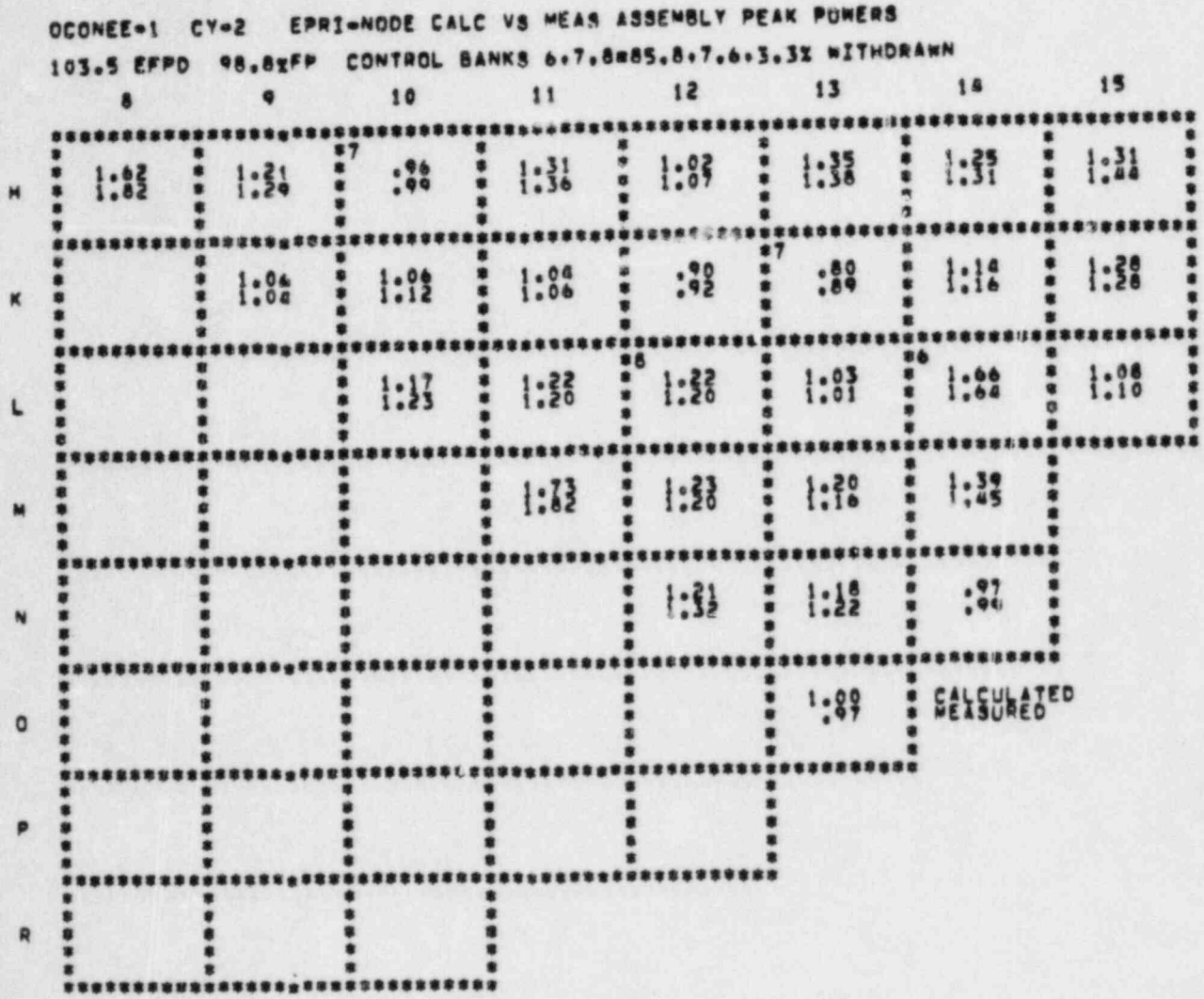
OCONEE-1 CY-2 EPRI-NODE CALC VS MEAS ASSEMBLY PEAK POWERS
103.5 EFPD 98.8%FP CONTROL BANKS 6,7,8=85.8,7.6,3.3% WITHDRAWN
8 9 10 11 12 13 14 15
H K L M N O P R
1.62 1.82
1.21 1.29
#7 .96 .99
1.31 1.36
1.02 1.07
1.35 1.38
1.25 1.31
1.31 1.44
1.04 1.04
1.06 1.12
1.04 1.06
.90 .92
#7 .80 .89
1.14 1.16
1.28 1.28
1.17 1.23
1.22 1.20
#8 1.22 1.20
1.03 1.01
#6 1.66 1.64
1.08 1.10
1.73 1.82
1.23 1.20
1.20 1.16
1.39 1.45
1.21 1.32
1.18 1.22
.97 .94
1.00 .97
CALCULATED
MEASURED

Figure 4-55

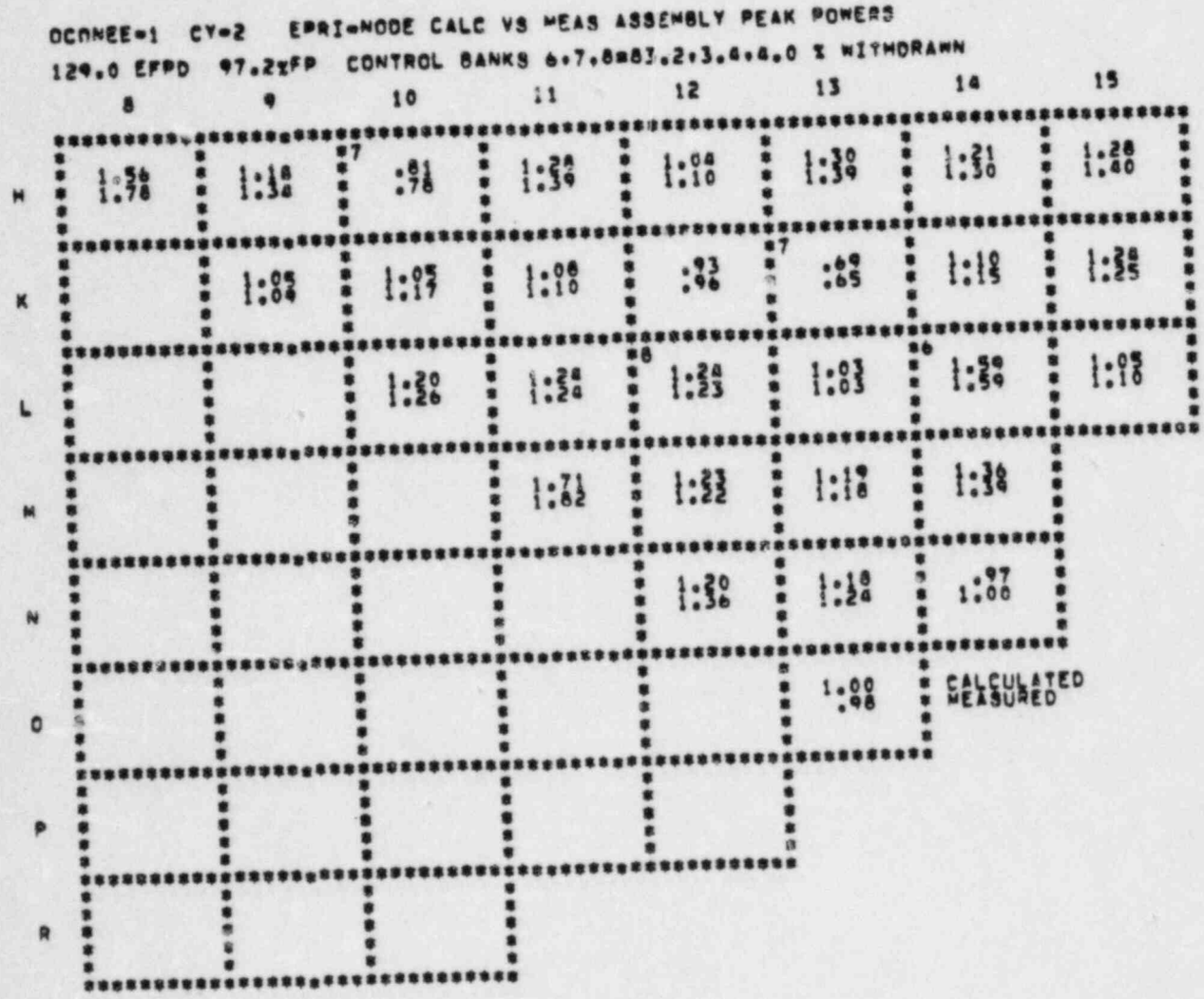
OCONEE-1 CY-2 EPRI-NODE CALC VS MEAS ASSEMBLY PEAK POWERS
129.0 EFPD 97.2%FP CONTROL BANKS 6,7,8=83.2,3.4,4.0 % WITHDRAWN
8 9 10 11 12 13 14 15
H
K
L
M
N
O
P
R
1.56 1.78
1.18 1.34
.81 .78
1.28 1.39
1.04 1.10
1.30 1.39
1.21 1.30
1.28 1.40
1.05 1.04
1.05 1.17
1.08 1.10
.93 .96
.69 .65
1.10 1.15
1.28 1.25
1.20 1.26
1.24 1.24
1.24 1.23
1.03 1.03
1.50 1.54
1.05 1.10
1.71 1.82
1.23 1.22
1.19 1.18
1.30 1.34
1.20 1.36
1.18 1.24
.97 1.00
1.00 .98
CALCULATED
MEASURED

Figure 4-56

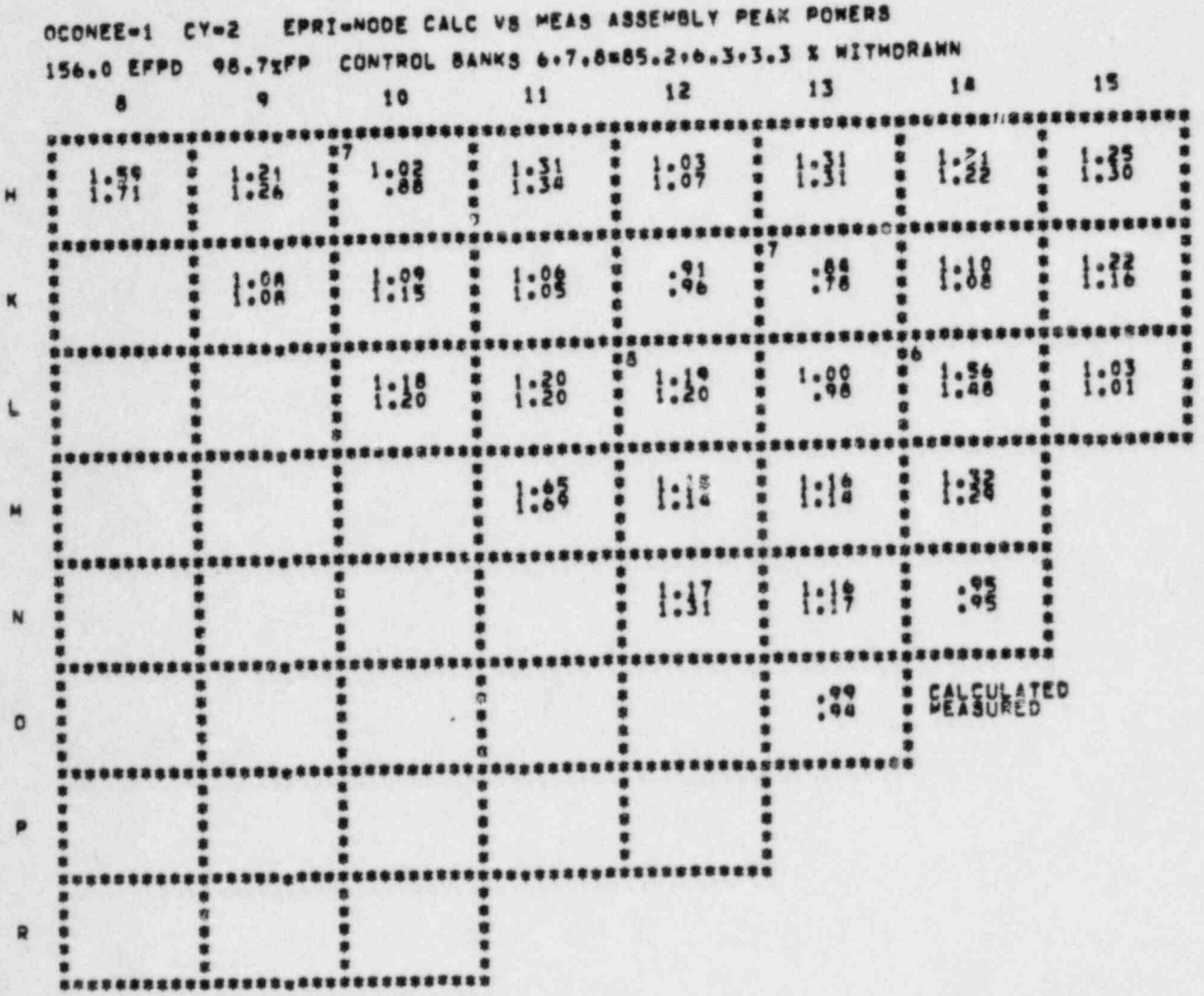
OCONEE-1 CY-2 EPRI-NODE CALC VS MEAS ASSEMBLY PEAK POWERS
156.0 EFPD 98.7%FP CONTROL BANKS 6,7,8=85.2,6.3,3.3 % WITHDRAWN
8 9 10 11 12 13 14 15
H
K
L
M
N
O
P
R
1.59 1.71
1.21 1.26
1.02 .88
1.31 1.34
1.03 1.07
1.31 1.31
1.21 1.22
1.25 1.30
1.08 1.08
1.09 1.15
1.06 1.05
.91 .96
.84 .78
1.10 1.08
1.22 1.16
1.18 1.20
1.20 1.20
1.19 1.20
1.00 .98
1.56 1.48
1.03 1.01
1.65 1.64
1.18 1.14
1.16 1.16
1.32 1.28
1.17 1.31
1.16 1.17
.95 .95
.99 .94
CALCULATED
MEASURED

Figure 4-57

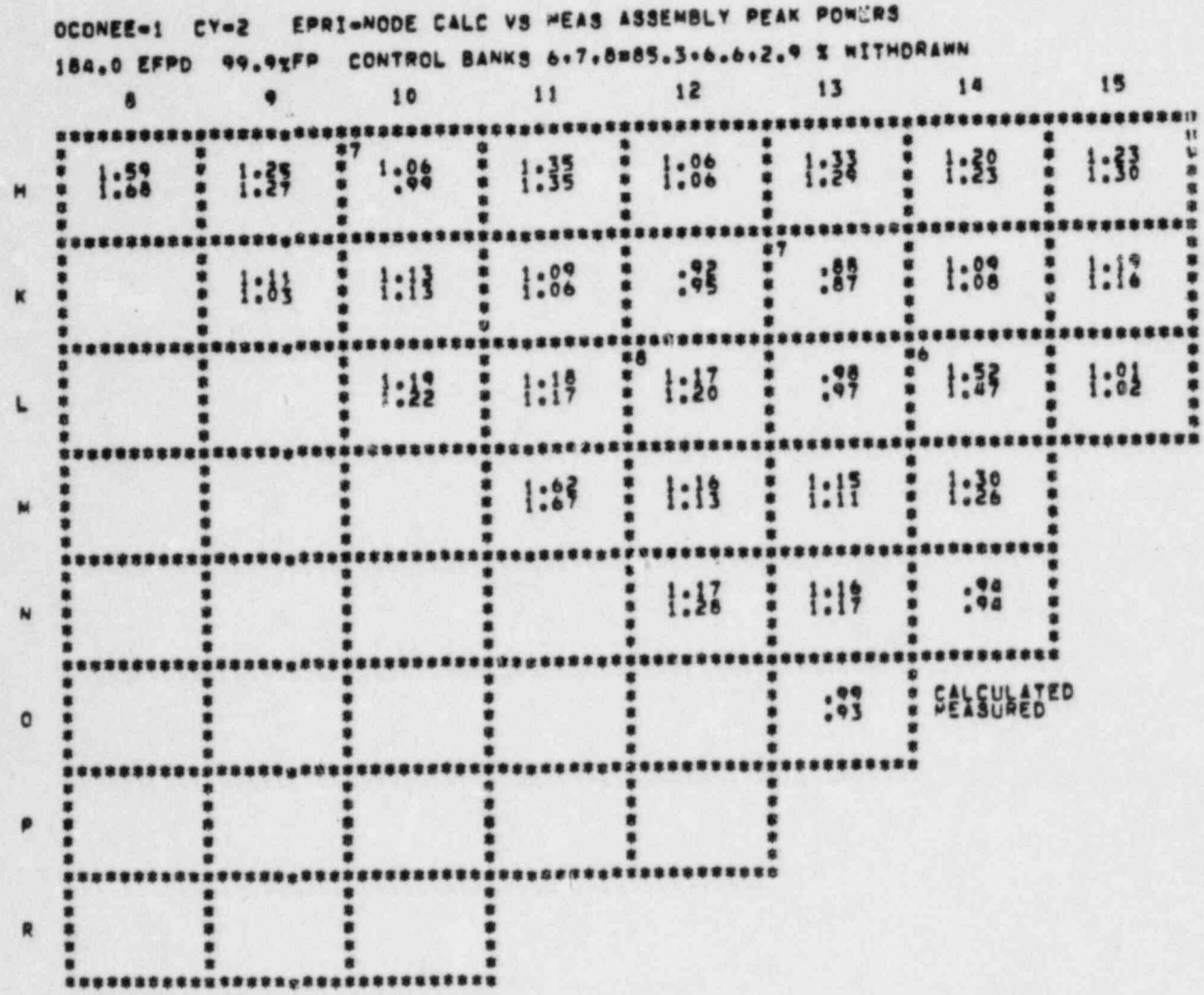
OCONEE-1 CY-2 EPRI-NODE CALC VS MEAS ASSEMBLY PEAK POWERS
184.0 EFPD 99.9%FP CONTROL BANKS 6,7,8=85.3,6.6,2.9 % WITHDRAWN
8 9 10 11 12 13 14 15
H
K
L
M
N
O
P
R
1.59 1.68
1.25 1.27
1.06 .94
1.35 1.35
1.06 1.06
1.33 1.24
1.20 1.23
1.23 1.30
1.11 1.03
1.13 1.13
1.09 1.06
.92 .95
.88 .87
1.09 1.08
1.19 1.16
1.19 1.22
1.18 1.17
1.17 1.20
.98 .97
1.52 1.47
1.01 1.02
1.62 1.67
1.16 1.13
1.15 1.11
1.30 1.26
1.17 1.26
1.16 1.17
.94 .94
.99 .93
CALCULATED
MEASURED

Figure 4-58

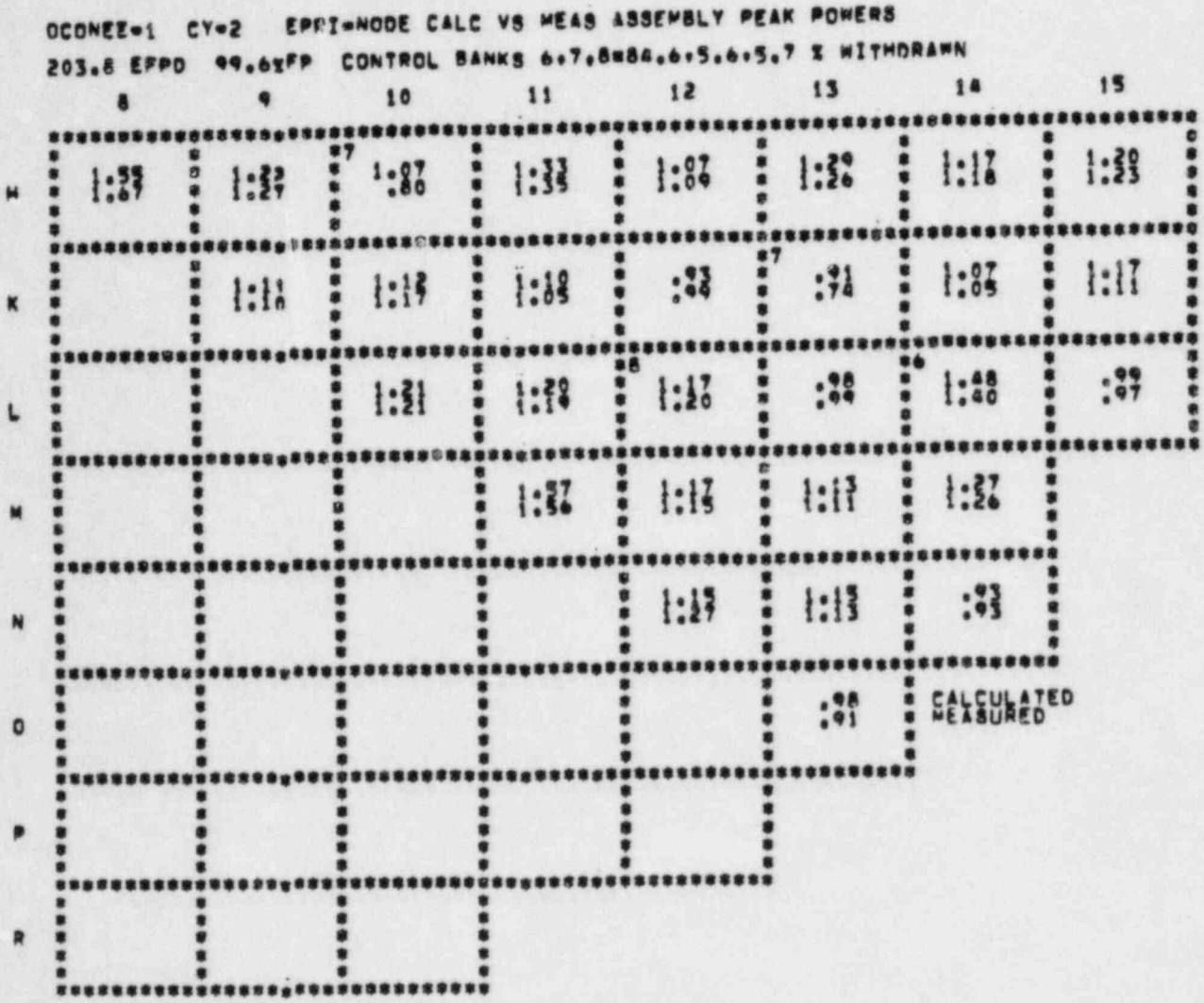
OCONEE-1 CY-2 EPRI-NODE CALC VS MEAS ASSEMBLY PEAK POWERS
203.8 EFPD 99.6%FP CONTROL BANKS 6,7,8=84.6,5.6,5.7 % WITHDRAWN
8 9 10 11 12 13 14 15
H
K
L
M
N
O
P
R
CALCULATED
MEASURED

Figure 4-59

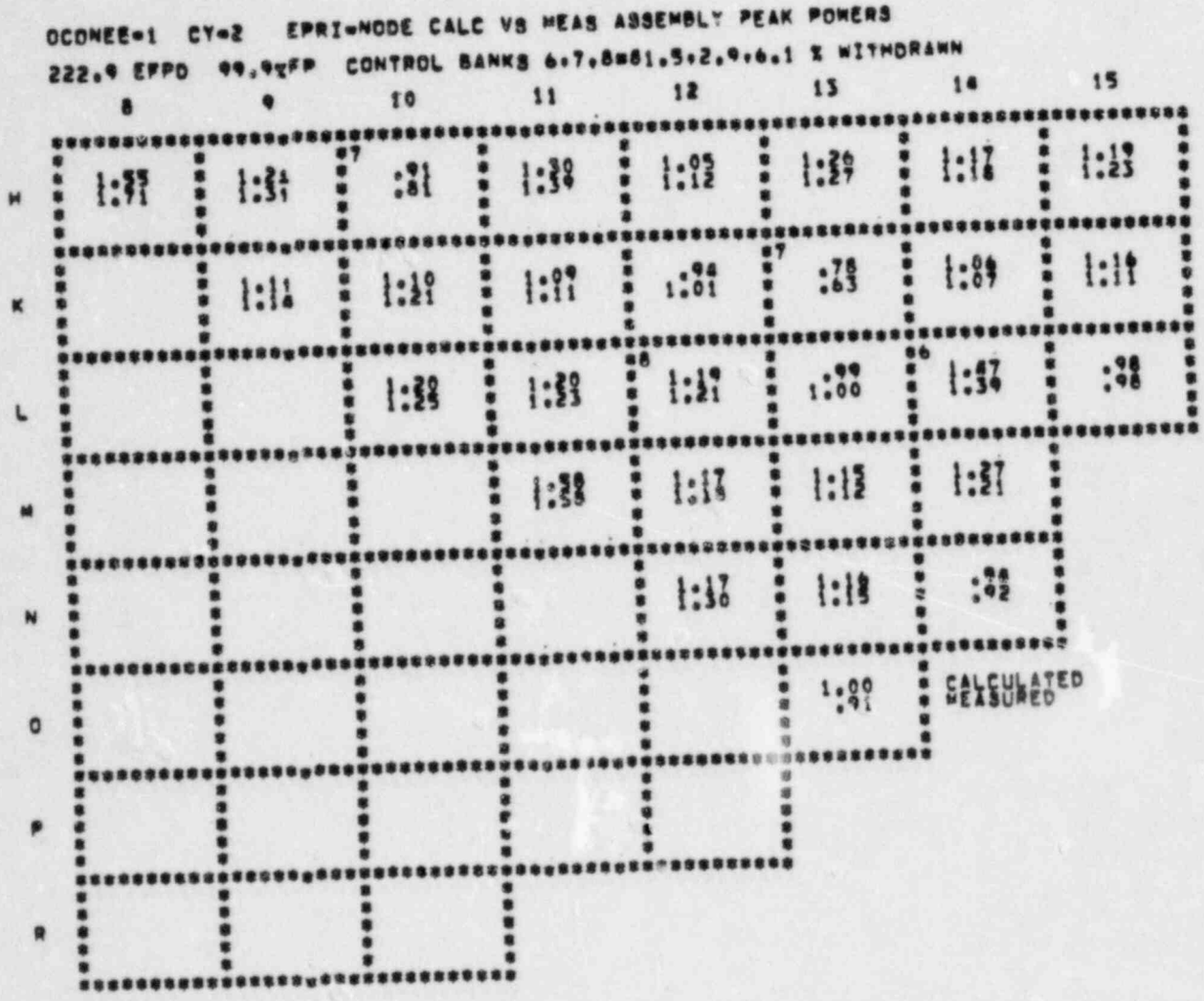
OCONEE-1 CY-2 EPRI-NODE CALC VS MEAS ASSEMBLY PEAK POWERS
222.9 EFPD 99.9%FP CONTROL BANKS 6,7,8=81.5,2,9,6,1 % WITHDRAWN
8 9 10 11 12 13 14 15
H
K
L
M
N
O
P
R
1.00
.91
CALCULATED
MEASURED

Figure 4-60

OCONEE-1 CY-2 EPRI-NODE CALC VS MEAS ASSEMBLY PEAK POWERS

259.9 EFPD 99.9%FP CONTROL BANKS 6,7,8= 100,83.7,15.6% WITHDRAWN

	8	9	10	11	12	13	14	15
H	1.81 1.76	1.52 1.48	7 1.52 1.42	1.61 1.55	1.27 1.26	1.69 1.60	1.24 1.24	1.11 1.18
K		1.31 1.21	1.35 1.27	1.23 1.14	1.17 1.11	7 1.21 1.15	1.18 1.13	1.07 1.04
L			1.28 1.20	1.23 1.12	8 1.21 1.22	1.07 1.03	6 1.35 1.32	.88 .90
M				1.49 1.41	1.07 1.01	1.00 .98	1.06 1.07	
N					.96 1.00	.92 .94	.79 .78	
O						.76 .74	CALCULATED MEASURED	
P								
R								

Figure 4-61
Oconee 1, Cycle 3
Control Rod Configuration

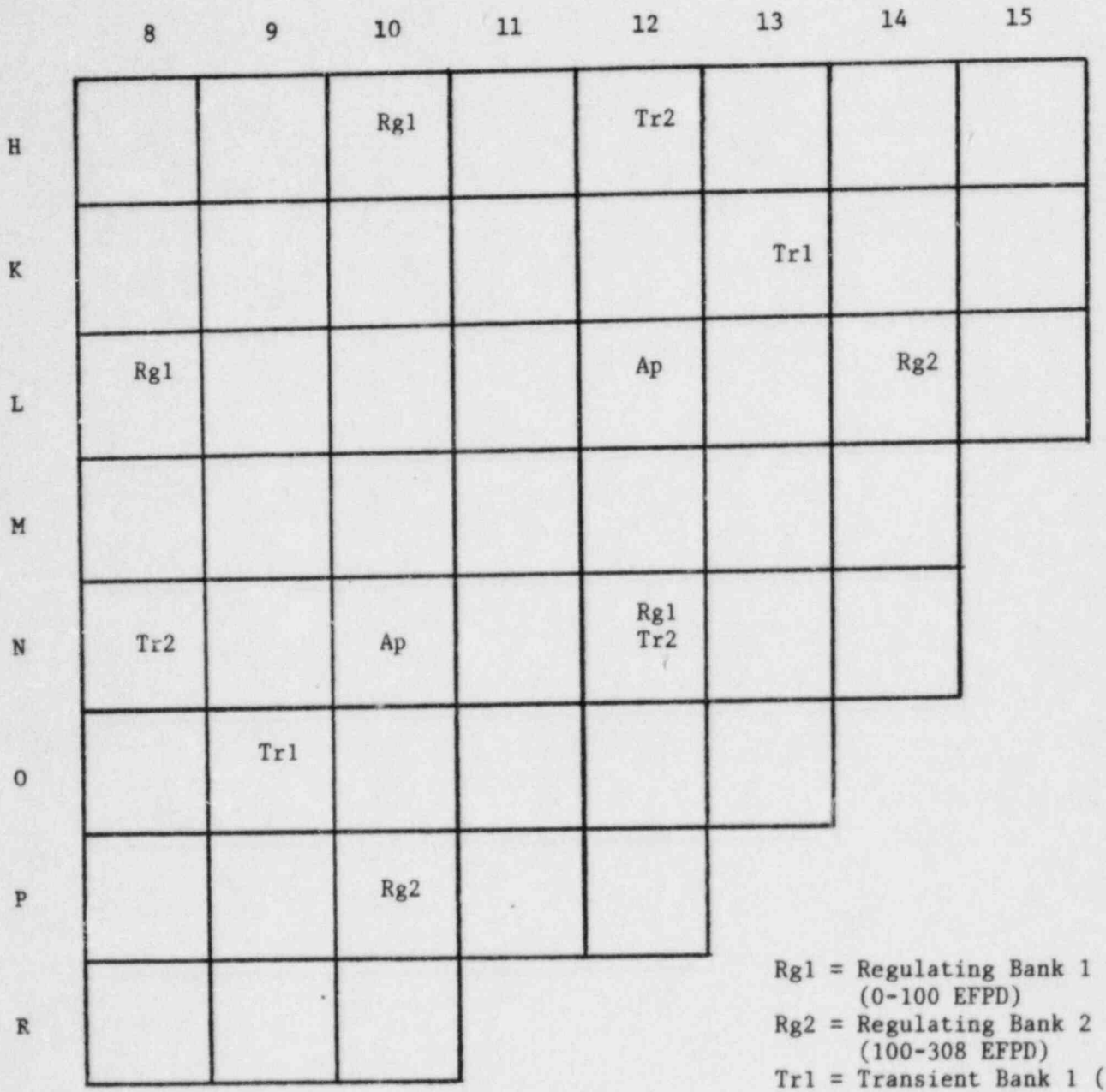

Rg1 = Regulating Bank 1 (6)
(0-100 EFPD)
Rg2 = Regulating Bank 2 (6)
(100-308 EFPD)
Tr1 = Transient Bank 1 (7)
(0-100 EFPD)
Tr2 = Transient Bank 2 (7)
(100-308 EFPD)
Ap = APSR (8)

Figure 4-62
Oconee 1, Cycle 3
Quarter Core Loading Diagram

	8	9	10	11	12	13	14	15
H	2.60 4A	2.15 3	2.60 4A	3.20 4B	2.15 3	2.75 5	2.15 3	2.75 5
K	2.15 3	3.20 4B	2.15 3	3.20 4B	3.20 4B	3.20 4B	2.15 3	2.75 5
L	2.60 4A	2.15 3	2.15 3	3.20 4B	2.15 3	3.20 4B	2.75 5	2.75 5
M	3.20 4B	3.20 4B	3.20 4B	3.20 4B	2.15 3	2.15 3	2.75 5	
N	2.15 3	3.20 4B	2.15 3	2.15 3	3.20 4B	2.75 5	2.75 5	
O	2.75 5	3.20 4B	3.20 4B	2.15 3	2.75 5	2.75 5		
P	2.15 3	2.15 3	2.75 5	2.75 5	2.75 5			
R	2.75 5	2.75 5	2.75 5					

W/O U-235
Batch No.

Figure 4-63
Oconee 1, Cycle 3
Quarter Core Shuffle Pattern

	8	9	10	11	12	13	14	15
H	H-8	H-10	H-11	H-15	H-14	F	H-9	F
K	L-8	0-13	K-10	L-14	K-15	M-14	K-14	F
L	M-8	L-9	L-10	L-15	L-12	N-14	F	F
M	R-8	P-10	R-10	M-11	N-13	M-13	F	
N	P-8	R-9	N-10	0-11	H-13	F	F	
O	F	P-11	P-12	0-11	F	F		
P	K-8	P-9	F	F	F			
R	F	F	F					

Previous cycle loc.

Figure 4-64

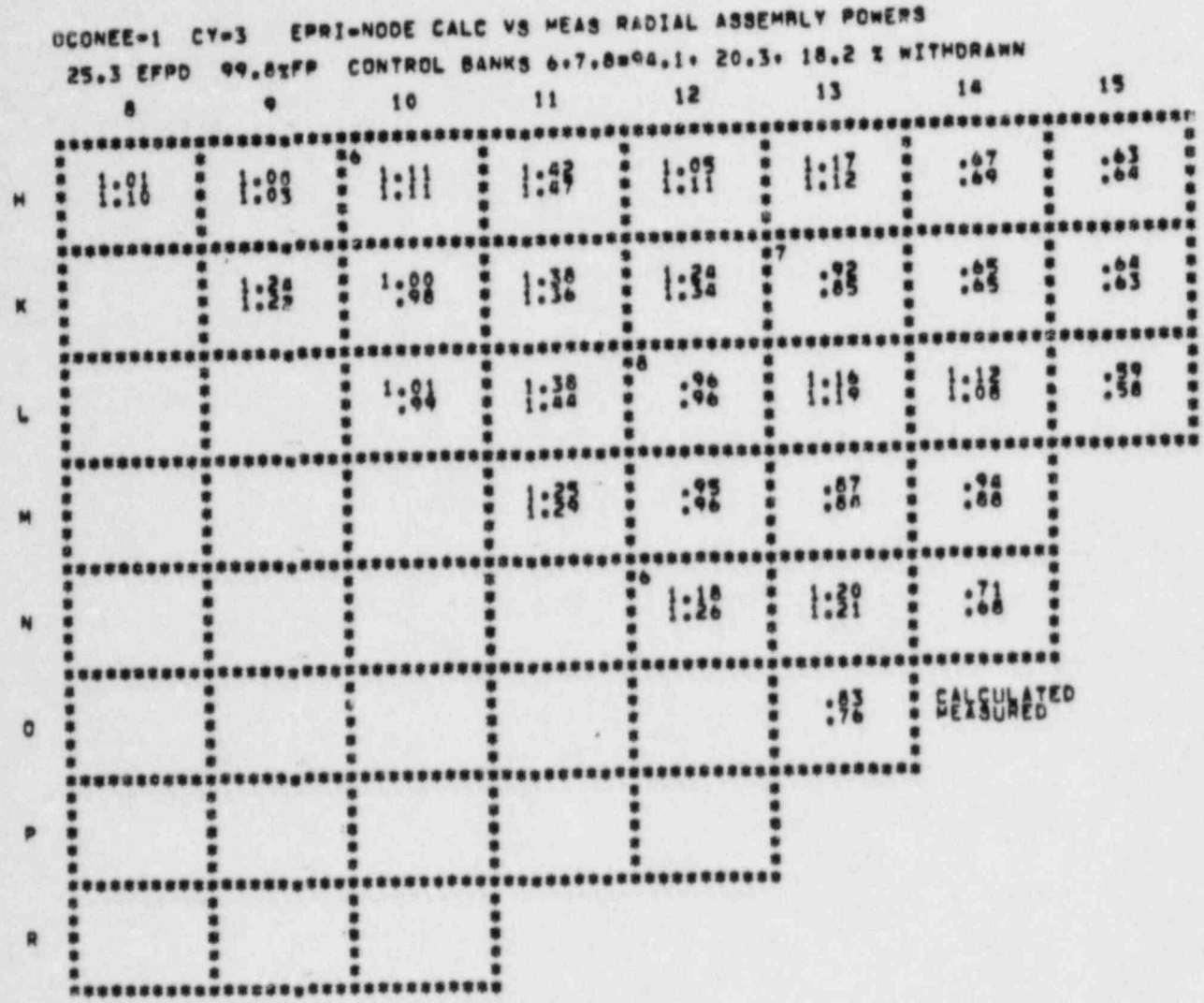
OCONEE-1 CY-3 EPRI-NODE CALC VS MEAS RADIAL ASSEMBLY POWERS
25.3 EFPD 99.8%FP CONTROL BANKS 6,7,8=94.1, 20.3, 18.2 % WITHDRAWN
8 9 10 11 12 13 14 15
H K L M N O P R
1:01 1:10
1:00 1:05
*6 1:11
1:42 1:49
1:05 1:11
1:17 1:12
:67 :69
:63 :64
1:24 1:29
1:00 1:08
1:38 1:36
1:24 1:34
*7 :92 :85
:65 :65
:64 :63
1:01 1:04
1:38 1:44
*8 :96 :96
1:19 1:19
1:12 1:08
:89 :58
1:25 1:24
:95 :96
:87 :86
:94 :88
*6 1:18 1:26
1:20 1:21
:71 :68
:83 :76
CALCULATED
MEASURED

Figure 4-65

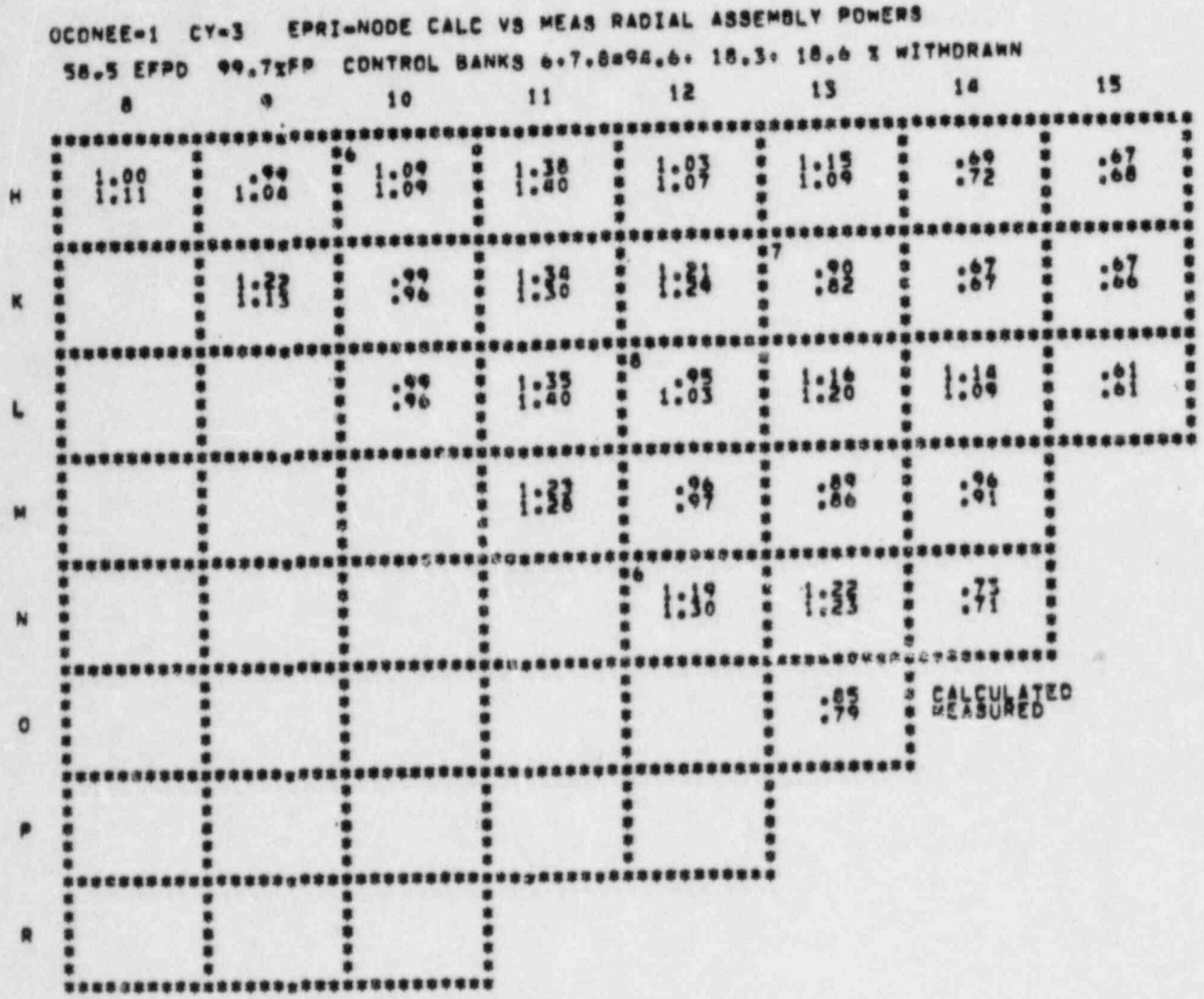
OCONEE-1 CY-3 EPRI-NODE CALC VS MEAS RADIAL ASSEMBLY POWERS
58.5 EFPD 99.7%FP CONTROL BANKS 6,7,8@94.6, 18.3, 18.6 % WITHDRAWN
8 9 10 11 12 13 14 15
H
K
L
M
N
O
P
R
1.00 1.11
.99 1.04
1.09 1.09
1.38 1.40
1.03 1.07
1.15 1.04
.69 .72
.67 .68
1.22 1.13
.99 .96
1.38 1.30
1.21 1.24
.90 .82
.67 .67
.67 .66
.99 .96
1.35 1.40
1.05 1.03
1.16 1.20
1.14 1.09
.81 .81
1.23 1.28
.94 .97
.89 .86
.96 .91
1.19 1.30
1.22 1.23
.73 .71
.85 .79
CALCULATED
MEASURED

Figure 4-66

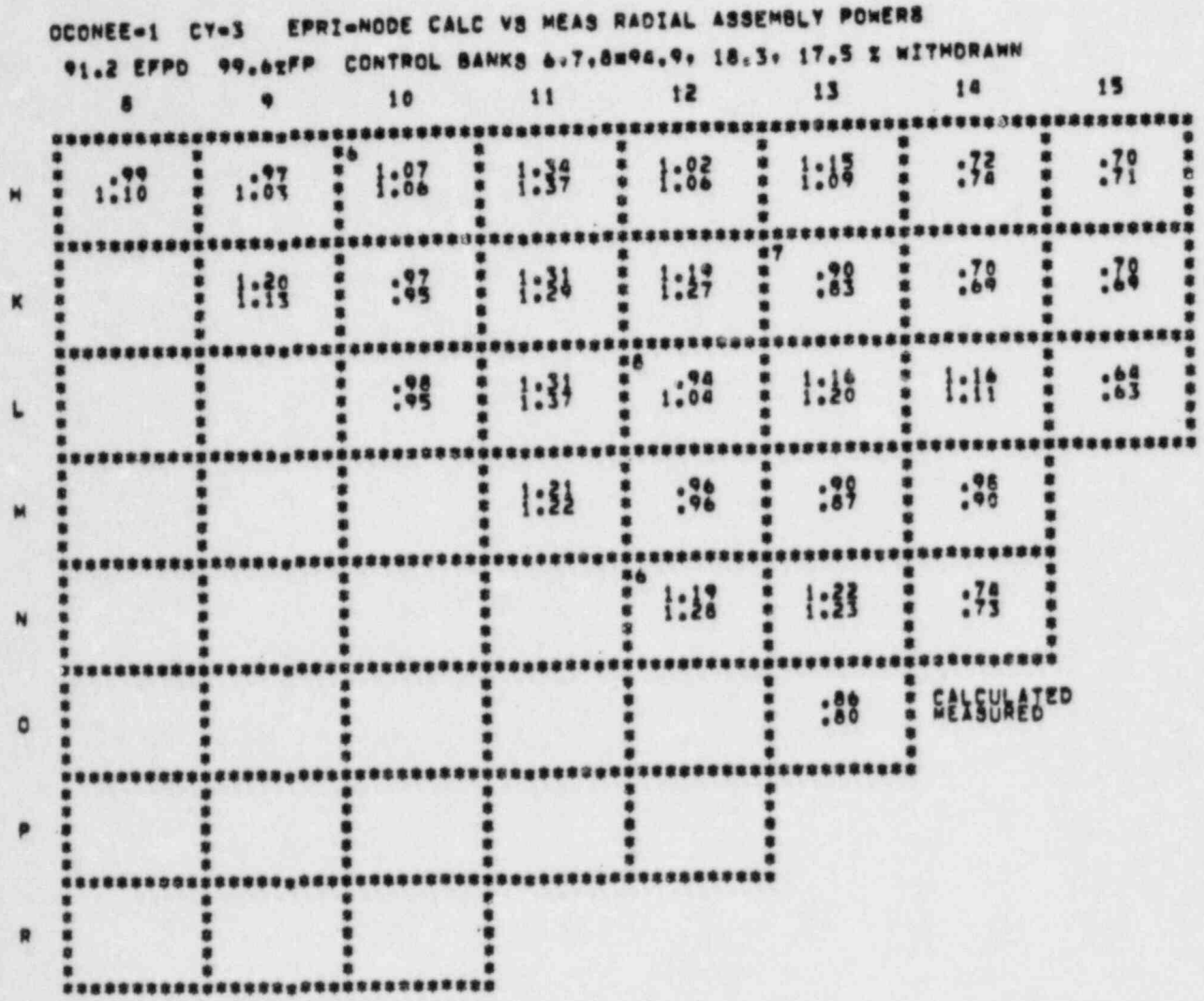
OCONEE-1 CY-3 EPRI-NODE CALC VS MEAS RADIAL ASSEMBLY POWERS
91.2 EFPD 99.6%FP CONTROL BANKS 6,7,8=94.9, 18.3, 17.5 % WITHDRAWN
8 9 10 11 12 13 14 15
H
K
L
M
N
O
P
R
.99 1.10
.97 1.03
1.07 1.06
1.34 1.37
1.02 1.06
1.15 1.09
.72 .74
.70 .71
1.20 1.13
.97 .95
1.31 1.24
1.19 1.27
.90 .83
.70 .69
.70 .69
.98 .95
1.31 1.37
1.04
1.16 1.20
1.16 1.11
.64 .63
1.21 1.22
.96 .96
.90 .87
.96 .90
1.19 1.28
1.22 1.23
.74 .73
.86 .80
CALCULATED
MEASURED

Figure 4-67

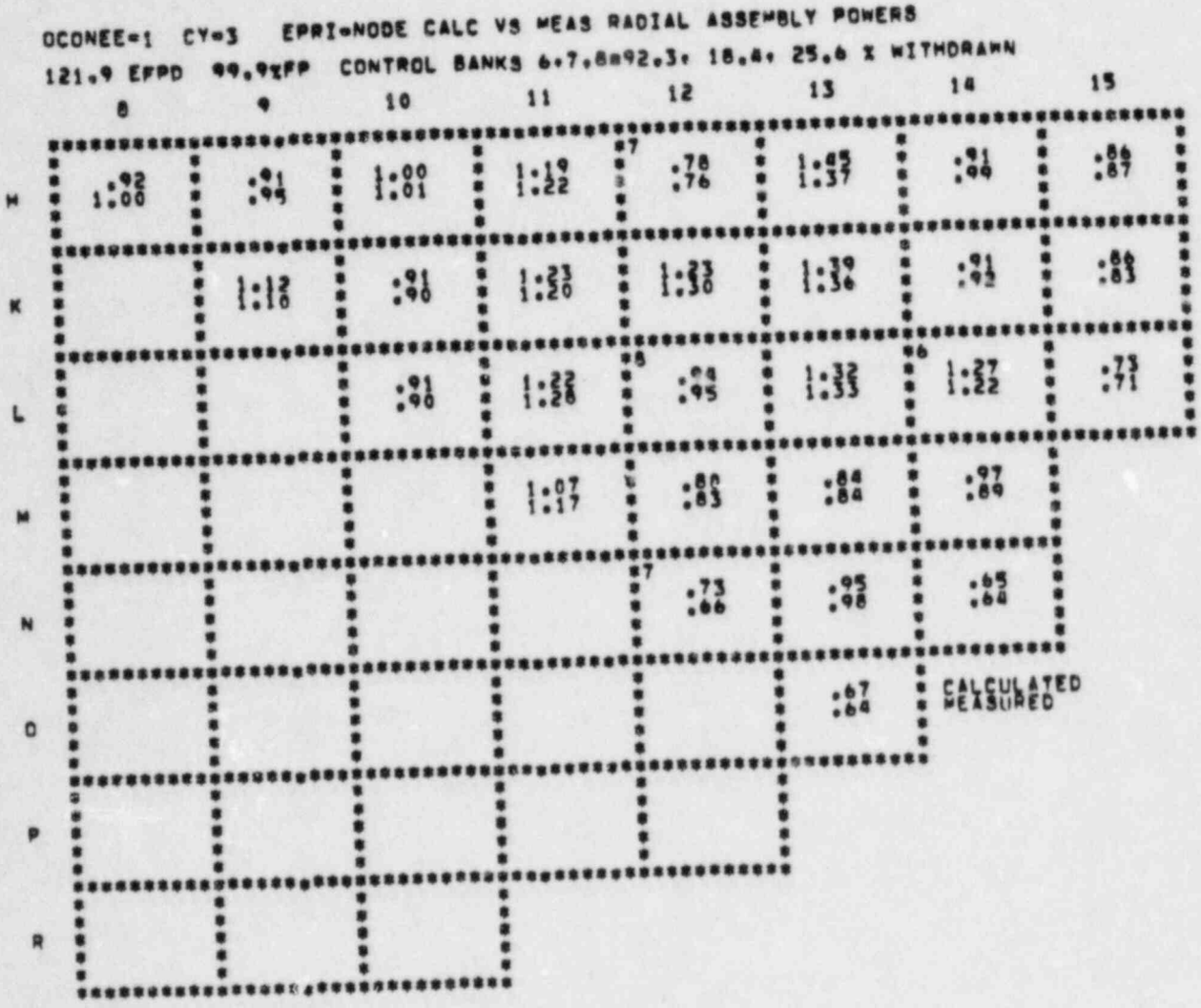
OCONEE-1 CY-3 EPRI-NODE CALC VS MEAS RADIAL ASSEMBLY POWERS
121.9 EFPD 99.9%FP CONTROL BANKS 6,7,8=92.3, 18.4, 25.6 % WITHDRAWN
8 9 10 11 12 13 14 15
H K L M N O P R
1.00 .92 .94 .91 1.01 1.00 1.22 1.19 .76 .78 1.37 1.45 .94 .91 .87 .86
1.10 1.12 .90 .91 1.20 1.23 1.30 1.33 1.36 1.39 .92 .91 .83 .86
.90 .91 1.28 1.22 .95 .94 1.33 1.32 1.22 1.27 .71 .73
1.17 1.07 .83 .80 .84 .84 .89 .97
.66 .73 .98 .95 .64 .65
.64 .67
CALCULATED
MEASURED

Figure 4-68

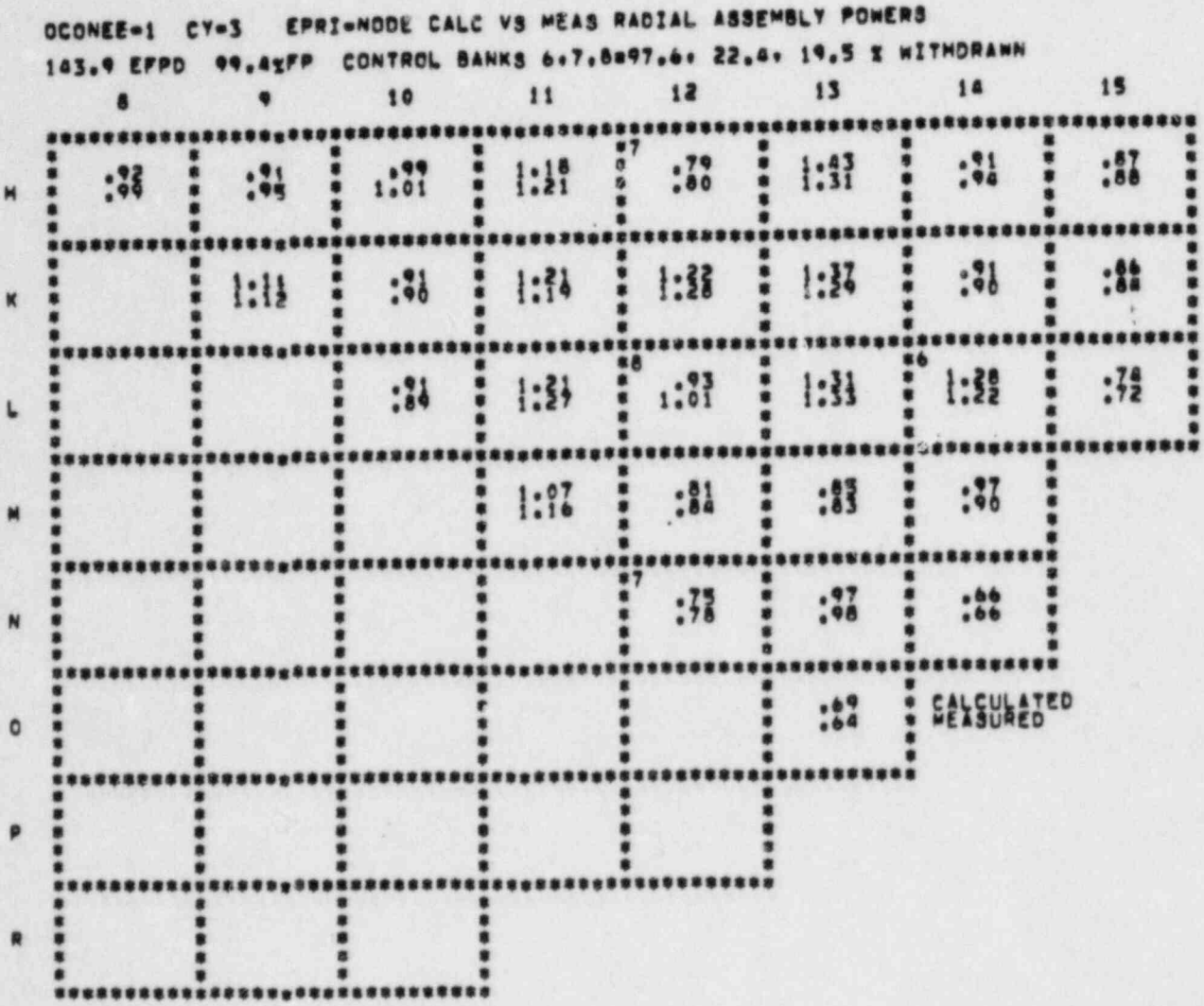
OCONEE-1 CY-3 EPRI-NODE CALC VS MEAS RADIAL ASSEMBLY POWERS
143.9 EFPD 99.4%FP CONTROL BANKS 6,7,8=97.6, 22.4, 19.5 % WITHDRAWN
8
9
10
11
12
13
14
15
H
K
L
M
N
O
P
R
.92 .90
.91 .95
.99 1.01
1.18 1.21
.79 .80
1.43 1.31
.91 .94
.87 .88
1.11 1.12
.91 .90
1.21 1.14
1.22 1.28
1.37 1.24
.91 .90
.84 .88
.91 .84
1.21 1.29
.93 1.01
1.31 1.33
1.28 1.22
.74 .72
1.07 1.16
.81 .84
.85 .83
.97 .90
.75 .78
.97 .98
.66 .66
.69 .64
CALCULATED
MEASURED

Figure 4-69

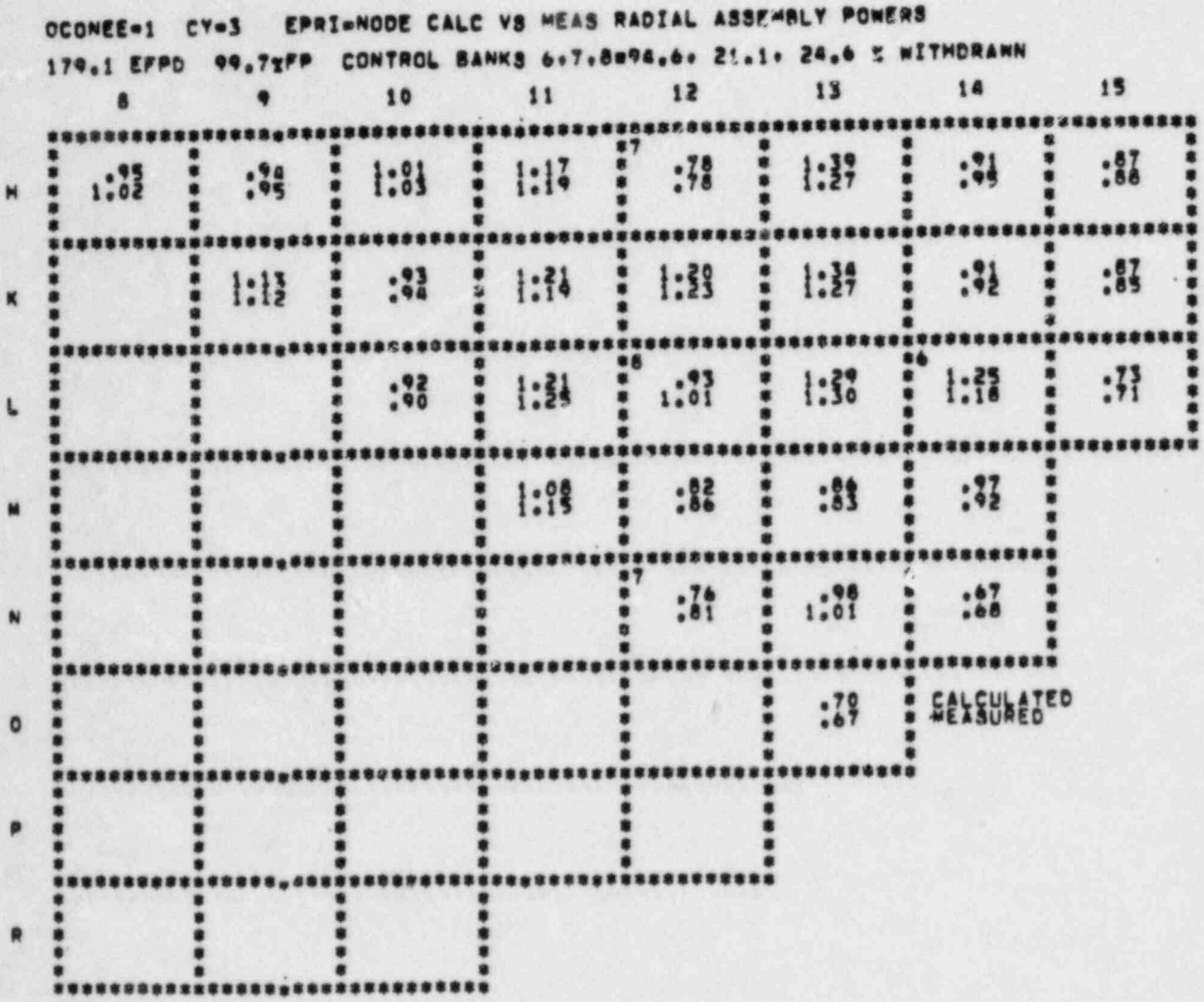
OCONEE-1 CY-3 EPRI-NODE CALC VS MEAS RADIAL ASSEMBLY POWERS
179.1 EFPD 99.7%FP CONTROL BANKS 6,7,8=94.6, 21.1, 24.6 % WITHDRAWN
8 9 10 11 12 13 14 15
H K L M N O P R
.95 1.02
.94 .95
1.01 1.03
1.17 1.14
.78 .78
1.39 1.27
.91 .95
.87 .88
1.13 1.12
.93 .94
1.21 1.14
1.20 1.23
1.34 1.27
.91 .92
.87 .85
.92 .90
1.21 1.24
.93 1.01
1.29 1.30
1.25 1.18
.73 .71
1.08 1.15
.82 .86
.86 .83
.97 .92
.76 .81
.98 1.01
.67 .68
.70 .67
CALCULATED
MEASURED

Figure 4-70

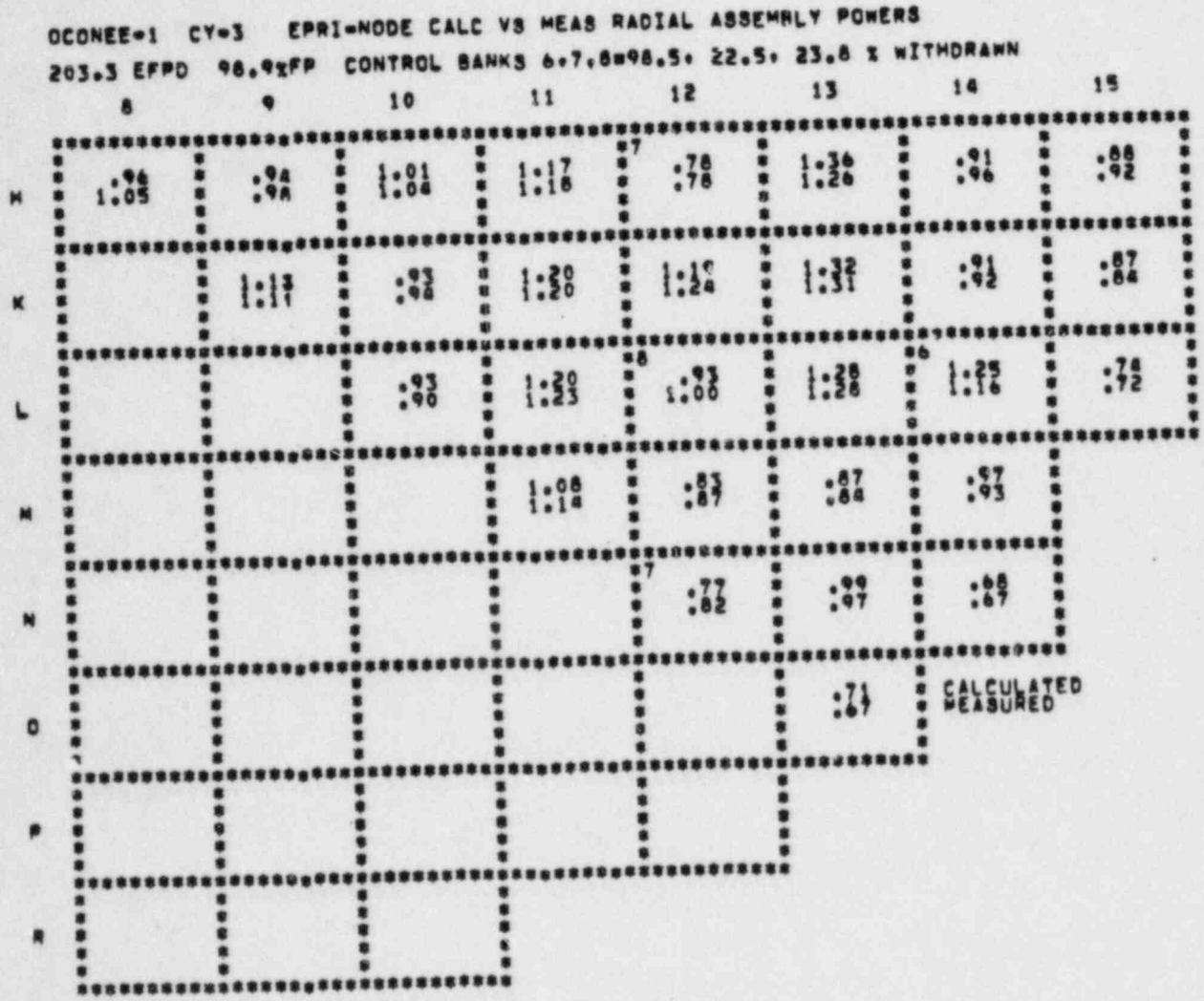
OCONEE-1 CY-3 EPRI-NODE CALC VS MEAS RADIAL ASSEMBLY POWERS
203.3 EFPD 98.9%FP CONTROL BANKS 6,7,8=98.5, 22.5, 23.8 % WITHDRAWN
8 9 10 11 12 13 14 15
H K L M N O P R
CALCULATED
MEASURED

Figure 4-71

OCONEE-1 CY-3 EPRI-NODE CALC VS MEAS RADIAL ASSEMBLY POWERS

232.6 EFPD 99.9%FP CONTROL BANKS 6,7,8=97.8, 22.5, 25.4 % WITHDRAWN

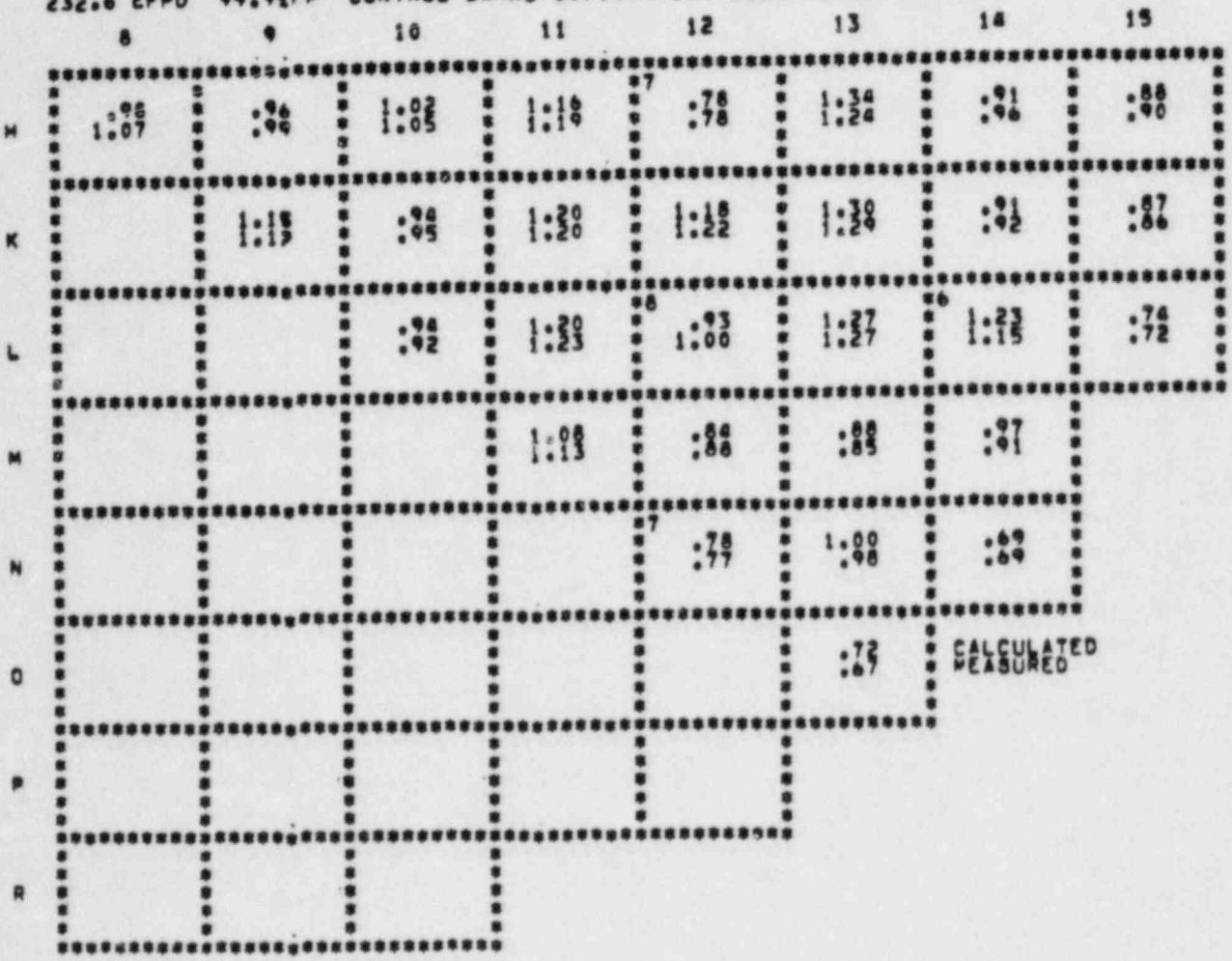

Figure 4-72

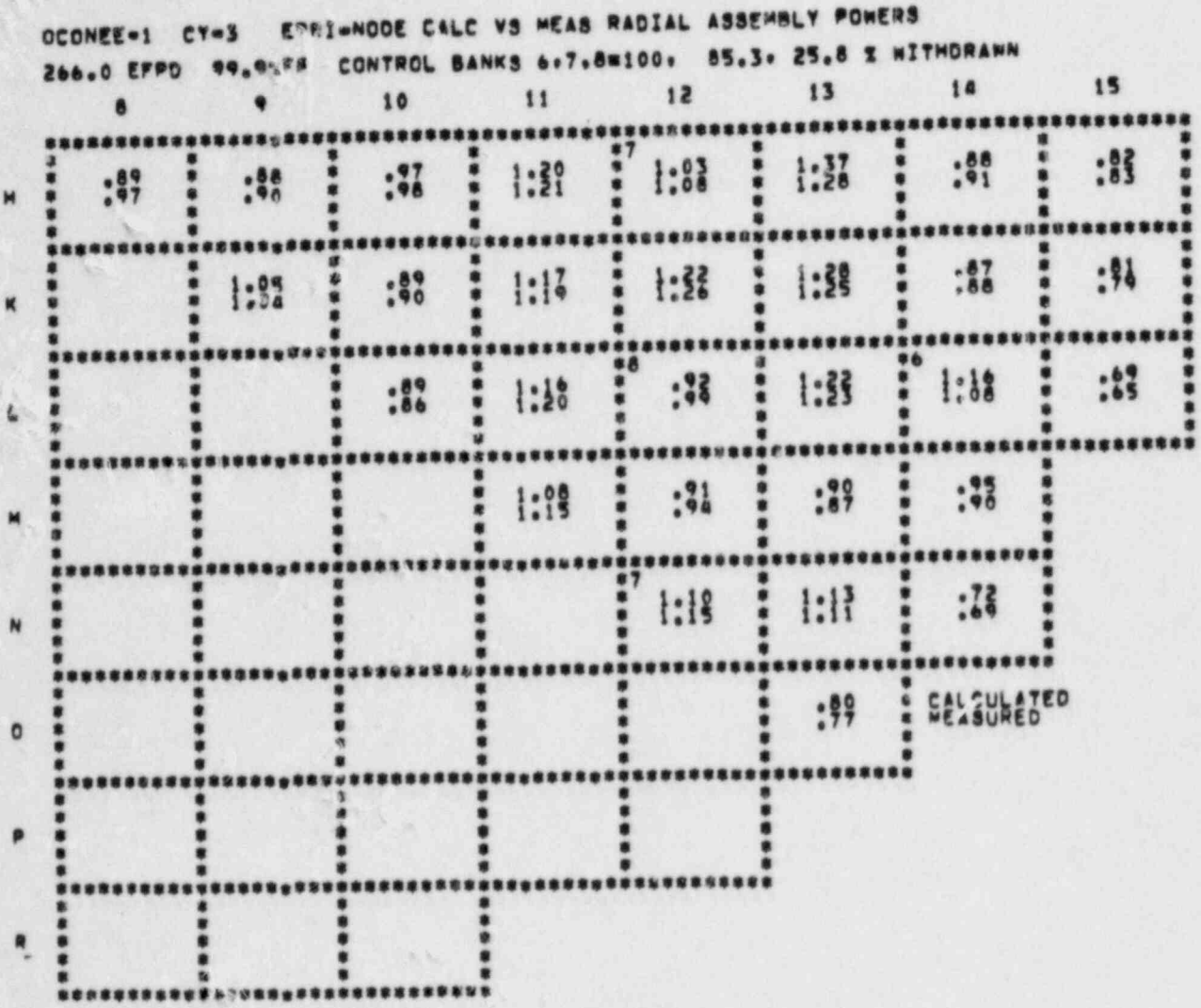
OCONEE-1 CY-3 EPRI-NODE CALC VS MEAS RADIAL ASSEMBLY POWERS
266.0 EFPD 99.9% CONTROL BANKS 6,7,8=100, 85.3, 25.8 % WITHDRAWN
8 9 10 11 12 13 14 15
H
K
L
M
N
O
P
R
.89 .97
.88 .90
.97 .98
1.20 1.21
1.03 1.08
1.37 1.28
.88 .91
.82 .83
1.09 1.04
.89 .90
1.17 1.19
1.22 1.26
1.28 1.25
.87 .88
.81 .74
.89 .86
1.16 1.20
.92 .94
1.22 1.25
1.16 1.08
.69 .65
1.08 1.15
.91 .94
.90 .87
.95 .90
1.10 1.15
1.13 1.11
.72 .69
.80 .77
CALCULATED
MEASURED

Figure 4-73

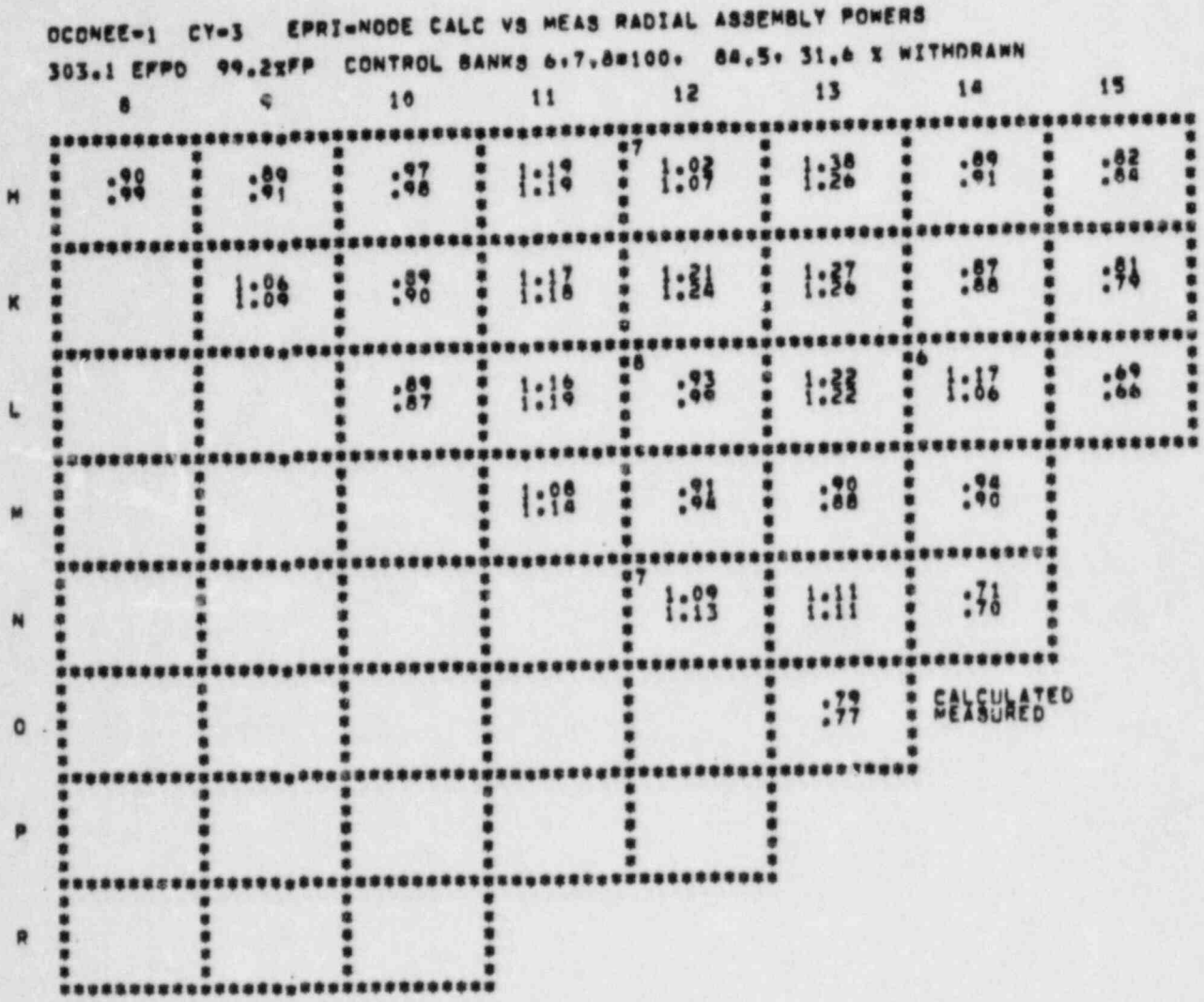
OCONEE-1 CY-3 EPRI-NODE CALC VS MEAS RADIAL ASSEMBLY POWERS
303.1 EFPD 99.2%FP CONTROL BANKS 6,7,8=100, 68.5, 31.6 % WITHDRAWN
8 9 10 11 12 13 14 15
H
K
L
M
N
O
P
R
.90 .99
.89 .91
.97 .98
1.19 1.19
1.02 1.07
1.38 1.26
.89 .91
.82 .84
1.06 1.04
.89 .90
1.17 1.18
1.21 1.24
1.27 1.26
.87 .88
.81 .79
.89 .87
1.16 1.19
.93 .96
1.22 1.22
1.17 1.06
.69 .66
1.08 1.14
.91 .94
.90 .88
.94 .90
1.09 1.13
1.11 1.11
.71 .70
.79 .77
CALCULATED
MEASURED

Figure 4-74

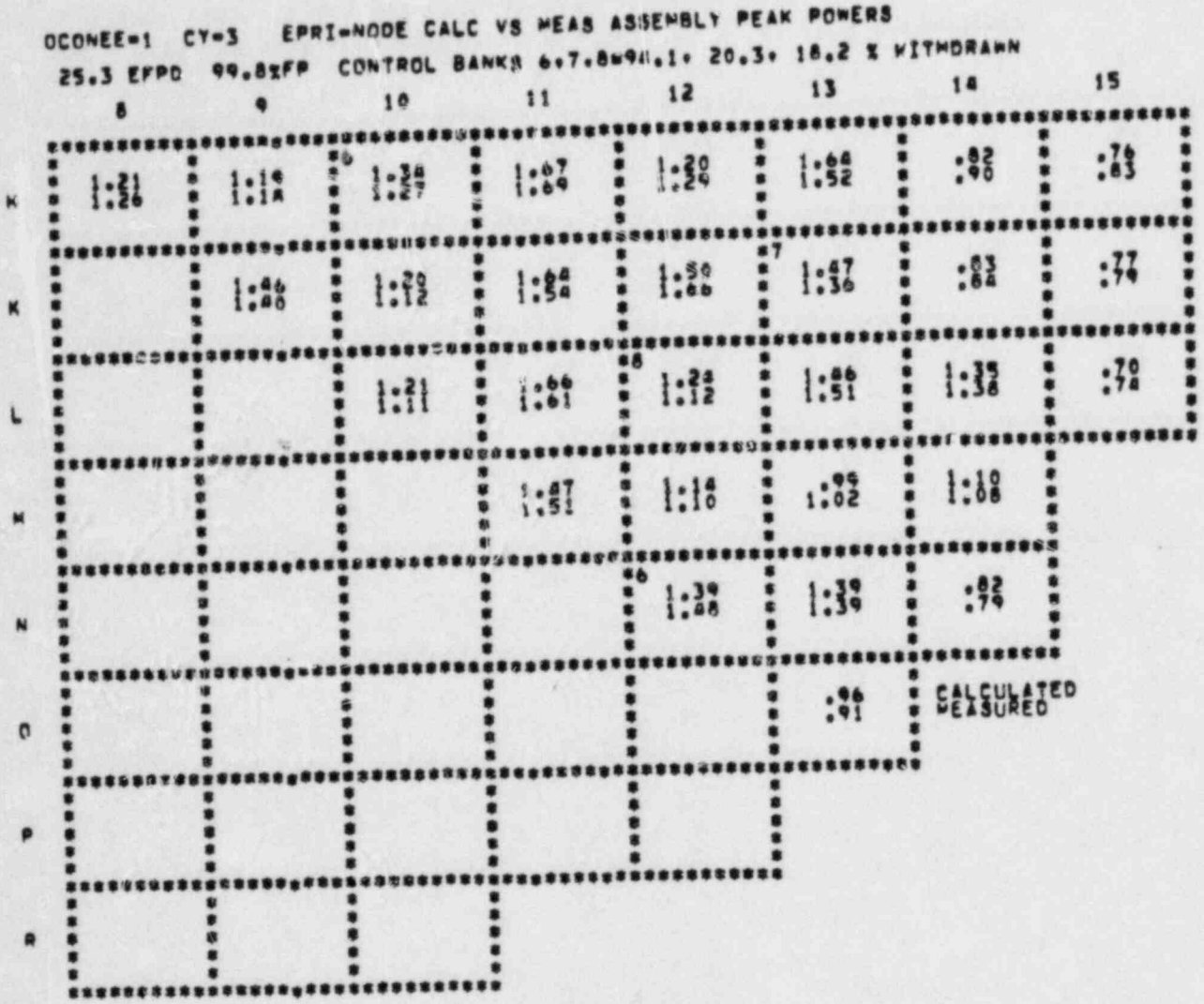
OCONEE-1 CY-3 EPRI-NODE CALC VS MEAS ASSEMBLY PEAK POWERS
25.3 EFPD 99.8%FP CONTROL BANKS 6,7,8W94.1, 20.3, 18.2 % WITHDRAWN
8 9 10 11 12 13 14 15
K
K
L
M
N
O
P
R
1.21 1.26
1.16 1.18
1.38 1.27
1.07 1.09
1.20 1.24
1.04 1.52
.82 .90
.76 .83
1.46 1.48
1.20 1.12
1.04 1.54
1.50 1.46
1.47 1.36
.83 .84
.77 .79
1.21 1.11
1.06 1.01
1.24 1.12
1.06 1.51
1.35 1.38
.70 .78
1.07 1.51
1.14 1.10
.96 1.02
1.10 1.08
1.39 1.48
1.39 1.39
.82 .79
.96 .91
CALCULATED
MEASURED

Figure 4-75

OCONEE-1 CY-3 EPRI-NODE CALC VS MEAS ASSEMBLY PEAK POWERS

58.5 EFPD 99.7±FP CONTROL BANKS 6,7,8=96.6, 18.3, 18.6 % WITHDRAWN

	8	9	10	11	12	13	14	15
H	1.16 / 1.24	1.14 / 1.16	#6 1.27 / 1.25	1.07 / 1.07	1.18 / 1.19	1.08 / 1.07	.83 / .86	.79 / .83
K		1.18 / 1.24	1.16 / 1.09	1.04 / 1.04	1.07 / 1.04	#7 1.02 / 1.02	.84 / .80	.80 / .78
L			1.15 / 1.09	1.07 / 1.07	#8 1.20 / 1.17	1.05 / 1.02	1.06 / 1.02	.73 / .73
M				1.01 / 1.06	1.12 / 1.11	.99 / 1.00	1.13 / 1.09	
N					#6 1.17 / 1.14	1.02 / 1.09	.85 / .82	
O						.99 / .93	CALCULATED / MEASURED	
P								
R								

Figure 4-76

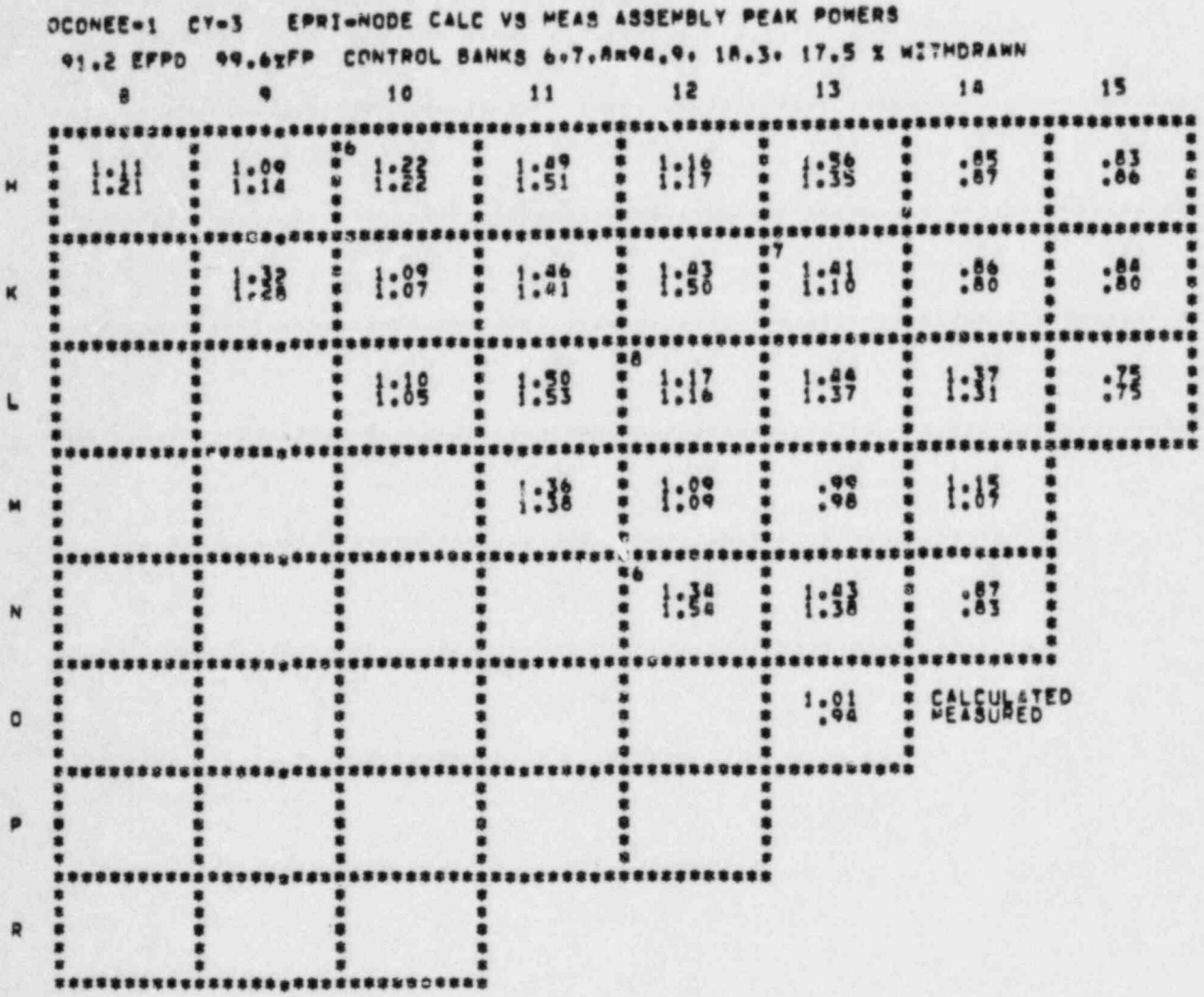
OCONEE-1 CY-3 EPRI-NODE CALC VS MEAS ASSEMBLY PEAK POWERS
91.2 EFPD 99.6%FP CONTROL BANKS 6,7,8=94.9, 18.3, 17.5 % WITHDRAWN
8 9 10 11 12 13 14 15
H
K
L
M
N
O
P
R
1.11 1.21
1.09 1.14
6
1.22 1.22
1.49 1.51
1.16 1.17
1.36 1.35
.85 .89
.83 .86
1.32 1.28
1.09 1.07
1.46 1.41
1.43 1.50
7
1.41 1.10
.86 .80
.84 .80
1.10 1.05
1.50 1.53
8
1.17 1.16
1.44 1.37
1.37 1.31
.75 .75
1.36 1.38
1.09 1.09
.99 .98
1.15 1.07
6
1.34 1.54
1.43 1.38
.87 .83
1.01 .94
CALCULATED
MEASURED

Figure 4-77

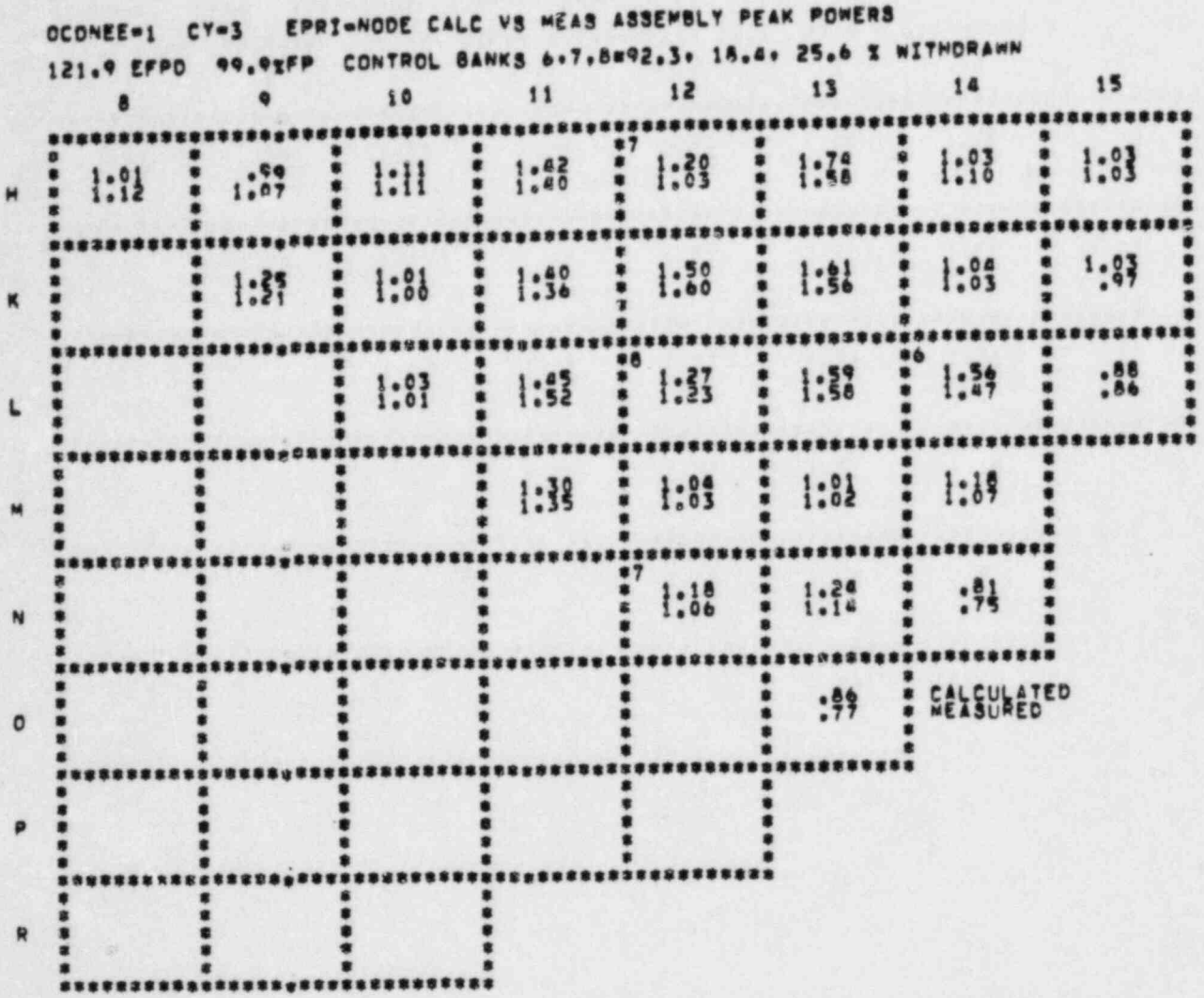
OCONEE=1 CY=3 EPRI=NODE CALC VS MEAS ASSEMBLY PEAK POWERS
121.9 EFPD 99.9%FP CONTROL BANKS 6,7,8=92.3, 18.4, 25.6 % WITHDRAWN
8 9 10 11 12 13 14 15
H
K
L
M
N
O
P
R
1.01 1.12
.99 1.07
1.11 1.11
1.42 1.40
1.20 1.03
1.74 1.58
1.03 1.10
1.03 1.05
1.25 1.21
1.01 1.00
1.40 1.36
1.50 1.60
1.61 1.56
1.04 1.03
1.03 .97
1.03 1.01
1.45 1.52
1.27 1.23
1.59 1.58
1.56 1.47
.88 .84
1.30 1.35
1.04 1.03
1.01 1.02
1.18 1.09
1.18 1.06
1.24 1.14
.81 .75
.86 .77
CALCULATED
MEASURED

Figure 4-78

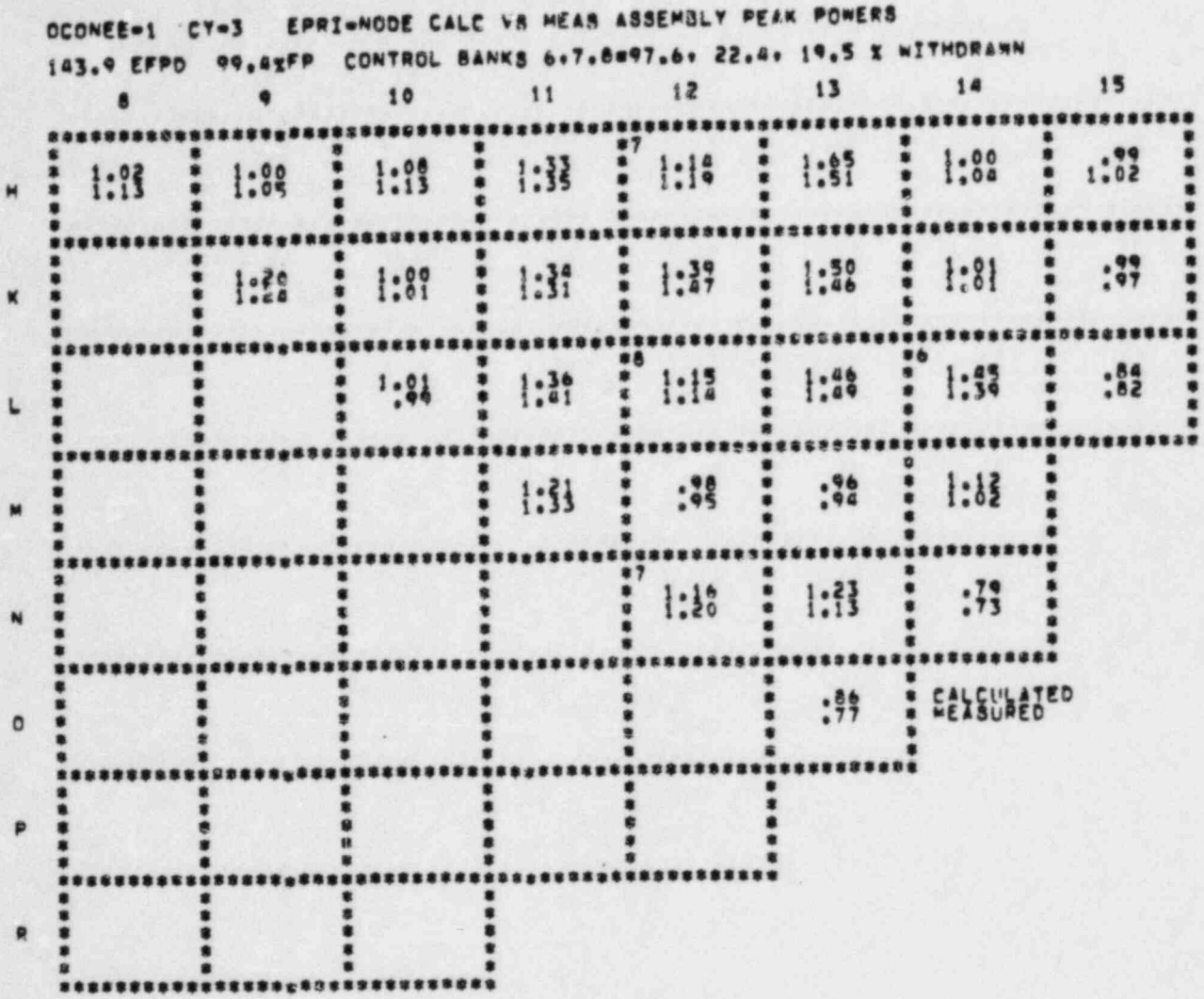
OCONEE-1 CY-3 EPRI-NODE CALC VS MEAS ASSEMBLY PEAK POWERS
143.9 EFPD 99.4%FP CONTROL BANKS 6,7,8=97.6, 22.4, 19.5 % WITHDRAWN
8 9 10 11 12 13 14 15
H K L M N O P R
1.02 1.13
1.00 1.05
1.08 1.13
1.33 1.35
#7 1.14 1.19
1.65 1.51
1.00 1.04
.99 1.02
1.20 1.28
1.00 1.01
1.34 1.31
1.39 1.47
1.50 1.46
1.01 1.01
.99 .97
1.01 .99
1.36 1.41
#8 1.15 1.14
1.46 1.49
#6 1.45 1.39
.84 .82
1.21 1.33
.98 .95
.96 .94
1.12 1.02
#7 1.16 1.20
1.23 1.13
.79 .73
.86 .77
CALCULATED
MEASURED

Figure 4-79

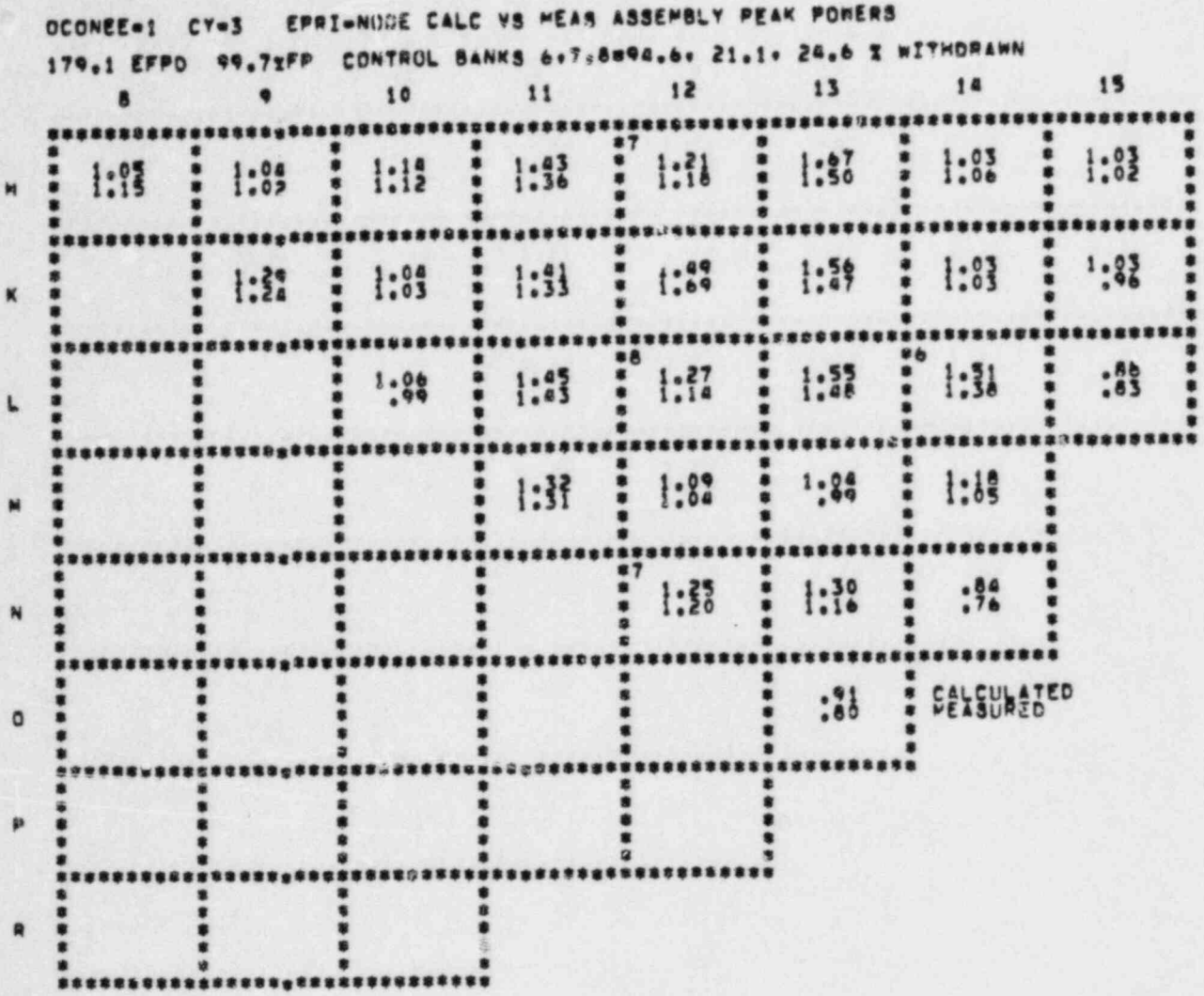
OCONEE-1 CY-3 EPRI-NODE CALC VS MEAS ASSEMBLY PEAK POWERS
179.1 EFPD 99.7%FP CONTROL BANKS 6,7,8=94.6, 21.1, 24.6 % WITHDRAWN
8 9 10 11 12 13 14 15
H K L M N O P R
1.05 1.15
1.04 1.07
1.18 1.12
1.43 1.36
#7 1.21 1.18
1.67 1.50
1.03 1.06
1.03 1.02
1.29 1.24
1.04 1.03
1.41 1.33
1.49 1.69
1.56 1.47
1.03 1.03
1.03 .96
1.06 .99
1.45 1.43
#8 1.27 1.14
#6 1.55 1.48
1.31 1.38
.86 .83
1.32 1.31
1.09 1.04
1.04 .99
1.18 1.05
#7 1.25 1.20
1.30 1.16
.84 .76
.91 .80
CALCULATED
MEASURED

Figure 4-80

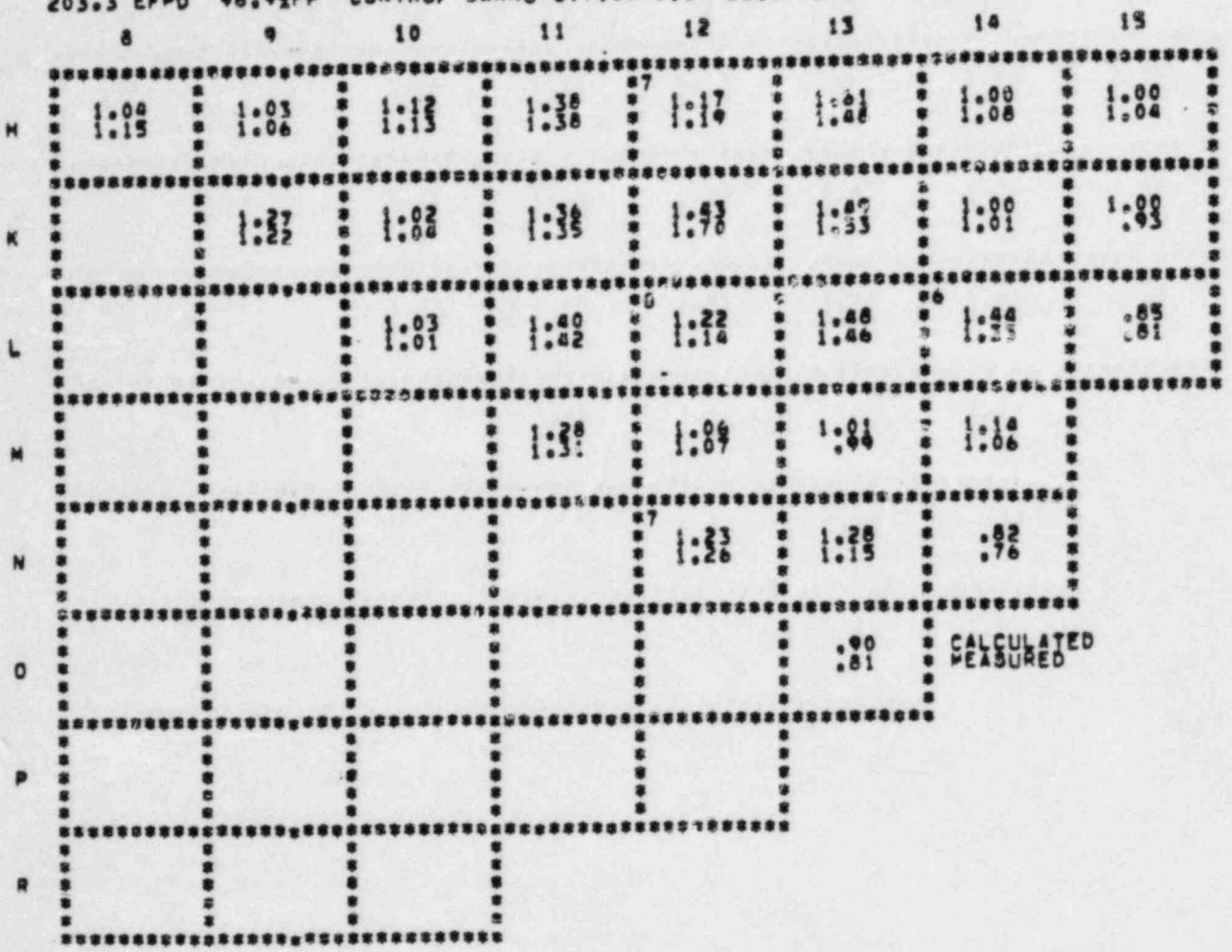
OCONEE-1 CY-3 EPRI-NODE CALC VS MEAS ASSEMBLY PEAK POWERS
203.3 EFPD 98.9%FP CONTROL BANKS 6,7,8=98.5, 22.5, 23.8 % WITHDRAWN
8 9 10 11 12 13 14 15
H
K
L
M
N
O
P
R
1.04 1.15
1.03 1.06
1.12 1.13
1.38 1.38
#7
1.17 1.14
1.01 1.02
1.00 1.08
1.00 1.04
1.27 1.22
1.02 1.04
1.36 1.35
1.43 1.70
1.02 1.03
1.00 1.01
1.00 .93
#8
#6
1.03 1.01
1.40 1.42
1.22 1.14
1.48 1.46
1.44 1.35
.85 .81
1.28 1.31
1.06 1.07
1.01 .94
1.14 1.06
#7
1.23 1.26
1.28 1.15
.82 .76
.90 .81
CALCULATED
MEASURED

Figure 4-81

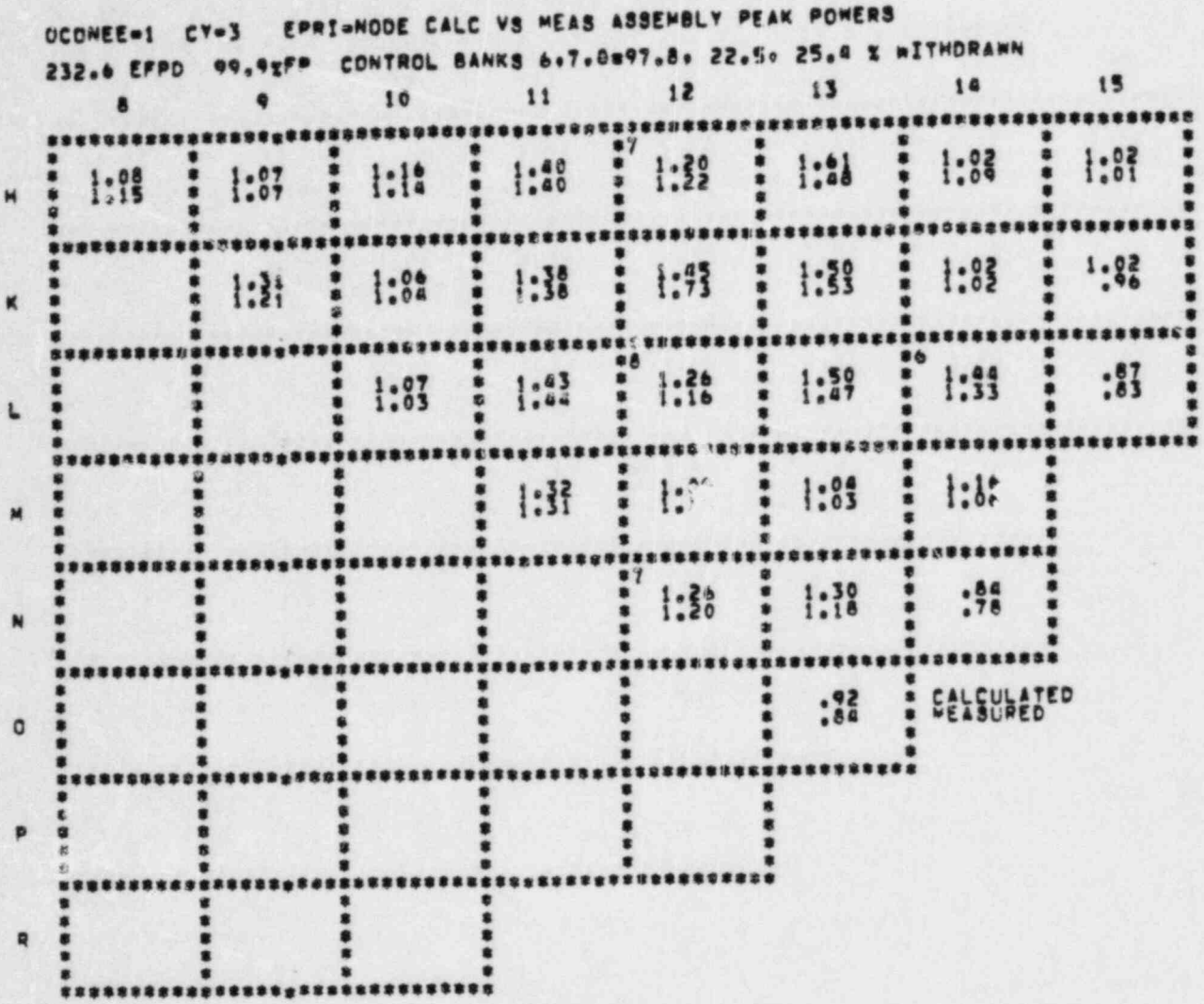
OCONEE-1 CY-3 EPRI-NODE CALC VS MEAS ASSEMBLY PEAK POWERS
232.6 EFPD 99.9%FP CONTROL BANKS 6,7,8=97.8, 22.5, 25.4 % WITHDRAWN
8 9 10 11 12 13 14 15
H
K
L
M
N
O
P
R
1.08 1.15
1.07 1.07
1.16 1.14
1.40 1.40
7
1.20 1.22
1.61 1.48
1.02 1.04
1.02 1.01
1.31 1.21
1.06 1.04
1.38 1.38
1.45 1.73
1.50 1.53
1.02 1.02
1.02 .96
8
1.07 1.03
1.43 1.44
1.26 1.16
1.50 1.47
6
1.44 1.33
.87 .83
1.32 1.31
1.04 1.03
7
1.26 1.20
1.30 1.18
.84 .78
.92 .84
CALCULATED
MEASURED

Figure 4-82

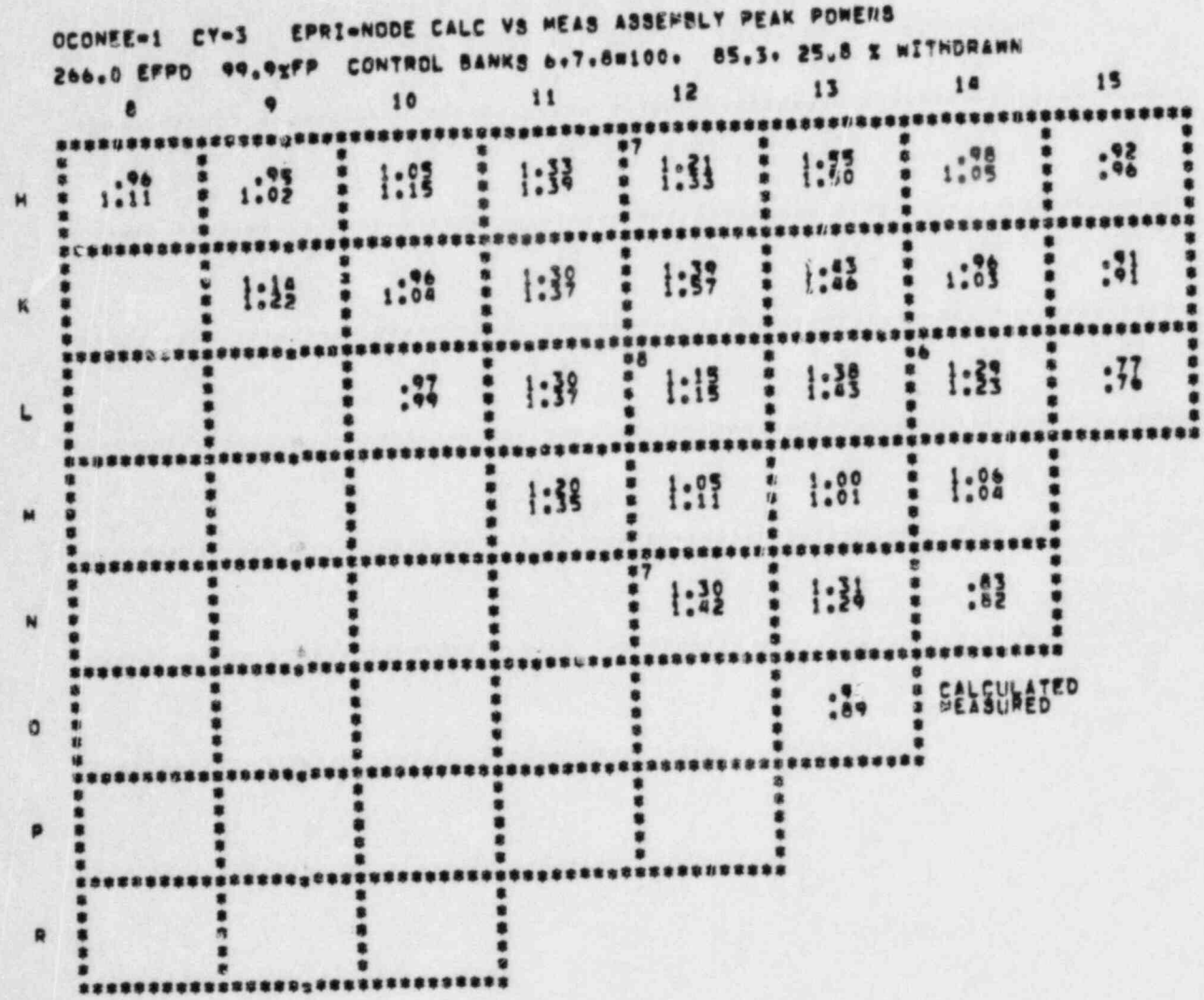
OCONEE-1 CY-3 EPRI-NODE CALC VS MEAS ASSEMBLY PEAK POWERS
266.0 EFPD 99.9%FP CONTROL BANKS 6,7,8@100, 85.3, 25.8 % WITHDRAWN
8 9 10 11 12 13 14 15
H
K
L
M
N
O
P
R
CALCULATED
MEASURED

Figure 4-83

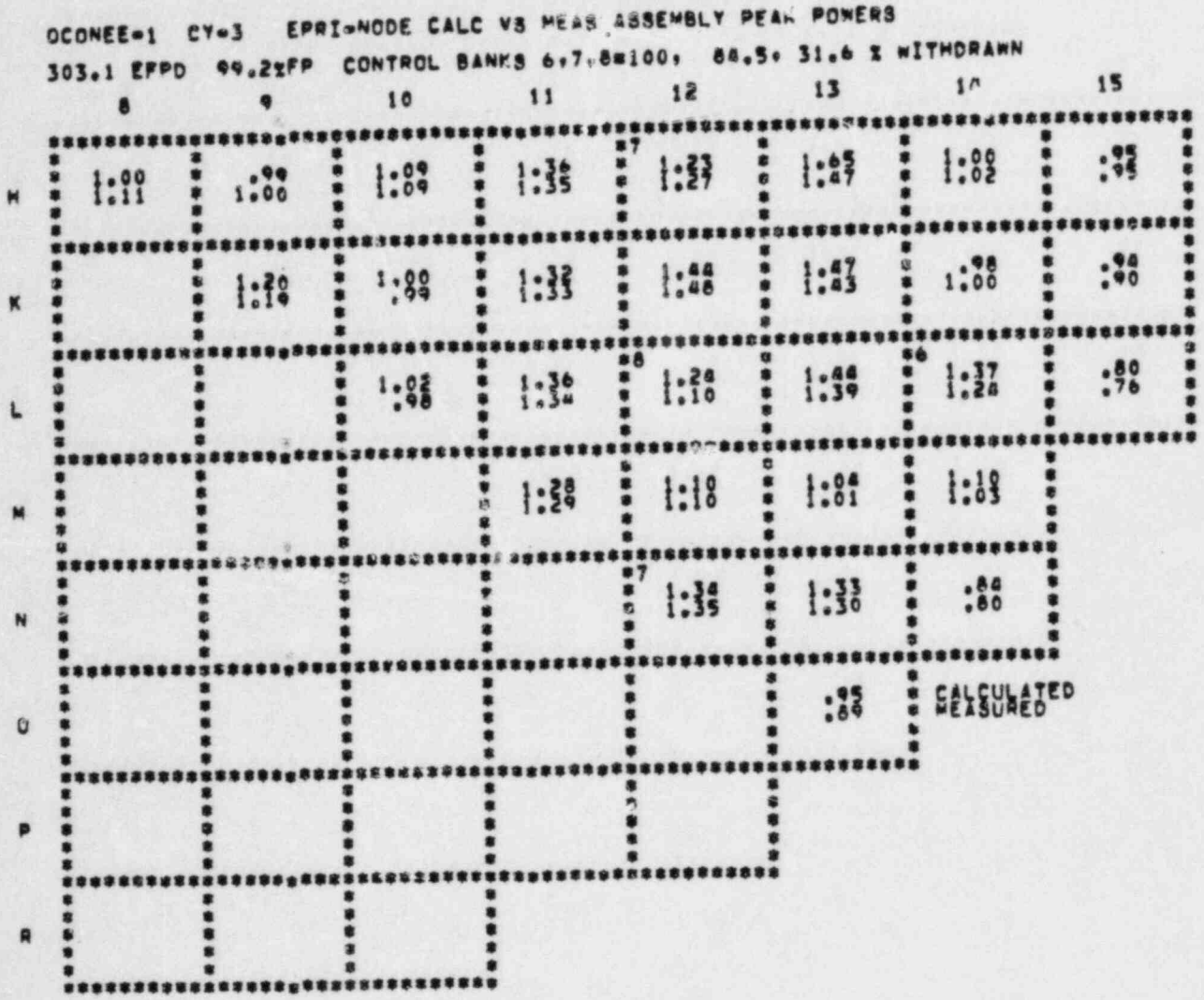
OCONEE=1 CY=3 EPRI=NODE CALC VS MEAS ASSEMBLY PEAK POWERS
303.1 EFPD 99.2%FP CONTROL BANKS 6,7,8=100, 88.5, 31.6 % WITHDRAWN
8 9 10 11 12 13 14 15
H K L M N O P R
1.00 1.11
.99 1.00
1.09 1.09
1.36 1.35
1.23 1.27
1.65 1.47
1.00 1.02
.95 .95
1.20 1.19
1.00 .99
1.32 1.33
1.44 1.46
1.47 1.43
.98 1.00
.94 .90
1.02 .98
1.36 1.34
1.28 1.10
1.44 1.39
1.37 1.28
.80 .76
1.28 1.29
1.10 1.10
1.04 1.01
1.10 1.03
1.34 1.35
1.33 1.30
.84 .80
.95 .89
CALCULATED
MEASURED

Figure 4-84
Oconee 1, Cycle 4
Control Rod Configuration

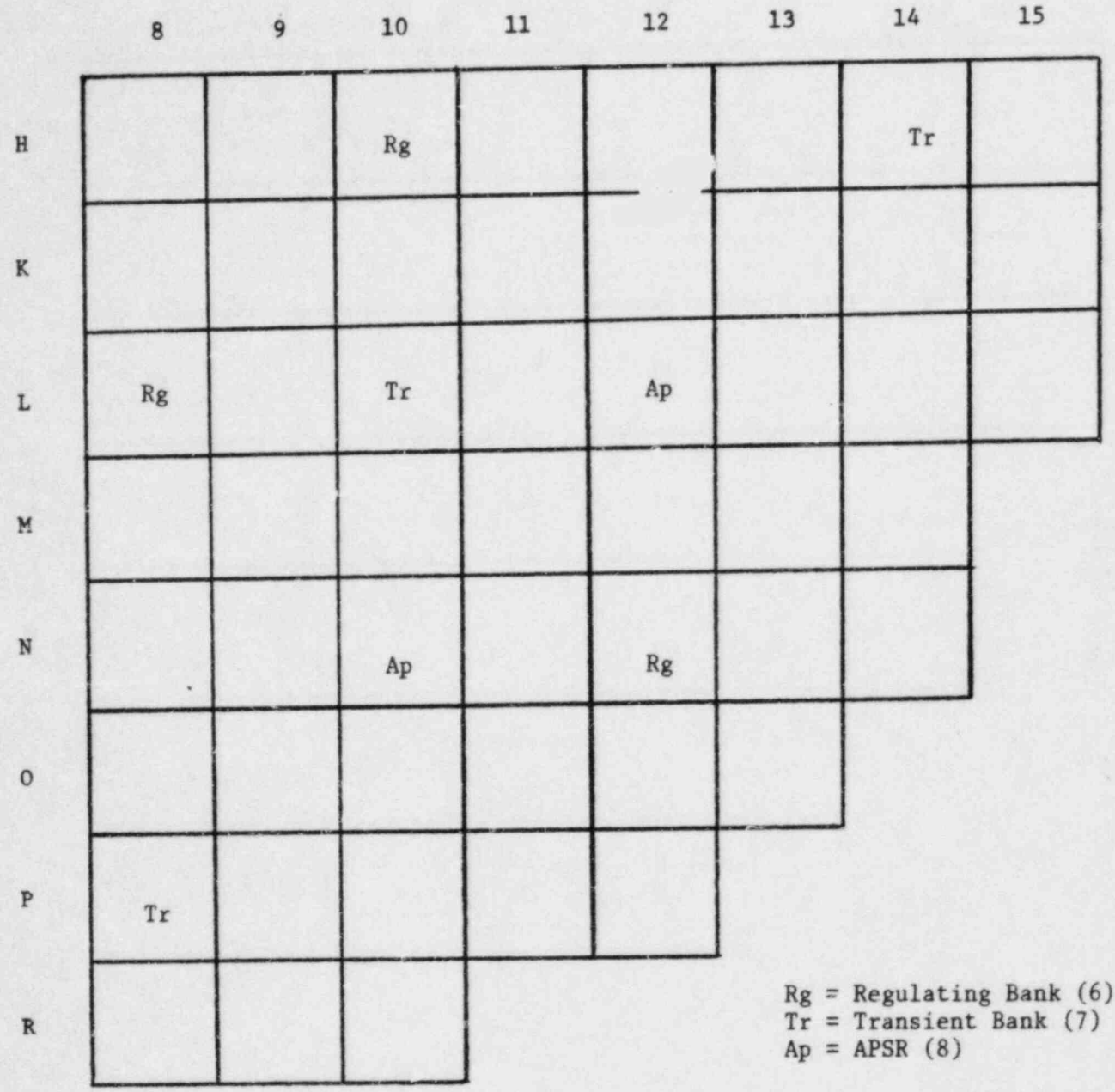

Figure 4-85
Oconee 1, Cycle 4
Quarter Core Loading Diagram

	8	9	10	11	12	13	14	15
H	2.60 4A	2.75 5	3.20 4B	2.60 4A	2.75 5	3.20 4B	3.20 4B	2.79 6
K	2.75 5	3.20 4B	2.75 5	2.75 5	3.20 4B	2.75 5	3.20 4B	2.79 6
L	3.20 4B	2.75 5	3.20 4B	3.20 4B	2.75 5	2.75 5	2.79 6	2.79 6
M	2.60 4A	2.75 5	3.20 4B	2.75 5	2.75 5	3.20 4B	2.79 6	
N	2.75 5	3.20 4B	2.75 5	2.75 5	2.10 2	2.79 6	2.79 6	
O	3.20 4B	2.75 5	2.75 5	3.20 4B	2.79 6	2.79 6		
P	3.20 4B	3.20 4B	2.79 6	2.79 6	2.79 6			
R	2.79 6	2.79 6	2.79 6					

W/O U-235
Batch No.

Figure 4-86
Oconee 1, Cycle 4
Quarter Core Shuffle Pattern

	8	9	10	11	12	13	14	15
H	H-8	H-13	L-13*	H-10	H-15	H-11	L-13*	F
K	O-8	N-12	L-15	K-15	L-11	M-14	K-12	F
L	O-10*	R-10	K-9	K-13	N-14	N-13	F	F
M	L-8	R-9	O-9	O-13	L-14	K-11	F	
N	R-8	M-10	P-12	P-10	** H-13 (CY-1)	F	F	
O	M-8	P-11	O-12	M-9	F	F		
P	O-10*	N-9	F	F	F			
R	F	F	F					

Previous cycle loc.

* Moved from eighth core symmetric location to quarter core symmetric location.
** Re-Insert Batch 2.

Figure 4-87

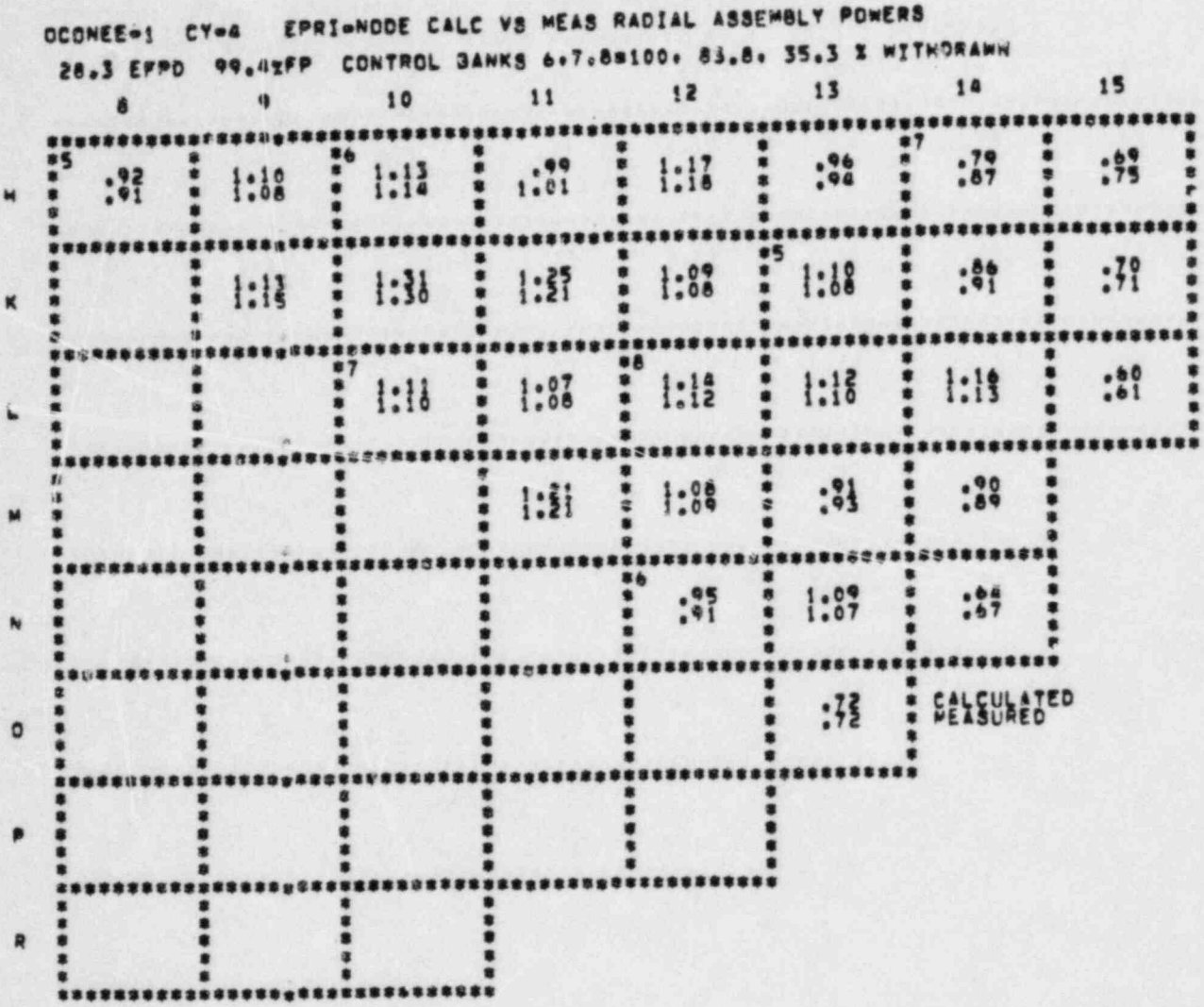
OCONEE-1 CY-4 EPRI-NODE CALC VS MEAS RADIAL ASSEMBLY POWERS
28.3 EFPD 99.4%FP CONTROL BANKS 6,7,8=100, 83.8, 35.3 % WITHDRAWN
8 9 10 11 12 13 14 15
H
K
F
M
N
O
P
R
.92 .91
1.10 1.08
1.13 1.14
.99 1.01
1.17 1.18
.96 .94
.79 .87
.69 .75
1.13 1.15
1.31 1.30
1.25 1.21
1.09 1.08
1.10 1.08
.86 .91
.70 .71
1.11 1.10
1.07 1.08
1.14 1.12
1.12 1.10
1.16 1.13
.80 .81
1.21 1.21
1.08 1.09
.91 .93
.90 .89
.95 .91
1.09 1.07
.64 .67
.72 .72
CALCULATED
MEASURED

Figure 4-88

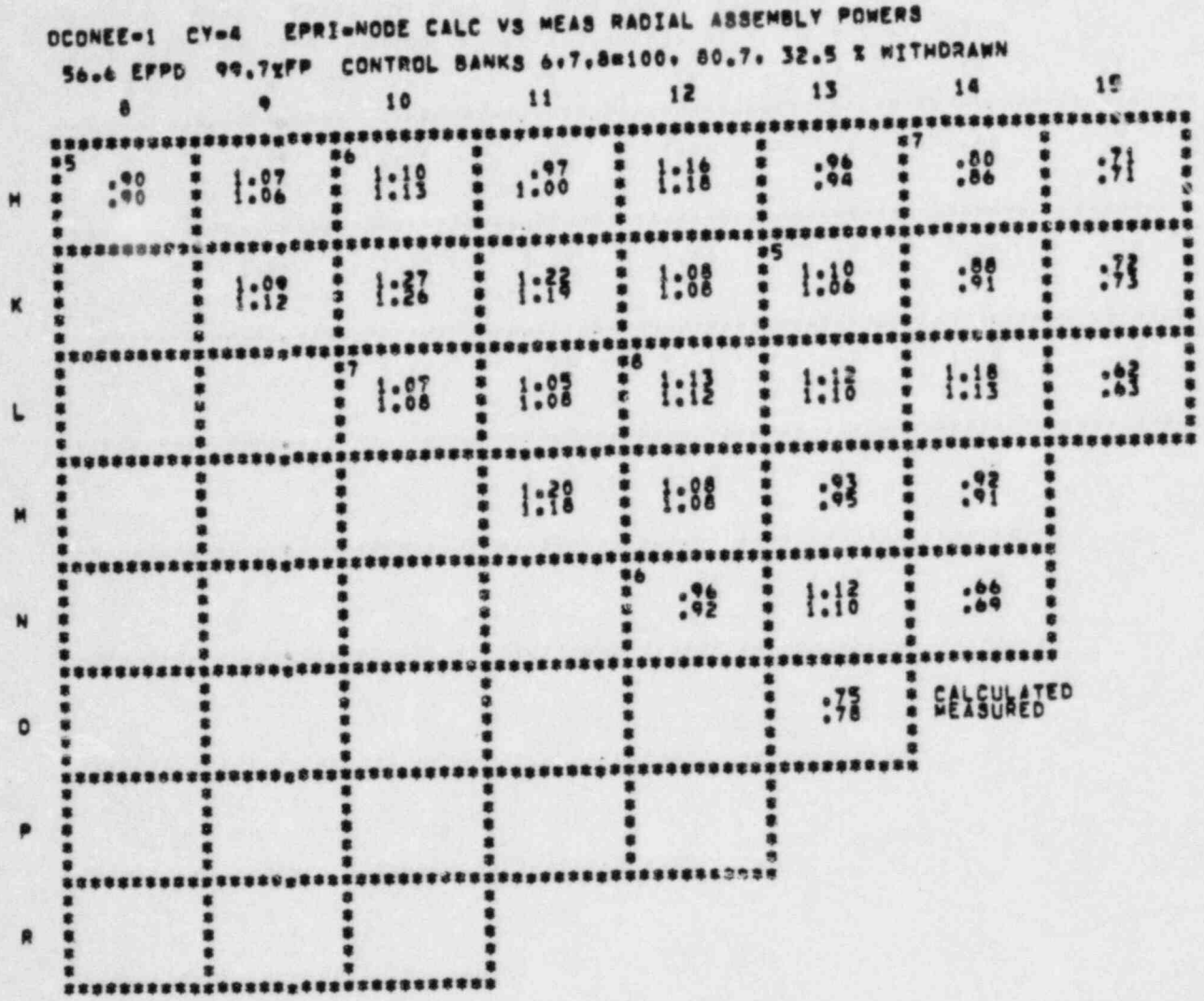
OCONEE-1 CY-4 EPRI-NODE CALC VS MEAS RADIAL ASSEMBLY POWERS
56.6 EFPD 99.7%FP CONTROL BANKS 6,7,8=100, 80.7, 32.5 % WITHDRAWN
8
9
10
11
12
13
14
15
H
K
L
M
N
O
P
R
CALCULATED
MEASURED

Figure 4-89

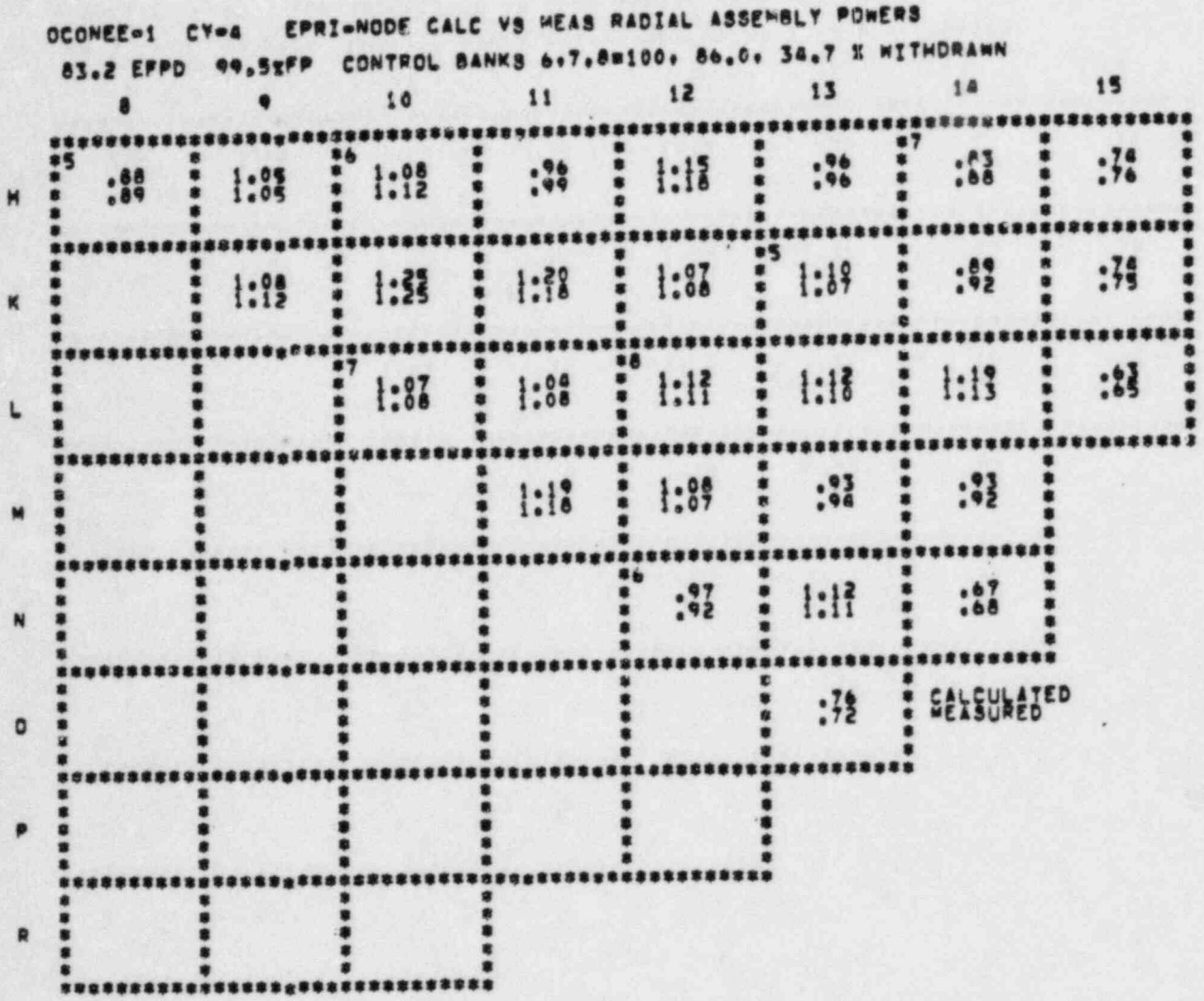
OCONEE-1 CY-4 EPRI-NODE CALC VS MEAS RADIAL ASSEMBLY POWERS
83.2 EFPD 99.5%FP CONTROL BANKS 6,7,8=100, 86.0, 34.7 % WITHDRAWN
8 9 10 11 12 13 14 15
H
K
L
M
N
O
P
R
CALCULATED
MEASURED

Figure 4-90

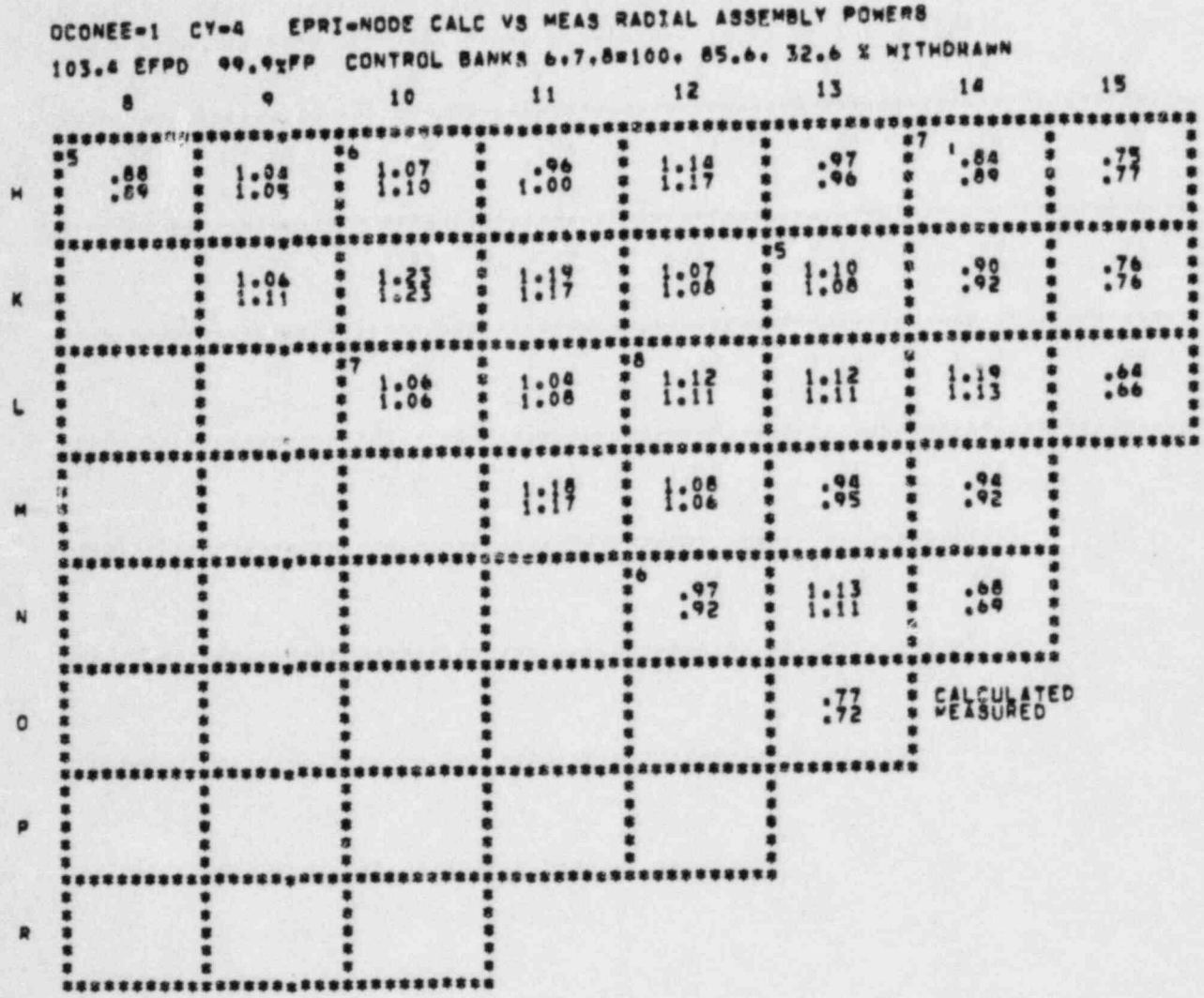
OCONEE-1 CY-4 EPRI-NODE CALC VS MEAS RADIAL ASSEMBLY POWERS
103.4 EFPD 99.9%FP CONTROL BANKS 6,7,8=100, 85.6, 32.6 % WITHDRAWN
8
9
10
11
12
13
14
15
H
K
L
M
N
O
P
R
.88 .89
1.04 1.05
1.07 1.10
.96 1.00
1.14 1.17
.97 .96
.84 .89
.75 .77
1.04 1.11
1.23 1.23
1.19 1.17
1.07 1.08
1.10 1.08
.90 .92
.76 .76
1.06 1.06
1.04 1.08
1.12 1.11
1.12 1.11
1.19 1.13
.64 .66
1.18 1.17
1.08 1.06
.94 .95
.94 .92
.97 .92
1.13 1.11
.68 .69
.77 .72
CALCULATED
MEASURED

Figure 4-91

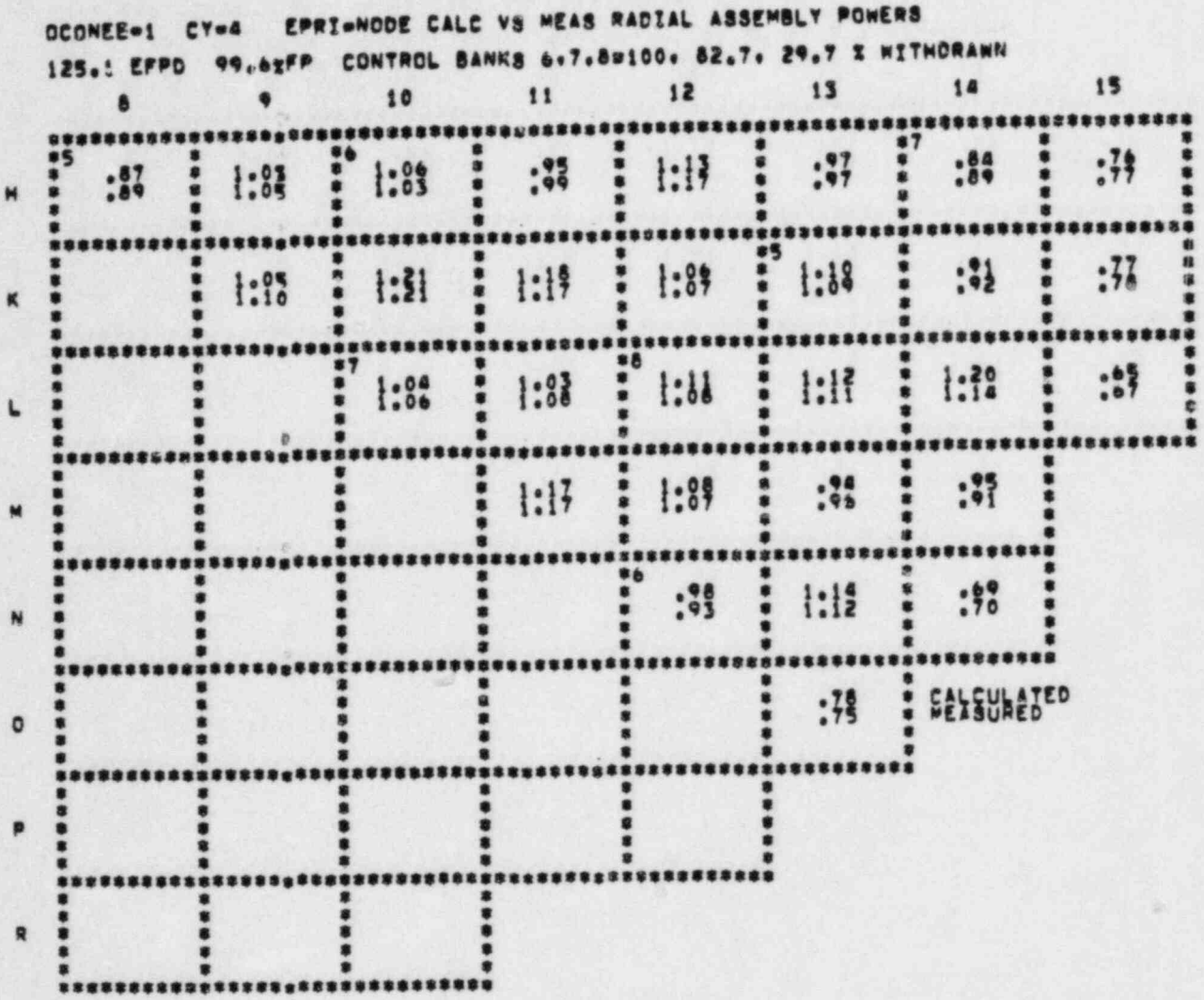
OCONEE-1 CY-4 EPRI-NODE CALC VS MEAS RADIAL ASSEMBLY POWERS
125.1 EFPD 99.6%FP CONTROL BANKS 6,7,8=100, 82.7, 29.7 % WITHDRAWN
8 9 10 11 12 13 14 15
H K L M N O P R
CALCULATED
MEASURED

Figure 4-92

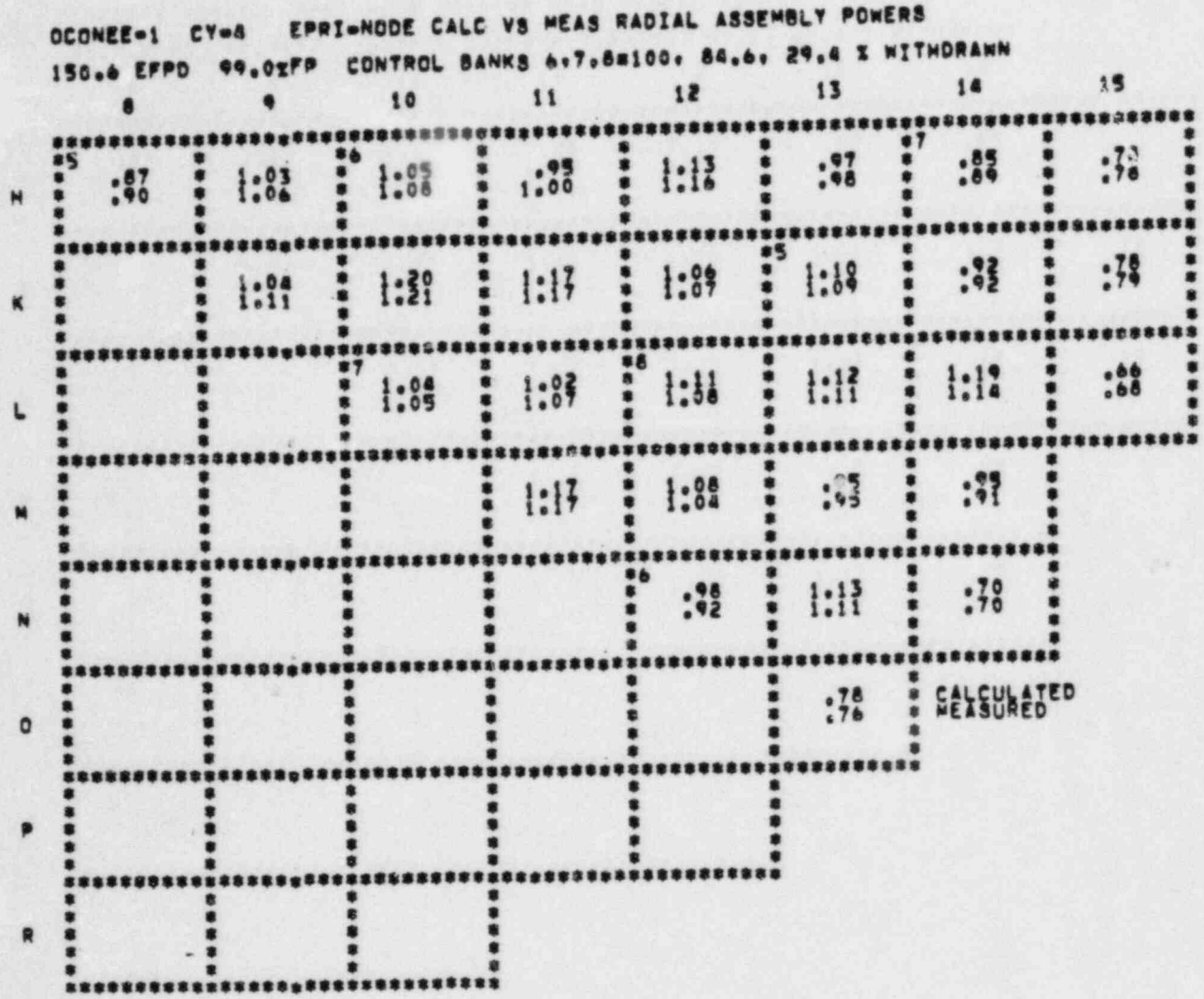
OCONEE-1 CY-8 EPRI-NODE CALC VS MEAS RADIAL ASSEMBLY POWERS
150.6 EFPD 99.0%FP CONTROL BANKS 6,7,8=100, 84.6, 29.4 % WITHDRAWN
8 9 10 11 12 13 14 15
H K L M N O P R
.87 .90
1.03 1.06
1.05 1.08
.99 1.00
1.13 1.16
.97 .98
.85 .89
.78 .78
1.04 1.11
1.20 1.21
1.17 1.17
1.06 1.07
1.10 1.04
.92 .92
.78 .79
1.04 1.05
1.02 1.07
1.11 1.08
1.12 1.11
1.19 1.14
.66 .68
1.17 1.17
1.08 1.04
.95 .95
.95 .91
.98 .92
1.13 1.11
.70 .70
.78 .76
CALCULATED
MEASURED

Figure 4-93

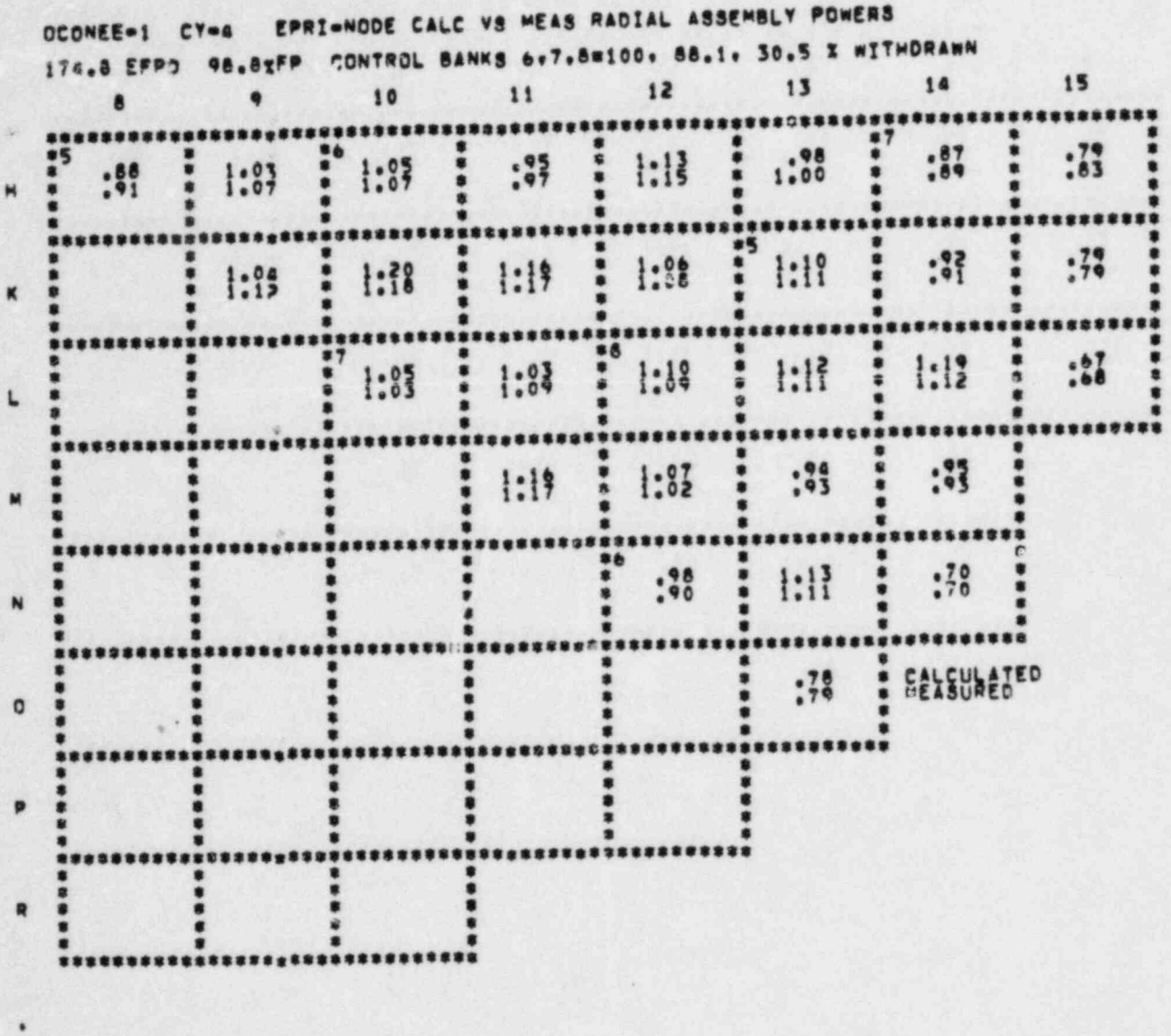
OCONEE-1 CY-4 EPRI-NODE CALC VS MEAS RADIAL ASSEMBLY POWERS
174.8 EFPD 98.8%FP CONTROL BANKS 6,7,8=100, 88.1, 30.5 % WITHDRAWN
8 9 10 11 12 13 14 15
H K L M N O P R
.88 .91
1.03 1.07
1.05 1.07
.95 .97
1.13 1.15
.98 1.00
.87 .89
.79 .83
1.06 1.15
1.20 1.18
1.19 1.17
1.06 1.08
1.10 1.11
.92 .91
.79 .79
1.05 1.03
1.03 1.04
1.10 1.04
1.12 1.11
1.19 1.12
.87 .88
1.19 1.17
1.07 1.02
.94 .93
.95 .93
.98 .90
1.13 1.11
.70 .70
.78 .79
CALCULATED
MEASURED

Figure 4-94

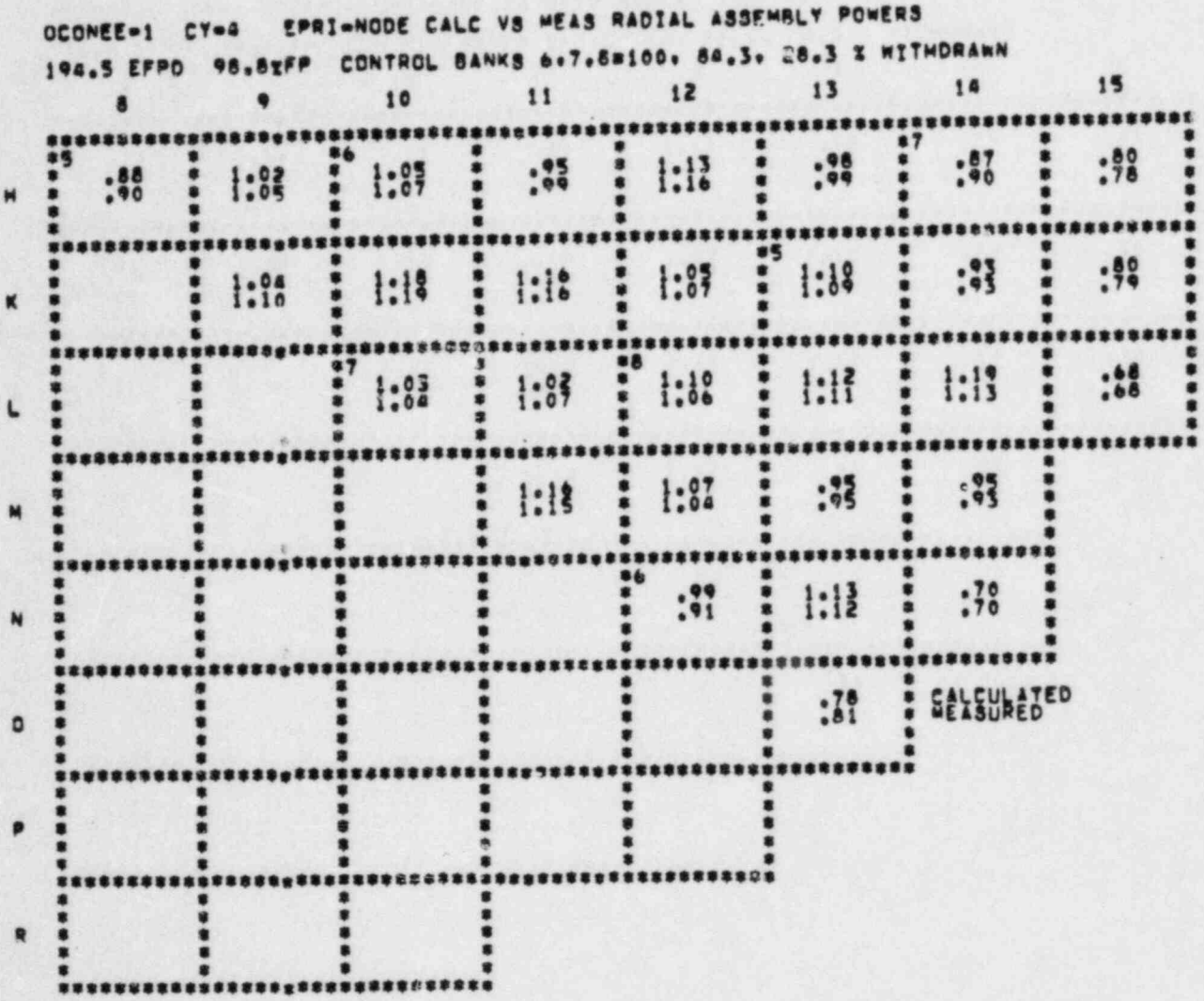
OCONEE-1 CY-4 EPRI-NODE CALC VS MEAS RADIAL ASSEMBLY POWERS
194.5 EFPD 98.8%FP CONTROL BANKS 6,7,8=100, 84.3, 28.3 % WITHDRAWN
8 9 10 11 12 13 14 15
H K L M N O P R
.88 .90
1.02 1.05
1.05 1.07
.95 .99
1.13 1.16
.98 .99
.87 .90
.80 .78
1.04 1.10
1.18 1.19
1.16 1.16
1.05 1.07
1.10 1.04
.93 .93
.80 .79
1.03 1.04
1.02 1.07
1.10 1.06
1.12 1.11
1.19 1.13
.68 .68
1.18 1.15
1.07 1.04
.95 .95
.95 .93
.99 .91
1.13 1.12
.70 .70
.78 .81
CALCULATED
MEASURED

Figure 4-95

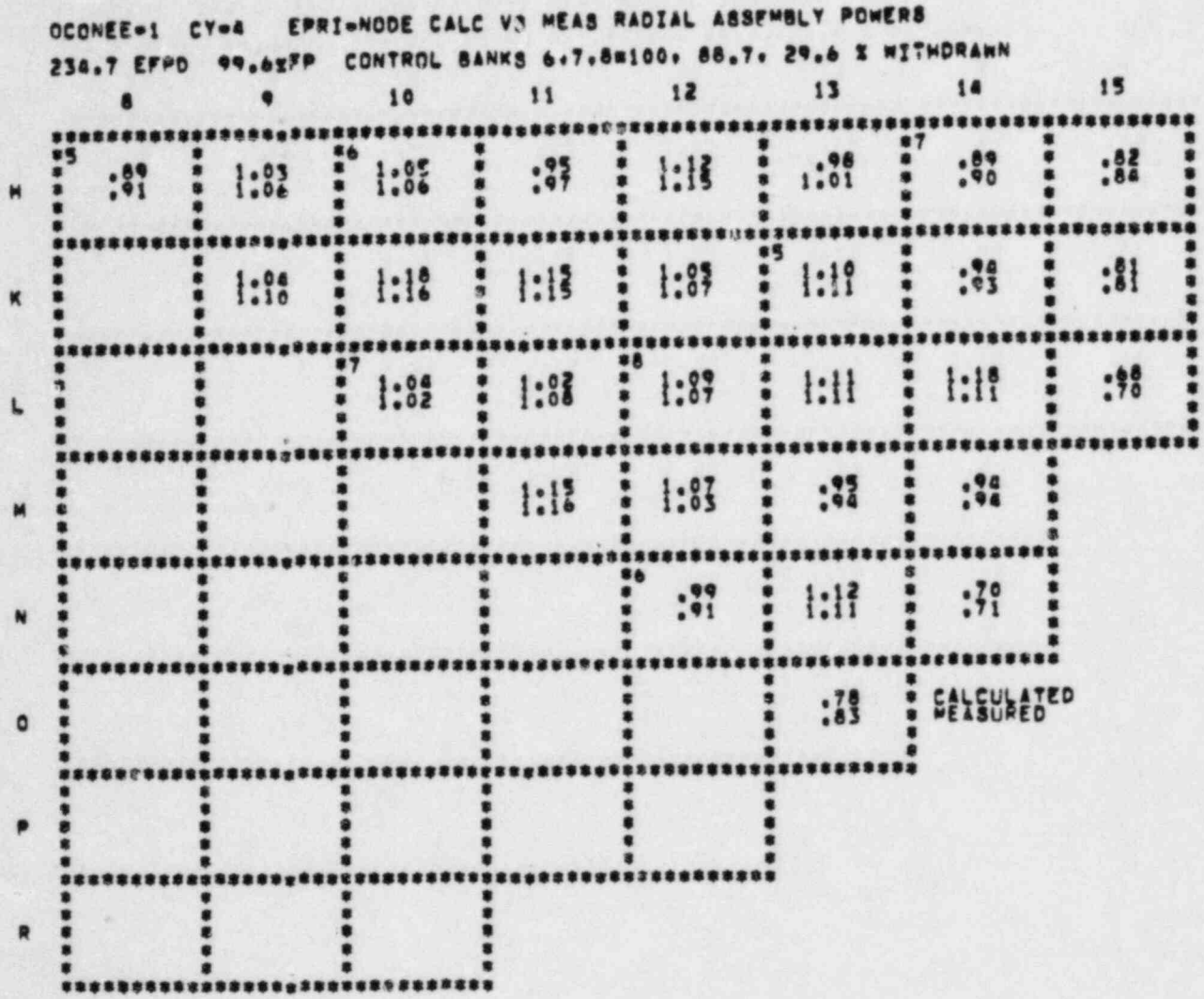
OCONEE-1 CY-4 EPRI-NODE CALC VS MEAS RADIAL ASSEMBLY POWERS
234.7 EFPD 99.6%FP CONTROL BANKS 6,7,8=100, 88.7, 29.6 % WITHDRAWN
8 9 10 11 12 13 14 15
H
K
L
M
N
O
P
R
CALCULATED
MEASURED

Figure 4-96

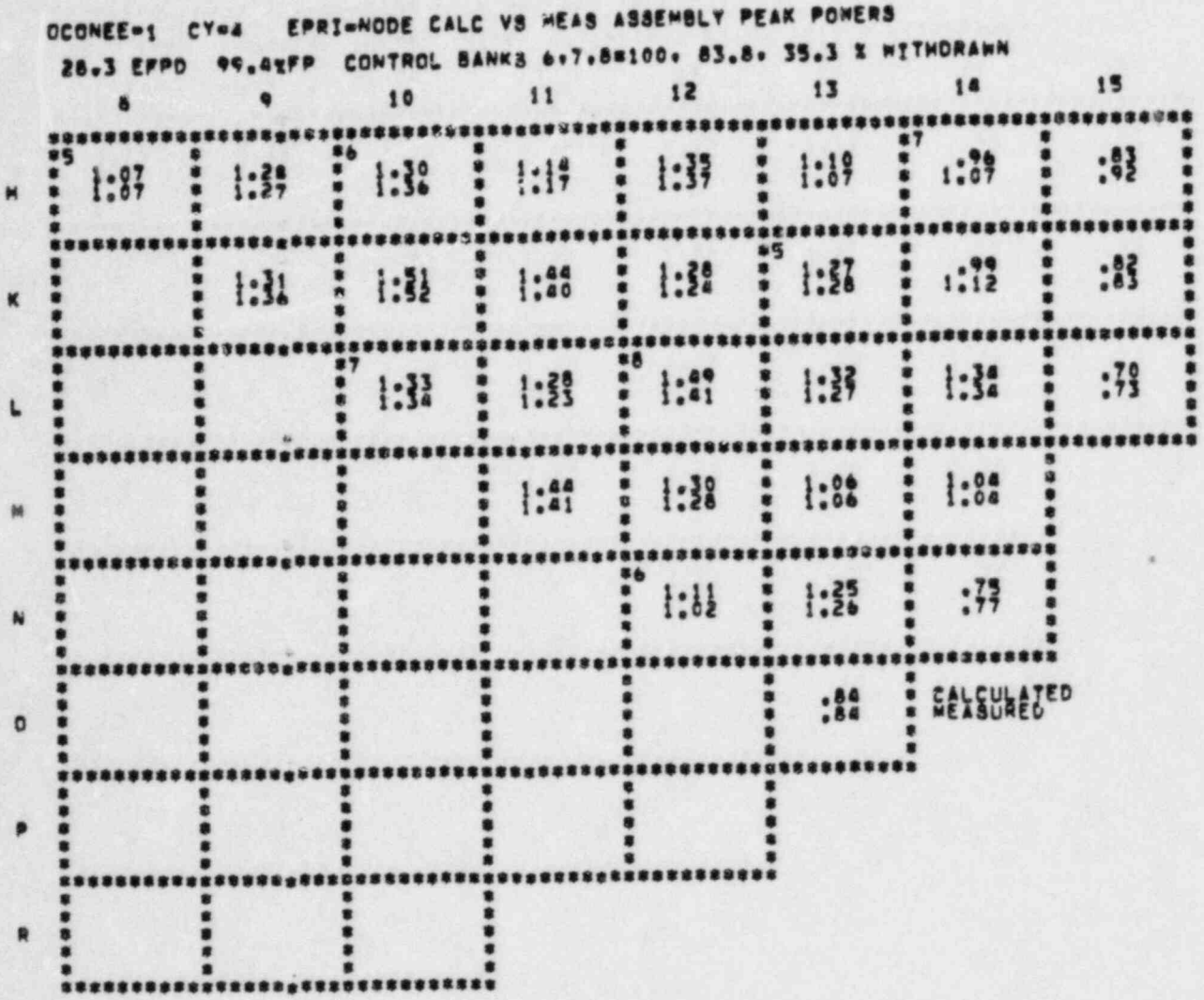
OCONEE-1 CY-4 EPRI-NODE CALC VS MEAS ASSEMBLY PEAK POWERS
28.3 EFPD 99.4%FP CONTROL BANKS 6,7,8=100, 83.8, 35.3 % WITHDRAWN
8 9 10 11 12 13 14 15
H
K
L
M
N
O
P
R
CALCULATED
MEASURED

Figure 4-97

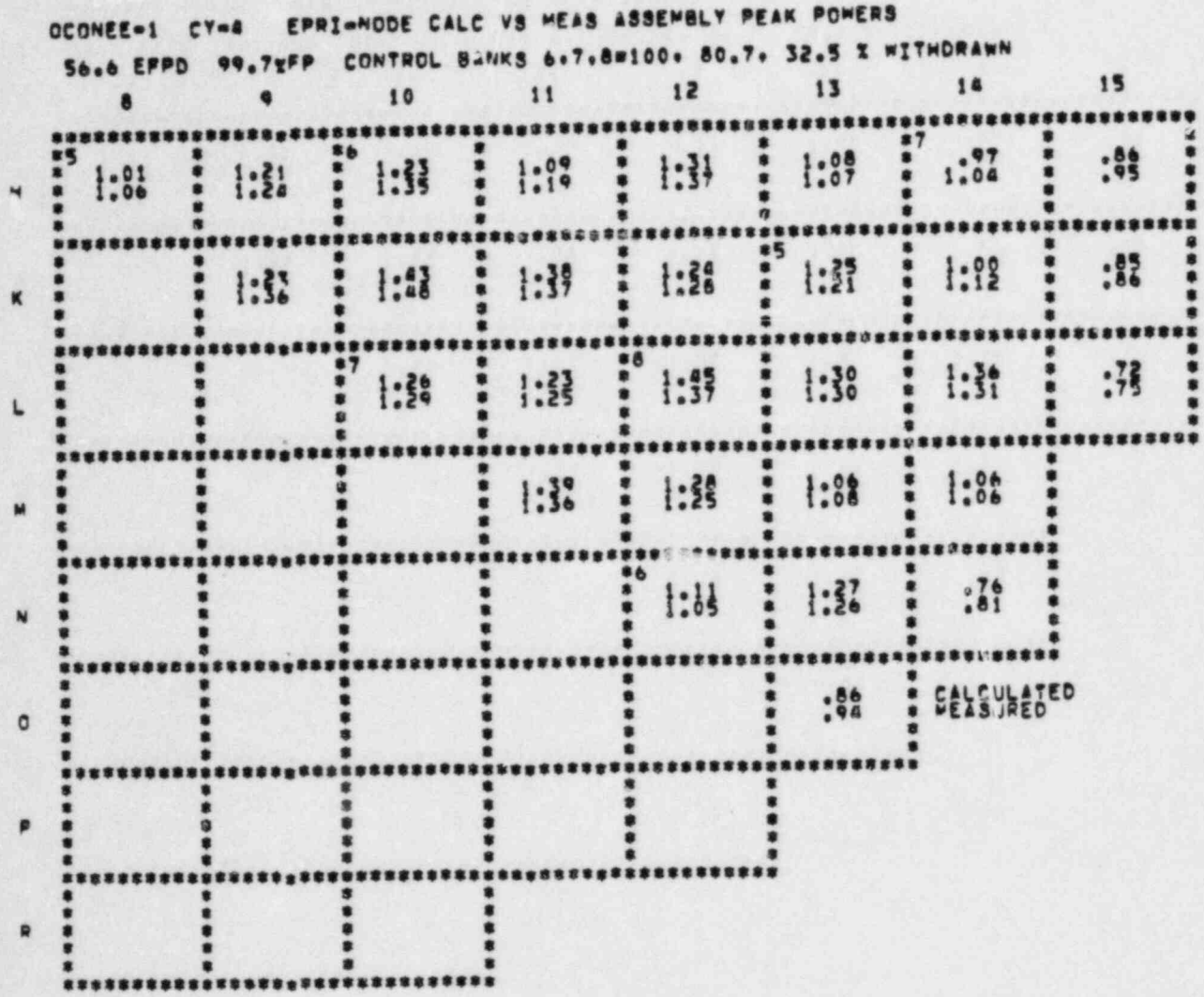
OCONEE-1 CY-4 EPRI-NODE CALC VS MEAS ASSEMBLY PEAK POWERS
56.6 EFPD 99.7%FP CONTROL BANKS 6,7,8@100, 80.7, 32.5 % WITHDRAWN
8
9
10
11
12
13
14
15
J
K
L
M
N
O
P
R
5
1.01
1.06
1.21
1.28
6
1.23
1.35
1.09
1.19
1.31
1.37
1.08
1.07
7
.97
1.04
.86
.95
7
1.23
1.36
1.43
1.48
1.38
1.37
1.24
1.28
5
1.25
1.21
1.00
1.12
.85
.86
7
1.26
1.29
1.23
1.25
8
1.45
1.37
1.30
1.30
1.36
1.31
.72
.75
1.39
1.36
1.28
1.25
1.06
1.08
1.06
1.06
6
1.11
1.05
1.27
1.26
.76
.81
.86
.94
CALCULATED
MEASURED

Figure 4-98

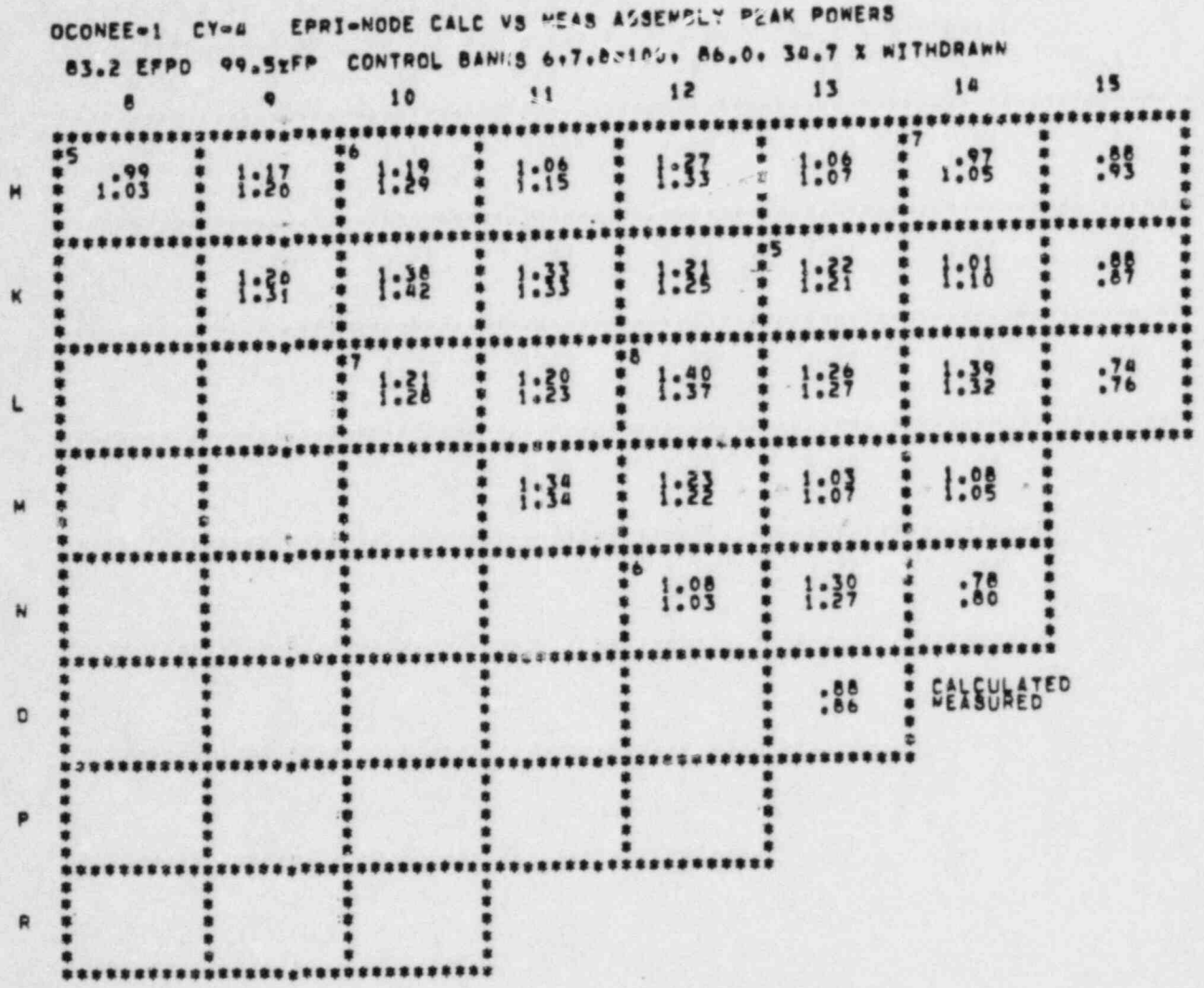
OCONEE-1 CY-4 EPRI-NODE CALC VS MEAS ASSEMBLY PEAK POWERS
83.2 EFPD 99.5%FP CONTROL BANKS 6,7,8@100, 86.0, 30.7 % WITHDRAWN
8 9 10 11 12 13 14 15
H K L M N D P R
.99 1.03
1.17 1.20
1.19 1.29
1.06 1.15
1.27 1.33
1.06 1.07
.97 1.05
.88 .93
1.20 1.31
1.38 1.42
1.33 1.33
1.21 1.25
1.22 1.21
1.01 1.10
.88 .87
1.21 1.28
1.20 1.23
1.40 1.37
1.26 1.27
1.39 1.32
.74 .76
1.34 1.34
1.23 1.22
1.03 1.07
1.08 1.05
1.08 1.03
1.30 1.27
.78 .80
.88 .86
CALCULATED
MEASURED

Figure 4-99

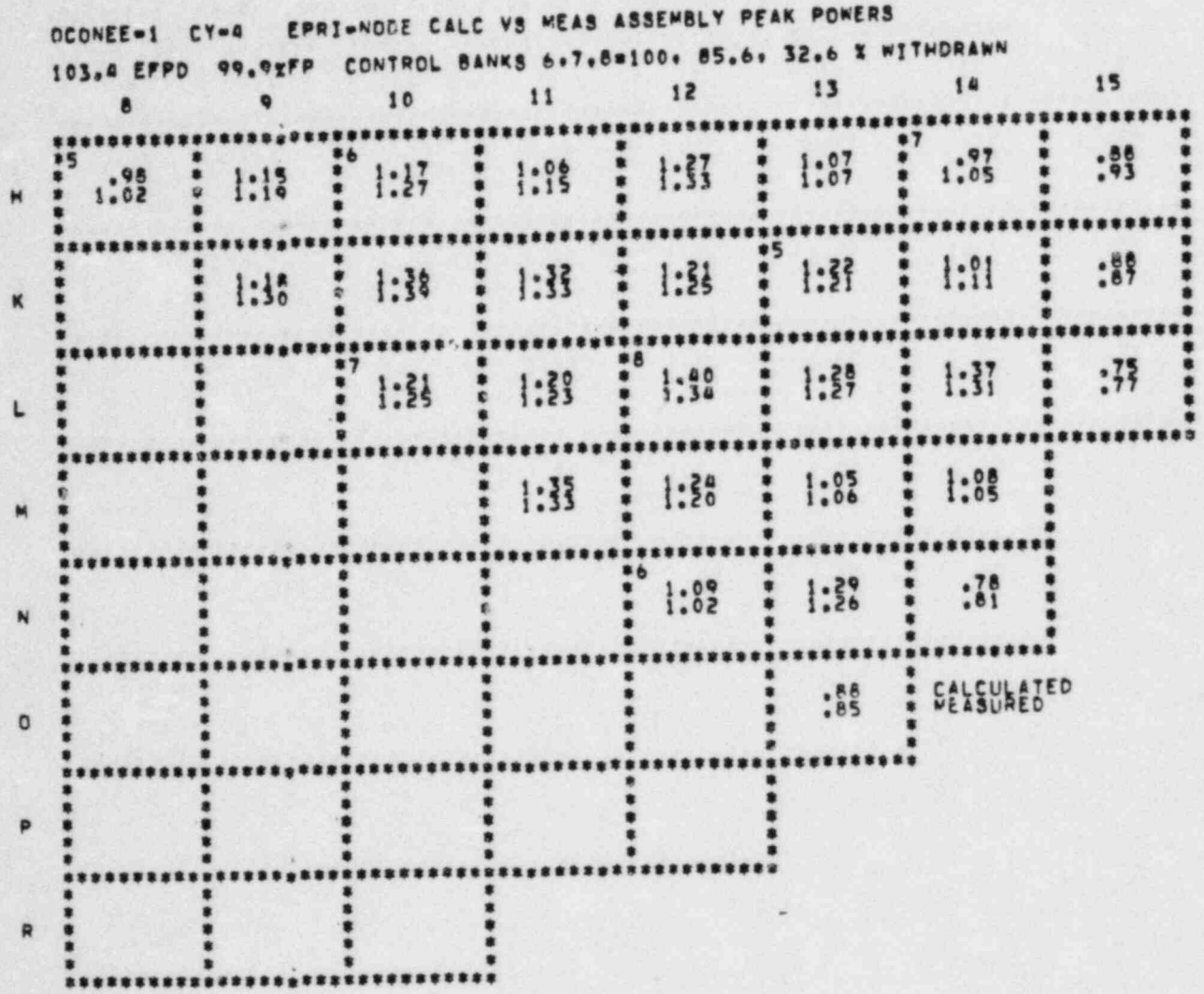
OCONEE-1 CY-4 EPRI-NODE CALC VS MEAS ASSEMBLY PEAK POWERS
103.4 EFPD 99.9%FP CONTROL BANKS 6,7,8=100, 85.6, 32.6 % WITHDRAWN
8 9 10 11 12 13 14 15
H K L M N O P R
.98 1.02
1.15 1.14
1.17 1.27
1.06 1.15
1.27 1.53
1.07 1.07
.97 1.05
.88 .93
1.18 1.30
1.36 1.38
1.32 1.33
1.21 1.25
1.22 1.21
1.01 1.11
.88 .87
1.21 1.25
1.20 1.23
1.40 1.34
1.28 1.27
1.37 1.31
.75 .77
1.35 1.33
1.24 1.20
1.05 1.06
1.08 1.05
1.09 1.02
1.29 1.26
.78 .81
.88 .85
CALCULATED
MEASURED

Figure 4-100

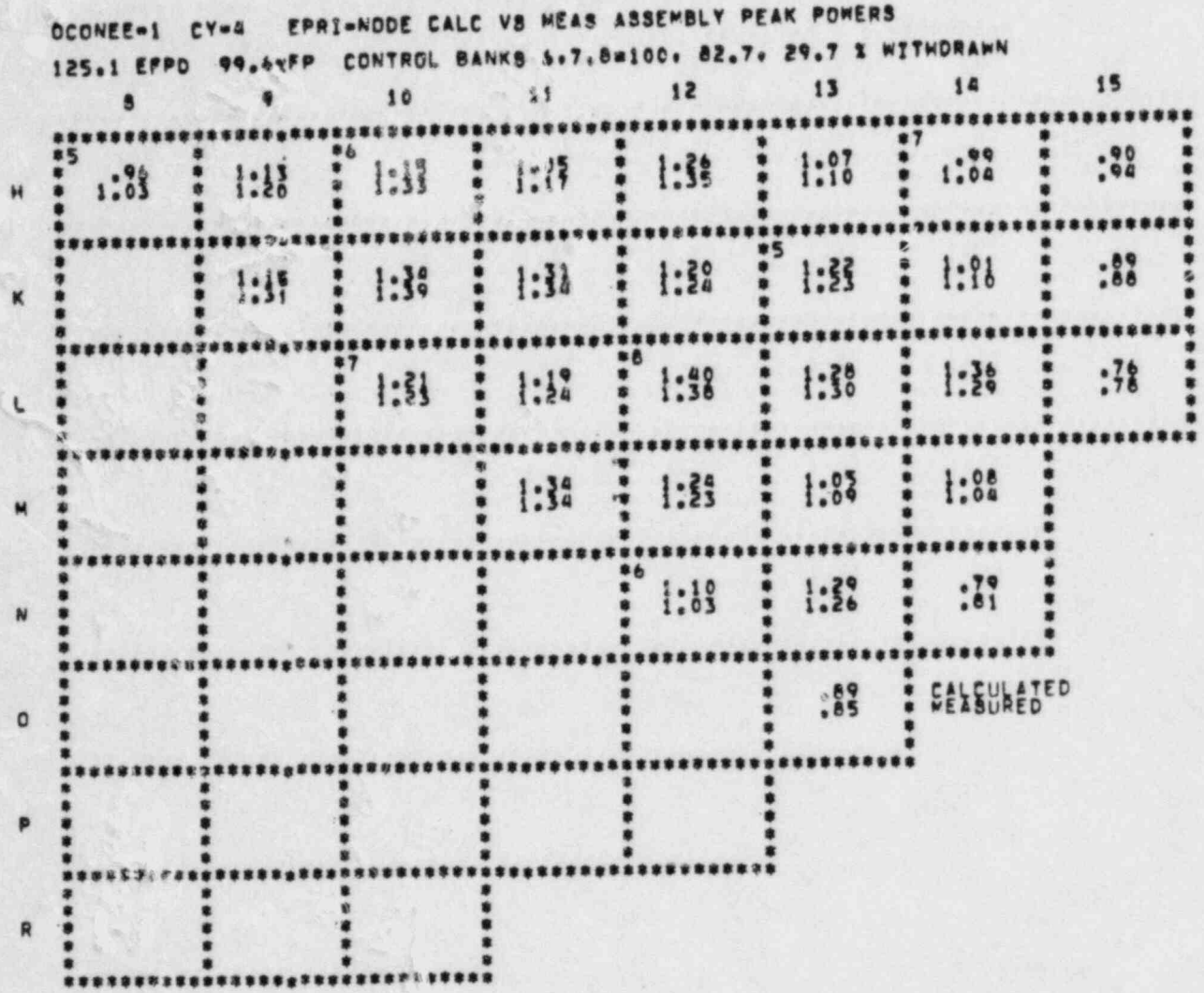
OCONEE-1 CY-4 EPRI-NODE CALC VS MEAS ASSEMBLY PEAK POWERS
125.1 EFPD 99.4 EFP CONTROL BANKS 5,7,8=100, 82.7, 29.7 % WITHDRAWN
8 9 10 11 12 13 14 15
H K L M N O P R
CALCULATED
MEASURED

Figure 4-101

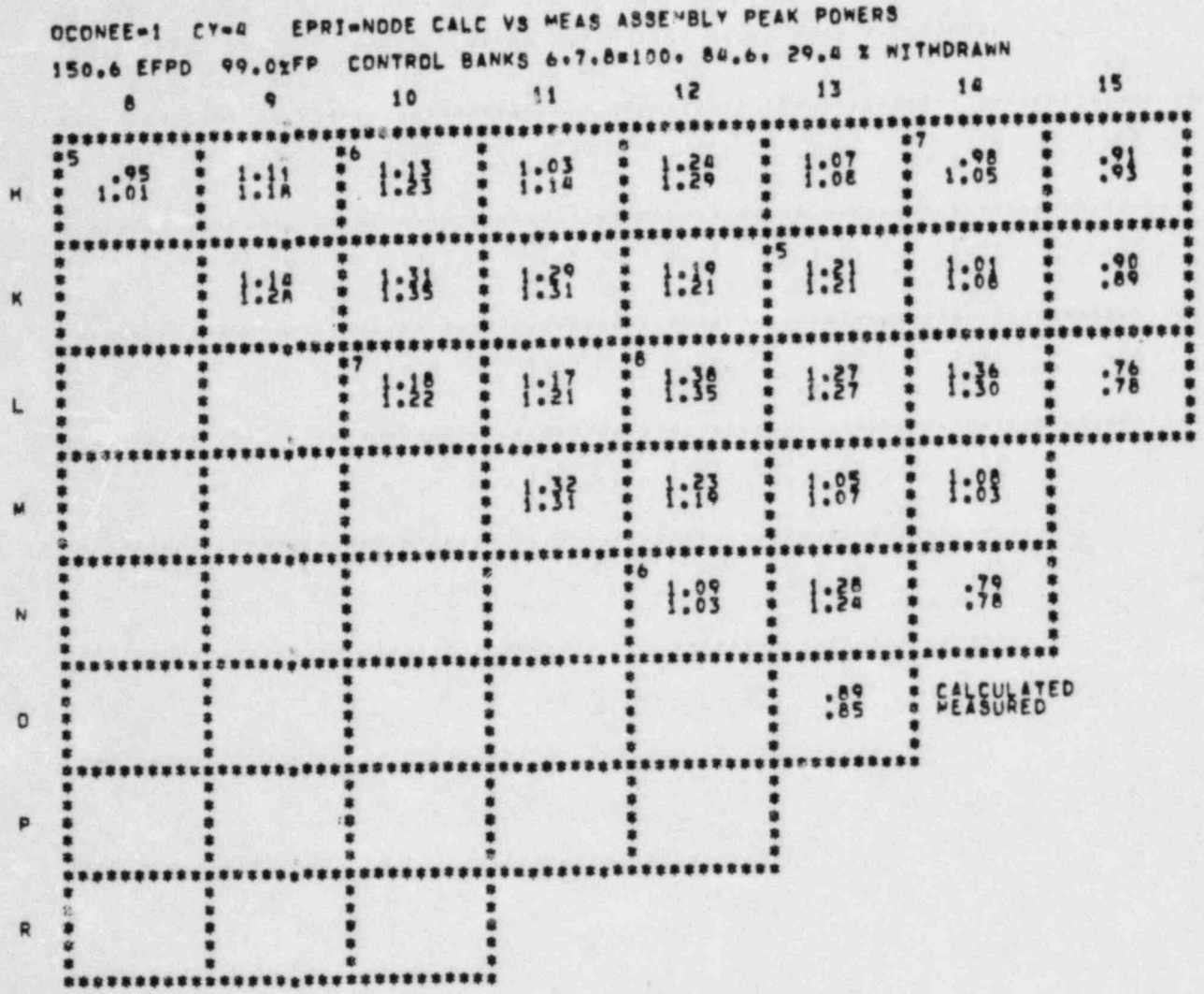
OCONEE-1 CY-4 EPRI-NODE CALC VS MEAS ASSEMBLY PEAK POWERS
150.6 EFPD 99.0%FP CONTROL BANKS 6,7,8=100, 84.6, 29.4 % WITHDRAWN
8 9 10 11 12 13 14 15
H K L M N O P R
.95 1.01
1.11 1.14
1.13 1.23
1.03 1.14
1.24 1.29
1.07 1.08
.98 1.05
.91 .93
1.14 1.24
1.31 1.35
1.29 1.31
1.19 1.21
1.21 1.21
1.01 1.08
.90 .89
1.18 1.22
1.17 1.21
1.38 1.35
1.27 1.27
1.36 1.30
.76 .78
1.32 1.31
1.23 1.14
1.05 1.07
1.08 1.03
1.09 1.03
1.28 1.24
.79 .78
.89 .85
CALCULATED
MEASURED

Figure 4-102

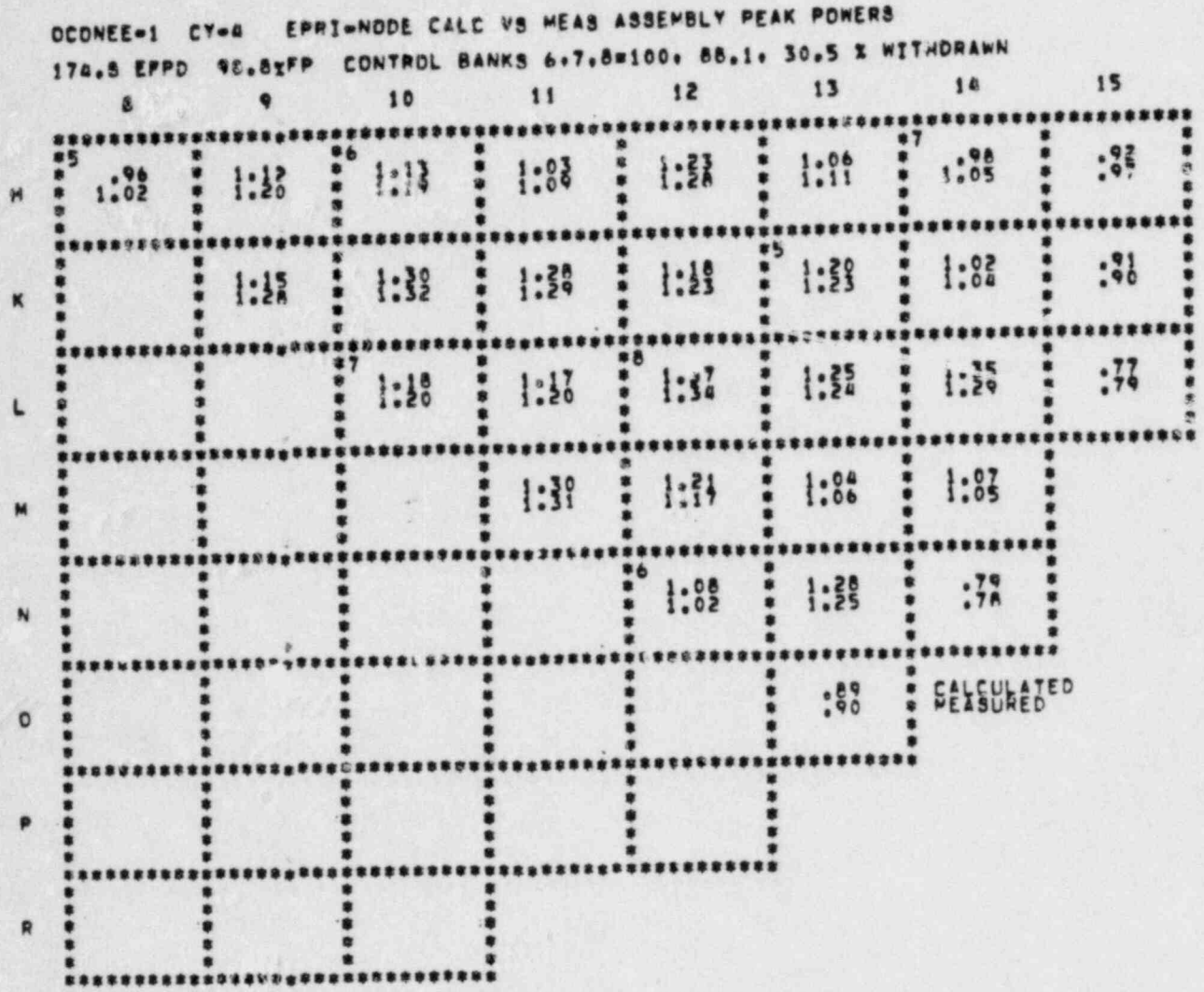
OCONEE-1 CY-8 EPRI-NODE CALC VS MEAS ASSEMBLY PEAK POWERS
174.8 EFPD 98.8%FP CONTROL BANKS 6,7,8=100, 88.1, 30.5 % WITHDRAWN
8 9 10 11 12 13 14 15
H
K
L
M
N
O
P
R
CALCULATED
MEASURED

Figure 4-103

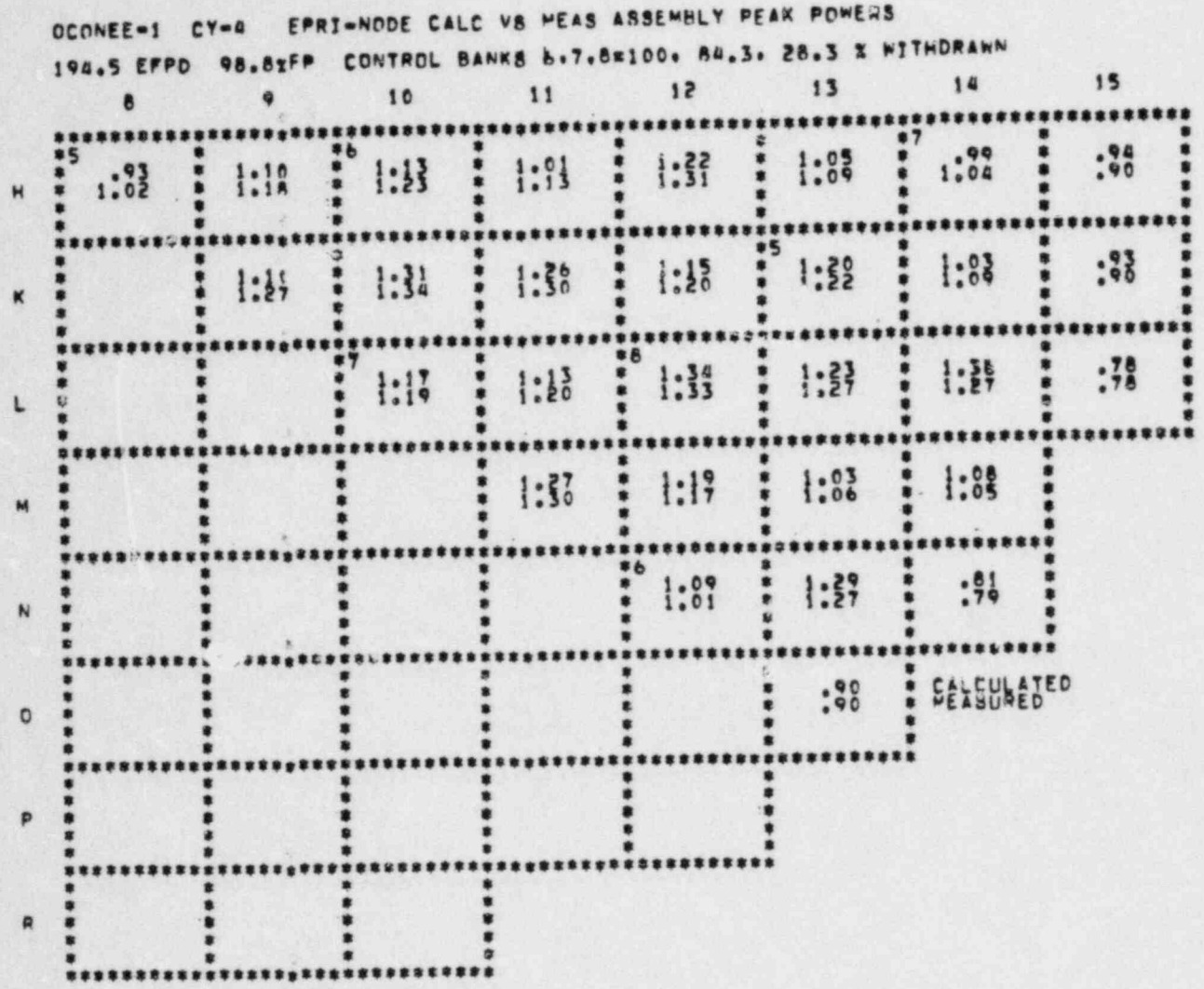
OCONEE-1 CY-8 EPRI-NODE CALC VS MEAS ASSEMBLY PEAK POWERS
194.5 EFPD 98.8%FP CONTROL BANKS 6,7,8=100, 84.3, 28.3 % WITHDRAWN
8 9 10 11 12 13 14 15
H
K
L
M
N
O
P
R
.93 1.02
1.10 1.18
1.13 1.23
1.01 1.13
1.22 1.31
1.05 1.09
.99 1.04
.94 .90
1.11 1.27
1.31 1.34
1.26 1.30
1.15 1.20
1.20 1.22
1.03 1.04
.93 .90
1.17 1.19
1.13 1.20
1.34 1.33
1.23 1.27
1.36 1.27
.78 .78
1.27 1.30
1.19 1.17
1.03 1.06
1.08 1.05
1.09 1.01
1.29 1.27
.81 .79
.90 .90
CALCULATED
MEASURED

Figure 4-104

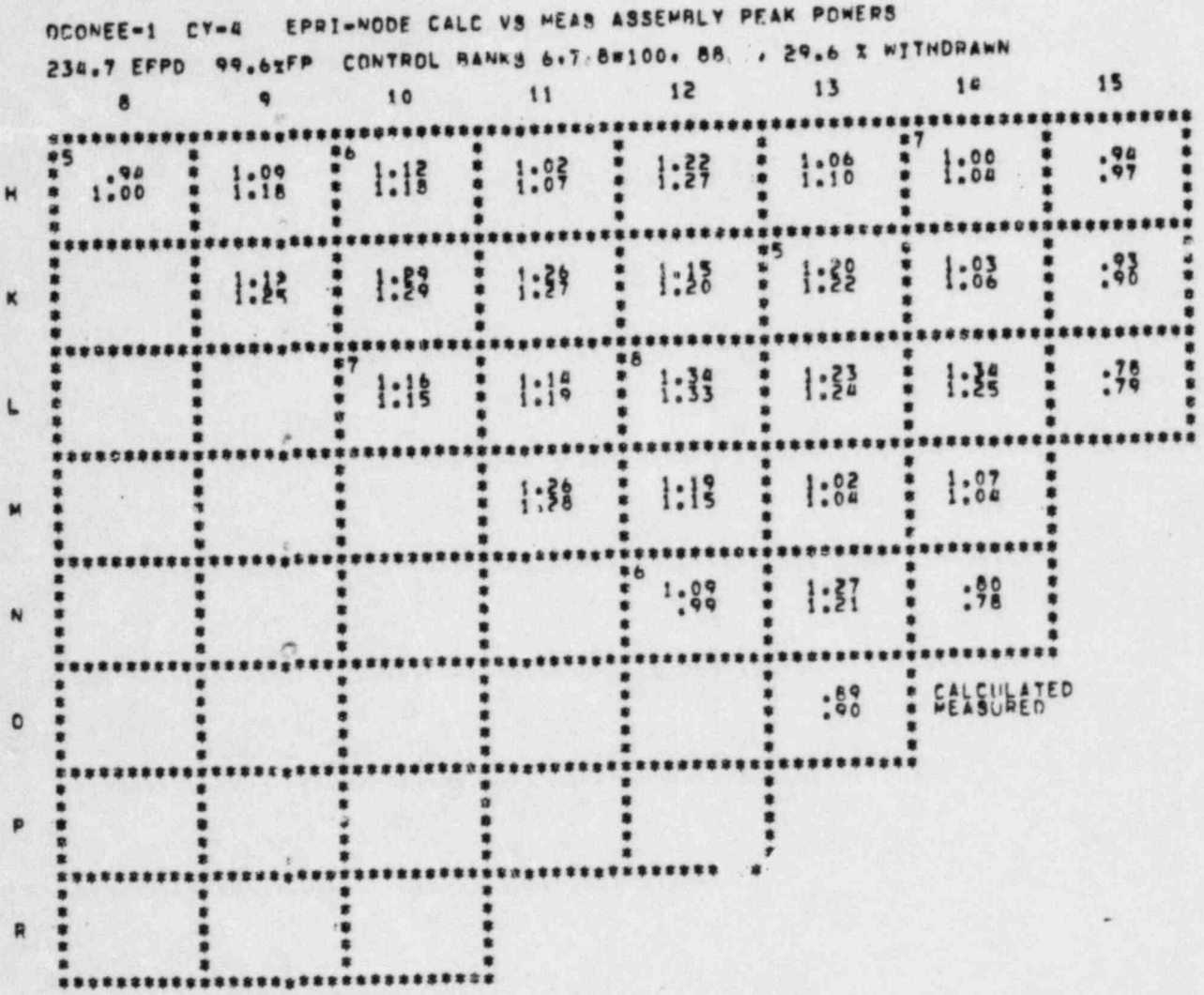
OCONEE-1 CY-4 EPRI-NODE CALC VS MEAS ASSEMBLY PEAK POWERS
234.7 EFPD 99.6%FP CONTROL BANKS 6,7,8=100, 88 , 29.6 % WITHDRAWN
8 9 10 11 12 13 14 15
H
K
L
M
N
O
P
R
.98 1.00
1.09 1.18
1.12 1.18
1.02 1.07
1.22 1.27
1.06 1.10
1.00 1.04
.98 .97
1.12 1.25
1.29 1.29
1.26 1.27
1.15 1.20
1.20 1.22
1.03 1.06
.93 .90
1.16 1.15
1.18 1.19
1.34 1.33
1.23 1.24
1.34 1.25
.78 .79
1.26 1.28
1.19 1.15
1.02 1.04
1.07 1.04
1.09 .99
1.27 1.21
.80 .78
.89 .90
CALCULATED
MEASURED

Figure 4-105
Oconee 1, Cycle 5
Control Rod Configuration

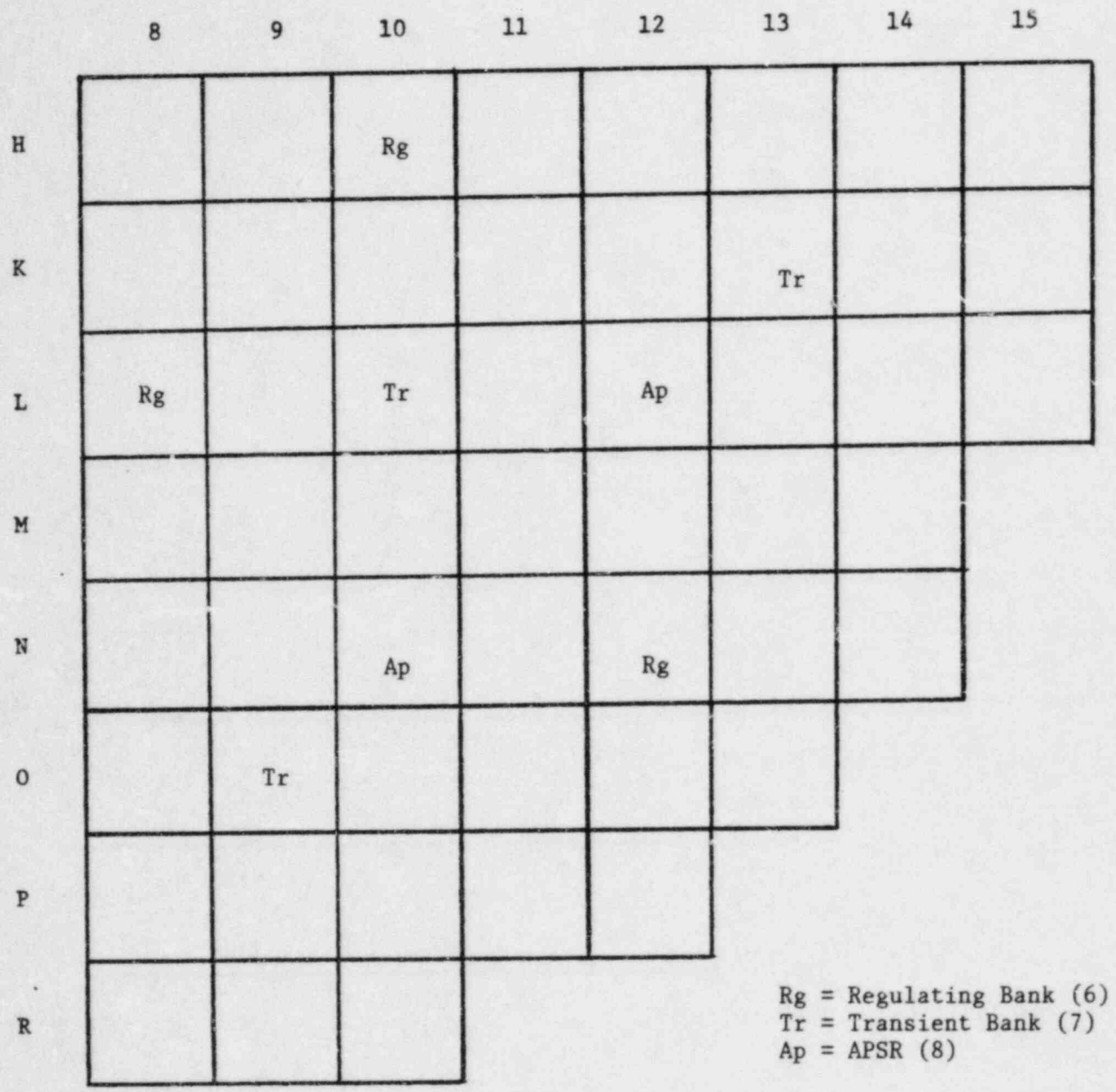

Figure 4-106
Oconee 1, Cycle 5
Quarter Core Loading Diagram

	8	9	10	11	12	13	14	15
H	* 3.20 4B	2.75 5	2.75 5	* 3.20 4B	3.02 7	2.75 5	2.79 6	3.02 7
K	2.75 5	3.02 7	2.75 5	2.79 6	2.75 5	2.79 6	2.75 5	3.02 7
L	2.75 5	2.75 5	2.75 5	2.79 6	2.79 6	2.75 5	3.02 7	3.02 7
M	* 3.20 4B	2.79 6	2.79 6	2.75 5	2.79 6	2.75 5	3.02 7	
N	3.02 7	2.75 5	2.79 6	2.79 6	2.79 6	2.79 6	3.02 7	
O	2.75 5	2.79 6	2.75 5	2.75 5	2.79 6	3.02 7		
P	2.79 6	2.75 5	3.02 7	3.02 7	3.02 7			
R	3.02 7	3.02 7	3.02 7					

W/O U-235
Batch No.

* Location of thrice burned 4B assemblies.

Figure 4-107
Oconee 1, Cycle 5
Quarter Core Shuffle Pattern

	8	9	10	11	12	13	14	15
H	K-14	H-9	H-12	M-13**	F	M-11*	H-15	F
K	K-8	F	L-12	N-14	M-12	L-14	K-11	F
L	N-8	N-10	K-13	K-15	N-13	K-10	F	F
M	M-13**	P-12	R-9	O-9	L-15	L-13	F	
N	F	N-11	O-12	R-10	O-13	M-14	F	
O	M-11*	P-10	L-9	O-10	P-11	F		
P	R-8	M-9	F	F	F			
R	F	F	F					

Previous cycle loc.

* Assembly location formerly on diagonal placed on the core flat.
** Moved from eighth core symmetric location to quarter core symmetric location.

Figure 4-108

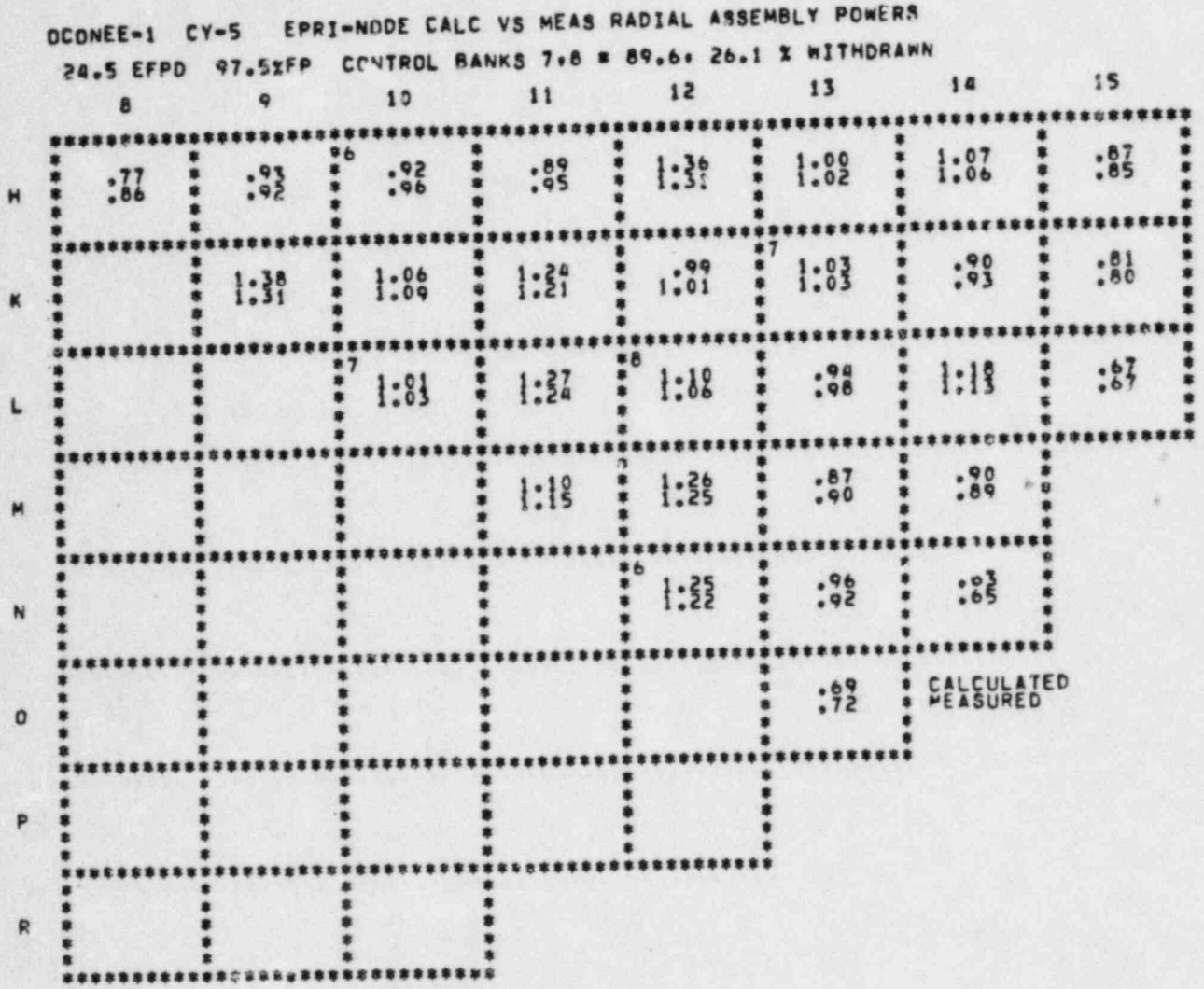
OCONEE-1 CY-5 EPRI-NODE CALC VS MEAS RADIAL ASSEMBLY POWERS
24.5 EFPD 97.5%FP CONTROL BANKS 7,8 = 89.6, 26.1 % WITHDRAWN
8 9 10 11 12 13 14 15
H K L M N O P R
.77 .86
.93 .92
.92 .96
.89 .95
1.36 1.31
1.00 1.02
1.07 1.06
.87 .85
1.38 1.31
1.06 1.09
1.24 1.21
.99 1.01
1.03 1.03
.90 .93
.81 .80
1.01 1.03
1.27 1.24
1.10 1.06
.94 .98
1.18 1.13
.87 .84
1.10 1.15
1.26 1.25
.87 .90
.90 .89
1.25 1.22
.96 .92
.93 .85
.69 .72
CALCULATED
MEASURED

Figure 4-109

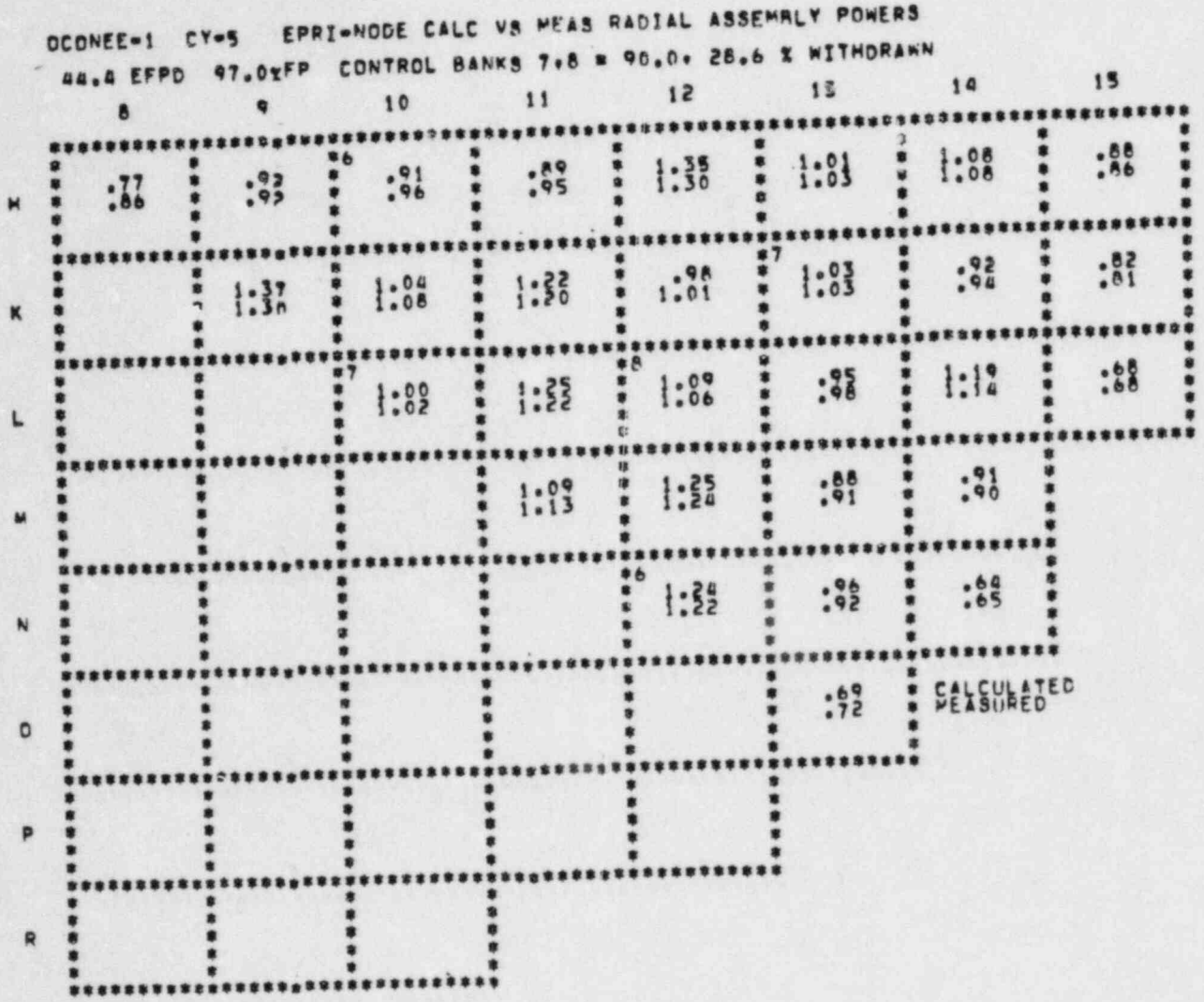
OCONEE-1 CY-5 EPRI-NODE CALC VS MEAS RADIAL ASSEMBLY POWERS
44.4 EFPD 97.0%FP CONTROL BANKS 7,8 = 90.0, 28.6 % WITHDRAWN
8 9 10 11 12 13 14 15
H
K
L
M
N
P
R
.77 .86
.92 .93
.91 .96
.89 .95
1.35 1.30
1.01 1.03
1.08 1.08
.88 .86
1.37 1.30
1.04 1.08
1.22 1.20
.98 1.01
1.03 1.03
.92 .94
.82 .81
1.00 1.02
1.25 1.22
1.09 1.06
.95 .98
1.19 1.14
.68 .68
1.09 1.13
1.25 1.24
.88 .91
.91 .90
1.24 1.22
.96 .92
.64 .65
.69 .72
CALCULATED
MEASURED

Figure 4-110

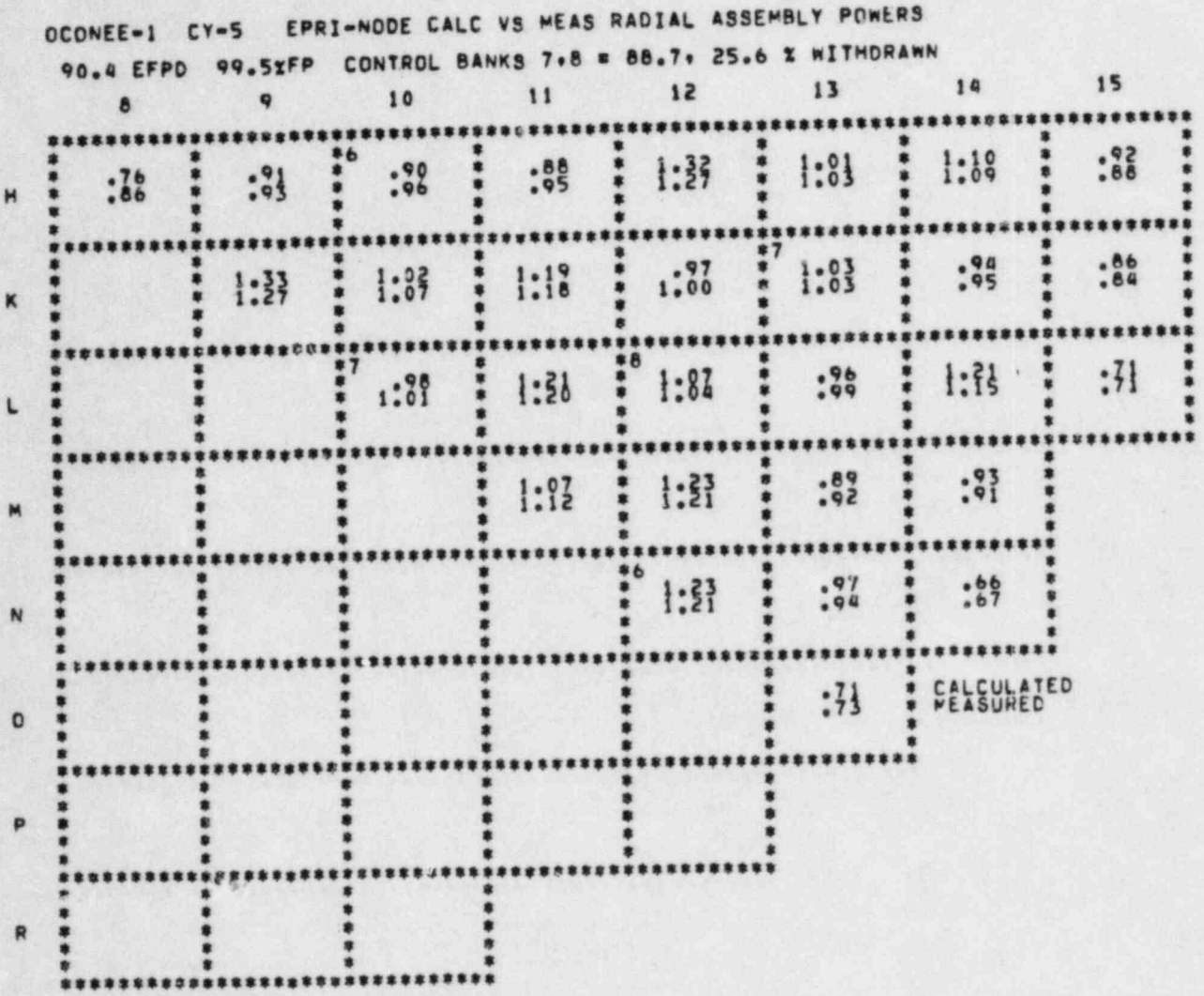
OCONEE-1 CY-5 EPRI-NODE CALC VS MEAS RADIAL ASSEMBLY POWERS
90.4 EFPD 99.5%FP CONTROL BANKS 7,8 = 88.7, 25.6 % WITHDRAWN
8 9 10 11 12 13 14 15
H K L M N O P R
.76 .86
.91 .93
6 .90 .96
.88 .95
1.32 1.27
1.01 1.03
1.10 1.09
.92 .88
1.33 1.27
1.02 1.07
1.19 1.18
.97 1.00
7
1.03 1.03
.94 .95
.86 .84
7 .98 1.01
1.21 1.20
8 1.07 1.04
.96 .99
1.21 1.15
.71 .71
1.07 1.12
1.23 1.21
.89 .92
.93 .91
6 1.23 1.21
.97 .94
.66 .67
.71 .73
CALCULATED
MEASURED

Figure 4-111

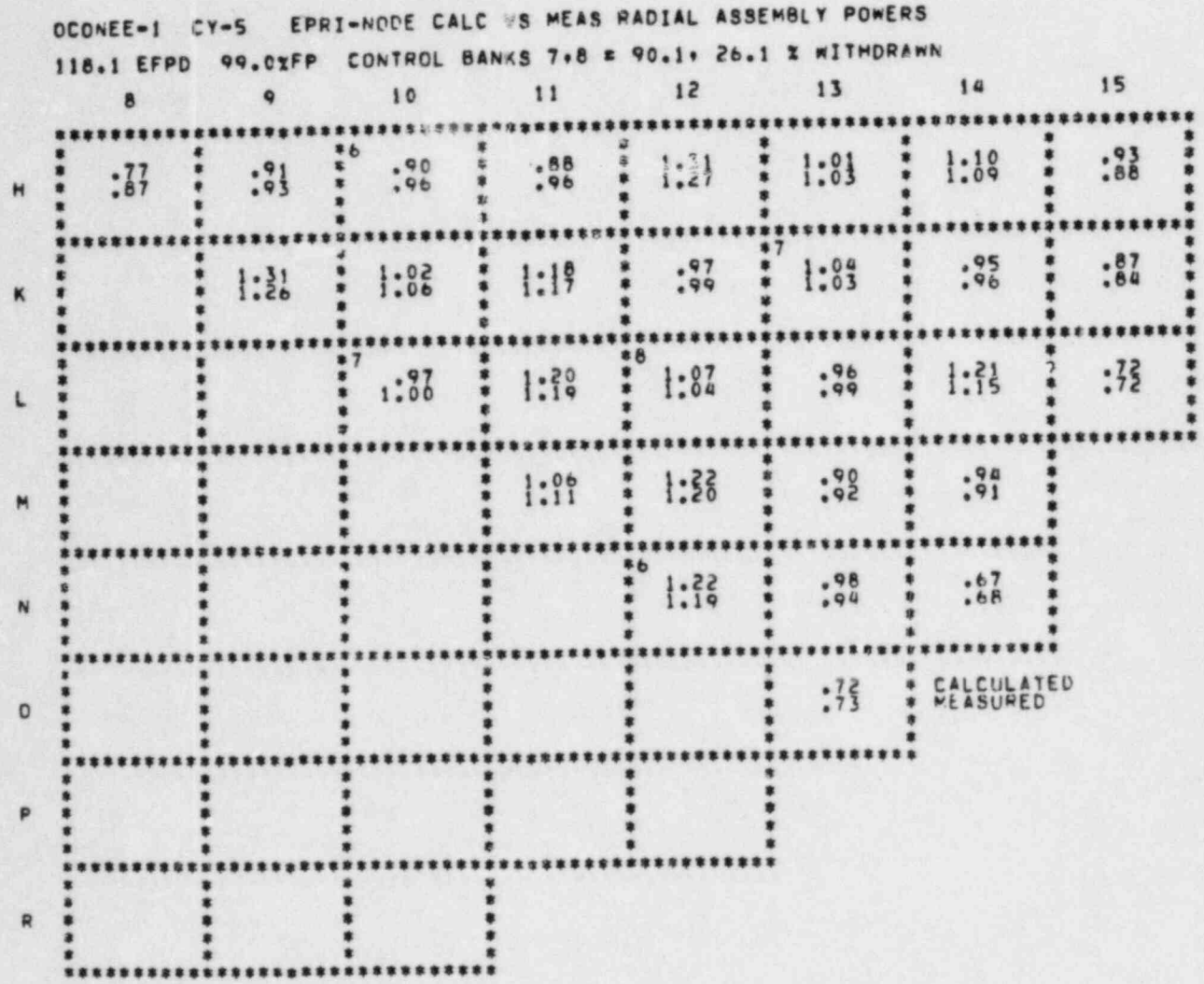
OCONEE-1 CY-5 EPRI-NODE CALC VS MEAS RADIAL ASSEMBLY POWERS
118.1 EFPD 99.0%FP CONTROL BANKS 7,8 @ 90.1, 26.1 % WITHDRAWN
8 9 10 11 12 13 14 15
H K L M N O P R
.77 .87
.91 .93
.90 .96
.88 .96
1.31 1.27
1.01 1.03
1.10 1.09
.93 .88
1.31 1.26
1.02 1.06
1.18 1.17
.97 .99
1.04 1.03
.95 .96
.87 .84
.97 1.00
1.20 1.19
1.07 1.04
.96 .99
1.21 1.15
.72 .72
1.06 1.11
1.22 1.20
.90 .92
.94 .91
1.22 1.19
.98 .94
.67 .68
.72 .73
CALCULATED
MEASURED

Figure 4-112

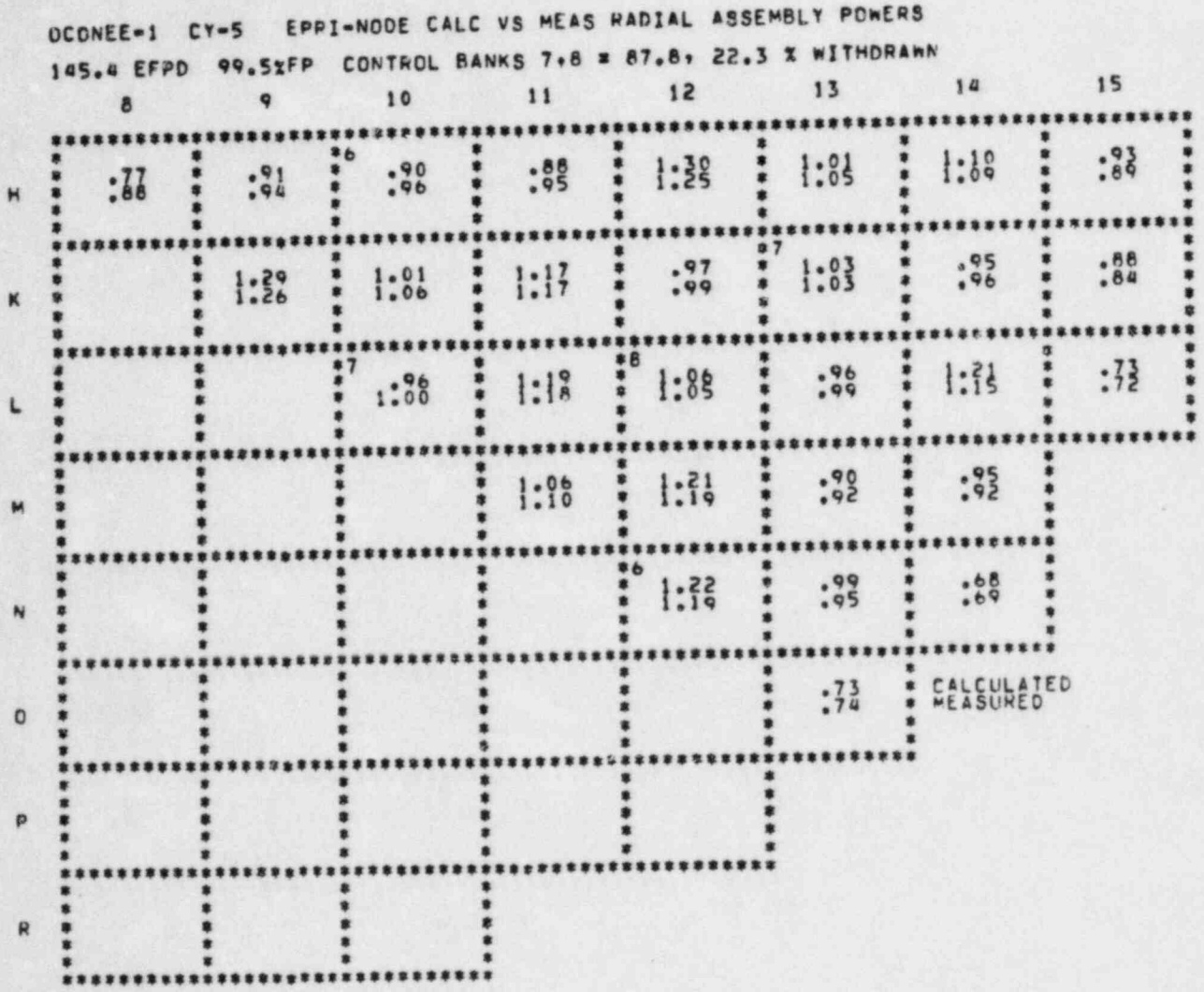
OCONEE-1 CY-5 EPRI-NODE CALC VS MEAS RADIAL ASSEMBLY POWERS
145.4 EFPD 99.5%FP CONTROL BANKS 7,8 = 87.8, 22.3 % WITHDRAWN
8 9 10 11 12 13 14 15
H
K
L
M
N
O
P
R
.77 .88
.91 .94
6 .90 .96
.88 .95
1.30 1.25
1.01 1.05
1.10 1.09
.93 .89
1.29 1.26
1.01 1.06
1.17 1.17
.97 .99
7 1.03 1.03
.95 .96
.88 .84
7 .96 1.00
1.19 1.18
8 1.06 1.05
.96 .99
1.21 1.15
.73 .72
1.06 1.10
1.21 1.19
.90 .92
.95 .92
6 1.22 1.19
.99 .95
.68 .69
.73 .74
CALCULATED
MEASURED

Figure 4-113

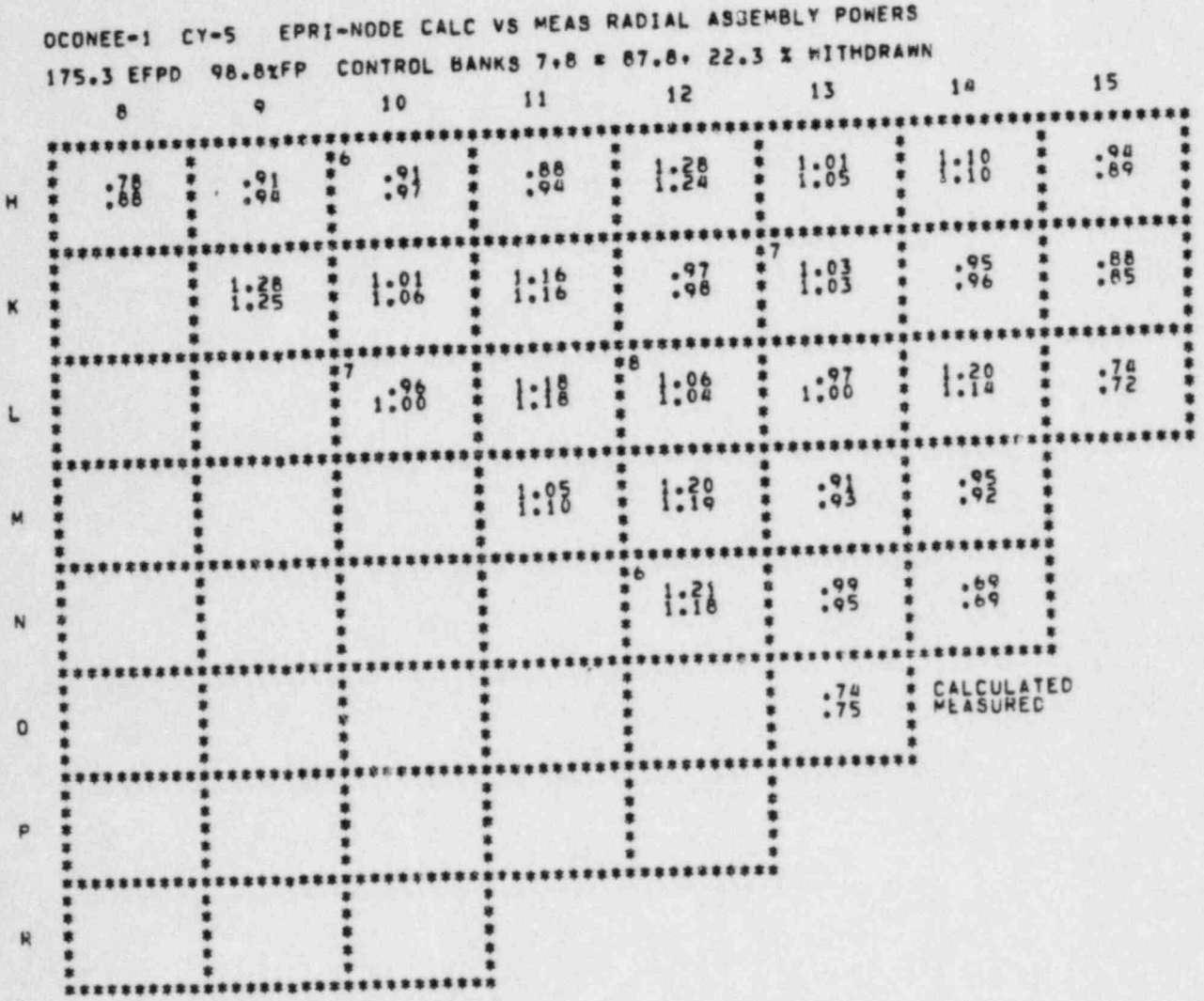
OCONEE-1 CY-5 EPRI-NODE CALC VS MEAS RADIAL ASSEMBLY POWERS
175.3 EFPD 98.8%FP CONTROL BANKS 7,8 @ 87.8, 22.3 % WITHDRAWN
8 9 10 11 12 13 14 15
H K L M N O P R
.78 .88
.91 .94
.6 .91 .97
.88 .94
1.28 1.24
1.01 1.05
1.10 1.10
.94 .89
1.28 1.25
1.01 1.06
1.16 1.16
.97 .98
.7 1.03 1.03
.95 .96
.88 .85
.7 .96 1.00
1.18 1.18
.8 1.06 1.04
.97 1.00
1.20 1.14
.74 .72
1.05 1.10
1.20 1.19
.91 .93
.95 .92
.6 1.21 1.18
.99 .95
.69 .69
.74 .75
CALCULATED
MEASURED

Figure 4-114

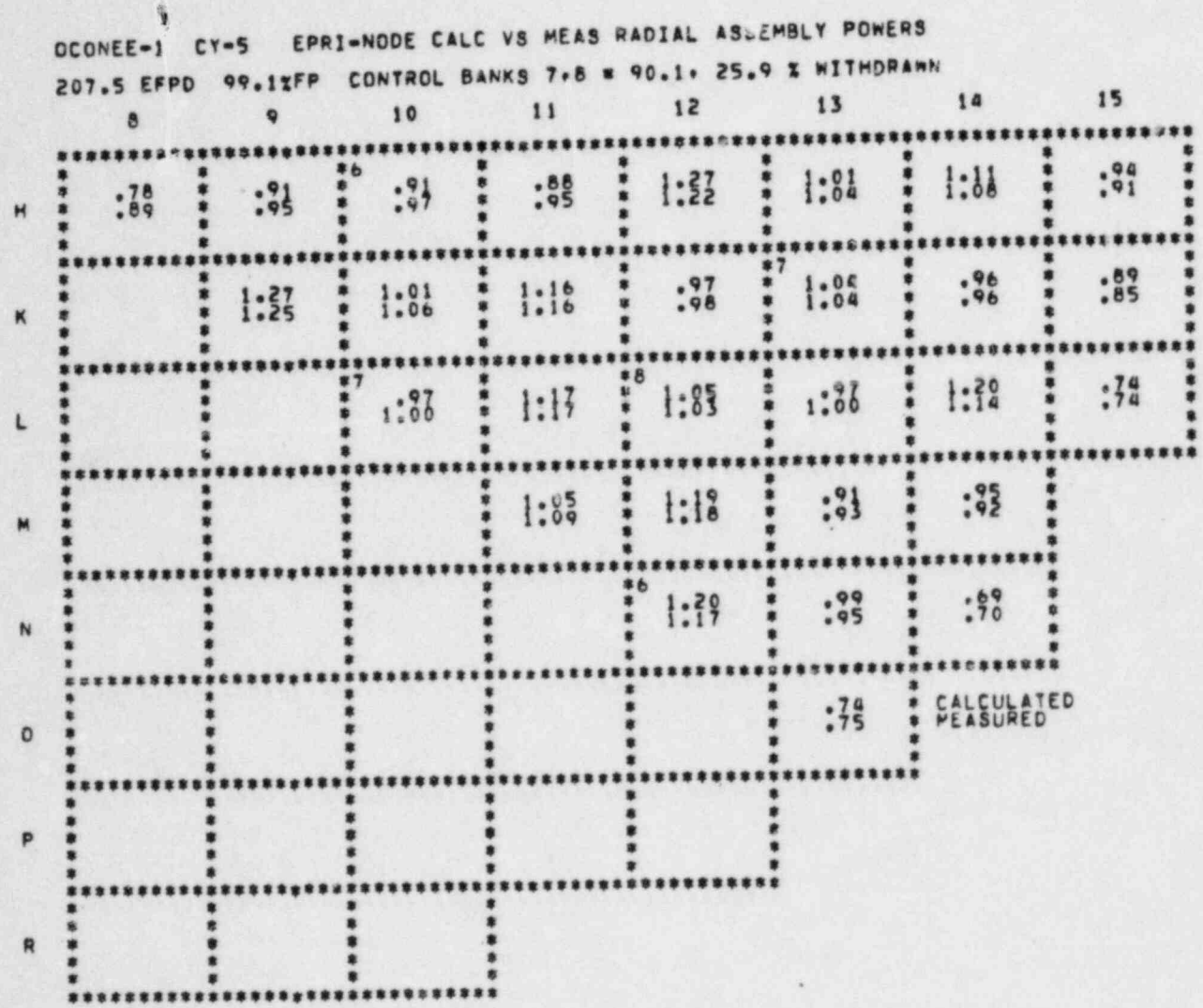
OCONEE-1 CY-5 EPRI-NODE CALC VS MEAS RADIAL ASSEMBLY POWERS
207.5 EFPD 99.1%FP CONTROL BANKS 7,8 @ 90.1, 25.9 % WITHDRAWN
8 9 10 11 12 13 14 15
H K L M N O P R
.78 .89
.91 .95
*6 .91 .97
.88 .95
1.27 1.22
1.01 1.04
1.11 1.08
.94 .91
1.27 1.25
1.01 1.06
1.16 1.16
.97 .98
*7 1.06 1.04
.96 .96
.89 .85
*7 .97 1.00
1.17 1.17
*8 1.05 1.03
.97 1.00
1.20 1.14
.74 .74
1.05 1.09
1.19 1.18
.91 .93
.95 .92
*6 1.20 1.17
.99 .95
.69 .70
.74 .75
CALCULATED
MEASURED

Figure 4-115

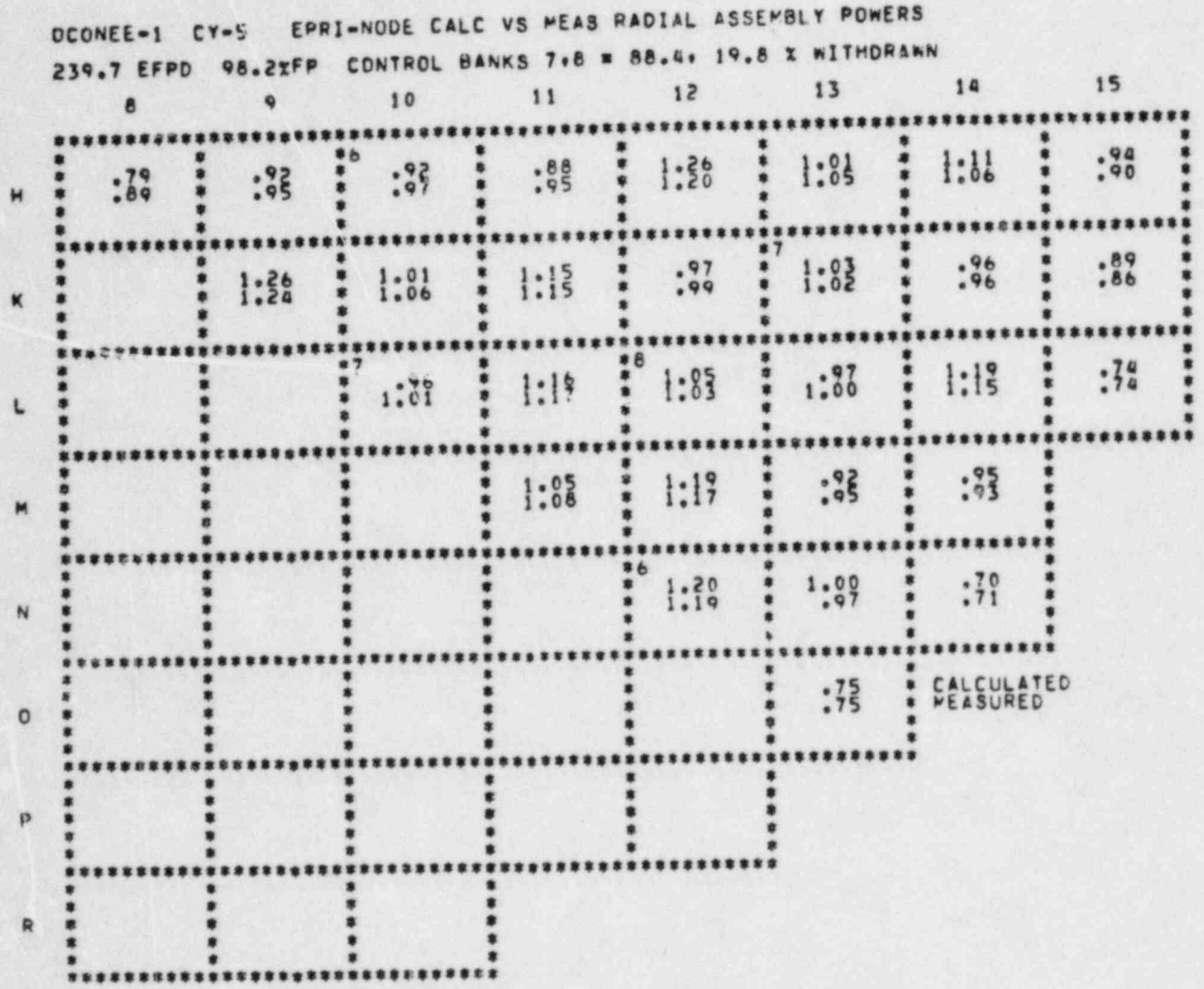
OCONEE-1 CY-5 EPRI-NODE CALC VS MEAS RADIAL ASSEMBLY POWERS
239.7 EFPD 98.2%FP CONTROL BANKS 7,8 = 88.4, 19.8 % WITHDRAWN
8 9 10 11 12 13 14 15
H
K
L
M
N
O
P
R
.79 .89
.92 .95
6 .92 .97
.88 .95
1.26 1.20
1.01 1.05
1.11 1.06
.94 .90
1.26 1.24
1.01 1.06
1.15 1.15
.97 .99
7 1.03 1.02
.96 .96
.89 .86
7 .79 1.01
1.16 1.17
8 1.05 1.03
.97 1.00
1.19 1.15
.74 .74
1.05 1.08
1.19 1.17
.92 .95
.95 .93
6 1.20 1.19
1.00 .97
.70 .71
.75 .75
CALCULATED
MEASURED

Figure 4-116

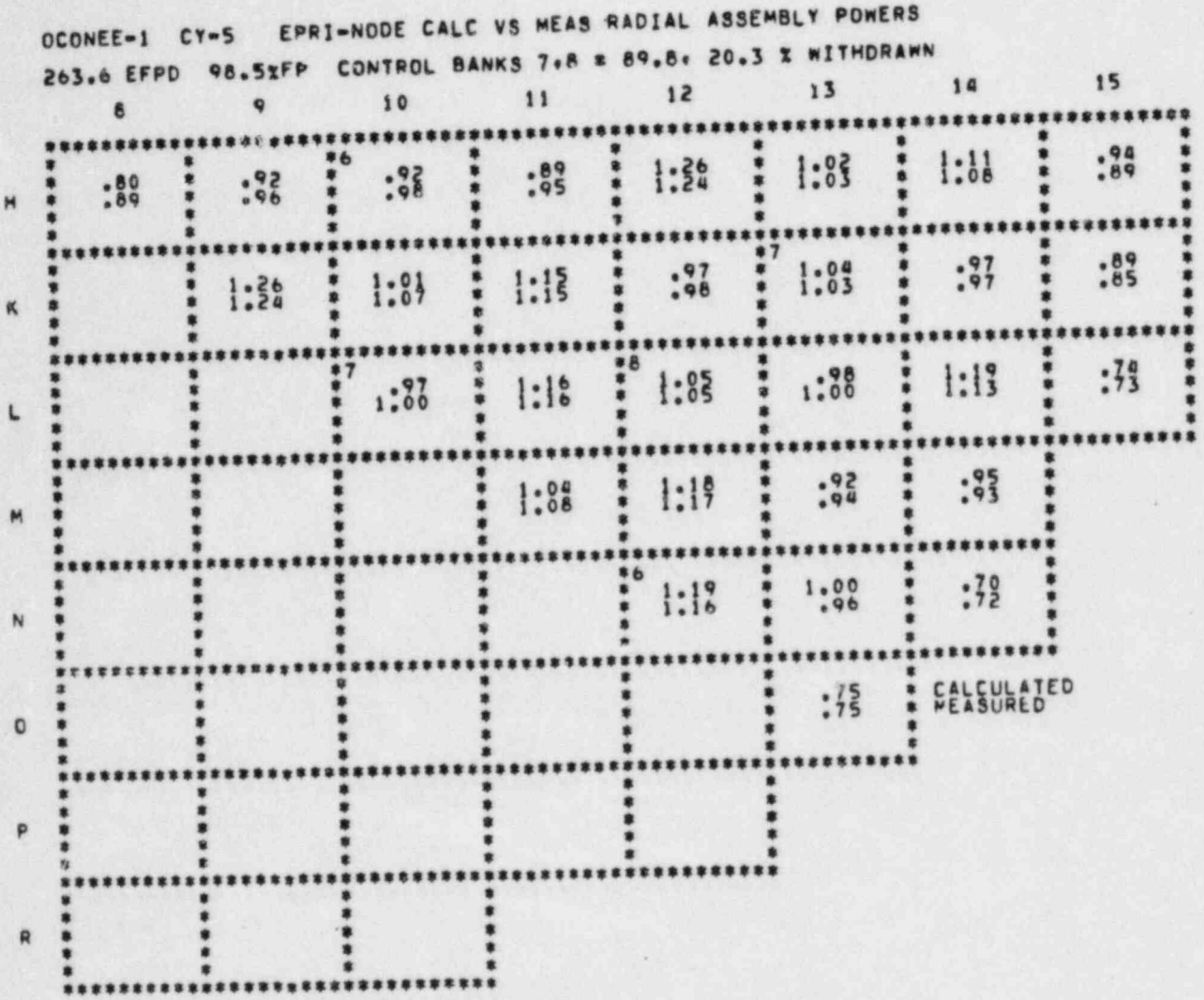
OCONEE-1 CY-5 EPRI-NODE CALC VS MEAS RADIAL ASSEMBLY POWERS
263.6 EFPD 98.5%FP CONTROL BANKS 7,8 @ 89.8, 20.3 % WITHDRAWN
8 9 10 11 12 13 14 15
H
K
L
M
N
O
P
R
.80 .89
.92 .96
.92 .98
.89 .95
1.26 1.24
1.02 1.03
1.11 1.08
.94 .89
1.26 1.24
1.01 1.07
1.15 1.15
.97 .98
1.04 1.03
.97 .97
.89 .85
.97 1.00
1.16 1.16
1.05 1.05
.98 1.00
1.19 1.13
.74 .73
1.04 1.08
1.18 1.17
.92 .94
.95 .93
1.19 1.16
1.00 .96
.70 .72
.75 .75
CALCULATED
MEASURED

Figure 4-117

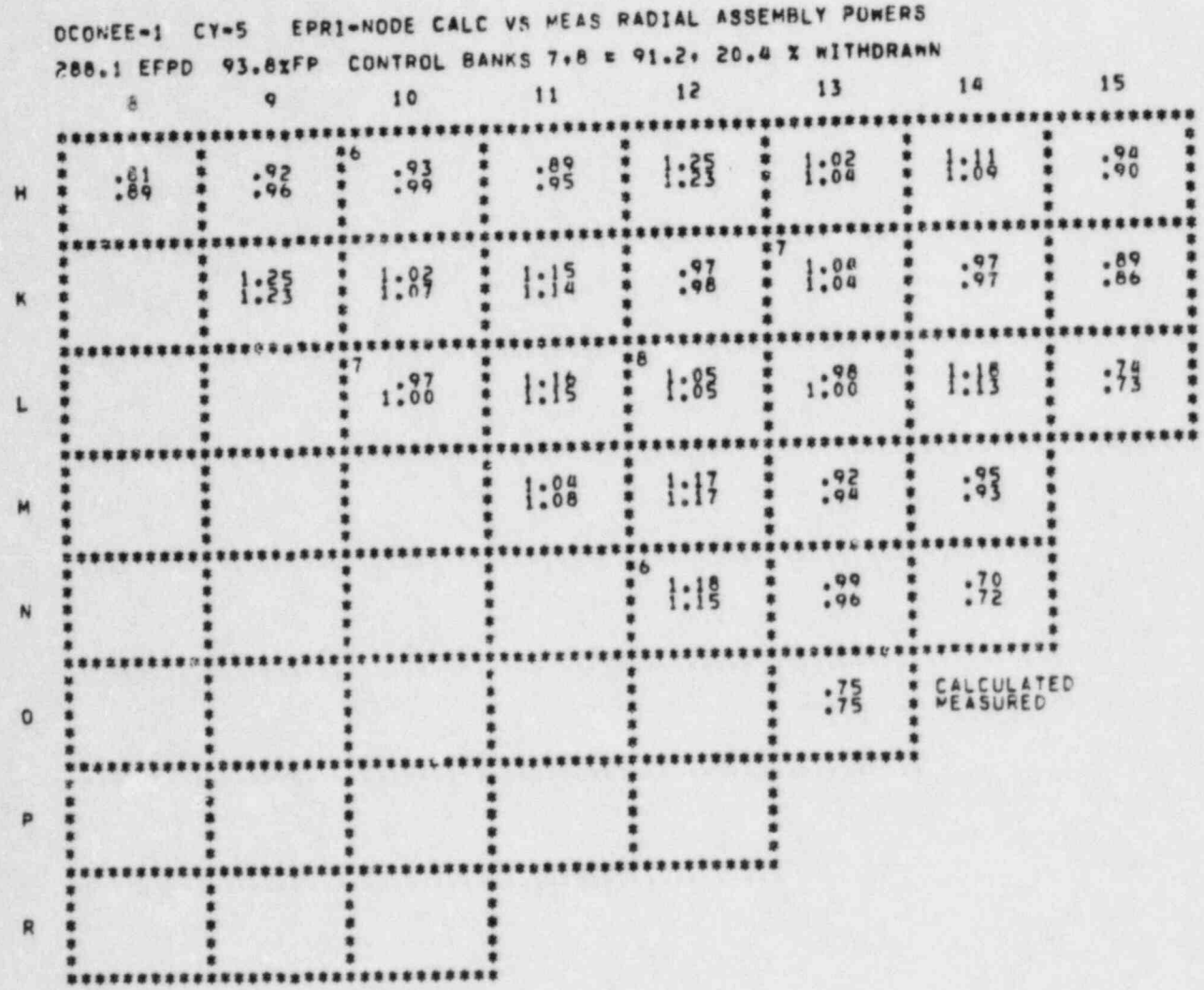
OCONEE-1 CY-5 EPRI-NODE CALC VS MEAS RADIAL ASSEMBLY POWERS
288.1 EFPD 93.8%FP CONTROL BANKS 7,8 = 91.2, 20.4 % WITHDRAWN
8 9 10 11 12 13 14 15
H K L M N O P R
.81 .89
.92 .96
#6 .93 .99
.89 .95
1.25 1.23
1.02 1.04
1.11 1.04
.90 .90
1.25 1.23
1.02 1.07
1.15 1.14
.97 .98
#7 1.00 1.04
.97 .97
.89 .86
#7 .97 1.00
1.16 1.15
#8 1.05 1.05
.98 1.00
1.16 1.13
.74 .73
1.04 1.08
1.17 1.17
.92 .94
.95 .93
#6 1.18 1.15
.99 .96
.70 .72
.75 .75
CALCULATED
MEASURED

Figure 4-118

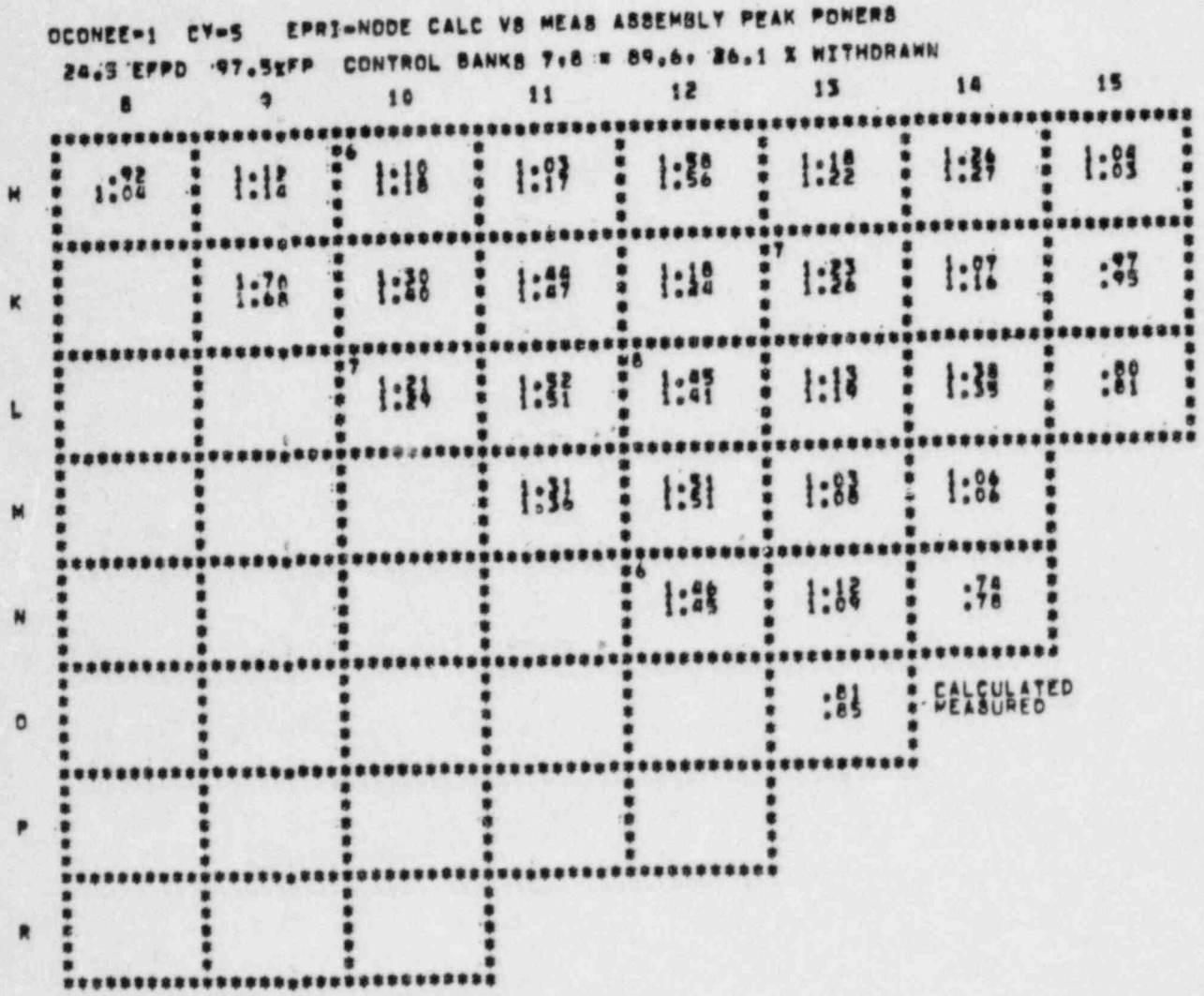
OCONEE-1 CY-5 EPRI-NODE CALC VS MEAS ASSEMBLY PEAK POWERS
24.3 EFPD 97.5%FP CONTROL BANKS 7,8 = 89.6, 86.1 % WITHDRAWN
8 9 10 11 12 13 14 15
H
K
L
M
N
O
P
R
CALCULATED
MEASURED

Figure 4-119

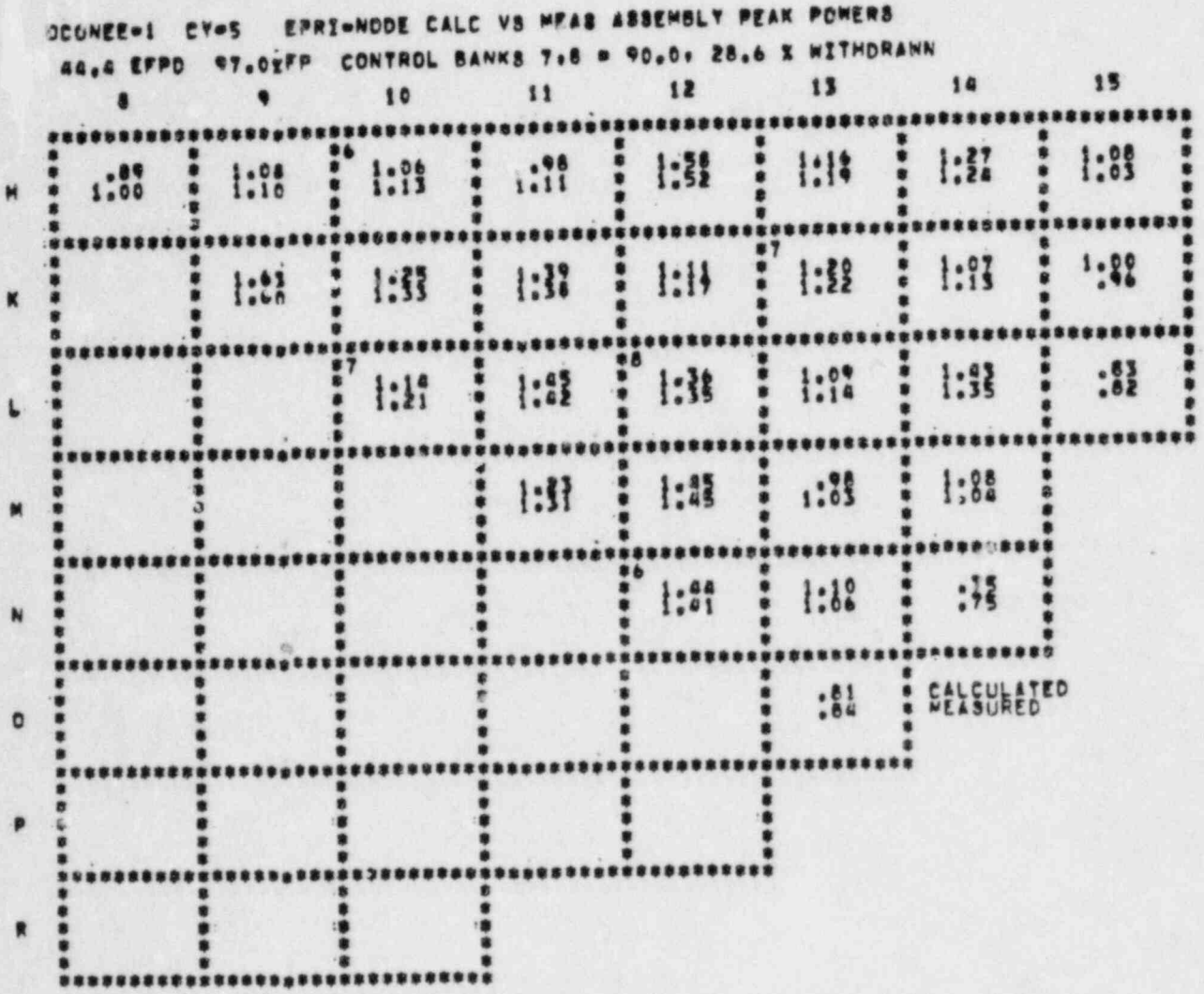
OCONEE-1 CY-5 EPRI-NODE CALC VS MEAS ASSEMBLY PEAK POWERS
440.4 EFPD 97.0%FP CONTROL BANKS 7,8 = 90.0, 28.6 % WITHDRAWN
8
9
10
11
12
13
14
15
H
K
L
M
N
O
P
R
1.00
1.10
1.13
1.11
1.52
1.14
1.24
1.03
1.00
1.00
1.21
1.02
1.35
.82
1.03
1.04
1.01
1.06
.75
.84
CALCULATED
MEASURED

Figure 4-120

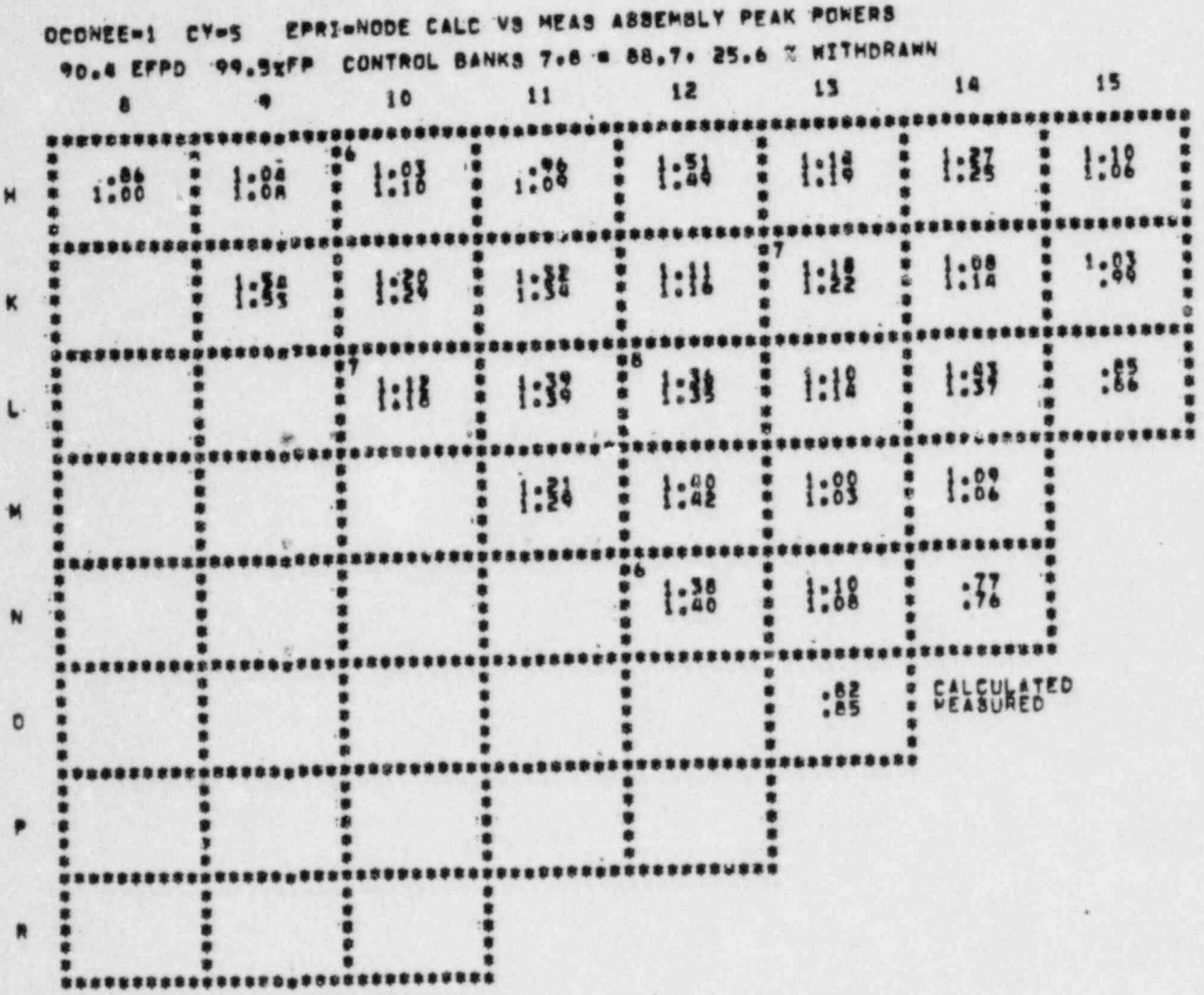
OCONEE-1 CY-5 EPRI-NODE CALC VS MEAS ASSEMBLY PEAK POWERS
90.4 EFPD 99.5%FP CONTROL BANKS 7-8 = 88.7, 25.6 % WITHDRAWN
8
9
10
11
12
13
14
15
H
K
L
M
N
O
P
R
CALCULATED
MEASURED

Figure 4-121

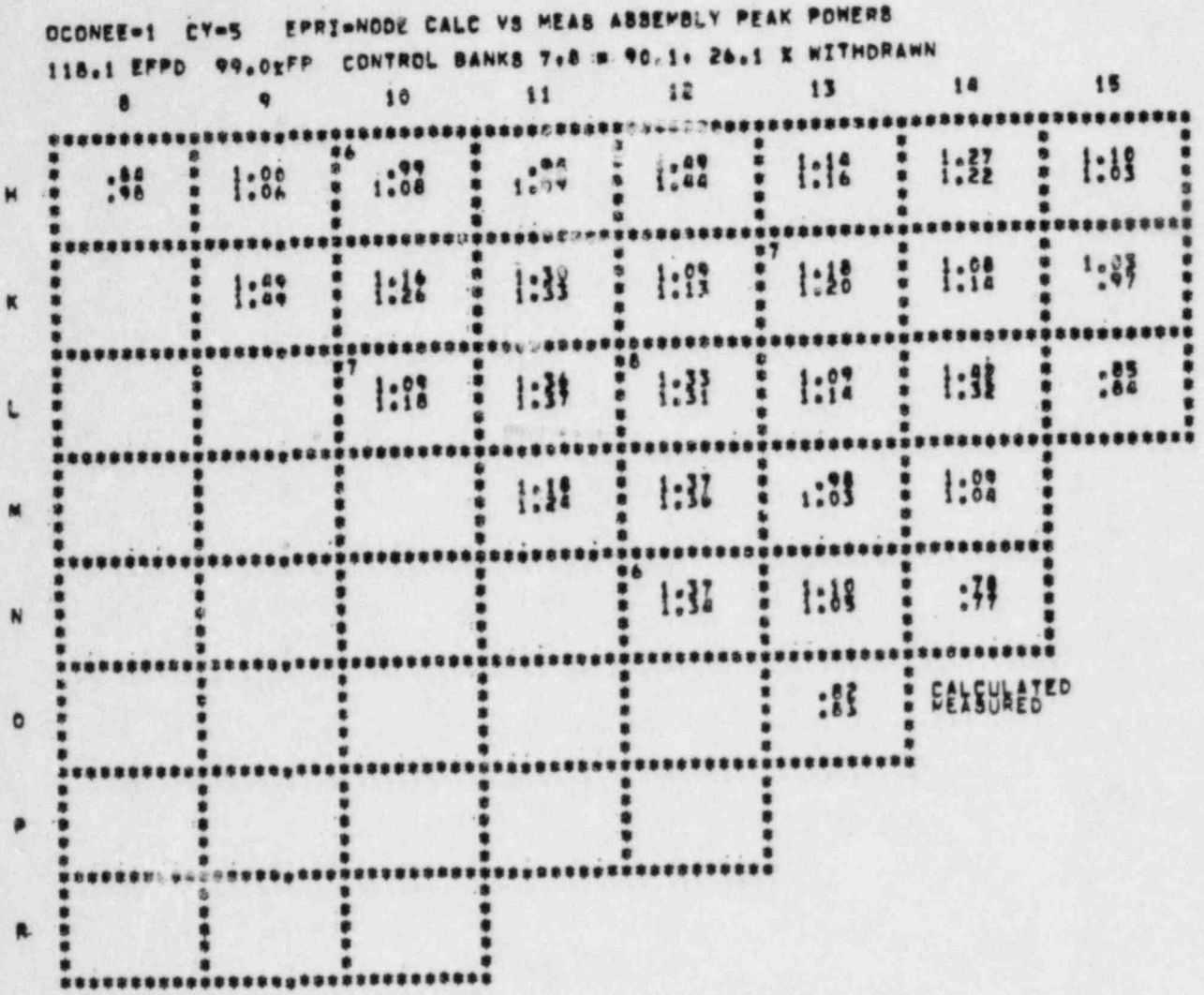
OCONEE-1 CY-5 EPRI-NODE CALC VS MEAS ASSEMBLY PEAK POWERS
118.1 EFPD 99.0%FP CONTROL BANKS 7,8 = 90.1, 26.1 % WITHDRAWN
8
9
10
11
12
13
14
15
H
K
L
M
N
O
P
R
CALCULATED
MEASURED

Figure 4-122

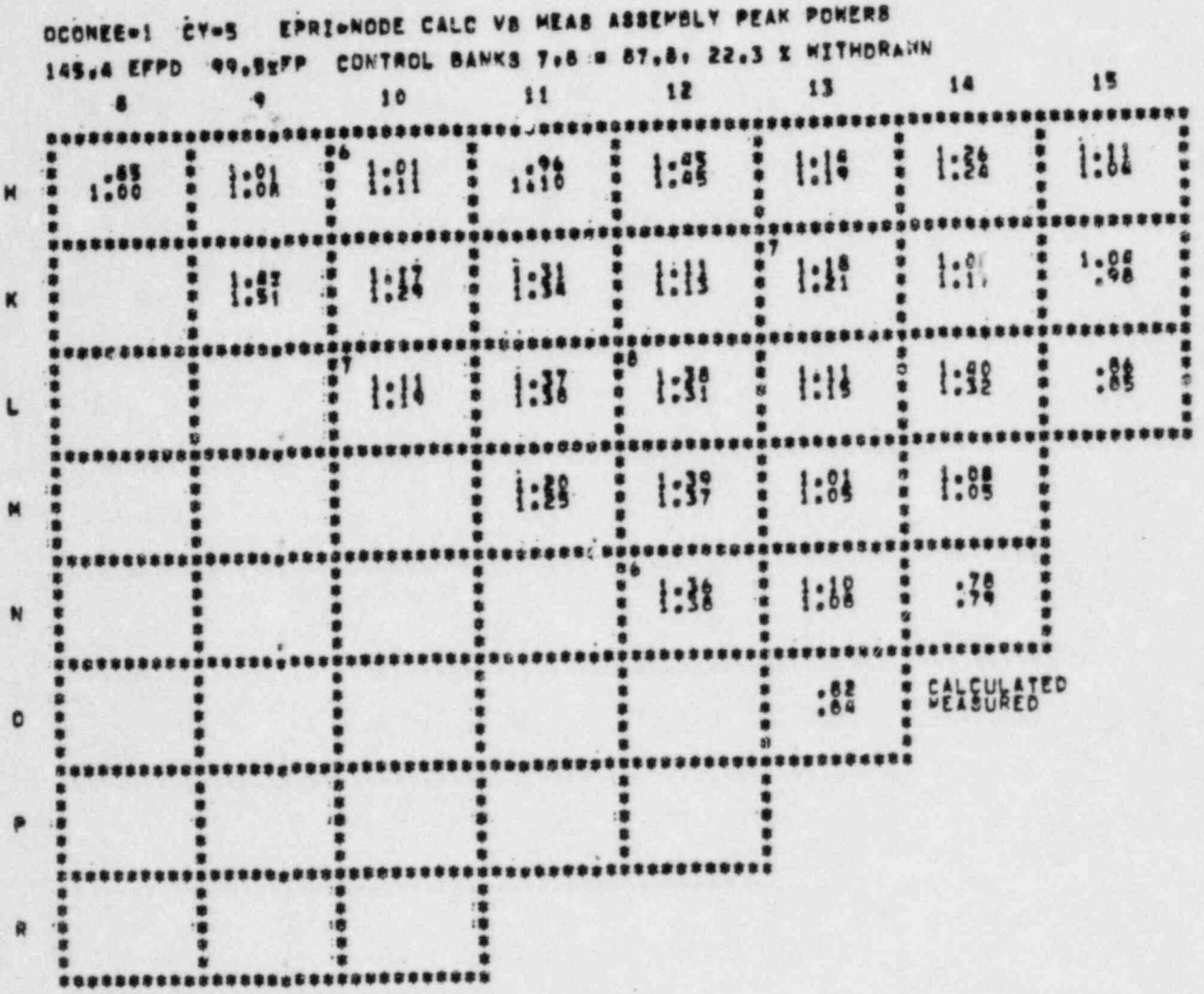
OCONEE-1 CY-5 EPRI-NODE CALC VS MEAS ASSEMBLY PEAK POWERS
145.4 EFPD 99.8%FP CONTROL BANKS 7,8 = 87.8; 22.3 % WITHDRAWN
8
9
10
11
12
13
14
15
H
K
L
M
N
O
P
R
CALCULATED
MEASURED

Figure 4-123

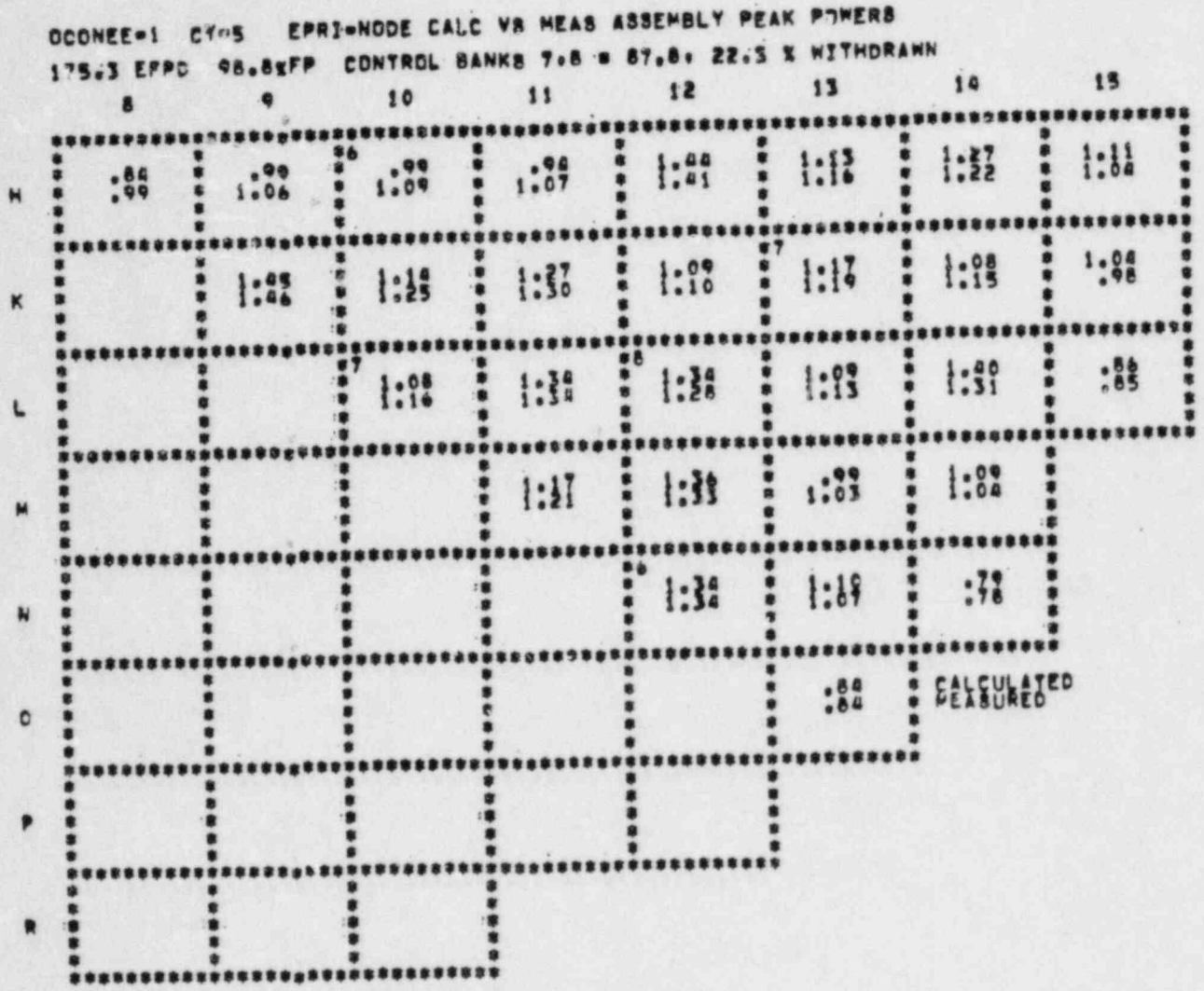
OCONEE-1 CY-5 EPRI-NODE CALC VS MEAS ASSEMBLY PEAK POWERS
175.3 EFPD 98.8%FP CONTROL BANKS 7,8 @ 87.8, 22.5 % WITHDRAWN
8 9 10 11 12 13 14 15
H K L M N O P R
.84 .99
.99 1.06
.99 1.09
.98 1.07
1.44 1.41
1.13 1.16
1.27 1.22
1.11 1.04
1.05 1.46
1.14 1.25
1.27 1.30
1.09 1.10
1.17 1.14
1.08 1.15
1.04 .98
1.08 1.16
1.34 1.34
1.34 1.28
1.09 1.13
1.40 1.31
.84 .85
1.17 1.21
1.34 1.33
1.09 1.03
1.09 1.04
1.34 1.34
1.10 1.09
.79 .78
.84 .84
CALCULATED
MEASURED

Figure 4-124

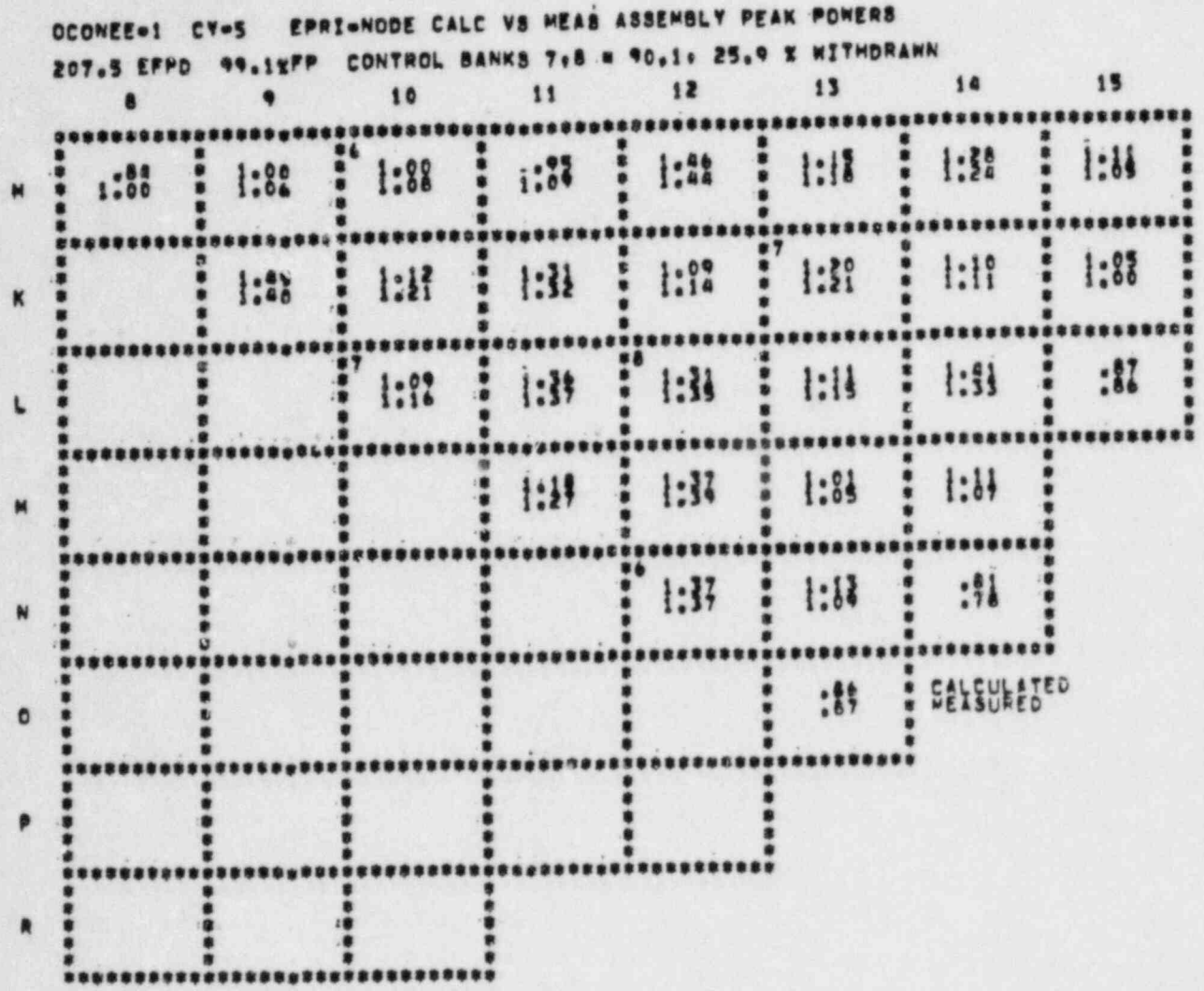
OCONEE-1 CY-5 EPRI-NODE CALC VS MEAS ASSEMBLY PEAK POWERS
207.5 EFPD 99.1%FP CONTROL BANKS 7,8 = 90.1, 25.9 % WITHDRAWN
8
9
10
11
12
13
14
15
H
K
L
M
N
O
P
R
CALCULATED
MEASURED

Figure 4-125

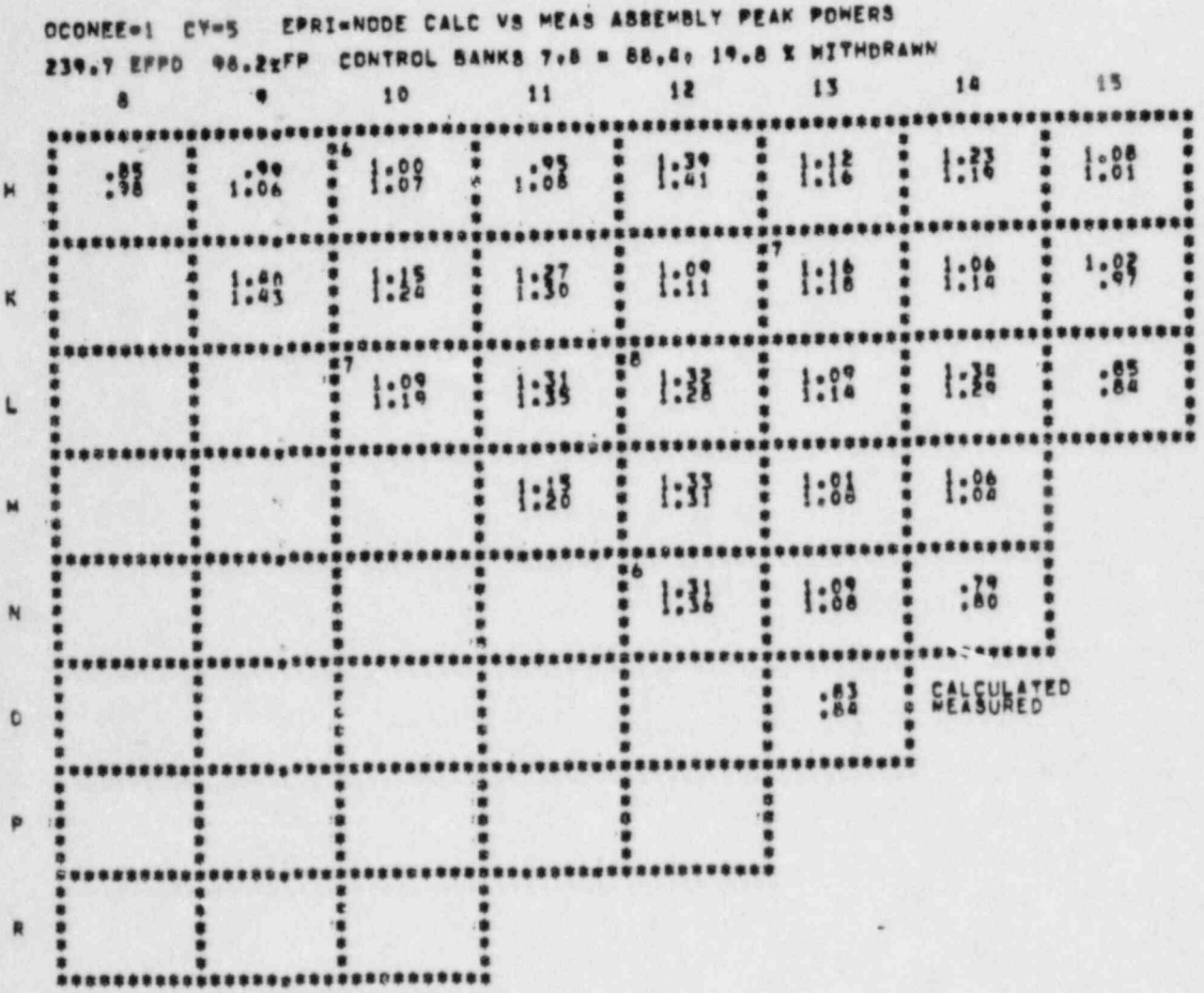
OCONEE-1 CY-5 EPRI-NODE CALC VS MEAS ASSEMBLY PEAK POWERS
239.7 EFPD 98.2%FP CONTROL BANKS 7,8 = 88.4; 19.8 % WITHDRAWN
8
9
10
11
12
13
14
15
H
K
L
M
N
O
P
R
.85 .98
.99 1.06
#6 1.00 1.07
.95 1.08
1.39 1.41
1.12 1.16
1.23 1.16
1.08 1.01
1.40 1.43
1.15 1.24
1.27 1.30
1.09 1.11
#7 1.16 1.18
1.06 1.14
1.02 .99
#7 1.09 1.19
1.31 1.35
#8 1.32 1.28
1.09 1.14
1.38 1.24
.85 .84
1.13 1.20
1.33 1.31
1.01 1.08
1.06 1.04
#6 1.31 1.36
1.09 1.08
.79 .80
.83 .84
CALCULATED
MEASURED

Figure 4-126

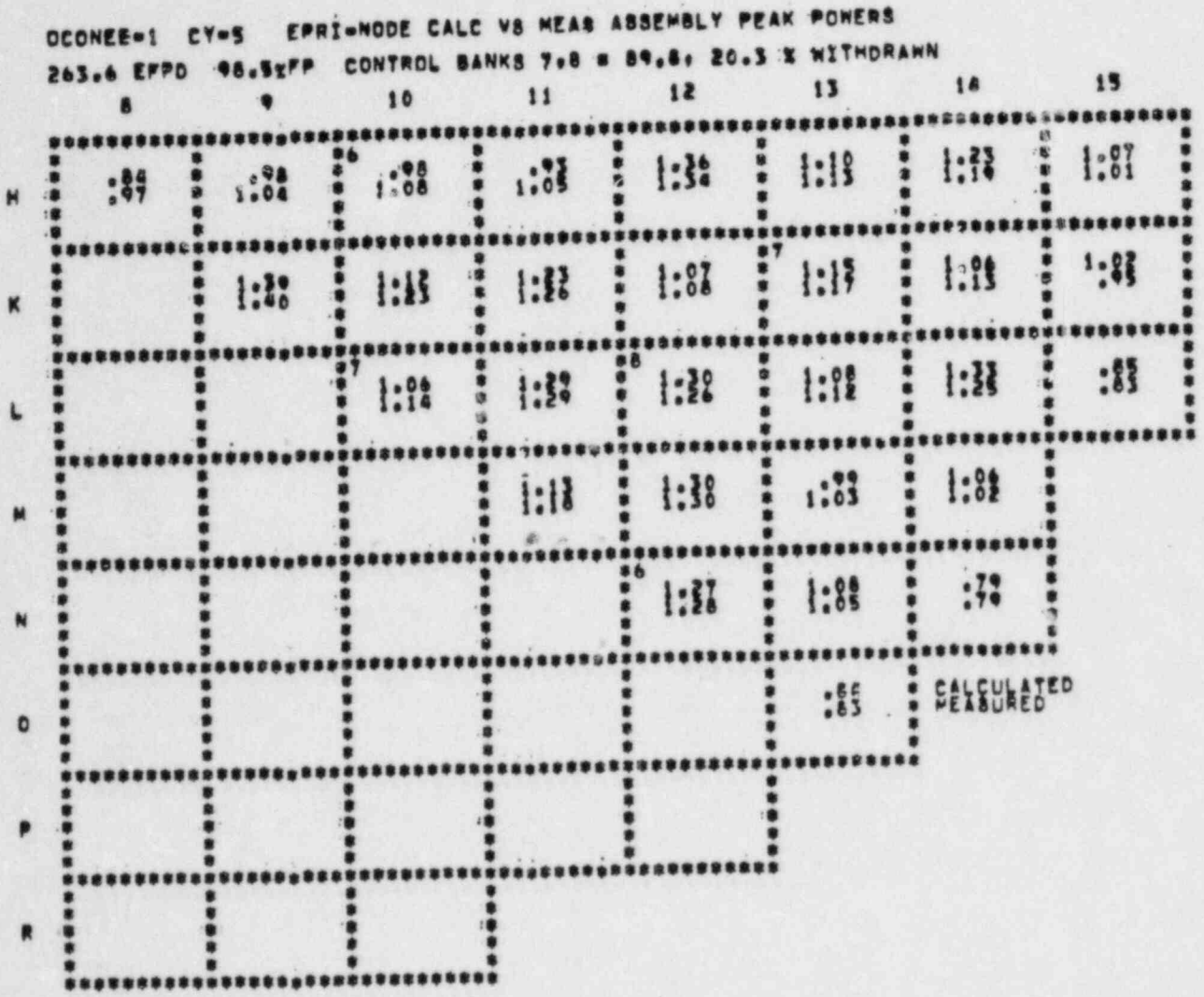
OCONEE-1 CY-5 EPRI-NODE CALC V8 MEAS ASSEMBLY PEAK POWERS
263.6 EFPD 98.5%FP CONTROL BANKS 7,8 @ 89.8, 20.3 % WITHDRAWN
8
9
10
11
12
13
14
15
H
K
L
M
N
O
P
R
CALCULATED
MEASURED

Figure 4-127

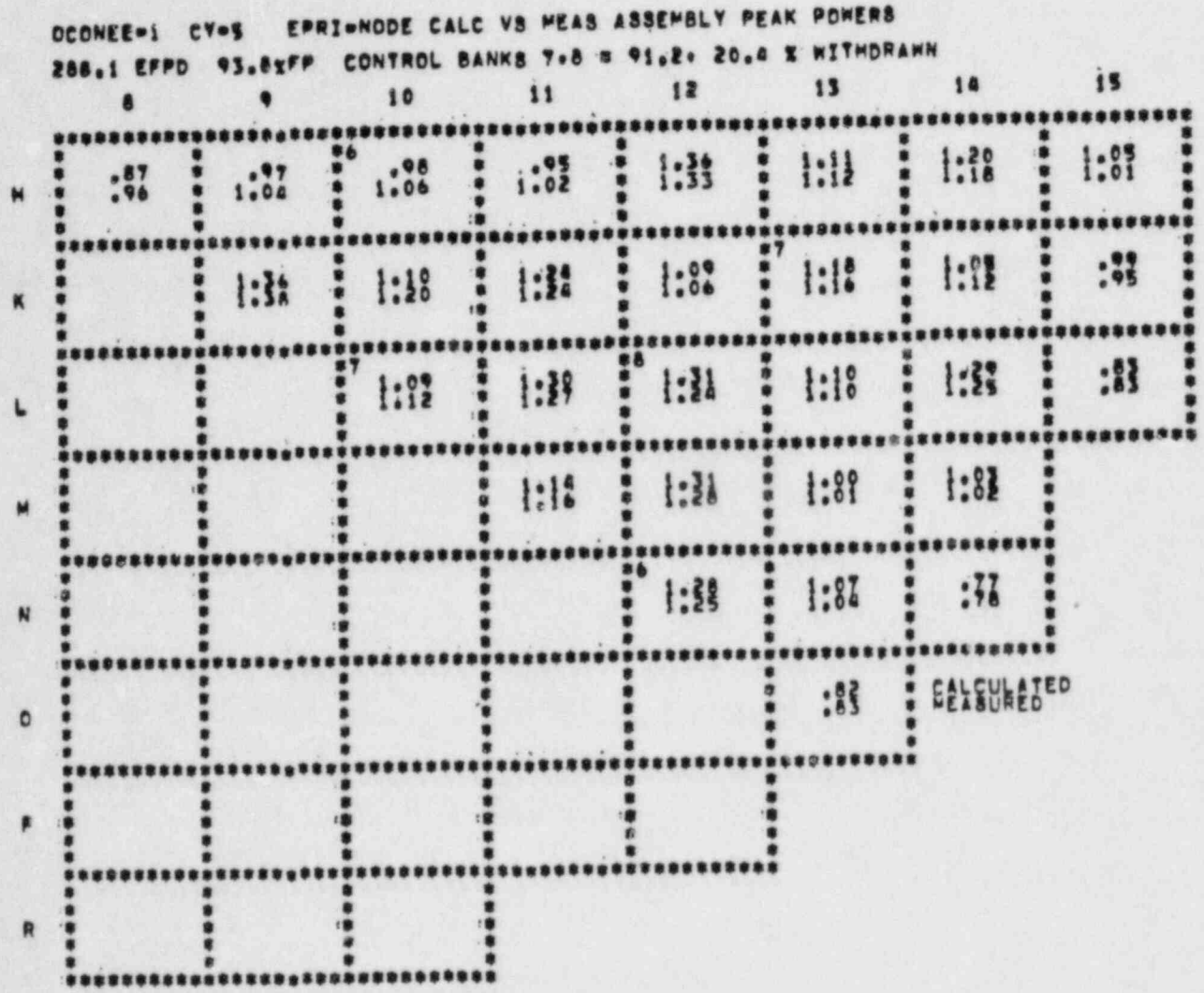
OCONEE-1 CY-5 EPRI-NODE CALC VS MEAS ASSEMBLY PEAK POWERS
288.1 EFPD 93.8%FP CONTROL BANKS 7-8 = 91.2, 20.4 % WITHDRAWN
8 9 10 11 12 13 14 15
H
K
L
M
N
O
P
R
.87 .96
.97 1.04
#6 .98 1.06
.95 1.02
1.36 1.33
1.11 1.12
1.20 1.18
1.05 1.01
1.34 1.34
1.10 1.20
1.24 1.24
1.09 1.06
#7 1.18 1.16
1.08 1.12
.99 .95
#7 1.09 1.12
1.30 1.29
#8 1.31 1.24
1.10 1.10
1.29 1.25
.83 .83
1.14 1.16
1.31 1.28
1.09 1.01
1.07 1.02
#6 1.28 1.25
1.07 1.04
.77 .78
.82 .83
CALCULATED
MEASURED

5. STATISTICAL ANALYSIS

5.1 Observed Nuclear Reliability Factor Derivation

The section will address quantitatively statistics arising from Section 4. Normal distribution theory will be used in deriving calculational uncertainties.

In deriving the calculational uncertainty for EPRI-NODE-P, the algebraic difference between a calculated and a measured value forms a normally distributed (refer to Section 5.2) random variable.

The difference variable is defined:

$$D_i = C_i - M_i \qquad (5\text{-}1)$$

where: D is the i^{th} difference; $1 \leq i \leq N$

C is the i^{th} calculated value (radial or peak)

M is the i^{th} measured value (radial or peak)

The mean of the difference as defined in equation 5-2 is:

$$\bar{D} = \bar{C} - \bar{M} \qquad (5\text{-}2)$$

where: $$\bar{C} = \left(\sum_{i=1}^{n} C_i\right) \div n \qquad (5\text{-}2a)$$

$$\bar{M} = \left(\sum_{i=1}^{n} M_i\right) \div n \qquad (5\text{-}2b)$$

$$\bar{D} = \left(\sum_{i=1}^{n} M_i\right) \div n \qquad (5\text{-}2c)$$

n = number of observations in sample

Now a one sided upper bound factor is derived by employing one sided upper tolerance limit (OSUTL) methodology. For a normal random variable X with a sample mean $\bar{X}$ and standard deviation S, the OSUTL of X is defined by:

$$OSUTL(X) = \bar{X} + K \times S \qquad (5\text{-}3)$$

where: $$\bar{X} = \left(\sum_{i=1}^{n} X_i\right) \div n \qquad (5\text{-}4)$$

$$S = \left[\left(\sum_{i=1}^{n} (X_i - \bar{X})^2\right) \div (n-1)\right]^{\frac{1}{2}} \qquad (5\text{-}5)$$

In equation 5-3, K is the one-sided tolerance factor. Equation 5-3 is formulated such that a predetermined proportion of the population (P) is below the OSUTL with a confidence factor (α)[18]. K is explicitly dependent on n, P, and α.

Following industry practice, P = 95% and α = 95%.

The OSUTL is given for D by:

$$OSUTL(D) = \bar{D} + K \times S(D) \qquad (5\text{-}6)$$

C is a deterministic variable and does not have an OSUTL per se, but a reasonable upper limit to C can be defined by:

$$UL(C) = \bar{M} + OSUTL(D) \qquad (5\text{-}7)$$

$$UL(C) = \bar{M} + \bar{D} + K \times S(D) \qquad (5\text{-}7a)$$

If one substitutes equations 5-2 into equation 5-7 you obtain the following:

$$UL(C) = \bar{M} + \bar{C} - \bar{M} + K \times S(D) \qquad (5\text{-}8)$$

or $$UL(C) = \bar{C} + K \times S(D) \qquad (5\text{-}8a)$$

From equation (5-8a), it is more obvious that the upper limit is a function of the calculated parameter. Also, it is obvious that the standard deviation being associated with the calculated limit is that of the difference distribution. This means that any error in the measurement of the radial or total power as well as any calculational error will be included in the UL(C) parameter.

While equation 5-7a and 5-8a are valid, the definition of $\bar{D} = \bar{C} - \bar{M}$ (equation 5-2) leads to UL(C) being smaller if the measured parameter is underpredicted. The conservative solution to this is to subtract $\bar{D}$ in equation 5-7a instead of adding it. This would yield the following equation:

$$UL(C) = \bar{M} - \bar{D} + K \times S(D) \qquad (5\text{-}9)$$

A further conservatism in equation 5-9 has been included by collapsing the 52 detector strings (seven detectors per string) into an octant of the reactor core consisting of 29 assembly locations (See Section 2.2). This averaging of symmetric detector values tends to smooth out some of the measurement uncertainty.

Finally, the Observed Nuclear Reliability Factor (ONRF) is defined as the quotient of UL(C) from equation 5-9 and the mean of the measurements:

$$ONRF = \frac{UL(C)}{\bar{M}} \qquad (5\text{-}10)$$

or,

$$ONRF = \frac{\bar{M} - \bar{D} + K \times S(D)}{\bar{M}} \qquad (5\text{-}11)$$

The ONRF from equation 5-11 will be used as a multiplicative factor applied to EPRI-NODE-P calculated powers such that:

$$ONRF \times C \leq M \qquad (5\text{-}12)$$

for 95% of the population and with a confidence factor of 95%. Separate ONRF's are derived for the assembly radial and assembly peak powers.

5.2 Normality Test Results

Using equation 5-1, the variable D was employed to form a frequency distribution. Histograms of these distributions are shown in Figures 5-1 to 5-10. The window width (WW) of each cell is displayed above the ordinate. Each frequency was analyzed for normality using the D' test from ANSI N15.15-1974.[19]

In analyzing the normality of the difference distributions, C,M data were grouped into the following categories:

1) reactor cycle: 1, 2, 3, 4, or 5
2) grouped cycles: 1, 2 (rodded); 4, 5 (feed and bleed), or 1, 2, 4, 5 (combined)
2) type: assembly peak or assembly radial

Using the engineering judgement that only RPDs greater than the core average area of concern, pairs of C,M where both are $\geq$ 1.0 will be treated. Table 5.1 displays the normality test results. The level of significance was chosen to be .05. Therefore, the D' statistic must be between the .025 and .975 percentage point D' values for normality. Here, 5 of 8 assembly radial power difference distributions were normal and 4 of 8 peak difference distributions were normal. The remainder of the difference distributions yielded D' statistics that were close to the critical values and were therefore classified as nearly normal.

Figures 5-1 to 5-10 are radial power difference distributions by cycle for all C,M pairs. The first five are radials and the next five are peak power pairs. Figures 5-11 to 5-15 are D histograms for the radials when C,M $\geq$ 1.0. Likewise, Figures 5-16 to 5-20 apply to the peaks by cycle. Grouped cycle histograms are shown in Figures 5-21 to 5-26. Finally, the maximum values of the radials and the peaks at each state point (regardless of location from calculation or measurement) were assembled for the combined cycles. The resultant histograms of the variable D are shown on Figures 5-27 and 5-28.

It is important to note that distributions which fail the normality test appear normal when plotted. Such is the case for Cycle 5 radial differences as shown in Figure 5-15. Therefore the assumption of normality will be used for all data sets.

5.3 Observed Nuclear Reliability Factors (ONRF) for EPRI-NODE-P

In this subsection the statistical treatment developed in Section 5.1 will be utilized to develop ONRF's for rodded, unrodded and a combination of rodded and unrodded fuel cycles. The Babcock and Wilcox Calculated Nuclear Reliability Factors (CNRF) currently being used in Oconee reload design (1.05 radial and 1.075 total) will be shown to be conservative for use with EPRI-NODE-P and unrodded fuel cycles. Since the EPRI-NODE-P power distributions times the ONRF times the pin to assembly average factor is used to determine margin to both centerline fuel melt and DNBR criteria, and since both of these criteria are limited by the maximum radial and total peaking in the reactor core, ONRF's will be developed based on the maximum peak or radial difference distribution at each burnup point.

Cycles 1 and 2 are grouped together as representative of rodded mode operation. Similarly, cycles 4 and 5 are grouped together for unrodded (feed and bleed) operation.

For each state point in these grouped cycles, the corewise maximum calculated and measured values are derived. The procedure is applied to the radial and repeated for the peak. The variables shown in equation 5-11 were then derived and the ONRF's calculated.

As an example, for the cycle 4 and 5 corewise maximum peaks:

$$\bar{M} = 1.44579$$
$$\bar{D} = .0018316$$
$$S(D) = .0229297$$
$$N = 19$$
$$K = 2.423 \text{ (N=19, 95\%/95\%)}$$

Therefore, the ONRF would be:

$$ONRF = \frac{1.44579 - .0018316 + (2.423 \times .0229297)}{1.44579} \qquad (5\text{-}13)$$

$$ONRF = 1.0372 \qquad (5\text{-}13a)$$

Peak and radial ONRF values for the grouped cycles are shown in Table 5-2.

5.4a Quantitative Comparisons of EPRI-NODE-P to Measurement

By analyzing the variable D as defined in equation 5-1, the accuracy of EPRI-NODE-P can be assessed. Four important statistical properties of D are discussed.

$\bar{D}$ is the mean of the differences between EPRI-NODE-P and measured assembly powers. For cycles 4 and 5, $\bar{D}$ is .023000 for the radial and .001832 for the peaks. The above means were derived from the core maximum calculated and measured state point values. Subsequent statistics are also derived from this consideration.

S(D), the standard deviation of the differences, indicates the spread of the values of D about $\bar{D}$. For Cycles 4 and 5, S(D) for the radial is .023557. S(D) for the peak is .022930.

The mean of the absolute differences ABS(D) and its standard deviation can be combined to give limits on this variable. 95% confidence limits on the means were given by:

$$\overline{\overline{ABS(D)}}_{U,L} = \overline{ABS(D)} \pm \frac{t(.05,n) \times S\,(ABS(D))}{\sqrt{n}} \qquad (5\text{-}14)$$

Equation 5-14 yields for the cycle 4 and 5 radials:

$$\overline{\overline{ABS(D)}}_{U,L} = .0245 \pm .0105$$

and for the peaks:

$$\overline{\overline{ABS(D)}}_{U,L} = .0194 \pm .0055$$

Table 5-3 shows corewise maximum data used to derive ONRF's in Table 5-2. Tables 5-4 and 5-5 present summary D statistics for peaks and radials, respectively, where $C,M \geq 1.0$ for all pairs considered.

5.4b Relative Percent Differences

The relative percent difference between EPRI-NODE-P calculated values and measured values will be defined:

$$\% \text{ Diff} = \frac{C - M}{M} \times 100 \qquad (5\text{-}15)$$

This section will address relative percent differences derived from:

a) the sample mean
b) the mean of the absolute value

Since negative percent differences represent calculational nonconservatisms, the minimum values will be more important. Relative percent differences for all $C,M \geq 1.0$ will be discussed.

Combining data for cycles 4 and 5, the following results were obtained. The average percent difference was .303% and the absolute 2.212% for the radial. Also, the average percent difference was -1.257% and the absolute 3.581% for the peak.

Table 5-6 shows summary data for percent differences derived from calculated and measured peaks. Values are presented by cycle and for grouped cycles. Table 5-7 is similar to Table 5-6 and provides data for radial percent differences.

5.5 Conclusions

A statistical analysis of EPRI-NODE-P calculated and plant measured power distributions has been performed. Data has been grouped into three methods of plant operation; rodded, unrodded, and a combination of rodded and unrodded. The resulting ONRF's for these combinations from Table 5-2 are:

		Radial ONRF	Total ONRF
1.	Rodded	1.03	1.10
2.	Unrodded	1.03	1.04
3.	Combined	1.04	1.08

Since present and future fuel cycle designs for Oconee are expected to be of the feed and bleed (unrodded) design, the appropriate factors for ONRF's are 1.03 radial and 1.04 total.

For additional conservatism and consistency with B&W, the values used will be established as 1.05 radial and 1.075 total for unrodded cycles.

These values while based upon calculations and measurements performed on Oconee Unit 1 are applicable to all three Oconee units for the following reasons:

1. All three units have identical incore detector systems.

2. All three units are manufactured by the same vendor and use similar fuel.

3. Calculations for all three units will be performed using the same calculational methods and procedures.

As an additional verification of the conservatism in the 1.05 radial and 1.075 total peak ONPF's, all calculated maximum radial powers were multiplied by 1.05 and compared to measured. Similarly all calculated maximum total peaks were multiplied by 1.075 and compared to measured.

In cycles 1 and 2, there were 27 state points; no maximum measured radials exceeded the 1.05 x maximum calculated radials, and only one measured peak exceeded the 1.075 x calculated peak. Cycles 4 and 5 consisted of 19 state points; no maximum measured radials exceeded 1.05 x maximum calculated radials, and no maximum measured peaks exceeded the 1.075 x maximum calculated radial peaks.

Therefore, the 1.05 radial factor was satisfactory for the entire population of rodded and unrodded cases. The 1.075 peak factor was satisfactory for 96% (26/27) of the rodded state points and satisfactory for all unrodded state points.

Table 5-1
Difference Distribution Normality Tests
For C,M $\geq$ 1.0 - 5% Level of Significance

Assembly Radial Power

Cycle	N	D'(P = .025)	D'	D'(P = .975)	Remarks
1	308	1504.2	1471.7	1540.0	nearly normal
2	147	492.7	495.0	509.8	normal
3	119	357.4	365.9	371.2	normal
4	144	477.4	483.1	494.1	normal
5	131	414.1	423.1	429.3	normal
1,2	455	2707.5	2660.1	2760.8	nearly normal
4,5	275	1267.5	1285.9	1300.0	normal
1,2,4,5	730	5516.5	5430.7	5602.0	nearly normal

Assembly Peak Power

Cycle	N	D'(P = .025)	D'	D'(P = .975)	Remarks
1	377	2039.7	2034.4	2083.4	nearly normal
2	235	1000.2	998.8	1027.6	normal
3	211	850.3	819.1	874.9	nearly normal
4	199	777.8	789.5	801.0	normal
5	216	880.6	909.5	905.8	normal
1,2	612	4230.8	4172.6	4302.6	nearly normal
4,5	415	2357.5	2397.5	2405.8	normal
1,2,4,5	1027	9220.0	9061.1	9340.2	nearly normal

Table 5-2

EPRI-NODE-P ONRF Values

ONRF

Cycle	Radial	Peak	Remarks
1 and 2	1.0316	1.1020	Rodded Operation
4 and 3	1.0274	1.0372	Unrodded Operation
1,2,4,5	1.0364	1.0821	Combined

Table 5-3

Maximum State Point Data Used In
ONRF Calculation

Corewise Maximum Radial

Cycle	N	$\bar{M}$	$\bar{D}$	S(D)
1,2	27	1.36537	-.009685	.014811
4,5	19	1.24238	.023000	.023557
1,2,4,5	46	1.31547	.003815	.024768

Corewise Maximum Peak

Cycle	N	$\bar{M}$	$\bar{D}$	S(D)
1,2	27	1.60339	-.044504	.052685
4,5	19	1.44579	.001832	.022930
1,2,4,5	46	1.53830	.025365	.048437

Table 5-4

Difference Means and Standard Deviations
for Peaks (C,M $\geq$ 1.0)

Cycle	N	$\bar{D}$	S(D)	$\overline{ABS(D)}$	S(ABS(D))
1	377	.004010	.077792	.061397	.047834
2	235	-.022739	.061448	.049263	.043104
3	211	.014339	.085612	.062537	.060055
4	199	-.018769	.053858	.044837	.035132
5	216	-.012163	.048515	.041721	.027453
1,2	612	-.006262	.073073	.056737	.046416
4,5	415	-.015331	.051191	.043215	.031371
1,2,4,5	1027	-.009926	.065246	.051273	.041524

Table 5-5

Difference Means and Standard Deviations
for Radials ($C,M \geq 1.0$)

Cycle	N	$\bar{D}$	S(D)	$\overline{ABS(D)}$	S(ABS(D))
1	308	-.018619	.038282	.032867	.027010
2	147	-.013606	.050752	.039850	.034107
3	119	-.004970	.053062	.043281	.030844
4	144	-.000243	.029224	.022964	.017974
5	131	.008747	.031790	.026906	.018926
1,2	455	-.016999	.042718	.035123	.029633
4,5	275	.004040	.030748	.024842	.018505
1,2,4,5	730	-.009074	.039949	.031250	.026466

Table 5-6

Percent Difference Means

(C,M $\geq$ 1.0) - Peak

Cycle	Mean % Difference	Mean Absolute % Difference
1	.6877	4.7280
2	-1.5748	3.7361
3	1.3627	4.8951
4	-1.5082	3.6941
5	-1.0253	3.4776
1,2	- .1811	4.3471
4,5	-1.2569	3.5814
1,2,4,5	- .6158	4.0377

Table 5-7

Percent Difference Means

(C,M $\geq$ 1.0) - Radials

Cycle	Mean % Difference	Mean Absolute % Difference
1	-1.5564	2.8345
2	-1.0207	3.3668
3	-0.3839	3.5875
4	-0.0260	2.081
5	0.6648	2.3568
1,2	-1.3833	3.0065
4,5	0.3031	2.2124
1,2,4,5	-0.7480	2.7074

FIGURE 5-1
NUCLEAR RELIABILITY ANALYSIS STAGE TWO
ANALYSIS OF RADIAL(CALC-MEAS) POWER DIFFERENCES
HISTOGRAM OF DIFFERENCE DISTRIBUTIONS FOR 01C1

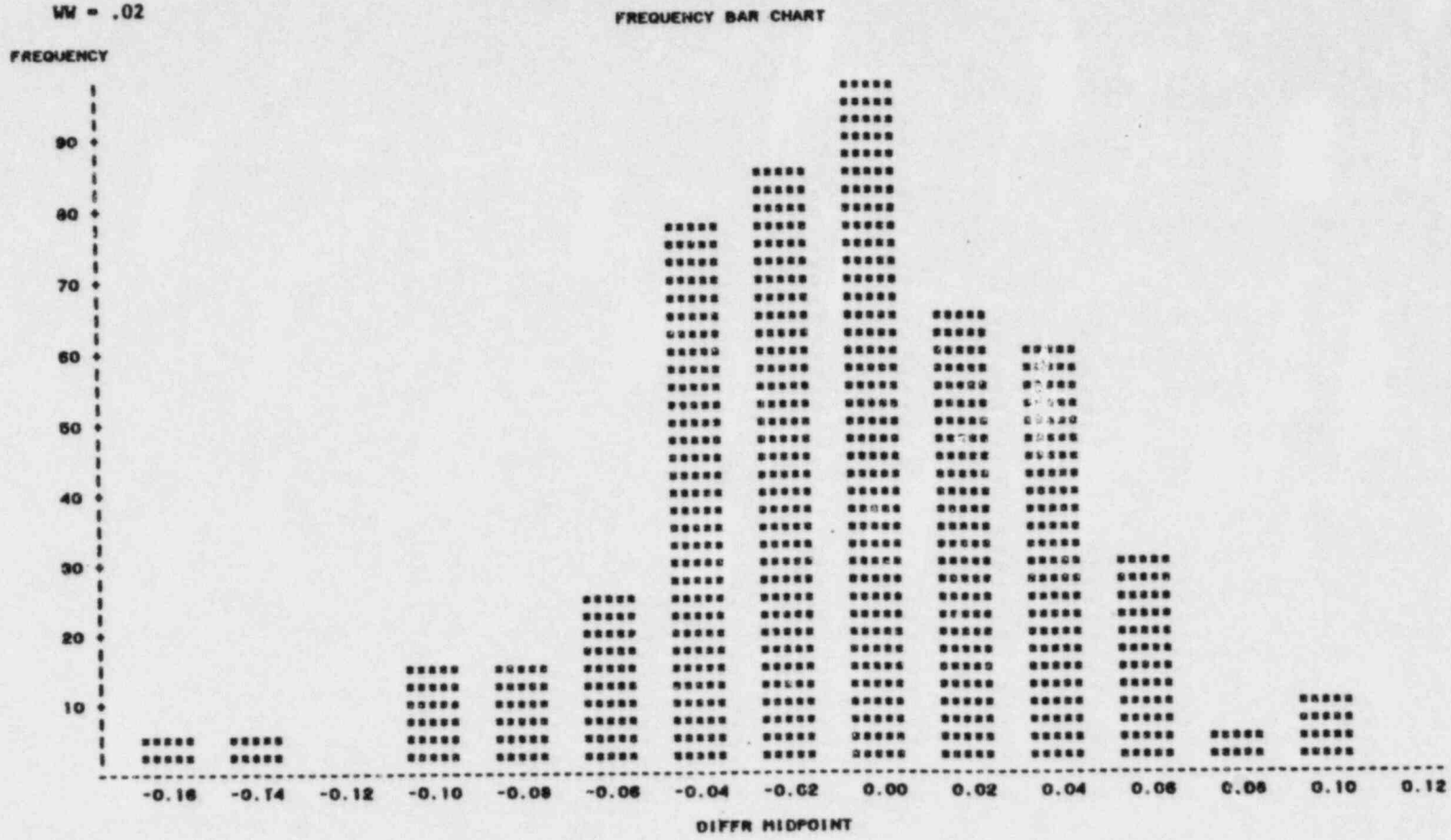

FIGURE 5-2

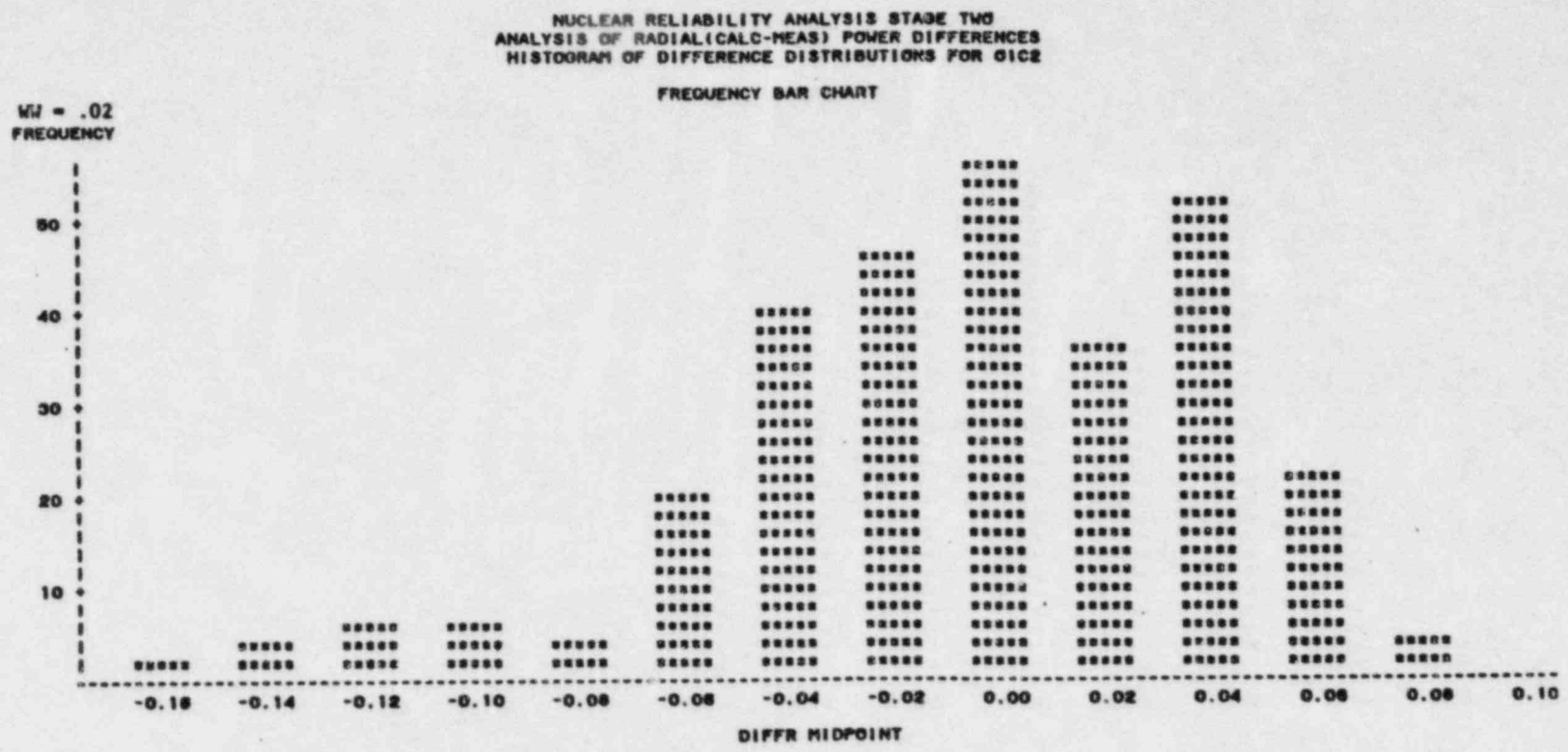
NUCLEAR RELIABILITY ANALYSIS STAGE TWO
ANALYSIS OF RADIAL(CALC-MEAS) POWER DIFFERENCES
HISTOGRAM OF DIFFERENCE DISTRIBUTIONS FOR GIC2
FREQUENCY BAR CHART
WW = .02
FREQUENCY
50
40
30
20
10
-0.16
-0.14
-0.12
-0.10
-0.08
-0.06
-0.04
-0.02
0.00
0.02
0.04
0.06
0.08
0.10
DIFFR MIDPOINT

FIGURE 5-3

NUCLEAR RELIABILITY ANALYSIS STAGE TWO
ANALYSIS OF RADIAL(CALC-MEAS) POWER DIFFERENCES
HISTOGRAM OF DIFFERENCE DISTRIBUTIONS FOR GIC3

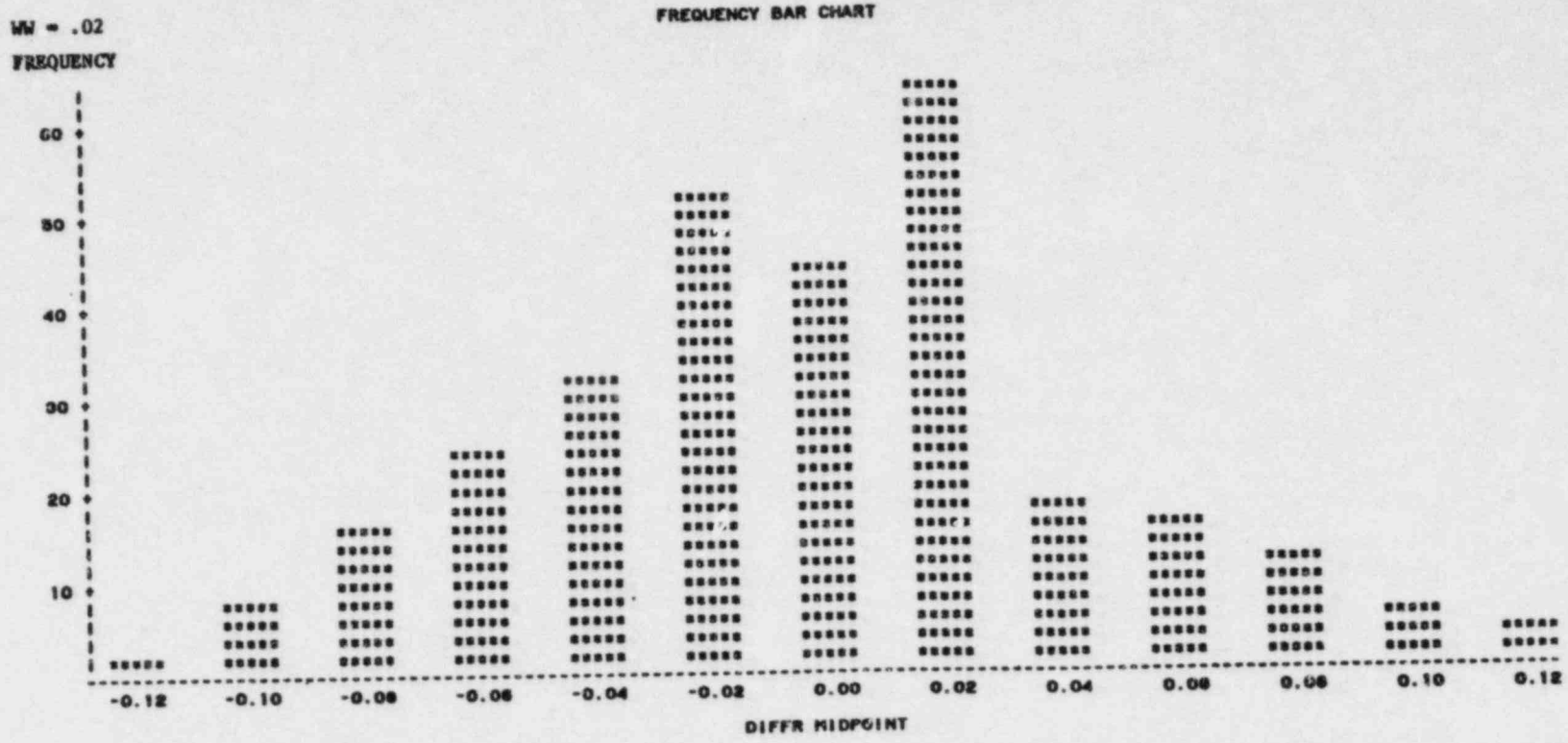

FIGURE 5-4
NUCLEAR RELIABILITY ANALYSIS STAGE TWO
ANALYSIS OF RADIAL(CALC-MEAS) POWER DIFFERENCES
HISTOGRAM OF DIFFERENCE DISTRIBUTIONS FOR 61C6

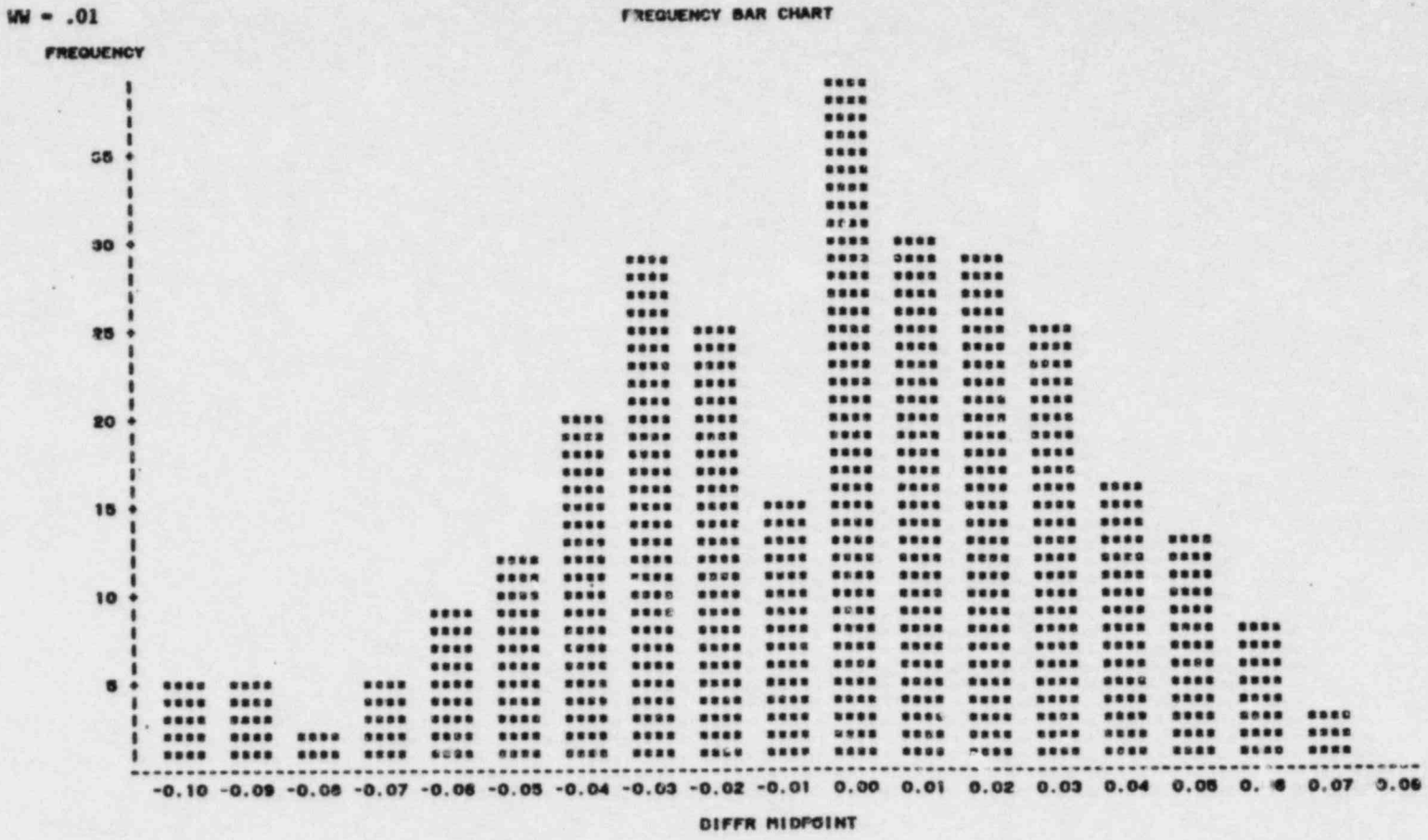

FIGURE 5-5

NUCLEAR RELIABILITY ANALYSIS STAGE TWO
ANALYSIS OF RADIAL(CALC-MEAS) POWER DIFFERENCES
HISTOGRAM OF DIFFERENCE DISTRIBUTIONS FOR CIC4

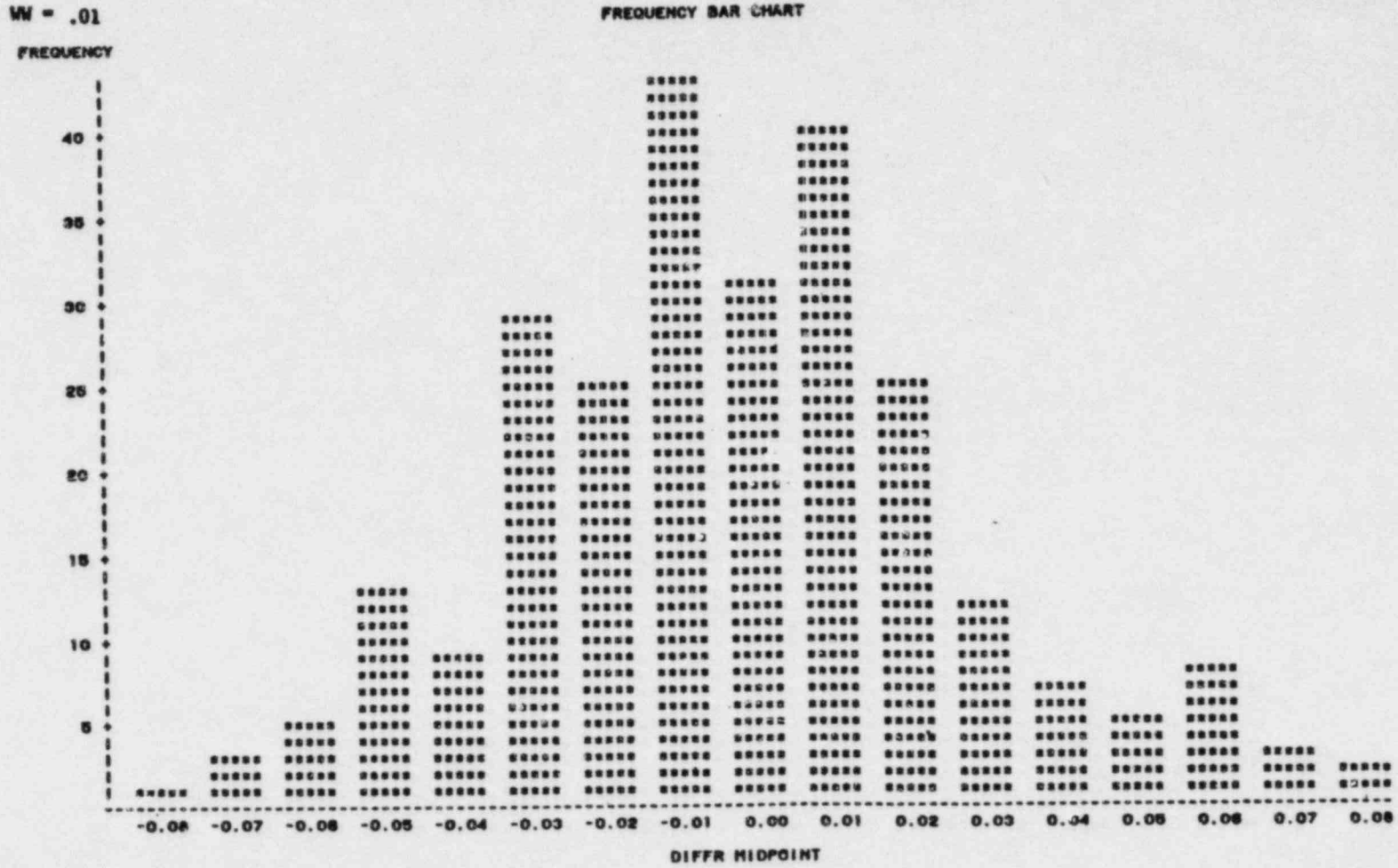

FIGURE 5-6

NUCLEAR RELIABILITY ANALYSIS STAGE TWO
ANALYSIS OF PEAK(CALC-MEAS) POWER DIFFERENCES
HISTOGRAM OF DIFFERENCE DISTRIBUTIONS FOR 01C1

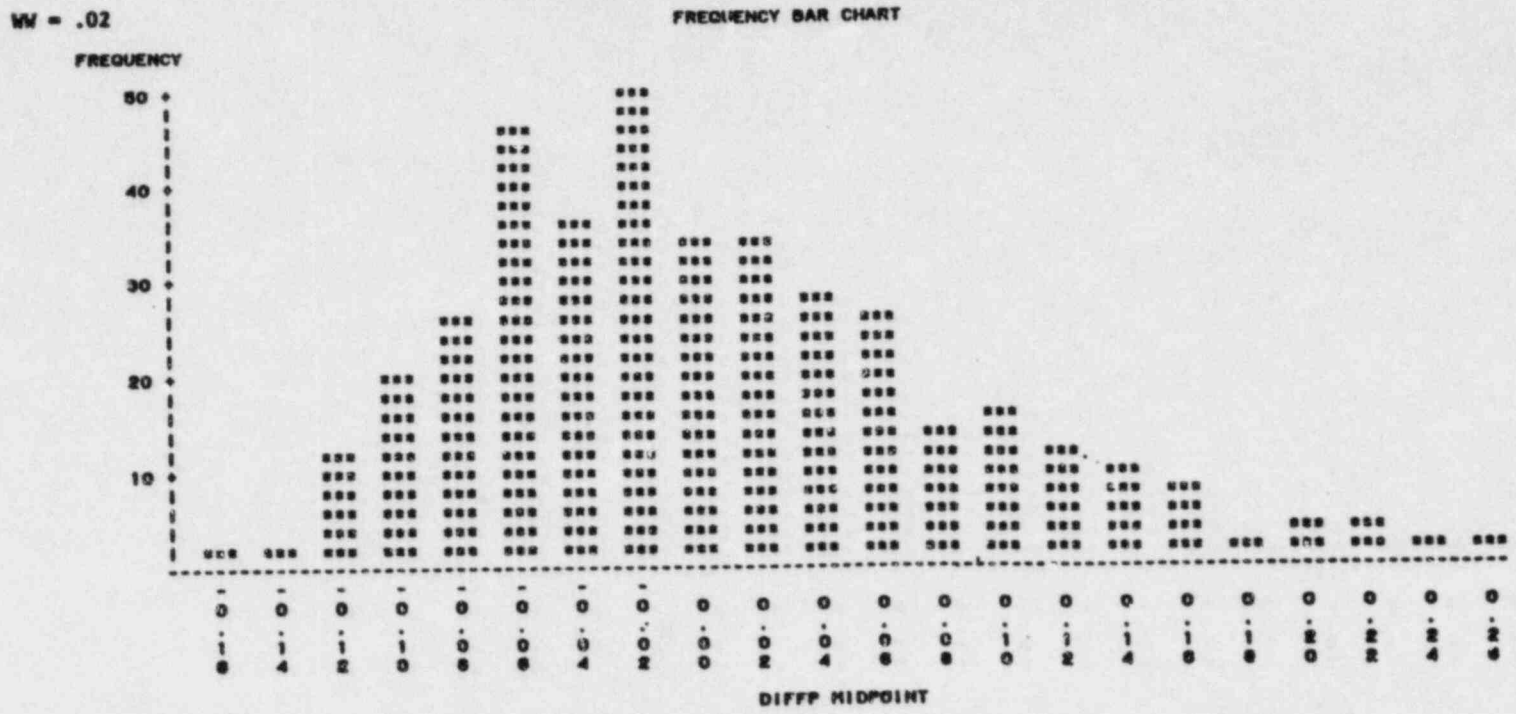

FIGURE 5-7
NUCLEAR RELIABILITY ANALYSIS STAGE TWO
ANALYSIS OF PEAK(CALC-MEAS) POWER DIFFERENCES
HISTOGRAM OF DIFFERENCE DISTRIBUTIONS FOR 01C2

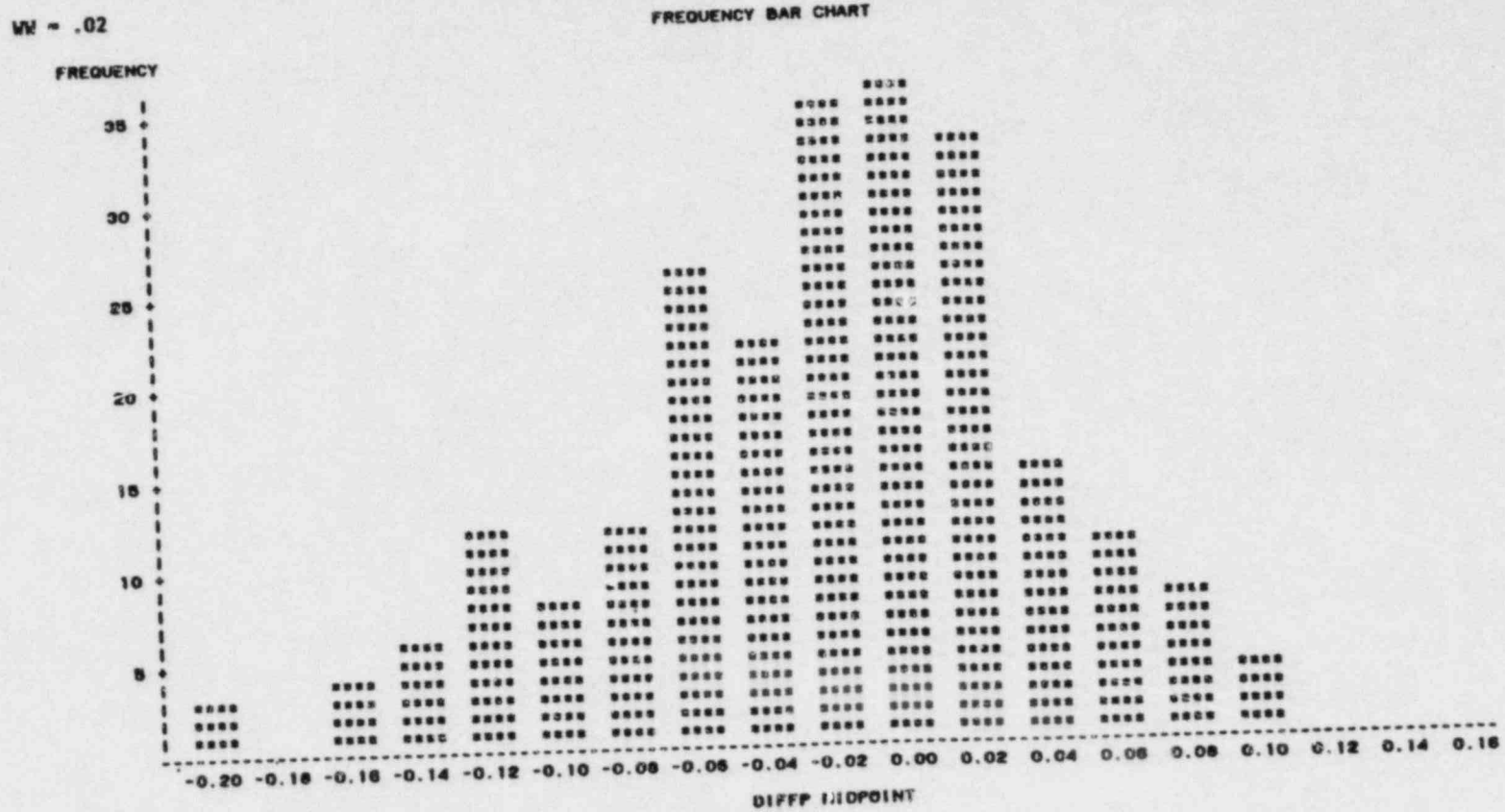

FIGURE 5-8
NUCLEAR RELIABILITY ANALYSIS STAGE TWO
ANALYSIS OF PEAK(CALC-MEAS) POWER DIFFERENCES
HISTOGRAM OF DIFFERENCE DISTRIBUTIONS FOR OIC3

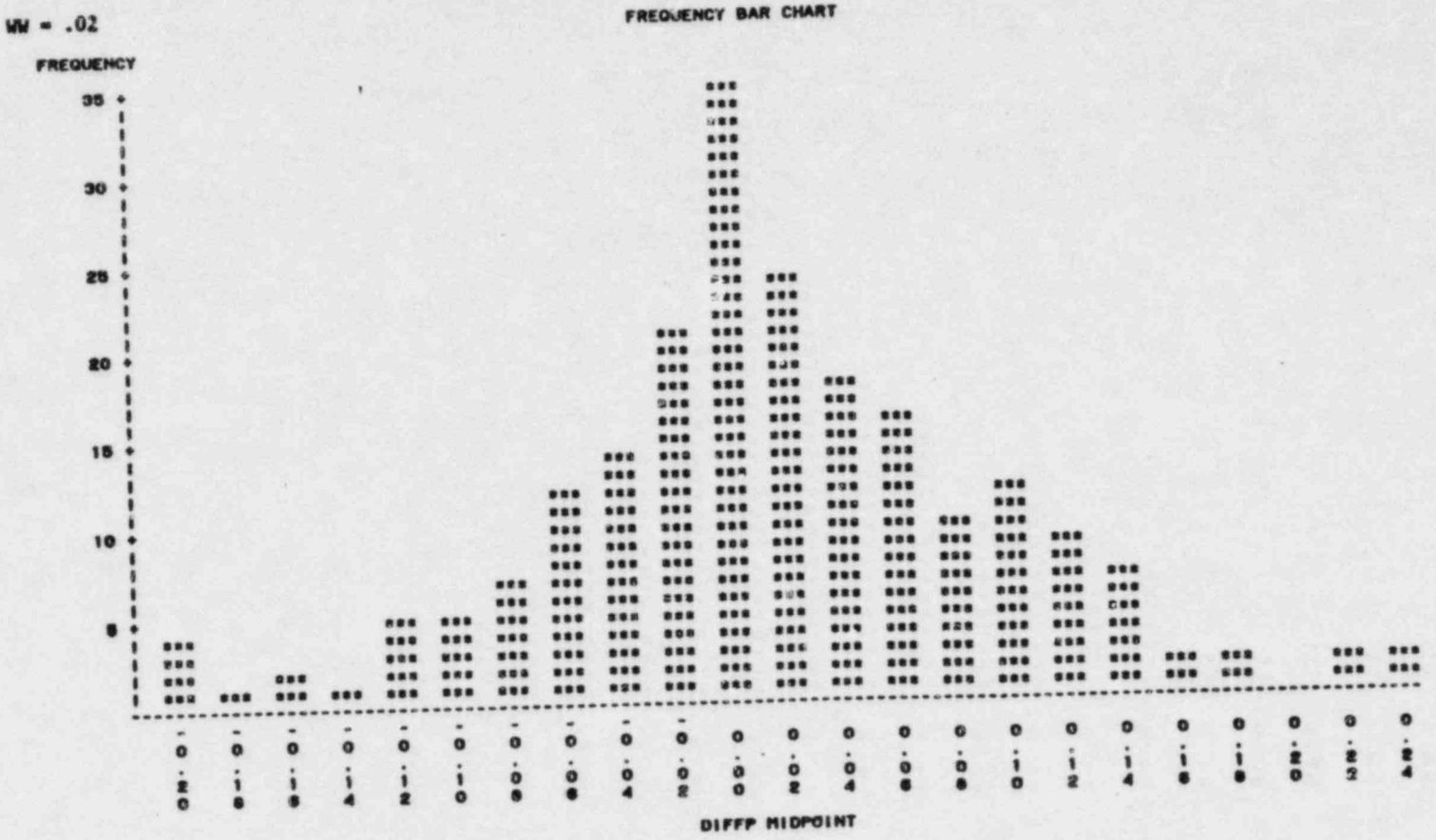

FIGURE 5-9
NUCLEAR RELIABILITY ANALYSIS STAGE TWO
ANALYSIS OF PEAK(CALC-MEAS) POWER DIFFERENCES
HISTOGRAM OF DIFFERENCE DISTRIBUTIONS FOR 61C4

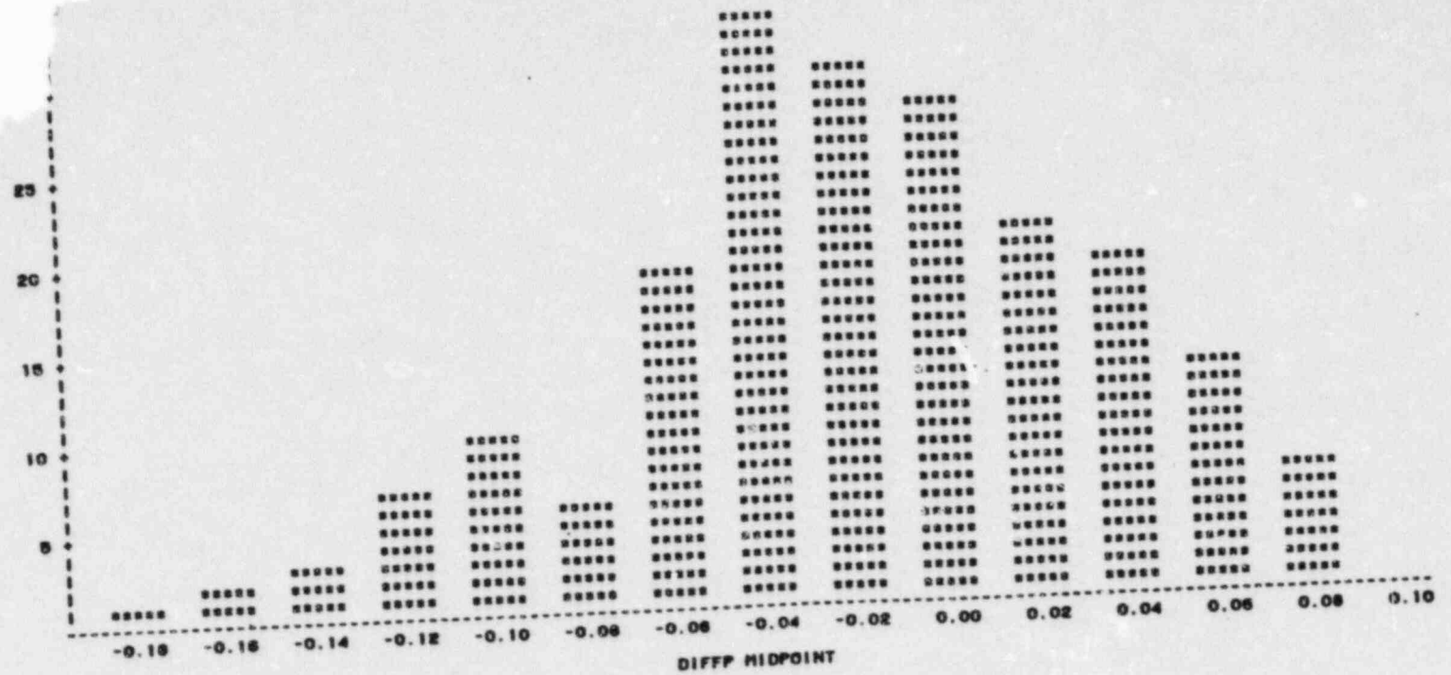

FIGURE 5-10

NUCLEAR RELIABILITY ANALYSIS STAGE TWO
ANALYSIS OF PEAK(CALC-MEAS) POWER DIFFERENCES
HISTOGRAM OF DIFFERENCE DISTRIBUTIONS FOR 01C5

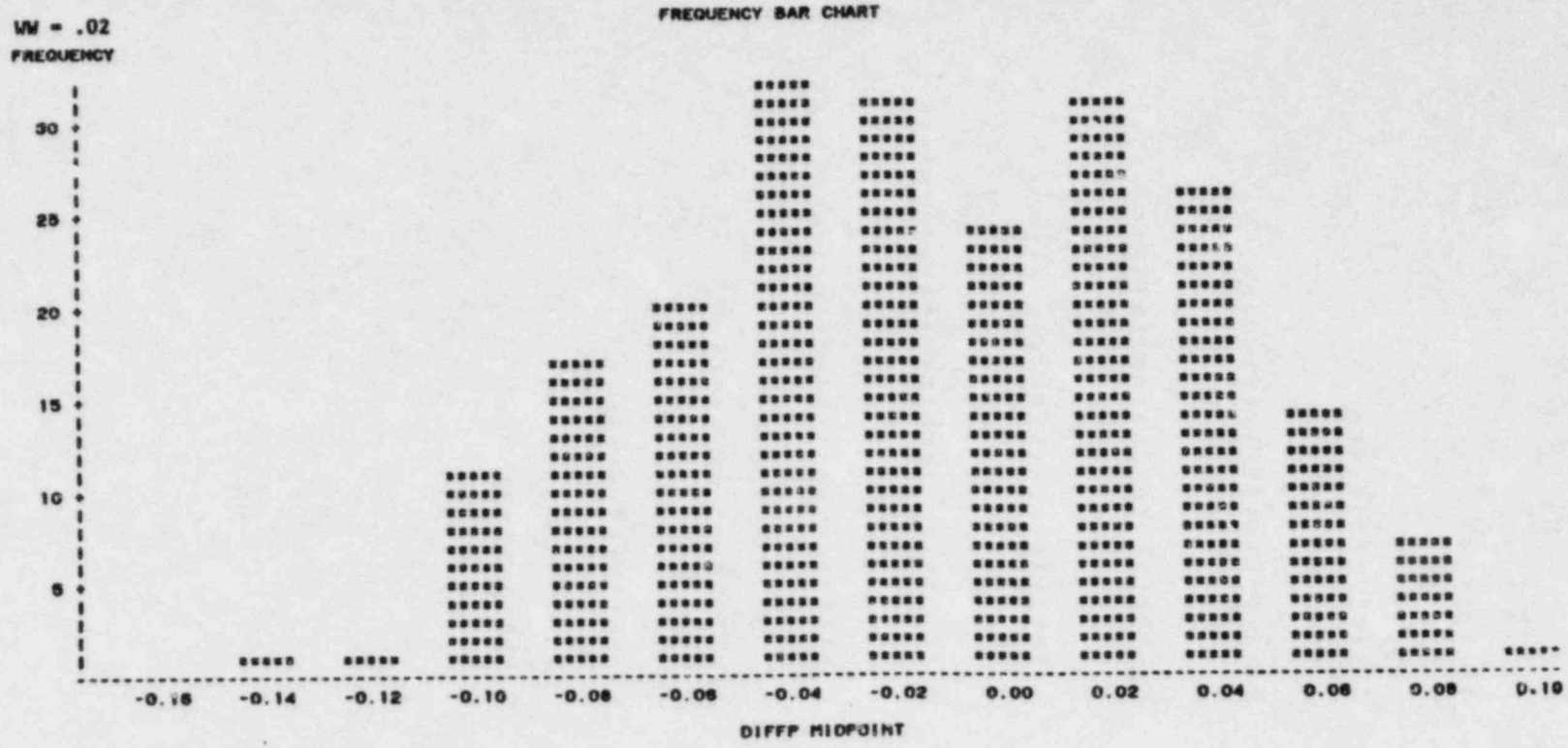

FIGURE 5-11
NUCLEAR RELIABILITY ANALYSIS STAGE TWO
ANALYSIS OF RADIAL(CALC-MEAS) POWER DIFFERENCES(>=1.0)
HISTOGRAM OF DIFFERENCE DISTRIBUTIONS FOR 01C1

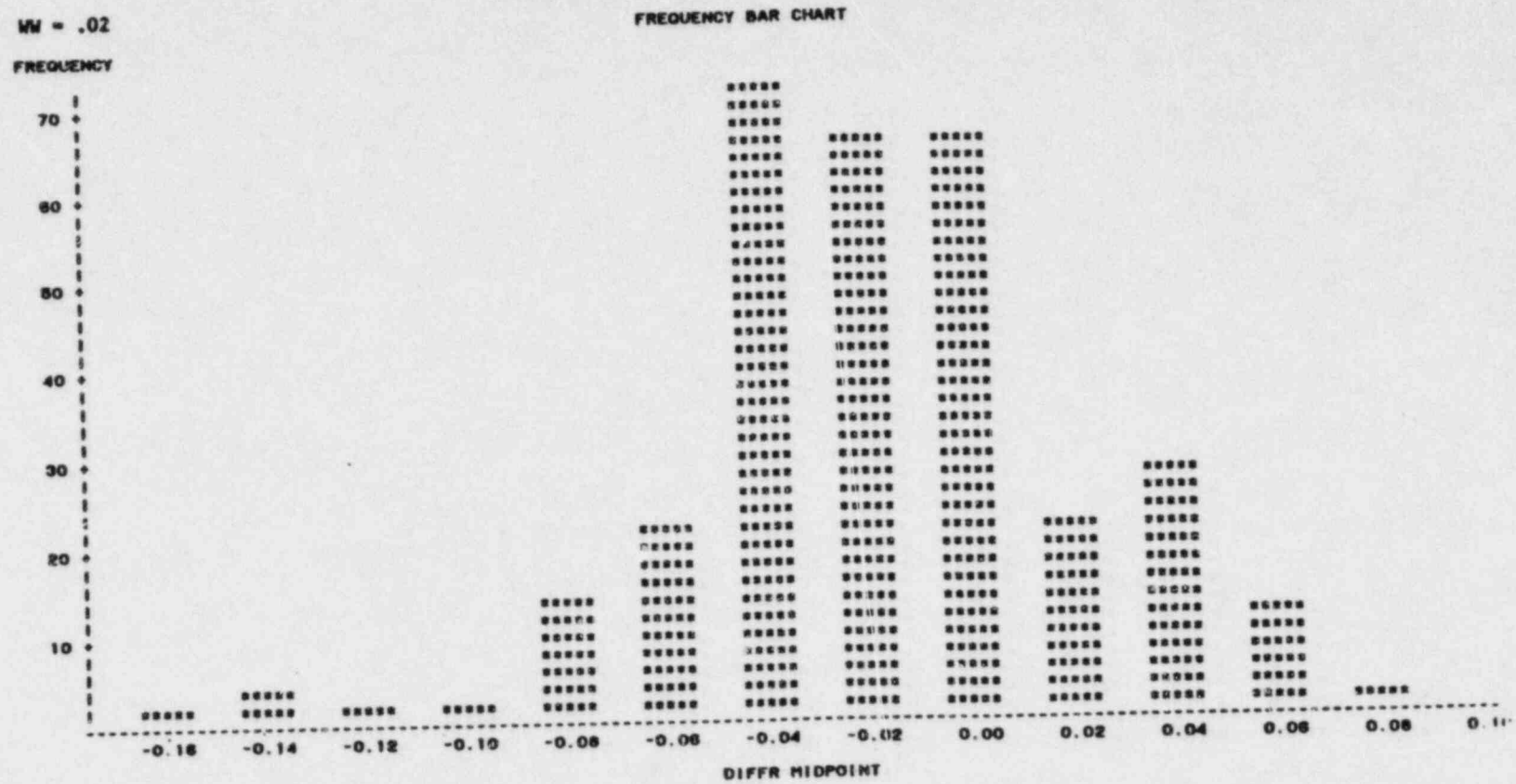

FIGURE 5-12

NUCLEAR RELIABILITY ANALYSIS STAGE TWO
ANALYSIS OF RADIAL(CALC-MEAS) POWER DIFFERENCES(>=1.0)
HISTOGRAM OF DIFFERENCE DISTRIBUTIONS FOR 01C2

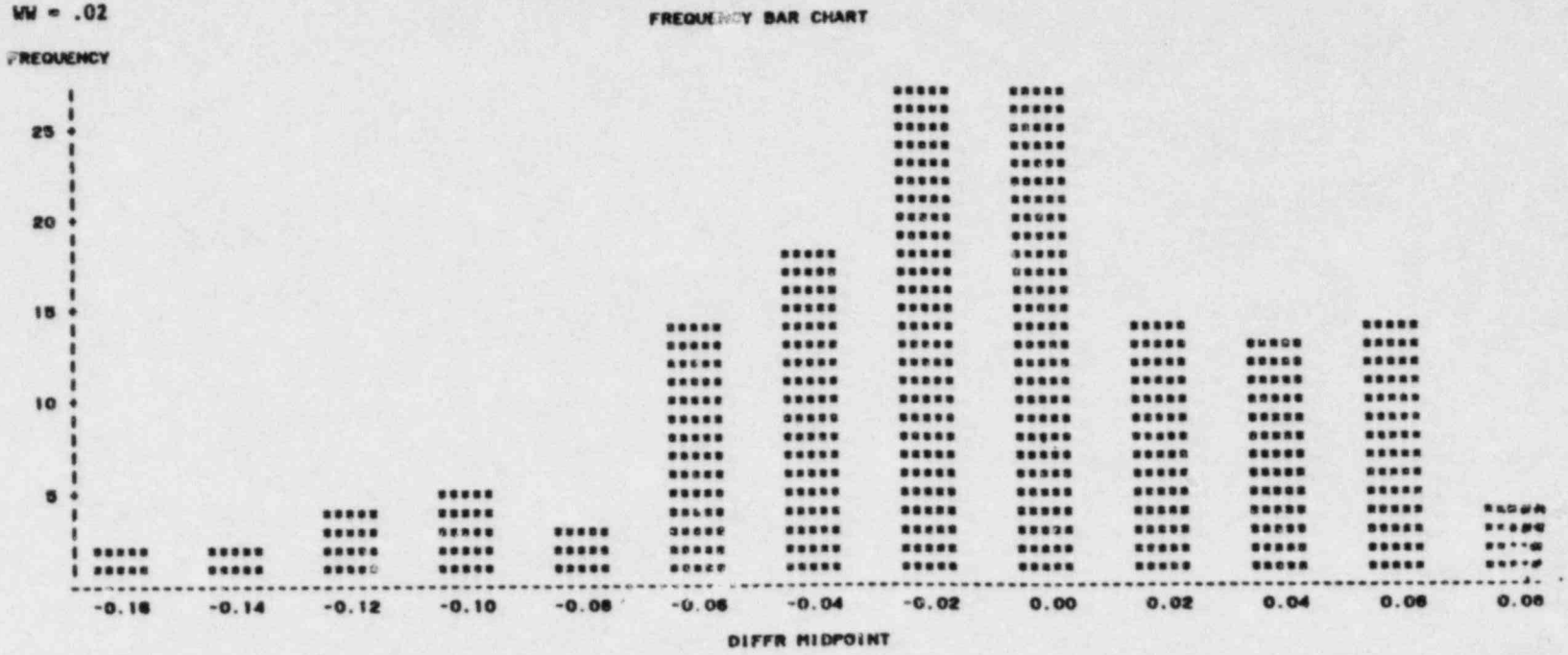

FIGURE 5-13
NUCLEAR RELIABILITY ANALYSIS STAGE TWO
ANALYSIS OF RADIAL(CALC-MEAS) POWER DIFFERENCES(>=1.0)
HISTOGRAM OF DIFFERENCE DISTRIBUTIONS FOR GICS

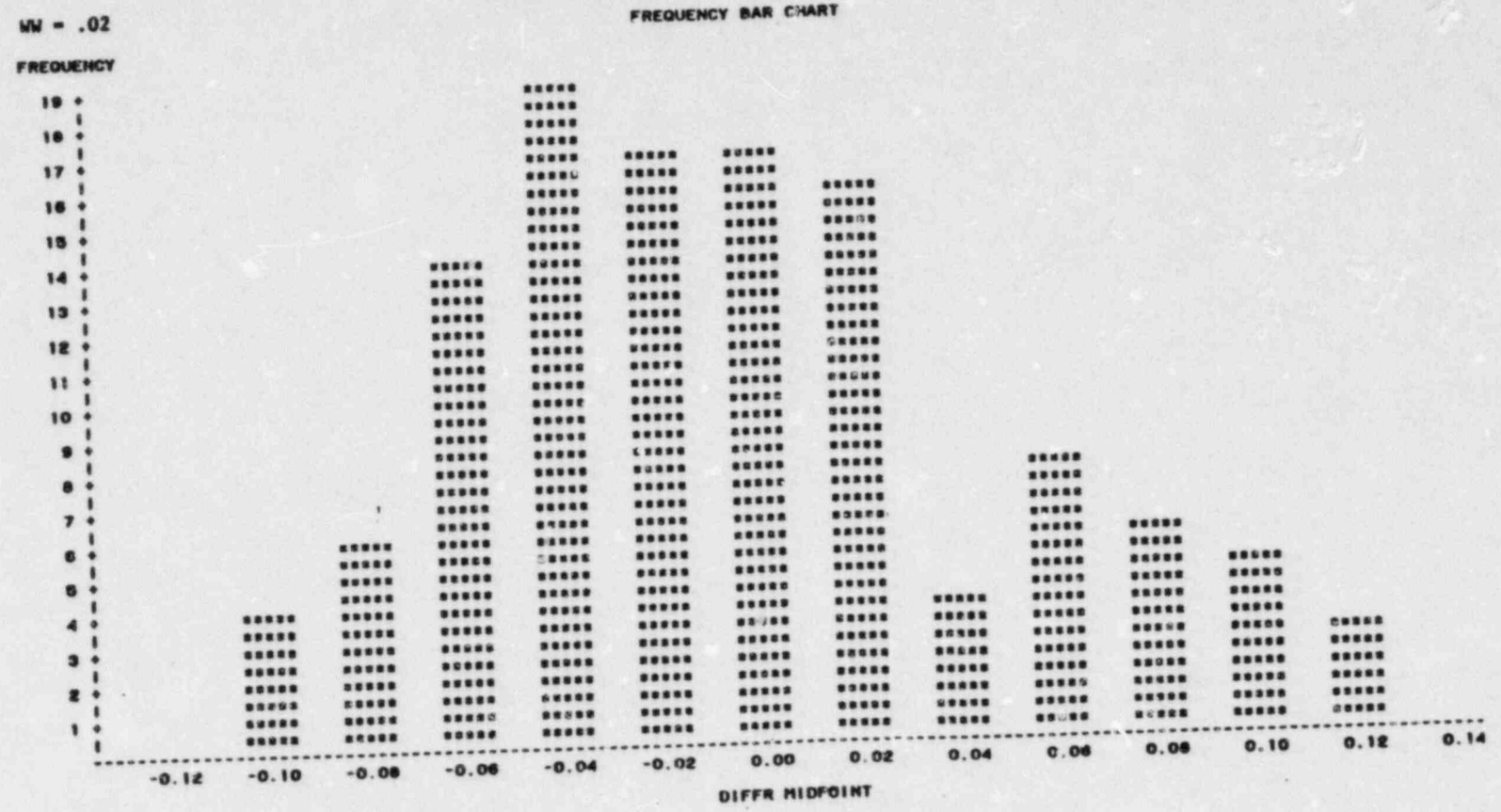

FIGURE 5-14

NUCLEAR RELIABILITY ANALYSIS STAGE TWO
ANALYSIS OF RADIAL(CALC-MEAS) POWER DIFFERENCES(>=1.0)
HISTOGRAM OF DIFFERENCE DISTRIBUTIONS FOR CIC4

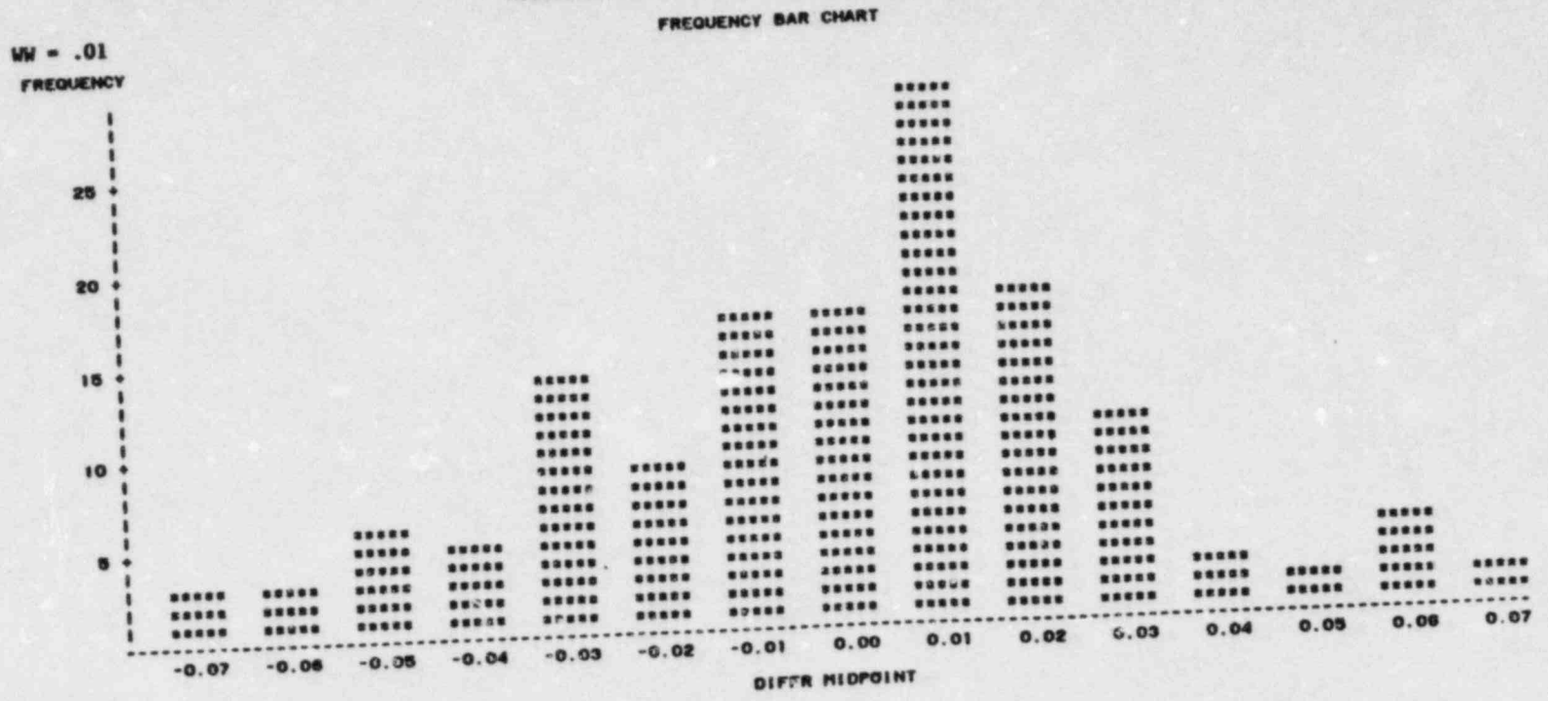

FIGURE 5-15

NUCLEAR RELIABILITY ANALYSIS STAGE TWO
ANALYSIS OF RADIAL(CALC-MEAS) POWER DIFFERENCES(>=1.0)
HISTOGRAM OF DIFFERENCE DISTRIBUTIONS FOR 0105

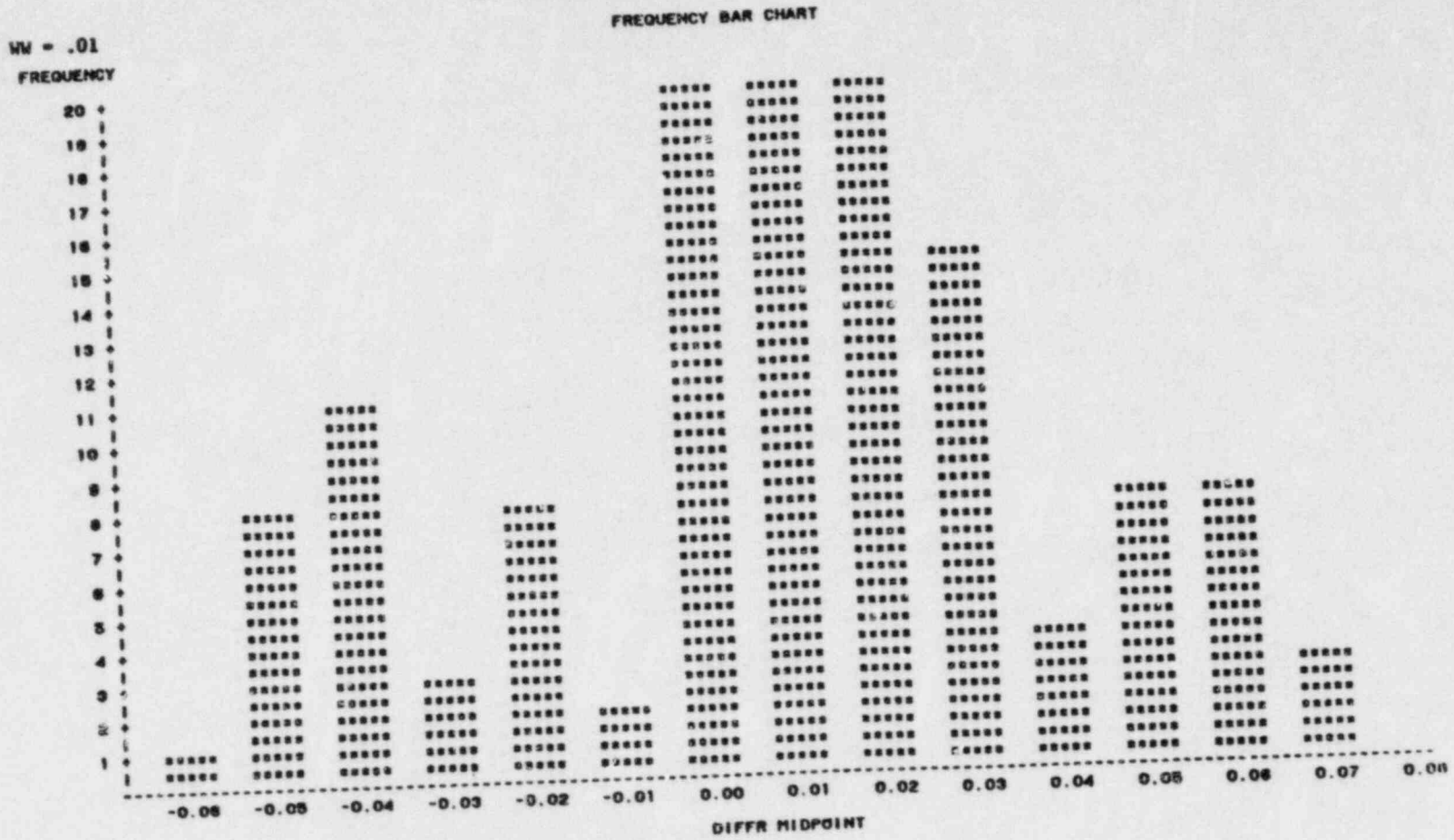

FIGURE 5-16

NUCLEAR RELIABILITY ANALYSIS STAGE TWO
ANALYSIS OF PEAK(CALC-MEAS) POWER DIFFERENCES(>=1.0)
HISTOGRAM OF DIFFERENCE DISTRIBUTIONS FOR 01C1

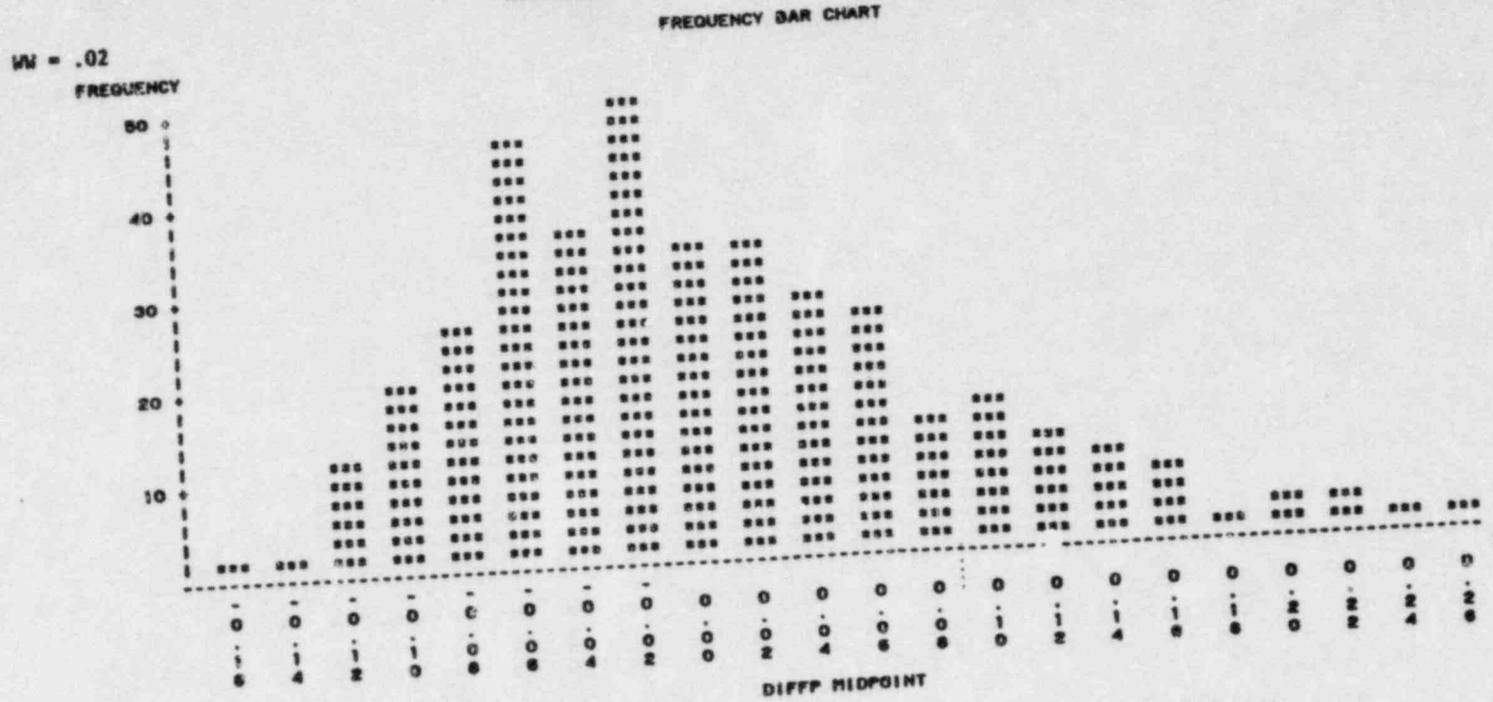

FIGURE 5-17

NUCLEAR RELIABILITY ANALYSIS STAGE TWO
ANALYSIS OF PEAK(CALC-MEAS) POWER DIFFERENCES(>=1.0)
HISTOGRAM OF DIFFERENCE DISTRIBUTIONS FOR G1C2

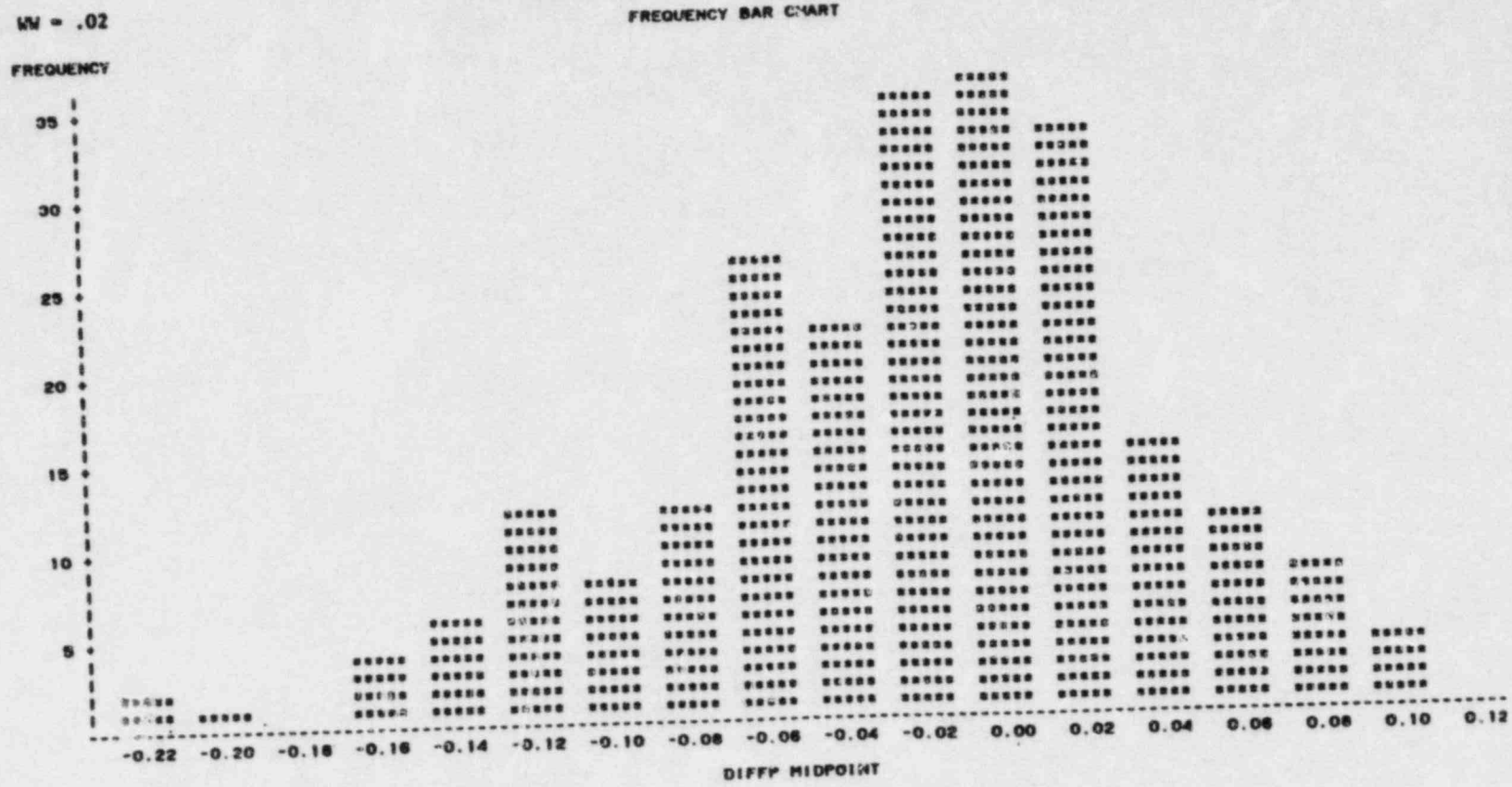

FIGURE 5-18
NUCLEAR RELIABILITY ANALYSIS STAGE TWO
ANALYSIS OF PEAK(CALC-MEAS) POWER DIFFERENCES(>=1.0)
HISTOGRAM OF DIFFERENCE DISTRIBUTIONS FOR 01C4

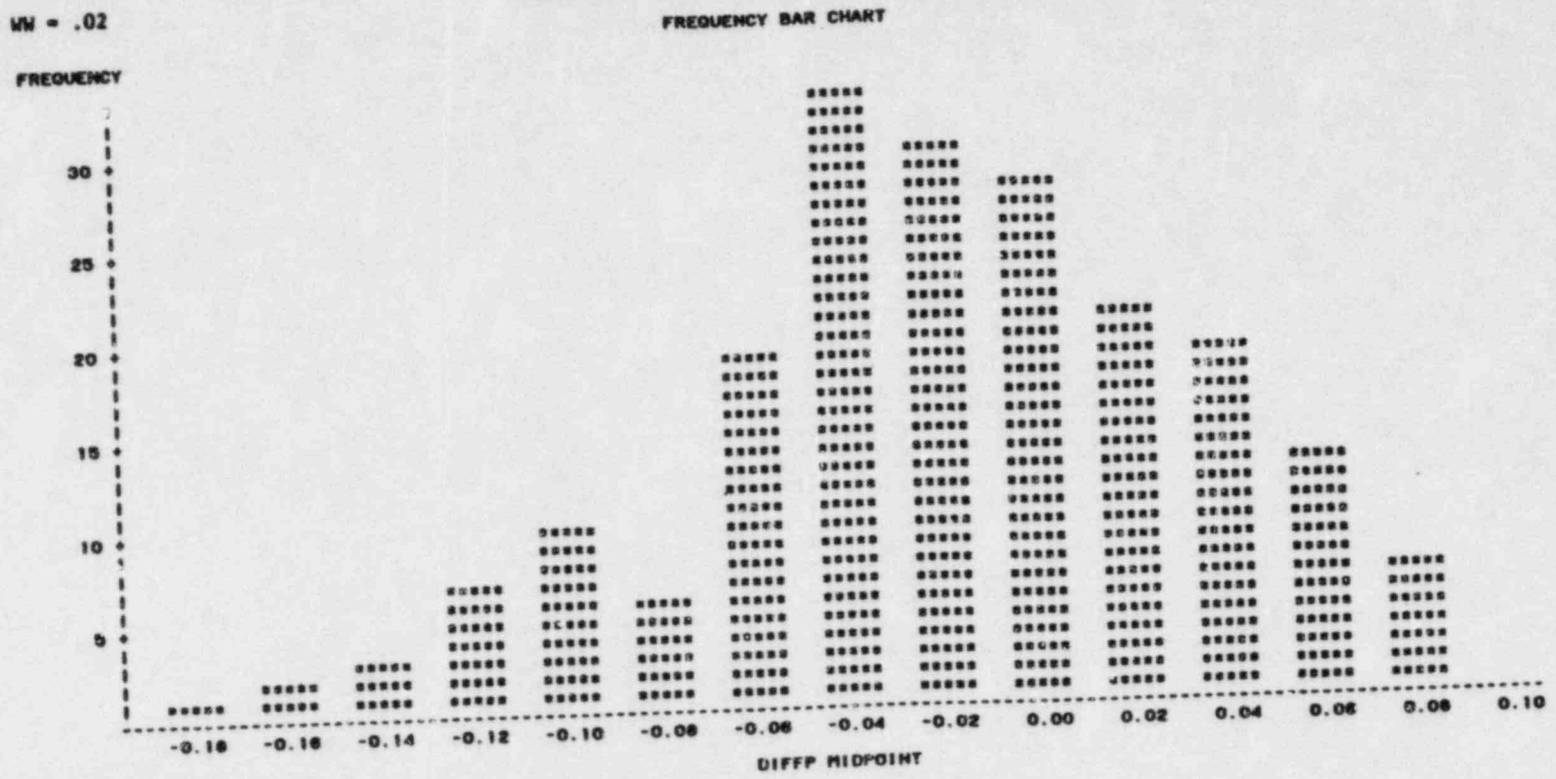

FIGURE 5-19

NUCLEAR RELIABILITY ANALYSIS STAGE TWO
ANALYSIS OF PEAK(CALC-MEAS) POWER DIFFERENCES(>=1.0)
HISTOGRAM OF DIFFERENCE DISTRIBUTIONS FOR OIC3

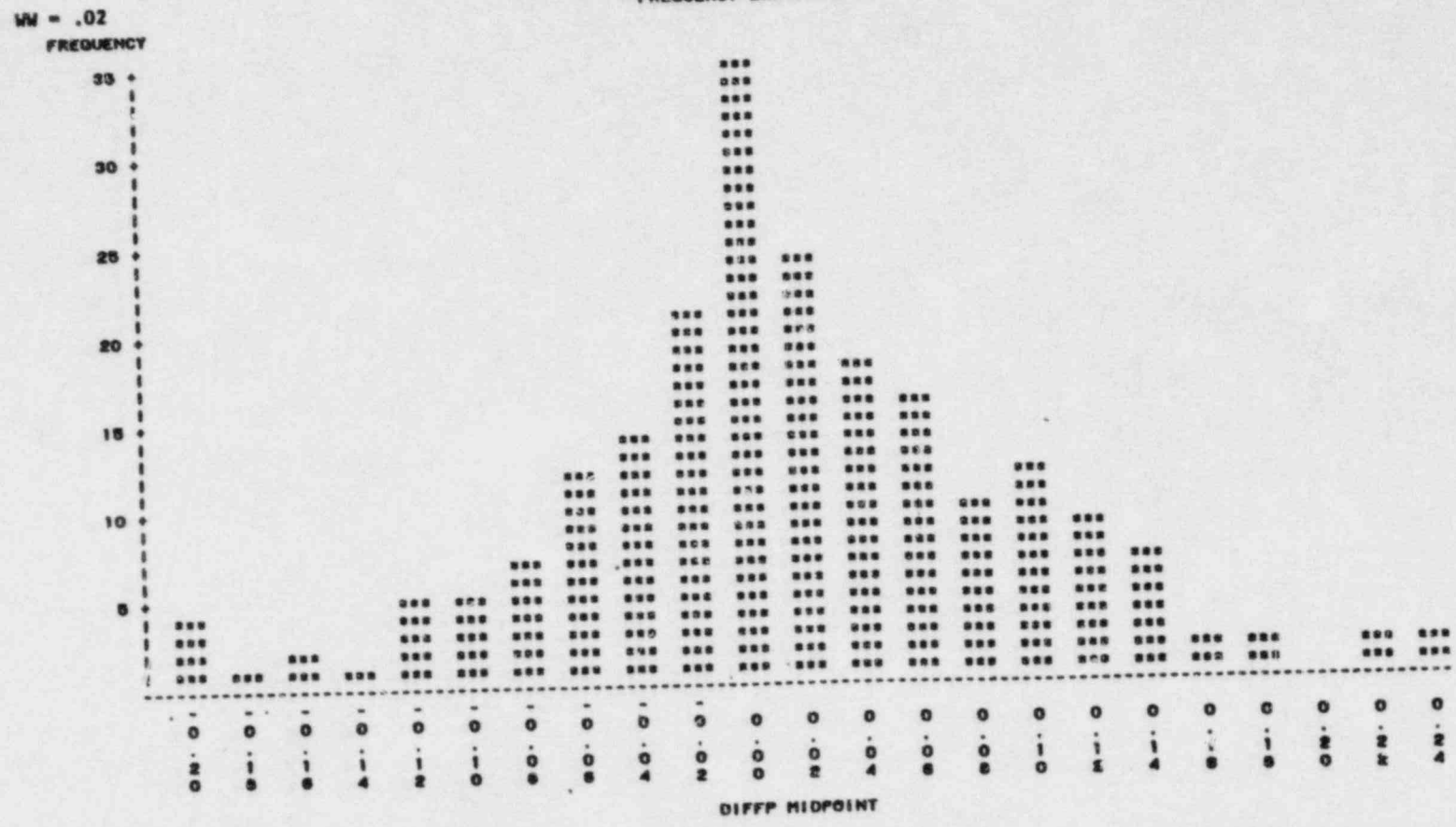

FIGURE 5-20

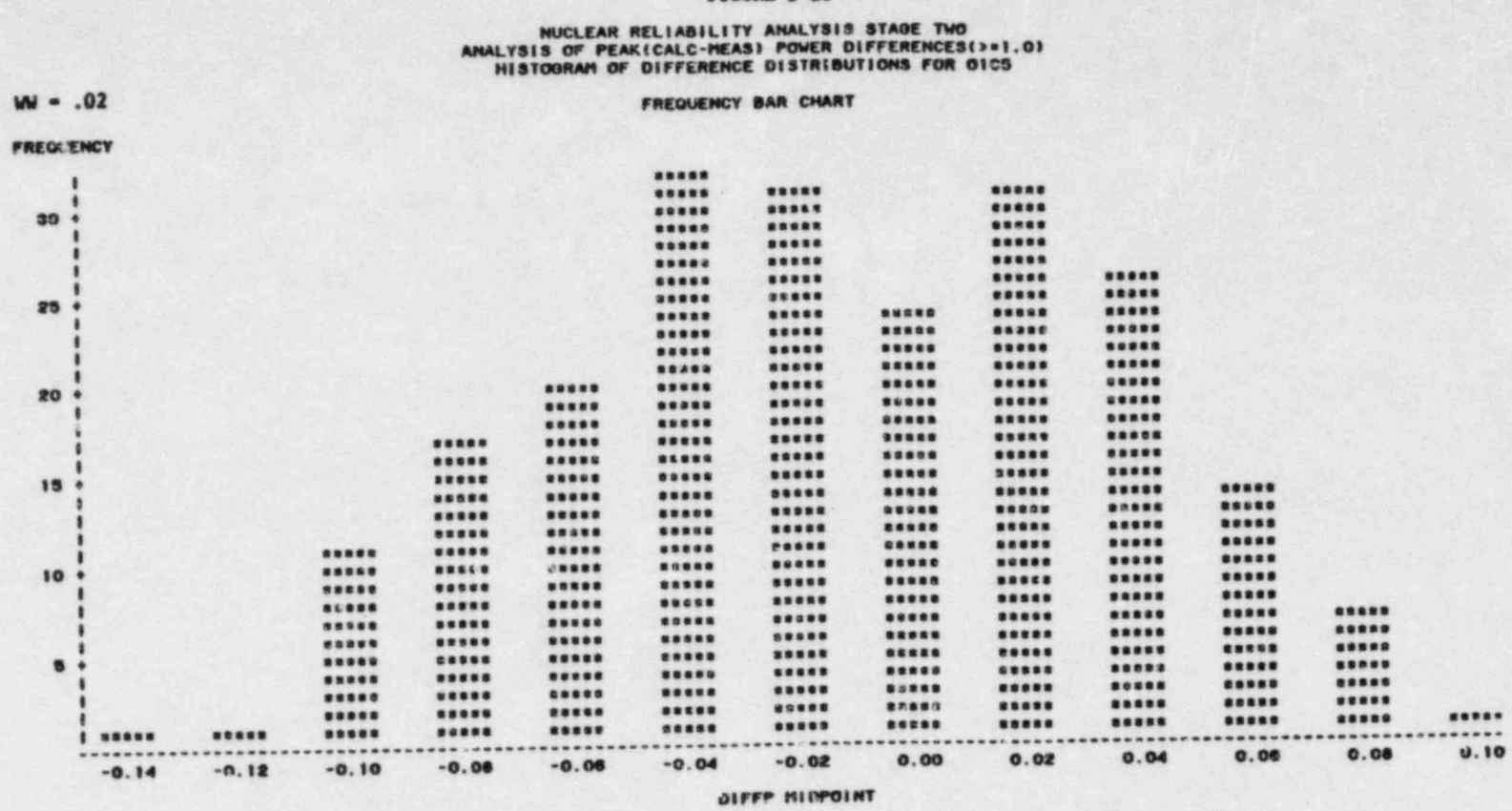
NUCLEAR RELIABILITY ANALYSIS STAGE TWO
ANALYSIS OF PEAK(CALC-MEAS) POWER DIFFERENCES(>=1.0)
HISTOGRAM OF DIFFERENCE DISTRIBUTIONS FOR OICS
FREQUENCY BAR CHART
W = .02
FREQUENCY
30
25
20
15
10
5
-0.14
-0.12
-0.10
-0.08
-0.06
-0.04
-0.02
0.00
0.02
0.04
0.06
0.08
0.10
DIFFP MIDPOINT

FIGURE 5-21
NUCLEAR RELIABILITY ANALYSIS STAGE TWO
ANALYSIS OF RADIAL(CALC-MEAS) POWER DIFFERENCES(>=1.0)
HISTOGRAM OF DIFFERENCE DISTRIBUTIONS FOR G1C1-2

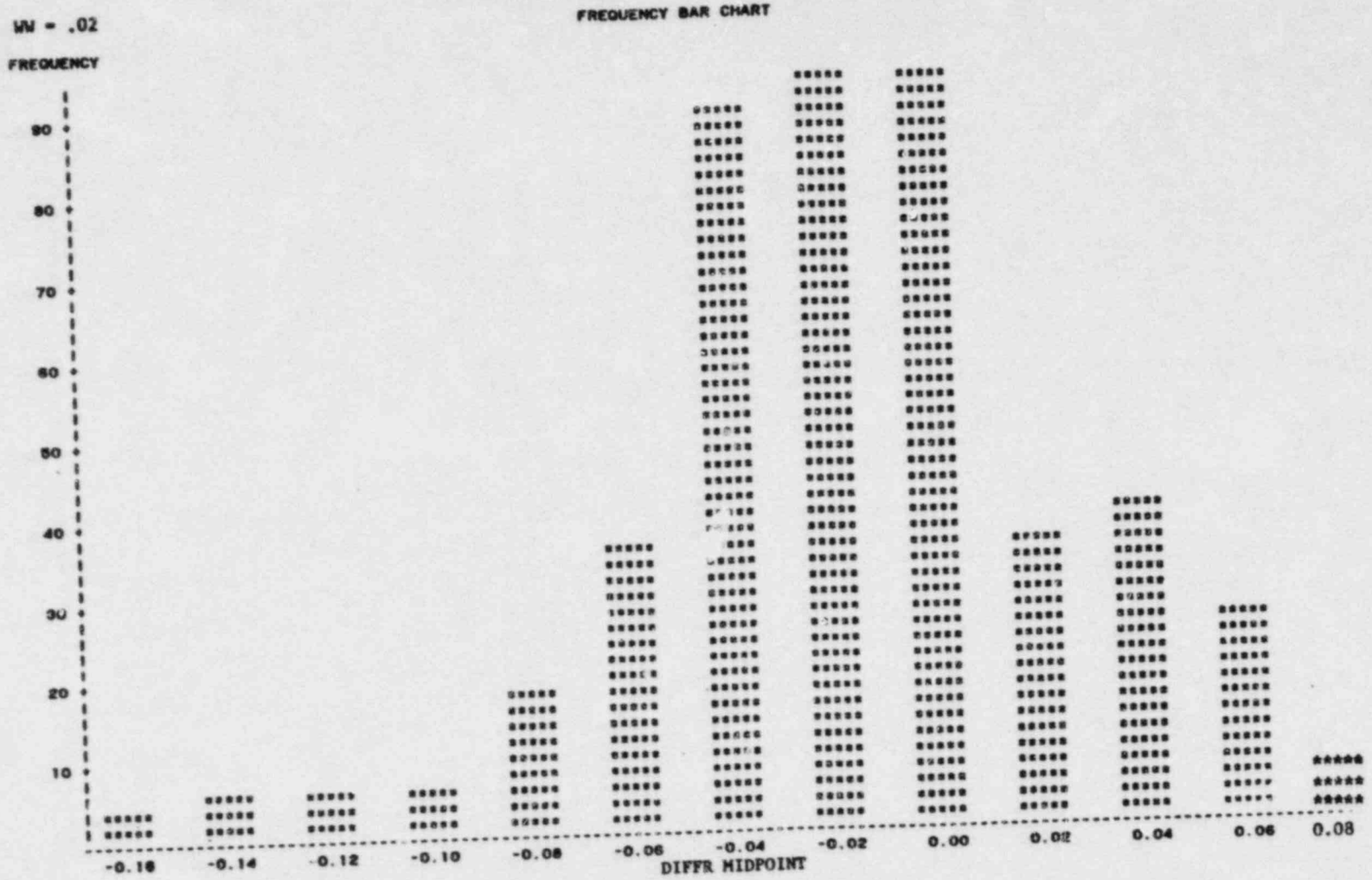

FIGURE 5-22
NUCLEAR RELIABILITY ANALYSIS STAGE TWO
ANALYSIS OF RADIAL(CALC-MEAS) POWER DIFFERENCES(>=1.0)
HISTOGRAM OF DIFFERENCE DISTRIBUTIONS FOR 61C4-5

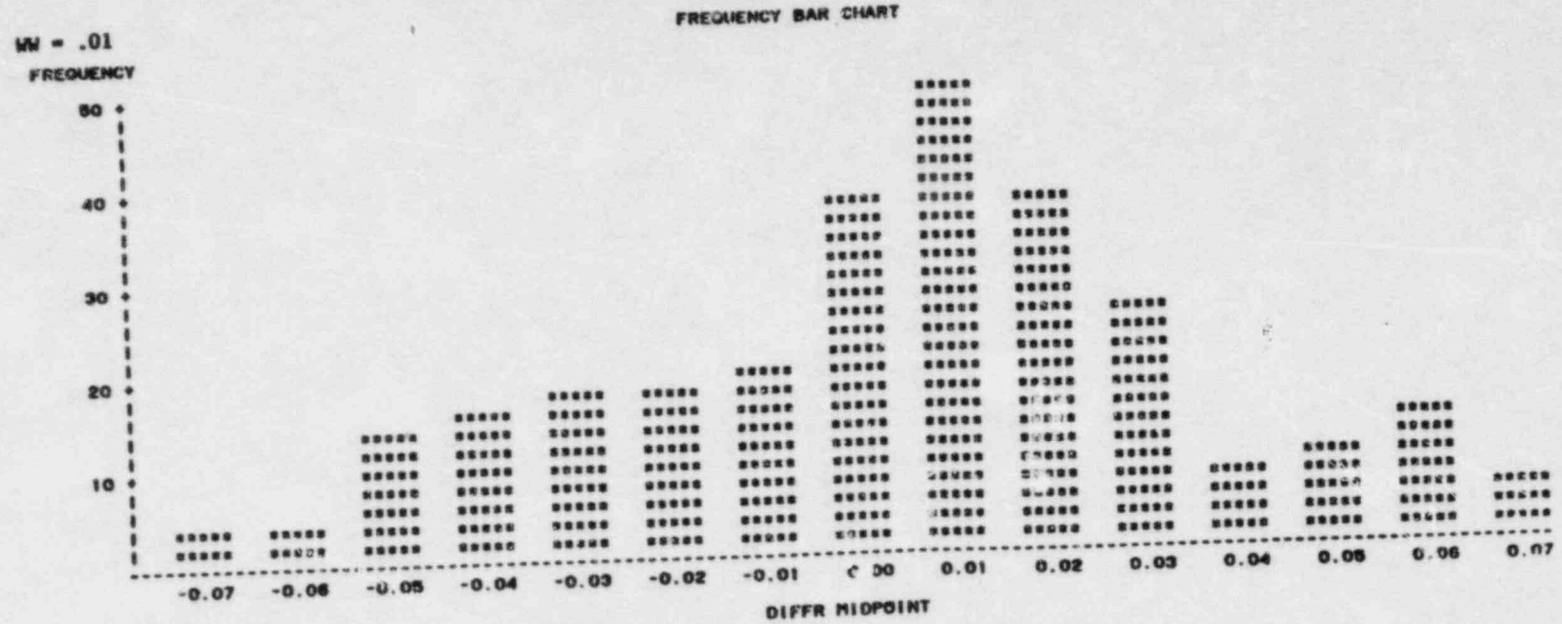

FIGURE 5-23

NUCLEAR RELIABILITY ANALYSIS STAGE TWO
ANALYSIS OF RADIAL(CALC-MEAS) POWER DIFFERENCES(>=1.0)
HISTOGRAM OF DIFFERENCE DISTRIBUTIONS FOR 01C1,2,4,5

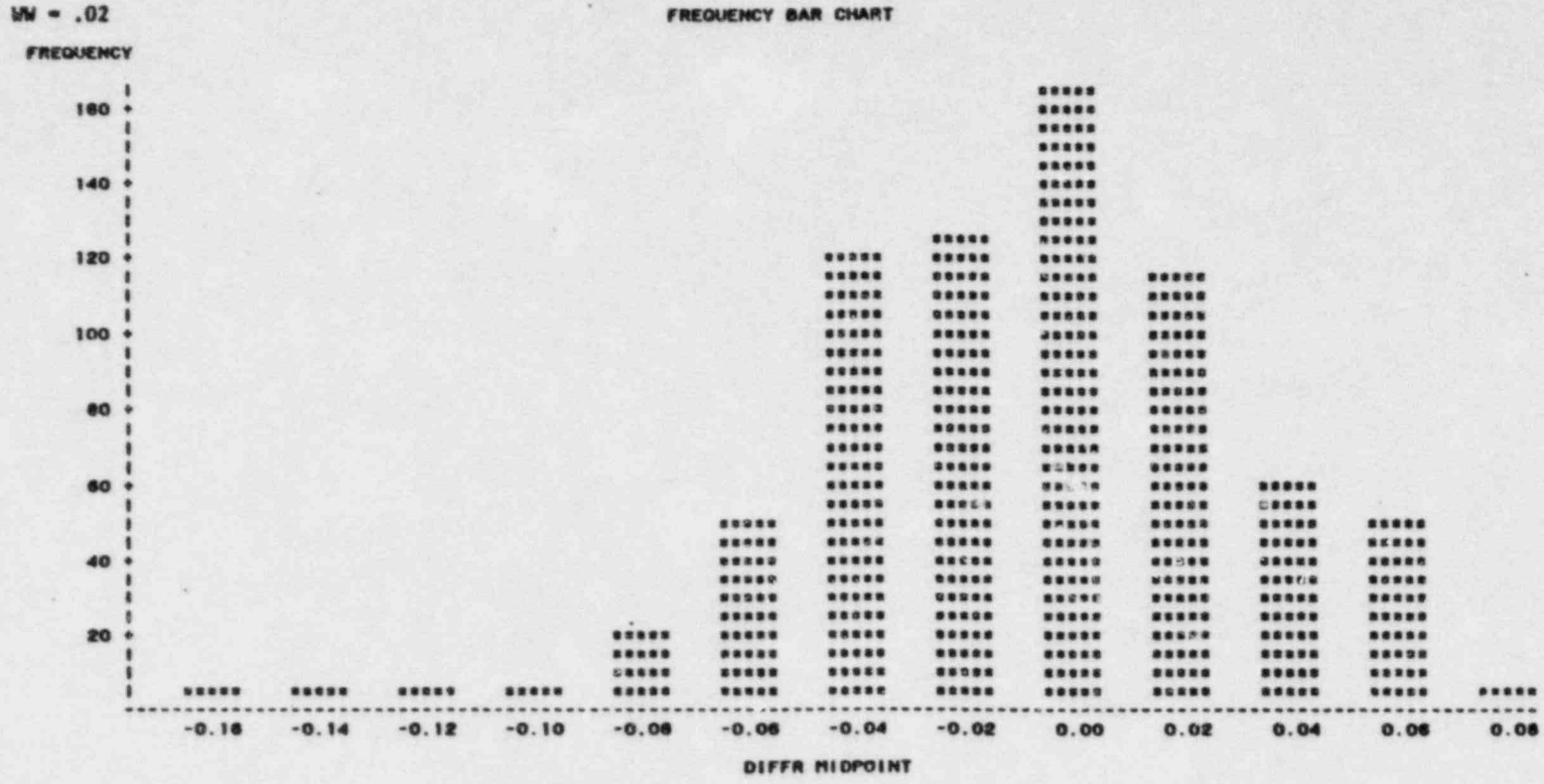

FIGURE 5-24

NUCLEAR RELIABILITY ANALYSIS STAGE TWO
ANALYSIS OF PEAK(CALC-MEAS) POWER DIFFERENCES(>=1.0)
HISTOGRAM OF DIFFERENCE DISTRIBUTIONS FOR CIC1-2

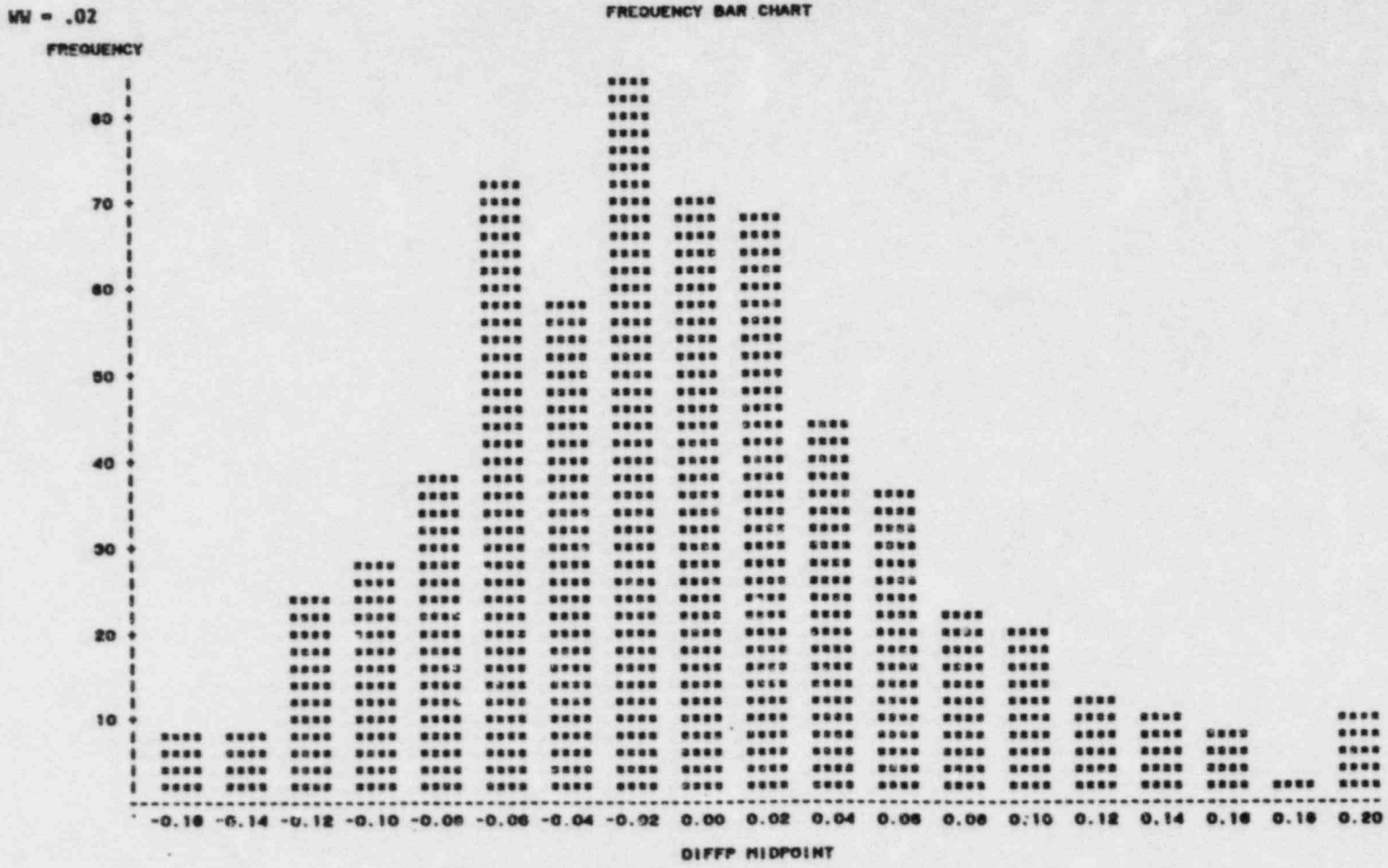

FIGURE 5-25

NUCLEAR RELIABILITY ANALYSIS STAGE TWO
ANALYSIS OF PEAK(CALC-MEAS) POWER DIFFERENCES(>=1.0)
HISTOGRAM OF DIFFERENCE DISTRIBUTIONS FOR G1C4-5

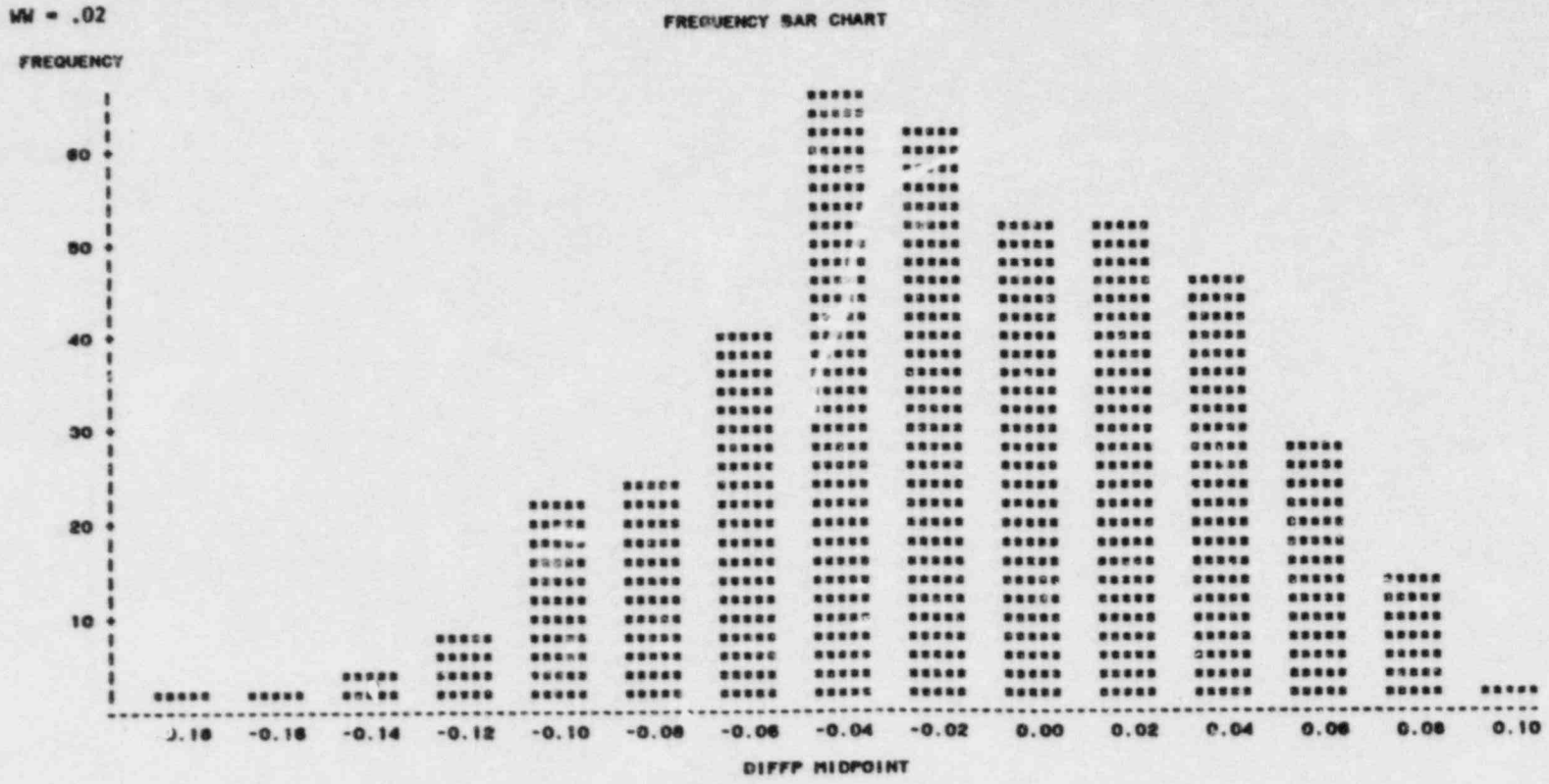

FIGURE 5-26

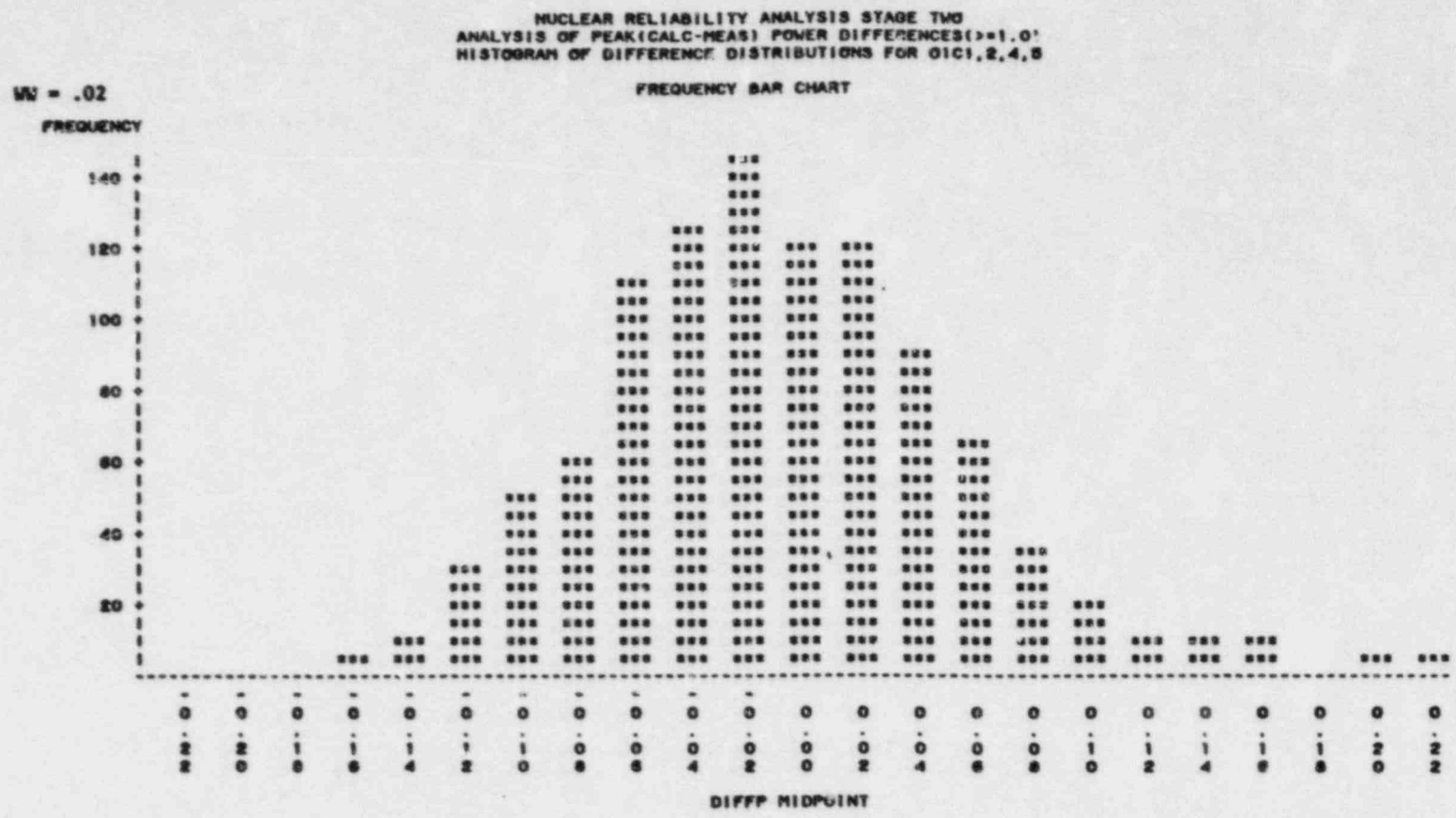
NUCLEAR RELIABILITY ANALYSIS STAGE TWO
ANALYSIS OF PEAK(CALC-MEAS) POWER DIFFERENCES(>=1.0'
HISTOGRAM OF DIFFERENCE DISTRIBUTIONS FOR 01C1,2,4,5
FREQUENCY BAR CHART
W = .02
FREQUENCY
140
120
100
80
60
40
20
0
DIFFP MIDPOINT

FIGURE 5-27
DIFFERENCE FREQUENCY DISTRIBUTION (MAX CALC) - (MAX MEAS)
RADIALS - BY STATE POINT

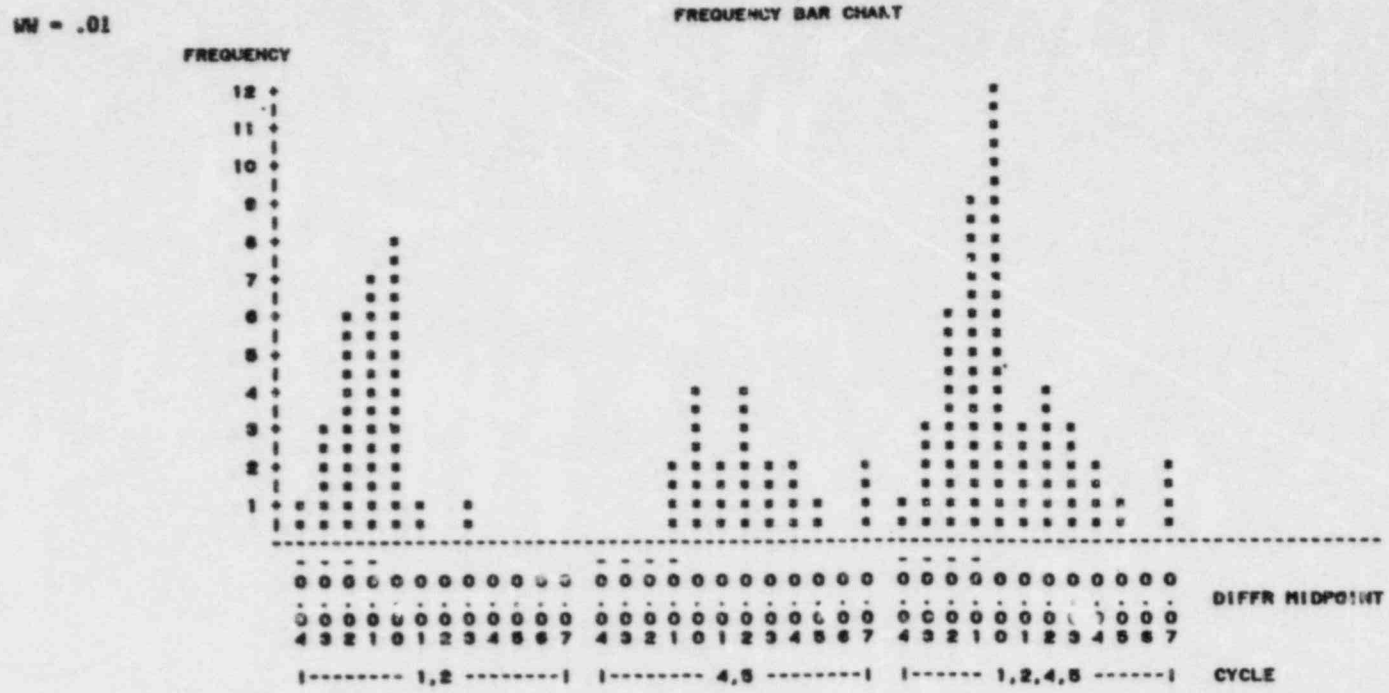

FIGURE 5-28
DIFFERENCE FREQUENCY DISTRIBUTION (MAX CALC) - (MAX MEAS)
PEAKS - BY STATE POINT

FREQUENCY BAR CHART

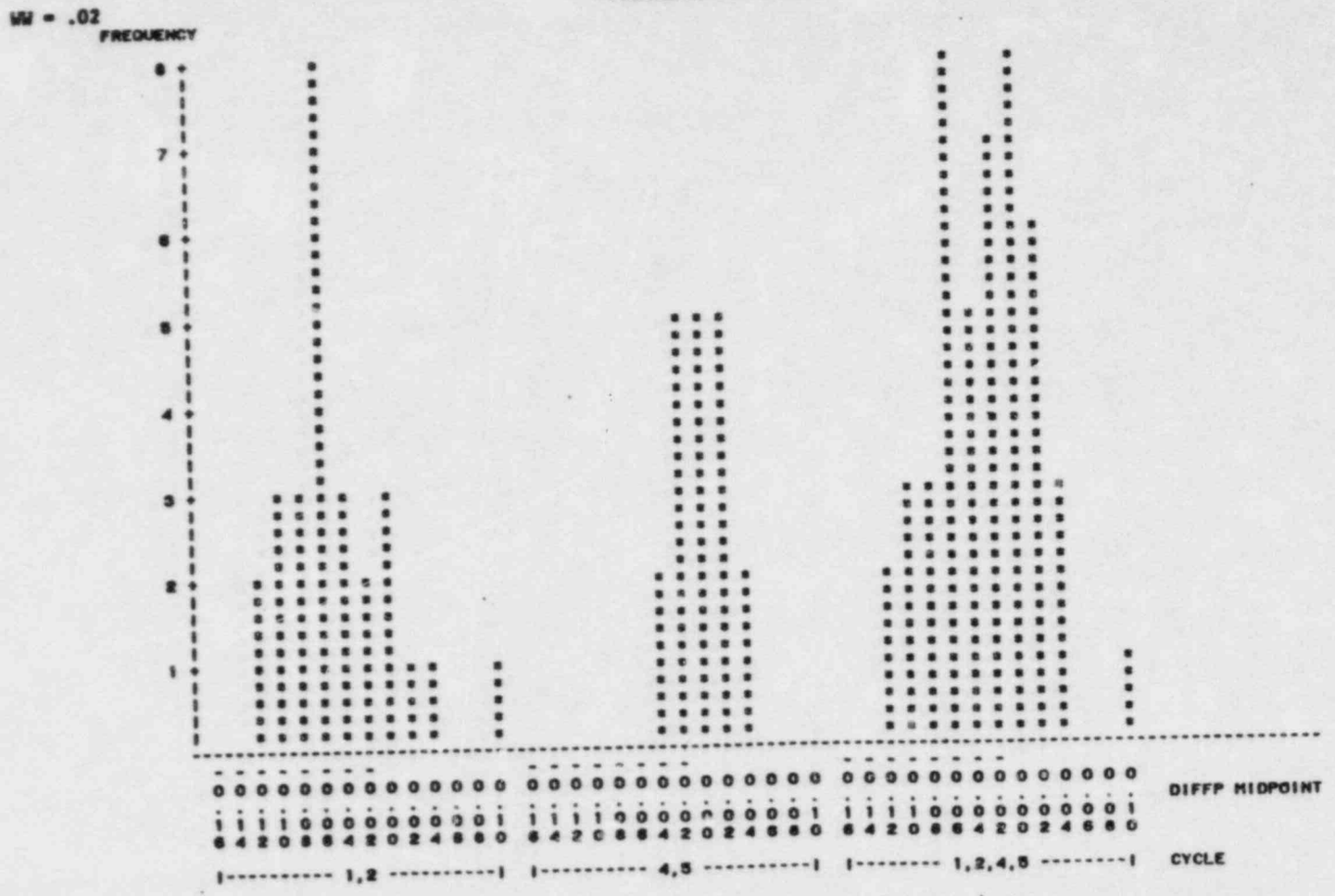

6.0 REFERENCES

1. Duke Power Company, "Oconee Nuclear Station Reload Design Methodology," NFS-1001, April, 1979.

2. B. M. Rothleder, J. R. Fisher, "EPRI-NODE-P," EPRI-ARMP System Documentation, Part II, Chapter 14, September, 1977.

3. Electric Power Research Institute, B. M. Rothleder et. al., "PWR Core Modeling Procedures for Advanced Recycle Methodology Program," RP 976-1, August, 1979.

4. Bettis Atomic Power Laboratory, C. J. Pfeifer, "PDQ-7 Reference Manual II," WAPD-TM-947(6), February, 1971.

5. Proprietary data transfer from Babcock & Wilcox, July 1979.

6. Proprietary data transfer from Babcock & Wilcox, August 1979.

7. Proprietary data transfer from Babcock & Wilcox, February 1980.

8. M. N. Baldwin and M. E. Stern, "Physics Verification Program - Part III, Task 4, Summary Report," BAW-3647, 1971.

9. Electric Power Research Institute, A. Ahlin, M. Edinius, "The Collision Probability Module, EPRI CPM," EPRI ARMP System Documentation, Part II, Chapter 6, September 1977.

10. A. B. Atomenergi, "CASMO USERS' GUIDE," RF-76-4158, April 1978.

11. Electric Power Research Institute, M. Edenius, "EPRI-CPM Benchmarking," EPRI ARMP System Documentaion, Part 1, Chapter 5, November 1975.

12. R. D. Mosteller, "PWR Poisons: Benchmark Criticals and Parameterization Unification," Electric Power Research Institute, RP1252-3, 1979.

13. Electric Power Research Institute, W. J. Eich, "Overview," EPRI ARMP System Documentation, Part 1, Chapter 1, September 1977.

14. M. A. Hannah, "Oconee Nuclear Station Unit 1, Cycle 1 - Core Operation Report," BAW-1413-2, Babcock & Wilcox, Lynchburg, Virginia, June 1975.

15. M. A. Hannah, "Oconee 1 Cycle 2 - Core Operation Report," BAW-1450, Babcock & Wilcox, Lynchburg, Virginia, March 1977.

16. T. N. Ake, "Core Operation Report - Oconee Unit 1, Cycle 3 Operation," BAW-1472, Babcock & Wilcox, Lynchburg, Virginia, October 1977.

17. B. A. Guthrie III, "Core Operation Report - Oconee Unit 1, Cycle 4 Operation," BAW-1515, Babcock & Wilcox, Lynchburg, Virginia, October 1977.

18. D. B. Owens, "Factors For One-Sided Tolerance Limits And For Variables Sampling Plans," SCR-607, Sandia Corporation Monograph, March 1963.

19. American National Standards Institute, Inc., "Assessment of the Assumption of Normality (Employing Individual Observed Values)," ANSI N15.15-1974, 1974.

APPENDIX A - POWER PEAK METHODOLOGY

A.1 Objective

The power produced at the assembly peak, like the local radial, is not a directly measurable quantity. It will be assumed that the assembly axial power shape is a continuous function of normalized assembly height. Therefore, the peak will be defined to be the maximum value of this function, evaluated over the vertical axis of the fuel assembly. The vertical axis will be normalized such that the level at the top of the active stack height will be 1.0.

When a core is simulated in an R-Z geometry using diffusion theory, the axial power shape can be approximated by the following Fourier series:

$$P(z) = A_o + \sum_{n=1}^{\infty} A_n \text{ Sin } (n\pi z) + B_n \text{ Cos } (n\pi z) \qquad \text{(A-1)}$$

where: A_o, A_n, B_n = Fourier series coefficients
z = normalized vertical axis variable
n = Fourier sequence number

A.2 Method of Series Evaluation

In evaluating the order of the series in Equation A-1, there are only seven measured points per assembly; therefore, the series was truncated to three sine and three cosine terms. It will be assumed that A_o is negligible.

Equation A-1 then becomes:

$$P(z) = \sum_{n=1}^{3} A_n \text{ Sin } (n\pi z) + B_n \text{ Cos } (n\pi z) \qquad \text{(A-2)}$$

Before the axial powers were fit, the normalized height variable was transformed in order to incorporate nonzero power production at the ends of the pellet stacks. Then, the seven-level measured powers were fit, yielding a

fitted "measured" axial power series for each assembly at each state point. The same procedure was followed for the twelve-level EPRI-NODE-P calculated powers.

The measured fits produced series which yielded residual sums of squares in the neighborhood of 3.8×10^{-4} to 4.8×10^{-6}. The calculated power fits likewise had small residuals ranging from 1.0×10^{-3} to 6.0×10^{-3}. Although the calculated residuals are larger, twelve points instead of seven were fitted to the same type of six term function.

These fitted functions were then evaluated over 2 inch increments of assembly length. Plots of fitted functions and fit points are shown in Figures A-1 to A-70. In these plots, the "+" is the fitted calculated power, the "*" fitted measured power; and C, M represent calculated and measured data points, respectively. Agreement between fit points and functions are very good even for highly convoluted power shapes.

Figure A-1

ASSEMBLY H-8 CYCLE 1

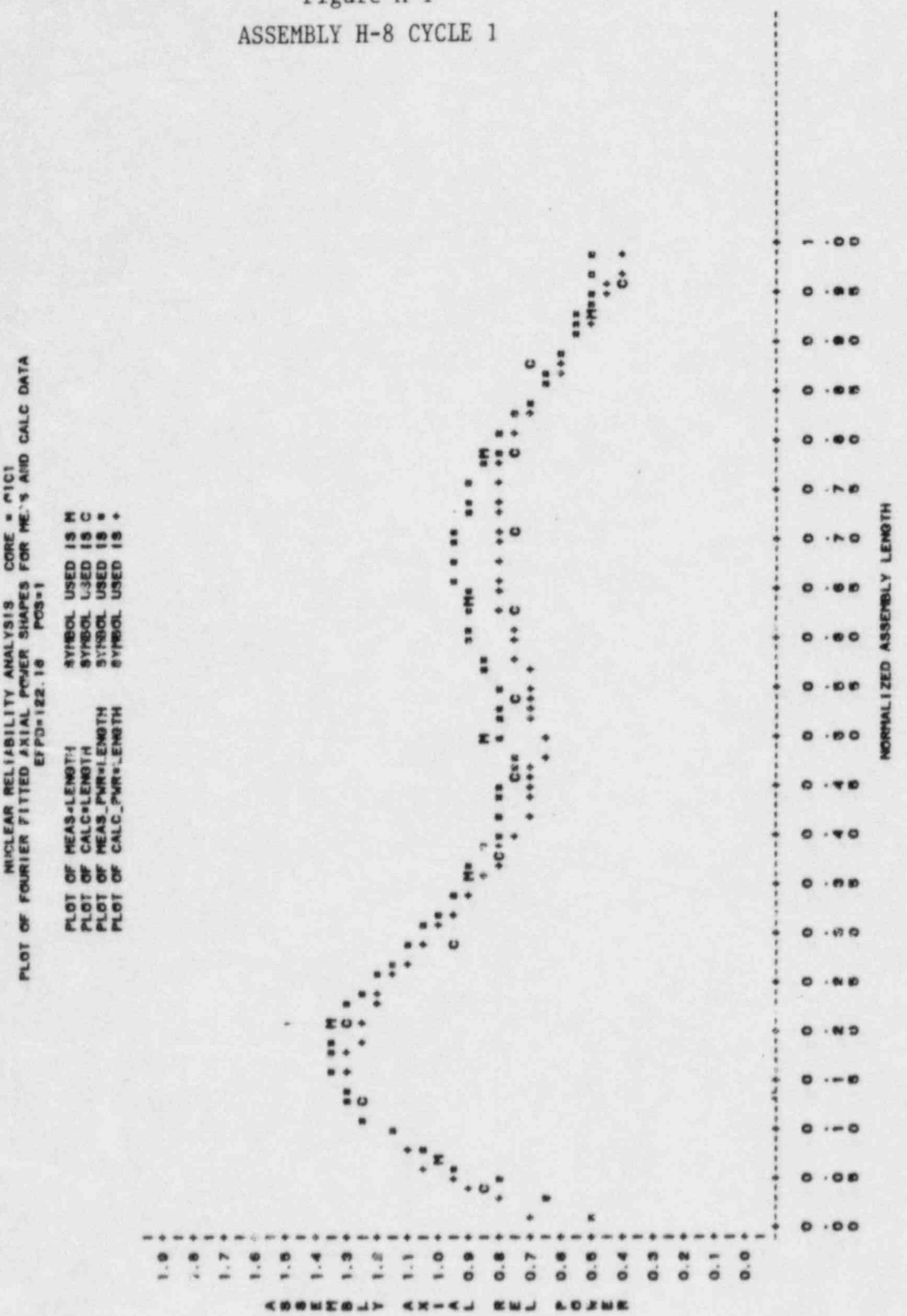

Figure A-2

ASSEMBLY H-10 CYCLE 1

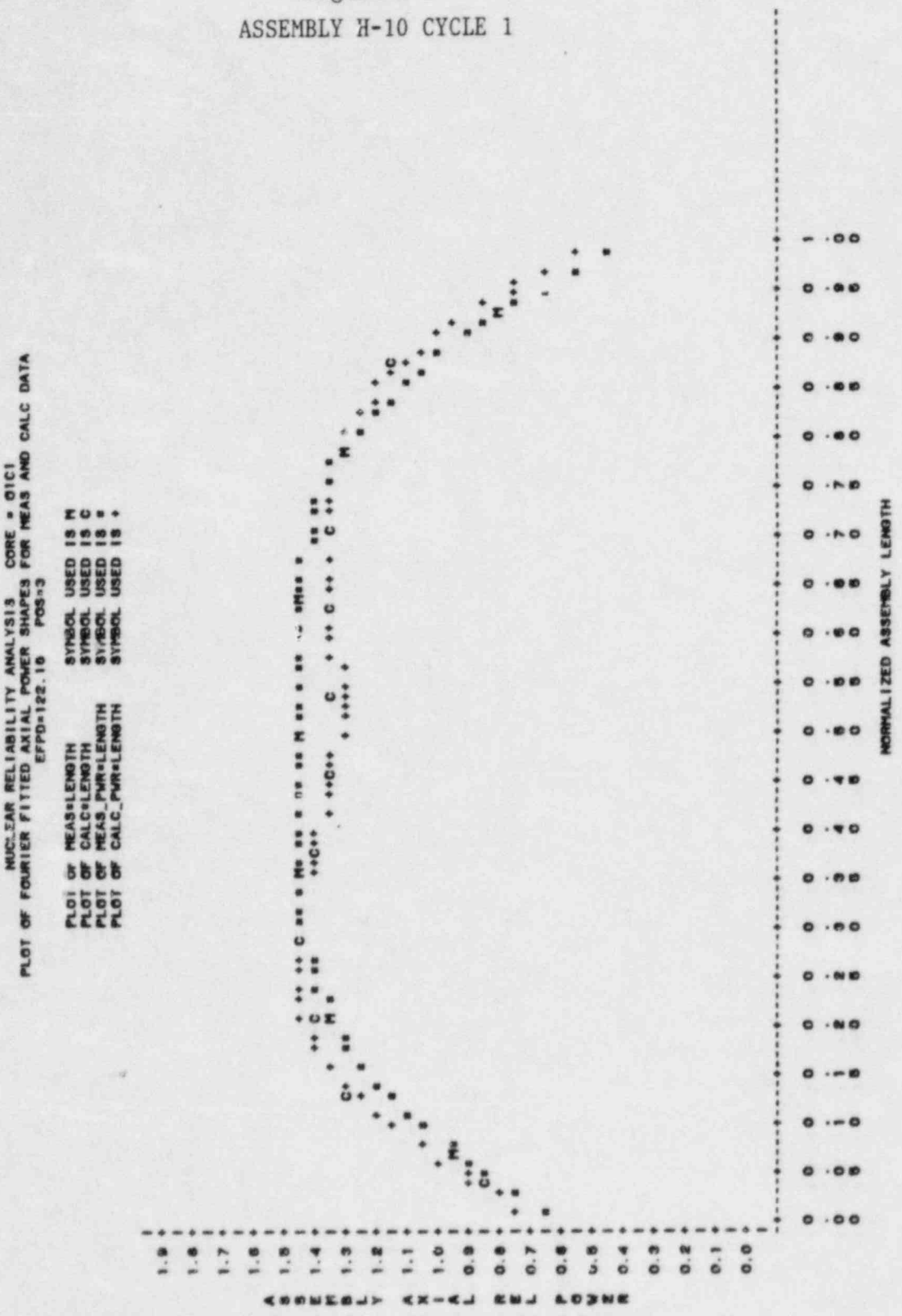

Figure A-3

ASSEMBLY K-9 CYCLE 1

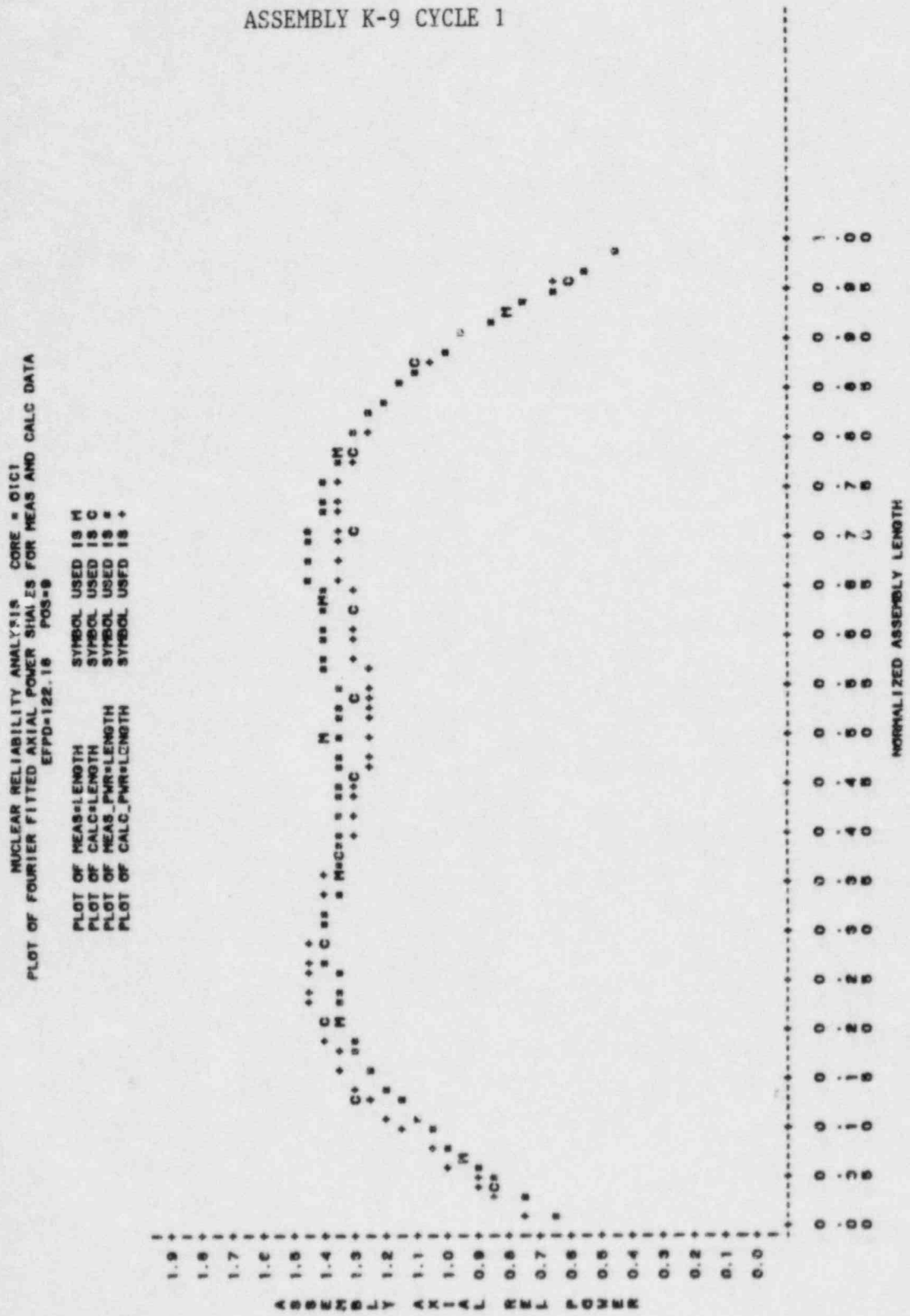

Figure A-4

ASSEMBLY L-12 CYCLE 1

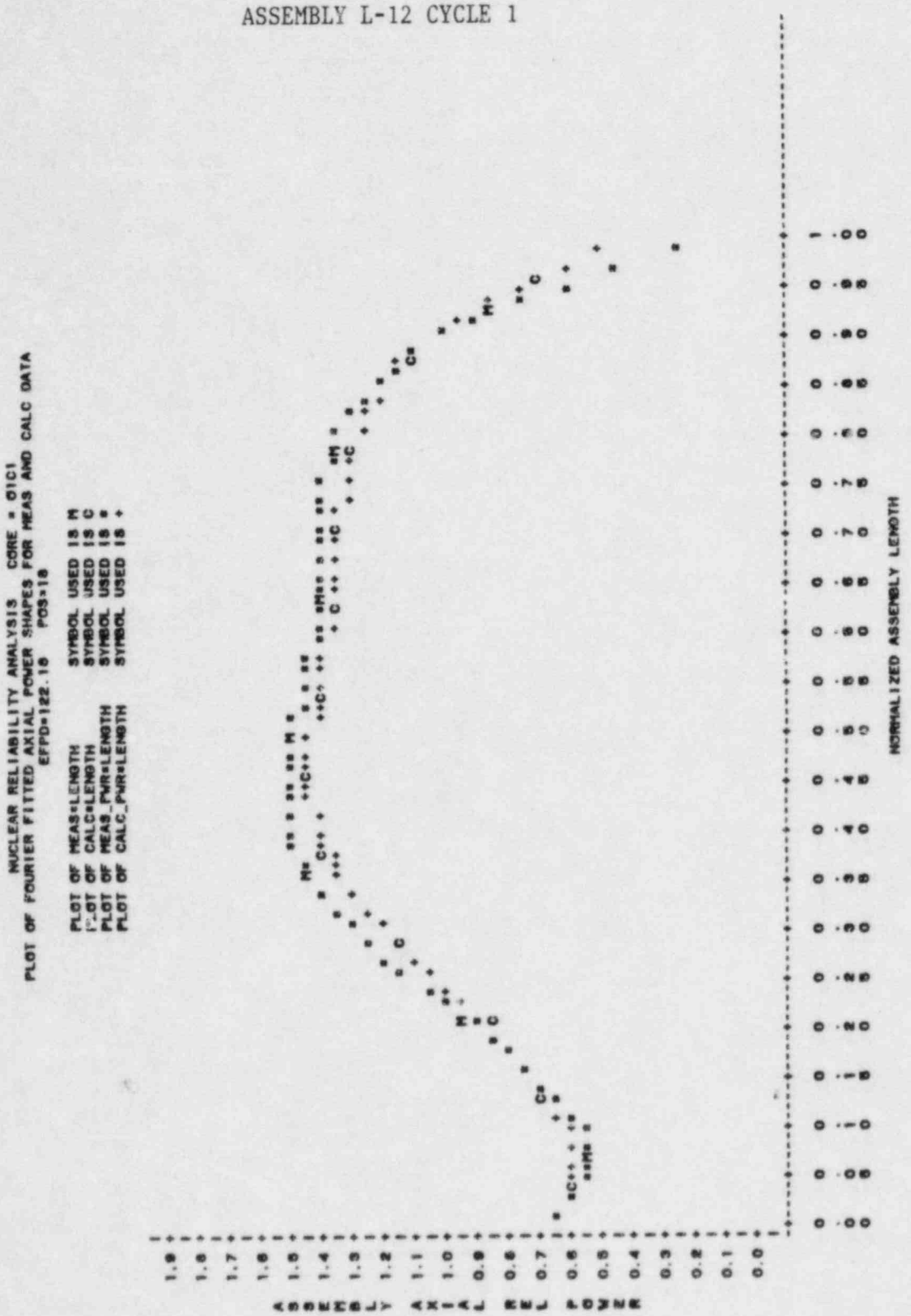

Figure A-5
ASSEMBLY H-8 CYCLE 1

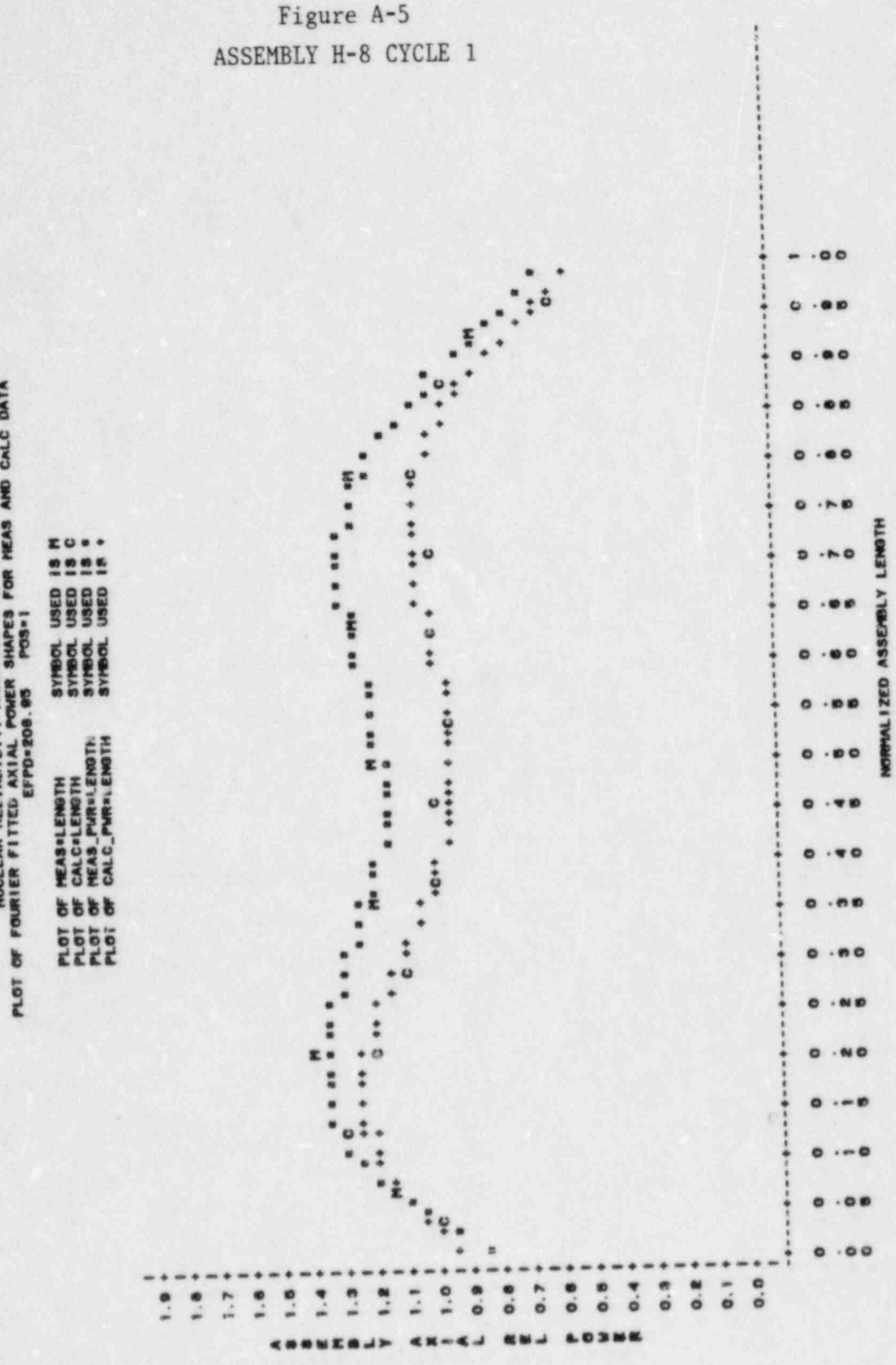

Figure A-6

ASSEMBLY H-10 CYCLE 1

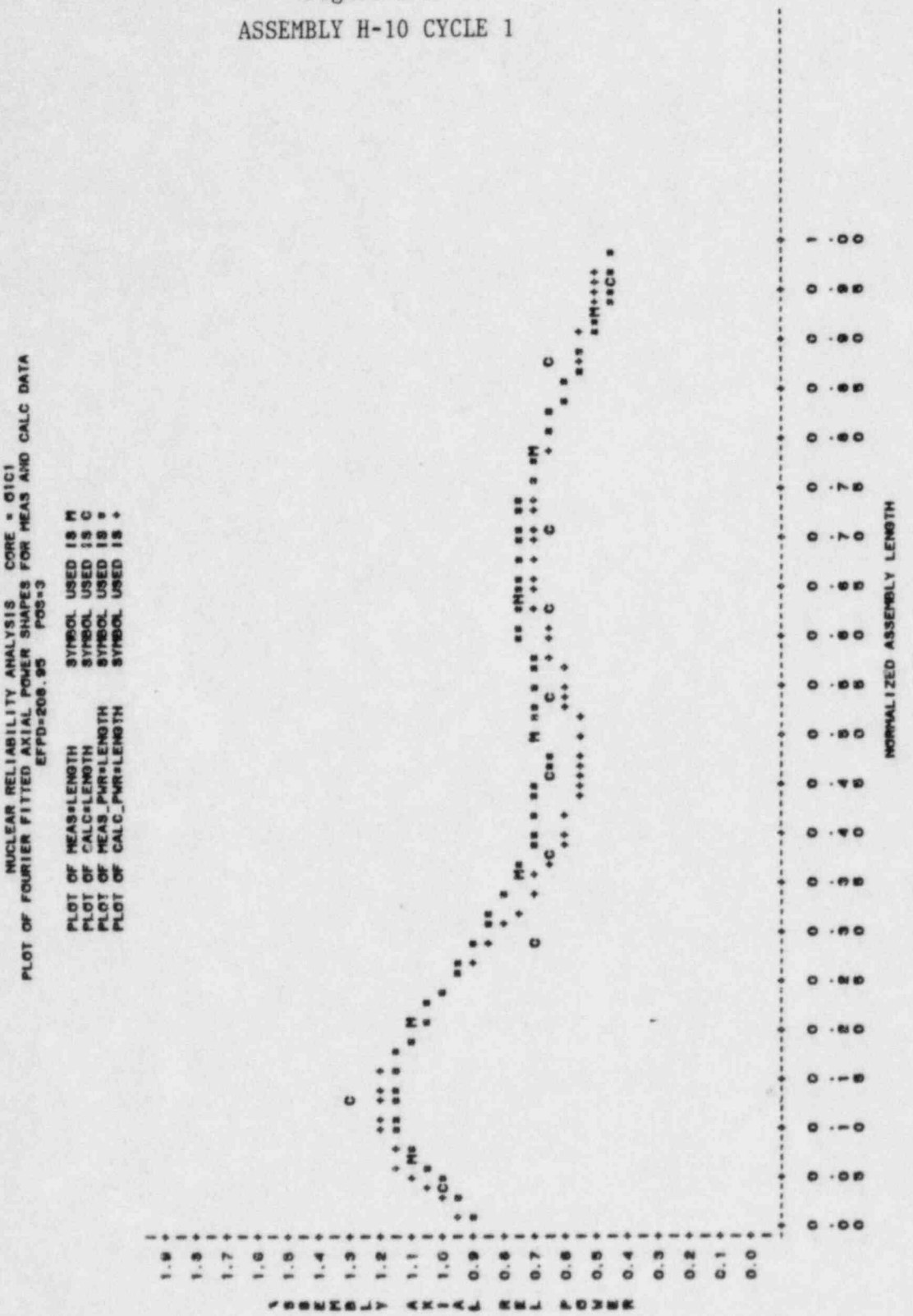

Figure A-7

ASSEMBLY K-9 CYCLE 1

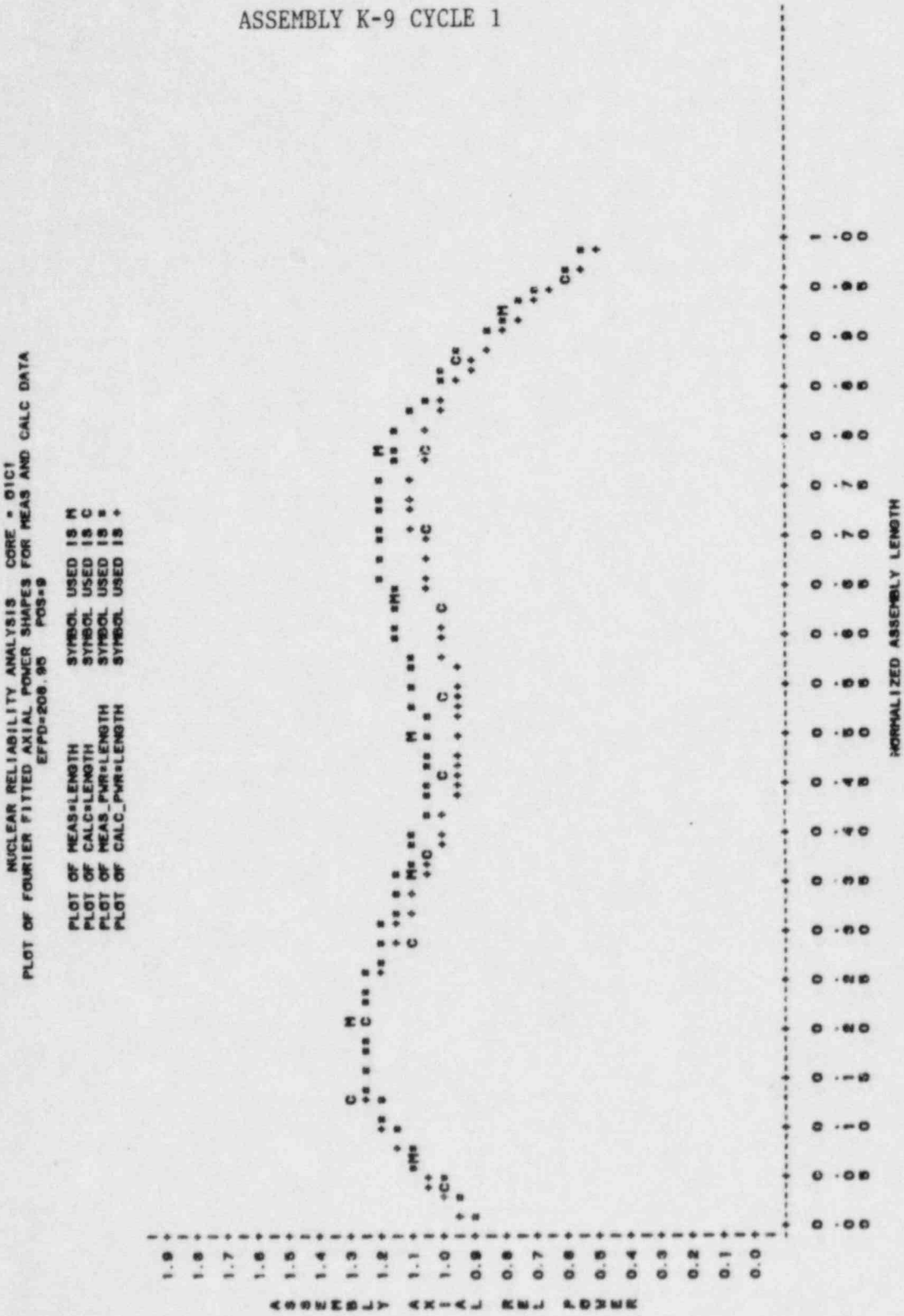

Figure A-8

ASSEMBLY L-12 CYCLE 1

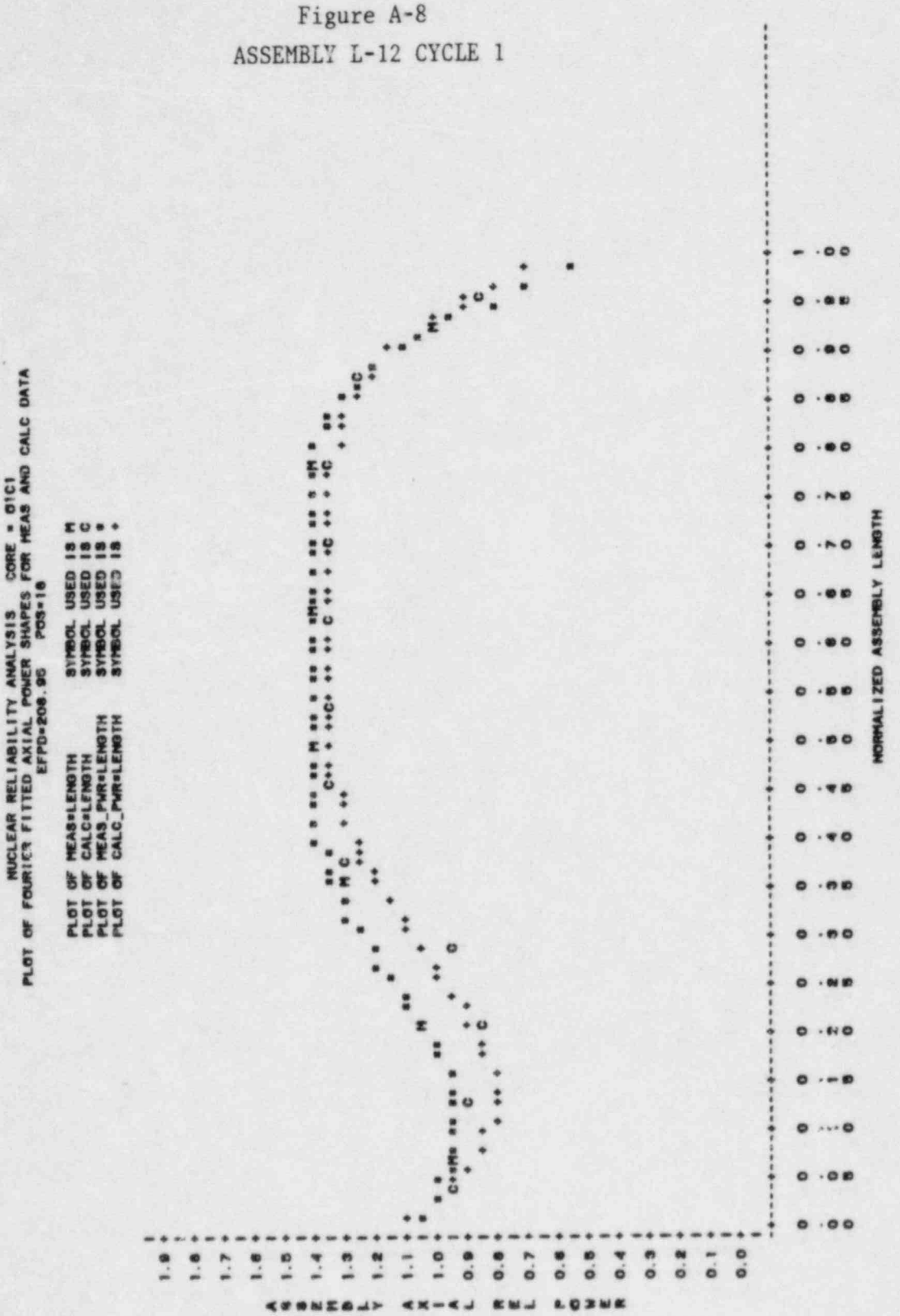

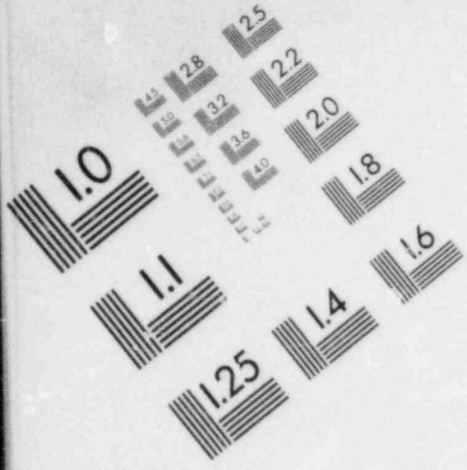

IMAGE EVALUATION TEST TARGET (MT-3)

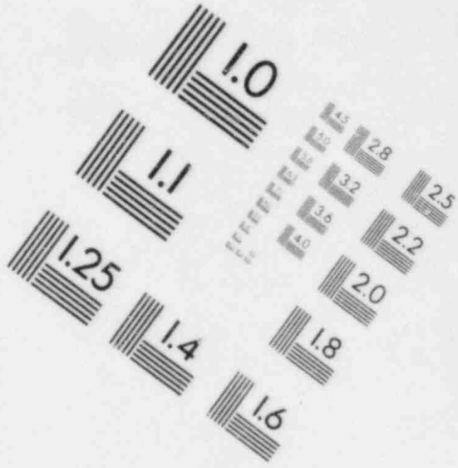

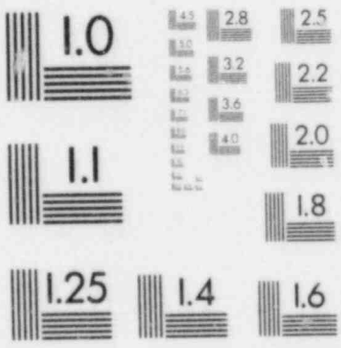

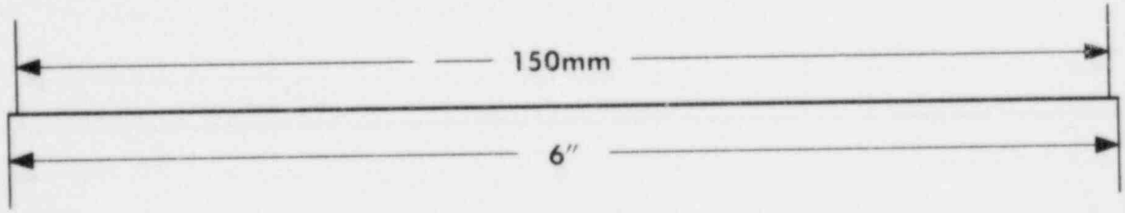

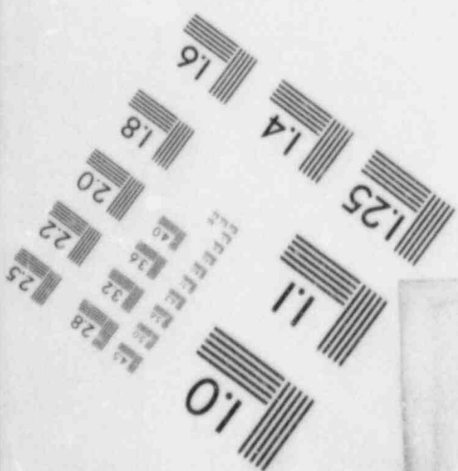

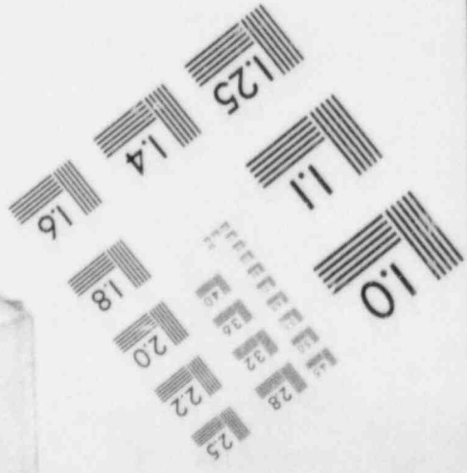

IMAGE EVALUATION TEST TARGET (MT-3)

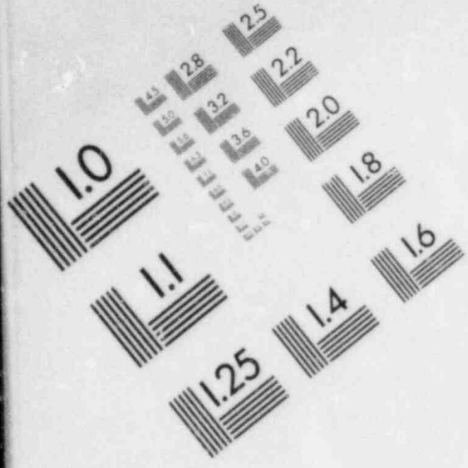

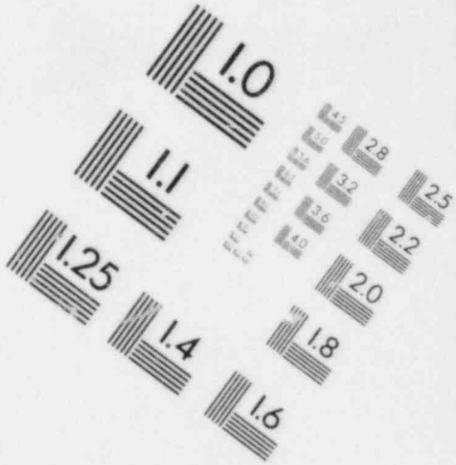

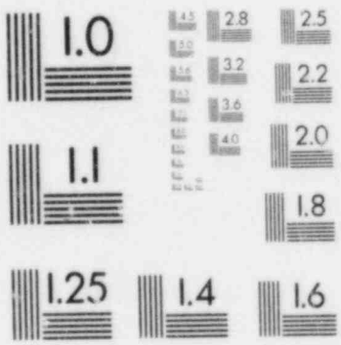

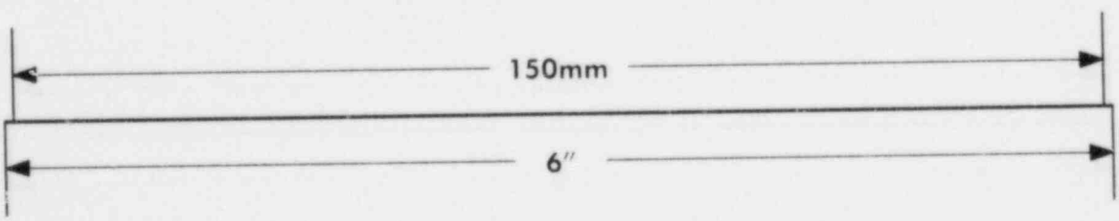

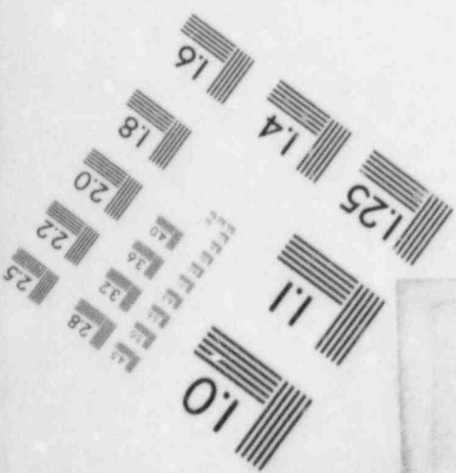

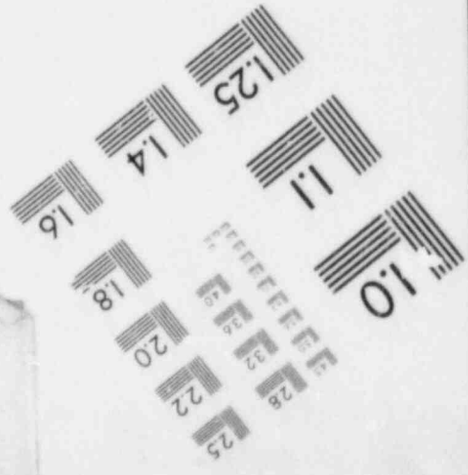

Figure A-9
ASSEMBLY H-8 CYCLE 1

Figure A-10

ASSEMBLY H-10 CYCLE 1

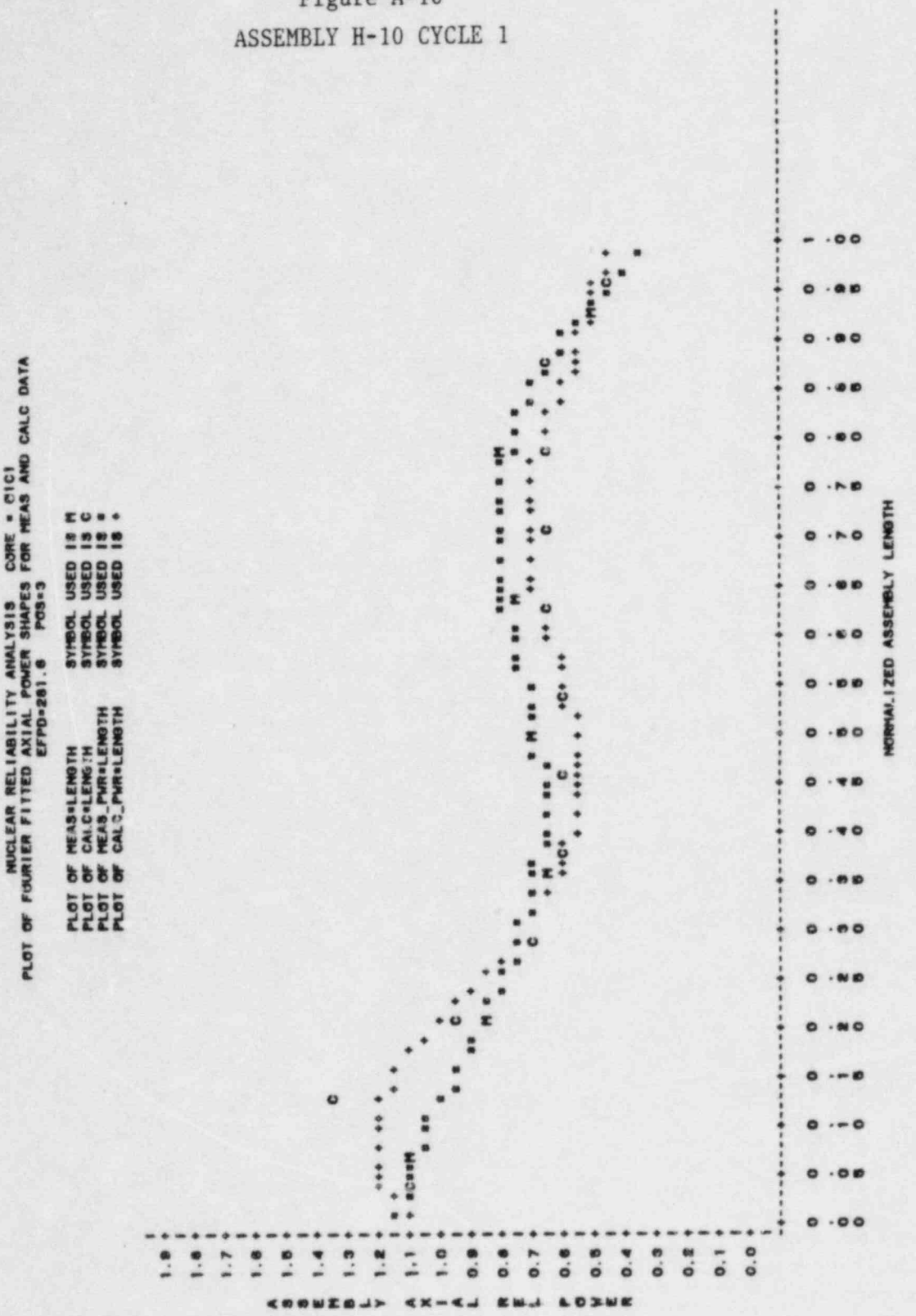

Figure A-11

ASSEMBLY K-9 CYCLE 1

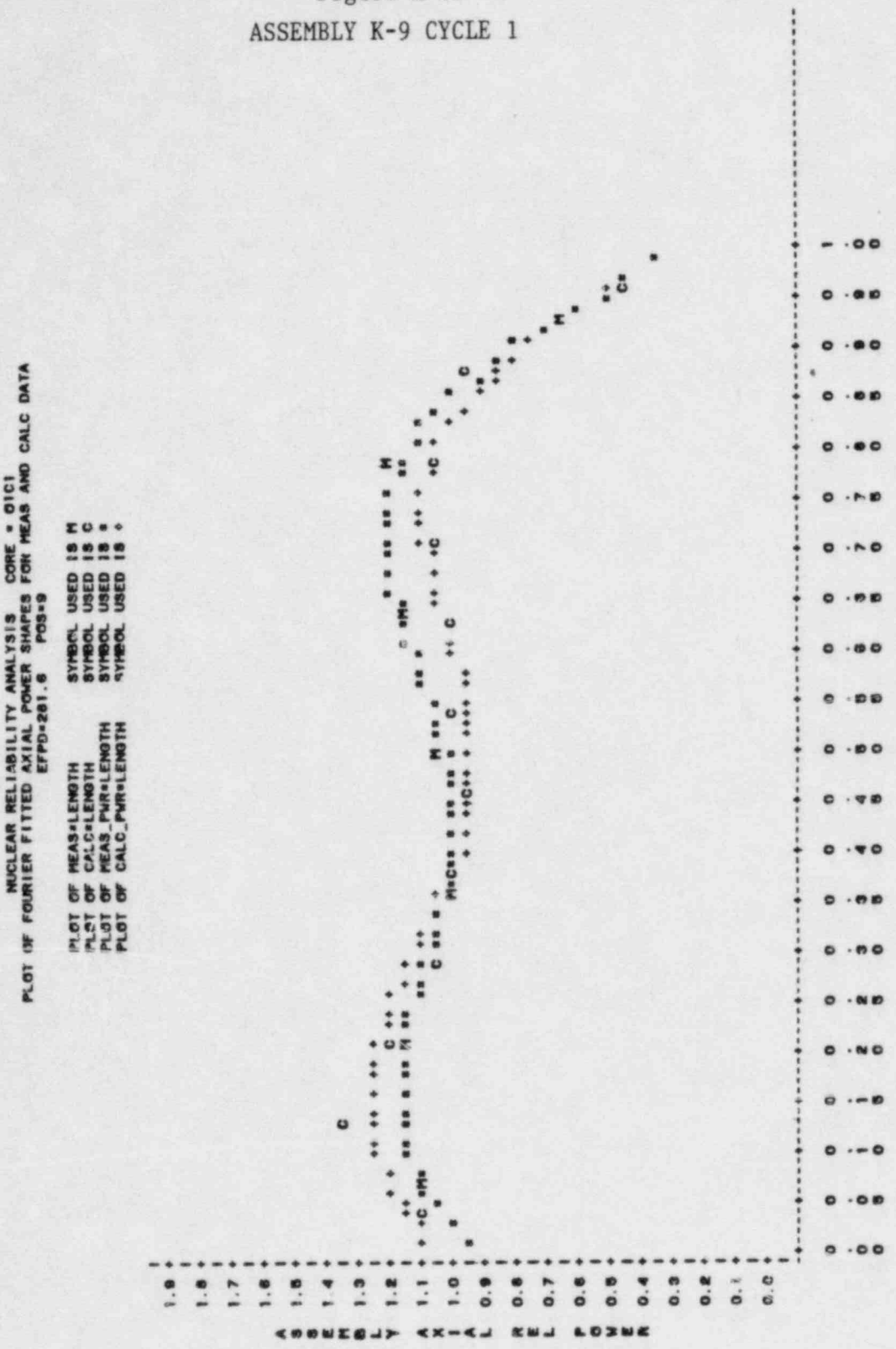

Figure A-12

ASSEMBLY L-12 CYCLE 1

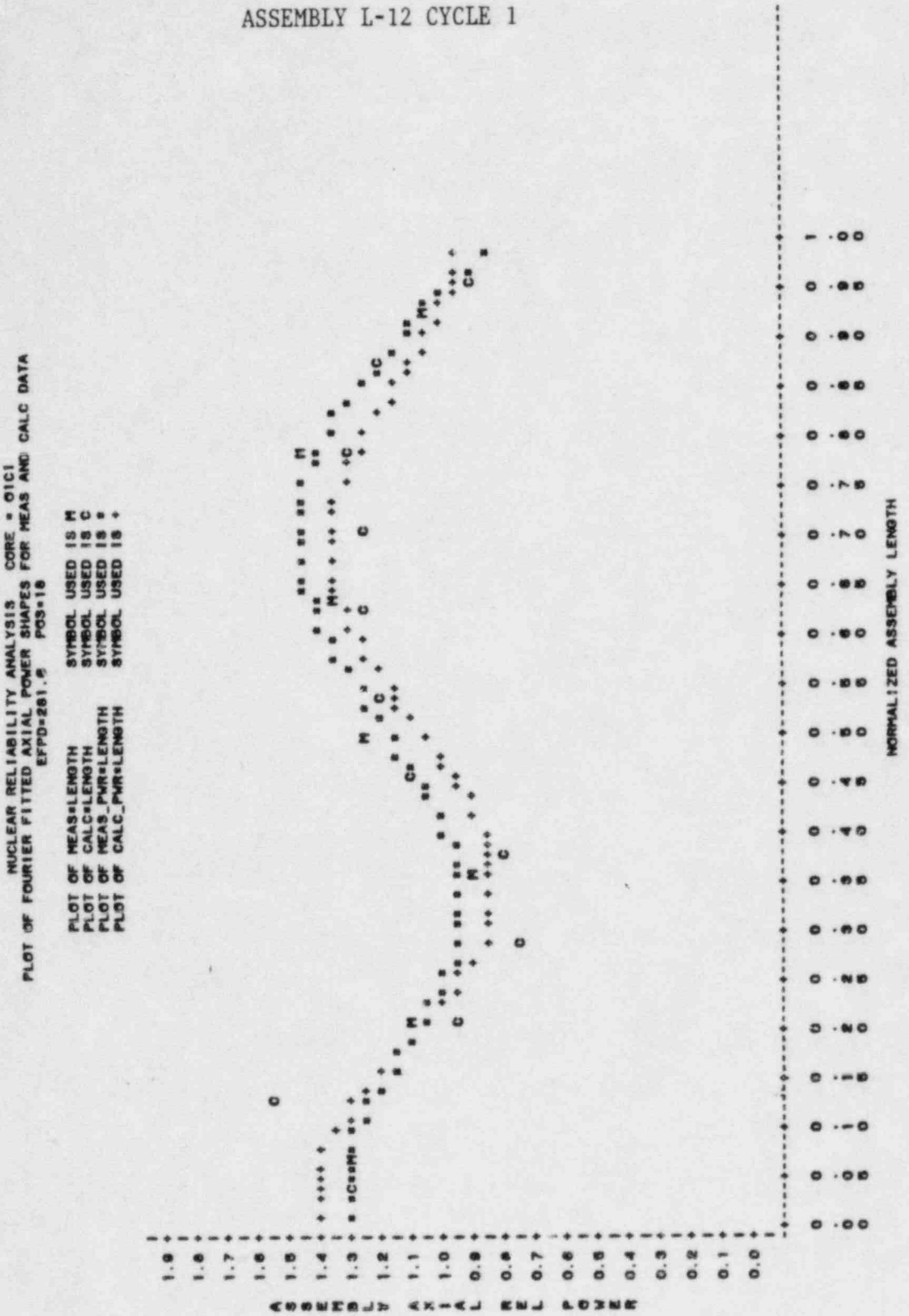

Figure A-13

ASSEMBLY M-11 CYCLE 1

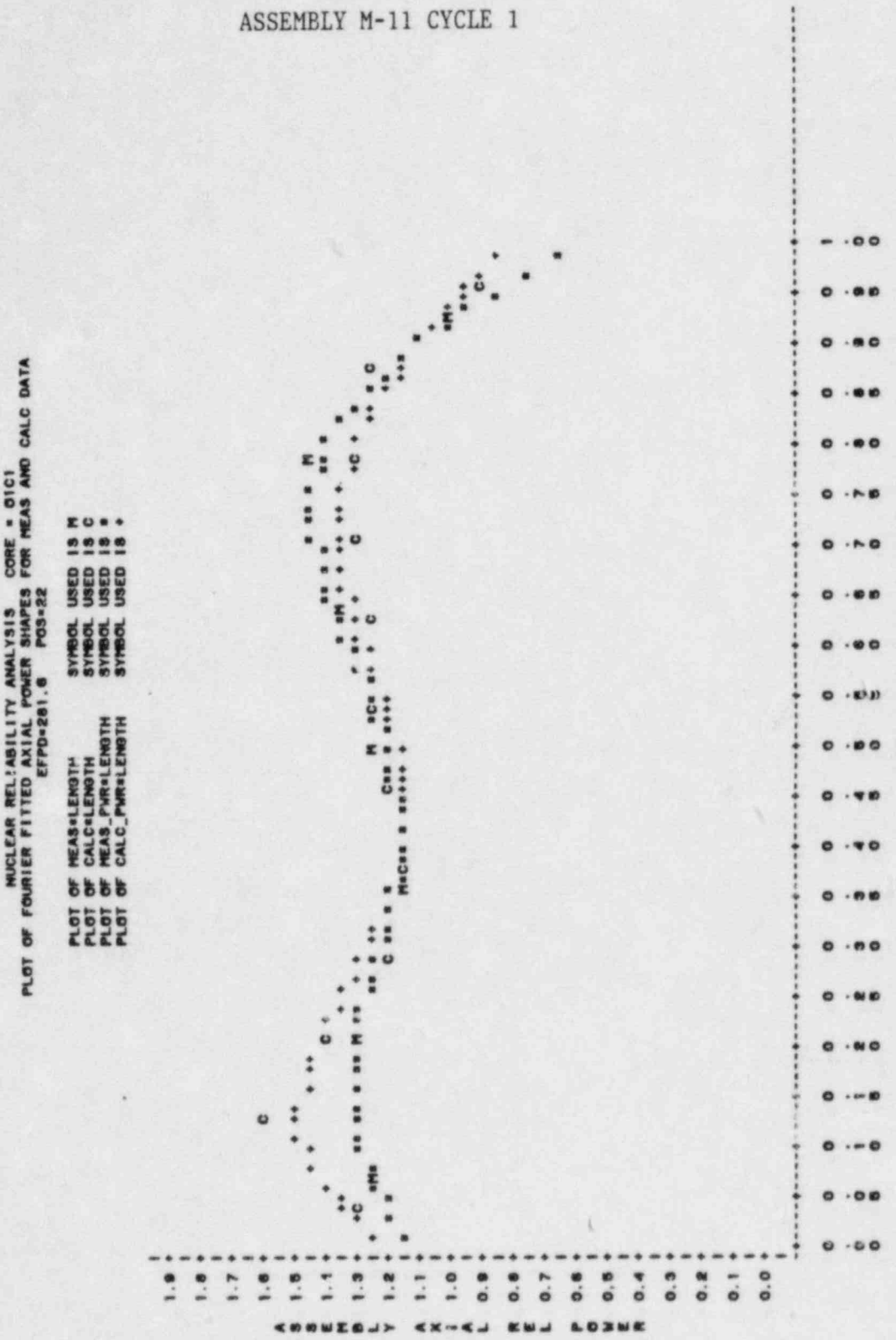

Figure A-14

ASSEMBLY H-8 CYCLE 2

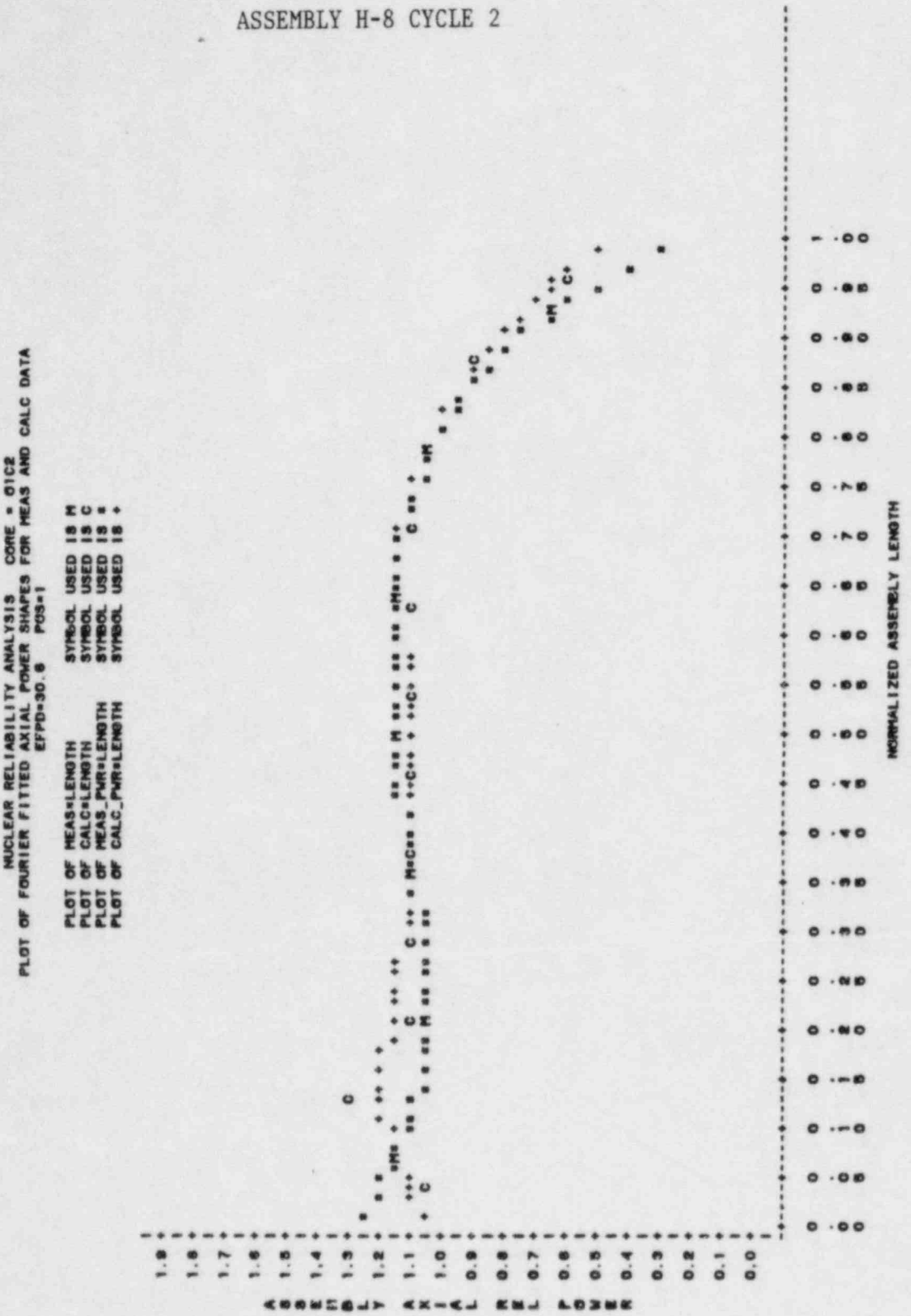

Figure A-15

ASSEMBLY H-11 CYCLE 2

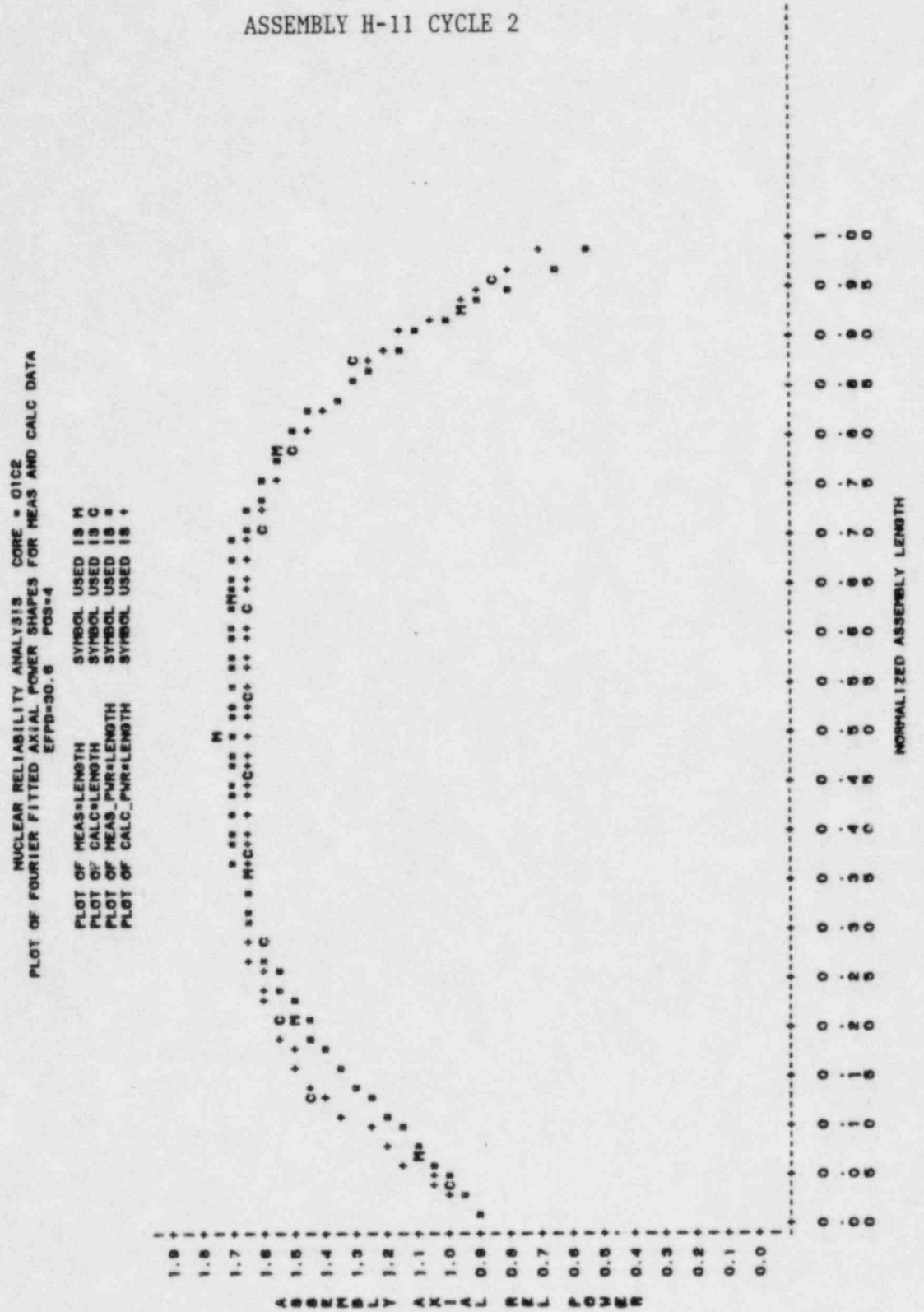

Figure A-16

ASSEMBLY K-13 CYCLE 2

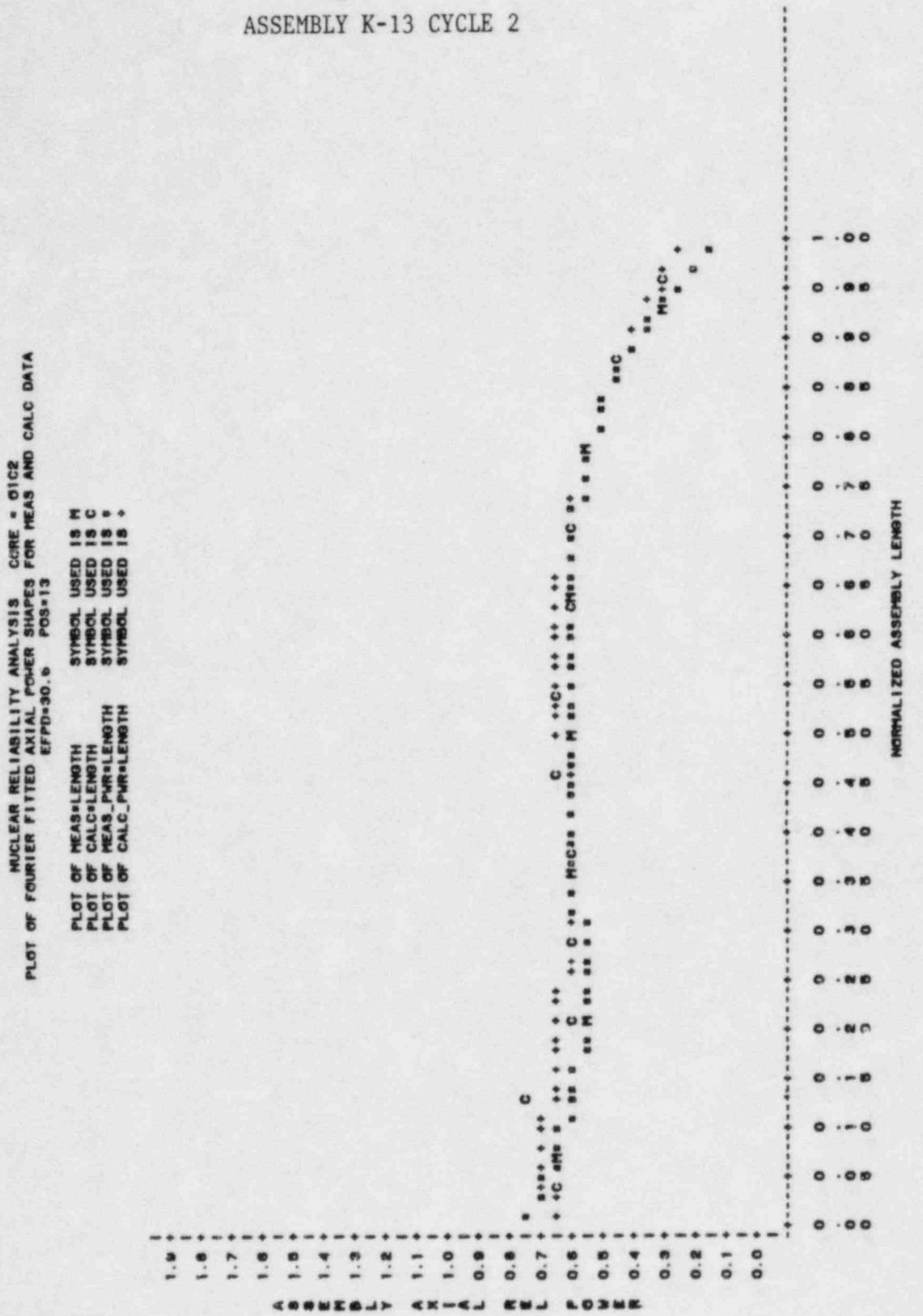

Figure A-17

ASSEMBLY L-12 CYCLE 2

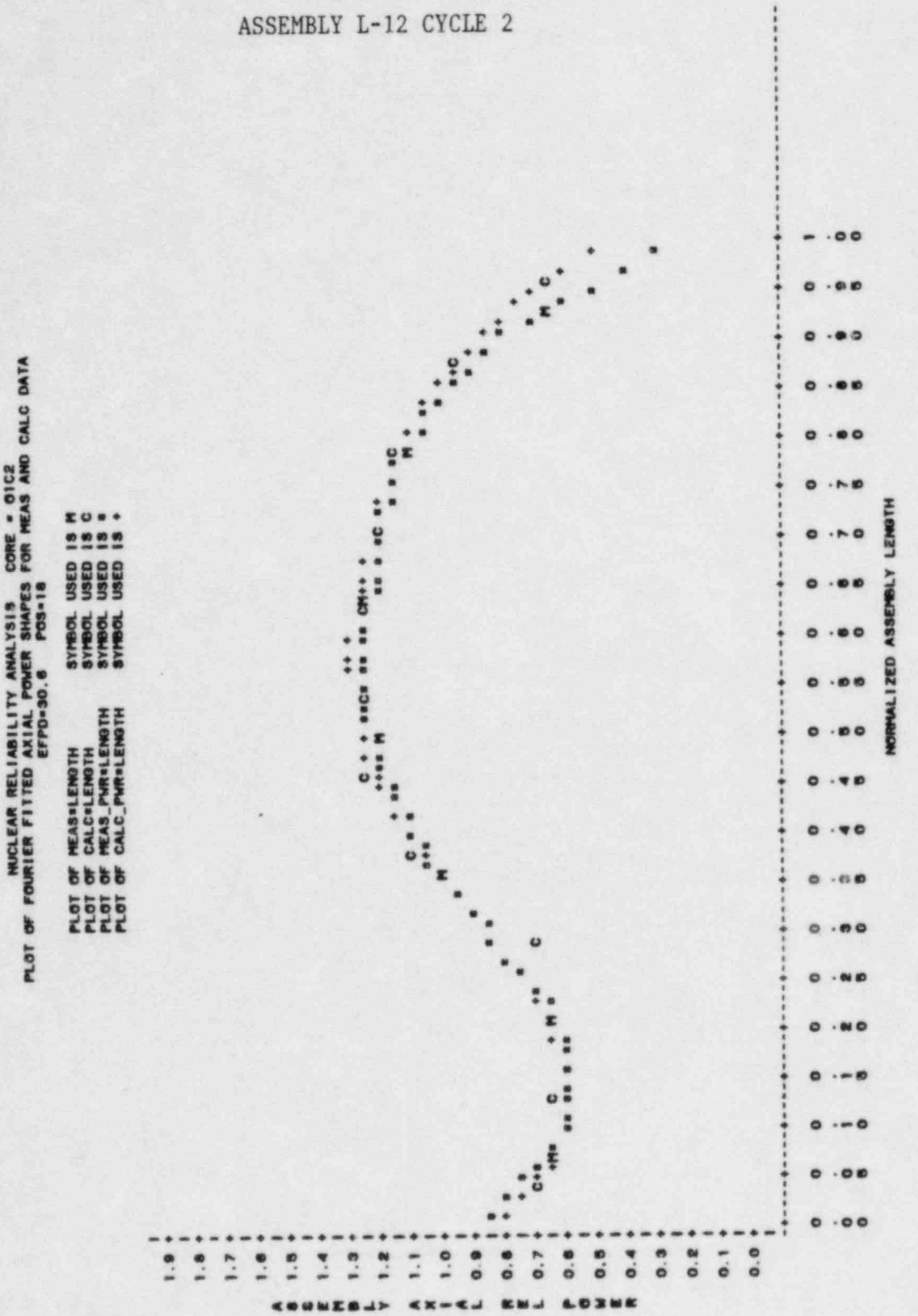

Figure A-18

ASSEMBLY L-15 CYCLE 2

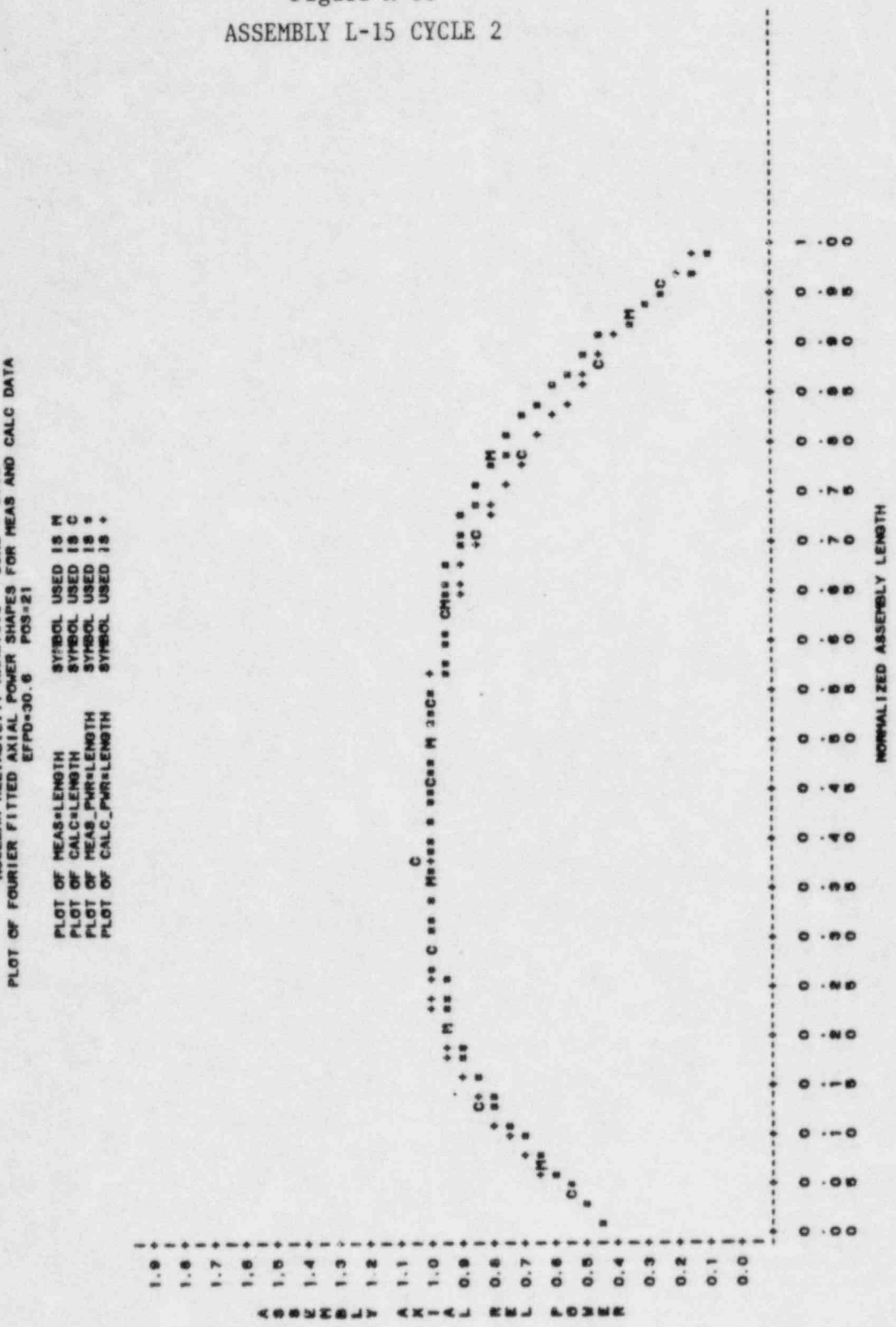

Figure A-19

ASSEMBLY H-8 CYCLE 2

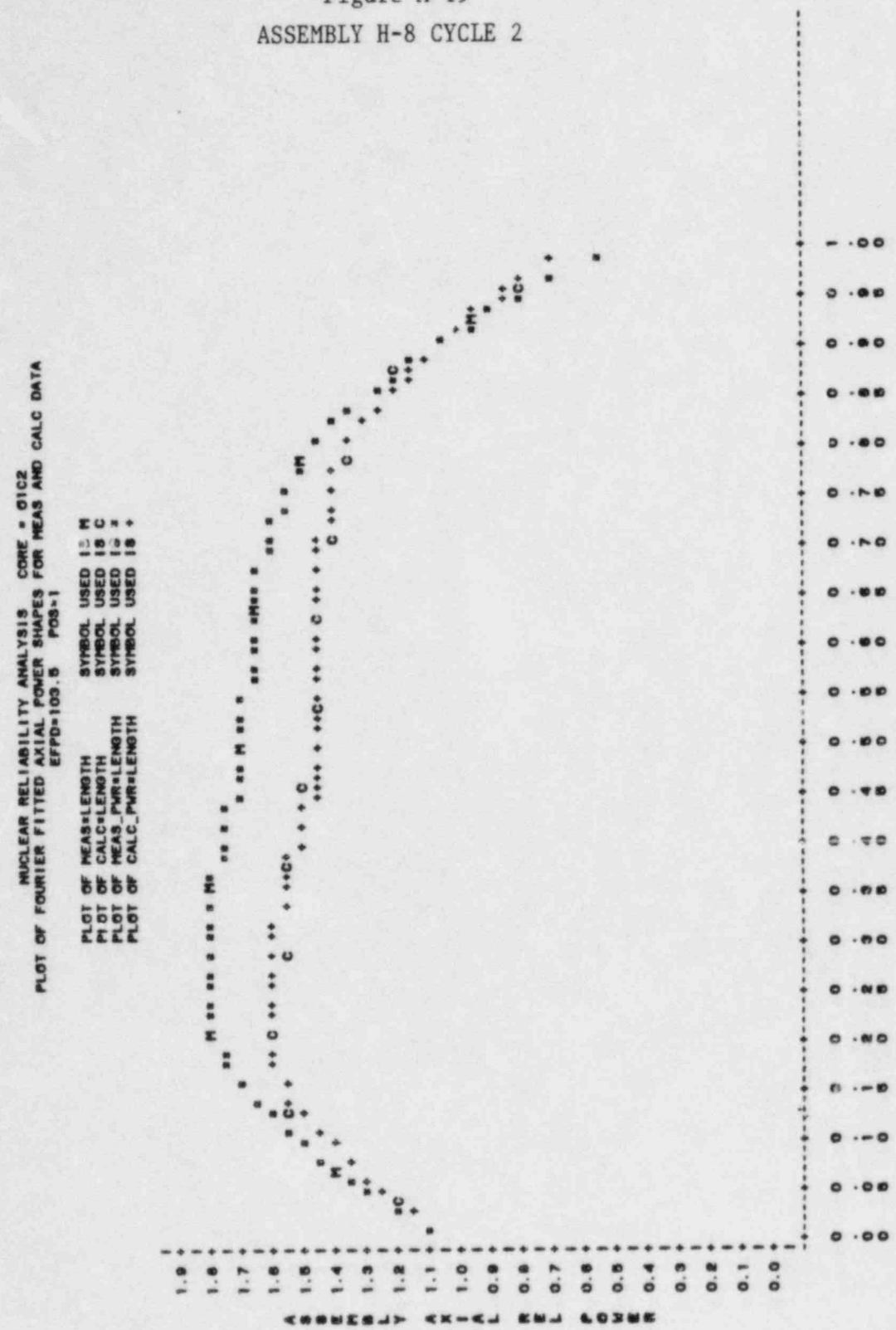

Figure A-20
ASSEMBLY H-11 Cycle 2

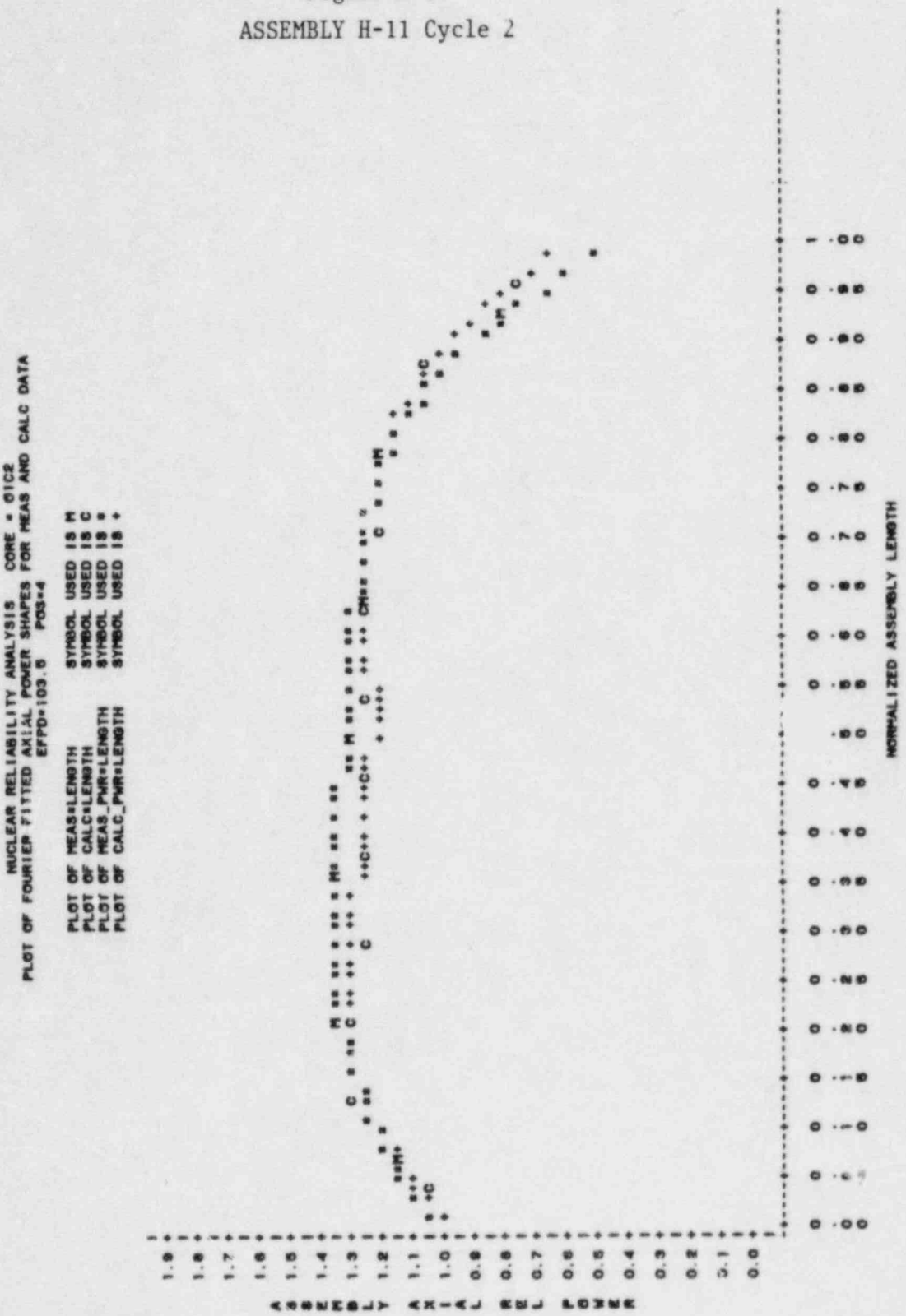

Figure A-21

ASSEMBLY K-13 CYCLE 2

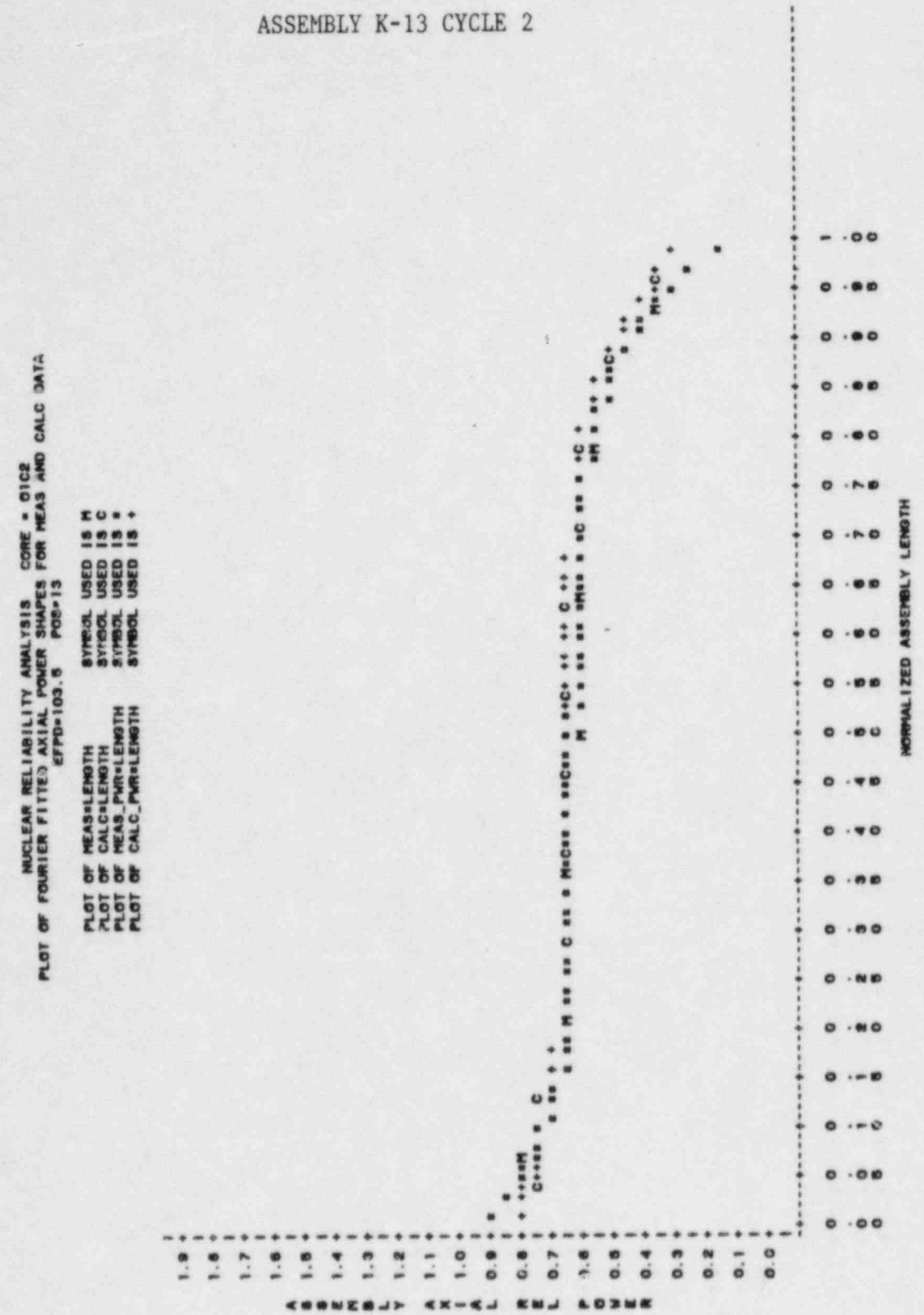

Figure A-22

ASSEMBLY L-12 CYCLE 2

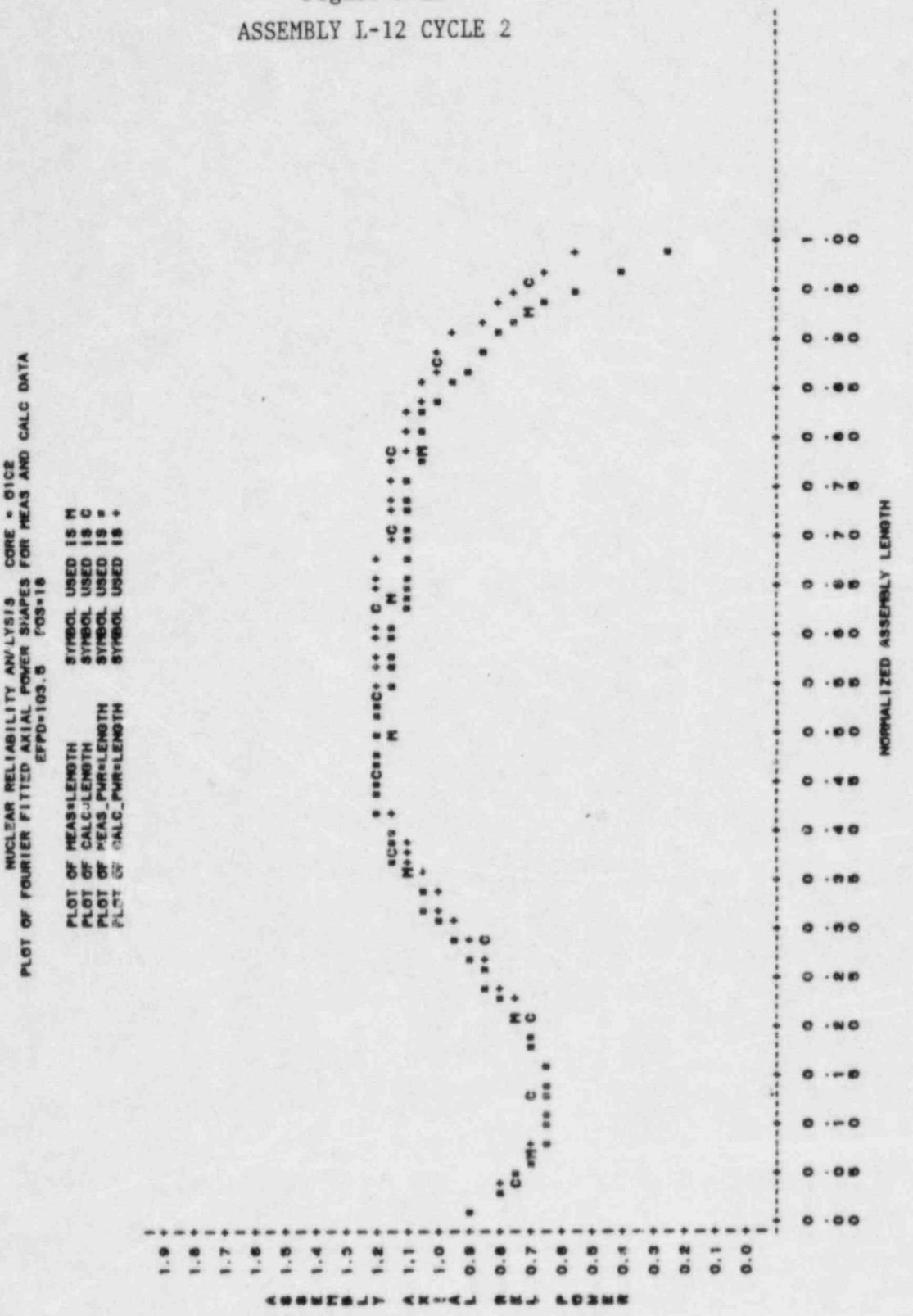

Figure A-23

ASSEMBLY L-15 CYCLE 2

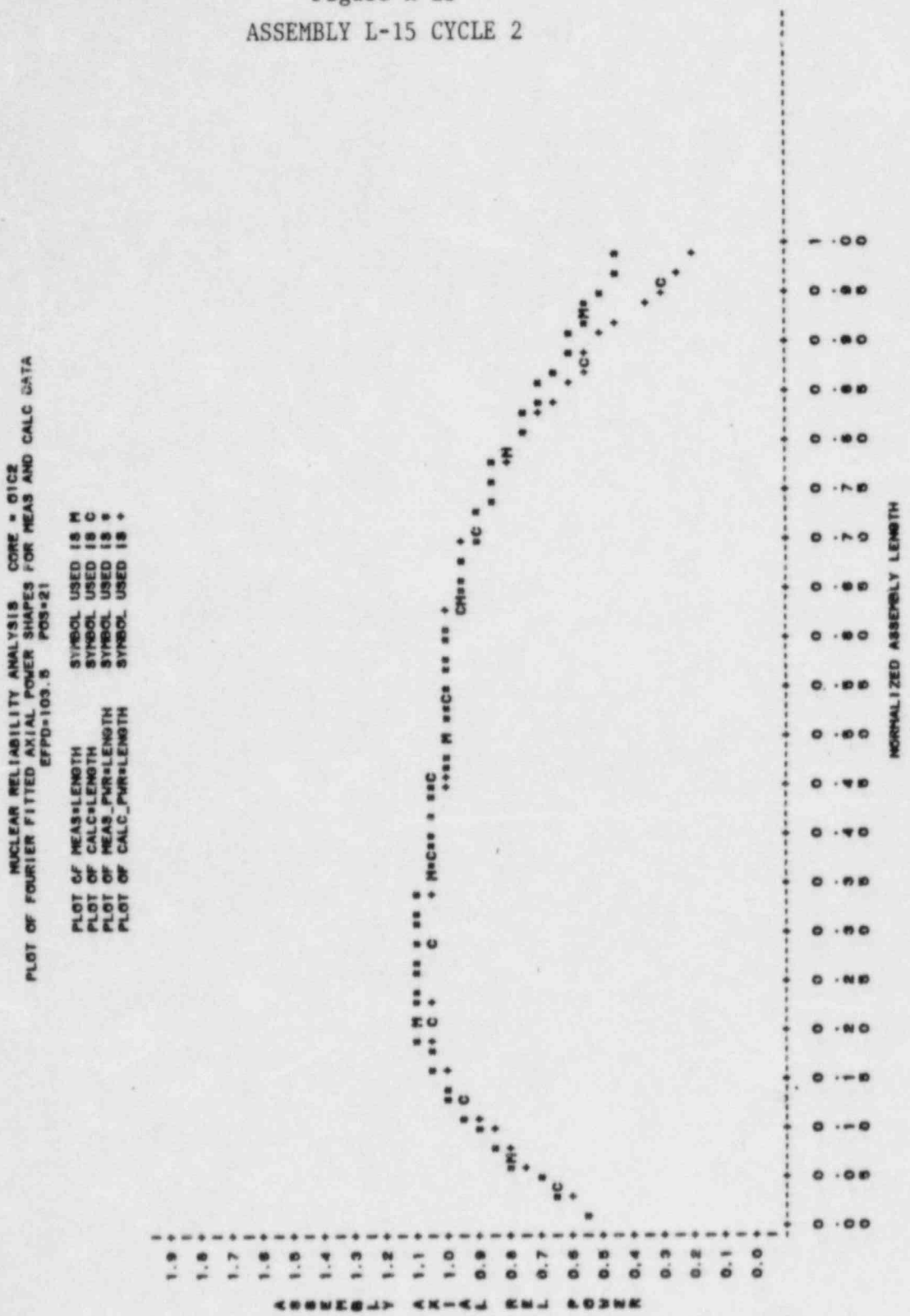

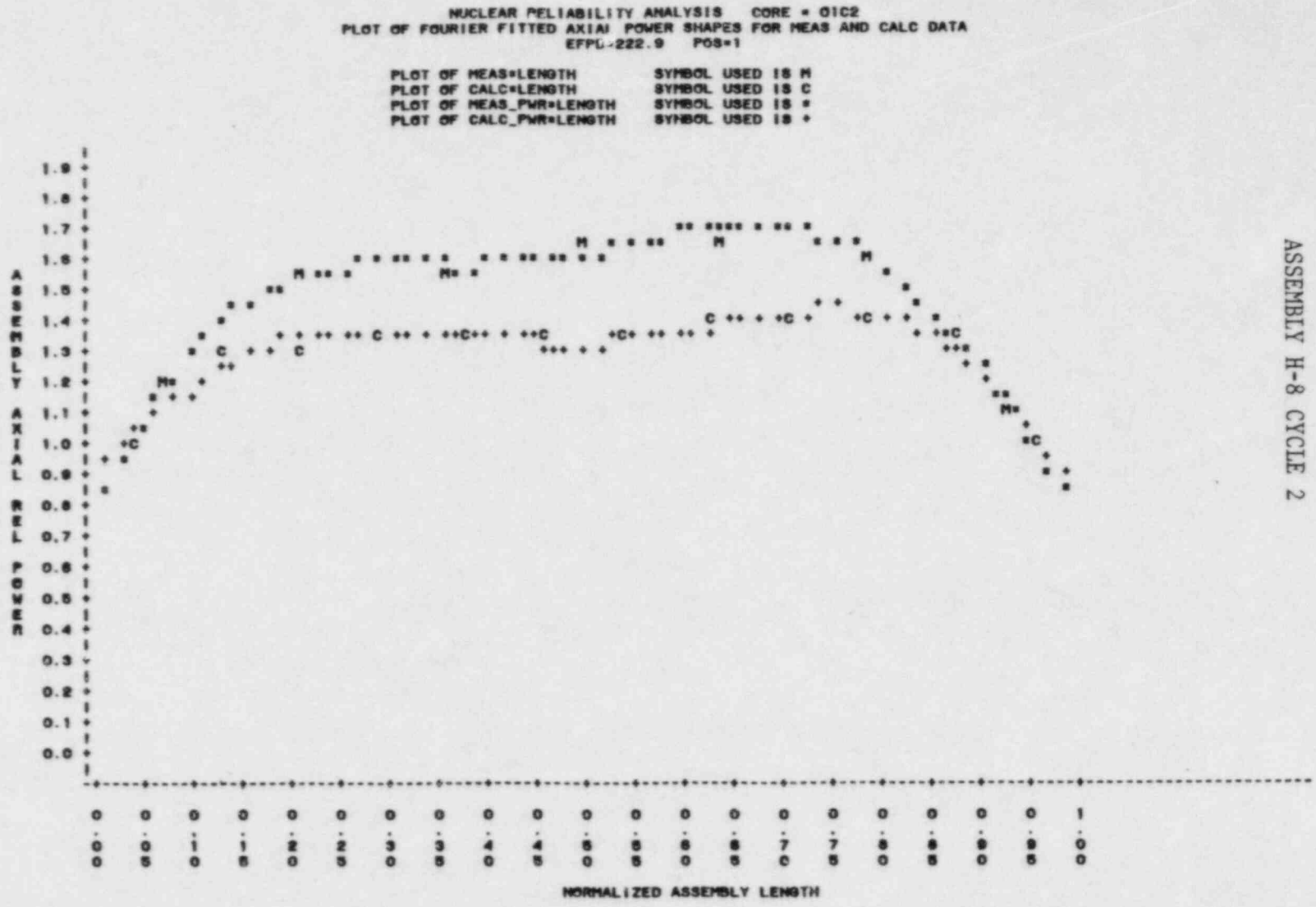

Figure A-24
ASSEMBLY H-8 CYCLE 2

Figure A-25
ASSEMBLY H-11 CYCLE 2

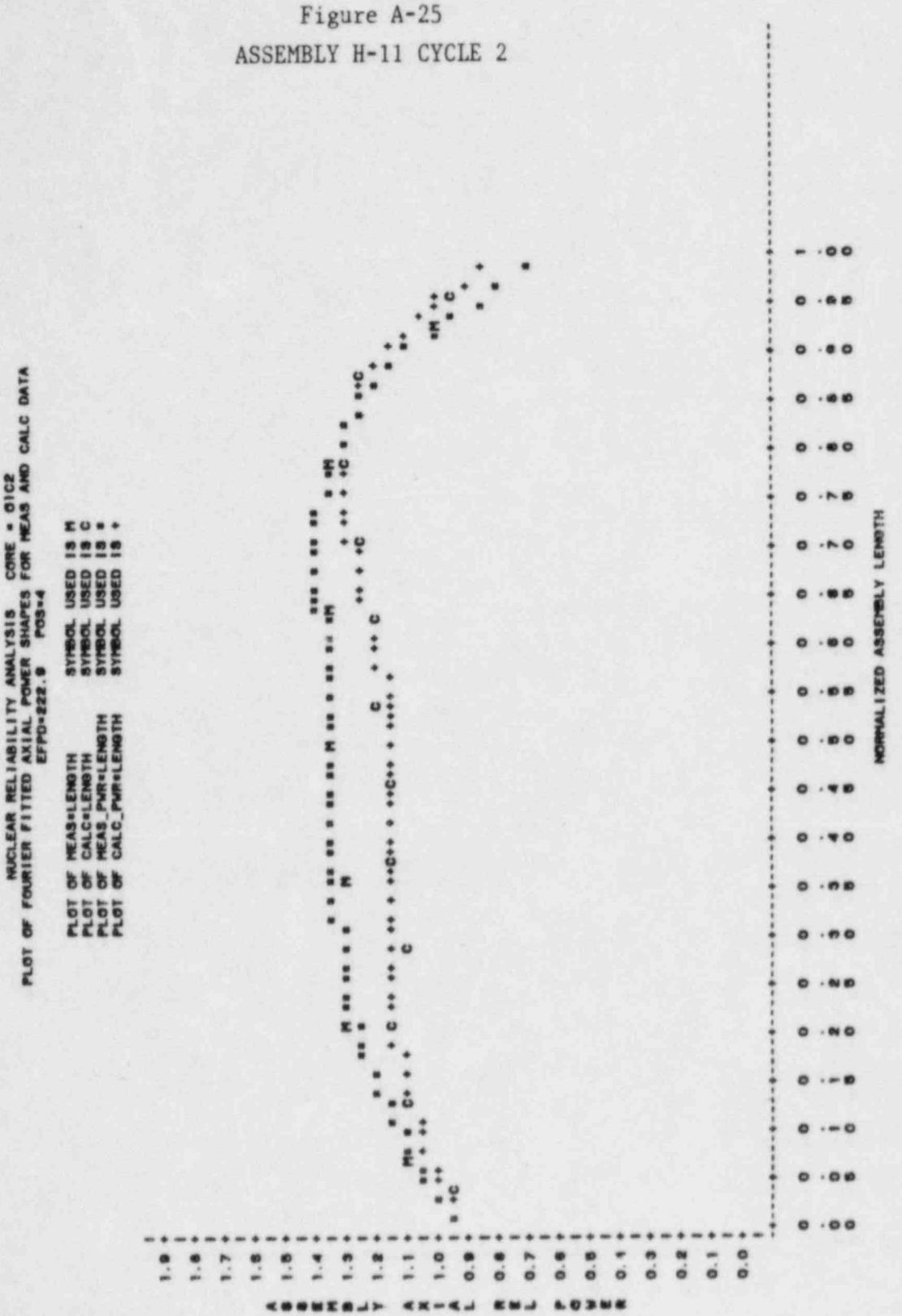

Figure A-26
ASSEMBLY K-13 CYCLE 2

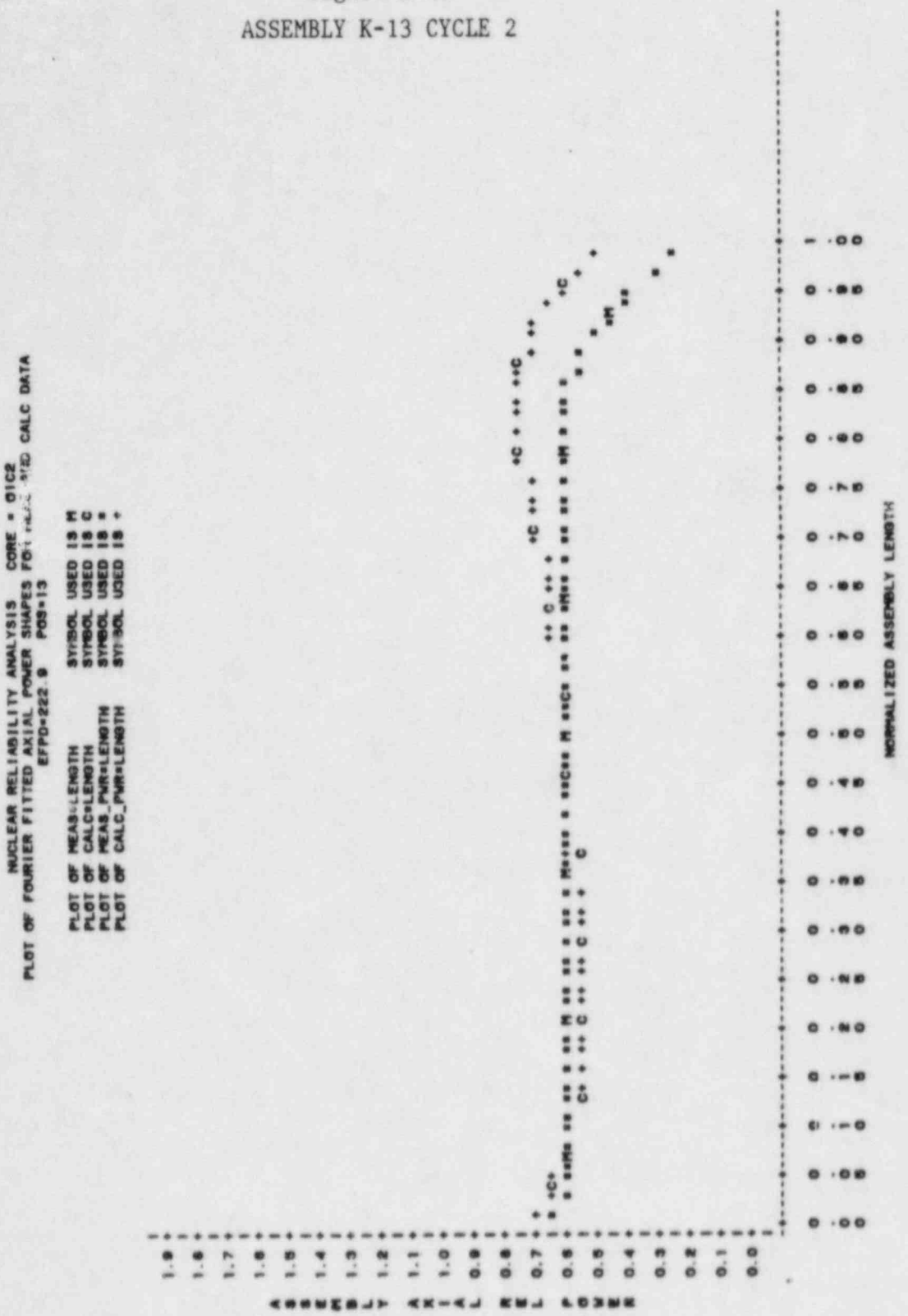

Figure A-27

ASSEMBLY L-12 CYCLE 2

Figure A-28

ASSEMBLY L-15 CYCLE 2

Figure A-29
ASSEMBLY H-11 CYCLE 3

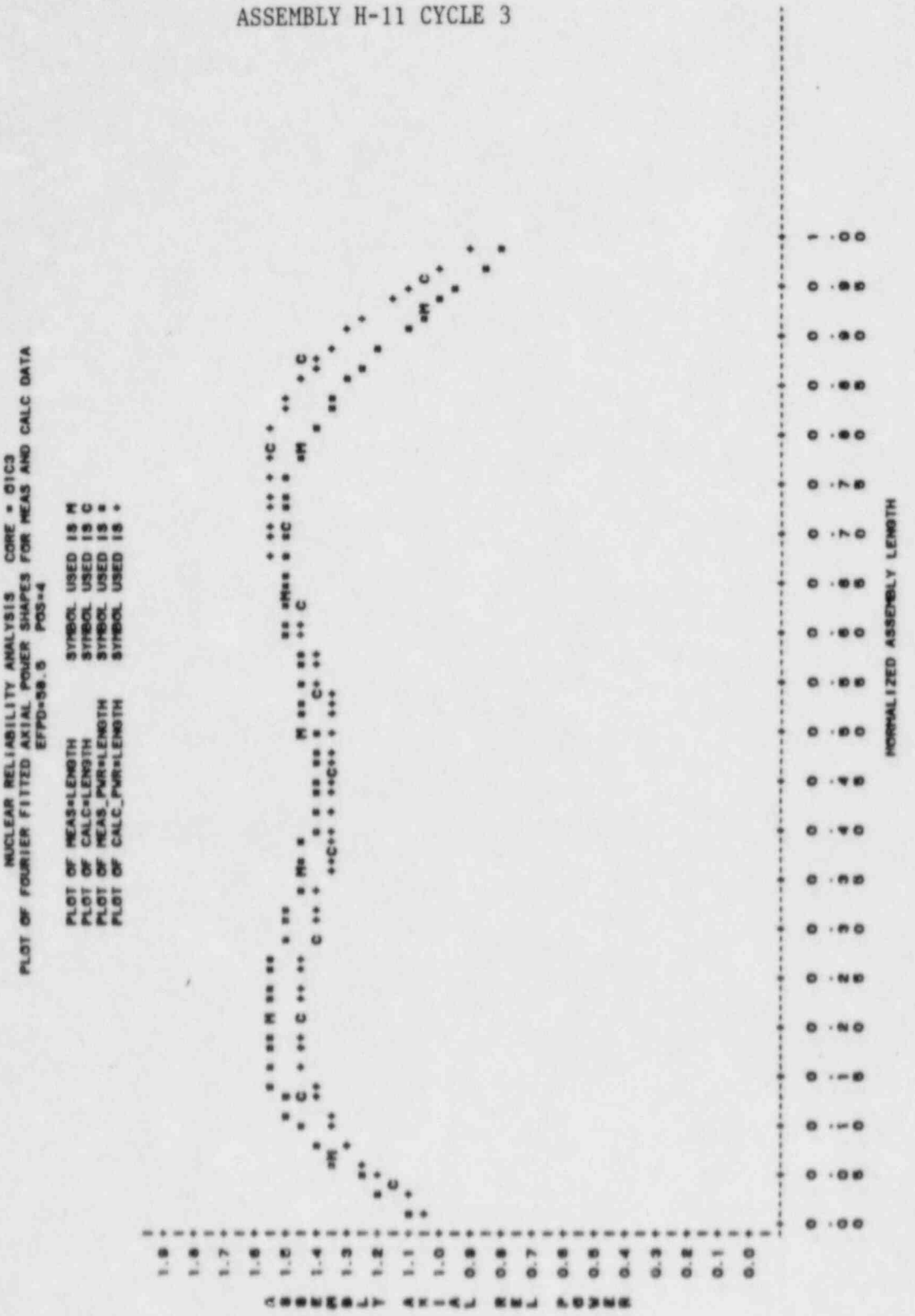

Figure A-30
ASSEMBLY H-13 CYCLE 3

Figure A-31
ASSEMBLY K-13 CYCLE 3

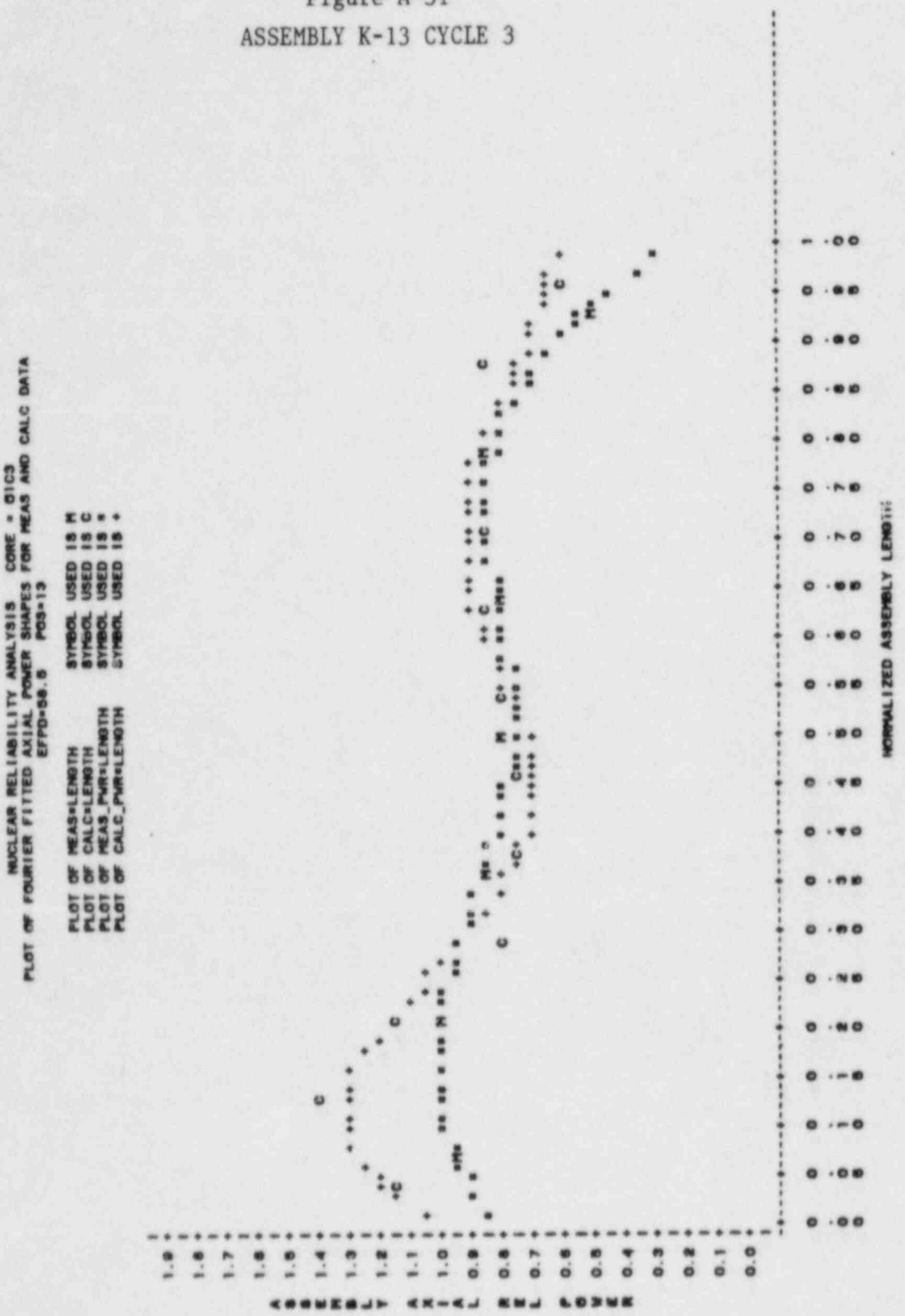

Figure A-32

ASSEMBLY L-11 CYCLE 3

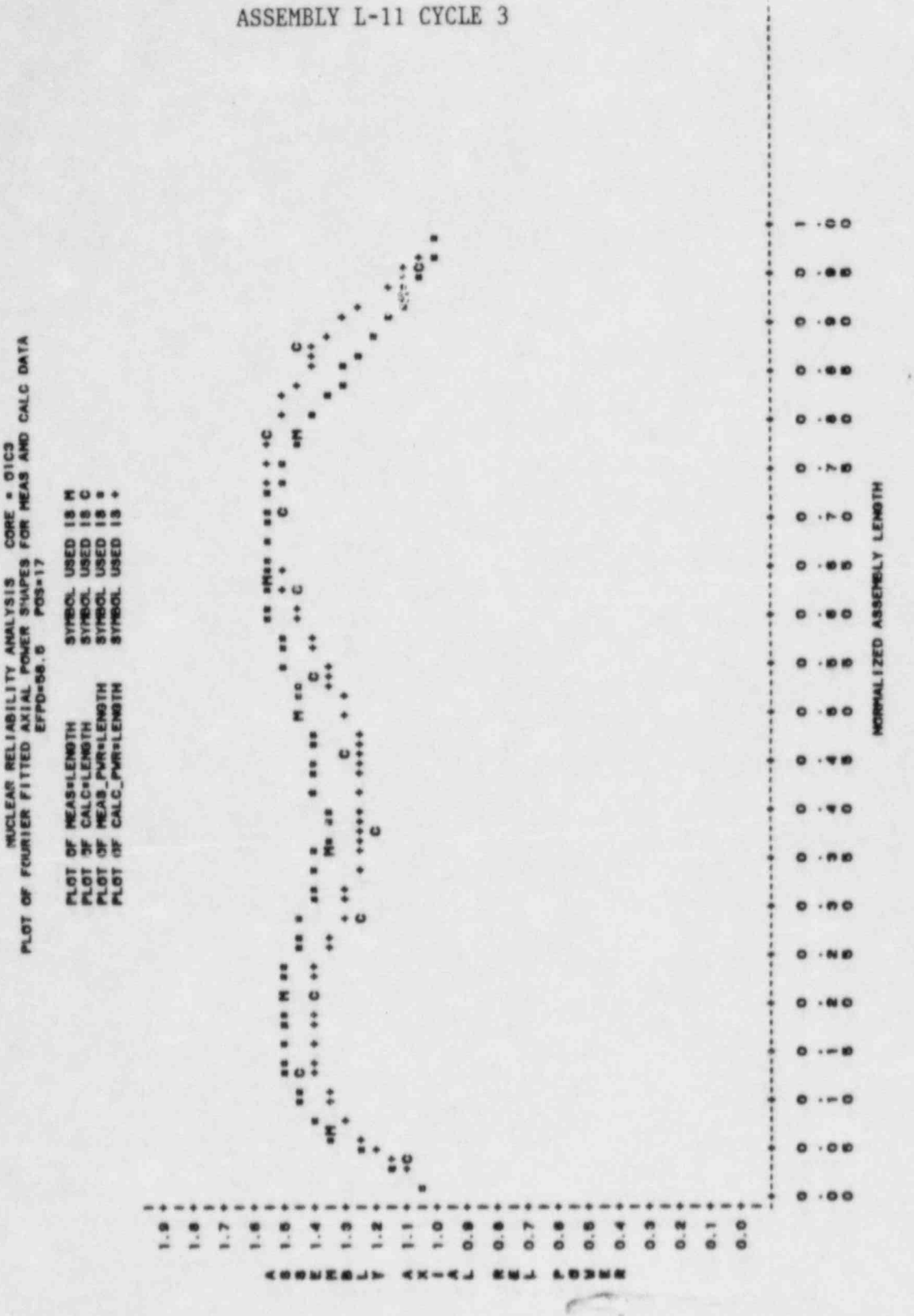

Figure A-33

ASSEMBLY N-12 CYCLE 3

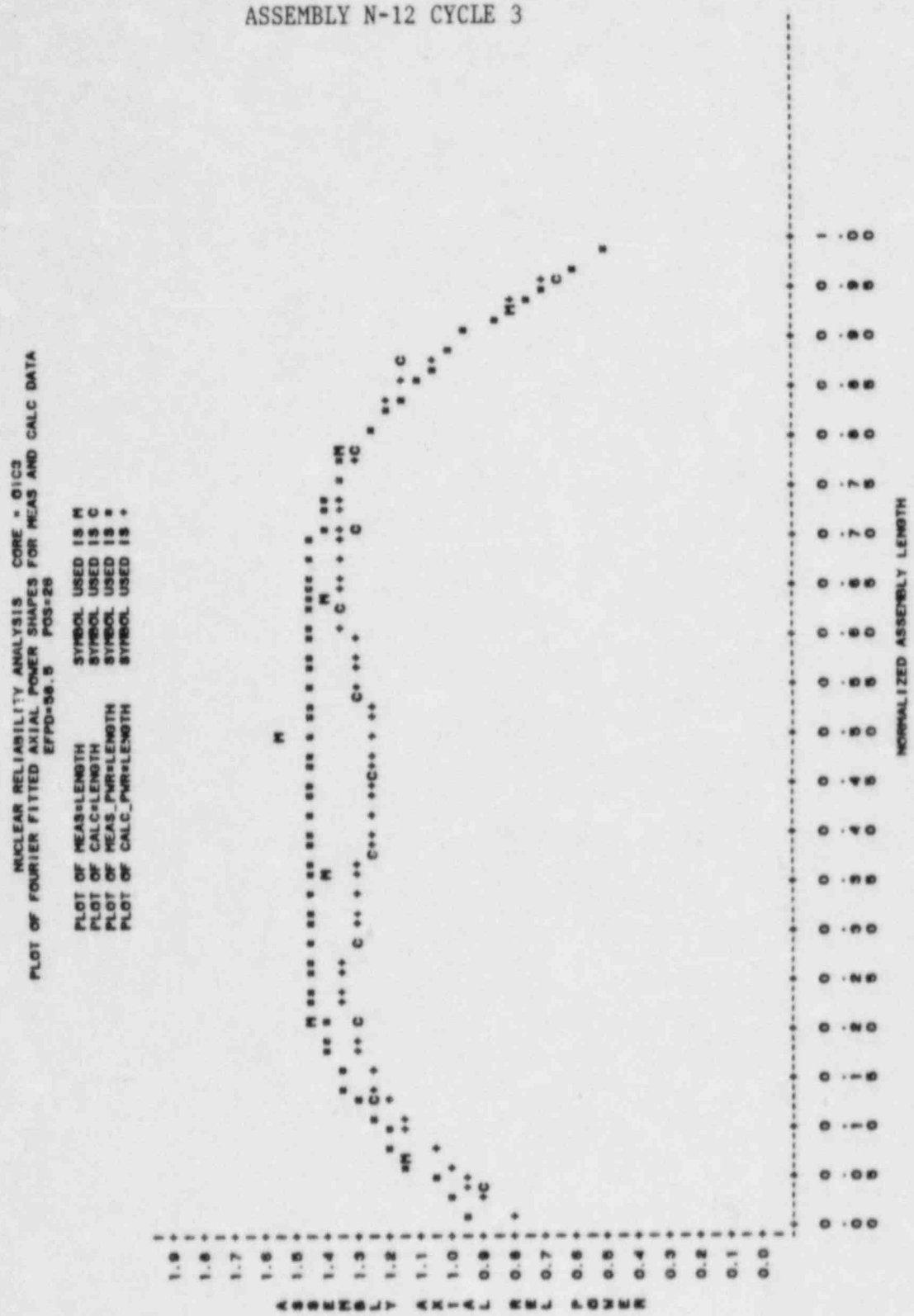

Figure A-34
ASSEMBLY H-11 CYCLE 3

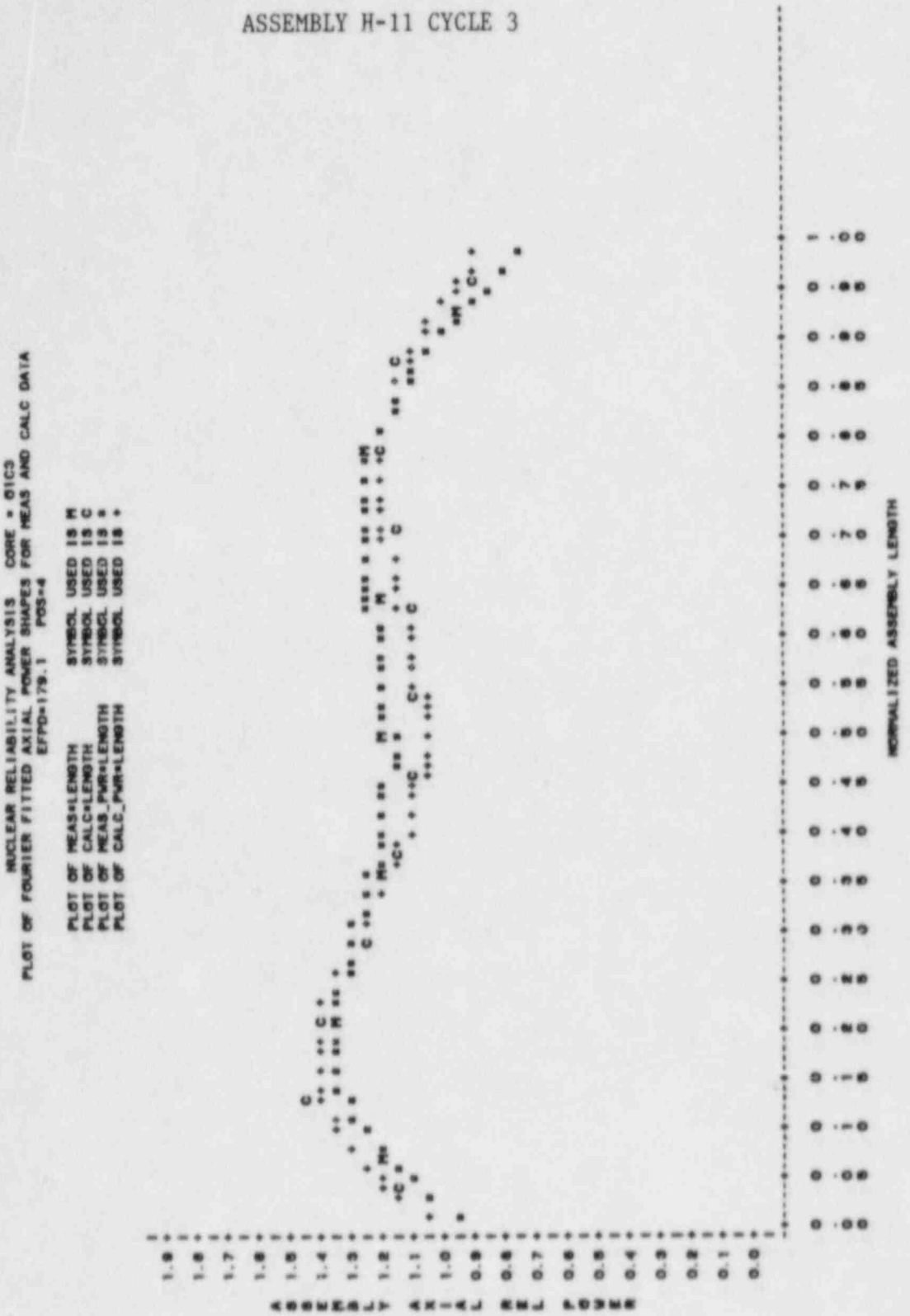

Figure A-35

ASSEMBLY H-13 CYCLE 3

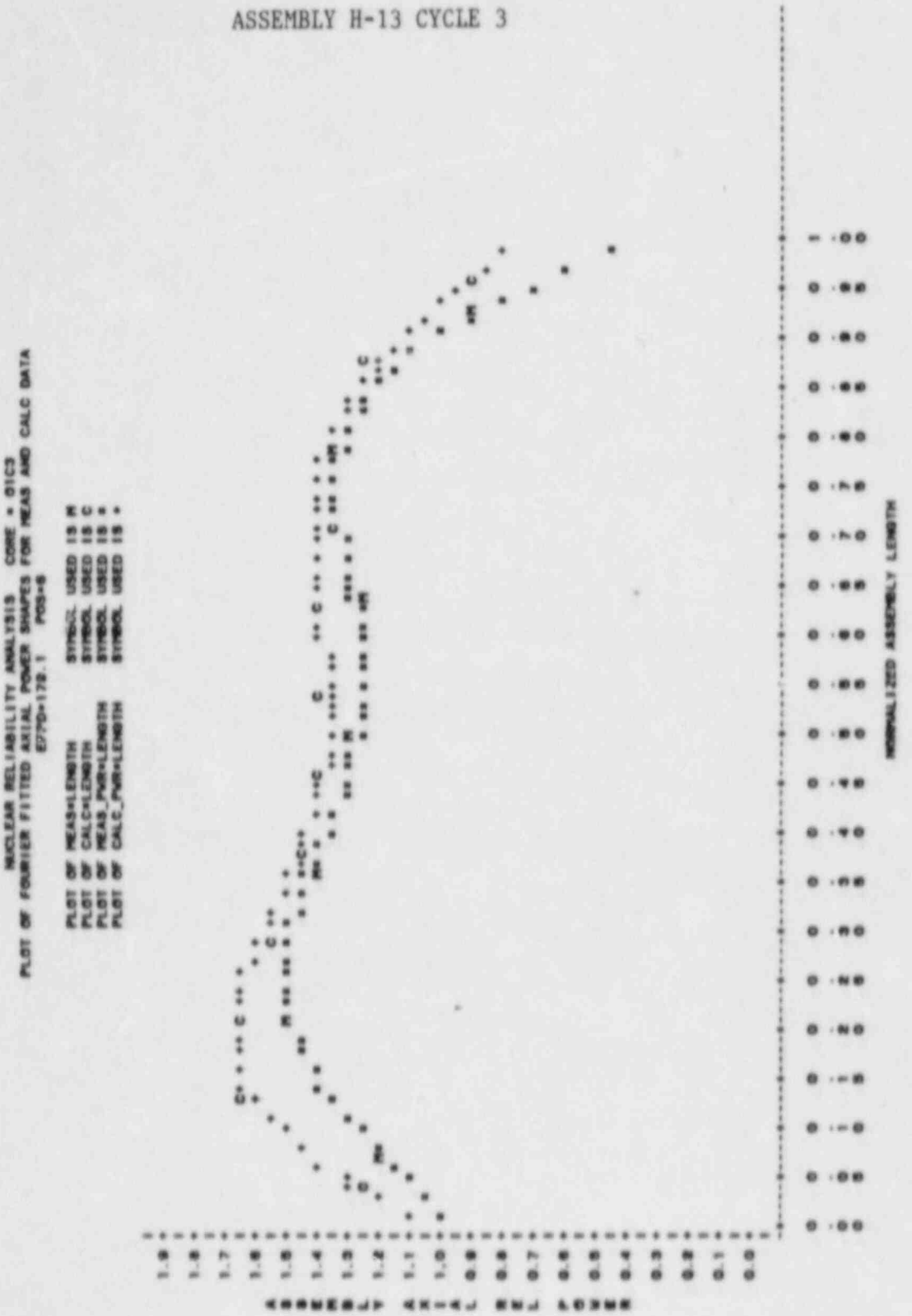

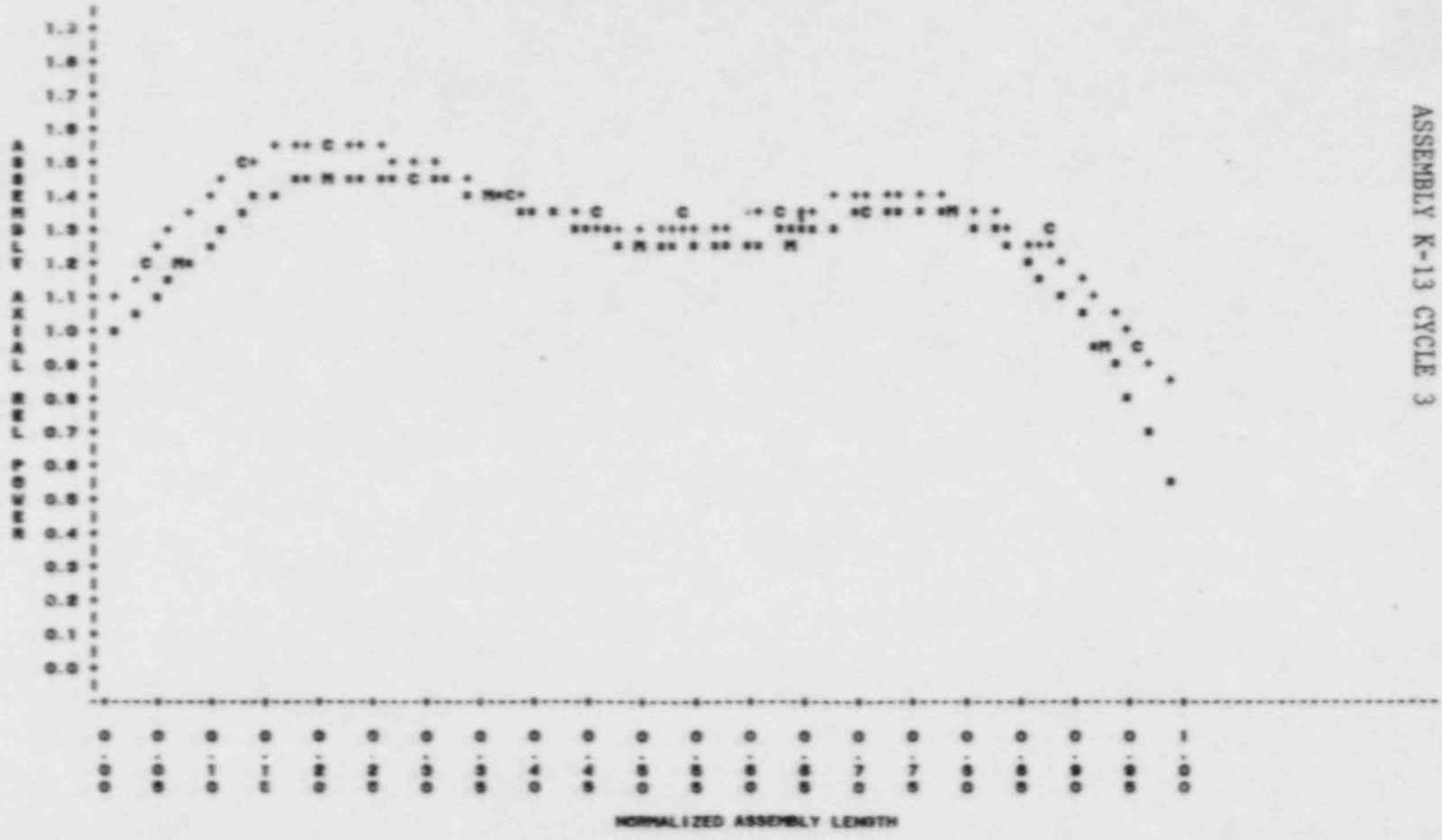

Figure A-36
ASSEMBLY K-13 CYCLE 3

Figure A-37

ASSEMBLY L-11 CYCLE 3

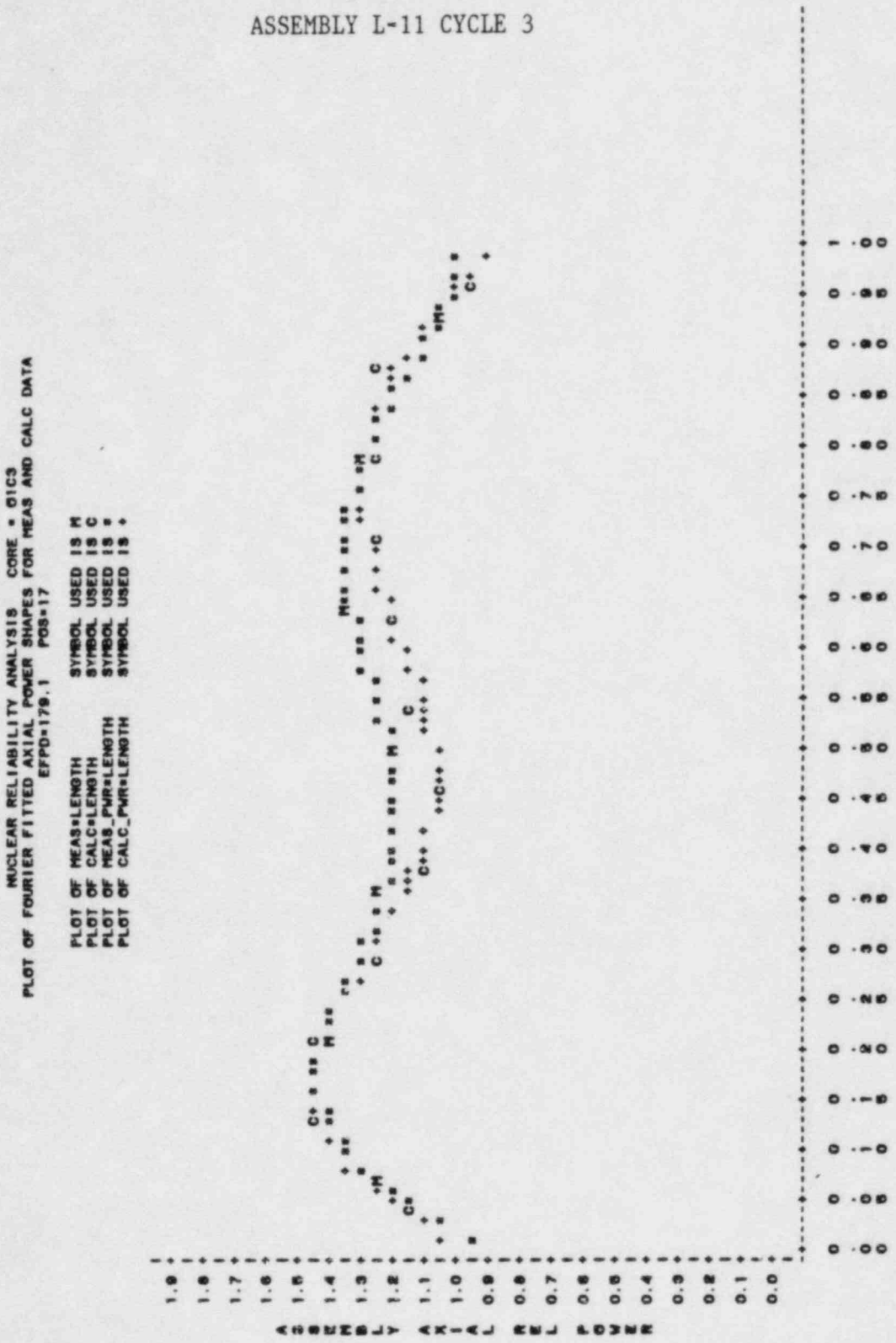

Figure A-38

ASSEMBLY N-12 CYCLE 3

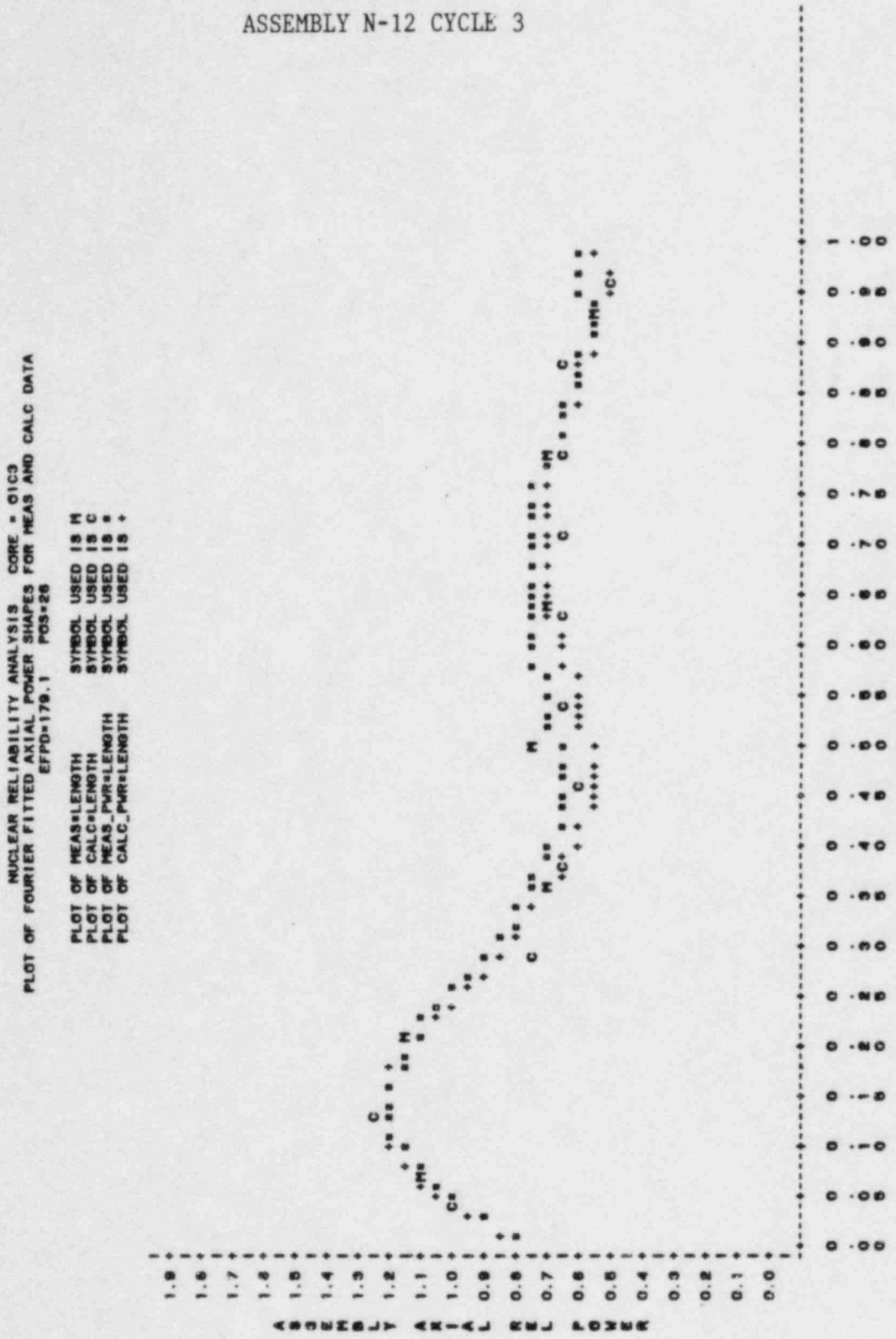

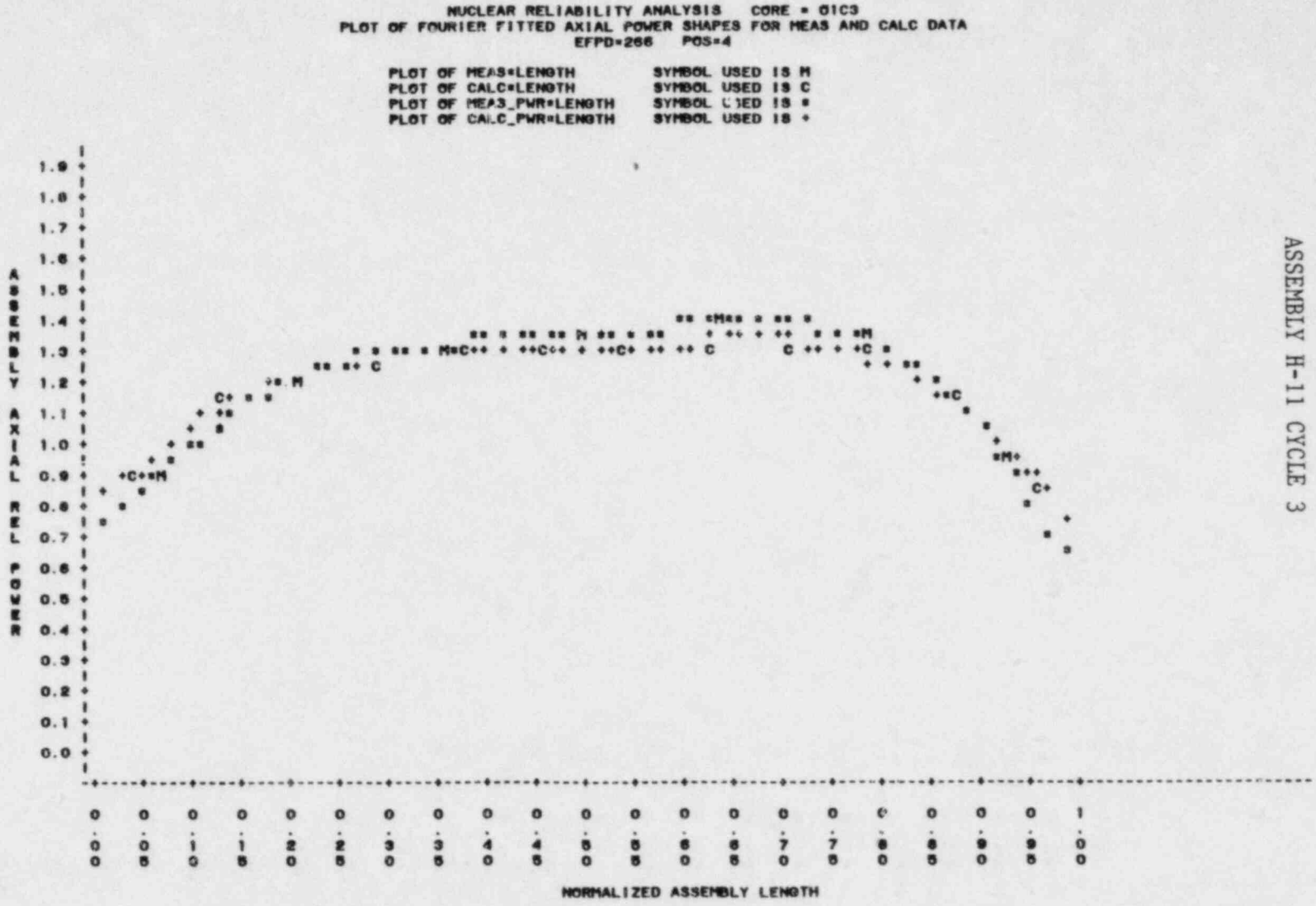

Figure A-39
ASSEMBLY H-11 CYCLE 3

Figure A-40
ASSEMBLY H-13 CYCLE 3

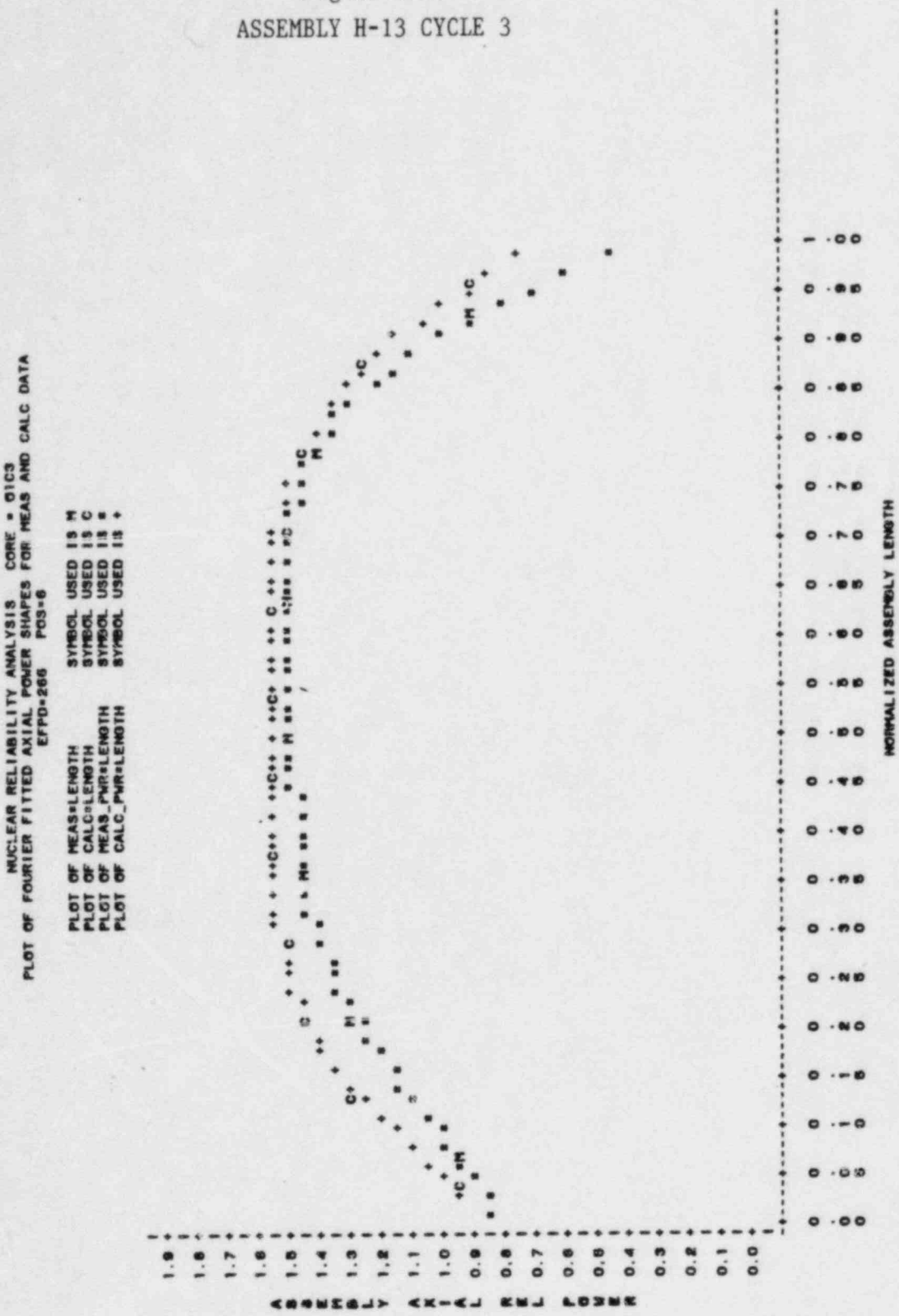

Figure A-41

ASSEMBLY K-13 CYCLE 3

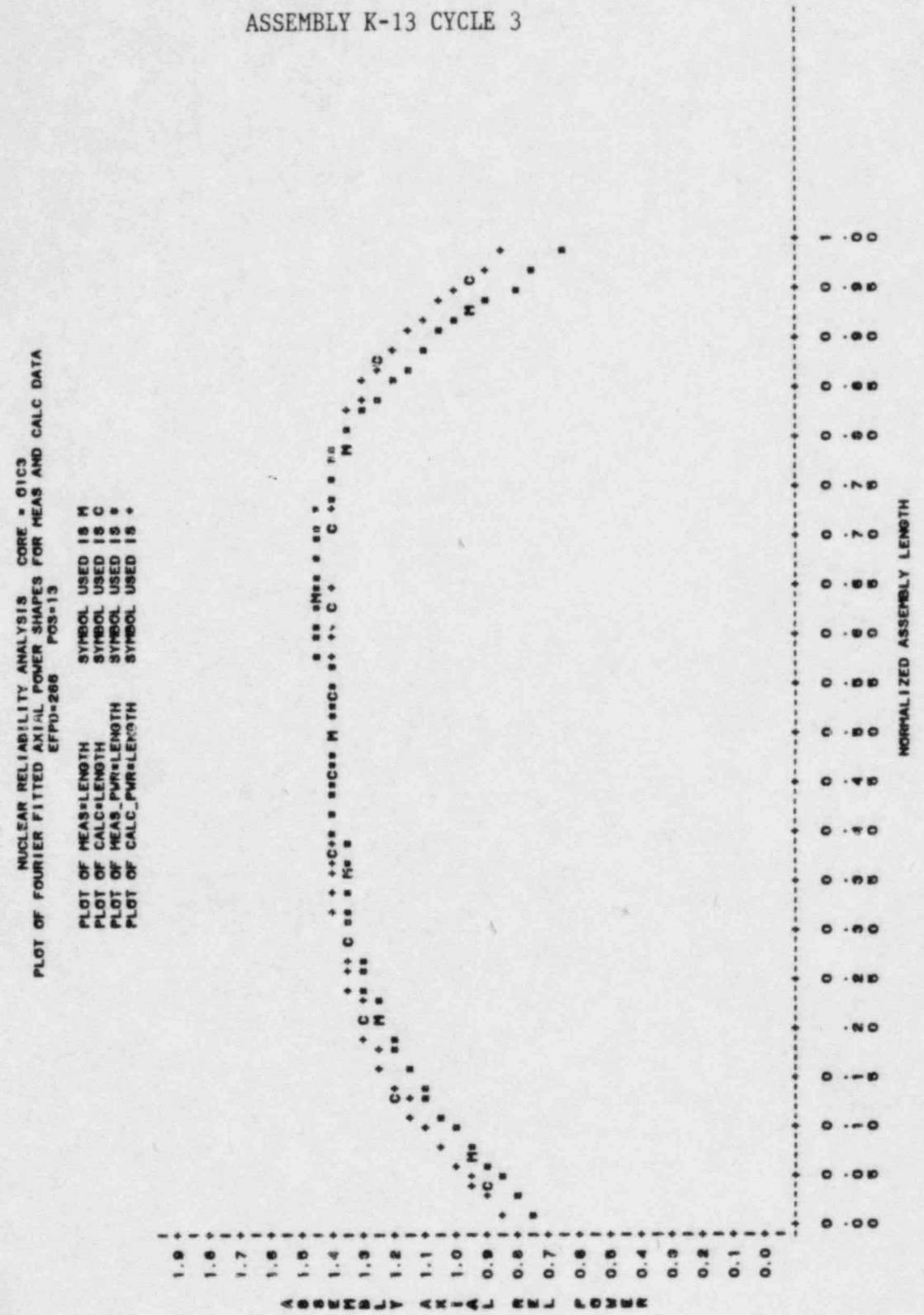

Figure A-42
ASSEMBLY L-11 CYCLE 3

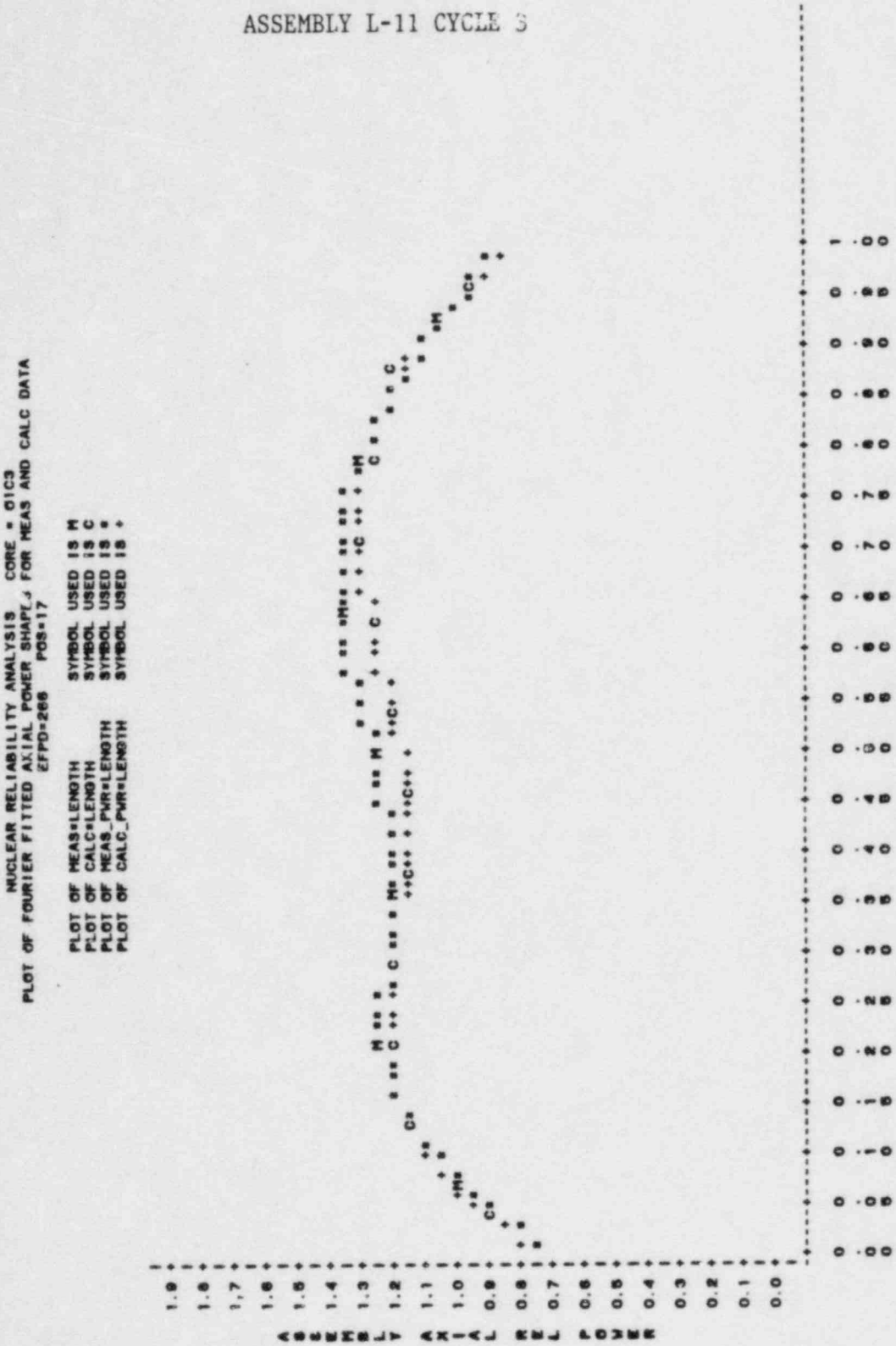

Figure A-43

ASSEMBLY N-12 CYCLE 3

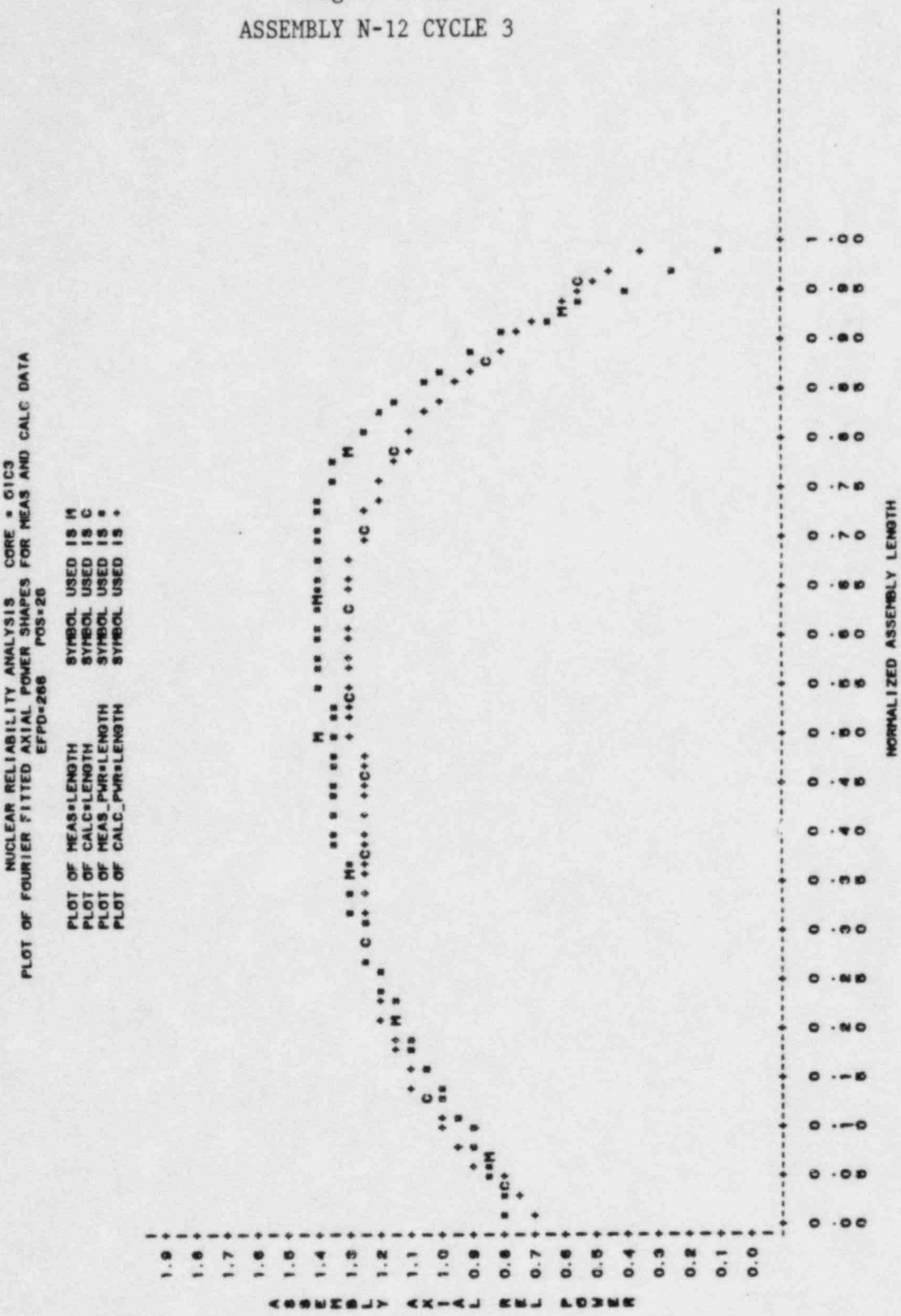

Figure A-44
ASSEMBLY H-11 CYCLE 4

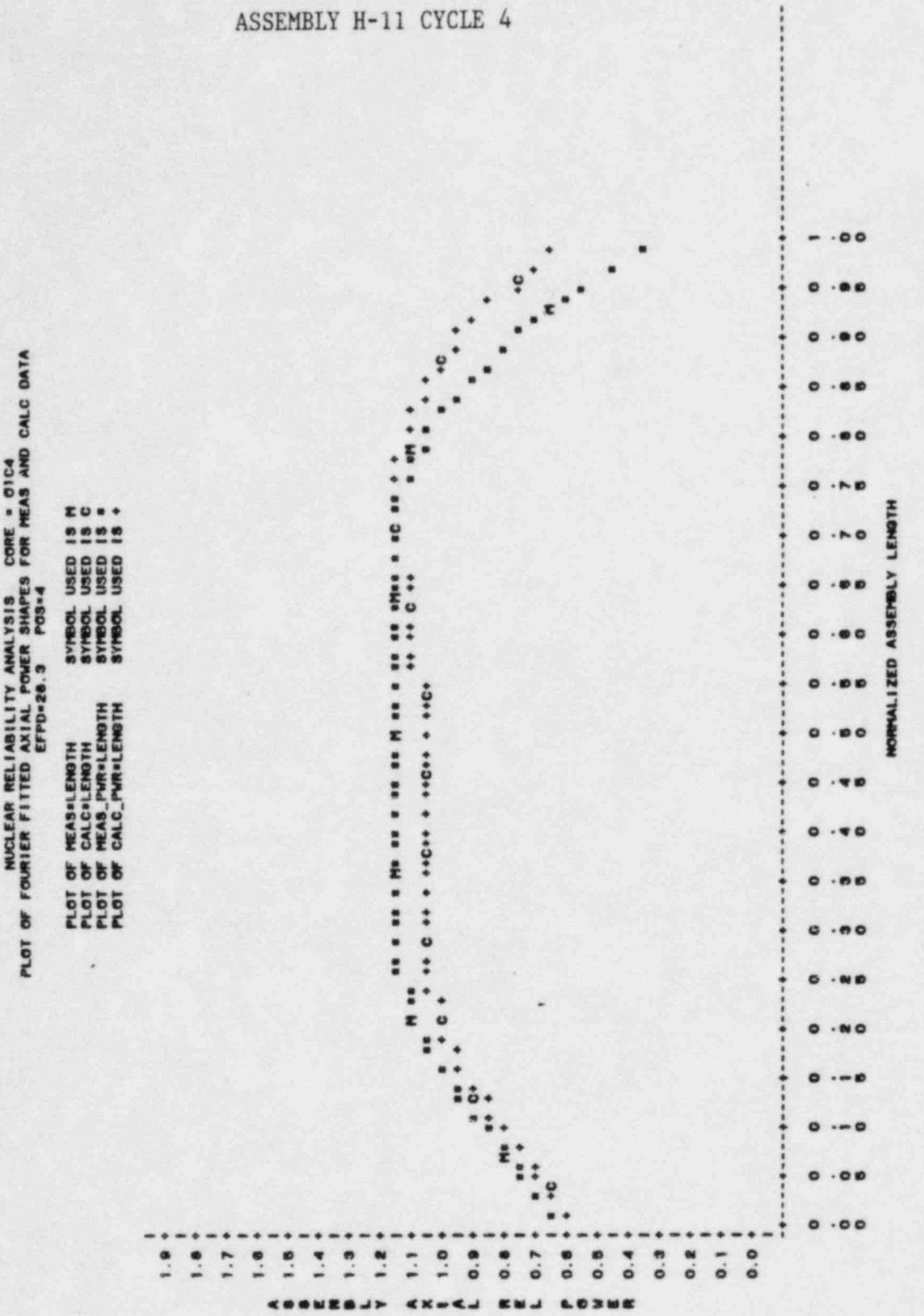

Figure A-45
ASSEMBLY H-12 CYCLE 4

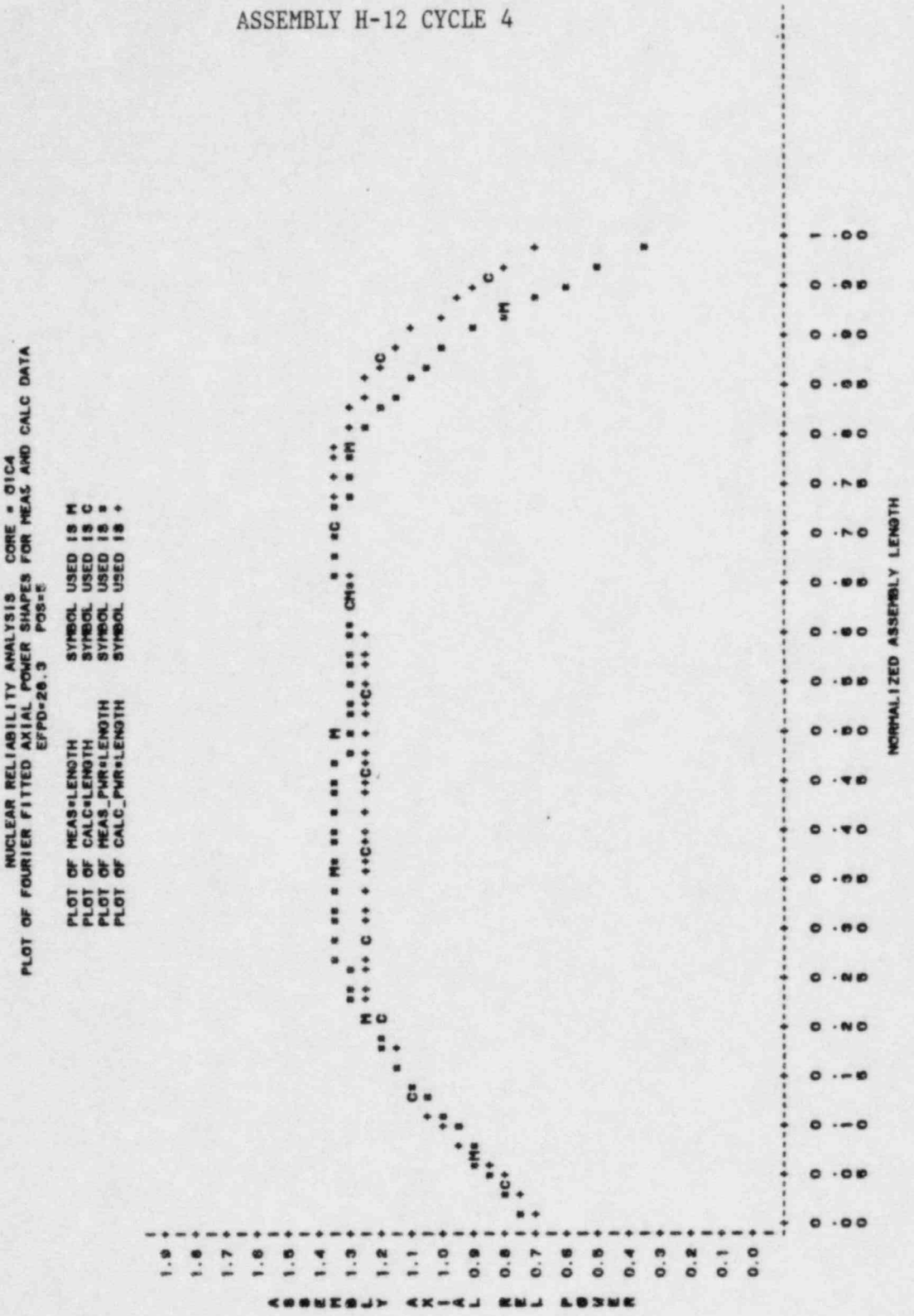

Figure A-46

ASSEMBLY H-14 CYCLE 4

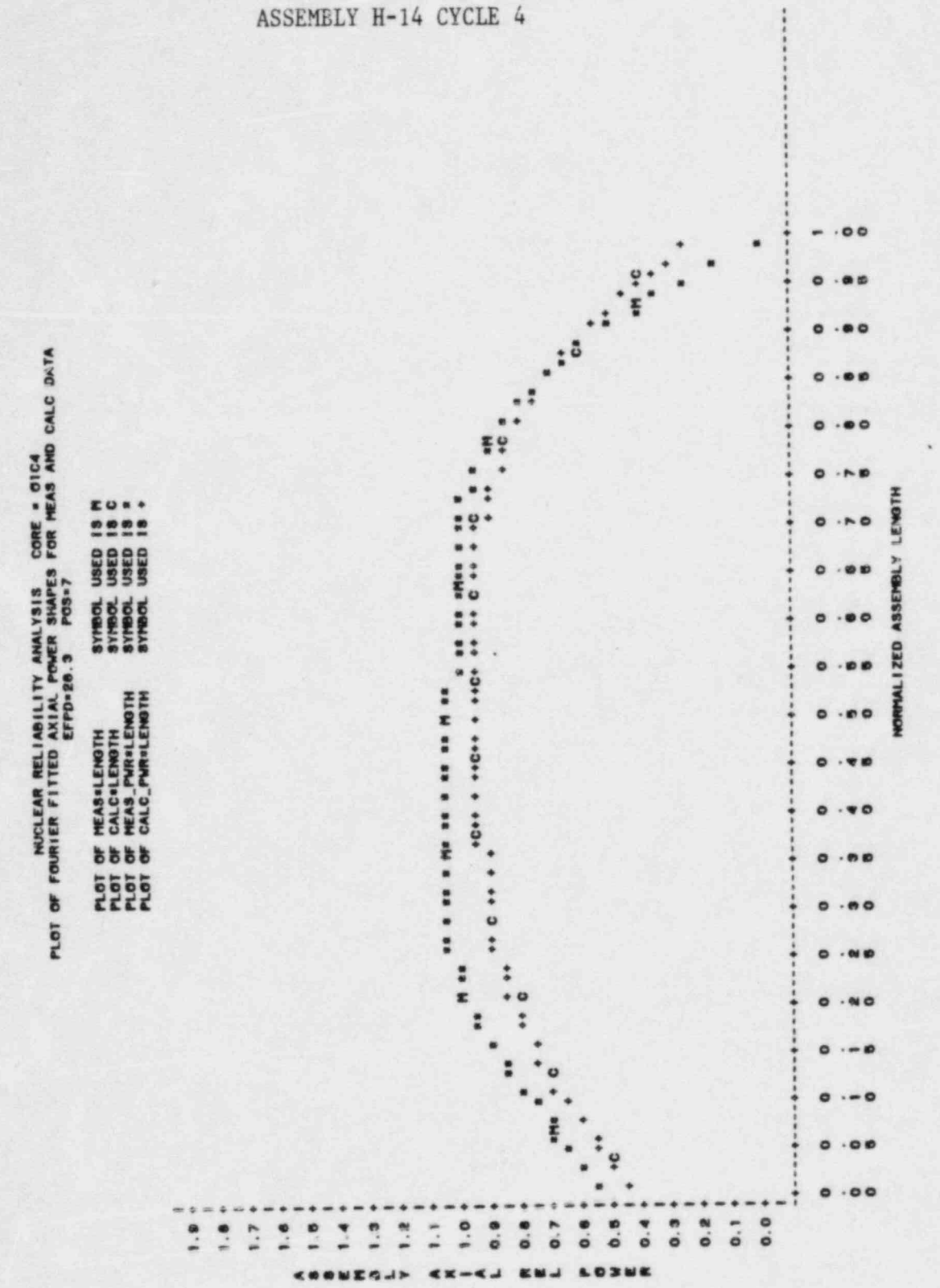

Figure A-47
ASSEMBLY K-13 CYCLE 4

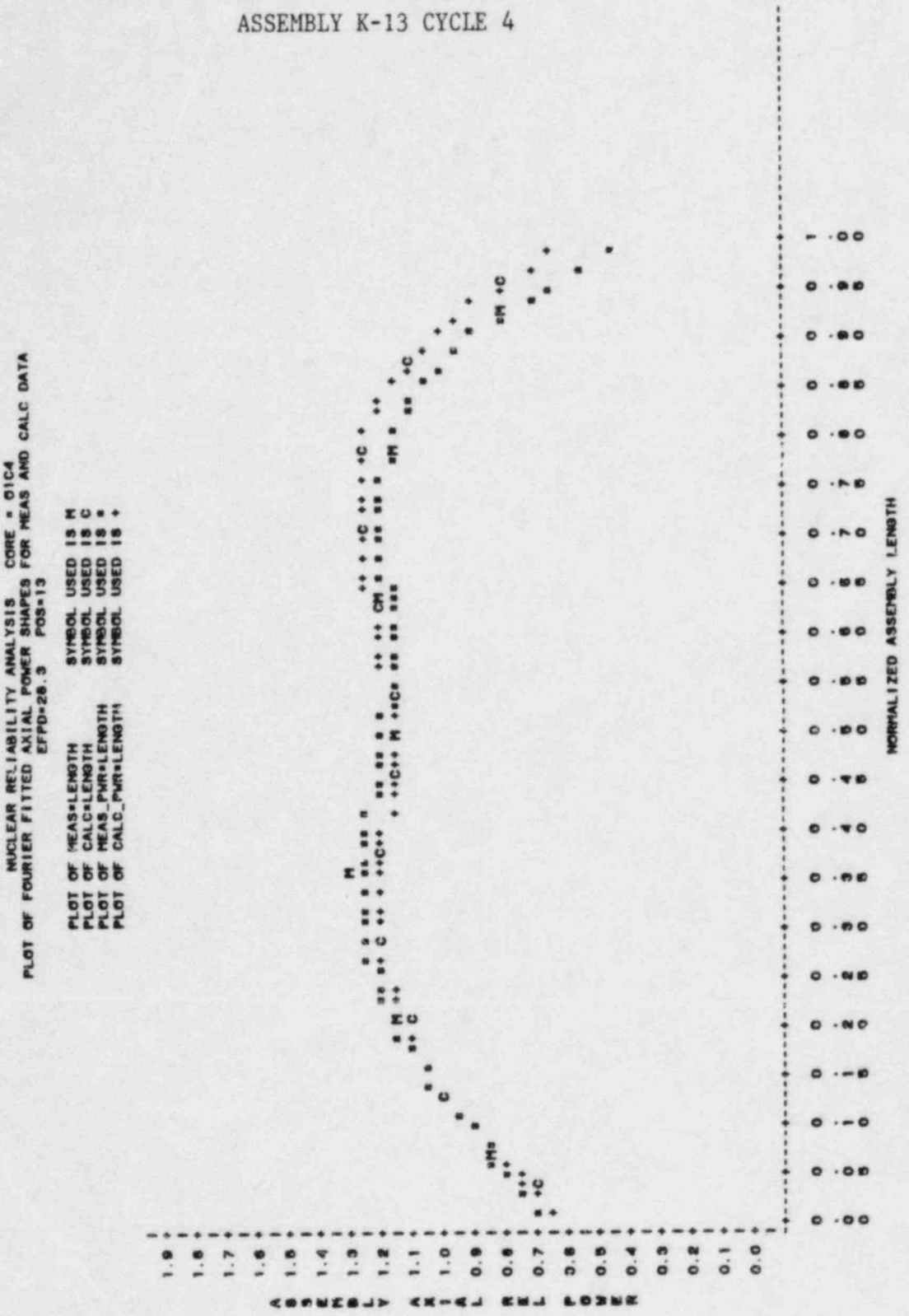

Figure A-48

ASSEMBLY L-11 CYCLE 4

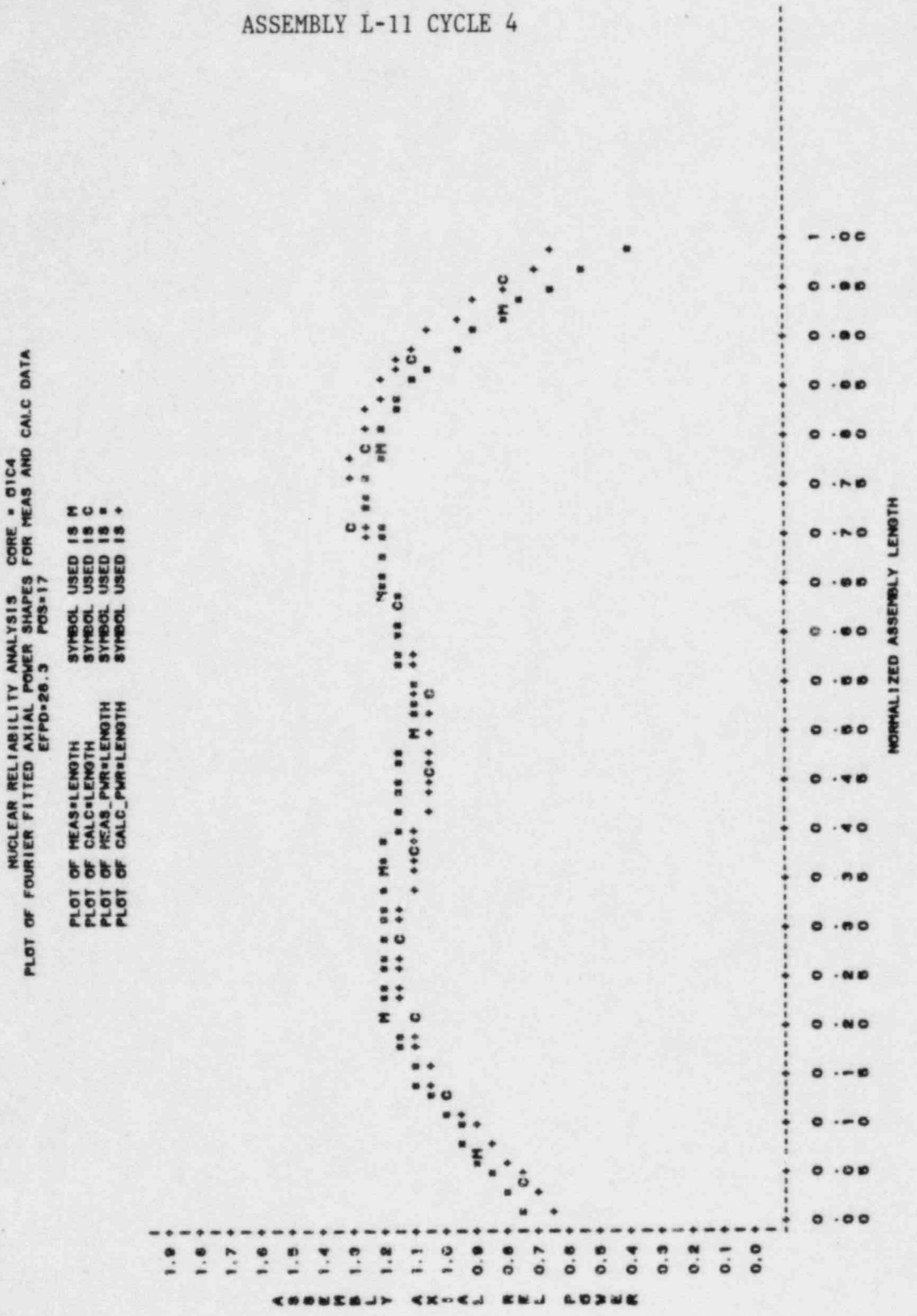

Figure A-49

ASSEMBLY H-11 CYCLE 4

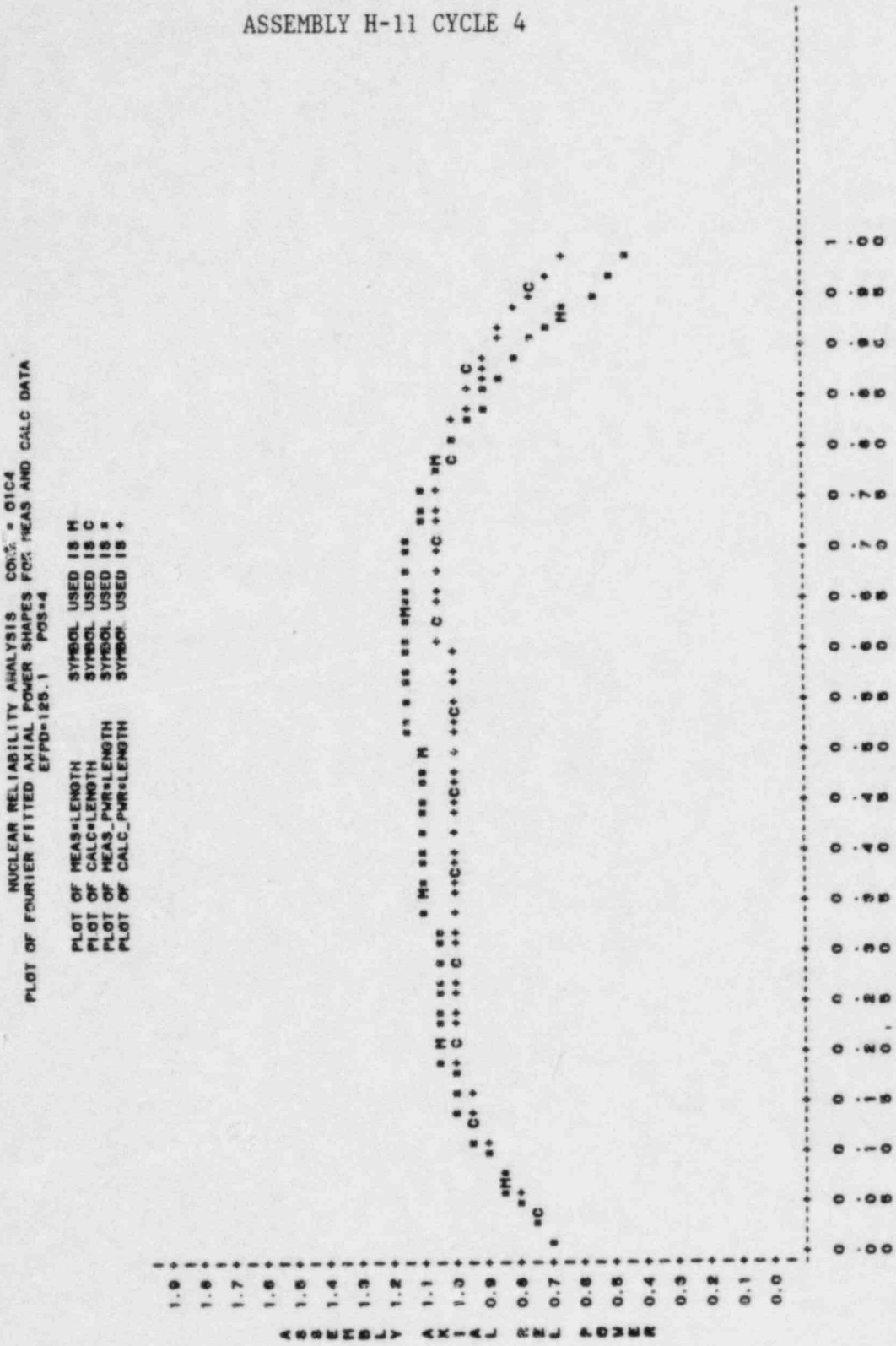

Figure A-50
ASSEMBLY H-12 CYCLE 4

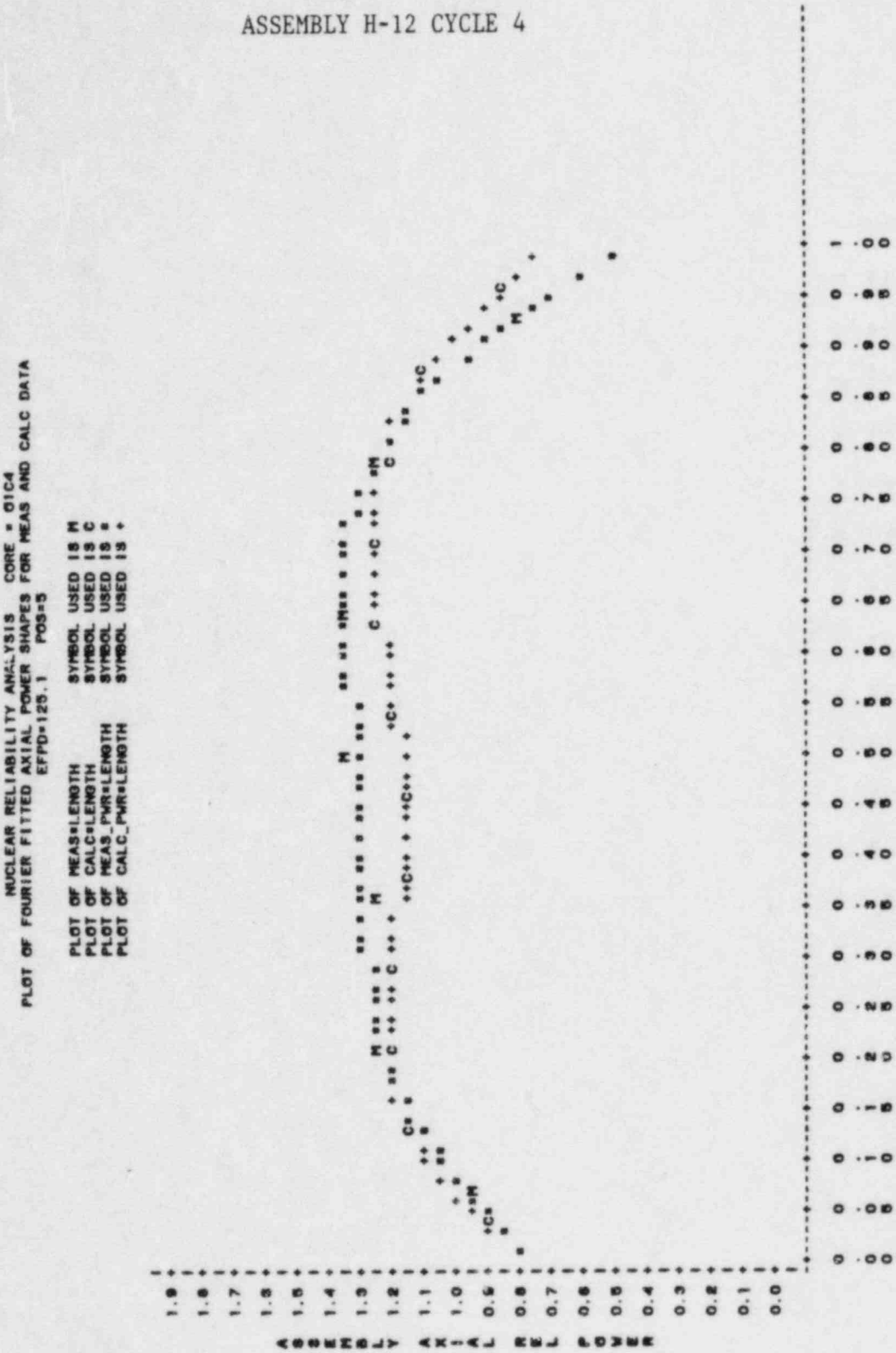

Figure A-51
ASSEMBLY H-14 CYCLE 4

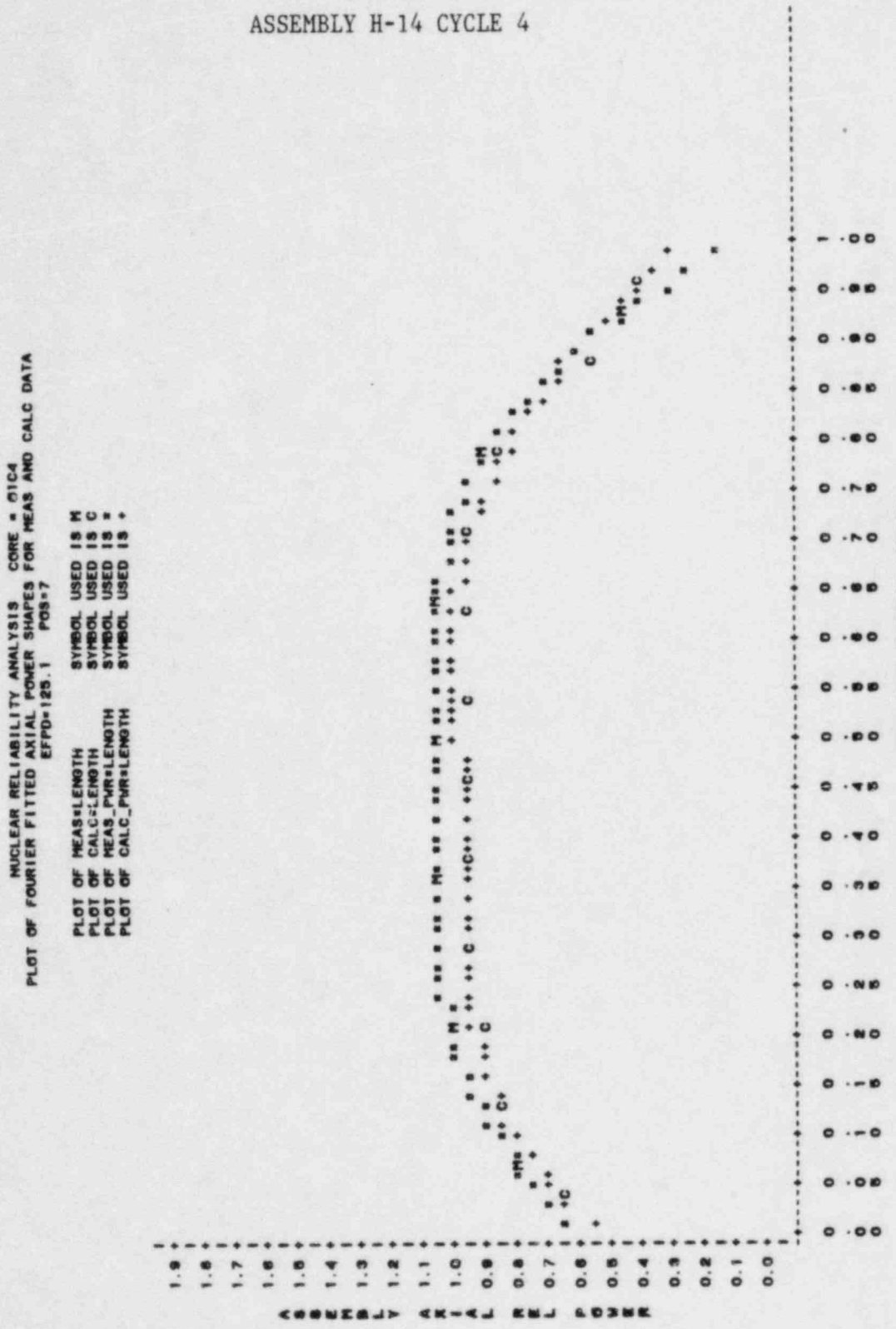

Figure A-52
ASSEMBLY K-13 CYCLE 4

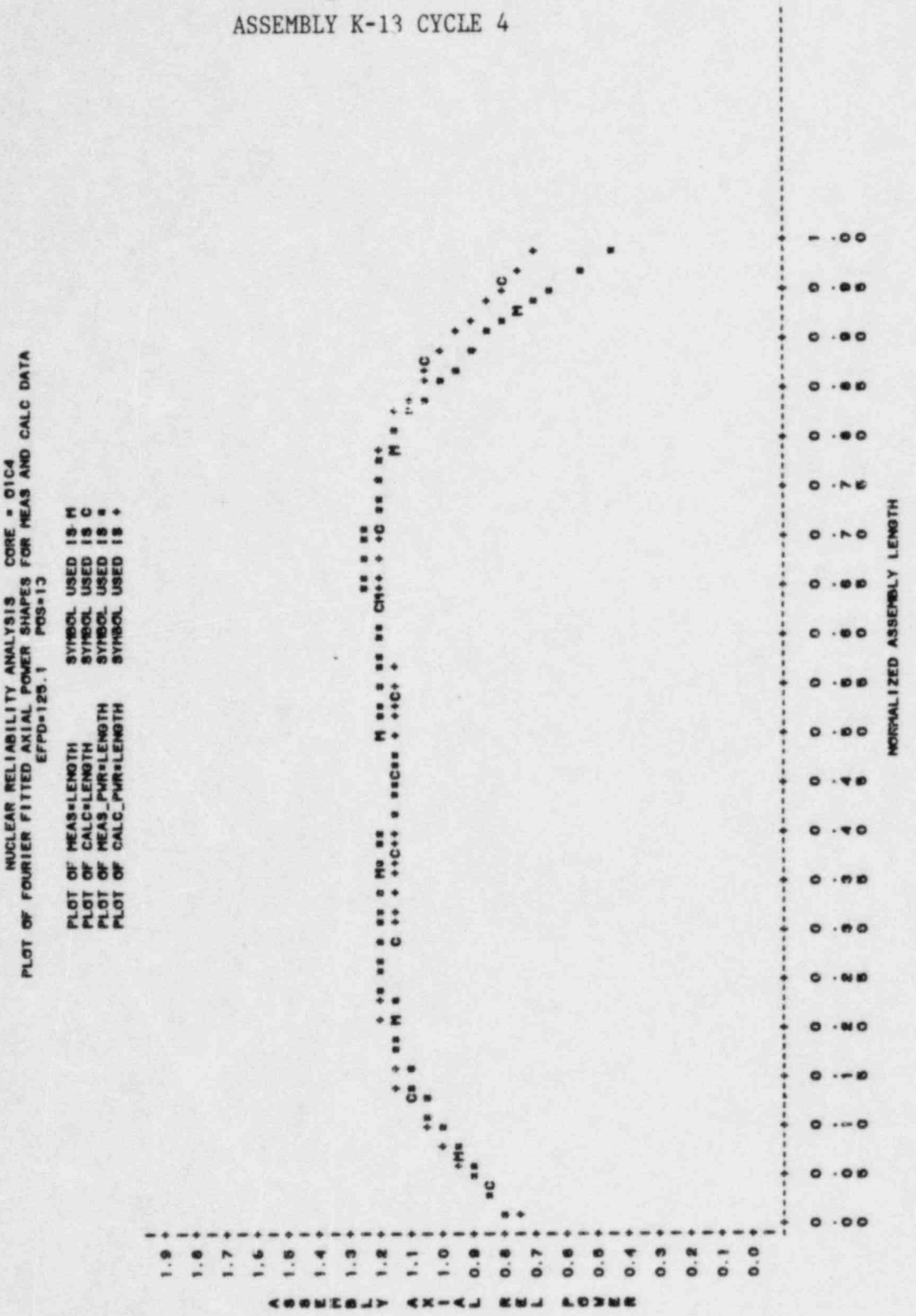

Figure A-53
ASSEMBLY L-11 CYCLE 4

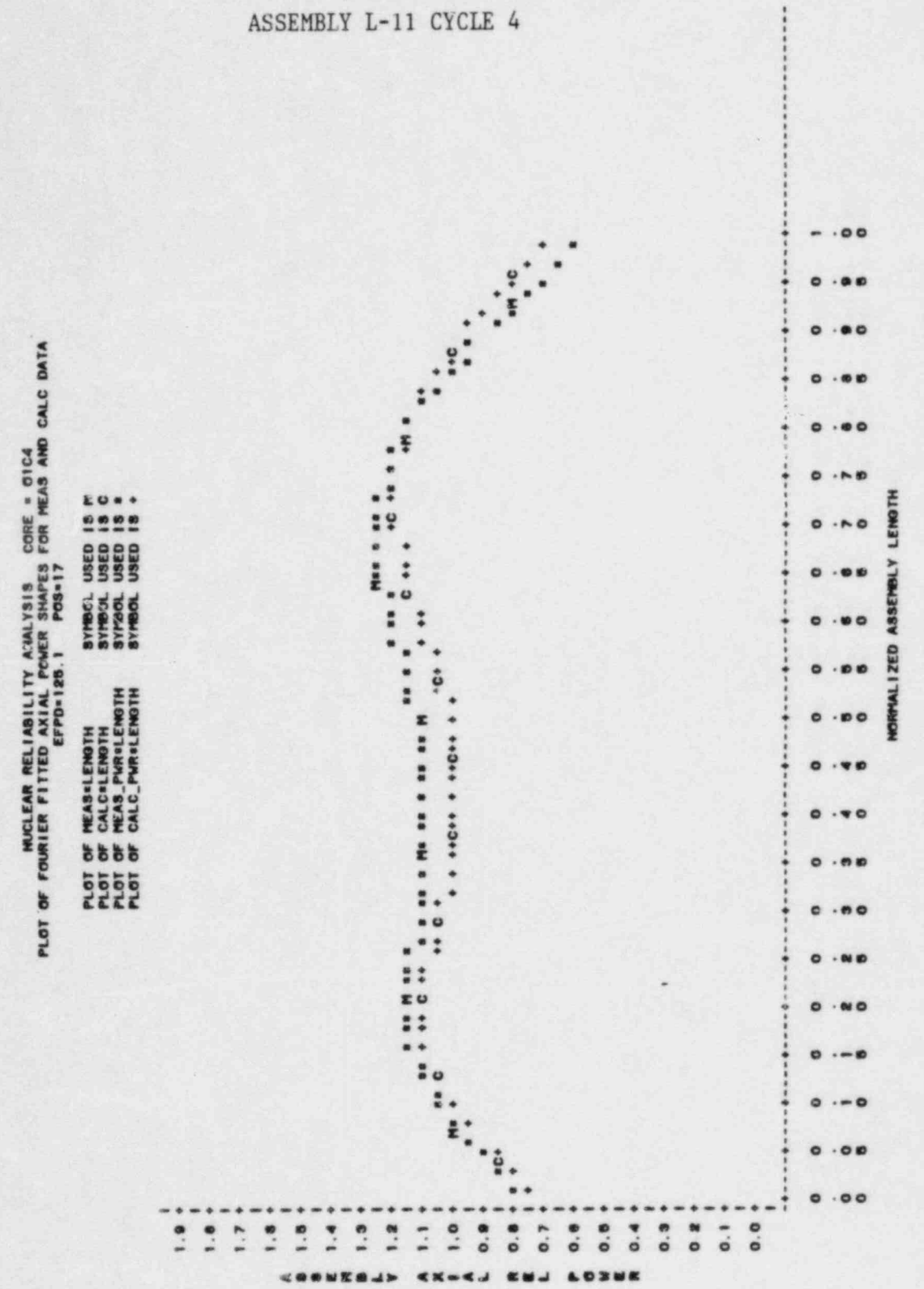

Figure A-54
ASSEMBLY H-11 CYCLE 4

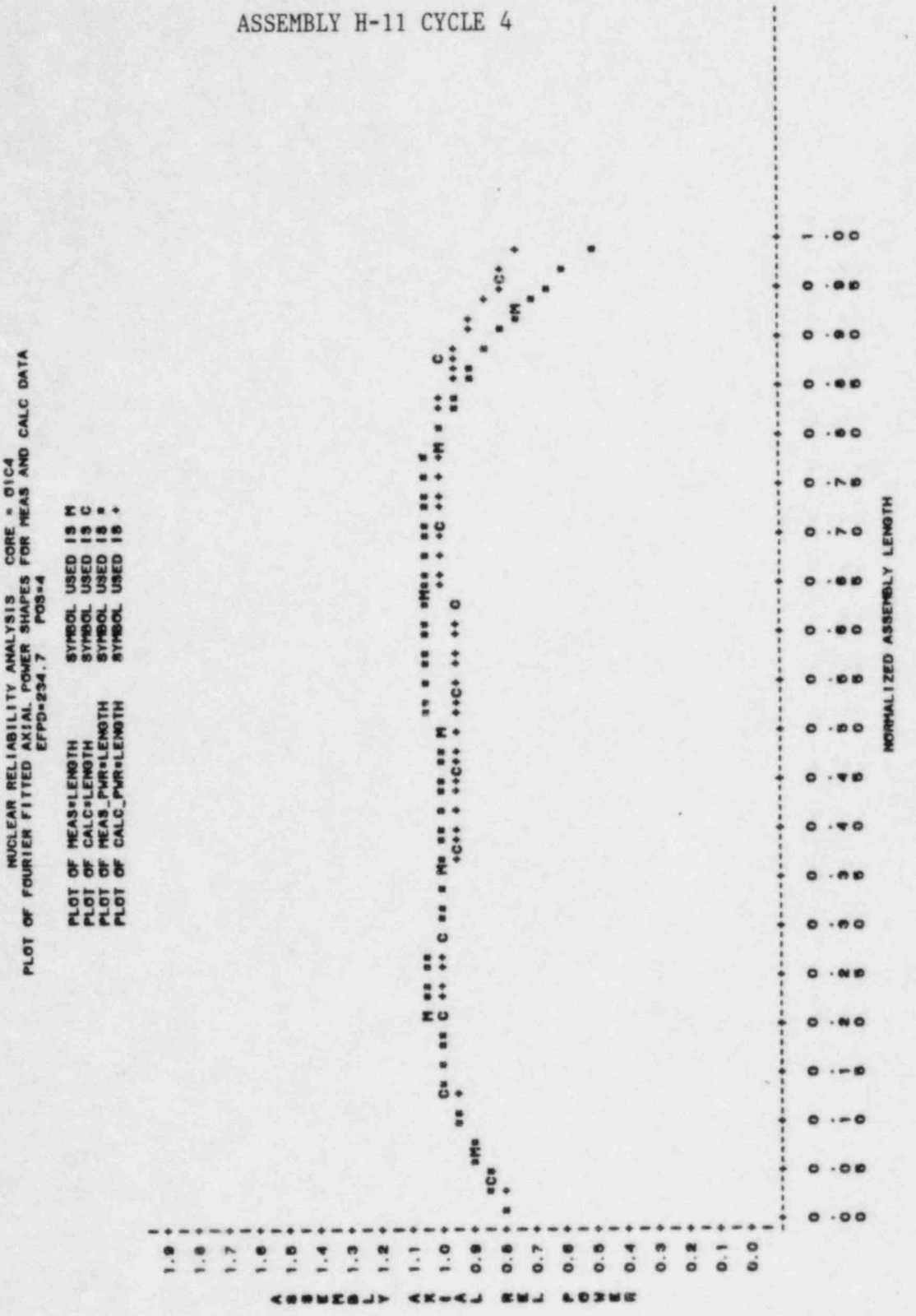

Figure A-55
ASSEMBLY H-12 CYCLE 4

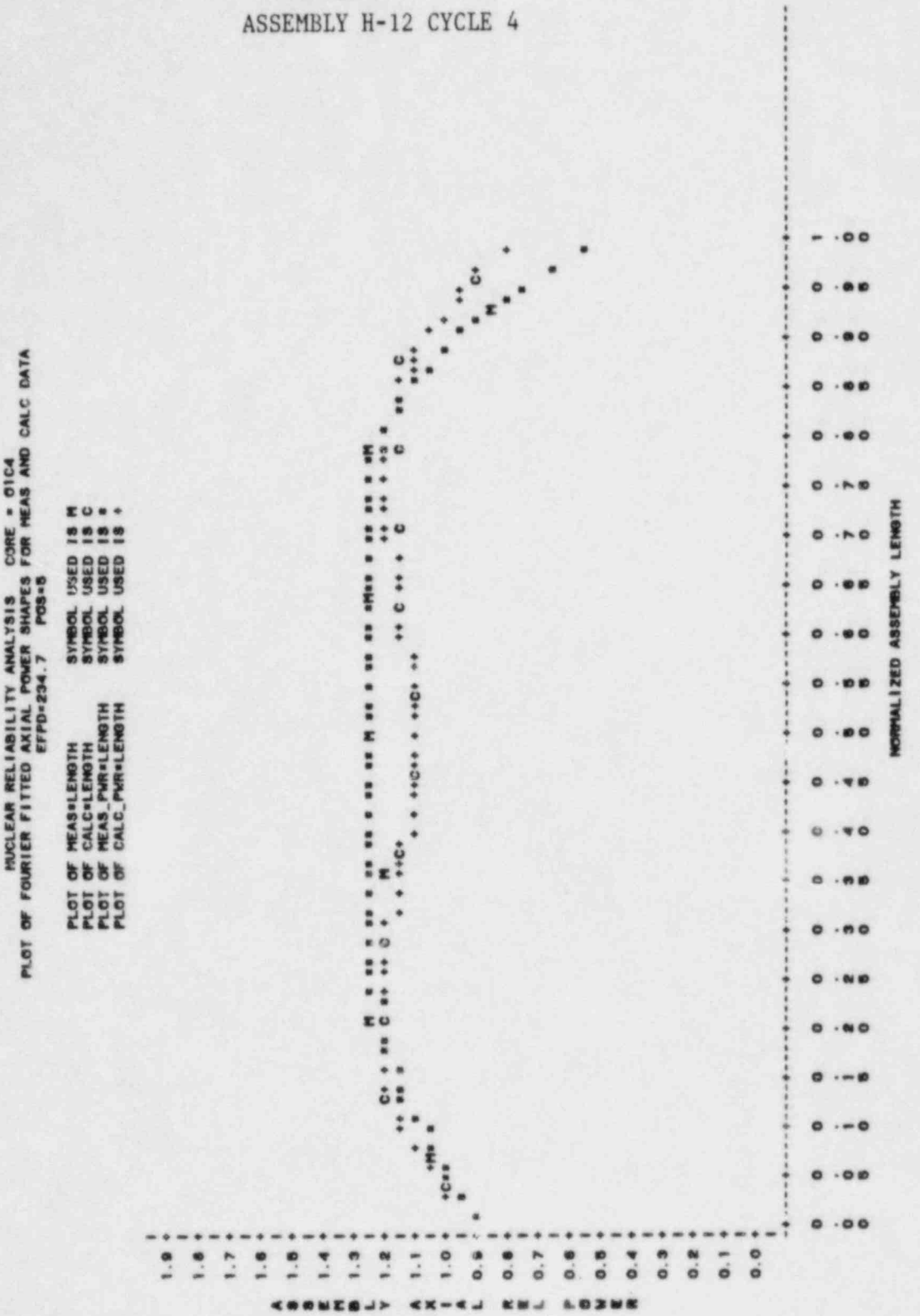

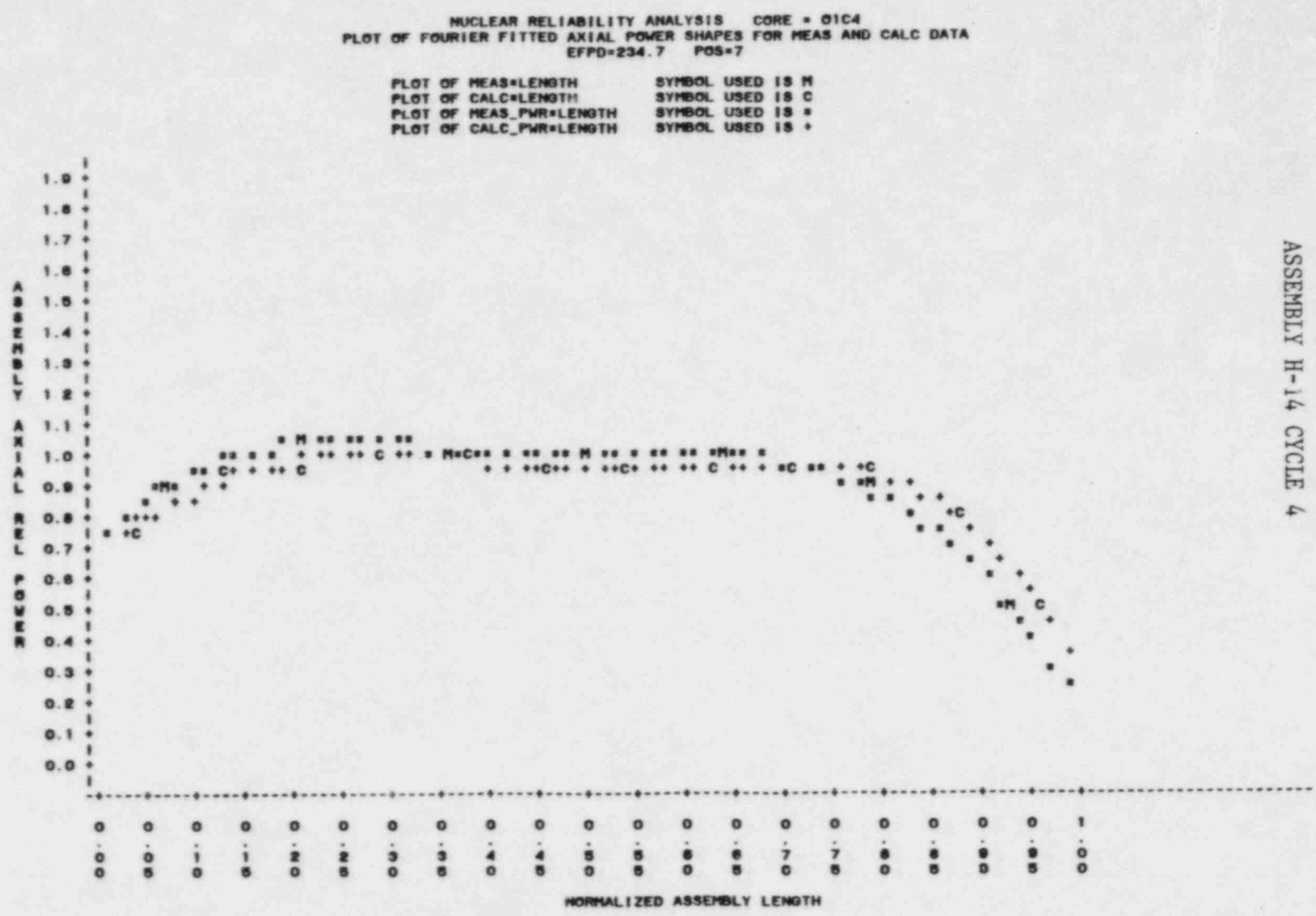

Figure A-56
ASSEMBLY H-14 CYCLE 4

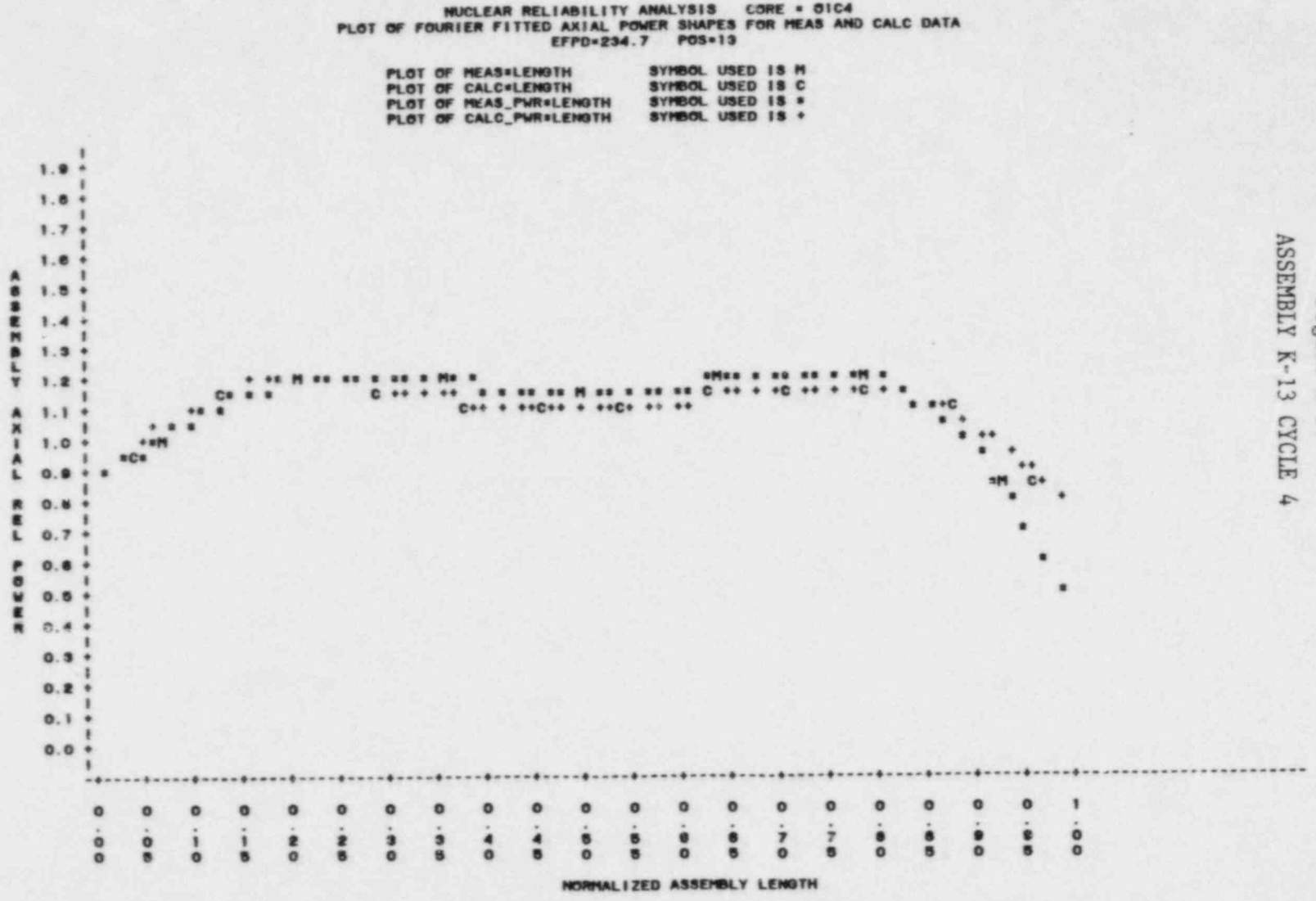

Figure A-57
ASSEMBLY K-13 CYCLE 4

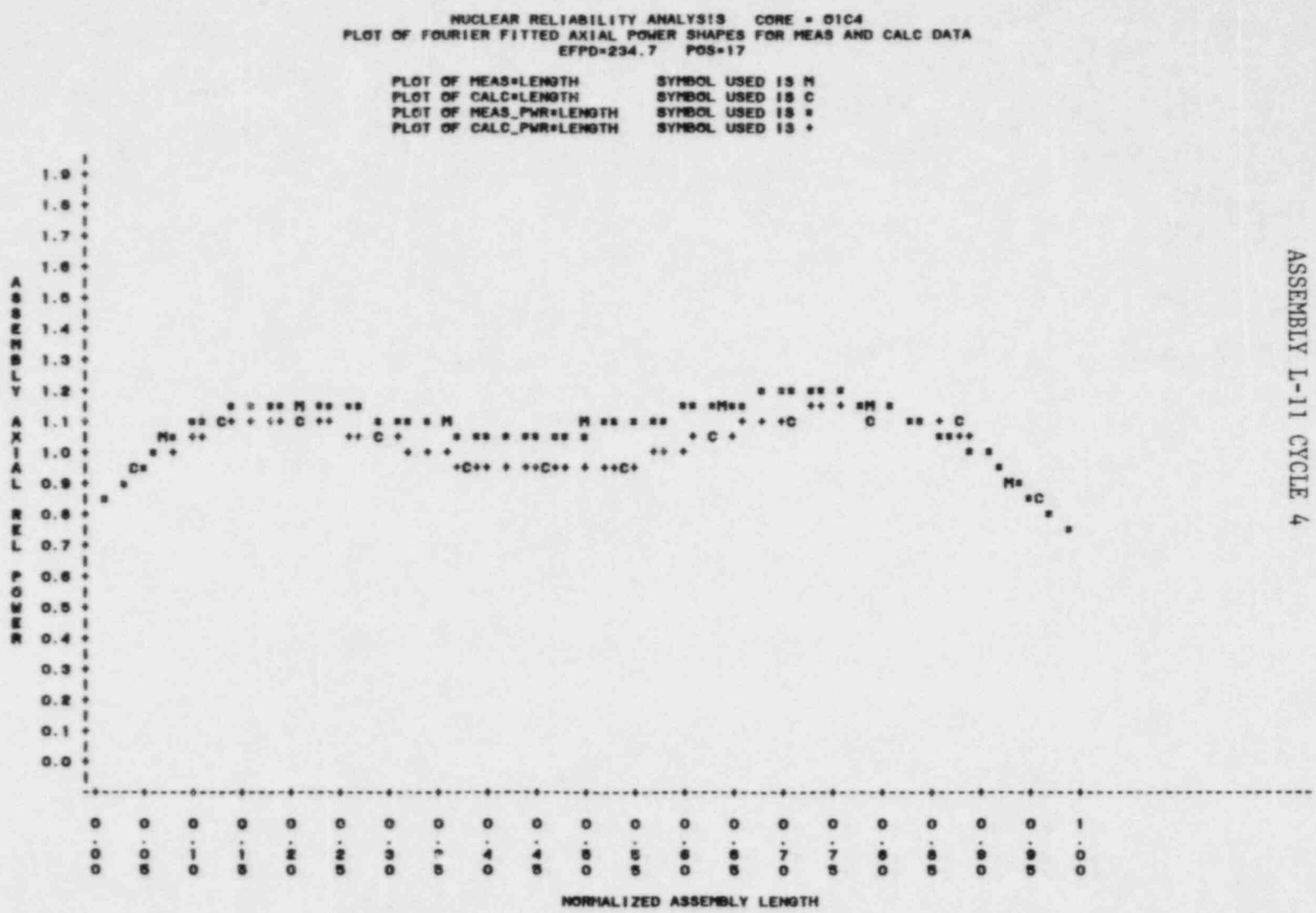

Figure A-58
ASSEMBLY L-11 CYCLE 4

Figure A-59

ASSEMBLY H-8 CYCLE 5

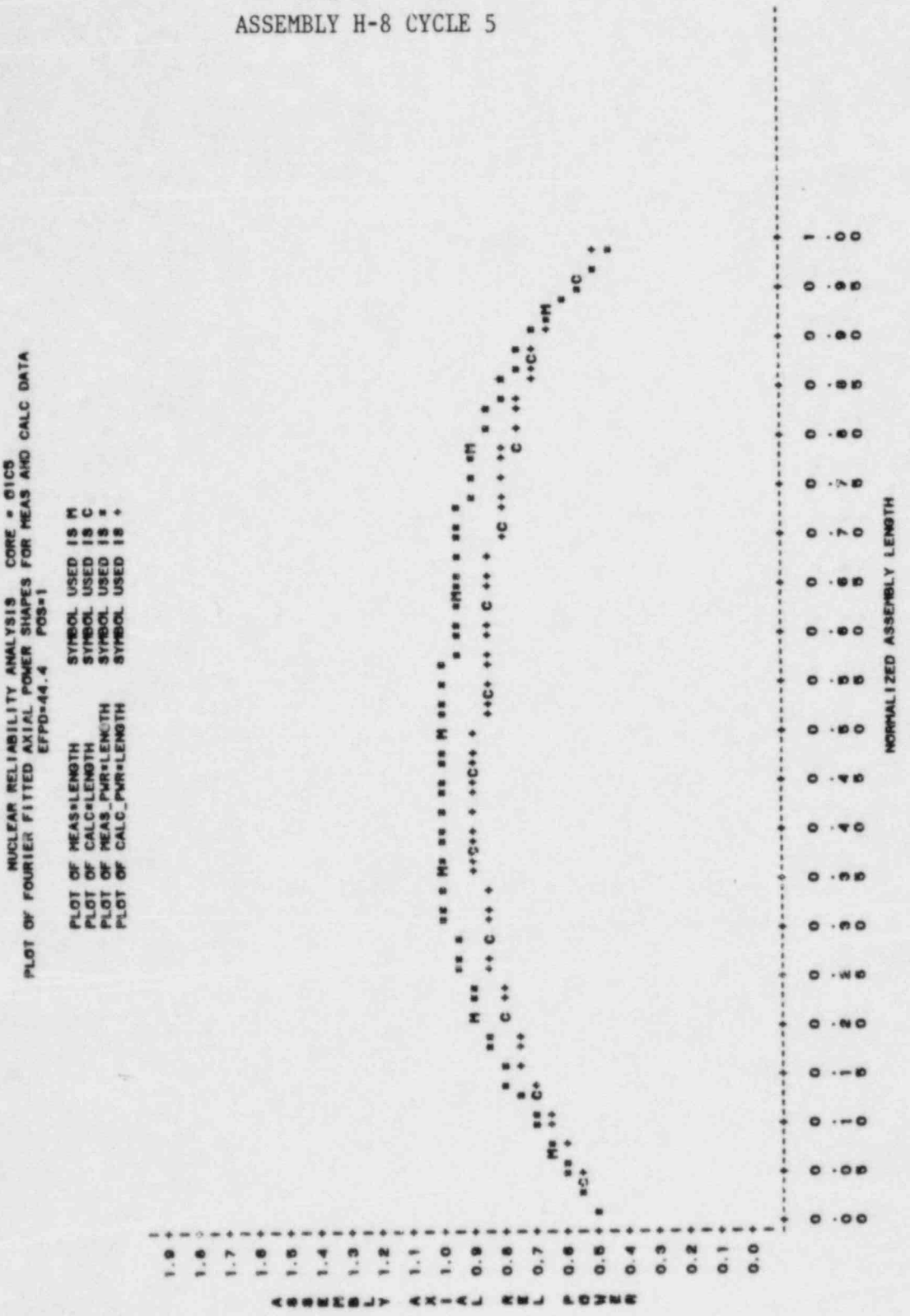

Figure A-60
ASSEMBLY L-10 CYCLE 5

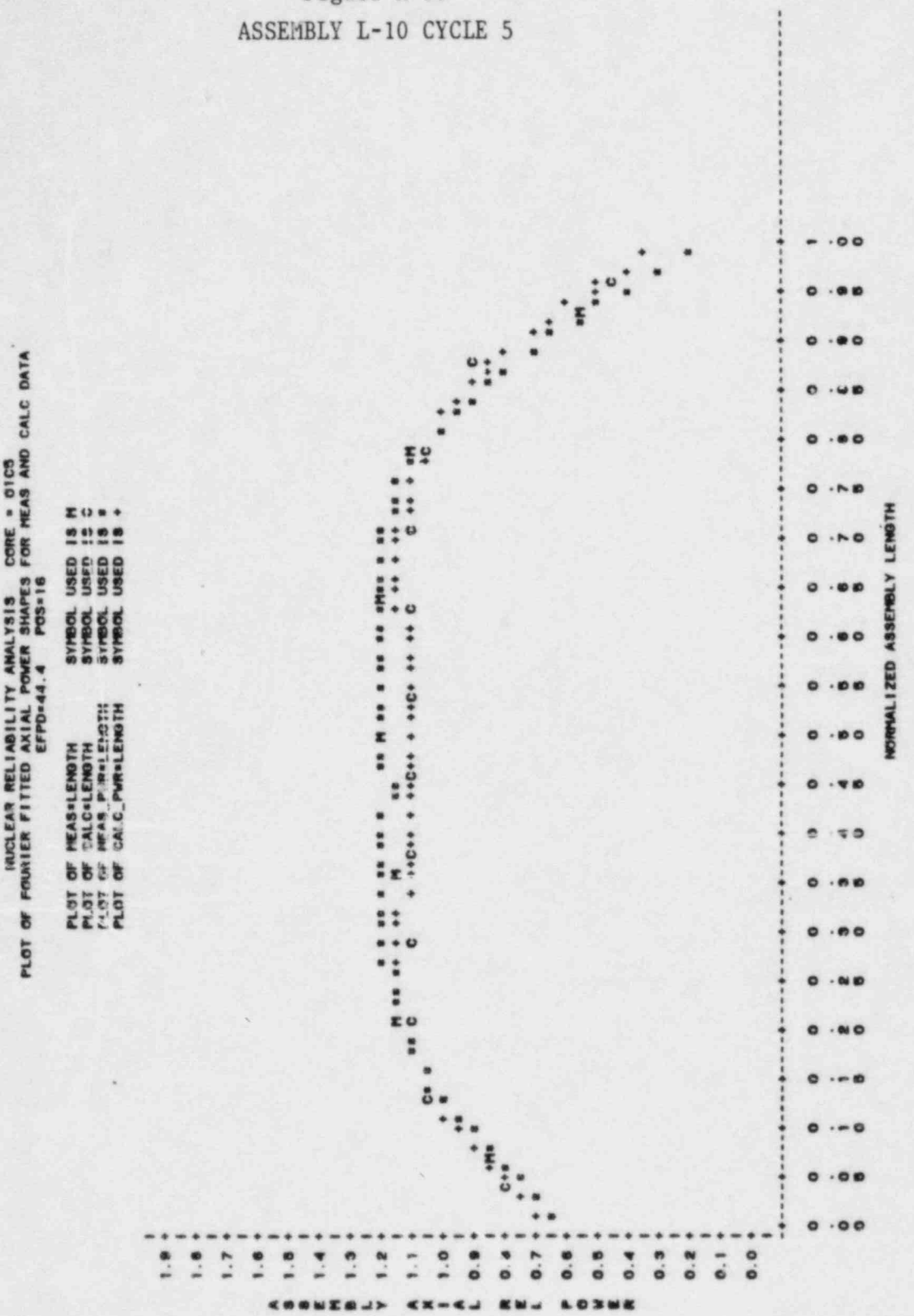

Figure A-61
ASSEMBLY L-12 CYCLE 5

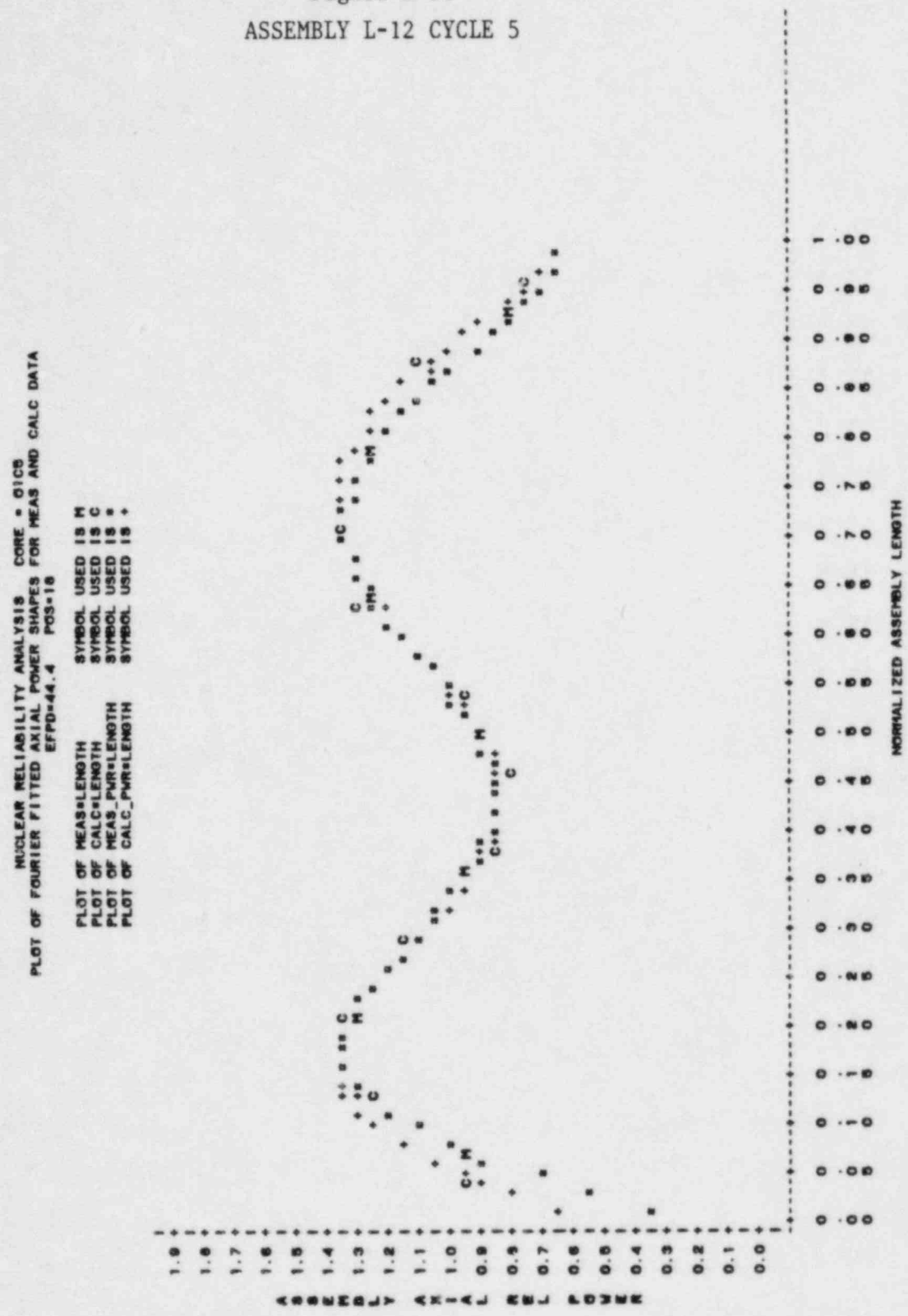

Figure A-62
ASSEMBLY L-14 CYCLE 5

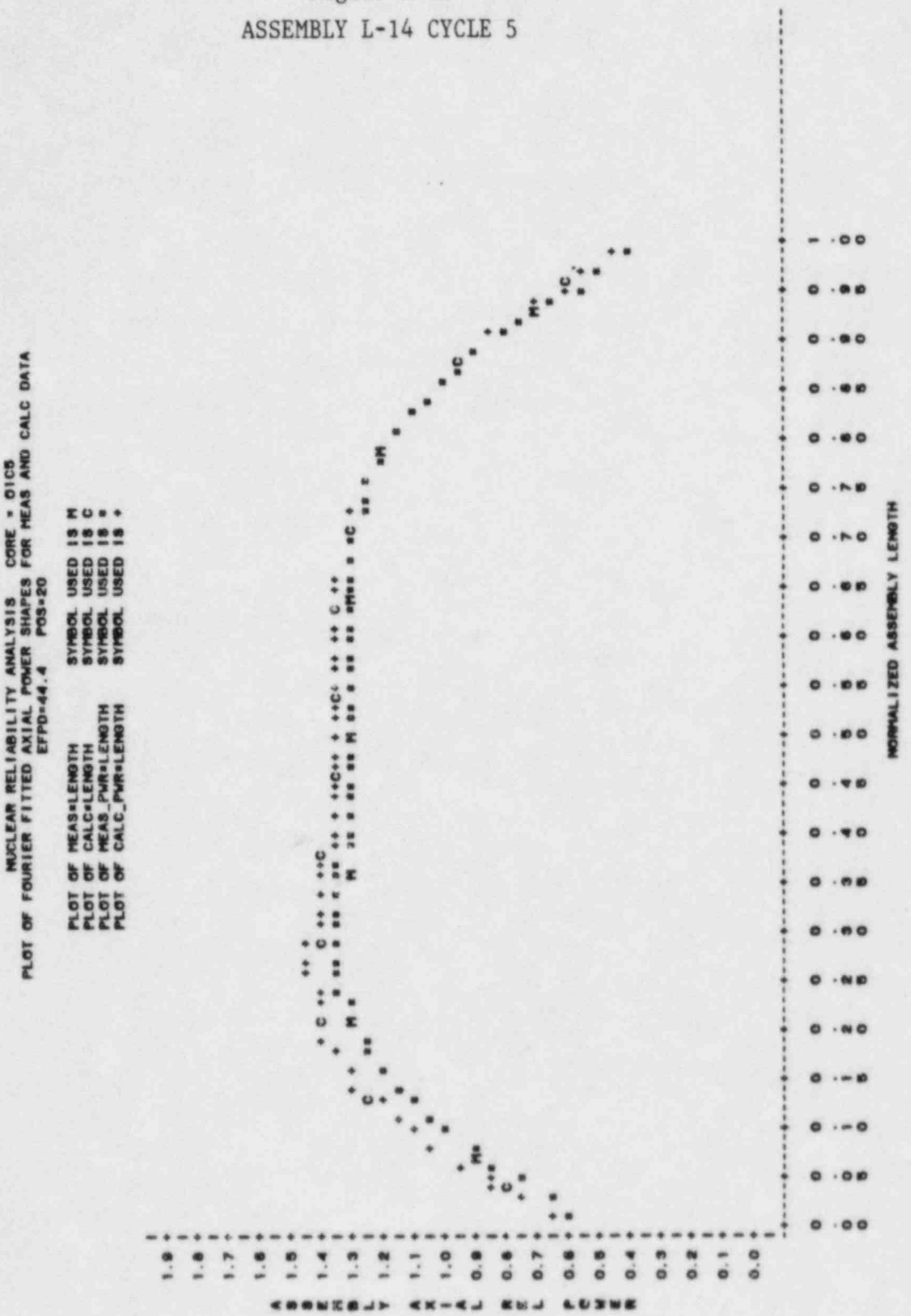

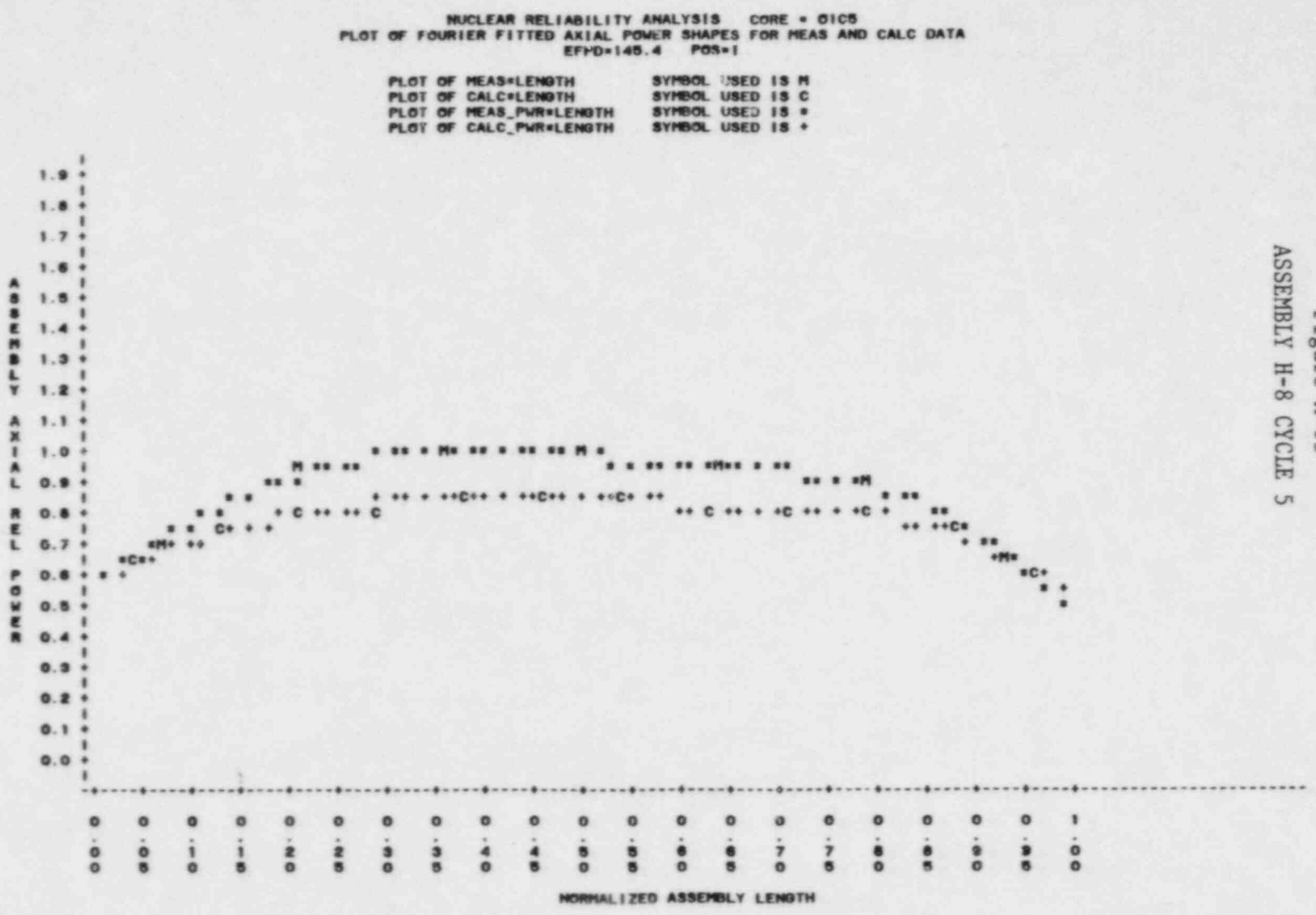

Figure A-63
ASSEMBLY H-8 CYCLE 5

Figure A-64

ASSEMBLY L-10 CYCLE 5

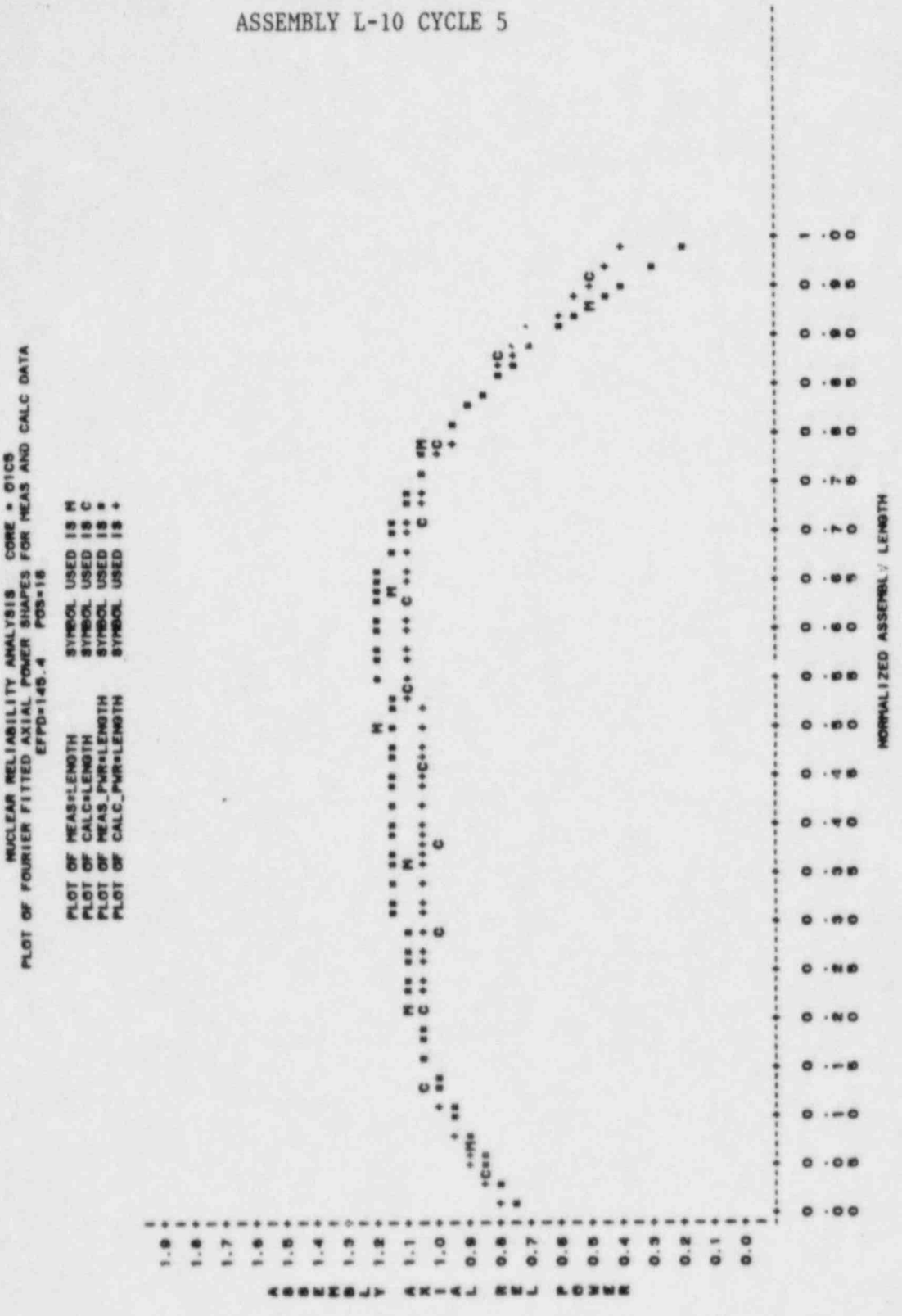

Figure A-65

ASSEMBLY L-12 CYCLE 5

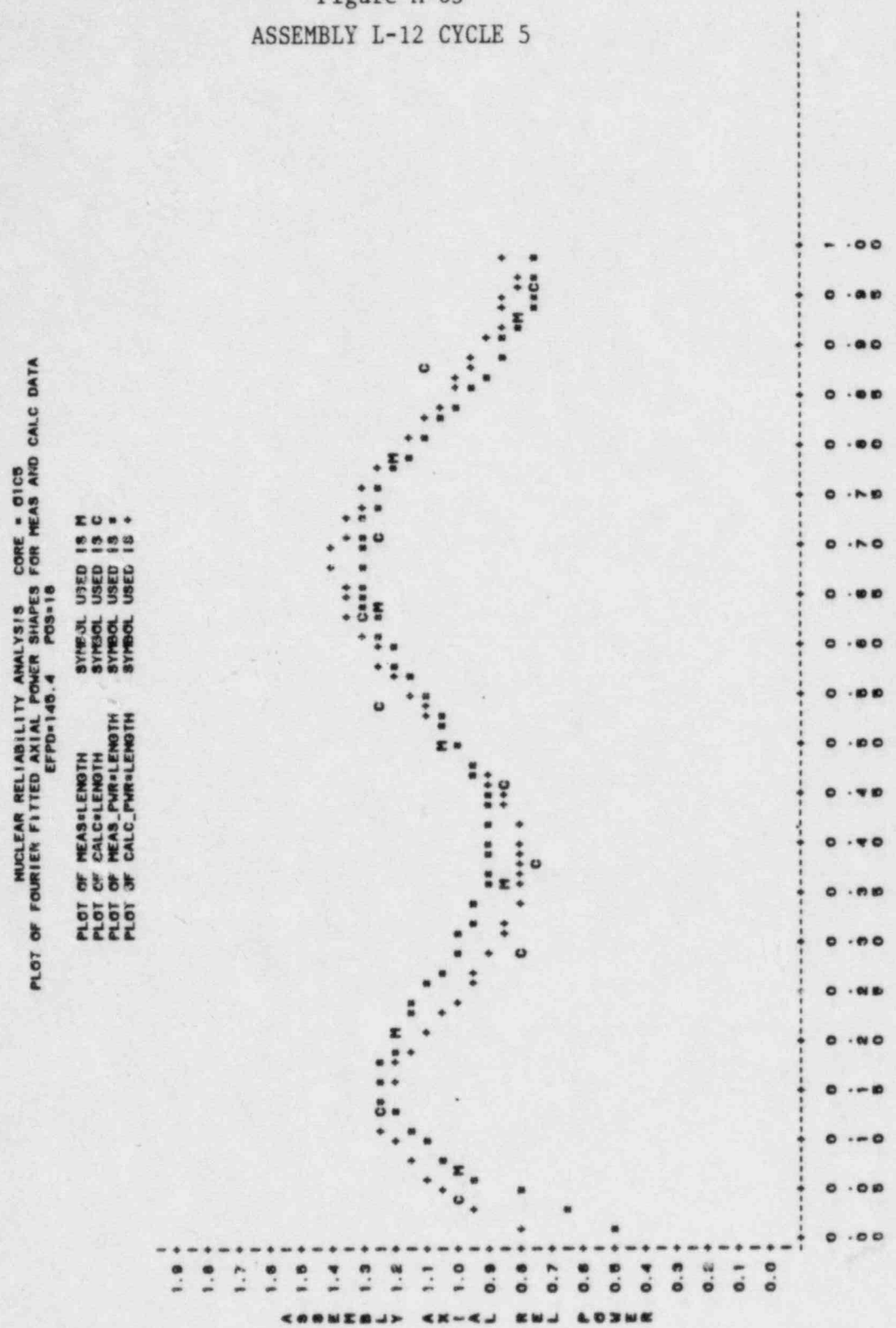

Figure A-66

ASSEMBLY L-14

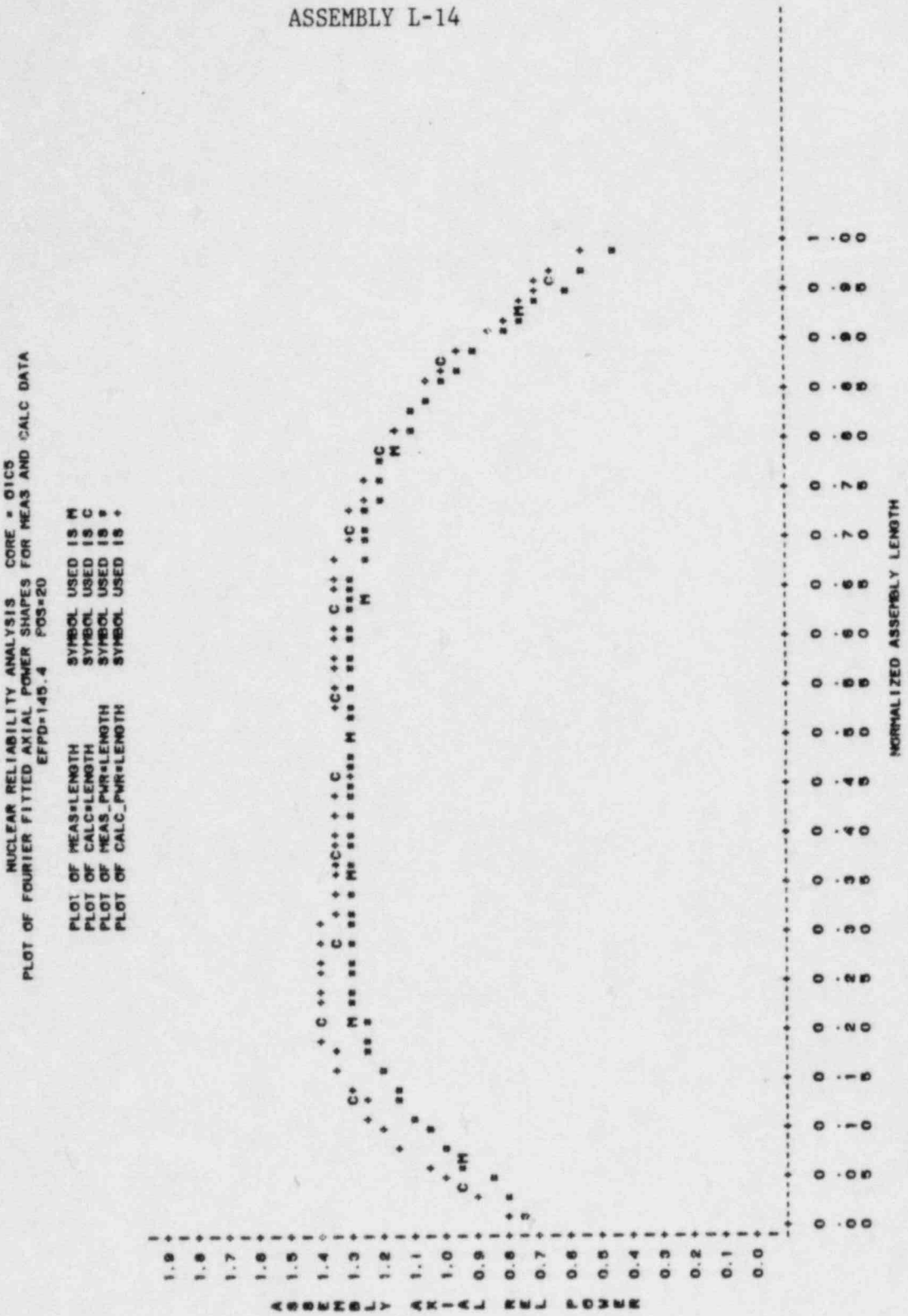

Figure A-67

ASSEMBLY H-8 CYCLE 5

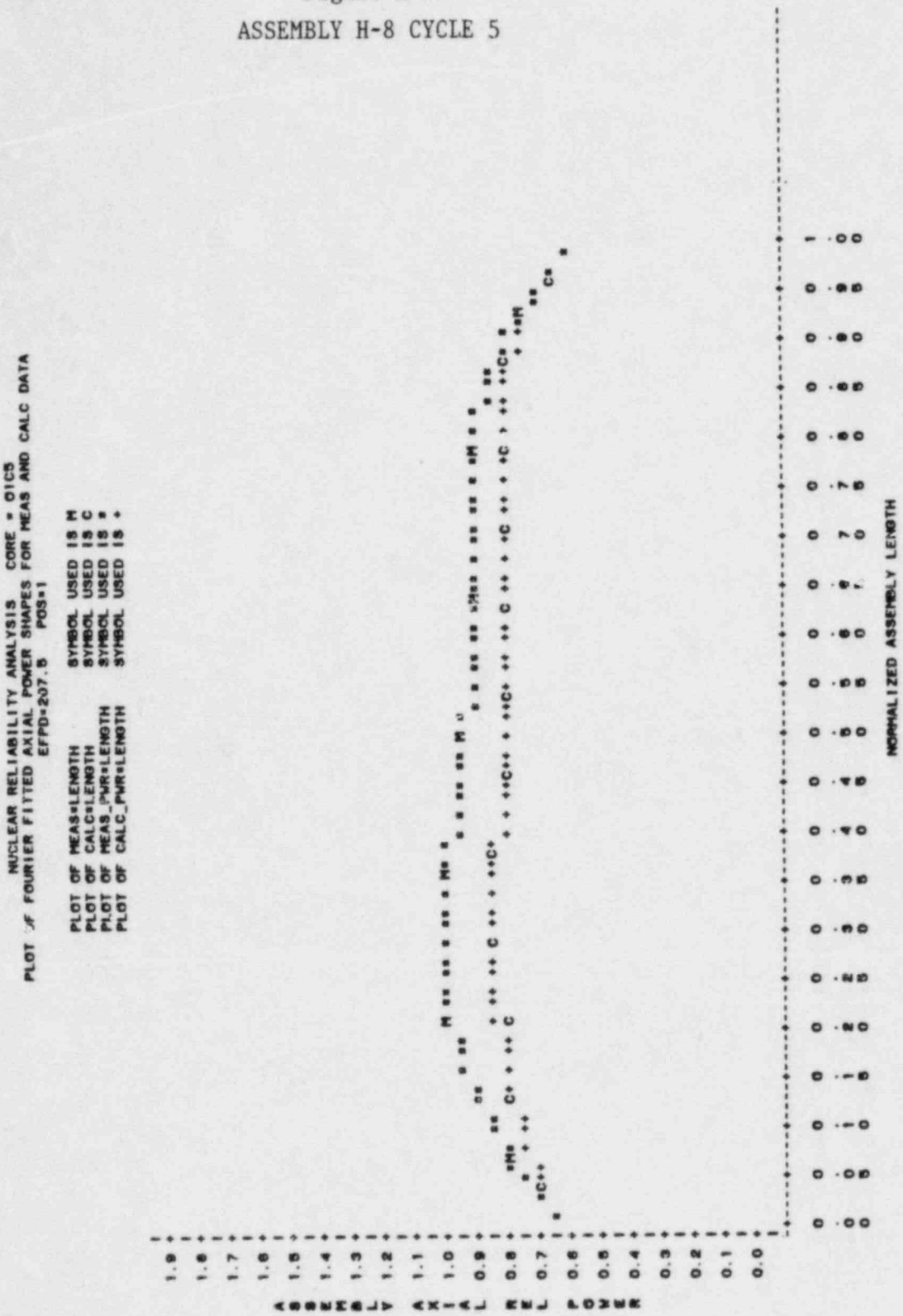

Figure A-68

ASSEMBLY L-10 CYCLE 5

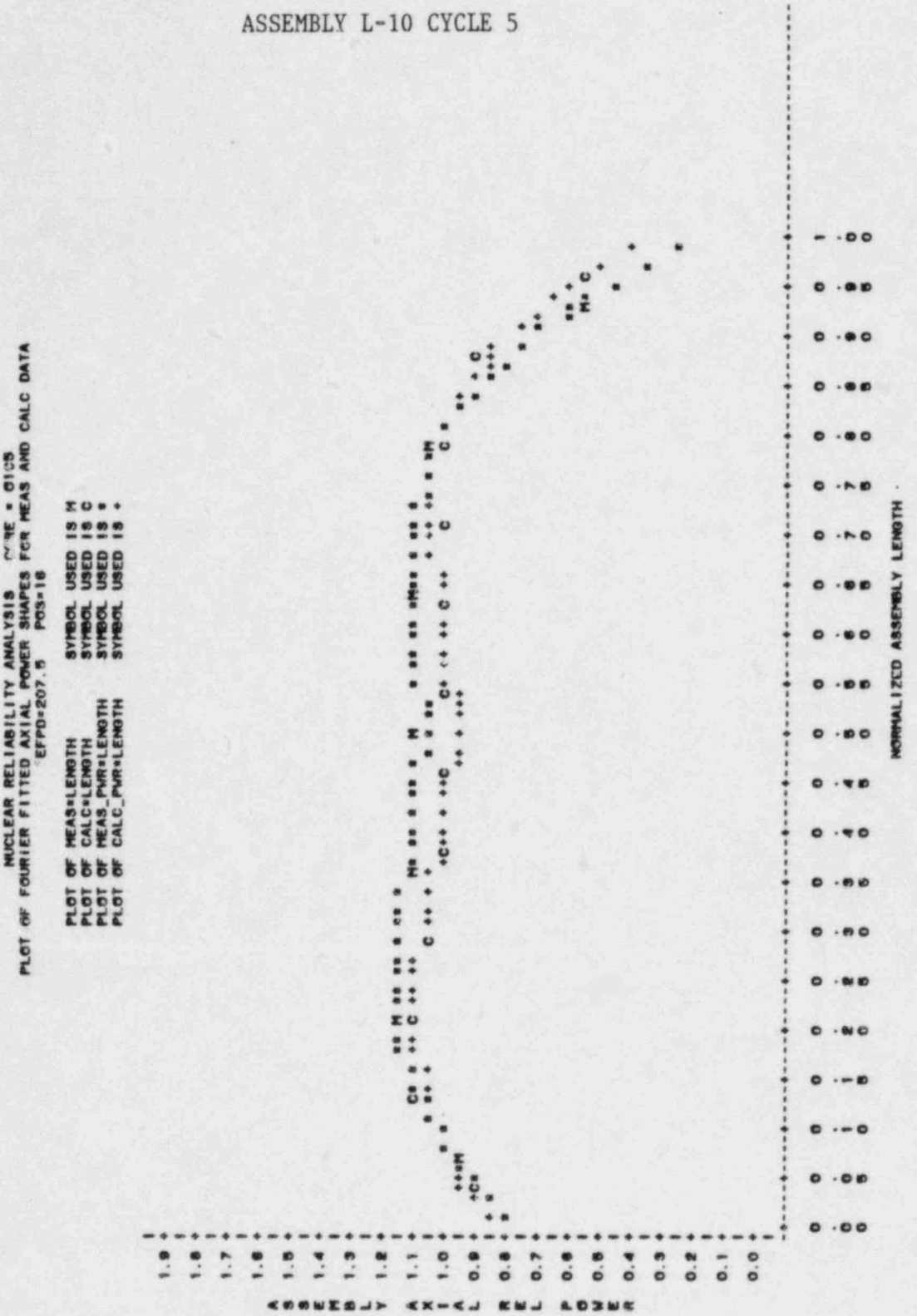

Figure A-69

ASSEMBLY L-12 CYCLE 5

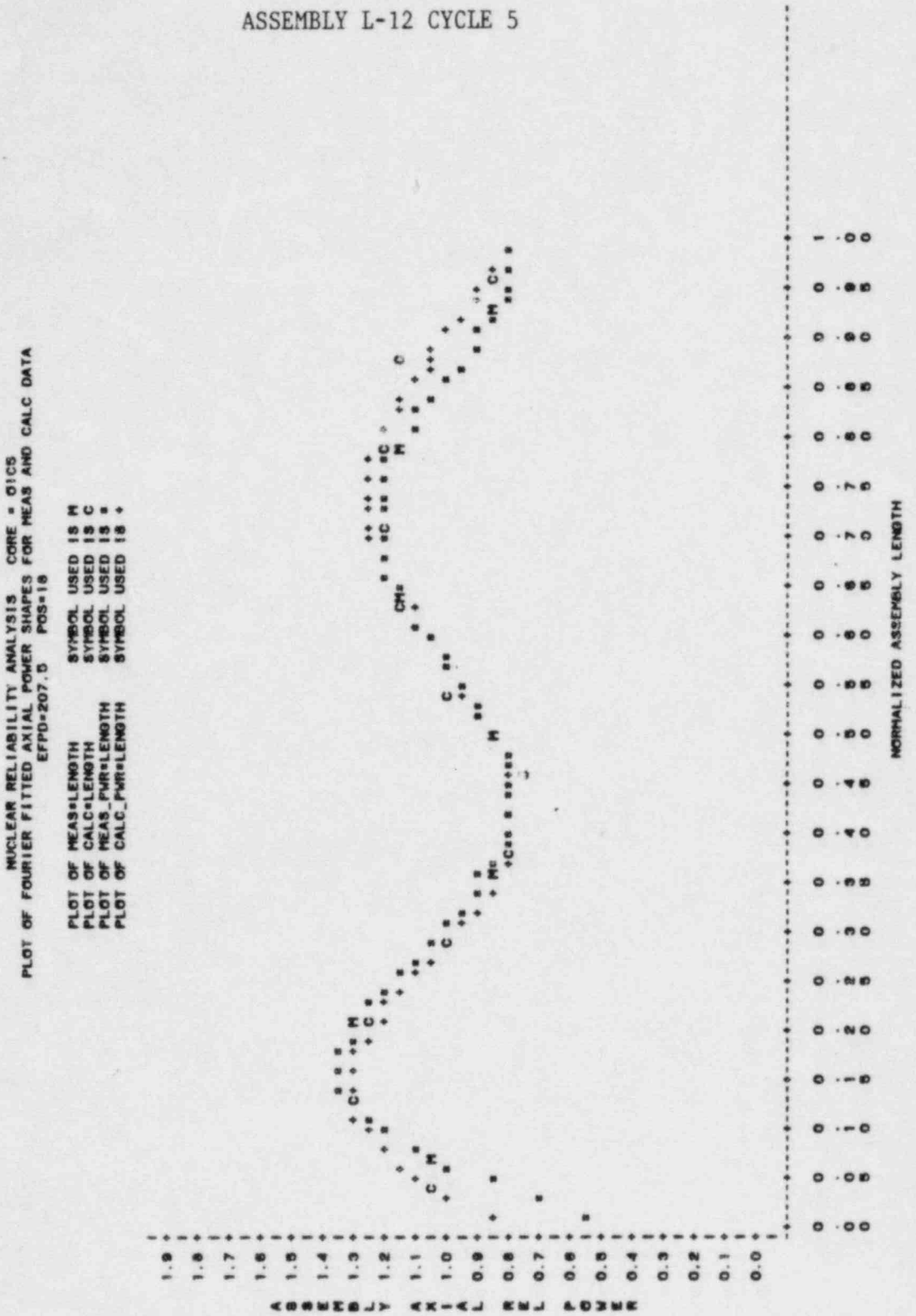

Figure A-70
ASSEMBLY L-14 CYCLE 5

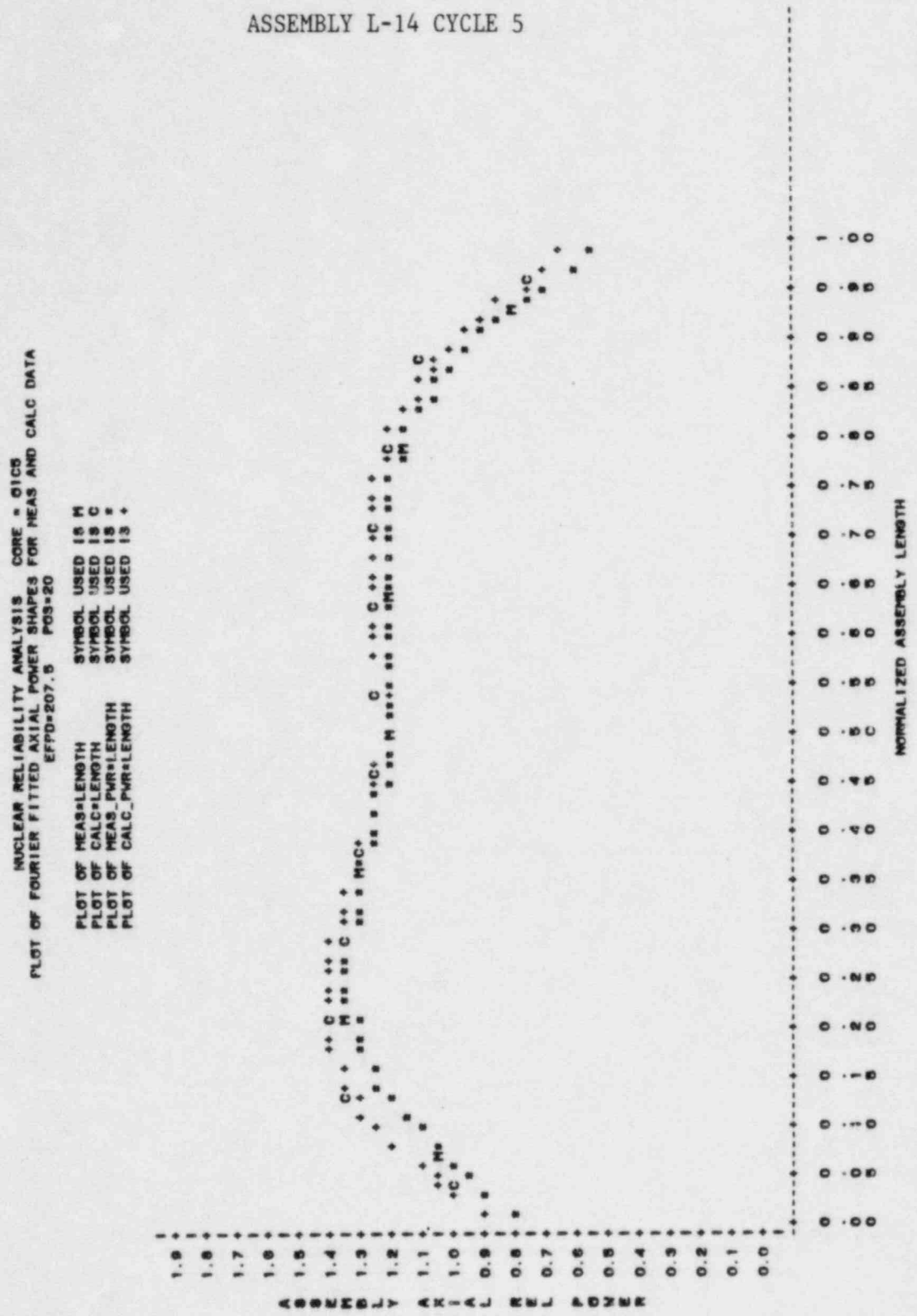

SAFETY EVALUATIONS

UNITED STATES
NUCLEAR REGULATORY COMMISSION
WASHINGTON, D. C. 20555

SAFETY EVALUATION BY THE OFFICE OF NUCLEAR REACTOR REGULATION

OF THE RELOAD DESIGN METHODOLOGY

TECHNICAL REPORT NFS-1001

FOR THE

DUKE POWER COMPANY

OCONEE NUCLEAR STATION, UNITS NOS. 1, 2 AND 3

DOCKETS NOS. 50-269, 50-270 AND 50-287

1.0 Introduction

Duke Power Company (DPC) submitted Technical Report NFS-1001, "Oconee Nuclear Station Reload Design Methodology" for NRC review on April 23, 1979 (Reference 1a). The report contains information pertaining to the design of core reloads for the Oconee Units 1, 2 and 3, and includes fuel design, mechanical and thermal-hydraulic design, Technical Specification and accident analysis review, and core physics parameters.

By letter dated May 20, 1981 (Reference 1b), DPC submitted Revision 1 to NFS-1001 which revised the original submittal in its entirety and included two supplements on comparison of predicted and measured physics parameters in addition to providing supplemental and clarifying information. Additional revisions (2, 3 and 4) were submitted by DPC on January 28, April 22, and June 16, 1981 (References 1c, 1d and 1e) to incorporate additional or clarifying information requested by the staff.

2.0 Summary of Report

Technical Report NFS-1001 describes the reload design methodology for the Oconee Nuclear Station. The topics included deal with nuclear fuel cycle

design, Technical Specifications, transient and accident analysis, the development of core physics parameters, fuel design and thermal-hydraulic analyses. All of the above are analytical procedures with the objective of designing a reload in a manner that the reactor can be operated at its power level within the specified safety margins for a given number of full power days. The nuclear fuel cycle design employs EPRI-CELL, NUPUNCHER and PDQ07 for the calculation of cross sections, assembly constants and quarter core power distributions, local pin peaking, and reactivity as a function of burnup. Finally, the results are processed by EPRI-FIT and SUPERLINK for EPRI-NODE-P which produces three dimensional information on power distribution, rod worths, etc. The Technical Specifications reflect certain Limiting Safety System Settings (LSSSs), and Limiting Conditions of Operation (LCOs) which are established on the basis of nuclear and thermal-hydraulic characteristics and the applicable transient and accident analyses. The limits refer to DNBR, linear heat generation rate, pressure-temperature regions of operation, power imbalance and centerline fuel melt limits.

The accident analysis section considers the safety analysis of postulated transient and accidents and is designed to demonstrate that the reactor is able to mitigate such events and that the calculated consequences are acceptable. Considerations of importance in the accident analysis are: values of pertinent plant parameters, performance of the assumed mitigating systems and the analytical methods. Analysis is presented for: startup accidents, uncompensated operating reactivity changes, rod withdrawal at rated power, moderator dilution, cold water injection, loss of coolant flow, stuck or dropped control rods, loss of electric power, steam line failure, steam generator tube failure, fuel handling accident, rod ejection, and loss of coolant.

The development of core physics parameters is based on measurements performed on Oconee Unit 1 Cycles 1-5 and were compared to analytical values obtained with the EPRI-NODE-P code. The measured parameters include critical boron concentration at hot, zero power (HZP) and hot, full power (HFP), control rod worths, ejected rod worths (using boron swap, rod swap and rod drop) and isothermal temperature coefficients. Comparison of calculated and measured values was used to estimate adequacy of the calculated procedures in predicting core physics parameters. Lastly, the benchmarking of the EPRI-NODE-P is described with the measured assembly powers, local radial power peaking comparisons, statistical analysis and the fitting procedure used.

Two sections of the report address reload aspects of the fuel design's material features, as apart from physics or thermal-hydraulic concerns: (1) Section 2.0 Fuel Design and (2) Section 4.0 Fuel Mechanical Performance. In the Fuel Design section, brief descriptions are provided of the fuel pellets, fuel rods, and fuel assembly design. As noted in the Fuel Mechanical Performance section, design analyses that envelope the operation of current fuel designs have been completed by the fuel vendor, and the approach taken by Duke Power Company for a specific fuel cycle (reload) design is to compare that design against the enveloping design analysis. The information contained in Section 4.0, therefore, is intended to (1) describe the types of comparisons that must be made to justify a fuel cycle design without reanalysis and (2) provide some detail concerning the types of analyses that must be performed if required by either the fuel cycle design or changes in the fuel design itself.

Section 6.0 of the report addresses the thermal-hydraulic design. A thermal-hydraulic analysis must be performed in conjunction with a reload when there is a change in fuel design, a change in the input assumptions of earlier analyses or a change in regulatory criteria. The general criterion for thermal-hydraulic performance is that no damage due to critical heat flux takes place during normal operations or anticipated transients. The thermal-hydraulic analyses, therefore establishes the maximum permissible core power and power distribution for various operating conditions and the permissible combination of core outlet pressure and reactor outlet temperature to ensure that a minimum departure from nucleate boiling ratio (DNBR) of 1.30 or greater can be maintained.

3.0 Evaluation

3.1 Core Physics Evaluation

The fuel cycle design section is divided into preliminary and final fuel cycle design. The design process is initiated with the generation of the necessary cross sections using EPRI-CELL for each of the subassemblies. They are then put into the proper tabular form by NUPUNCHER and inputed to PDQ07 which solves the diffusion-depletion problem in one, two, or three dimensions. The PDQ07 results are processed by EPRI-FIT and SUPERLINK and are input to EPRI-NODE-P which yields three dimensional power distribution, rod worths etc. The objective of this phase of the analysis is to estimate cycle lifetime, power peaking and number, and enrichment of fuel assemblies. The final fuel cycle design phase aims at optimizing the placement of the burned and fresh assemblies, control rod grouping, and burnable poison assemblies. At this point, the design must meet several criteria; radial pin peak power, moderator temperature

coefficient, maximum pellet burnup, shutdown margin and ejected rod worth at HZP and HFP. The control rod worths are calculated for operation at either the "rods in" or "rods out" mode, for several groupings, shutdown margin, ejected and dropped rod. The power distribution is calculated for the assemblies and the rods and ascertained that they meet the requirements such as the ones on linear heat generation rate and centerline melting.

The reactivity coefficients are calculated including Doppler, moderator temperature, and power and power defect. The boron related parameters, i.e., boron critical concentrations at beginning of cycle (BOC) and end of cycle (EOC) for HZP and HFP and various rod positions are computed. Finally, xenon worths and the kinetics parameters are calculated.

The technical specifications are developed for safe reactor operation under applicable transient and accident analyses. Those affected by the reload design and within the interest of this review are core safety limits emanating from or involving core physics parameters. The allowable total peaking factor is determined from the ratio of the center fuel melt linear heat rate limit over the product of the average linear heat rate times the fraction of rated power. This peaking factor is then increased by (a) the nuclear uncertainty factor of 1.075 , (b) spacer grid effect factor of 1.026, (c) radial local power peaking factor, (1.10, typical value), (d) an engineering hot channel factor of 1.014, and (e) a densification power spike factor depending on core location. From the above factors limiting safety settings have been developed for the Reactor Protection System (RPS).

The transient and accident evaluation was a systematic analysis of all postulated accidents. The accidents considered were:

(a) Uncompensated operating reactivity changes: on the basis of a Doppler coefficient of -1.17×10^{-5} $\Delta K/K/^{o}F$ and moderator temperature coefficient 0.5×10^{-4} $\Delta K/K/^{o}F$ at the BOC it was concluded that no safety limits would be exceeded.

(b) Start-up accident: during which it is assumed that a control rod is inadvertently withdrawn. Assuming total control rod worth of 10% $\Delta K/K$ and the parameters of (a) above it is concluded that the overpower limit of 112% applicable in this case is not exceeded.

(c) Rod withdrawal at rated power: the analysis in this case was carried out under the same assumptions as (b) above and the result indicated that the reactor power and pressure will remain within acceptable limits.

(d) Moderator dilution accident: occurs when the boron concentration of the coolant make up flow is less than the concentration of the primary coolant. With power and pressure assumptions as in (c) above and reactor minimum shutdown margin of 1% $\Delta K/K$ it is estimated that no safety limits will be exceeded.

(e) Cold water injection accident, i.e., the abrupt introduction of cold water was treated assuming conservative values of EOC Doppler coefficient of -1.3×10^{-5} $\Delta K/K/^{o}F$ and a moderator coefficient of -3.0×10^{-4} $\Delta K/K/^{o}F$. The minimum value of 1.3 for DNBR is not exceeded.

(f) Loss of coolant flow; which could be caused by loss of power or be due to mechanical damage to one or more coolant pumps. Assuming a Doppler coefficient of -1.2×10^{-4} $\Delta K/K/^{o}F$, moderator temperature coefficient of -0.5×10^{-4} $\Delta K/K/^{o}F$, coolant flow of 352,000 gpm, radial local power peaking factor 1.783 and axial peaking of 1.50 the criterion of 1.3 minimum DNBR for loss of power or 1.0 for mechanical failure are not violated.

(g) Control rod misalignment accident, could cause significant distortion of power distribution and result in excessive local power peaking. The requirement of 1% $\Delta K/K$ shutdown margin prevents exceeding 1.3 minimum of DNBR. The coefficients are assumed as in (e) above.

(h) Loss of electrical power will cause a reactor trip on overpower-overpressure after loss of load. This accident is the same as the analysis in the FSAR.

(i) Steam line failure, when the heat sink is essentially assumed to be lost; assuming Doppler coefficient of -1.2×10^{-5} $\Delta K/K/^{o}F$, moderator temperature coefficient of -3.0×10^{-4} $\Delta K/K/^{o}F$ and available scram worth of 3.46% $\Delta K/K$, the potential radioactivity release is within 10 CFR 100 limits.

(j) Steam generator tube failure has been analyzed in the FSAR. The analysis is valid for the reload.

(k) Fuel handling accidents are the same as those presented and analyzed in the FSAR.

(l) Rod ejection accident would result in rapid reactivity insertion. Assuming conservative parameter values for BOC and EOC it is shown that no safety limits are exceeded.

(m) The loss of coolant accident consequences are primarily dependent on the size of the break. Reactor trip and injection of borated water will limit the consequences of the LOCA. The criteria for this accident are set forth in 10 CFR 50.46 and it is shown not to be exceeded.

Development of Physics Parameters, is based upon PDQ07 and EPRI-NODE-P depletion calculations and are used to predict startup and cycle physics parameters. The comparison of calculated and measured values from Cycles 1-5 of Oconee Unit 1 confirm the adequacy of the calculational procedure. This procedure, based on EPRI-NODE-P was benchmarked with measured assembly powers and local radial peaking factors. Adequate statistical analyses and fitting procedures were discussed and documented.

The predictive capability of EPRI-NODE-P was confirmed with comparisons to measured data from Oconee 1, Cycles 1 to 5. The predictive capability discussed in the report refers to measurements before the calculation. In this manner there was assurance of the correct input. The comparisons were presented by means of the differences of measured and calculated data and their corresponding standard deviation. Calculated and measured power distributions were statistically combined to derive 95/95 Observed Nuclear Reliability Factors (ONRF) for EPRI-NODE-P calculations.

Local radial peaking factor reliability analysis involved cold criticals as well as simulated hot full power condition comparisons. The codes PDQ07, CASMO, and CPM were used. The comparisons indicated that there was a conservative overprediction of the peak pin powers for both the cold and hot criticals.

Three-dimensional Oconee simulations were performed using the EPRI-NODE-P in quarter core configurations. Auxiliary calculations were performed by CPM, EPRI-CELL and PDQ07/HARMONY. K_{eff}, critical boron concentration, power distributions and reactivity coefficients were calculated as a function of operating conditions and depletion. The results of these calculations were compared to extensive measured data from Oconee 1, Cycles 1-5.

The differences of the measured from the calculated value of a parameter were treated as on a normal distribution. On this assumption the Observed Nuclear Reliability Factor (ONRF) were calculated, for the rodded, unrodded, and combined cycles. For the unrodded cycle the radial and total ONRFs were found to be 1.03 and 1.04 respectively. However, for consistency with B&W values and for increased conservatism they are to be taken as 1.05 and 1.075 respectively. Finally, normality tests for the differences are shown.

The following is a brief description of the physics related codes. (Use the following abbreviations: MG = multigroup, 2D = two dimensional, 3D = three dimensional, TT = transport theory, DT = diffusion theory, DP = depletion.)

CASMO: MG, 2D, TT for DP calculations.

DELAY: Computes delayed neutron fractions decay constants, neutron lifetime and reactivity vs period.

EPRI-CELL: Computes fuel cell neutron spectrum dependence on space and burnup.

EPRI-CPM: MG, 2D, collision probability for PWR DP.

EPRI-FIT: A PDQ07 editor.

EPRI-NODE: 3D, computes K_{eff}, power, flow, temperature, and fuel exposure distributions. Accounts for part length rods and can be used for fuel management.

EPRI-NUPUNCHER: Cross section preparation.

EPRI-PDQ07: MG, 2D, and 3D, DT, DP.

EPRI-SHUFFLE: File manager and editor for PDQ07.

The report NFS-1001 has been reviewed within the guidelines provided by the Standard Review Plan, Section 4.3 and the applicable parts of Section 15, i.e., 15.4.1, 2, 3, 7, and 8. Sufficient information is provided in the report to permit a knowledgeable person to ascertain that the methods and techniques used are satisfactory and the data employed are adequate. On the basis of our review we concluded that Technical Report NFS-1001 may be referenced in licensing actions by the Duke Power Company for the physics calculations for the Oconee Nuclear Power Station reloading procedures. We recommend that the Duke Power Company continue to perform periodic reevaluations of the reload methodology to provide continuing assurance of model applicability.

3.2 Fuel Design Evaluation

Our review of Section 2.0 and 4.0 of Technical Report NFS-1001 was performed in conformance with the design limits and acceptance criteria used in the Safety Evaluation of the Oconee FSAR. In addition, we examined the Technical Report Sections to determine if the same fuel performance parameters and concerns were addressed there as in the original Oconee FSAR. Those parameters and issues included fission gas release, fuel rod dimensional changes, corrosion or irradiation effects of mechanical properties, fretting, seismic disturbances, temperature gradients, and cladding stress and strain.

As noted in Section 2.0 of the report, the fuel design consists of (a) fuel assembly design (material selection, fuel rod lattice, and fuel rod number specification); (b) spacer grid design (number of grids, material selection and fuel assembly end fittings); and (c) fuel rod design (rod dimensions, cladding type and dimensions, pellet density and dimensions, design of fuel stack spacers, fuel stack length, fuel rod fill gas pressure and composition, and specified tolerances on fuel rod design parameters). The fuel pellet radius is stated to be such that the cladding plastic strain will not exceed one percent. The fuel rod internal volume is said to be designed to maintain the internal pin pressures below the primary system pressure at temperatures greater than 425^{o}F for Conditions I and II operation, and all rods are to be pre-pressurized with helium to aid heat transfer, to prevent cladding collapse, and to avoid hydrogen contamination. Thus, the criteria (one percent cladding strain, fuel pin pressure less than system pressure, and no creep collapse) are consistent with the Oconee FSAR acceptance criteria and the current Standard Review Plan criteria, as well, and are, therefore, acceptable.

It is stated in report Section 4.0 Fuel Mechanical and Thermal Performance that differences in the reload fuel design (from previous design analyses) must be assessed in regard to cladding creep collapse, cladding stress and strain, fuel pin temperature, and fuel pin pressure. These parameters are all consistent with the parameters listed above for the Oconee FSAR. Individual subsections of report Section 4.0 address cladding collapse, cladding strain analysis, cladding stress analysis, fuel pin pressure analysis, linear heat rate capability, power spike model, and rod bow calculations.

With respect to creep collapse, the CROV computer code (Ref. 2) is said to be used to calculate ovality changes in the fuel rod cladding due to thermal and irradiation creep and is used to perform the fuel rod creep analysis when required. CROV predicts the conditions necessary for collapse and the resultant time to collapse. CROV is a reviewed and approved code, and its use for these purposes is acceptable. Among the inputs to the CROV code, however, are the internal pin pressures and cladding temperatures, which were stated to be calculated by TACO 2 (Ref. 3). TACO 2 is still under review and has not yet been approved. Thus, at the time of the submittal of the Oconee 3 Cycle 7 reload analysis, a reanalysis of the cladding creep-down and collapse may be

required, using an approved code such as TAFY 3 (Ref. 4)* or TACO (Ref. 5)** for input to CROV. To demonstrate acceptability, the maximum expected residence time of any fuel rod during the cycle should be less than the number of effective full power hours required for cladding collapse, as calculated by the approved codes. By letter dated June 16, 1981 (Ref. 1e) the licensee committed to use the approved TACO Code until the TACO2 Code is approved by the staff.

A generic strain analysis is said to have been completed by the fuel vendor, again using TACO 2. The same restrictions and requirements apply to its use in this application as those listed above for the cladding collapse calculation.

The cladding stress analysis is stated to be bounded by a design analysis that uses Section III of the ASME boiler and pressure vessel code as a guide in classifying the stresses into various categories, assigning appropriate limits to those categories, and combining those stresses to determine stress intensity. Although as stated in the report, reanalysis should not be required for standard mark B fuel assembly reloads (because the stress analysis "is very conservative"), each new fuel cycle design will be assessed in terms of cladding stress, taking into account such parameters as cladding O.D., I.D., and thickness, pellet diameter and

---

* TAFY-3 is acceptable provided peak rod exposures do not exceed 42 GWd/mtU.

** TACO is acceptable provided the approved version of the code is used (see reference 5).

density, and initial pre-pressure within the fuel rods. This is consistent with standard industry practice and is, therefore, acceptable. The limits for (a) fuel cladding stresses and (b) stress intensity value of the primary membrane stresses are also consistent with industry practice and are, therefore, acceptable for the same reason. Inasmuch as (a) the methods used to calculate and to combine worst case compressive loads with other loads and to analyse worst core tensile loads, as described in the technical report, are conservative, (b) the limits for cladding stresses and stress intensity are consistent with present industry practice, and (c) ovality bending stresses, flow induced vibration, and differential fuel rod growth stresses are also addressed, we conclude that the technical report provides an adequate description of cladding stress limits and methods of calculation and that the Duke reload methodology for cladding stresses is acceptable.

For the fuel pin pressure analysis, the report indicates that the same parameters as listed earlier for the cladding stress calculation are used, along with one additional parameter, pin power history versus burnup. The pin pressure analysis is said to be performed using TACO 2, which as noted earlier, is an unapproved code. Therefore, a reanalysis will be required using an approved code, if the Oconee 3 Cycle 7 reload analysis is submitted prior to approval of TACO 2. Similarly, the linear heat rate to melt (LHRTM) analysis may have to be redone because it was also performed with TACO 2.

As indicated in Section 4.8 of the technical report, the NRC rod bowing correlation is used by Duke Power in the reload design. We conclude, therefore, that the effect of rod bowing on DNBR will be appropriately accounted for up to the maximum burnup assumed in the technical report (33,000 MWd/t).

Based on our evaluation of the information provided in Technical Report NFS-1001 and in discussions held with representatives of Duke Power Company, we conclude that reasonable assurance has been provided that the Duke reload methodology is appropriately conservative with respect to the mechanical and thermal aspects of fuel performance in the reload design, and is, therefore, acceptable.

3.3 Thermal-Hydraulics Evaluation

The thermal-hydraulic analysis establishes the maximum permissible core power level and power distribution and the permissible combination of core outlet pressure and temperature to ensure that the minimum departure from nucleate boiling ratio (MDNBR) of 1.30 is not violated during steady-state operation or during anticipated transients. This criterion of 1.30 will prevent core damage for the types of operations mentioned above.

The DNBR is calculated using the Babcock and Wilcox Critical Heat Flux (CHF) correlation BAW-2. The minimum DNBR limit of 1.30 assures that there is a 95% probability at a 95% confidence of not experiencing DNB. However, the effects of rod bowing on DNBR must be accounted for in the form of a penalty applied to the MDNBR.

The rod bow penalty has an initial value of 11.2%. The staff has given a 1% credit due to a flow area reduction factor included in the thermal hydraulic analysis. Thus a penalty of 10.2% is applied to the MDNBR. This results in a MDNBR of 1.4326. This penalty is only applicable for burnups less than or equal to 33,000 MwD/MTU. If an increase in burnup is desired the applicant must submit a change to the Technical Specifications to provide for a modified rod bow penalty.

The methodology used in the steady-state analysis determines the maximum allowable pressure-temperature operating limits at 112% overpower and a set of generic DNBR curves. These curves show the allowable pressure-temperature matchups which ensure that the minimum DNBR is not violated.

The approach used in generating the curves is to determine the core mass flow rate and core inlet temperature for each operating condition. Once the core flow rate is known the core wide flow distribution is determined using the CHATA computer code. CHATA determines the assembly flow by varying this flow until each assembly has the same pressure drop and the total of the assembly flows equals the core flow. The core is modeled on an eighth-core symmetric basis and the primary output is the hot assembly flow.

The major input parameters used by CHATA are core flow effective for heat transfer, individual fuel assembly geometries, form loss coefficients, the radial peaking distribution, the 1.5 design cosine axial flux shape, and the core operating conditions.

The core flow rate is a limiting parameter in the thermal-hydraulic analysis. The Technical Specifications for the Oconee Units list the system flow rate for four pump operation as 374,880 GPM or 106.5% of the original design flow rate. This value is obtained from the lowest value of flow rate measurements and a downward adjustment of measurement uncertainty, and is acceptable. However,

reactor coolant flow reduction may occur in future cycles due to system degradation such as plugging of steam generation tubes. Therefore, the coolant flow rate listed in the Technical Specifications must be evaluated to ensure that it is the minimum acceptable flow rate needed to obtain adequate cooling. The core bypass flow is also cycle dependent. Its value depends on the number of orifice rods and burnable poison rod assemblies. A value of 8.10% is given as a typical value in this report.

The isothermal flow distribution is assumed to be relatively flat with a maximum deviation of 5% for 4 pump flow conditions. The hot assembly is assumed to receive only 95% of the total nominal assembly flow based on the assumption given above. Those values were approved in the design review of the Oconee Units (Ref. 7).

The flow maldistribution factors are considered by the use of an additional form loss coefficient located at the entrance of the hot assembly.

Once the hot assembly flow rate is known a hot assembly/hot channel analysis is performed. The hot assembly is that fuel assembly which has the highest radial peaking factors. This assembly is not an individual fuel assembly but is the intersection of four 1/4 assemblies.

The hot assembly flow rate, calculated in the CHATA analysis, is input into the TEMP code. The calculations performed by TEMP account for energy interchange between channels at each calculational increment. Mass interchange between subchannels is not included in this model. The minimum DNBR and hot channel flow rates are the outputs of importance from this analysis and are

used to establish the equivalent hot channel model discussed below. The minimum DNBR for 112% overpower analysis is the reference design DNBR. The output from this analysis is used as input in the hot channel analysis. The hot channel is that subchannel which has the highest single pin peaking factors.

The hot channel factors used in the hot assembly/hot channel analysis are listed in Table 1. A comparison of these hot channel factors and those used in the Cycle 5 and 6 Oconee Unit 3 reloads is included.

An equivalent two channel model is used for all subsequent parametric analyses. This model contains a hot channel (the results from the TEMP analysis) and an average channel. The CHATA code is used to model these two channels. The hot channel contains all the conservatisms used in TEMP. An engineering hot channel factor on enthalpy rise, $F_{\Delta h}$, is applied in the CHATA analysis. This factor is used to match the CHATA hot channel with the TEMP hot channel. The $F_{\Delta h}$ value is varied until the MDNBR calculated by CHATA equals the TEMP MDNBR. The average channel serves as a driver of the hot channel. This parametric analysis will be used to determine the pressure-temperature core protection safety limits and the generic DNBR curves.

The pressure-temperature safety limits are obtained by using the equivalent two channel model. For a given outlet pressure the inlet temperature is varied until the MDNBR of 1.4326 has been determined. Using a reactor vessel heat balance, the reactor vessel outlet temperature, for the given pressure and inlet temperature, is determined. This process is repeated for a series of different pressures, typically 1800, 1900, 2000, 2100, 2200, and 2300 psia.

The results of these calculations are the temperature-pressure points corresponding to the MDNBR of 1.4326. This analysis is performed for a combination of 4-, 3- and 2-pump cases. The most limiting type of operation is 4-pump operation. This is the same method used by Babcock & Wilcox.

The generic DNBR curves are used to determine the power-power imbalance limits based on the DNBR criterion. How the power-power imbalance limits are calculated is discussed in the SER for Section 7.2 "Technical Specifications." This report deals only with the method used to calculate the generic DNBR curves. For each series of axial peaking factors the parametric hot channel analysis uses axial power shapes which are a series of smooth curves whose peak can be specified at various distances up the channel. The Technical Report states that the power shapes used were smooth cosine curves. The licensee explained, during subsequent discussions, that the curves were derived from a polynomial without tails. The staff concludes that the use of these flux shapes in the thermal-hydraulic design is acceptable.

The power input of each channel is increased until the limiting DNBR is obtained. The maximum allowable total peak for a specified axial peak and its location are then determined. The final results of this analysis are two sets of generic DNBR curves or Maximum Allowable Peaking (MAP) curves. One generic DNB curve is used for DNB operational offset limits and the other is used for Reactor Protection System offset limits. Finally, the actual power shapes which yielded the lowest DNBR are input into the hot channel code to confirm the conservatism of the corresponding smoothed curves used in the development of the generic DNBR curves.

The thermal-hydraulic analysis used to determine the generic DNBR curves utilized two additional hot channel factors on local heat flux. A penalty of 1.026 was incurred to increase calculated axial powers since flux depression at the spacer grids is neglected and the ratio of the total nuclear uncertainty (1.075) to the radial nuclear uncertainty (1.05) resulted in a penalty of 1.024. These additional penalties increased the value of Fq" from 1.014 to 1.065.

The reactor to flow setpoint is used to initiate a reactor trip. The trip ensures that the MDNBR of 1.4326 is not violated during loss of one or more pumps. The coastdown analysis assumes the loss of two pumps because it is possible that the loss of one coolant pump may not be detected by the reactor protection system, and therefore, the reactor will not immediately trip. Since a two pump coastdown is more conservative than the one pump coastdown, and for a loss of four pumps the reactor trips immediately; the two pump coastdown is the most limiting.

The RADAR code is used for the transient analysis to assure that the 1.4326 MDNBR is not violated during the transient. The initial conditions are the results from the steady-state thermal-hydraulic analysis. The power-flow setpoint is determined by varying the time of reactor trip following the loss of two RC pumps until the minimum ratio (Flux/flow) required to maintain the MDNBR of 1.4326 has been determined.

Our review of the thermal-hydraulic design of the Duke reload methodology included the CHF correlation, the computer codes used, the method of combining the codes, the peaking factors used, the method of determining pressure-temperature core protection safety limits and the method of generating the generic DNBR curves.

The staff has previously approved the BAW-2 CHF correlation (Ref. 16) and the TEMP computer code. The use of the BAW-2 CHF correlation in a subchannel analysis performed by CHATA is still under staff review. Also, the CHATA computer code is being reviewed by the staff. However, the CHATA code with the BAW-2 correlation has been used in the thermal-hydraulic design of Babcock & Wilcox reactors and found to be acceptable for preliminary design approval by the staff (Refs. 11 and 12). Based on these previous approvals and the current advanced status of our CHATA review, the staff concludes that the use of the BAW-2 correlation in a CHATA subchannel analysis and the use of CHATA are acceptable in this analysis. Any limitations resulting from our completion of the CHATA review will be compensated for by appropriate operating restrictions; however, none are anticipated.

The method of combining the CHATA core wide analysis and the TEMP hot assembly/hot channel analysis; the equivalent two channel analysis; and the initial conditions, from the TEMP steady-state analysis, for the RADAR transient analysis are acceptable based on our preliminary review of CHATA. Once again any limitations identified during completion of the CHATA review will be appropriate by compensated for by operating restrictions.

The values and use of the peaking factors, both local and total, can be easily verified in either the Oconee FSAR or approved B&W topical reports. Therefore, the staff concludes that their use in the Oconee Reload Methods is acceptable. The peaking factors Fq, Fq" and FA, and the design radial-local peaking factor, have all been approved by the staff in the Oconee Units SER (Ref. 21). The reactor flow of 106.5% and the bypass flow of 8.10% were approved in the Cycle 6 reload but can vary from reload to reload; therefore, the staff can not give a generic approval to these items.

In summary, the staff concludes that the methodology used by Duke is an acceptable means of performing the thermal-hydraulic analysis necessary for a reload with the limitations discussed above. If any of the parameters are changed such as the DNBR penalty for rod bow, the licensee should justify the use of these new numbers in their thermal-hydraulic analysis. If the DNBR penalty is changed, the licensee should insert into the basis of the technical specifications any generic or plant specific margin that has been used to offset the reduction in DNBR due to rod bow and identify the source and reference previous staff approval of each generic margin.

Table 1

Thermal-Hydraulic Design Comparisons

	Cycle 5 Unit 3	Cycle 6 Unit 3	Reload Methodology
Reactor Coolant Flow % Design	106.5	106.5	106.5
Core Bypass Flow % Total	10.4	8.10	8.10
Ref. Design radial-local power	1.71	1.71	1.71
Hot Channel Factors: Enthalpy Rise	1.011	1.011	1.011
Heat Flux	1.014	1.014	1.014
Flow Area	0.98	0.98	0.98
Min. DNBR w/o Densification Penalty	1.4326	1.4326	1.4326
CHF Correlation	BAW-2	BAW-2	BAW-2

The P-T limits are used to determine the core outlet pressure - vessel outlet temperature conditions which will ensure a MDNBR of 1.30 when other pertinent parameters are at their design limit (maximum or minimum). The design MDNBR of 1.4326 was calculated for 4-pump operation at 112% overpower. The SER for Section 6 tells how the DNBR-core outlet pressure - vessel outlet temperature curves are generated. These curves used a DNBR of 1.4326 as their parameter and were generated for 4-, 3- and 2-pump operation. These curves serve as the basis of the Tech. Spec. P-T limits.

Since the curves where generated for DNBR of 1.4326, the staff concludes that the method used to determine the Tech. Spec. P-T limits is conservative and therefore, acceptable.

The method used to determine the Power-Power Imbalance limits is to first perform a maneuvering analysis which generates the power distribution in the core for various design conditions and various times in the cycle. The calculated maximum total peaking factors of each assembly are increased by a radial uncertainty factor of 1.05, and a radial-local factor, and the resulting adjusted peak is compared to the allowable peaking factor for that axial peaking factor and axial peak location. The DNBR margin is then calculated for each assembly in the 1/4-core, and then the MDNBR margin in the core for each power distribution is determined.

Finally the axial offset limits that correspond to the acceptable DNBR margin are determined. The licensee stated that these limits "are determined in a manner similar to that used to establish the center fuel melt limited offset limits." The staff has reviewed this methodology and concludes that the methodology used to determine the power-power imbalance limits is acceptable for preliminary design considerations.

The RPS P-T trip setpoints are derived by error adjusting the P-T core safety limits generated in Section 7.2.1 and also considering the high RCS pressure, low RCS pressure, and high RCS outlet temperature setpoints.

First the high RCS pressure setpoint (2300 psig), the low RCS pressure setpoint (1800 psig) and the high RCS temperature setpoint (619 F) are identified on the Core Safety P-T Limit Curve. The locus of P-T points constrained by the high RCS pressure trip, low RCS pressure trip, and high RCS temperature is determined using the trip points and the P-T safety curve discussed in Section 6 and 7.2-1. The pressure-temperature points are adjusted to account for the difference between core pressure and the RCS pressure at the measurement location and for errors in measurements. The net error adjustment for pressure is 0 psi and the error-adjustment for Temperature is $+1\ ^{o}F$. The temperature adjustment accounts for the maximum temperature error in the instrumentation string. The pressure measurement error is ± 30 psia which is added to the difference between the hot leg and core outlet, P = +30 psi. Therefore, the net error-adjustment is 0 psi.

The staff has reviewed this method and compared it with the method used by Babcock and Wilcox. Based on our review and the fact that the Duke method is comparable to the Babcock and Wilcox method, the staff concludes that the Duke method is an acceptable method. However, Duke should supply adequate justification to show that the error-adjustments do not change for each reload.

The power-flow-imbalance trip setpoint is the value of reactor power at which a RPS trip should occur. The trip should occur whenever the combinations of power, flow and their uncertainties produce values of power and flow which result in the design MDNBR during a flow transient and whenever the combination of power, imbalance, and their uncertainties correspond to the core safety limits on power imbalance.

This setpoint is determined by first calculating the maximum power/flow or flux/flow ratio. This calculation is described in the SER on Section 6. The ratio is then reduced by an error adjustment factor. This factor accounts for noise in the RPS flow signal and other electronic erros in RPS flow instrumentation. Next, an error adjustment factor of 6.5% FP is used to adjust the power level limit and the imbalance limit. The 6.5% adjustment factor is comprised of a 4% FP allowance for neutron flux error, 2% FP allowance for the calorimetric error, and 0.5% FP allowance for any setpoint error. The error adjustment factor for imbalance is a function of the imbalance limit and power level limit and is used to account for the uncertainty in the measurement of axial imbalance by the out-of-core detector system.

Finally, a set of curves are produced which envelop the allowable operation. The curves are flux/flow setpoints for 4-, 3-, and 2-pump operation.

The staff has reviewed the method used to determine the Flux/Flow setpoint and compared it with the method used by Babcock and Wilcox. Based on our review and comparison the staff concludes that it is an acceptable method.

4.0 Conclusion

The staff has reviewed Technical Report NFS-1001, "Oconee Nuclear Station Reload Design Methodology", as revised through Revision 4 (References 1a, 1b, 1c, 1d and 1e) and has concluded, based on the considerations and approval of the individual issues discussed above, that the use of this methodology is an acceptable means of performing reload design calculations for future Oconee Nuclear Station Units 1, 2 and 3 reloads.

Dated: July 29, 1981

References

1. a) William O. Parker, Jr. (Duke Power Company) letter to H. R. Denton (NRC), April 23, 1979.

   b) William O. Parker, Jr. letter to H. R. Denton, May 20, 1980.

   c) William O. Parker, Jr. letter to H. R. Denton, January 28, 1981.

   d) William O. Parker, Jr. letter to H. R. Denton, April 22, 1981.

   e) William O. Parker, Jr. letter to H. R. Denton, June 16, 1981.

2. "Program to Determine In-Reactor Performance of B&W Fuels - Cladding Creep Collapse," Babcock and Wilcox report BAW-10084P, Rev. 1, October 1976.

3. Y. A. Hsii, et al, "TACO-2: Fuel Pin Performance Analyses," Babcock and Wilcox Company Report BAW-10141P, January 1979.

4. C. D. Morgan and H. S. Kao, "TAFY - Fuel Pin Temperature and Gas Pressure Analysis," Babcock and Wilcox Company Report BAW-10044, May 1972.

5. "TACO - Fuel Pin Performance Analysis," Babcock and Wilcox Company Report BAW-10087P-A, Rev. 2, August 1977.

6. "Rules for Construction of Nuclear Power Plant Components," ASME Boiler and Pressure Vessel Code, Section III, 1977.

7. Oconee Nuclear Station, Units 1, 2, and 3 Final Safety Analysis Report Docket Nos. 50-269, 50-270 and 50-287.

8. J. M. Alcorn, R. H. Wilson, "CHATA-Core Hydraulic and Thermal Analysis," BAW-10110, Rev. 1, May 1977.

9. C. D. Morgan, H. C. Cheatwood, and J. R. Gloudemans, "RADAR-Reactor Thermal and Hydraulic Analysis During Reactor Flow Coastdown," BAW-10069, July, 1973.

10. "TEMP-Thermal Enthalpy Mixing Program" BAW-10021, April, 1970.

11. D. F. Ross, Jr., (AD for Reactor Safety, DSS) to D. B. Vassallo, (AD for LWRs, DPM) Memorandum, "BSAR-205 SER Input," May 25, 1977.

12. D. F. Ross, Jr., (AD for Reactor Safety, DSS) to D. B. Vassallo, (AD for LWRs, DPM) Memorandum, "Midland 1 and 2 - Round 2 Questions," September 28, 1978.

13. Oconee Unit 3, Cycle 5 - Reload Report BAW-1522, Babcock & Wilcox, March, 1979.

14. Oconee Unit 3, Cycle 6 - Reload Report BAW-1634, Babcock & Wilcox, August, 1980.

15. L. S. Rubenstein (AD for Core and Containment Systems, DSI) to T. M. Novak, (AD for Operating Reactors, DL), Memorandum, "CPB Thermal-Hydraulic SE Input on Oconee, Unit 3, Reload Safety Analysis", Feb. 2, 1981.

16. D. F. Ross, Jr., (AD for Reactor Safety, DSS) to R. C. Young (Ad for LWRs), Memorandum, "Topical Report Evaluation - BAW-10000, Correlation of Critical Heat Flux in a Bundle Cooled by Pressurized Water", March 2, 1976.

17. Midland Plant, Units 1 and 2 Final Safety Analysis Report, Docket Nos. 50-329, 50-330.

18. D. F. Ross, Jr., (AD for Reactor Safety, DSS) to D. B. Vassallo (AD for LWRs, DPM), Memorandum, "Evaluation of the Effect of a Change in the Flow Maldistribution Factor on DNB for Babcock and Wilcox 205 Fuel Assembly Plants (Reissued)," May 23, 1978.

19. H. A. Hassan, et al.,"Power Peaking Nuclear Uncertainty Factors,", BAW-10119-P-A, February, 1979.

20. "Safety Evaluation Report of the Duke Power Company Oconee Nuclear Power Station Unit 1" Docket 50-269 U. S. Atomic Energy Commission, December 29, 1970.

21. "Safety Evaluation of the Oconee Nuclear Power Station Units 2 and 3" Docket 50-270; 50-287, U. S. Atomic Energy Commission, July 6, 1973.

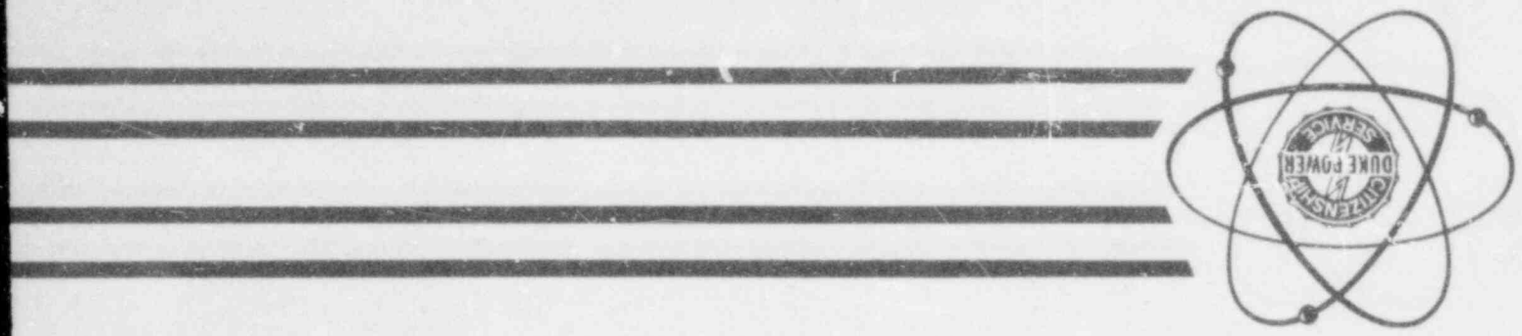
CITIZENSHIP
BY
DUKE POWER
SERVICE